Facies analysis and correlations in complex mineralised submarine volcanic successions: Mount Read Volcanics, western Tasmania

by

Pedro David Pereira da Fonseca
B.Sc. Honours
University of Lisbon, Portugal

Submitted in fulfilment of the requirements for the degree of Doctor of Philosophy

ARC CENTRE OF EXCELLENCE IN ORE DEPOSITS
University of Tasmania, Australia
February 2016

Statement

This thesis contains no material which has been accepted for the award of a degree or diploma by the University or any other institution and, to the best of my knowledge and belief, contains no copy or paraphrase of material previously published or written by any other person, except where due acknowledgement is made in the text of this thesis.

Pedro David Pereira da Fonseca
1 February 2016

Authority of access

This thesis may be made available for loan and limited copying in accordance with the Copyright Act 1968.

Abstract

Volcanic-hosted massive sulfide (VHMS) deposits provide a significant contribution to world zinc, copper, lead, silver, and gold and continue to be a target for significant base metal exploration. The Middle to Late Cambrian Mount Read Volcanics in western Tasmania are altered, deformed and metamorphosed submarine volcanic facies interfingered with sedimentary rocks, comprising one of the richest VHMS provinces worldwide. The Mount Read Volcanics host six world-class VHMS deposits ranging from polymetallic Zn-Pb-Cu-rich (Hellyer, Que River, Rosebery and Hercules) to Cu-rich (Mount Lyell) and Au-rich (Henty).

Previous studies and recent high-precision dating conducted in the Mount Read Volcanics have led to the hypothesis that ore formation occurred during a single chronostratigraphic interval. However, the Hellyer, Que River, Rosebery and Hercules VHMS deposits in the northern Mount Read Volcanics occur in a range of local geological settings and within very different host volcanic successions, hampering stratigraphic correlations both on regional and local scales.

These major deposits occur at two stratigraphic levels; the stratigraphically higher level (Hellyer and Que River) is associated with polymictic, basaltic to dacitic, volcanic breccia and coarse-grained sandstone of the mixed sequence of the Que-Hellyer Volcanics (Mount Charter Group), and the lower level (Rosebery and Hercules) is associated with feldspar-phyric fiamme breccias and interbedded pumice-rich sandstone and siltstone of the Hercules Pumice Formation (upper Central Volcanic Complex). Furthermore, the Hellyer and Que River VHMS deposits are accepted to have formed dominantly by seafloor massive sulfide deposition whereas several different genetic models have been proposed for the formation of the Rosebery and Hercules VHMS deposits, both by syn-volcanic sub-seafloor replacement and seafloor massive sulfide accumulation.

In this study, the integration of diamond drill core logging, geological mapping, facies analysis, thin-section petrography and whole-rock compositional data of the upper Central Volcanic Complex and overlying western volcano-sedimentary sequences (Mount Charter and Dundas Groups) is used to establish local and regional lithostratigraphic correlations in the Sock Creek-Burns Peak area with the adjacent VHMS-hosting areas to the NE (Hellyer-Mount Charter) and SSW (Rosebery-Howards Road). These techniques are combined with the examination of the different genetic models, local geological settings and host volcanic successions of the Hellyer, Que River, Rosebery and Hercules VHMS deposits in order to constrain the most prospective stratigraphic position in the Sock Creek-Burns Peak area.

The Sock Creek-Burns Peak area of the northern Mount Read Volcanics comprises the upper Central Volcanic Complex and the Mount Charter Group. The stratigraphy of the Sock Creek-Burns Peak area can be considered in terms of seven regional stratigraphic units (USB), one of which (USB4b, polymictic volcanic breccia and sandstone) has been correlated with the mixed sequence of the Que-Hellyer Volcanics. This unit overlies dacitic facies that are possible equivalents of lithologies occurring in the footwall succession of the Hellyer and Que River VHMS deposits, and underlies black mudstone (USB5) and polymictic quartz-bearing, mass flow-type volcaniclastic units that are likely equivalents of lithologies occurring above the Hellyer, Que River, Rosebery and Hercules VHMS deposits.

Assuming that a syn-volcanic, sub-seafloor replacement model best accounts for the formation of the Rosebery and Hercules VHMS deposits, this study proposes that the emplacement of USB4b in the Sock Creek-Burns Peak North area occurred immediately before, to at the same time as, the formation of the Hellyer and Que River seafloor and the Rosebery and Hercules sub-seafloor VHMS deposits in the northern Mount Read Volcanics. This major VHMS-forming event coincided with a period of quiescence in volcanic activity during which deposition of black mudstone (USB5 and possible correlates) occurred in the northern Mount Read Volcanics.

Prior to the formation of the VHMS deposits, at approximately 503 Ma, major explosive eruptions generated the rhyolitic pumice breccia of the Footwall Member of the Hercules Pumice Formation in the Rosebery-Hercules area (SSW of Sock Creek-Burns Peak), and feldspar-phyric rhyolitic to dacitic and minor feldspar-quartz-phyric rhyolitic lavas, domes and minor cryptodomes were emplaced in the Sock Creek-Burns Peak (USB1) and White Spur-Howards Road area (correlated with the Central Volcanic Complex), and presumably also in the Hellyer-Mount Charter area (NE of Sock Creek-Burns Peak). Dacitic-andesitic volcanic centres in the Sock Creek-Burns Peak area and basaltic-andesitic-dacitic volcanic centres in the Hellyer-Mount Charter area developed probably at the same time as the Host-rock Member of the Hercules Pumice Formation and back mudstone accumulated slowly over an approximately 3-million-year period in the Rosebery-Hercules area.

The VHMS deposits mark the only chronostratigraphic horizon at approximately 500 Ma. The mixed sequence of the Que-Hellyer Volcanics accumulated in the Hellyer-Mount Charter area and its correlate (USB4b, polymictic volcanic breccia and sandstone) was deposited in the Sock Creek-Burns Peak North area while black mudstone continued accumulating in the Rosebery-Howards Road area. Regional, basin-wide deposition of black mudstone followed in the Hellyer-Mount Charter (Que River Shale) and Sock Creek-Burns Peak (USB5) areas at the same time as black mudstone was still accumulating in the Rosebery-Howards Road area. Following the major phase of massive sulfide formation, explosive eruptions produced the volcanic quartz-bearing units of the Hangingwall Volcaniclastics in the Rosebery-Hercules area and the White Spur Formation in the White Spur-Howards Road area. Similar volcanic quartz-bearing lithofacies were deposited at approximately the same time in the Sock Creek and Burns Peak areas (USB7) while the Que River Shale continued accumulating in the Hellyer-Mount Charter area.

Despite the lack of evidence for the presence of economically significant mineral deposits in the Sock Creek-Burns Peak area, USB4b represents the lithostratigraphic unit in the Sock Creek-Burns Peak area favorable for the formation of Hellyer-Que River-like seafloor VHMS deposits, and the volcano-sedimentary succession in the Sock Creek-Burns Peak area below the top of USB4b is potentially prospective for Rosebery-Hercules-like sub-seafloor VHMS deposits. This stratigraphic interval includes dominantly coherent feldspar-quartz-phyric rhyolite and feldspar-phyric dacite, and monomictic rhyolite and dacite breccia facies of USB1 (upper Central Volcanic Complex) that are equivalent to the stratigraphic level at which the Rosebery and Hercules sub-seafloor VHMS deposits occur. Tracing USB4b to the SW and further investigating the volcano-sedimentary succession below the top of USB4b in the Sock Creek-Burns Peak area may assist in future VHMS exploration.

The volcanic footwall and host successions to the VHMS deposits at Hellyer and Que River (feldspar-phyric andesites and basalts, and polymictic volcanic breccia, sandstone and mudstone) and at Rosebery and Hercules (feldspar-phyric fiamme breccia, and pumice-rich sandstone and siltstone) are very different in character and do not constitute good exploration guides to other VHMS deposits elsewhere in the northern MRV. They were deposited synchronously with the emplacement of partly extrusive rhyolite and dacite cryptodomes, domes and lavas, and andesitic to basaltic lavas and domes in the Sock Creek-Burns Peak area. However, the hangingwall successions at all deposits comprise black mudstone and mass flow-type, volcanic quartz-bearing volcaniclastic units that are excellent stratigraphic markers for VHMS exploration.

Acknowledgements

This research was financially supported by the Fundação para a Ciência e a Tecnologia (FCT, Portugal) and the ARC Centre of Excellence in Ore Deposits (CODES, Tasmania).

First, I would like to thank my supervisors Jocelyn McPhie, Andrew McNeill and Jorge Relvas for their guidance, support, encouragement, friendship and thorough reviews of chapters. Thank you Jocelyn for your invaluable patience, time and effort you have so kindly provided, and for reviewing all the chapters repeatedly and tirelessly during the last year. You have been crucial for the construction of this thesis, and have constantly given me focus, determination and motivation in completing the PhD. Thank you Andrew for your enthusiasm, huge smile and precious feedbacks during the countless meetings while you were at CODES. Thank you for your help during fieldwork and for sharing your stories and adventures in Tasmania and your perseverance and skills in finding shortcuts... You surely deserve extra chips for that! And thank you Jorge for your companionship, joy and valuable advice in keeping me intact. Thank you for making the Tasmanian journey possible. Now we can finally have lunch!

I must thank Mineral Resources Tasmania and Minerals and Metals Group for the logistic and technical support provided to this research and for arranging access to drill core in Mornington and Tullah. I especially thank Craig Archer, Shane Heawood and Todd McGilvray for all the insightful conversations and for letting me know a few hidden treasures about Australians. I would like to thank all the past and present researchers and staff at CODES for making me feel at home and for always being available with a smile.

I would especially like to thank Gina Zalmstra, Karen Mollross, Rose Pongratz, Keith Dobson, Peter Cornish and Steve Calladine for all the administrative and technical assistance. I am grateful to Al Cuison for the lapidary work and Ian Little for the XRF analyses. I am indebted to Izzy von Lichtan for all the help with the rock cataloguing and June Pongratz for putting my thesis together.

Thank you to all my friends and PhD students at CODES. I am very grateful for everything you have taught me and for all the funny moments. A special thank you goes to Martin Jutzeler for all the helpful discussions, and for first picking me up at the Hobart airport and introducing me to Tasmania. Special thanks also go to Jeff Steadman for making me laugh with his terrific Yoda voice, Nic Jansen for teaching me how to cook delicious turkey and for reminding me to bring a plate, Heidi Berkenbosch for her kindness and precious advice, and Paul Ferguson for sharing his computer skills.

I am also extremely grateful to the CODES SEG Student Chapter for organizing the memorable Geology and Ore Deposits of Thailand and Laos fieldtrip in 2012. What an eye-opening and rewarding experience that was.

To all my friends in Tasmania and mainland Australia, thank you for your friendship and all the great memories. Thank you for making my stay so enjoyable and unforgettable, and for your rock solid, heart touching support during the good and rough moments. I would especially like to thank Helen Kollias and her family for the unwavering love, friendship and support, and for providing me with a second home where I know I will always be welcome. Thank you Helen for your unconditional love, true friendship and all that you have done for me. I am extremely grateful to Joanna Langman, Gregorio and Maria, and the Kerr family for their generosity and kindness in providing me with a home in which to live during my last year in Tasmania when my scholarship expired. Thank you Richard, Sue and Esther for putting up with my portuguese habits in your home. You set an example and inspire me to pay it forward. To my dearest friends Bud and Win, thank you for believing in me and for all your support, friendship and hospitality. Thank you Imma and John for offering your home and for always making me welcome. I must thank all the beautiful people from "Casa Cubana" and "SALSAme" for your hospitality and for accepting a foreigner's point of view. I am especially grateful for all the dances and all that you have shared and taught me. I especially thank Ildiko Nagy for all the help during my last months in Tasmania, Barry Dickson for all the insightful conversations and countless cups of tea with extra honey, Neil Carbery for the contagious enthusiasm, energy and support, Christine Swan for the beautiful, inspirational words before I left Tasmania, Mandy Lorelei for all the support and motivation, Matt and June Scriber for your hospitality and endless joy, Lyndel Dean and Tunde Frisnyak for your kindness and support, Cathy Walker for your beautiful music and for making my dream come true, Chris Morehead for being such a great friend, and Adrienne Andrew for pointing your bazooka at me...!

I would also like to thank all my Portuguese friends who inspired and helped me in completing my PhD. I especially thank Inês Pereira for her friendship and support, particularly during my first year. I am also very grateful to all my university collegues and teachers who shaped me and made this journey possible. I would sincerely like to thank Fernando Ornelas for being such an inspirational and motivational force, and for having visited me in Tasmania!

A very special thank you is due to Ana. Her love, passion, presence, insight and resourcefulness are deeply acknowledged and were always a strong motivation for me to complete my PhD. Thank you for making me a better person and for sharing tears of happiness and sorrow. You take a special place in my heart. Thank you for having never given up on me. I dedicate figure 3.34I to you. Now we can finally celebrate properly!

Finally, I would like to thank my family for the unconditional love, support and encouragement during and before my PhD years. I especially thank my parents for everything they have done for me and for always being there when I most needed. To my brother, I say Brother to Brother, yours in life and death, as you once quoted. I would like to dedicate this thesis to my deceased grandparents. Rest in peace. I have finally finished!

Table of contents

CHAPTER 6
Volcanic setting of mineralisation in the northern Mount Read Volcanics

CHAPTER 7
Conclusions, discussion and recommendations

List of figures

List of tables

Appendices

CHAPTER 1

Introduction

1.1 Aims and significance

This thesis presents research on the Western Volcano-Sedimentary Sequences (Mount Charter and Dundas groups) and Central Volcanic Complex of the Middle to Late Cambrian Mount Read Volcanics in western Tasmania (Figure 1.1). The Mount Read Volcanics are an altered, deformed and metamorphosed belt of dominantly submarine volcanic facies interfingered with sedimentary rocks, comprising one of the richest volcanic-hosted massive sulfide (VHMS) provinces in the world (Corbett, 1992).

This study uses lithofacies analysis to establish local and regional stratigraphic correlations in the northern Mount Read Volcanics. The focus is the Sock Creek-Burns Peak area which is relatively poorly understood and under-explored, and lies between major VHMS deposits to the N (Hellyer and Que River) and S (Rosebery and Hercules) (Figure 1.1). It presents new data and brings together scattered information from previous research in an attempt to reconstruct and clarify the volcanic and sedimentary facies architecture and paleogeography of the northern Mount Read Volcanics during the late Middle Cambrian.

The principal aims of this thesis are:

- to establish the lithostratigraphic correlations of the Sock Creek-Burns Peak area with the areas to the NE (Hellyer-Mount Charter) and SSW (Rosebery-Howards Road)
- to determine the position of the known VHMS deposits and prospects in the northern Mount Read Volcanics in the regional stratigraphic framework;
- to identify the location of the most prospective stratigraphic position(s) in the Sock Creek-Burns Peak area, considering both sub-seafloor replacement and seafloor styles of VHMS deposits;
- to reconstruct the volcanic and sedimentary settings before, during and after the hydrothermal activity that formed the VHMS deposits in the northern Mount Read Volcanics.

VHMS deposits are stratabound accumulations of sulfide minerals that form in extensional tectonic settings on and beneath the seafloor through the focused discharge of hot, metal-rich hydrothermal fluids (Franklin et al., 1981; Large et al., 2001c; Doyle and Allen, 2003; Galley et al., 2007). VHMS deposits are a major source of zinc, copper, lead, silver, and gold and continue to be a target for base metal exploration (Franklin et al., 2005). The Mount Read Volcanics in western Tasmania are highly prospective for VHMS deposits, with six known economic deposits ranging from polymetallic Zn-Pb-Cu-rich (Hellyer, Que River,

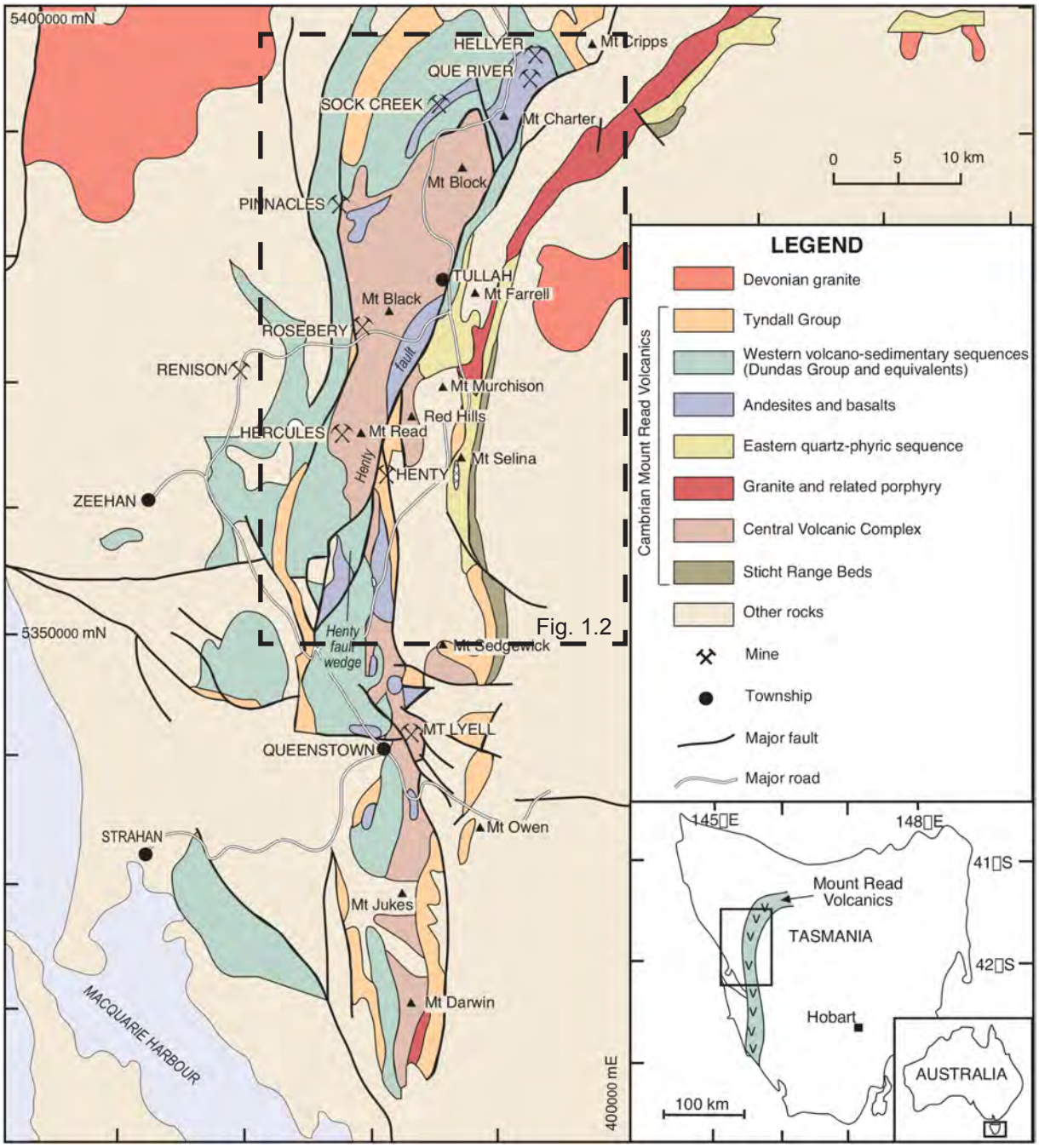

Figure 1.1: Geological map of the Mount Read Volcanics in central western Tasmania, showing the distribution of the principal lithostratigraphic units and major VHMS deposits (Gifkins et al., 2005). The box shows the location of Figure 1.2.

Rosebery and Hercules) to Cu-rich (Mount Lyell) and Au-rich (Henty) formed in a variety of local geological settings (Solomon et al., 1988; Corbett, 1992; Large, 1992; Large et al., 2001c).

Despite the broad spectrum of VHMS deposits and host successions, it is widely acknowledged that VHMS hydrothermal systems are synchronous with the formation of spatially associated volcanic rocks (syn-volcanic) and that in many provinces, VHMS deposits can be linked to a particular stratigraphic level or favorable horizon (Sangster, 1972; Franklin et al., 1981; Lydon, 1984, 1988; Large, 1992; Doyle and Allen, 2003). Previous studies (Corbett, 1981, 1992; Crawford et al., 1992; McPhie and Allen, 1992) and recent high-precision dating (Mortensen et al., 2015) conducted in the Mount Read Volcanics have led to the hypothesis that ore formation occurred during a single time interval.

In the northern Mount Read Volcanics, the local stratigraphy of the host successions to the Hellyer-Que River-Mount Charter (NE) and Rosebery-Hercules (SSW) VHMS deposits is well established (Komyshan, 1986a; Corbett and Komyshan, 1989; Corbett, 1992; Waters and Wallace, 1992; Gifkins and Allen, 2001; Large et al., 2001a). The Sock Creek-Burns Peak area is located between these VHMS-hosting and economically significant areas (Figure 1.2), but the internal stratigraphy is poorly known. The accurate characterization of the stratigraphic framework and reconstruction of the volcanic and sedimentary facies architecture in the Sock Creek-Burns Peak area are thus critical in order to further improve general understanding of the geological setting of VHMS deposits and to determine the likely stratigraphic positions of yet undiscovered VHMS deposits in the northern Mount Read Volcanics.

Tracing lithostratigraphic intervals, constraining their stratigraphic location and spatial distribution, and identifying the key facies, present an opportunity to develop a framework for VHMS ore genesis studies and exploration in the Mount Read Volcanics. In addition, it is imperative to develop appropriate lithofacies analysis and correlation techniques within and among the complex lithostratigraphic units of the northern Mount Read Volcanics, particularly in the Sock Creek-Burns Peak area and the areas to the NE (Hellyer-Mount Charter) and SSW (Rosebery-Howards Road).

The dominantly submarine volcanic and sedimentary facies in the northern Mount Read Volcanics are compositionally and texturally diverse and have been subjected to various degrees of alteration, deformation, fault disruptions, metamorphism and granitic intrusions (Corbett, 1992), hampering stratigraphic correlations both on regional and local scales. Stratigraphic correlations depend on finding distinctive, laterally extensive volcaniclastic units and are particularly difficult in the Mount Read Volcanics due to the scarcity of laterally extensive facies and relatively poor outcrop. The presence of intrusions in the volcanic succession further complicates the stratigraphy, as intrusions have a relationship with the enclosing successions that is different from that of lavas or domes. The correct identification and distinction between intrusions and lavas is critical in stratigraphic analysis.

The precise manner of massive sulfide deposition, particularly sub-seafloor replacement versus seafloor accumulation, must be considered very carefully in any research on the stratigraphic positions of VHMS deposits. Sub-seafloor VHMS deposits may be the same age as seafloor deposits that occur higher in the

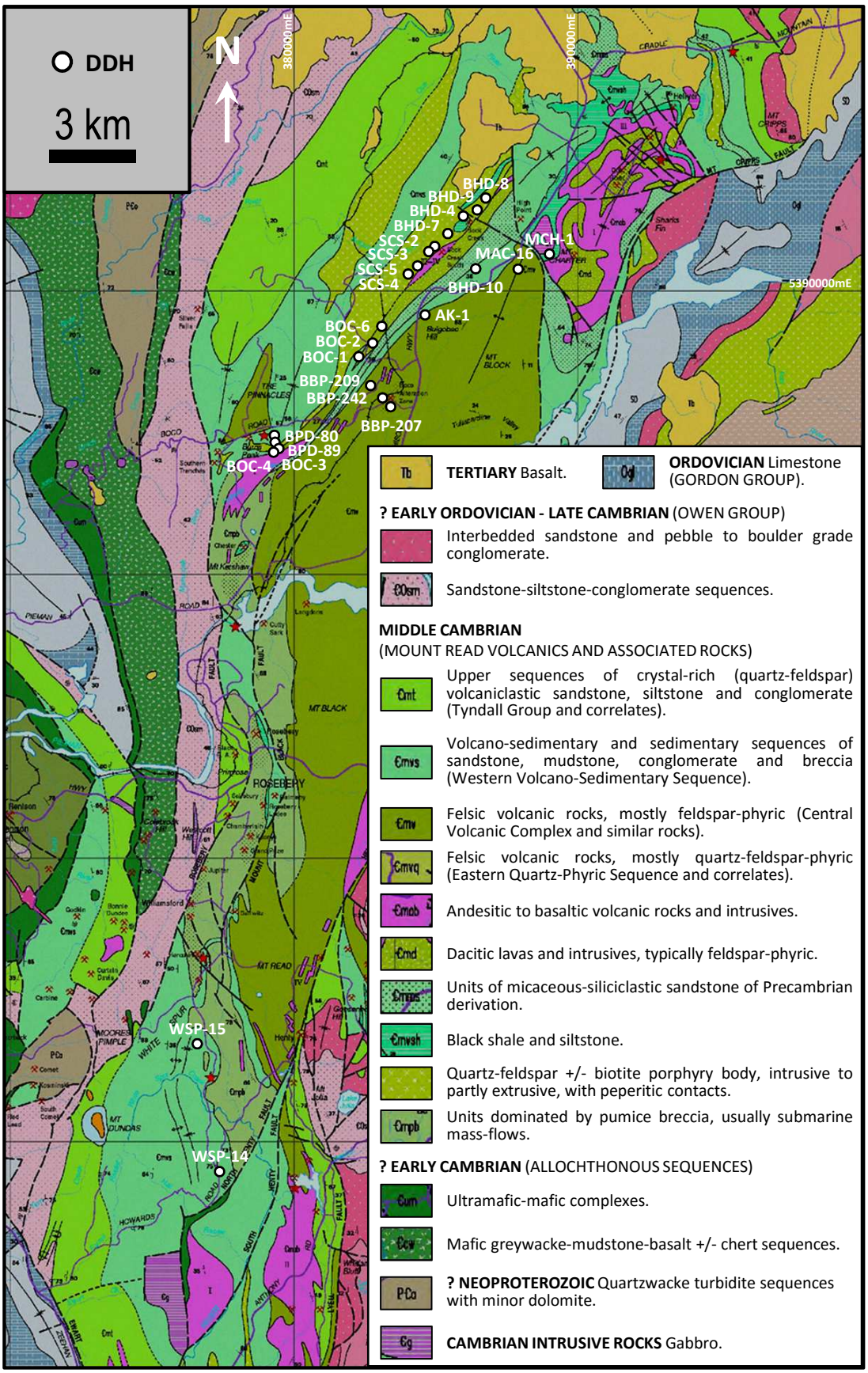

Figure 1.2: Bedrock geological map of the northern Mount Read Volcanics, showing the location of the diamond drill holes (DDH) in this study, after Corbett (2002a). The Sock Creek-Burns Peak area is located north of Lake Rosebery, where most samples were collected from DDH.

stratigraphy so the VHMS deposits cannot be simply linked to a single chronostratigraphic unit. Single lenses or parts of a single VHMS deposit can form by different processes, and both the VHMS deposits and the host successions can be very complex and diverse (Large, 1992; Large et al., 2001c; Doyle and Allen, 2003). In the northern Mount Read Volcanics, genetic models involving both seafloor massive sulfide deposition and sub-seafloor replacement have been proposed for the Hellyer, Que River, Rosebery and Hercules VHMS deposits (Aerden, 1990, 1991, 1992, 1993, 1994a, 1994b; Brathwaite, 1974; Solomon and Walshe, 1979; Green et al., 1981; Sainty, 1986; Huston and Large, 1988; Solomon et al., 1990; Solomon and Groves, 1994; Gemmell and Large, 1992; Zaw and Large, 1992; Waters and Wallace, 1992; Allen, 1994b; Solomon and Khin Zaw, 1997; Gemmell and Fulton, 2001; Doyle and Allen, 2003; Martin, 2004).

1.2 Location, access and exposure

The Sock Creek-Burns Peak area is an approximately 14-km-long, NE-striking section of the northern Mount Read Volcanics and lies approximately midway between the Hellyer and Que River VHMS deposits, in the NE, and the Rosebery and Hercules VHMS deposits, in the SSW (Figure 1.2). It is located N of Lake Rosebery and NW of Lake Mackintosh, approximately 10 km NNW of Tullah. The area is covered by the 1:25 000 Block (Pemberton et al., 1995), Charter (Corbett, 1995) and Parsons (Everard, 2000) geological map sheets.

Road access to the area is mainly via the Murchison Highway. A limited network of forestry roads (e.g., Boco Road) and vehicular side-tracks, developed for logging and mineral exploration, extend to the W from the highway, SW of Bulgobac Hill, and provide excellent access to parts of the area. Access to the rest of the area is commonly difficult and by foot only along old tramways overgrown logging tracks, creeks (e.g., Animal Creek) and mountain slopes with thick, nearly impenetrable rainforest (Figure 1.3).

In western Tasmania, the rugged topography comprises mountain ranges with sharp ridges and angular peaks, separated by steep-sided U-shaped valleys produced during the Pleistocene glaciation. The Mount Read Volcanics are commonly concealed, either by glacial deposits or siliciclastic conglomerate and quartz sandstone of the Late Cambrian to Early Ordovician Owen Conglomerate (Corbett, 1992). Evergreen temperate rainforests cover most areas with dense and nearly impenetrable vegetation. As a result, the Mount Read Volcanics are generally very poorly exposed.

Natural exposure is restricted to mountain slopes, rivers, and creeks that are typically difficult to access. A limited number of roads, tracks, dams and canals provide access to some of the best rock exposures. The rugged topography, dense vegetation, poor exposure and difficult access make geological mapping very arduous. However, high quality data are locally available from numerous diamond drill holes. This study focuses on the Sock Creek-Burns Peak area, where most samples were collected from diamond drill holes (Figure 1.2).

Figure 1.3: Nearly impenetrable vegetation, known locally as horizontal scrub, along a creek traversed during mapping in the northern Mount Read Volcanics.

1.3 Methods of investigation

Field work for this research included diamond drill core logging and geological mapping and was completed over four consecutive summer field seasons. Twenty-four diamond drill holes (DDH) intersecting the Mount Read Volcanics (twenty one in the Sock Creek-Burns Peak area, one in the Mount Charter area and two in the White Spur-Howards Road area) were logged at 1:400 scale both at the Minerals and Metals Group's Tullah core shed in western Tasmania and at Mineral Resources Tasmania's Mornington core store in Hobart. The logs record information on the grain size, components and mineralogy, textures, deformation structures, contact relationships and geometry, and sample locations (appendix A).

Geological mapping was done using a 1:5 000 scale topographic map published by the Mineral Resources Tasmania and made available by the Minerals and Metals Group at Rosebery. One available approximately 2-km-long road section (Boco Road) located E of Burns Peak and W of the Boco Alteration Zone was mapped and the data acquired were transposed onto a true-thickness log to allow direct correlations with the logs from the surrounding areas.

Field data were compiled using Illustrator® and both regional and local stratigraphic correlations were produced from the construction of fence diagrams in order to reconstruct the facies architecture and paleogeography of the volcano-sedimentary successions. Facies analysis was used to assist in determining provenance, eruption and emplacement processes and depositional environments.

Thin-section petrography and whole-rock compositional data for representative samples were used to assist and refine the macroscopic description and identification of textures of the different lithofacies. Polished thin-section petrography was an important tool in identifying the composition and distribution of mineral assemblages, mineral textures and overprinting relationships, and ultimately provided the basis for correlations and interpretations.

1.4 Terminology

The terminology used in this thesis follows the nomenclature outlined in McPhie et al. (1993). Descriptive nomenclature was used during field work, both in diamond drill core logging and geological mapping. Genetic nomenclature and facies interpretations focus on eruption style, emplacement processes, depositional setting and proximity to source.

Terminology used in this thesis includes:

Autobreccia - A volcaniclastic facies composed of irregularly shaped lava fragments produced by the non-explosive fragmentation of the cooler, more viscous parts of lava flows (Fisher, 1960, 1966).

Autoclasts - Fragments produced by the non-explosive fragmentation (autobrecciation and quenching) of lavas (Fisher, 1960, 1966).

Breccia - Rock composed of more than 50% of angular to sub-angular fragments greater than 2 mm in size set in a subordinate matrix of any composition and texture, or with no matrix (Fisher, 1958).

Cryptodome - A dome-shaped shallow intrusion. Cryptodome intrusion typically lifts the overlying rock or sediments, producing a bulge or mound at the surface.

Facies - A body of rock or deposit with unique definable characteristics distinct from other bodies of rock or deposits (e.g., Selley, 1978). In volcanic successions, facies are commonly defined on the basis of a combination of components or composition, textures and structures. A primary distinction is made between coherent facies, formed from cooling and solidification of lava or magma, and volcaniclastic facies, which are composed predominantly of volcanic particles (McPhie et al., 1993).

Facies association - A group of facies that have a spatial, compositional, textural or genetic relationship (Cas and Wright, 1987). In volcanic successions, facies associations commonly represent particular eruption and/or emplacement processes.

Facies architecture - The spatial organization of different facies and facies associations (Allen and Allen, 2005).

Fiamme - Elongate lenses or domains of the same mineralogy, texture and composition, which define a pre-tectonic foliation, and are separated by domains of different mineralogy, texture or composition (Bull and McPhie, 2007). This descriptive term can be used regardless of the origin of the texture. In the Sock Creek-Burns Peak succession, this term was also applied to elongate, flame-like domains with wispy, smoothly curved margins that are not necessarily aligned.

Hyaloclastite - A volcaniclastic facies composed of glassy or partly glassy lava clasts produced by the quench fragmentation of hot lava on contact with water, ice or unconsolidated wet sediment (Pichler, 1965). Fragmentation not followed by transport of the clasts produces in situ hyaloclastite; transport accompanying or following fragmentation produces resedimented hyaloclastite (Yamagishi, 1987).

Lithic - Non-juvenile, pertaining to rock fragments. In the Sock Creek-Burns Peak succession, this term was applied to fine-grained clasts that lack any internal structure or texture, and that could not be identified in terms of type (igneous, sedimentary or metamorphic) or composition (e.g., rhyolitic, dacitic, siliceous) at hand specimen scale.

Peperite - A rock formed essentially in situ by disintegration of magma intruding and mingling with unconsolidated or poorly consolidated, typically wet sediments (White et al., 2000). This term also refers to similar textures generated by the same processes operating at the contacts of lavas and hot pyroclastic flow deposits with such sediments. Peperite is characterized by a clastic texture in which either the sediment or the igneous components may form the clasts. In volcanic successions, peperite provides evidence of magma/lava-water/sediment interaction and is important in distinguishing lavas from intrusions (Skilling et al., 2002).

Perlite - Volcanic glass cut by a network of delicate, arcuate, intersecting fractures surrounding cores of intact glass.

Pumice - A low density highly vesicular glassy volcanic rock.

Pyroclasts - Fragments (pumice, ash, scoria, shards, crystals and rock fragments) produced by explosive eruptions (Fisher, 1960, 1966).

Volcanic glass - A thermodynamically unstable, non-crystalline solid produced by the rapid quenching of silicate melts.

Volcaniclastic - A descriptive term applied to deposits composed predominantly of volcanic particles (Fisher, 1961).

1.5 Criteria for distinguishing intrusions from extrusions

In subaqueous environments, magmas may be extruded as lava flows and domes, or form sills, dykes, and intrusive to partly extrusive cryptodomes. Distinguishing intrusions from extrusions in submarine volcanic successions is commonly difficult because internal textures in both settings may be identical. Interpretations of the mode of emplacement should be consistent with all the available lithofacies information and not rely exclusively on one criterion.

Criteria used in this research to help differentiate syn-volcanic intrusions from lavas and domes include contact relationships and the character and distribution of associated facies. The upper contact relationships are crucial because basal contacts of intrusions and lavas can be very similar. In this thesis, field data come mainly from drill core logging, and the remainder from an incomplete road section (Boco Road) in which contacts are not exposed. A single contact intersected in drill core may be very difficult to interpret even where well preserved, and obviously different facies are involved. Hence, wherever possible, the same contact has been examined in multiple drill holes. In addition, the limitations imposed by drill core have meant that the character and distribution of associated facies (coherent facies, autobreccia, in situ and resedimented hyaloclastite, and peperite) has also been critically important in determining the mode of emplacement.

Syn-volcanic or syn-sedimentary intrusions have been interpreted on the basis of upper contact relationships involving tongues or lobes of coherent facies projecting upward from the main interval of coherent facies into the host, the presence of peperite (fluidal peperite or intrusive hyaloclastite), induration or alteration of the host, and destruction or disturbance of bedding of sedimentary facies at the contact (e.g., Kokelaar, 1982; Branney and Suthren, 1988; McPhie, 1993; Skilling et al., 2002). Abundant, relatively thin (<10 m thick) andesitic to basaltic units were interpreted as intrusions because they cross cut thick (up to tens of metres), felsic (rhyolite and dacite) successions and have sharp passive contacts. Locally, thicker basaltic units that are discordant with adjacent facies and have tabular geometries were traced between adjacent drill holes, and are also interpreted as intrusions.

Units in the northern Mount Read Volcanics interpreted as intrusions comprise either wholly coherent facies or combinations of coherent and typically strictly monomictic breccia facies with jigsaw-fit to clast-rotated textures (in situ and clast-rotated intrusive autoclastic facies). The monomictic breccia facies is not bedded, and no clasts derived from the intrusion are present in adjacent or overlying facies. However, irregular enclaves of host sediment or adjacent coherent facies can be completely detached and incorporated into the interior parts of intrusions.

In contrast, units interpreted as extrusions (lavas, domes and partly extrusive cryptodomes) have upper contacts that are typically sharp (planar or irregular) (Figure 1.4), or gradational (McPhie et al., 1993). Gradational upper contacts show uphole grading of coherent facies into jigsaw-fit monomictic breccia, through clast-rotated monomictic breccia to bedded monomictic or weakly polymictic breccia. As with intrusions, units interpreted as lavas and domes may comprise wholly coherent facies or combinations of coherent and monomictic breccia with jigsaw-fit to clast-rotated textures (in situ autoclastic facies). However, the associated autoclastic facies may be stratified and locally polymictic (McPhie et al., 1993), and clasts within overlying facies can be matched with the extrusive units (Figure 1.4).

The intrusive versus extrusive nature of some rhyolitic and dacitic units could not be confidently interpreted and remains unclear. These units occur in thick (hundreds of metres) successions comprising distinct, adjacent units of coherent rhyolite and/or dacite with or without associated monomictic rhyolite and/or dacite breccia, separated by contacts that are ambiguous in drill core. Adjacent rhyolitic and/or dacitic units

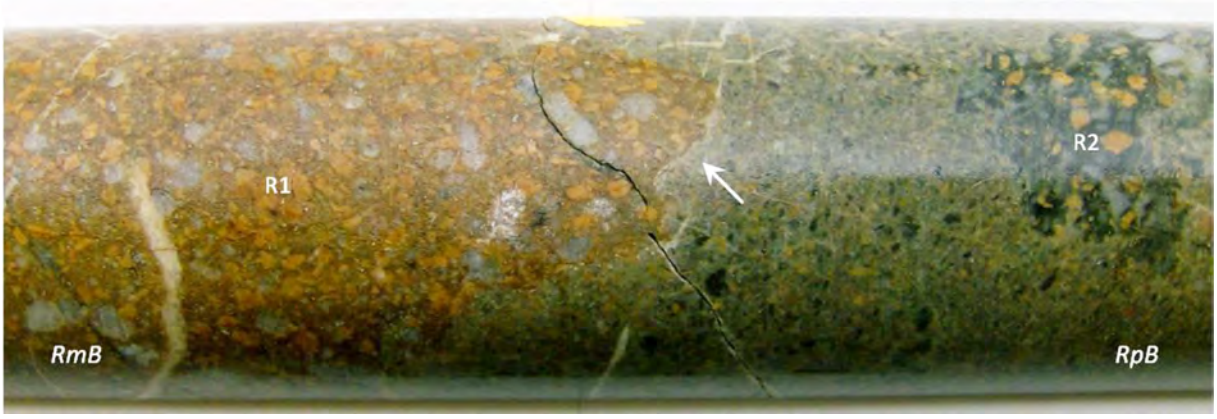

Figure 1.4: Sharp irregular contact between monomictic (RmB) and polymictic (RpB) rhyolite breccia facies (DDH BHD-4; 60.5 m) (Uphole and younging direction: left to right). Rhyolite clasts (R2) within the polymictic rhyolite breccia facies are very similar to larger rhyolite clasts (R1) within the monomictic rhyolite breccia facies, indicating that the contact (white arrow) is extrusive.

typically have similar textures, but different phenocryst populations (e.g., feldspar-phyric versus feldspar-quartz-phyric).

1.6 Stratigraphic nomenclature

Many of the stratigraphic units in the Mount Read Volcanics have not been formally defined (e.g. Central Volcanic Complex), including those represented on the 1:25 000 geological map sheets published by the Mineral Resources Tasmania. Nevertheless, the names have been used in international and national refereed publications and are well established.

In this thesis, the use of upper case for names of units where that has been the convention is purely for convenience and simplicity, even though some units are strictly still informal. New names have not been created and pre-existing names have not been modified. The stratigraphic unit names are fully explained in Chapters 2, 4 and 5.

1.7 Thesis organization

This thesis contains seven chapters.

Chapter 1 (*Introduction)* provides the aims and significance of this research, the location of the study areas, and the methods of investigation used. It also includes terminology and criteria for discriminating intrusions from extrusions used in this study.

Chapter 2 (*Geological setting of the Mount Read Volcanics)* includes important background information for this research. The regional geology, stratigraphy, geochronology, geochemistry, tectonic setting, and mineralisation in the Mount Read Volcanics are summarized.

Chapter 3 (*Facies associations in the northern Mount Read Volcanics)* presents detailed descriptions and interpretations of the main volcanic facies associations in the Sock Creek-Burns Peak area, N of Lake Rosebery, and also in the Mount Charter (NE) and White Spur-Howards Road (SSW) areas. Facies textures and geometry, depositional structures and contact relationships are used to constrain the eruption style, environment of deposition, proximity to source, and transport and depositional processes. This chapter forms the core of this research and provides new data for interpretations presented in subsequent chapters.

Chapter 4 (*Stratigraphy, correlations and facies architecture in the Sock Creek-Burns Peak area)* introduces the geological setting of the Sock Creek-Burns Peak area and discusses the relationships among the different volcanic successions identified in the area. Correlation problems are addressed. The correlations and the major interpretations from Chapter 3 are used to reconstruct the volcanic facies architecture in the Sock Creek-Burns Peak area.

Chapter 5 (*Stratigraphy and correlations in the northern Mount Read Volcanics)* introduces the geology of the Hellyer-Mount Charter and Rosebery-Howards Road areas. It also includes summaries of the stratigraphy of the host sequences to the Hellyer-Que River and Rosebery-Hercules VHMS deposits. This chapter combines the major interpretations from Chapters 3 and 4 to discuss the stratigraphic correlations between the Sock Creek-Burns Peak area (Chapter 4) and the areas to the NE (Hellyer-Mount Charter) and SSW (Rosebery-Howards Road).

Chapter 6 (*Volcanic setting of mineralisation in the northern Mount Read Volcanics)* presents the stratigraphic context of mineralisation in the Hellyer-Mount Charter and Rosebery-Hercules areas and discusses the implications of the regional correlations (Chapter 5) for the timing and setting of VHMS deposits in the northern Mount Read Volcanics. This chapter assembles the main interpretations and conclusions from previous chapters to propose the paleogeography and pre-, syn- and post-mineralisation reconstructions of the northern Mount Read Volcanics. It also discusses the implications of these reconstructions and offers directions for VHMS exploration in the Mount Read Volcanics.

Chapter 7 (*Conclusions, discussion and recommendations)* provides a discussion and a summary of the main outcomes of this research and recommendations for future work in submarine volcanic successions.

The original logs of the diamond drill holes, the original 1:5000 scale topographic map of the approximately 2-km-long Boco Road section with the lithologies mapped and the calculations made in order to transpose the acquired data onto a true-thickness log, a short description of the analytical methods and the whole rock compositional data of the samples used in this study are given in the appendices.

In order to facilitate the reader, and because this thesis relies mainly on facies analysis and drill core logging and correlations, the link between the nomenclature of the facies/stratigraphic units identified in this study and the correlated formal stratigraphic units has been constantly mentioned, particularly in sections of Chapters 4, 5 and 6. Apart from Chapters 1 and 7, a summary is provided at the end of each chapter where the reader may find a synthesis of the main conclusions.

CHAPTER 2

Geological setting of the Mount Read Volcanics

2.1 Introduction

The Cambrian Mount Read Volcanics (MRV) of western Tasmania are one of the most highly mineralised, polymetallic, volcanic-hosted massive sulfide (VHMS) provinces in the world. The MRV are the most important metallogenic province in Tasmania, containing nearly 397 million tons of pre-mining resources with an in-ground total value estimate of approximately 79 billion Australian dollars (Seymour et al., 2007) (Figure 2.1). The MRV were first described by Campana and King (1963) and the ore deposits and associated rocks have been intensely studied by Brathwaite (1974), Corbett (1981, 1989, 1992, 2001a), Solomon (1981), Eastoe et al. (1987), Solomon et al. (1988, 2004), Crawford et al. (1992), McPhie and Allen (1992, 2003), Gemmell and Large (1992), Waters and Wallace (1992), Zaw and Large (1992), Large et al. (1996, 2001a), White and McPhie (1996), and Gifkins and Allen (2001).

The MRV form an arcuate belt occupying an approximately 200 km long and 20 km wide area in western Tasmania from Elliot Bay, in the southwest coast, to near Deloraine (Figure 2.1). They comprise a thick sequence of dominantly submarine volcanic rocks interfingered with sedimentary rocks (Corbett, 1992; McPhie and Allen, 1992). The MRV have been affected by regional deformation, diagenetic and hydrothermal alteration, greenschist facies metamorphism and contact metamorphism (Corbett and Lees, 1987; Corbett, 1992). The MRV host six major VHMS deposits (Solomon et al., 1988) formed in a variety of geological settings and environments (McPhie and Allen, 1992) during a narrow time interval (Mortensen et al., 2015).

This chapter provides an overview of the geology and geotectonic history of Tasmania and introduces the regional geology of the MRV in western Tasmania. The stratigraphy, geochronology, geochemistry, tectonic setting, and mineralisation of the MRV are summarised.

2.2 Geology of western Tasmania

The geology of Tasmania is divided by the Tamar Fracture System, a major NNW-striking arcuate discontinuity that runs from N of Beaconsfield to E of Hobart (Figure 2.1). The Tamar Fracture System separates two extremely different terranes. The Eastern Tasmanian Terrane comprises the Mathinna Supergroup, a quartzwacke-mudstone turbidite succession of Ordovician-Devonian age, intruded by Late Devonian granites. The Western Tasmanian Terrane is much more complex and consists of deformed and metamorphosed Proterozoic sedimentary and volcanic rocks, Cambrian volcano-sedimentary sequences and mafic-ultramafic complexes, and Late Cambrian-Devonian siliciclastic sequences and carbonates, intruded

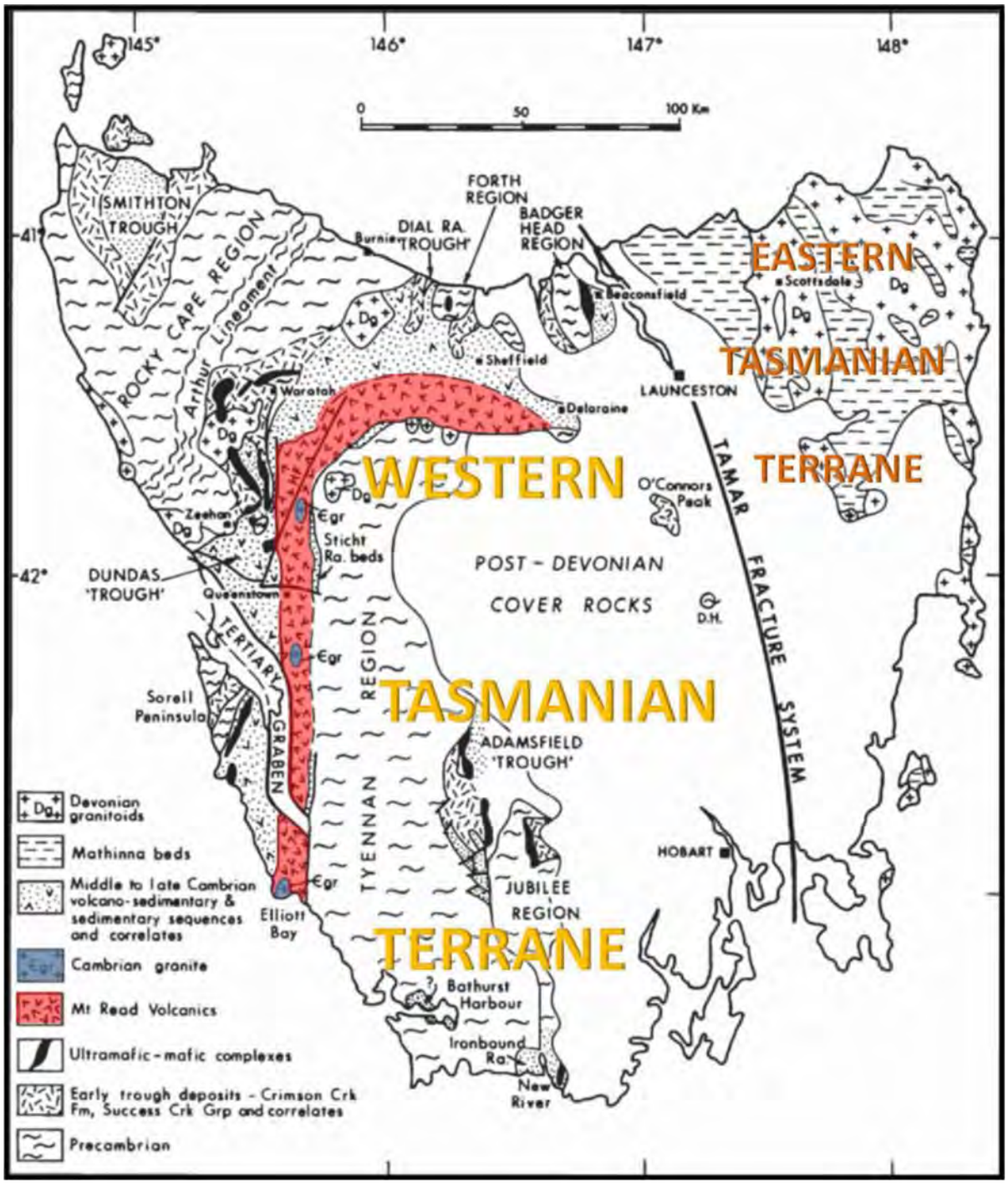

Figure 2.1: Simplified geological map of early Palaeozoic geology of Tasmania, after Corbett and Turner, 1989. The Tamar Fracture System is a major arcuate discontinuity in Tasmania. The Mount Read Volcanics occur along the eastern margin of the Cambrian *Dundas Trough*. Most of the Ordovician and Siluro-Devonian cover rocks are not shown.

by Devonian granites. Post-Devonian rocks cover central and southeastern Tasmania and most of the Tamar Fracture System (Figure 2.1) (Corbett, 1992; Laurie et al., 1995; Corbett et al., 2014).

2.2.1 Mesoproterozoic and Neoproterozoic rocks

The oldest rocks in Tasmania outcrop on the western part of King Island and consist of Middle Mesoproterozoic, amphibolite-grade metasedimentary rocks and minor amphibolites of the Surprise Bay Formation (Calver, 2007) that are younger than 1350 Ma (Black et al., 2004; Berry et al., 2005). In western Tasmania, the oldest rocks occur in the Tyennan and Rocky Cape Regions (Figure 2.1) and consist of phyllite and quartzite (Rocky Cape Group and correlates; Oonah Formation and correlates). SHRIMP detrital zircon dating indicates that at least parts of these two successions are younger than 1000 Ma (Black et al., 2004). Proterozoic rocks in both western Tasmania and King Island are strongly deformed and metamorphosed (Seymour et al., 2007; Corbett et al., 2014).

The Tyennan Region is the largest area of exposed Proterozoic rocks, extending from the southwestern coast to the Cradle Mountain area (Figure 2.1). The Tyennan Region comprises two assemblages of polydeformed metamorphic rocks: an autochthonous assemblage of metaquartzite and metapelite with metamorphic grades up to greenschist facies, and an allochthonous assemblage of schist, quartzite and amphibolite with amphibolite-eclogite metamorphic grades (Spry, 1962, 1963; Turner, 1989; Meffre et al., 2000; Seymour et al., 2007; Corbett et al., 2014). The Jubilee Region is a smaller Precambrian block in central southern Tasmania, at the eastern margin of the Tyennan Region (Figure 2.1) (Seymour et al., 2007; Corbett et al., 2014).

In northwestern Tasmania, the Proterozoic Rocky Cape Region (Figure 2.1) includes the Rocky Cape Group (Spry, 1957; Gee, 1968), a Late Mesoproterozoic to Early Neoproterozoic (Black et al., 2004), thick (approximately 10 km) succession of quartzite, siltstone, mudstone and minor carbonate rocks deposited in an open marine shelf (passive margin) environment (Corbett et al., 2014). A widespread low-angle unconformity (Gee, 1967) separates the Rocky Cape Group from the overlying Middle Cryogenian (Middle Neoproterozoic) to Cambrian Togari and Ahrberg Groups (next section). The Tyennan, Rocky Cape and Jubilee Regions (Figure 2.1) are probably broadly correlates on the basis of similar lithologies (Turner, 1989), detrital zircon age distributions (Black et al., 2004) and similarities in the overlying Late Neoproterozoic successions (Corbett et al., 2014).

To the E of the Rocky Cape Region (Figure 2.1), the Oonah Formation (Spry, 1958; Brown, 1986) and correlates, including the Burnie Formation (Spry, 1957) and Badger Head Group (Reed et al., 2002), are a thick (at least 5 km on the north coast; Gee, 1977), polydeformed, continent-derived turbidite succession of Late Mesoproterozoic to Early Neoproterozoic age (Adams et al., 1985; Turner et al., 1998; Black et al., 2004) with generally low metamorphic grades up to low greenschist facies (Corbett et al., 2014). The Oonah Formation is overlain by the Middle Cryogenian (Middle Neoproterozoic) Success Creek Group (next section).

The Arthur Lineament (Figure 2.1) is an 8-km-wide by 110-km-long NE-striking belt of strongly sheared metamorphic rocks separating the Rocky Cape Region to the NW from the eastern Oonah Formation and correlates (Holm and Berry, 2002; Corbett et al., 2014). It extends from the western to the northern coasts of Tasmania and represents a major structure hosting economically important mineral deposits (e.g., Savage River - Fe, Arthur River and Main Creek - Mg) (Seymour et al., 2007; Corbett et al., 2014).

The Arthur Metamorphic Complex is located in the Arthur Lineament and contains mostly amphibolite with sodic blue amphibole (Turner and Bottrill, 2001) and minor garnet-bearing schist (Corbett et al., 2014). It includes the poorly dated Bowry Formation, an allochthonous blueschist unit consisting of amphibolite and chloritic and albitic schist, which hosts the Savage River high-grade magnetite deposit (Bottrill and Taheri, 2008).

Other than the Arthur Metamorphic Complex, numerous high-grade Mesoproterozoic to Neoproterozoic metamorphic complexes have been identified in western and northern Tasmania (Figure 2.1) (Meffre et al., 2000; Corbett et al., 2014) and are known to have undergone metamorphic conditions estimated around 550 to 740°C and 600-1700 MPa (McNeill, 1985; Reed et al., 2002; Chmielowski, 2009; Palmeri et al., 2009). U-Th-Pb dating of monazite gave a mean Cambrian age of 505 ± 1 Ma for the peak episode of metamorphism, and the range is approximately 511 to 497 Ma (Chmielowski, 2009).

2.2.2 Neoproterozoic and Cambrian rocks

The Togari Group and correlates are widespread in the Western Tasmania Terrane and comprise sedimentary and mafic volcanic successions of Middle Cryogenian (Middle Neoproterozoic) to Early Cambrian age (Seymour et al., 2007; Corbett et al., 2014). The Togari Group is preserved in the Smithton Synclinorium of the Rocky Cape Region (Figure 2.1) and can be sub-divided into four lithostratigraphic sub-units (Corbett et al., 2014), from oldest to youngest: 1) Black River Dolomite (Spry, 1957, 1964; Re-Os age of 641 ± 5 Ma, Kendall et al., 2009), 2) Kanunnah Subgroup (SHRIMP U-Pb age of 582 ± 4 Ma, Calver et al. 2004), 3) Smithton Dolomite (Calver, 1998), and 4) Salmon River Siltstone.

The Cryogenian (Middle Neoproterozoic) Success Creek Group, a succession of mostly unfossiliferous shallow marine carbonate and clastic sedimentary rocks, is conformably overlain by the Ediacaran (Late Neoproterozoic) Crimson Creek Formation, deeper marine greywacke-mudstone-chert deposits, also mainly unfossiliferous, associated with tholeiitic basalts (Brown, 1986; Collins and Williams, 1986; Corbett and Lees, 1987; Corbett, 1992; Adabi, 1997; Corbett et al., 2014). The Success Creek Group and Crimson Creek Formation represent the lowermost and westernmost stratigraphy of the Dundas Trough (Corbett, 1992; Laurie et al., 1995; Corbett et al., 2014).

Cambrian units include mafic-ultramafic complexes (MUC), the MRV and formations in the Dundas Trough. The Dundas Trough is a 20- to 30-km-wide arcuate zone between the western and northern margins of the Tyennan Region and the southeastern margin of the Rocky Cape Region (Figure 2.1). The upper stratigraphy of the Dundas Trough includes the Dundas Group, an early Middle to middle Late Cambrian

fossiliferous conglomeratic flysch sequence about 3800 m thick (Elliston, 1954; Campana and King, 1963; Jago, 1979; Brown, 1983, 1986; Collins and Williams, 1986; Corbett and Lees, 1987; Corbett, 1992; Corbett et al., 2014) that is partly equivalent to and interfingers with the MRV. Both the Dundas Group and the MRV are disrupted by several major faults, including the Henty, Great Lyell and Rosebery Faults (section 2.8) (Corbett et al., 2014).

At Dundas, the Judith Formation is the earliest unit of the Dundas Group, comprising trilobites identified as being of *P. gibbus* Zone late Templetonian (early Middle Cambrian) age (Jago and Brown, in Burrett and Martin, 1989) (Figure 2.2). The Red Lead Conglomerate follows the Judith Formation and is conformably overlain by the Hodge Slate, which has a trilobite fauna of probably *P. punctuosus* Zone Undillan (middle Middle Cambrian) age (Jago and Bentley, 2010). The Hodge Slate is conformably overlain by the Razorback Conglomerate, which grades up into the Lower Brewery Junction Formation (Jago, 1979; Corbett and Lees, 1987; Laurie et al., 1995; Corbett et al., 2014) (Figure 2.2).

A significant number of MUC (Crawford and Berry, 1992) of late Early Cambrian age are exposed along the western margin of the Dundas Trough and farther E (e.g., Adamsfield; Mount Mueller) and N (e.g., Andersons Creek, Beaconsfield; Claytons Rivulet, Forth) of the Tyennan Region (Corbett et al., 2014) (Figure 2.3). The crystallisation age of the McIvor Hill gabbro at 516.0 ± 0.6 Ma (Mortensen et al., 2015) constrains the age of the MUC in western Tasmania. A tonalite from the Heazlewood River Ultramafic Complex records a crystallisation age of 513.6 ± 5.0 Ma, which dates the last phase of igneous activity in this mafic-ultramafic complex (Black et al., 1997). The MUC host numerous small mineral deposits comprising platinum group elements (PGE), nickel, lead-zinc-silver, copper, gold, chromite, stichtite, iron, ochre, chrysotile asbestos and talc (Corbett et al., 2014). The MUC represent sheets of allochthonous forearc oceanic crust and upper mantle thrust onto the Neoproterozoic continental crust of Tasmania during the early Middle Cambrian (section 2.3) (Berry and Crawford, 1988; Crawford and Berry, 1992).

The Dial Range Trough is a northward extension of the Dundas Trough located on the northern coast of Tasmania, N of the Tyennan Region (Figure 2.1). The Fossey Mountain Trough is an eastward extension of the Dundas Trough about 30 km wide, occurring in central northern Tasmania. The Dundas-Dial Range-Fossey Mountain Trough includes the Middle to Late Cambrian MRV to the E and SE, and overall constitutes the largest exposed area of Late Neoproterozoic to Cambrian rocks in mainland Tasmania (Corbett et al., 2014).

Other Late Neoproterozoic-Cambrian troughs occur throughout the Western Tasmanian Terrane, including the Smithton, Beaconsfield and Adamsfield troughs (Figure 2.1) (Jago, 1979; Baillie and Jago, 1995; Laurie et al., 1995; Corbett et al., 2014). In southern Tasmania, E of the Tyennan Region, Cambrian rocks outcrop in the Ironbound Range, Bathurst Harbour, De Witt Island, and Rocky Boat Inlet-Pretty's Inlet areas (Seymour et al., 2007; Corbett et al., 2014).

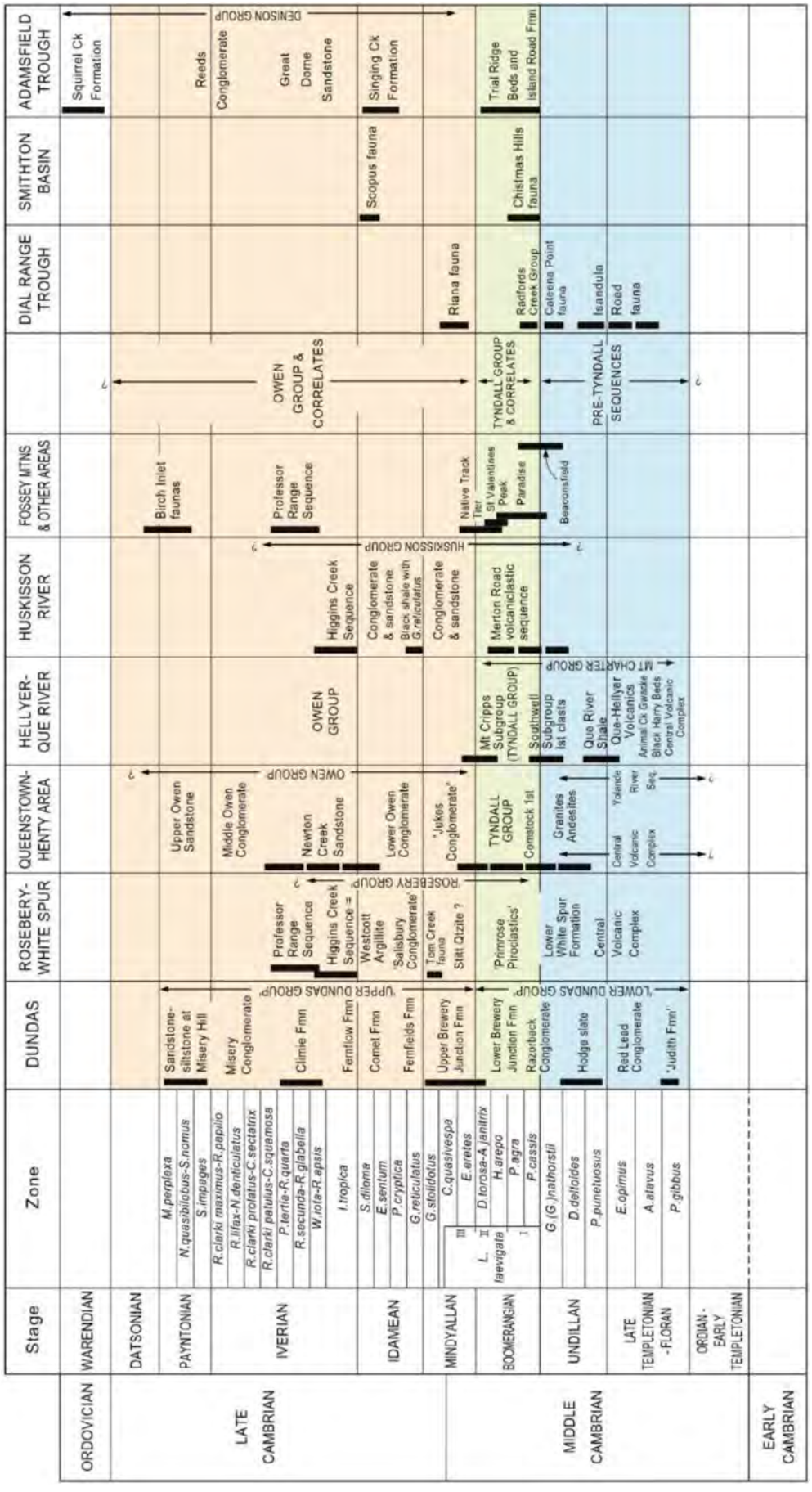

Figure 2.2: Biostratigraphic correlation chart for Middle and Late Cambrian sequences in western Tasmania (from Corbett, 2002b).

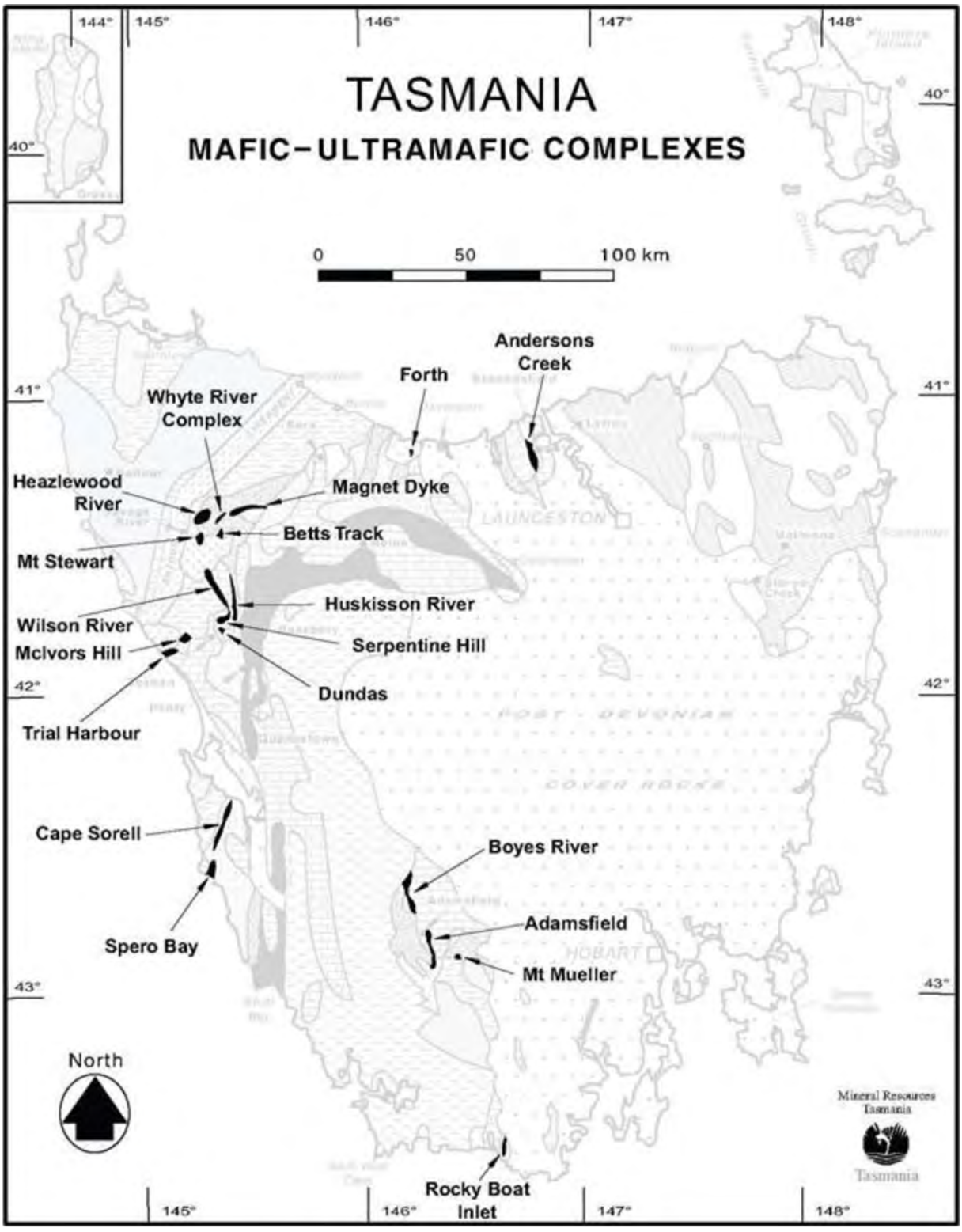

Figure 2.3: Simplified geological map of Tasmania, with the location of the Cambrian mafic-ultramafic complexes (from Brown, 1998).

2.2.3 Late Cambrian and younger rocks

The Wurawina Supergroup (Banks and Williams, 1986) occurs throughout the Western Tasmanian Terrane and comprises five distinct Late Cambrian to Early Devonian successions:

1. The Owen Group contains a thick sequence of siliceous conglomerate and quartz sandstone of Late Cambrian to Early Ordovician age, mostly derived from Precambrian rocks of the Tyennan and Rocky Cape Regions (Figure 2.1), that conformably and unconformably overlies older sequences within the Dundas Trough, including the MRV (Collins and Williams, 1986; Laurie et al., 1995; Corbett et al., 2014).
2. The Denison Group occurs at the eastern margin of the Tyennan Region in the Adamsfield area (Figure 2.1) and comprises a Late Cambrian marine sequence of Idamean (early Late Cambrian) age (Corbett, 1970, 1975; Jago, 1987, 1989), a fluvial to shallow marine conglomerate-sandstone sequence, and an Early Ordovician shallow marine sandstone-mudstone sequence (Stait and Laurie, 1980; Laurie, 1996).
3. The Gordon Group is an Ordovician sequence of predominantly micritic, dolomitic limestone and sandstone of variable thickness which conformably overlies the Denison Group, and unconformably and disconformably overlies the Owen Group (Corbett et al., 2014).
4. The Silurian to Lower Devonian Eldon Group conformably and disconformably overlies the Gordon Group and comprises a thick sequence of quartz sandstone, siltstone shale and minor limestone (Seymour et al., 2007; Corbett et al., 2014).
5. The Mathinna Supergroup (Baillie et al., 1989; Powell and Baillie, 1992; Powell et al., 1993; Reed, 2001) occurs in the Eastern Tasmanian Terrane and consists of an Early Ordovician to Early Devonian quartzwacke-mudstone turbidite succession deposited in a deep marine environment (Seymour et al., 2007; Corbett et al., 2014).

Post-Devonian rocks of the Tasmania Basin cover the Tamar Fracture System (Figure 2.1) and comprise two lithological associations of Late Carboniferous to Late Triassic age, the Upper and Lower Parmeener Supergroups (Corbett et al., 2014). Thick and extensive Jurassic dolerite sills (Leaman, 1995, 1997, 2012) intrude the Parmeener Supergroup (Corbett et al., 2014). Paleogene to Miocene volcanic rocks, mainly basaltic lavas, are widespread across Tasmania (Stacey and Berry, 2004; Seymour et al., 2007; Corbett et al., 2014).

2.3 Geotectonic history of Tasmania

The separation of Australia and Antarctica from North America during the breakup of the supercontinent Rodinia between approximately 827 and 780 Ma (Wingate et al., 1998, 2002) represented a major extensional phase which eventually caused the development of a Late Proterozoic rifted margin (Dalziel, 1991; Crawford and Berry, 1992; Li et al, 1997, 2008). The earliest stages of this major tectonic event are recorded by the deposition of the Rocky Cape Group and Oonah Formation and correlates (Burnie Formation and Badger Head Group) in the Early to Middle Neoproterozoic (Meffre et al., 2000). These sequences, together

with the metamorphic rocks of the Tyennan Region (Figure 2.1), were later extensively folded during the Cryogenian (Middle Neoproterozoic) Wickham Orogeny (Corbett et al., 2014).

The separation of Tasmania from the Australian craton may not have occurred until a second rifting event at approximately 600 to 580 Ma (Calver and Walter, 2000; Direen and Crawford, 2003a; Meffre et al., 2004), which led to the intrusion of the Rocky Cape Dyke Swarm, extrusion of tholeiitic basalts and deposition of the Togari Group and correlates, including the Success Creek Group and Crimson Creek Formation (Holm and Berry, 2002). The emplacement of the tholeiitic basalts in Tasmania and southeastern Australia (Crawford et al., 1997) is believed to record the development of an east-facing volcanic passive margin (Direen and Crawford, 2003b; Corbett et al., 2014).

The Cambrian Tyennan Orogeny in Tasmania was a very complex tectonic event with rapidly changing large-scale stress patterns (Stacey and Berry, 2004; Corbett et al., 2014) (Figure 2.4). The peak metamorphic

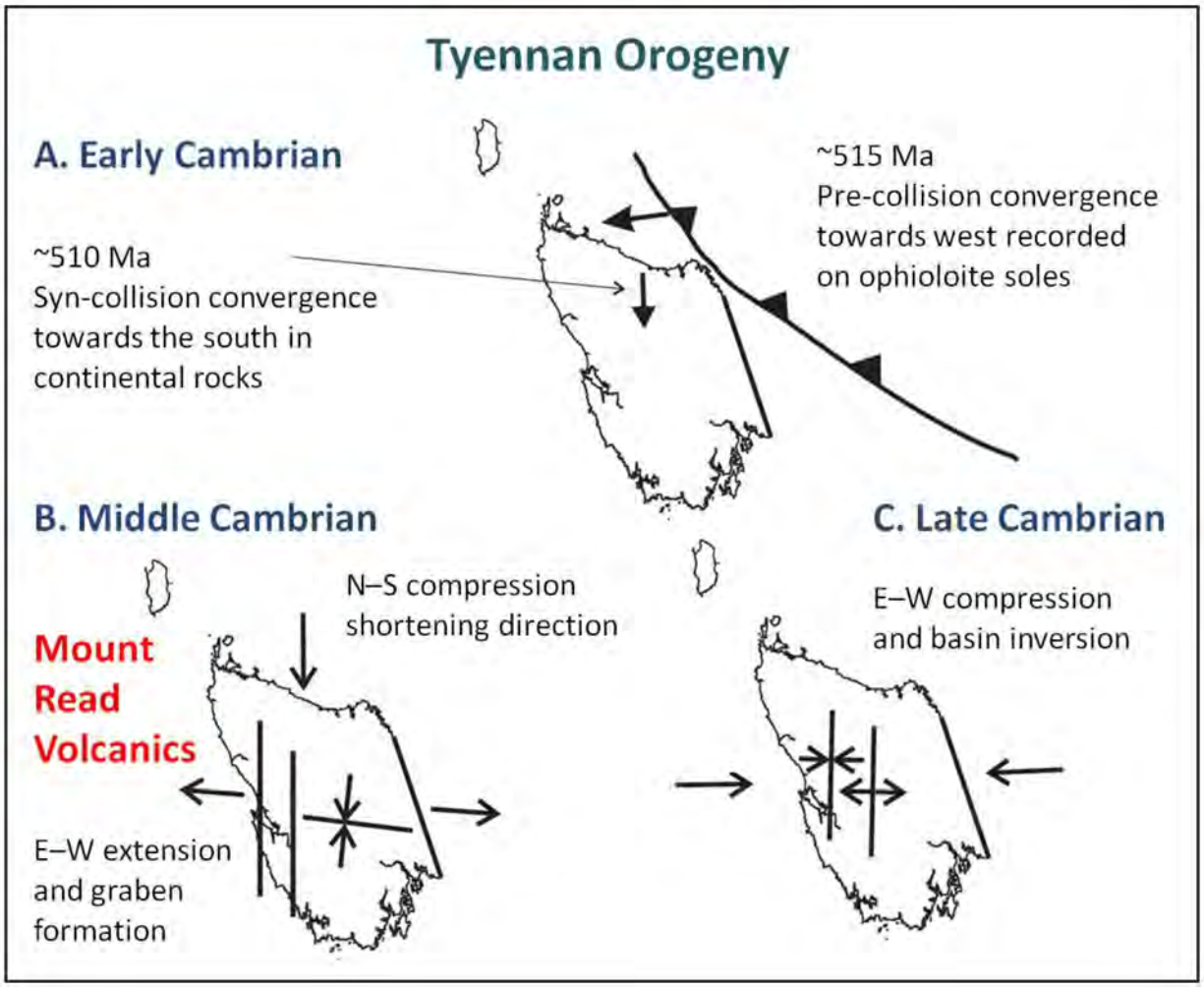

Figure 2.4: Summary diagram of the three major tectonic episodes during the Cambrian Tyennan Orogeny, after Stacey and Berry (2004).

age of the Tyennan Orogeny in central and western Tasmania is approximately 510 Ma (Berry et al., 2007). In the late Early Cambrian, during the first stage of the Tyennan Orogeny (515 to 508 Ma) (Figure 2.4), the eastern passive margin of the Western Tasmanian Terrane collided with an intra-oceanic island arc resulting in westward obduction of forearc lithologies, now represented by the allochthonous sheets of MUC of western and northern Tasmania (Berry and Crawford, 1988; Crawford and Berry, 1992; Turner et al., 1998; Meffre et al., 2000; Crawford et al., 2003; Stacey and Berry, 2004; Berry et al., 2007; Cayley, 2011). The western margin of the obduction complex is presently preserved as the Arthur Lineament, which was multiply deformed during the Middle and Late Cambrian (Holm and Berry, 2002).

The second stage of the Tyennan Orogeny occurred during the Middle Cambrian (Figure 2.4) and was dominated by E-W extension, producing rapid subsidence, active syn-orogenic deposition and post-collisional felsic-dominated volcanism of the MRV (Solomon, 1962, 1981; Stacey and Berry, 2004; Seymour et al., 2007; Corbett et al., 2014). Crustal relaxation and continued extension contributed to the formation of half grabens and the increasingly mafic volcanism of the MRV occurred along the eastern side of the Dundas Trough (Crawford and Berry, 1992; Crawford et al., 1992). The extensional phase was closely followed by a N-S compressional event that produced E-W-trending folds to the E of the MRV (Stacey and Berry, 2004).

The third and last stage of the Tyennan Orogeny occurred during the Late Cambrian to Early Ordovician (Figure 2.4) and produced major reverse faults and N-S-trending open folds, and inverted earlier extensional faults (e.g., Henty Fault) (Stacey and Berry, 2004; Corbett et al., 2014). E-W compression and isostatic uplift led to exhumation of the metamorphic complexes of the Tyennan and Rocky Cape Regions, as a rebound back-thrusting response to obduction (Crawford and Berry, 1992; Meffre et al., 2000; Corbett et al., 2014). The siliciclastic Owen Group and correlates were deposited in the Dundas Trough (Stacey and Berry, 2004; Corbett et al., 2014).

The Eastern Tasmanian Terrane joined the Western Tasmanian Terrane between Early Ordovician and Middle Devonian, separated by the Tamar Fracture System (Figure 2.1) (Varne and Foden, 1987; Corbett et al., 2014). In the Middle Ordovician, a new cycle of sedimentation began in central and western Tasmania. Deposition of the Ordovician Gordon Group and the Silurian-Devonian Eldon Group occurred in a shelf-type shallow-marine environment. Simultaneously, the Ordovician to Lower Devonian Mathinna Supergroup was deposited in northeastern Tasmania (Stacey and Berry, 2004; Seymour et al., 2007; Corbett et al., 2014).

The Middle Devonian Tabberabberan Orogeny affected all of Tasmania and reactivated or tightened older structures, creating complex fold and fault orientations (Corbett, 1981; Collins and Williams, 1986; Berry, 1989; Stacey and Berry, 2004; Seymour et al, 2007; Corbett et al., 2014). The regional prehnite-pumpellyite to local greenschist metamorphism associated with the Tabberabberan Orogeny was accompanied and followed by large-scale granitic intrusions from the Early Devonian to the Early Carboniferous, producing wide contact metamorphic aureoles (White and Chappell, 1977; Leaman and Richardson, 2003; Corbett et al., 2014).

Tasmania was affected by large-scale erosion after the Tabberabberan Orogeny and a new cycle of sedimentation commenced in the Late Carboniferous. The Tasmania Basin received a thick sequence of sedimentary rocks of Late Carboniferous to Triassic age (Parmeener Supergroup; Corbett et al., 2014) which were deposited and preserved in northern and southeastern Tasmania, unconformably overlying Late Devonian to Early Carboniferous granites and older deformed rocks (Stacey and Berry, 2004; Seymour et al., 2007; Corbett et al., 2014).

During the late Early Jurassic (approximately at 180 Ma), huge volumes of tholeiitic dolerite were intruded as sills in central and southeastern Tasmania, occupying an area of approximately 15 000 km^2 and an estimated volume of 15 000 km^3 (Hergt et al., 1989; Seymour et al., 2007; Corbett et al., 2014). The Tasmanian Jurassic dolerite is part of the Ferrar Magmatic Province (FMP), an example of a Large Igneous Province (LIP) that extends across Antarctica in a narrow belt approximately 3500 km long and 150 km wide (e.g., Brewer et al., 1992; Elliot and Fleming, 2004), and that, together with the Mesozoic Karoo and Parana-Etendeka LIPs of southern Africa and South America, have been linked to the breakup of Gondwana (e.g., Hergt et al., 1991).

Rifting-related extension between Australia and Antarctica developed the Bass, Sorell and Durroon basins in the Late Jurassic to Early Cretaceous. In the Middle to Late Cretaceous a high geothermal gradient affected Tasmania and several episodes of rifting, uplift, erosion and sedimentation occurred in the Bass, Sorell and Durroon basins (Seymour et al., 2007; Corbett et al., 2014). Following the opening of the Tasman Sea during the Late Cretaceous to Eocene (Middle Paleogene), basaltic lavas, mainly olivine melilitites to quartz tholeiites (Everard et al., 2004), were extruded during the Eocene to Miocene, and are widespread in mainland Tasmania. Tasmania witnessed several major glaciation phases in the Pleistocene and is actively rising at present in response to a regionally high geothermal gradient (Seymour et al., 2007; Corbett et al., 2014).

2.4 Regional geology of the Mount Read Volcanics

The Middle to Late Cambrian MRV extend along the western and northern margins of the Tyennan Region and form the eastern margin of the Dundas Trough (Jago et al., 1972; Corbett, 1992) (Figure 2.5). The MRV comprise a 5-km-thick succession of volcanic rocks interfingered with sedimentary rocks, most of which were emplaced in submarine environments below wave base (McPhie and Allen, 1992). The main volcanic facies include dominantly calc-alkaline lavas, mostly rhyolite and dacite with locally abundant andesite and basalt, volcaniclastic rocks and syn-volcanic intrusions. The principal sedimentary facies consist of interbedded sandstone turbidites and mudstone; non-volcanic conglomerate, and fossiliferous carbonate facies are also present. In the northern MRV, the principal volcanic facies are silicic, intermediate and mafic lavas, juvenile volcaniclastic rocks and syn-volcanic intrusions (McPhie and Allen, 1992; McPhie et al., 1993; Gifkins et al., 2005).

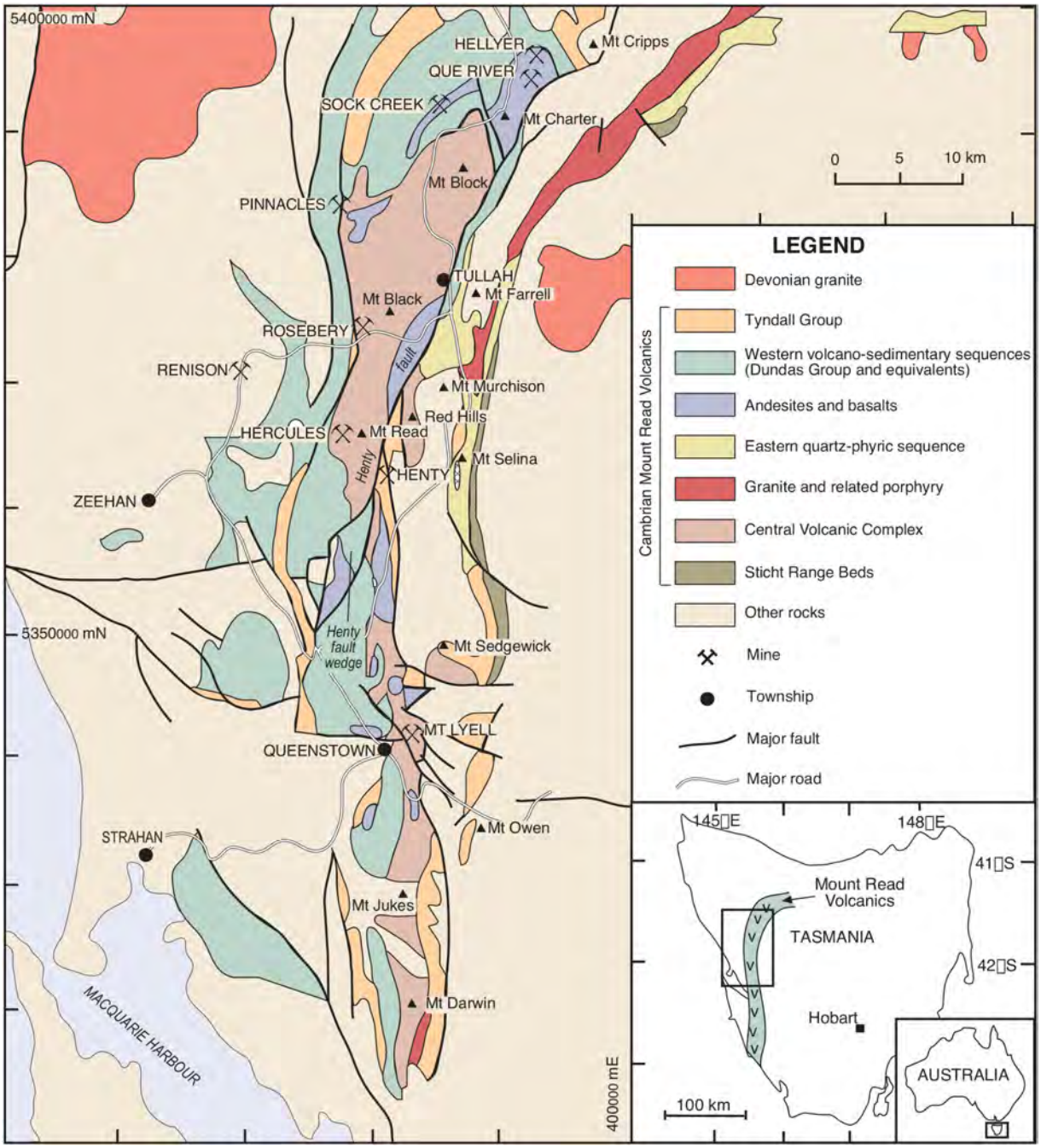

Figure 2.5: Geological map of the Mount Read Volcanics in central western Tasmania, showing the distribution of the principal lithostratigraphic units and major VHMS deposits (Gifkins et al., 2005).

In the MRV, there is a main eastern-central zone comprising volcanic rocks and intrusions and a wider western zone including mainly volcano-sedimentary sequences (Corbett, 1992). The MRV is divided by the N-NE-striking and W-dipping Henty Fault (Berry, 1989) (Figure 2.5). Significant lithostratigraphic, compositional, structural and metallogenic differences occur either side of this major fault zone (Corbett and Lees, 1987; Corbett, 1992; Corbett et al., 2014).

2.5 Lithostratigraphy of the Mount Read Volcanics

The MRV comprise five major lithostratigraphic associations: 1) the Sticht Range Beds, 2) the Eastern Quartz-Phyric Sequence (EQPS), 3) the Central Volcanic Complex (CVC), 4) the Western Volcano-Sedimentary Sequences (WVSS) and 5) the Tyndall Group (Corbett, 1992) (Figure 2.5). Three other lithological associations also occur in the MRV: andesites and basalts, tholeiitic mafic and ultramafic rocks, and granites and related porphyries (Corbett, 1992; Gifkins, 2001). These lithostratigraphic and lithological associations are complexly interfingered (Corbett et al., 2014).

The Henty Fault (Berry, 1989) divides the MRV into two major areas. To the S of the Henty Fault, the Sticht Range Beds, the EQPS, the CVC, the WVSS and the Tyndall Group occur. To the N of the Henty Fault, the CVC, the WVSS and the Tyndall Group are the only lithostratigraphic units present (Figure 2.6). The Henty Fault bifurcates into the North and South Henty Faults, S of Mount Read (Figure 2.5). The two branches enclose a complex sequence of volcanic, volcano-sedimentary and intrusive facies (Corbett and Lees, 1987; Corbett, 1992; Corbett et al., 2014).

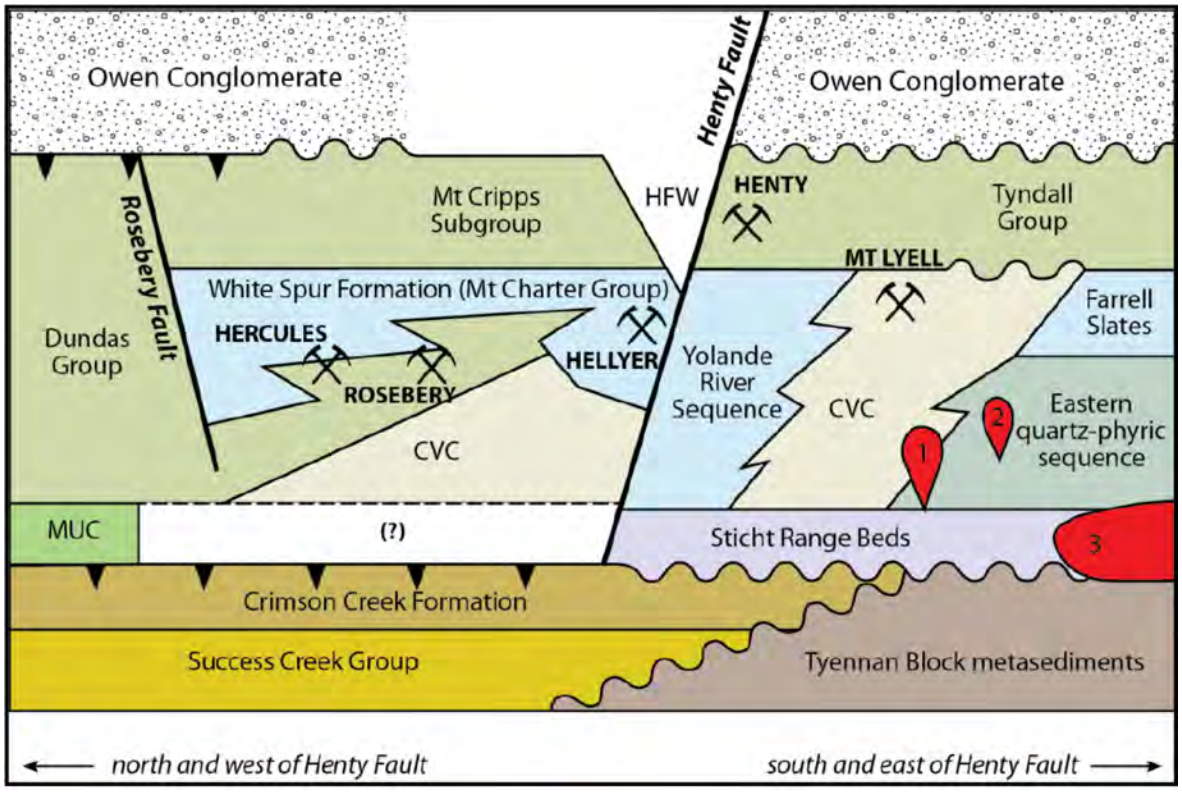

Figure 2.6: Distribution of the major lithostratigraphic units in the Mount Read Volcanics to the north and west, and south and east of the Henty Fault, after Mortensen et al. (2015). MUC = Mafic-ultramafic complexes; CVC = Central Volcanic Complex; HFW = Henty Fault Wedge. The numbered units are the Darwin (1) and Murchison (2) Granites and the Bonds Range Porphyry (3).

2.5.1 Sticht Range Beds

The Sticht Range Beds are present in the Lake Dora-Sticht Range area, where they comprise a W-dipping and W-younging, 1200-m-thick (maximum thickness) succession of siliciclastic pebble-cobble conglomerate and sandstone interbedded with micaceous siltstone, and include variable amounts of volcanic rocks (Corbett, 1992; McNeill and Corbett, 1992; Corbett et al., 2014). This succession occurs along the eastern side of the MRV (Figure 2.5) and is mainly derived from Precambrian metamorphic rocks (Baillie, 1989). The Sticht Range Beds unconformably overlie the Proterozoic Tyennan Region and show evidence of progression from fluvial to shallow-marine and deeper marine environments (Corbett, 1982; Baillie, 1989). Poorly preserved trilobite fossils near the top of the succession at Lake Dora indicate a probable Middle Cambrian age (Baillie, 1989).

2.5.2 Eastern Quartz-Phyric Sequence

The Eastern Quartz-Phyric Sequence (EQPS; also named Eastern sequence or Murchison Volcanics; Polya et al., 1986) comprises a thick (approximately 2.5 km) succession of quartz-feldspar-phyric rhyolite, dacite and minor andesite, volcaniclastic units and quartz-feldspar-phyric syn-volcanic intrusions (Corbett, 1992; Corbett et al., 2014). This succession occurs on the eastern margin of the MRV and is best exposed in the Murchison Gorge-Mount Murchison area (Polya et al., 1986; Pemberton et al., 1991; McNeill and Corbett, 1992) (Figure 2.5). The EQPS overlies the Sticht Range Beds to the E and N of Mount Murchison, interfingers with the CVC, and is conformably overlain by the Farrell Slates of the WVSS (section 2.5.4) at the western end of the Murchison Gorge-Mount Murchison area (Corbett, 1992; McNeill and Corbett, 1992). Units of bedded sandstone, siltstone and shard-rich mudstone from within the EQPS and correlates in the Back Peak area (Back Peak Beds; Pemberton et al, 1991) comprise Precambrian-derived detritus (McNeill and Corbett, 1992) and suggest deposition in a subaqueous environment (Corbett, 1992; Crawford et al., 1992).

2.5.3 Central Volcanic Complex

The Central Volcanic Complex (CVC) consists of a thick (approximately 3 km) assemblage of feldspar-phyric rhyolitic and dacitic lavas, pumiceous volcaniclastic rocks, and syn-volcanic intrusions (Corbett, 1979, 1992). Locally intercalated andesites and basalts are also present. These rocks occur in the central part of the MRV extending from S of Mount Darwin to N of Mount Murchison, S of the Henty Fault (southern CVC), and from SSW of Mount Read to NNE of Mount Block, N of the Henty Fault (northern CVC) (Figure 2.5). Rocks from the northern CVC have also been mapped in the Pinnacles area, N of Burns Peak.

Relatively thin and scattered intervals of mudstone and turbidites are evidence of a submarine depositional environment (Allen and Cas, 1990; Corbett, 1992; McPhie and Allen, 1992, 2003; Gifkins, 2001); this setting is consistent with the abundance of hyaloclastite and the presence of thick (up to approximately 100 m), massive to weakly graded beds of fiamme breccia (former pumice breccia). The CVC hosts the Rosebery-Hercules VHMS deposits N of the Henty Fault, and the Mount Lyell VHMS deposit S of the

Henty Fault (Figure 2.5). The CVC has complex interfingering relationships with most of the other major lithostratigraphic units of the MRV (Corbett, 1992; Corbett et al., 2014).

The southern CVC consists of feldspar-phyric rhyolitic and dacitic lavas, pumiceous pyroclastic rocks, syn-volcanic intrusions, minor shale and epiclastic units, and andesite in the Queenstown and Zig Zag Hill areas and W of the Tyndall Range (Corbett and Lees, 1987; Corbett, 1992) (Figure 2.5). The southern CVC interfingers with the EQPS in the Mount Murchison area (Polya et al., 1986; McNeill and Corbett, 1992; Corbett, 1992). To the N of Queenstown and W of the Tyndall Range, it interfingers and partly overlies the Yolande River sequence, which is part of the WVSS (next section). To the E, the southern CVC is intercalated with andesites (e.g., Anthony Road and Comstock Valley) and is overlain by the Tyndall Group (e.g., Mount Sedgwick, Mount Huxley and Mount Darwin areas) (Corbett, 1992).

The northern CVC comprises feldspar-phyric rhyolitic and dacitic lavas, pumiceous volcaniclastic rocks and syn-volcanic intrusions, and includes locally significant andesitic units. It is bounded to the E by the W-dipping Henty Fault and to the W by the E-dipping Rosebery Fault (Corbett and Lees, 1987; Corbett, 1992) (Figure 2.5). Andesitic and basaltic rocks occur E of Rosebery in the hanging wall of the Henty Fault (Sterling Valley Volcanics; Gifkins, 2001), S of Burns Peak, and in the Mount Charter area. A significant number of tholeiitic basaltic, doleritic and gabbroic dykes also occur throughout the northern CVC (Henty Dyke Swarm). To the NW, the northern CVC interfingers with and is overlain by the WVSS (next section) (Corbett and Lees, 1987; Corbett, 1992).

Gifkins (2001) revised the stratigraphy of the northern CVC and subdivided it into four formations: 1) Sterling Valley Volcanics, 2) Mount Black Formation, 3) Kershaw Pumice Formation, and 4) Hercules Pumice Formation.

Sterling Valley Volcanics

The Sterling Valley Volcanics have a minimum lateral extent of 7 km and a true stratigraphic thickness of 1.5 km, and occur in the core of a regional anticline at the eastern margin of the northern CVC. They comprise polymictic mafic breccia, mafic sandstone and siltstone, and dacitic to basaltic lavas and sills that have a gradational and conformable upper contact with dacitic to rhyolitic felsic units of the Mount Black Formation; the contact is exposed on the Murchison Highway E of Rosebery (Gifkins, 2001). The Sterling Valley Volcanics are exposed on the Murchison Highway between the Henty Fault and the summit of Mount Black, and are interpreted to represent the medial to proximal facies of a submarine basaltic volcanic centre that formed during a period of extension (Gifkins, 2001).

Mount Black Formation

The Mount Black Formation has a minimum lateral extent of 20 km and a minimum stratigraphic thickness of 1.6 km, and is exposed in a N-striking belt from Mount Read to Mount Block. It consists of massive, flow-banded and autobrecciated lavas, domes, cryptodomes and syn-volcanic sills that are interpreted to represent

Table 2.1: Geochronological data and fossil zones for lithostratigraphic units of the Mount Read Volcanics

LITHOLOGY AND LITHOSTRATIGRAPHIC UNITS		RADIOMETRIC AGES	TRILOBITE ZONES AND BIOSTRATIGRAPHIC AGE	DATING TECHNIQUE
Tyndall Group	Mount Julia Member (**Comstock Formation**)	494.4 ± 3.8 Ma	*L. laevigata* to *E. eretes* Zones (Boomeragian to early Mindyallan)	U-Pb in zircon SHRIMP[3]
	Volcaniclastic sandstone (Lynchford Member, **Comstock Formation**)	502.5 ± 3.3 Ma		U-Pb in zircon SHRIMP[3]
	Winter Brook lava	500.4 ± 6.9 Ma		U-Pb in zircon SHRIMP[5]
	Link Road ignimbrite	505.3 ± 3.6 Ma		U-Pb in zircon SHRIMP[5]
	Welded ignimbrite (**Mount Cripps Subgroup**)	496.0 ± 0.9 Ma		U-Pb in zircon ID-TIMS[6]
WVSS	Rhyolite lava (**Southwell Subgroup**)	503.2 ± 3.8 Ma	*G. nathorsti* to early *L. laevigata* Zones (late Undillan to early Boomerangian)	U-Pb in zircon SHRIMP[3]
	Rhyolite intrusion (**White Spur Formation**)	499.6 ± 0.8 Ma	*G. deltoides* to *G. nathorsti* Zones (middle to late Undillan)	U-Pb in zircon ID-TIMS[6]
	Rhyolite intrusion (**White Spur Formation**)	500.4 ± 0.8 Ma		U-Pb in zircon ID-TIMS[6]
	"Lower rhyolite" intrusion (**Southwell Subgroup** and **Que River Shale**)	499.3 ± 0.9 Ma	*E. opimus* to *P. punctuosus* Zones (late Floran to early Undillan)	U-Pb in zircon ID-TIMS[6]
	Andesite (Hellyer footwall, **Que-Hellyer Volcanics**)	500.4 ± 1.0 Ma	---	U-Pb in zircon ID-TIMS[6]
	Dacite (Que River footwall, **Que-Hellyer Volcanics**)	500 ± 16 Ma	---	U-Pb in zircon SHRIMP[3]
CVC	K-Lens Porphyry	499.4 ± 0.9 Ma	---	U-Pb in zircon ID-TIMS[6]
	Flow-banded rhyolite (Phylosopher's Ridge, **Central CVC**)	500.4 ± 0.9 Ma		U-Pb in zircon ID-TIMS[6]
	Rhyolite intrusion (Mount Jukes Road, **Central CVC**)	502.0 ± 0.9 Ma		U-Pb in zircon ID-TIMS[6]
	Quartz-phyric rhyolite (Mount Jukes Road, **Central CVC**)	503.9 ± 1.0 Ma		U-Pb in zircon ID-TIMS[6]
	Mount Jukes lava	503.3 ± 6.9 Ma		U-Pb in zircon SHRIMP[5]
	Pumice breccia (***Hercules Pumice Formation***)	502.6 ± 0.9 Ma		U-Pb in zircon ID-TIMS[6]
	Pumice breccia (***Hercules Pumice Formation***)	502.8 ± 1.0 Ma		U-Pb in zircon ID-TIMS[6]
	Pumice breccia (***Hercules Pumice Formation***)	503.0 ± 1.0 Ma		U-Pb in zircon ID-TIMS[6]
	Feldspar-phyric dacite (***Kershaw Pumice Formation***)	503.4 ± 0.9 Ma		U-Pb in zircon ID-TIMS[6]
	Feldspar-hornblende-phyric dacite (***Mount Black Formation***)	504.3 ± 1.0 Ma		U-Pb in zircon ID-TIMS[6]
	Feldspar-hornblende-phyric dacite (***Mount Black Formation***)	506.8 ± 1.0 Ma		U-Pb in zircon ID-TIMS[6]
Murchison Granite		497.3 ± 0.9 Ma	---	U-Pb in zircon ID-TIMS[6]
		501.0 ± 5.7 Ma		$^{40}Ar/^{39}Ar$ in hornblende[3]
		501.5 ± 5.7 Ma		$^{40}Ar/^{39}Ar$ in hornblende[3]
		523 ± 11 Ma		K-Ar in hornblende[3]
		524 ± 15 Ma		K-Ar in hornblende[1]
Darwin Granite		510 (+61,-21) Ma	---	U-Pb in zircon[2]
Bonds Range porphyry		500.4 ± 0.8 Ma	---	U-Pb in zircon ID-TIMS[6]
Crown Hill Andesite		489 ± 9 Ma	---	$^{40}Ar/^{39}Ar$ in hornblende[4]
Anthony Road Andesite		501.5 ± 5.7 Ma	---	$^{40}Ar/^{39}Ar$ in hornblende[3]
		502.2 ± 3.5 Ma		U-Pb in zircon SHRIMP[3]

Radiometric age data compiled from: (**1**) McDougall and Leggo (1965), (**2**) Adams et al. (1985), (**3**) Perkins and Walshe (1993), (**4**) Everard and Villa (1994), (**5**) Black et al. (1997) and (**6**) Mortensen et al. (2015). Trilobite zones and biostratigraphic age data compiled from Jago (1977), Jago and Brown (1989), Pemberton et al. (1991), Laurie et al. (1995), Jago and McNeill (1997), Corbett (2002b) and Kruse et al. (2009).

Abbreviations: **CVC** = Central Volcanic Complex; **WVSS** = Western Volcano-Sedimentary Sequences; **SHRIMP** = Sensitive High Resolution Ion Microprobe; **ID-TIMS** = Isotope Dilution Thermal Ionization Mass Spectroscopy

the proximal facies of a dacitic to rhyolitic, mainly effusive and intrusive volcanic complex (Gifkins, 2001). The Mount Black Formation is conformably overlain by pumice breccia and pumice-lithic clast-rich breccia units of the Kershaw Pumice Formation, and the contact is exposed between Mount Read and Dallwitz (Gifkins, 2001). Two feldspar-hornblende-phyric dacite units have recently been dated at 506.8 ± 1.0 Ma and 504.3 ± 1.0 Ma (Mortensen et al., 2015) (Table 2.1).

Kershaw and Hercules Pumice Formations

The Kershaw Pumice Formation has a minimum lateral extent of 16 km and a maximum measured stratigraphic thickness of 800 m, and occurs in a narrow (>800 m) N-striking belt from Jones Creek to Mount Kershaw and then in NE-striking fault slices from Mount Kershaw to north of Mount Block (Gifkins, 2001). In the Pinnacles-Burns Peak area, the top of the Kershaw Pumice Formation is defined as the base of the quartz-phyric volcaniclastic facies of the Dundas Group (Gifkins, 2001). The Kershaw Pumice Formation includes a 503.4 ± 0.9 Ma feldspar-phyric dacite (Mortensen et al., 2015) (Table 2.1). The Hercules Pumice Formation has a lateral extent of 12 km and a minimum stratigraphic thickness of 550 m (Allen, 1992b). Three pumice breccia samples from the Hercules Pumice Formation have recently been dated at 503.0 ± 1.0 Ma, 502.8 ± 1.0 Ma and 502.6 ± 0.9 Ma (Mortensen et al., 2015) (Table 2.1). The Kershaw Pumice Formation and Hercules Pumice Formation are laterally equivalent and dominated by regionally extensive pumice-rich and pumice-lithic clast-rich facies associations, and rhyolitic and dacitic lavas, sills and cryptodomes (Gifkins, 2001). The pumice breccia and rhyolitic to dacitic lavas and sills of these formations are compositionally similar to the rhyolite and dacite of the Mount Black Formation, and are considered to be the products of explosive and effusive eruptions that originated from a single felsic volcanic centre (Gifkins, 2001).

2.5.4 Western Volcano-Sedimentary Sequences

The Western Volcano-Sedimentary Sequences (WVSS) are a thick (>3 km) extensive succession of black and micaceous mudstone, and lithic sandstone interbedded with quartz-feldspar-phyric massive or graded volcaniclastic facies; rhyolitic, andesitic and basaltic lavas and syn-volcanic intrusions are locally important (Corbett, 1992; Crawford et al., 1992; McPhie and Allen, 1992; Gifkins et al., 2005). They represent the western and northernmost lithostratigraphic association within the MRV, occurring along the western and northern margins of the CVC from W of South Darwin Peak to the Cradle Mountain Link Road, N of Hellyer (Figure 2.5). The WVSS interfinger with the CVC in different parts of the MRV, and overlie the Success Creek Group and Crimson Creek Formation to the W (Corbett, 1981). Massive sulfide deposits and fossil occurrences, together with thick black mudstone, pillow basalts, hyaloclastite and turbidites, provide evidence for a submarine environment below storm wave base (McPhie and Allen, 1992). The WVSS include the Yolande River Sequence, the Dundas Group, the Mount Charter Group and the Henty Fault Wedge Sequence (Figure 2.5).

2.5.4.1 Yolande River Sequence

The Yolande River Sequence (Corbett, 1979) outcrops NW and SSW of Queenstown, S of the Henty Fault (Figure 2.5). It includes the siliceous-micaceous Miners Ridge Sandstone, overlain by the tholeiitic Guilfoyle Creek Basalt, which occupies the core of the steeply N-plunging Miners Ridge anticline (Corbett et al., 2014). Andesitic to basaltic rocks of the Lynch Creek Basalts occur at Lynchford and andesitic, dacitic and rhyolitic units occur NW of Queenstown, including the hornblende-phyric Crown Hill Andesite (Corbett, 1992; Crawford et al., 1992; Everard and Villa, 1994). The Yolande River Sequence interfingers with and is partly overlain by the CVC (Corbett, 1992).

2.5.4.2 Dundas Group

The Dundas Group extends from S of Mount Dundas up to the Rosebery-Pinnacles area (Figure 2.5), and consists of an approximately 3800-m-thick, early Middle to middle Late Cambrian fossiliferous flysch sequence of laminated mudstone and siltstone intercalated with turbiditic conglomerate and felsic volcanic rocks (Elliston, 1954; Campana and King, 1963; Jago, 1979; Brown, 1983, 1986; Collins and Williams, 1986; Corbett and Lees, 1987; Corbett, 1992; Corbett et al., 2014). To the NE, the Dundas Group contains highly altered andesitic and basaltic rocks of the Curtin-Davis Volcanics (Corbett and Lees, 1987; Corbett, 1992).

In the Huskisson River area, the lower part of the Dundas Group comprises mudstone, sandstone and conglomerate containing middle Middle Cambrian fossils; the upper part is equivalent to the Tyndall Group (next section). In the Dundas-Zeehan area, the three oldest formations of the Dundas Group (Judith Formation, Red Lead Conglomerate and Hodge Slate; section 2.2.2) are regarded as equivalents of the WVSS, but the overlying Razorback Conglomerate and Lower Brewery Junction Formation (section 2.2.2; Figure 2.2) are probably of Tyndall Group age (Corbett et al., 2014).

White Spur Formation

In the Rosebery-Howards Road area, the White Spur Formation (WSF) occurs at the base of the Dundas Group and comprises a W-younging, 5- to 400-m-thick, weakly fossiliferous succession of quartz-feldspar-phyric volcaniclastic facies with a compositionally wide range of clasts, intercalated with non-volcanic or mixed provenance mudstone and turbidites (Corbett, 1985, 1992; Corbett and Lees, 1987; Gikfins, 2001; McPhie and Allen, 2003; Jago, 2005). It is well exposed E and SE of Mount Dundas, particularly at the western end of Howards Road (Corbett, 1992). Fossils found in the WSF indicate an early Late Cambrian age (Jago, 1986), but in the Dundas area a Middle Cambrian age has been reported (Jago and Brown, 1989). The WSF is intruded by two rhyolite sills dated at 499.6 ± 0.8 Ma and 500.4 ± 0.8 Ma (Mortensen et al., 2015) (Table 2.1). The WSF disconformably overlies the CVC (Corbett and Lees, 1987) and the upper part of the sequence in the W has been correlated with the Tyndall Group (section 2.5.5) on the basis of its magnetic signature and stratigraphic position (Corbett, 2002b).

2.5.4.3 Mount Charter Group

The Mount Charter Group (Corbett, 1992) occurs in Hellyer-Burns Peak area between the CVC below and the Owen Group above. The Mount Charter Group has complex stratigraphic relationships with both the EQPS and the CVC along, and N of, the Henty Fault (Corbett, 1992; Corbett et al., 2014). The Mount Charter Group has been sub-divided into seven units: 1) Black Harry Beds, 2) Animal Creek Greywacke, 3) Que-Hellyer Volcanics, 4) Que River Shale, 5) Southwell Subgroup, 6) Mount Cripps Subgroup, and 7) Farrell Slates (Corbett, 1992). The Black Harry Beds, Animal Creek Greywacke, Que-Hellyer Volcanics, Que River Shale and Southwell Subgroup will be considered in more detail in Chapters 4 and 5.

Black Harry Beds

The Black Harry Beds (Corbett, 1992) comprise black mudstone, weakly micaceous siltstone, tuffaceous sandstone, and volcaniclastic breccia. They overly, or occur in faulted-contact with, the CVC on the Murchison Highway, SW of Sock Creek, and are gradationally overlain by the Animal Creek Greywacke.

Animal Creek Greywacke

The Animal Creek Greywacke (Collins, 1981) consists of well-bedded micaceous sandstone and siltstone interbedded with black mudstone and minor volcaniclastic breccia beds. The Animal Creek Greywacke is conformably overlain by the Que-Hellyer Volcanics.

Que-Hellyer Volcanics

The Que-Hellyer Volcanics (Corbett and Komyshan, 1989) comprise dominantly andesitic and basaltic lavas and volcaniclastic rocks, NE of the Mount Charter Fault. The Que-Hellyer Volcanics host the Hellyer, Fossey, Que River and Mount Charter VHMS deposits.

Que River Shale

The Que River Shale (Gee et al., 1970) conformably overlies the Que-Hellyer Volcanics and consists of pyritic black mudstone and siltstone. Fossils within the Que River Shale indicate a late Middle Cambrian Floran-Undillan age (E. opimus Zone to P. punctuosus Zone) (Figure 2.2) and deposition in a deep marine environment (Gee et al., 1970; Jago, 1977; Laurie et al., 1995). The Que River Shale is intruded by a 499.3 ± 0.9 Ma rhyolite sill (Mortensen et al., 2015) (Table 2.1).

Southwell Subgroup

The Southwell Subgroup (Corbett and Komyshan, 1989) conformably and gradationally overlies the Que River Shale and comprises quartz-feldspar-phyric and pumiceous volcaniclastic rocks interbedded with sedimentary rocks and minor felsic lava and intrusions. Trilobite fossils preserved within rare shallow water limestone clasts indicate a G. nathorsti Zone (late Undillan) to early L. laevigata Zone (early Boomerangian)

late Middle Cambrian age (Jago and McNeill, 1997) (Figure 2.2). The 499.3 ± 0.9 Ma rhyolite sill intruding the Que River Shale (previous section) also intrudes the lowermost unit of the Southwell Subgroup (Mortensen et al., 2015) (Table 2.1).

Mount Cripps Subgroup

The Mount Cripps Subgroup (Corbett, 1992) occurs E and NE of Hellyer and on the Cradle Mountain Link Road, and consists of quartz crystal-rich sandstone, volcanic conglomerate and sandstone and minor ignimbrite, andesite, and non-volcanic, Precambrian-derived conglomerate. The Mount Cripps Subgroup is considered to be a correlate of the Tyndall Group (next section) (Figure 2.2).

Farrell Slates

The Farrell Slates extend from Tullah to Mount Charter along the North Henty Fault (McNeill and Corbett, 1989), and comprise black mudstone, tuffaceous and micaceous sandstone, and minor volcaniclastic breccia (Corbett, 1992). The Farrell Slates contain important Devonian granite-related Pb-Zn-Ag veins (Corbett and Lees, 1987).

2.5.4.4 Henty Fault Wedge Sequence

The Henty Fault Wedge Sequence comprises a complex succession of sedimentary, volcanic (mainly andesite and basalt) and intrusive rocks, including gabbro and serpentinized ultramafic rocks (Corbett, 1992; Crawford et al., 1992). Fossils from the Henty Fault Wedge Sequence have a Middle Cambrian age (Corbett and Lees, 1987; Corbett, 1992).

2.5.5 Tyndall Group

The Tyndall Group (Corbett et al., 1974) comprises a thick succession (350 to 1300 m) of quartz-feldspar crystal-rich rocks, including tuffaceous sandstone, rhyolitic breccia and lithic-rich conglomerate, and minor rhyolitic ignimbrite, felsic to mafic lavas and intrusions, limestone, and non-volcanic mudstone and sandstone (White and McPhie, 1996; Corbett et al., 2014). It discontinuously extends along the eastern margin of the MRV, from South Darwin Peak to E of Mount Read (Figure 2.5). To the N and W of the Henty Fault, the Tyndall Group is also found NE of Mount Charter, in the Cradle Mountain Link Road area, N of the Pinnacles area, W of Rosebery, S of Serpentine Hill, and further S (Corbett et al., 2014). Fossiliferous limestone contains a late Middle Cambrian trilobite fauna (Jago et al., 1972). The depositional setting of the Tyndall Group was submarine below wave base although some parts accumulated in a shallow marine setting (White and McPhie, 1996, 1997).

The lower part of the Tyndall Group (Comstock Formation) comprises quartz-feldspar crystal-rich volcaniclastic sandstone, volcaniclastic breccia, welded ignimbrite, rhyolite, carbonate, mudstone and sandstone. The upper part (Zig Zag Hill Formation) is dominated by volcaniclastic conglomerate and

sandstone interbedded with mudstone and sandstone units (White and McPhie, 1996). A welded ignimbrite yielded an age of 496.0 ± 0.9 Ma (Mortensen et al., 2015) (Table 2.1).

The Tyndall Group is the youngest lithostratigraphic association in the MRV (Jago, 1979; Corbett, 1992; Perkins and Walshe, 1993; White and McPhie, 1996, 1997; Corbett, 2002b; Mortensen et al., 2015), unconformably overlying rocks of the Tyennan Region, the Sticht Range Beds, the EQPS, the southern CVC, the WVSS, and the Darwin Granite (next section). The Tyndall Group is conformably, unconformably, and disconformably overlain by the Late Cambrian to Early Ordovician Owen Group (Corbett, 1992; Corbett et al., 2014). Regional stratigraphic relationships between the Tyndall Group and other lithostratigraphic associations (Figure 2.7) are complex and laterally variable (Corbett, 1992). Significant parts of the WVSS have been reassigned as Tyndall Group correlates (Corbett, 2002b; Corbett et al., 2014). The Tyndall Group hosts the Henty gold deposit (section 2.9) between Mount Read and Mount Julia (Callaghan, 2001).

2.5.6 Cambrian granites

Five Cambrian granites were recognized in western Tasmania by Leaman and Richardson (1989), including the Murchison, Darwin, Elliot Bay, Dove and Timber Tops granites. Based on regional aeromagnetic surveys, Large et al. (1996) showed that these granites comprise a discontinuous belt which extends subsurface for 60 km N-S and 2 to 4 km E-W along the eastern margin of the CVC in the MRV, between Mount Darwin and Mount Murchison. They are interpreted to be sub-volcanic intrusions (Large et al., 1996), and are characterized by medium-grained (2-6 mm) quartz, K-feldspar, plagioclase, biotite and hornblende, and minor apatite, zircon and rutile (McNeill and Corbett, 1992). These granites and granodiorites intrude the EQPS, the CVC and the WVSS of the MRV, and are unconformably overlain by the Tyndall Group in the Darwin and Murchison areas (McNeill and Corbett, 1992). The granites were locally unroofed in the late Middle Cambrian (Corbett and Lees, 1987; Corbett, 1992).

The Cambrian Murchison and Darwin granites have high magnetic susceptibility and Fe2O3/FeO ratios, are typically high-K, and exhibit perthitic texture (Adams et al., 1985; Large et al., 1996). These granites are characterized by medium-grained (2-6 mm) quartz, K-feldspar, plagioclase, biotite and hornblende, and minor apatite, zircon and rutile, and have well-developed K-feldspar chlorite and sericite alteration zones (McNeill and Corbett, 1992). Recently, Mortensen et al. (2015) obtained a highly precise U-Pb age of 497.3 ± 0.9 Ma for the Murchison Granite (Table 2.1).

2.6 Age of the Mount Read Volcanics and the VHMS deposits

The MRV were first assigned a late Middle Cambrian age based on fossils in interbedded sedimentary units (Gee et al., 1970; Jago et al., 1972). Recently, Mortensen et al. (2015) provided highly precise chemical abrasion (CA) ID-TIMS (Isotope Dilution Thermal Ionization Mass Spectroscopy) U-Pb zircon crystallization age dates that further constrain the emplacement ages of MRV successions (Table 2.1; Figure

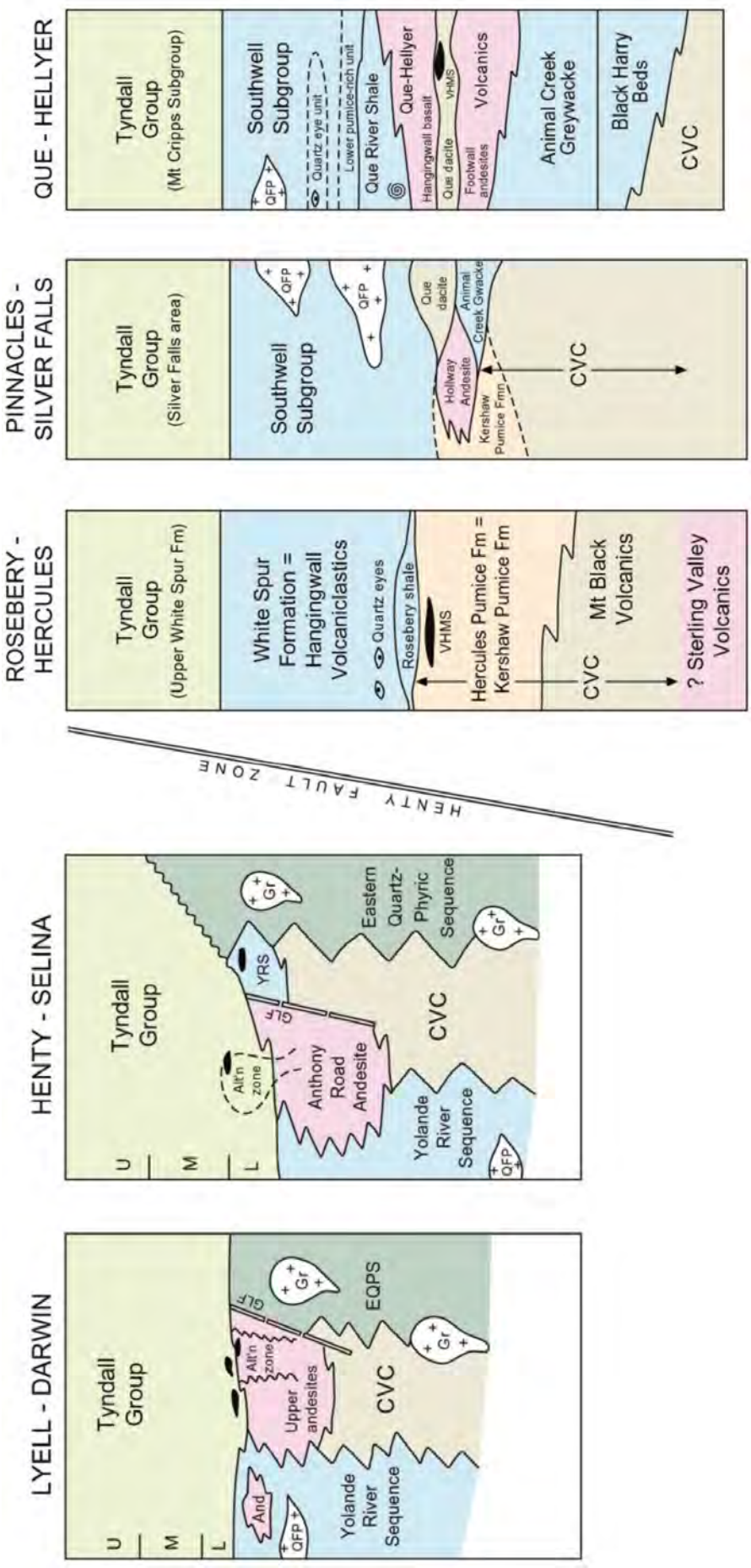

Figure 2.7: Correlation diagram for major units of the Mount Read Volcanics (from Corbett, 2002b).

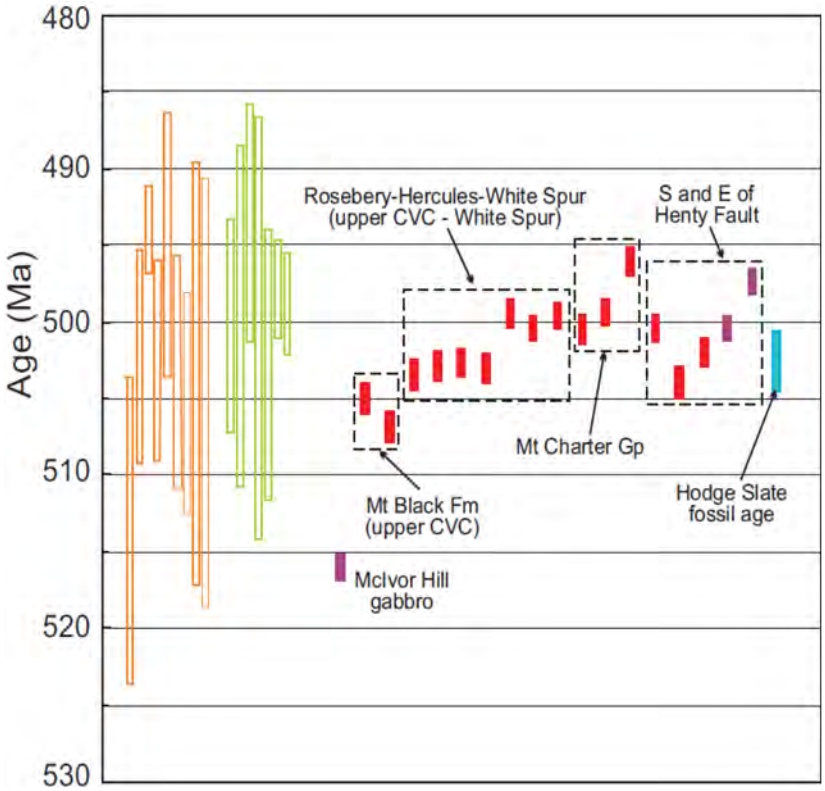

Figure 2.8: Compilation of U-Pb age constraints for the timing of magmatism within the Mount Read Volcanics (from Mortensen et al., 2015). Previous SHRIMP U-Pb zircon results from the Mount Read Volcanics (open orange bars) and from extensions of the Mount Read Volcanics to the northeast and south (open green bars) were obtained by Perkins and Walshe (1993) and Black et al. (1997, 2005). Solid bars are the CA ID-TIMS U-Pb zircon results from Mortensen et al. (2015). Purple bars represent ages for intrusive rock units. The solid blue bar shows the macrofossil age from Jago and Bentley (2010).

2.8). The volcanism in the central MRV is presently considered to have lasted at least 12.7 million years, from 506.8 ± 1.0 Ma for a feldspar-hornblende-phyric dacite unit in the lower part of the CVC to 496.0 ± 0.9 Ma for a welded ignimbrite in the Mount Cripps Subgroup (lower Tyndall Group) (Table 2.1). The new results of Mortensen et al. (2015) suggest that the volcanism in the northern MRV, N of the Henty Fault, occurred in three discrete pulses, separated by at least two periods of sedimentation, and that the VHMS deposits at Hellyer, Que River, Rosebery, Hercules and Mount Lyell formed during a narrow time interval at approximately 500 ± 1.0 Ma.

2.7 Petrology and geochemistry of the Mount Read Volcanics

The MRV have been subjected to locally intense diagenetic and hydrothermal alteration, and regional greenschist facies metamorphism. Hence, geochemical research has relied on least-altered samples and only relatively immobile element data are considered reliable (e.g., Crawford et al., 1992).

Table 2.2: Characteristics of geochemical suites of the Mount Read Volcanics.

FEATURES	SUITE I	SUITE II	SUITE III	SUITE IV
Lithostratigraphic units	EQPS; CVC; WVSS; Tyndall Group; Henty Fault Wedge	Yolande River Sequence; top of CVC	Yolande River Sequence (Lynch Creek Basalts); Hellyer Basalt	Henty Dyke Swarm; Henty Fault Wedge; Sterling Valley Volcanics
Rock types	Andesite, dacite and rhyolite; Darwin and Murchison Granites	Andesite and dacite	Basalt and andesite; shoshonite	Basalt and dolerite
Association	Medium to high-K calc-alkaline	High-K calc-alkaline	Calc-alkaline; shoshonitic	Tholeiitic
SiO_2 (wt. %)	58 - 78	58 - 68	49 - 57	50 - 54
TiO_2 (wt. %)	0.1 - 0.8	0.3 - 0.6	0.4 - 0.8	0.4 - 2
P_2O_5/TiO_2 (at any SiO_2 content)	< 0.40	0.35 - 0.75	0.40 - 1.25	0.05 - 0.25
Ti/Zr	< 40	14 - 21	18 - 41	73 - 107
$(La/Yb)_N$	Andesite (5 - 8); Rhyolite (10 - 14); Darwin Granite (16)	20 - 26 (andesite)	< 34	1.4 - 3.4
Other characteristics	$(Gd/Yb)_N$ values close to chondritic	0.60 - 0.75% K_2O in hornblende phenocrysts	up to 1.3 wt.% Cr_2O_3 in clinopyroxene in ankaramitic basalts	Nb < 3 ppm

Data compiled from Crawford et al. (1992), Gifkins (2001) and Corbett et al. (2014).

Phenocryst phases in the MRV typically include primary plagioclase, quartz, hornblende, clinopyroxene, magnetite, and minor biotite, ilmenite, apatite and K-feldspar. Most volcanic facies would have originally been at least partly glassy, but no glass is preserved. Secondary assemblages consist of major quartz, albite, chlorite, sericite and other white micas, calcite and other carbonates, epidote and K-feldspar, and minor biotite, sphene, pyrite, hematite, magnetite, rutile and leucoxene. Apatite, allanite, tourmaline, barite, garnet and monazite are locally present (Eastoe et al., 1987; Varne and Foden, 1987; Crawford et al., 1992; Gemmell and Large, 1992; McPhie et al., 1993; Large et al., 2001a, 2001b; Gifkins and Allen, 2001; Corbett et al., 2014).

Crawford et al. (1992) subdivided the MRV into five geochemical suites and two associations, based on major, minor and rare earth (REE) elements. One suite (suite V) is now known to pre-date the MRV (Corbett et al., 2014). The calk-alkaline association is represented by suites I, II, and III, and shows a progressive decrease in FeO_{total}, TiO_2, and Ti/Zr with increasing fractionation. Suite IV belongs to the tholeiitic magma association, which shows an increase in FeO_{total} and TiO_2 with increasing fractionation (Table 2.2).

Suite I includes lavas and shallow intrusions from the EQPS, the CVC, the WVSS, the Tyndall Group, and the Murchison and Darwin Granites (Table 2.2). Suite I is the volumetrically most abundant suite of coherent facies in the MRV and comprises plagioclase-phyric or quartz-plagioclase-phyric rhyolite, plagioclase-augite-phyric and minor hornblende-plagioclase-phyric dacite, and augite-plagioclase-phyric andesite. These rocks are typically medium- to high-K calk-alkaline and might represent a combination of variable degrees of crustal assimilation and simultaneous crystal fractionation (Crawford et al., 1992).

Suite II comprises hornblende-phyric andesite and dacite that are restricted to the S of the Henty Fault at the top of the CVC and the Yolande River Sequence (WVSS) (Table 2.2). They are more P_2O_5- and light REE-enriched than suite I. Suite II shows a typical high-K calk-alkaline trend and FeO_{total} and TiO_2 decrease with increasing fractionation (Crawford et al., 1992).

Suite III occurs both N and S of the Henty Fault and comprises olivine-chromite-clinopyroxene-phyric and clinopyroxene-rich ankaramitic basalt and andesite in the WVSS (Lynch Creek Basalt and Hellyer Basalt) (Table 2.2). Suite III shows general calk-alkaline affinities (decreasing FeO_{total} and TiO_2 with increasing fractionation), but the abundance of basalt and andesite distinguishes it from suites I and II. Also, FeO_{total} abundances overlap with those from tholeiitic suite IV, placing suite III closer to tholeiitic affinities. The Sock Creek basalts are considered to belong to suite III, but are compositionally distinct, showing much higher Ti/Zr (88), and lower Nb, Y, P_2O_5 (0.06-0.07%), (La/Yb)N (4-4.4), and REE abundances. These values might represent a transition between the suite III rocks and the tholeiitic suite IV (Crawford et al., 1992).

Suite IV includes tholeiitic augite-plagioclase-phyric to aphyric basalt and dolerite from the Henty Fault Wedge and the Henty Dyke Swarm (Table 2.2), which intrudes the northern CVC, N of the Henty Fault Wedge (Crawford et al., 1992). It also includes andesite and basalt of the Sterling Valley Volcanics (Gifkins, 2001).

Crawford et al. (1992) proposed that the MRV recorded evolution from transitional medium- to high-K calc-alkaline (suite I), through high-K calc-alkaline (suite II and III), to shoshonitic calc-alkaline (suite III) compositions. The Sock Creek basalts (suite III) may represent a transition to tholeiitic magmatism (suite IV) associated with rifting. Suite IV tholeiites are comparable to supra-subduction zone basalts erupted during the earliest stage of continental margin-arc and back-arc basin opening (Crawford et al., 1992).

2.8 Tectonic setting and structural geology of the Mount Read Volcanics

The MRV were affected by regional deformation during the last stages of the Cambrian Tyennan Orogeny and the Devonian Tabberabberan Orogeny. The rocks have been extensively faulted and folded, and are locally cleaved (Corbett et al., 2014).

2.8.1 Tectonic setting

The MRV have been interpreted to have formed in a diversity of tectonic settings (Campana and King, 1963; Corbett et al., 1972; Solomon and Griffiths, 1972; Williams, 1978; Crook, 1980; Green, 1983, 1984; Brown, 1986; Collins and Williams, 1986; Corbett and Lees, 1987; Varne and Foden, 1987). The formation of the MRV is considered in the tectonic model presented by Berry and Crawford (1988) and Crawford and Berry (1992) (Figure 2.9), and refined by Crawford et al. (2000) and Crawford et al. (2003). This model is constrained by geochemical studies and comparison with modern analogues, and interprets the Early to Middle Cambrian MUC in western Tasmania to be sheets of allochthonous forearc oceanic crust thrust onto the Neoproterozoic continental margin of Tasmania during the early stages of the Tyennan Orogeny (section 2.3) from approximately 515 to 508 Ma (Berry and Crawford, 1988; Crawford and Berry, 1992; Crawford et al., 2003).

The MUV were originally formed in an intra-oceanic island arc, the forearc of which was composed of boninites and low-Ti high-magnesian basalts. The intra-oceanic island arc collided with the passive continental margin at approximately 510 Ma and the forearc crust was thrust westward onto the thinned continental crust (Figure 2.9). The formation of a foreland basin, the Dundas Trough, occurred at this

Figure 2.9 (opposite): Hypothetical tectonic development of the Tasmanian section of southeastern Australia shown as crustal cross-section between 600 and 480 Ma (from Crawford et al., 2003). A) ~600 Ma: plume-triggered rifting at ca 600 Ma produces an east-facing volcanic margin with thick seaward-dipping reflector packages (SDRS). ~580 Ma: eventual continental crustal rupturing and ocean opening. B) ~520-515 Ma: east-dipping subduction commences, and produces a boninitic forearc lithospheric section and a primitive intra-oceanic arc. C) ~510 Ma: arc-continent collision leads to emplacement of allochthons first of SDRS-type volcanic passive-margin basalts, which are overridden by nappes of forearc-derived boninitic lithospheric sections, leading to collapse of the margin and development of the *Dundas Trough* foreland basin. D) 515 Ma: the new crustal collage had commenced to collapse due to post-collisional extension, and Mount Read Volcanics post-collisional lavas were erupted in the half-graben formed between ~505 and 497 Ma. E) ~497 Ma: continued extension led to exhumation of the underthrust continental crust of the volcanic passive margin, and the production of large amounts of coarse proximal siliciclastic molasse (Owen Conglomerate) that filled grabens formed along the collision zone.

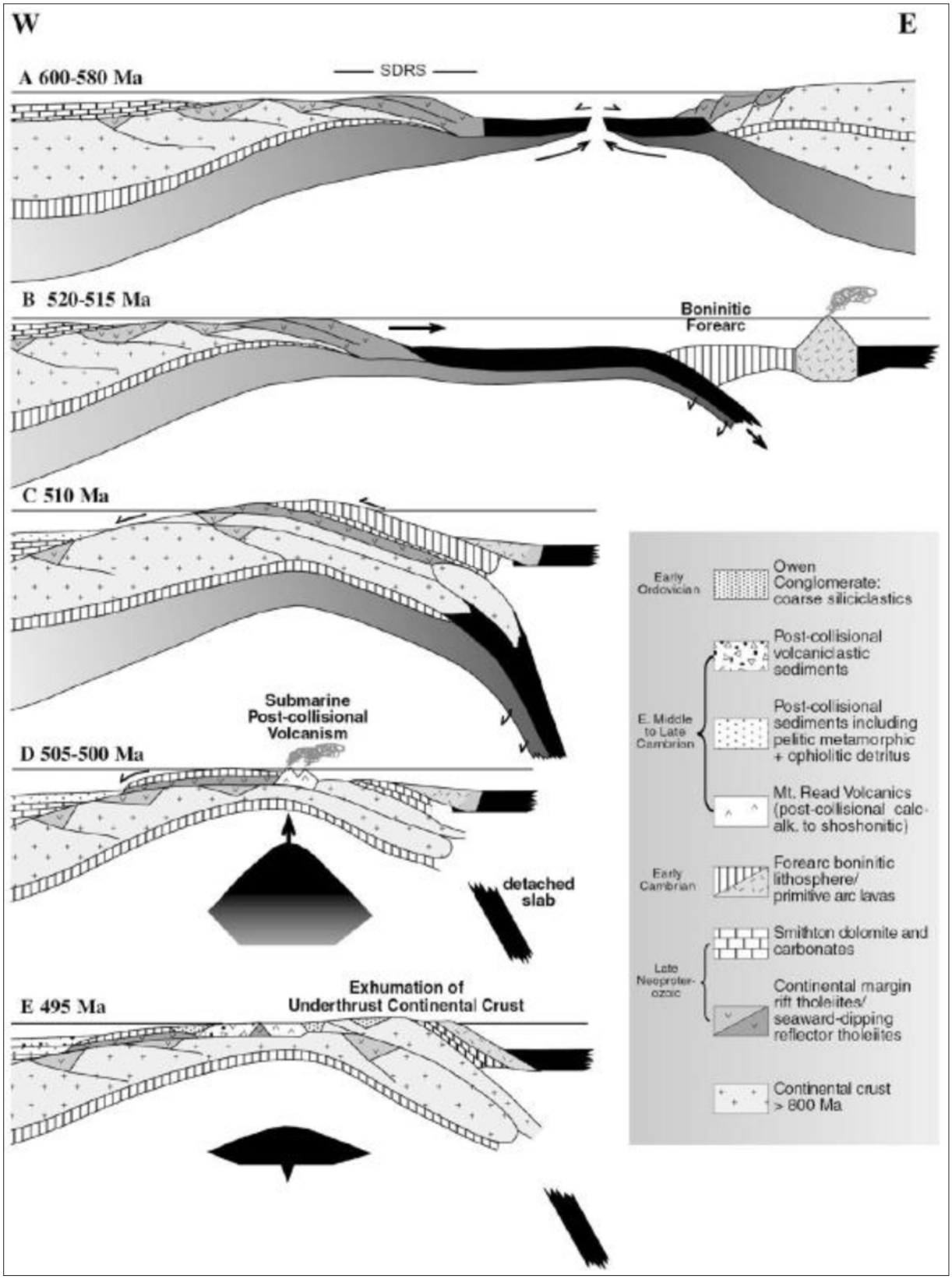
W
E
A 600-580 Ma
SDRS
B 520-515 Ma
Boninitic
Forearc
C 510 Ma
Submarine
Post-collisional
Volcanism
D 505-500 Ma
detached
slab
E 495 Ma
Exhumation of
Underthrust Continental Crust
Early Ordovician
Owen Conglomerate: coarse siliciclastics
Post-collisional volcaniclastic sediments
E. Middle to Late Cambrian
Post-collisional sediments including pelitic metamorphic + ophiolitic detritus
Mt. Read Volcanics (post-collisional calc-alk. to shoshonitic)
Early Cambrian
Forearc boninitic lithosphere/ primitive arc lavas
Smithton dolomite and carbonates
Late Neoprotero-zoic
Continental margin rift tholeiites/ seaward-dipping reflector tholeiites
Continental crust > 800 Ma

stage, and syn-orogenic sedimentation, mainly derived from local uplift of Precambrian basement rocks, immediately followed.

The MRV formed along the eastern margin of the Dundas Trough, W of the Tyennan Region, in a relatively deep submarine setting. A period of extension followed the post-collisional volcanism, producing the tholeiitic Henty Dyke Swarm and Henty Fault Wedge rocks (suite IV, Crawford et al., 1992). Along the eastern margin of the MRV, the Tyennan Region was exposed, uplifted and eroded as a result of prolonged backthrusting, filling the Dundas Trough with siliciclastic sediments (Owen Group).

2.8.2 Cambrian faults

The MRV are disrupted by several major Cambrian faults, including the Henty Fault and the Great Lyell Fault. The NNE-striking and W-dipping Henty Fault runs for about 70 km from the Mount Charter area, in the N, to W of Queenstown, in the S, and is best exposed in the Red Hills area. The Henty Fault has had a very complex movement history involving at least five episodes (Berry, 1989). The Great Lyell Fault is a N-striking and W-dipping fault extending from S of South Darwin Peak to W of Red Hills, just NNE of the Henty Fault Wedge, where it intersects the North Henty Fault (Corbett and Turner, 1989; Corbett, 2001a, 2001b; Noll and Hall, 2005).

2.8.3 Devonian deformation

Many Cambrian structures were reactivated during the Middle Devonian Tabberabberan Orogeny, including the Henty and Great Lyell Faults (Berry, 1989; Berry and Keele, 1993; Stacey and Berry, 2004; Seymour et al, 2007; Corbett et al., 2014). The early stage of E-W compression generated NNW- to NE-trending folds, and tightened N-trending Cambrian folds (Corbett, 1981; Collins and Williams, 1986; Carey and Berry, 1988; Seymour et al., 2007; Corbett et al., 2014). The second phase produced NW- to W-NW-trending folds and thrusts, which are best represented between Queenstown and Zeehan (Corbett, 1981; Corbett et al., 2014).

Rosebery Fault

The Rosebery Fault is a 45° E-dipping thrust fault that has been mapped from Mount Dundas to N of the Pinnacles area for at least 30 km, and is best exposed beside the Pieman River, near Bastyan Dam (Corbett and Lees, 1987). The Rosebery Fault is considered to be a Devonian thrust fault with no direct evidence of Cambrian movement (Berry and Keele, 1997) despite the presence of felsic intrusions near White Spur that suggest it may have been active in the Cambrian (Corbett and Lees, 1987).

2.8.4 Devonian granites

During the Late Devonian and Early Carboniferous, numerous post-tectonic, I- and S-type granites intruded eastern and western Tasmania at high crustal levels, generating tourmaline-bearing veins and considerable shallow, narrow, biotite-pyrite-tourmaline contact metamorphic aureoles (White and Chappell, 1977;

Adams et al., 1985; Corbett and Lees, 1987; Corbett, 1992; Black et al., 2005, 2010; McClenaghan, 2006; Corbett et al., 2014). The emplacement ages vary from 373.6 ± 1.8 Ma (northwest Tasmania) to 359.9 ± 1.8 Ma (west coast of Tasmania) (Black et al., 2005). Studies of the gravity field of Tasmania led Leaman et al. (1980) to interpret that the Devonian granites underlie large areas of western Tasmania and extend up to a few kilometers deep into the crust (Leaman and Richardson, 1989, 2003). These granites are important sources of Sn and are spatially associated with several economically important mineral deposits, including the Sn-rich Renison Bell and Mount Bischoff ore deposits, and the Zn-Pb-Ag vein deposits at Mount Farrell (Solomon, 1981; Seymour et al., 2007; Corbett et al., 2014).

2.9 Cambrian VHMS deposits in the Mount Read Volcanics

The MRV host economic VHMS deposits at Hellyer, Que River, Rosebery, Hercules and Mount Lyell, the Henty gold mine, and a large number of smaller ore deposits (Corbett et al., 2014). The total accumulated reserve amounts to approximately 12 million tons of base metals (Solomon, et al., 1988; Large, 1992). The deposits formed in a diversity of settings (McPhie and Allen, 1992), and both seafloor and sub-seafloor deposits have been recognized (e.g., Waters and Wallace, 1992; Allen, 1994b; Solomon and Zaw, 1997; Solomon and Groves, 2000; Gemmell and Fulton, 2001; Doyle and Allen, 2003; Martin, 2004). Almost all economic mineralisation took place in a narrow time interval during the late Middle Cambrian at approximately 500 ± 1 Ma (Mortensen et al., 2015).

North of the Henty Fault, polymetallic Zn-Pb-Au-Ag-Cu massive sulfide deposits dominate (Hellyer, Que River, Rosebery and Hercules) whereas S of the Henty Fault, the deposits are Cu-Au and Au-type (Mount Lyell and Henty) (Seymour et al., 2007; Corbett et al., 2014) (Figure 2.6). The ore deposits are hosted by the CVC (Rosebery, Hercules and Mount Lyell), the WVSS (Hellyer and Que River), and the Tyndall Group (Henty gold mine) (Gifkins et al., 2005; Corbett et al., 2014). The large VHMS deposits in the MRV are apparently clustered (e. g. Hellyer-Fossey-Que River-Mount Charter, Rosebery-Hercules-South Hercules, Mount Lyell field; Corbett et al., 2014).

2.9.1 Hellyer, Fossey, Que River and Mount Charter

The Hellyer, Fossey, Que River and Mount Charter VHMS deposits occur NE of Mount Charter Fault over a strike length of 6 km. They are hosted within the Que-Hellyer Volcanics, which is a sub-unit of the Mount Charter Group (northern subdivision of the WVSS; section 2.5.4) (Corbett, 1992; Waters and Wallace, 1992; Corbett et al., 2014).

The Hellyer VHMS deposit was an elongated, mound-shaped, high-grade, polymetallic ore deposit located within the hinge area of a broad anticline plunging 20°-30° NNE, and has been bisected by the N-striking, sub-vertical Jack Fault (McArthur, 1986; McArthur and Dronseika, 1990; Waters and Wallace, 1992; Gemmell and Fulton, 2001; Solomon and Gaspar, 2001; Solomon et al., 2004). The pre-mining resource is estimated at 16.9 million tons at 0.4 wt.% Cu, 7.2 wt.% Pb, 13.8 wt.% Zn, 167 g/t Ag and 2.5 g/t Au, and

an inferred resource of 0.75 million tons at 0.4 wt.% Cu, 4.1 wt.% Pb, 7.0 wt.% Zn, 86 g/t Ag and 1.3 g/t Au remains (Corbett et al., 2014).

The Fossey VHMS deposit is located approximately 100 m S of Hellyer between the NW-striking Easy Street and Tailings Dam Faults, and consists of an irregular, stratiform zone of barite ± minor "glassy silica-pyrite" (GSP) associated with high-grade base-metal sulfide (BMS) (Corbett et al., 2014). The published resource amounts to 800 thousand tons at 0.4 wt.% Cu, 5.8 wt.% Pb, 9.9 wt.% Zn, 137 g/t Ag and 2.5 g/t Au (Corbett et al., 2014).

The Que River VHMS deposit was located approximately 3 km to the SW of Hellyer, and comprised five NNE-striking, sub-vertical and sub-parallel lenses of massive and banded sulfides occurring in a complex synclinal structure (McArthur and Dronseika, 1990; McGoldrick and Large, 1992; Offler and Whitford, 1992). The pre-mining resource is 3.3 million tons at 0.7 wt.% Cu, 7.4 wt.% Pb, 13.3 wt.% Zn, 195 g/t Ag and 3.3 g/t Au (Corbett et al., 2014).

The Mount Charter VHMS deposit is located approximately 3 km SSW of the Que River VHMS deposit. It consists of a network of Au-Ag-rich barite veins and breccia associated with an extensive sericite-quartz-pyrite-barite-altered zone that is exposed at surface at the intersection between a NNE-striking high-strain zone and the ENE-striking Barite Creek Fault (Murphy, 2007; Corbett et al., 2014), and is similar to the footwall alteration associated with the Hellyer and Que River VHMS deposits in the NE (Murphy, 2007). The inferred resource is 6.1 million tons at 0.5 wt.% Zn, 35 g/t Ag and 1.2 g/t Au (Corbett et al., 2014).

2.9.2 Rosebery, Hercules and South Hercules

The Rosebery, Hercules and South Hercules VHMS deposits occur over a strike length of 9 km in a structural corridor bound to the E by the E-dipping Mount Black Fault and to the W by the E-dipping Rosebery Fault (Corbett and Lees, 1987; Allen, 1991; Berry and Keele, 1997; Gifkins, 2001). The Rosebery, Hercules and South Hercules VHMS deposits all occur in felsic pyroclastic facies at the top of the CVC (Allen, 1991, 1992b; Gifkins, 2001; Gifkins and Allen, 2001; Large et al., 2001a).

Rosebery is the largest polymetallic VHMS deposit in the MRV. It consists of 19 stacked, stratiform, sheet-like, Zn-Pb-Au-Ag-Cu ore lenses that sit sub-parallel and approximately 400 m above the 45° E-dipping Rosebery Fault (Brathwaite, 1974; Green et al., 1981; Corbett and Lees, 1987; Lees et al., 1990; Large et al., 2001a; Corbett et al., 2014). The global resource is 54.0 million tons at 3.9 wt.% Pb, 12.2 wt.% Zn, 0.5 wt.% Cu, 132g/t Ag and 1.9g/t Au as of December 2012 (Denwer, K., 2012).

The Hercules and South Hercules VHMS deposits are located approximately 7 km S of Rosebery on the western slope of Mount Hamilton, and lie on the eastern limb of a N-trending anticline (Briggs and McNeill, 2005). The Hercules polymetallic Zn-Pb-Au-Ag-Cu VHMS deposit consisted of numerous, relatively small, sheet- to pod-like, discontinuous sulfide lenses consistently dipping E at 60° to 70° (Zaw and Large, 1992). The total production and remaining reserve amounted to 2.57 million tons at 16.7 wt.% Zn, 5.2 wt.% Pb, 0.42 wt.% Cu, 160g/t Ag, and 2.7g/t Au (Briggs and McNeill, 2005). The South Hercules VHMS deposit

consists of a lenticular zone sub-parallel to bedding 1 km along strike from the main Hercules VHMS deposit. The calculated resource is 0.71 Mt at 3.5% Zn, 1.9% Pb, 0.11% Cu, 150g/t Ag and 2.7 g/t Au (Briggs and McNeill, 2005).

2.9.3 Mount Lyell field

The Mount Lyell field is located near Queenstown and comprises 21 different VHMS deposits enclosed in a relatively large (7 x 1 km), N-striking alteration zone focused along the Great Lyell Fault. The most economically important deposits are disseminated pyrite-chalcopyrite orebodies in alteration assemblages dominated by quartz-sericite or quartz-chlorite-sericite (e. g. Prince Lyell, Cape Horn, Western Tharsis) (Walshe and Solomon, 1981; Cox, 1981; Corbett, 2001a, 2001b; Huston and Kamprad, 2001; Corbett et al., 2014). The occurrence of pyrophyllite, enargite, digenite, tennantite, covellite, topaz, fluorite, zunyite, and woodhouseite, but also abundant massive to vuggy silica, collectively suggest conditions of high-sulfidation and advanced argillic alteration associated with acidic fluids, resembling epithermal environments (Large et al., 1996; Corbett et al., 2014).

2.9.4 Henty gold mine

The Henty gold mine is located just N of the Henty Fault Wedge, 20 km N of Mount Lyell, and consists of a series of small high-grade (10-30 g/t Au) sheet-style lenses, hosted within altered volcanic rocks at the base of the Tyndall Group (McNeill and Corbett, 1992; Halley and Roberts, 1997; Callaghan, 2001; Seymour et al., 2007). The estimated resource is 500 thousand tons at 12 g/t Au (Corbett et al., 2014).

2.10 Summary

The oldest rocks in Tasmania record the existence of a Proterozoic continent that underwent extension to form a passive margin at about 600 Ma (Corbett et al., 2014). This passive margin was overthrust by allochthonous intra-oceanic forearc crust and upper mantle during a continent-forearc collision event at about 510 Ma (Berry and Crawford, 1988; Crawford and Berry, 1992; Crawford et al., 2003). The MRV are a post-collisional succession of submarine volcanic facies interbedded with non-volcanic and mixed provenance mudstone and sandstone (Corbett et al., 2014).

The MRV extend along the western and northern margins of the Tyennan Region and form the eastern margin of the Dundas Trough in western Tasmania. They comprise five major lithostratigraphic associations (Sticht Range Beds, Eastern Quartz-Phyric Sequence, Central Volcanic Complex, Western Volcano-Sedimentary Sequences and Tyndall Group) (Corbett, 1992). The main volcanic facies associations include lavas and syn-volcanic intrusions, dominantly calc-alkaline rhyolite and dacite with locally abundant andesite and basalt, and a variety of pumiceous and crystal-rich volcaniclastic facies. The principal sedimentary facies comprise sandstone turbidites and black mudstone (Corbett, 1992; McPhie and Allen, 1992).

The bulk of the MRV is constrained by U-Pb dating and numerous fossil occurrences to a narrow time interval of approximately 12.7 Ma between Middle to Late Cambrian (Gee et al., 1970; Laurie et al., 1995; Mortensen et al., 2015). The MRV have been affected by regional deformation, locally intense diagenetic and hydrothermal alteration, and greenschist facies metamorphism and contact metamorphism (Corbett and Lees, 1987; Corbett, 1992). The MRV host economic VHMS deposits at Hellyer, Que River, Rosebery, Hercules, Mount Lyell and Henty (Solomon et al., 1988) that formed at approximately 500 ± 1.0 Ma (Mortensen et al., 2015).

CHAPTER 3

Facies associations in the northern Mount Read Volcanics

3.1 Introduction

This chapter focuses on the detailed descriptions and interpretations of the facies and facies associations of the Sock Creek-Burns Peak, White Spur-Howards Road and Mount Charter areas of the northern Mount Read Volcanics. The identification of facies and their genetic interpretation are based on detailed observations of the rock components and textures in drill core, hand samples, polished thin sections and field exposures. Identification of facies in the Mount Read Volcanics is challenging as they are commonly interfingered within different successions and are laterally discontinuous. Furthermore, primary textures and mineral assemblages have been modified by post-depositional diagenesis, hydrothermal alteration, deformation and metamorphism. However, graphic logs of 24 drill holes, data from 85 representative thin-sections and field exposures along the Boco Road, and whole-rock compositional data from 21 representative samples were used to identify 33 distinct facies and 2 sub-facies.

Phenocryst assemblages and ratios were used to discriminate among different coherent lithofacies and as a guide to the primary composition of clasts within associated volcaniclastic facies. Felsic facies are either feldspar-quartz-phyric or feldspar-phyric. Rhyolites are feldspar-quartz-phyric and feldspar-phyric; dacites are feldspar-phyric (section 3.2). The mafic facies are feldspar-pyroxene-phyric, feldspar-phyric or aphyric and typically amygdaloidal and/or vesicular.

The facies and sub-facies identified have been given descriptive names that reflect their primary mineralogy, texture and composition. Associated drill holes have also been assigned to assist in identifying and locating these facies and sub-facies in the northern Mount Read Volcanics.

Coherent and volcaniclastic facies that are spatially, texturally, mineralogically and compositionally related have been grouped into five facies associations: 1) rhyolite facies association (R), 2) dacite facies association (D), 3) mafic facies association (M), 4) polymictic volcaniclastic facies association (P), and mudstone facies association (Mud). Facies of the mudstone facies association are spatially or closely associated with almost every facies of the different facies associations.

The physical processes of emplacement, eruption and transport, and the provenance and environment of deposition are interpreted from volcanic and sedimentary components, textures and structures. The stratigraphy, correlations and facies architecture are discussed in Chapters 4, 5 and 6.

3.2 Criteria for distinguishing rhyolites from dacites

The criteria used in this study for distinguishing rhyolites from dacites are presented in Table 3.1. The criteria are in many cases progressive, which means that when criteria 1 is ambiguous or not available, criteria 2 and 3 were used to make the distinction.

Criterion 1 is a geochemical one, and is based on the Ti/Zr ratio and on the SiO_2 and Sc contents of rhyolite and dacite samples included in this study (Figure 3.1; Table 3.2). It is considered in this thesis that rhyolites have 68 to 77 wt. % SiO_2, 0 to 10 ppm Sc, and a Ti/Zr ratio of 0 to 10 whereas dacites have 63 to 68 wt. % SiO_2, 10 to 20 ppm Sc and a Ti/Zr ratio of 10 to 20 (Winchester and Floyd, 1977; Mielke, 1979).

The use of trace elements that are immobile during alteration has been very useful in the classification of primary rock types in the Mount Read Volcanics (Crawford et al., 1992). Elements such as Ti, Zr, Nb, Y, Lu, Yb, Hf, Ta, Th, P, Sc, V and Cr are considered to be relatively immobile during hydrothermal alteration (Pearce and Cann, 1973; Winchester and Floyd, 1977; MacLean and Kranidiotis, 1987; Ashley et al., 1988; Barrett and MacLean, 1994; Barrett and Sherlock, 1996).

Criterion 2 is based on thin-section observations and attributes the presence of quartz phenocrysts to be indicative of rhyolite (Corbett, 1981, 1989, 1992; McPhie et al., 1993). The absence of quartz phenocrysts in an otherwise feldspar-phyric sample has been considered to be more typical of dacite (Corbett, 1981, 1989, 1992; McPhie et al., 1993). Criterion 3 is based on observations of rhyolite and dacite samples in drill core and follows the same distinction used for Criterion 2. Corbett (1981) used SiO_2 content as an indicator of composition of primary rock types; as the effects of alteration in volcanic rocks of the Mount Read Volcanics became better understood, the phenocryst mineralogy was used as a criterion to distinguish rhyolites from dacites (Corbett, 1989, 1992; McPhie et al., 1993). In particular, rhyolites of the Central Volcanic Complex are largely feldspar-phyric (Corbett, 1989), but do contain sparse quartz phenocrysts.

Distinguishing rhyolites from dacites based on their phenocryst content alone may be unreliable, but it was not possible to analyse all the relevant samples.

Table 3.1: Criteria used in this study for distinguishing rhyolites from dacites

Rhyolite vs. Dacite	Criteria 1 - Geochemistry			Criteria 2 - Microscopy	Criteria 3 - Hand specimen
	SiO_2 (wt. %)	Ti/Zr	Sc (ppm)	Quartz phenocrysts	Quartz phenocrysts
Rhyolite	68-77	0-10	0-10	Yes	Yes
Dacite	63-68	10-20	10-20	No	No

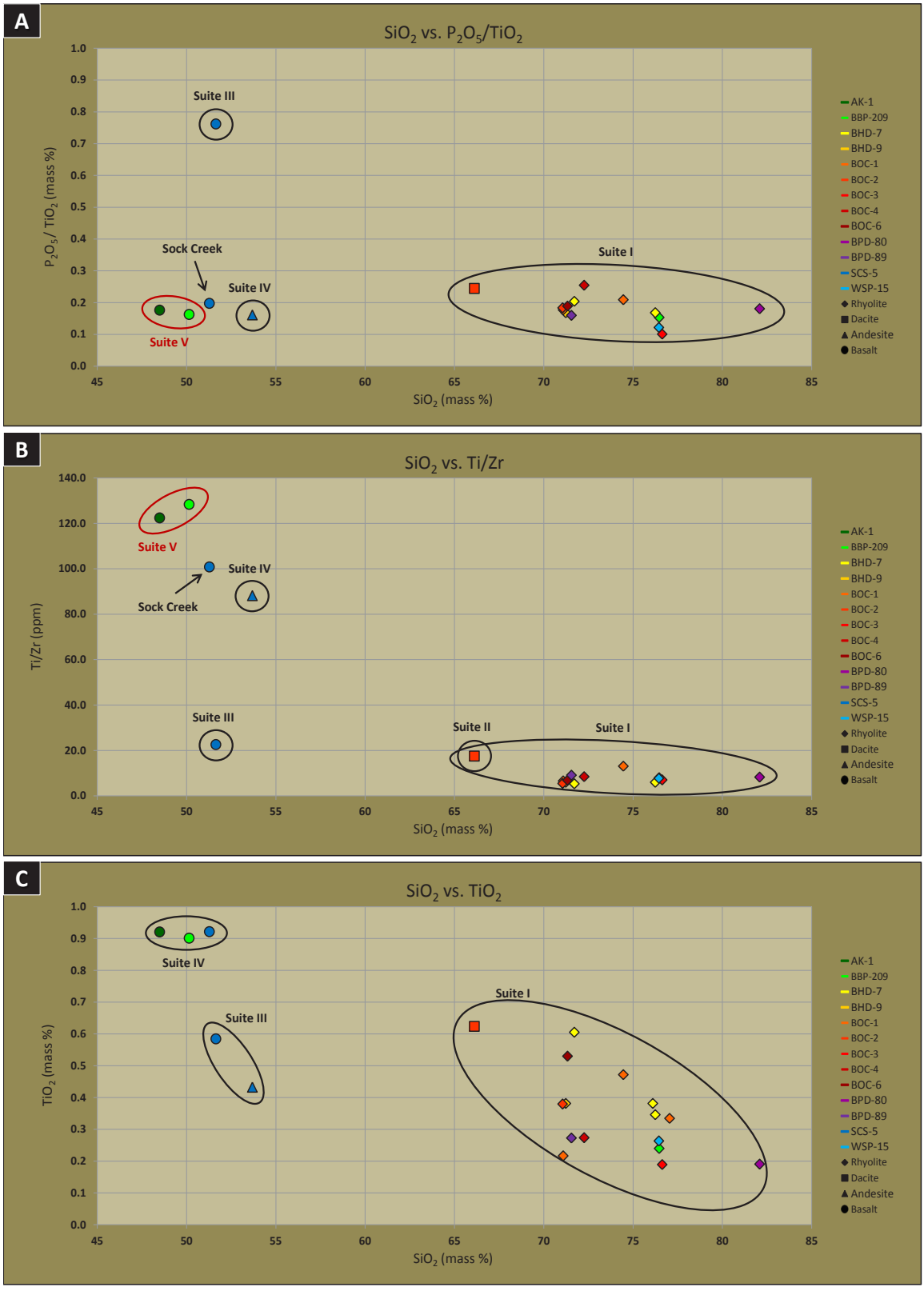

Figure 3.1: Discrimination diagrams for 21 least-altered samples of rhyolitic and dacitic lavas and syn-volcanic intrusions, and basaltic to andesitic syn-volcanic intrusions from the Sock Creek-Burns Peak and White Spur areas. The criteria used for selecting the least-altered samples were 1) the preservation of feldspars and ferromagnesian phases and 2) the absence of or minimal abundance of obvious hydrothermal phases such as chlorite and sulfides.
A: SiO_2 versus P_2O_5/TiO_2. B: SiO_2 versus Ti/Zr. C: SiO_2 versus TiO_2. Fields for Suite I, II, III, IV and V from Crawford et al. (1992). Suite V is now known to pre-date the Mount Read Volcanics (Corbett et al., 2014).

Table 3.2: Representative whole-rock analysis, recalculated 100% anhydrous

Sample	179333	179336	179337	179356	179359	179361	179376	179383	179391	179392	179394	179400	179411	179416	179421	179441	179443	179463	179464	179470	179486
Location	AK-1 (304.7 m)	BBP-209 (102.8 m)	BBP-209 (152.4 m)	BHD-7 (40.7 m)	BHD-7 (121.2 m)	BHD-7 (277.5 m)	BHD-9 (351.1 m)	BOC-1 (91.7 m)	BOC-1 (483.5 m)	BOC-1 (543.4 m)	BOC-2 (160.9 m)	BOC-2 (612.5 m)	BOC-3 (400.1 m)	BOC-4 (382.6 m)	BOC-6 (156.4 m)	BPD-80 (377.4 m)	BPD-89 (85.5 m)	SCS-5 (96.3 m)	SCS-5 (152.0 m)	SCS-5 (397.0 m)	WSP-15 (388.8 m)
Facies[1]	*Mfp*	*Mfp*	*Rqp*	*Rqr*	*Df*	*Rf*	*Rf*	*Rqp*	*PfS*	*Rqr*	*Rf*	*Df*	*Rf*	*Rf*	*Rqp*	*Rqr*	*Rqr*	*Mfp*	*Mfp*	*Mfp*	*Rf*
Rock type	Basalt	Basalt	Rhyolite	Rhyolite	Dacite	Rhyolite	Rhyolite	Rhyolite?	Pol. sst.[2]	Rhyolite	Rhyolite	Dacite	Rhyolite	Rhyolite	Rhyolite	Rhyolite	Rhyolite	Basalt	And/Bas	And/Bas	Rhyolite
Major elements (wt. %)																					
SiO_2	48.49	50.14	76.46	76.11	71.71	76.24	71.24	77.04	71.09	74.46	71.05	66.11	76.63	72.26	71.33	82.09	71.55	51.28	53.68	51.64	76.44
TiO_2	0.92	0.90	0.24	0.25	0.60	0.35	0.38	0.22	0.47	0.33	0.38	0.62	0.19	0.27	0.53	0.19	0.27	0.43	0.58	0.92	0.26
Al_2O_3	18.11	17.27	13.10	13.29	14.10	13.43	15.09	13.09	13.53	12.94	15.40	14.61	13.54	14.33	16.07	11.20	15.73	15.05	11.42	17.30	13.08
Fe_2O_3	13.19	12.08	2.43	2.07	4.54	1.49	2.18	1.79	3.48	4.12	3.19	5.98	0.97	3.42	3.53	0.31	4.46	9.89	9.88	11.22	1.82
MnO	0.45	0.15	0.06	0.05	0.18	0.03	0.05	0.06	0.16	0.11	0.12	0.53	0.05	0.08	0.13	0.02	0.11	0.19	0.30	0.26	0.04
MgO	6.18	6.31	0.50	0.58	1.68	0.64	0.66	0.54	0.82	0.82	1.61	2.90	0.29	0.58	1.36	0.23	0.88	9.44	13.52	5.51	0.39
CaO	9.67	10.50	0.19	0.20	1.73	0.41	1.60	0.25	2.28	0.96	0.40	4.14	0.46	1.05	0.59	0.95	0.35	11.92	8.84	8.45	0.90
Na_2O	1.89	1.53	3.81	5.40	3.29	4.17	4.18	5.64	2.25	4.40	4.08	3.53	6.67	5.66	2.99	3.80	5.10	1.36	1.27	3.44	4.15
K_2O	0.94	0.97	3.17	2.01	2.05	3.19	4.56	1.34	5.83	1.79	3.71	1.41	1.19	2.27	3.37	1.18	1.50	0.37	0.04	1.08	2.87
P_2O_5	0.16	0.15	0.04	0.04	0.12	0.06	0.06	0.04	0.10	0.06	0.07	0.15	0.02	0.07	0.10	0.03	0.04	0.07	0.45	0.18	0.03
Total	100.00	100.00	100.00	100.00	100.00	100.00	100.00	100.00	100.00	100.00	100.00	100.00	100.00	100.00	100.00	100.00	100.00	100.00	100.00	100.00	100.00
L.O.I.	5.01	2.70	1.05	0.83	2.90	1.79	2.07	0.76	1.99	2.06	1.72	2.73	0.83	1.52	2.32	1.83	1.95	2.58	5.52	2.76	1.37
Trace elements (ppm)																					
Ba	1341	514	1338	806	802	767	1322	988	1779	496	2470	753	498	871	818	463	528	217	112	1150	874
Ce (ICP-MS)	37.3	35.1	116.9	45.3	101.5	77.4	121.0	108.9	90.3	124.7	52.6	94.7	28.2	110.8	190.8	38.2	68.8	17.9	159.3	35.3	92.3
Cr	9.1	7.1	<1	2	1.7	2.4	1.5	1.4	4.8	2.8	<1	21.7	1.6	<1	3.9	1.8	1.5	347	1185	25.4	2.5
Cu (ICP-MS)	105.6	12.8	1.6	0.7	8.1	0.7	1.8	5.8	9.5	1.7	3.6	3.2	1.3	1.2	10.2	1.5	1.8	25.2	51.5	22.4	1.1
Ga	17.4	17.3	10.3	11.8	13.9	10.5	14.4	10.1	11.5	13.7	15.2	14.6	5.4	15.1	16.2	7.2	15.7	12.9	11.5	16.5	12.8
La (ICP-MS)	18.4	17.4	56.3	22.8	50.6	39.0	61.4	60.8	44.3	64.6	21.8	46.6	14.8	55.4	103.5	19.5	34.9	8.7	83.2	17.0	45.7
Mo (ICP-MS)	1.2	2.7	2.3	0.2	2.9	0.6	0.7	0.6	5.0	0.9	4.8	4.1	0.9	1.0	2.2	0.6	1.7	0.7	1.0	0.7	0.3
Ni	9.4	9.4	2.9	1.2	1.5	1.8	2	1.1	5	2.6	3.2	10.2	1.1	1.4	2.5	1.5	2.4	119	319	10.8	2.7
Nb	2.5	2.3	11.1	8.9	11.9	12.2	13.8	8.4	10.5	11	12.8	11.1	9.6	11	11.5	7.3	9.4	1.6	6.5	3.3	13.6
Nd (ICP-MS)	19.0	17.8	46.7	17.5	43.1	29.1	48.5	36.5	39.4	50.5	27.6	41.6	11.6	44.3	68.5	14.4	26.7	8.8	67.5	18.0	38.0
Pb (ICP-MS)	405.3	8.8	18.8	3.8	14.0	3.1	4.1	45.1	156.8	3.2	22.6	6.8	6.8	3.8	17.2	15.5	12.3	2.8	10.0	70.8	3.7
Rb	38.6	33.7	103	35.5	84.8	79.7	94.6	32.1	167	70.8	89.2	34.4	27.6	47.9	145	35.6	43.2	11.2	1.6	27.8	112
Sc	35.3	31.7	4.1	5.5	16.2	5.7	8.9	5.8	8.3	9.6	5.8	19	2.8	5.1	10.7	4.9	9.2	38.8	31.9	29.8	4.4
Sm (ICP-MS)	4.4	4.1	8.5	3.4	8.5	4.9	8.6	5.7	7.7	9.4	6.0	8.3	2.6	7.9	10.2	2.8	4.9	2.1	11.9	4.1	7.3
Sn (ICP-MS)	0.4	<1	3.9	0.9	1.4	1.3	1.5	<1	<1	4.5	<1	<1	<1	<1	<1	<1	<1	0.3	0.9	0.7	1.8
Sr	481	527	176	133	213	88.7	169	221	195	148	212	457	156	161	205	142	213	315	242	582	192
Th	2	3	22.2	12.4	20.2	21.5	24.8	18.6	17.6	24.6	28.8	19	19.8	20.3	26	12.6	17.9	2.4	22.8	3.5	20.7
U (ICP-MS)	0.9	0.9	5.4	2.9	5.4	5.4	6.2	3.8	4.6	5.8	6.2	4.6	5.2	4.6	5.6	3.1	3.9	0.6	4.6	1.2	5.8
V	348	364	8.9	20.4	31.7	16.7	15.8	<3	38.6	49	17.7	104	<3	7.6	43.6	7.6	18	259	221	322	4.6
Y	18.4	16.8	34.6	26.2	34.6	21.1	34.6	19.5	31.9	31.2	31.3	35.1	28.4	33	31.4	17.1	28.2	13.3	21.2	18.9	32.5
Yb (ICP-MS)	1.9	1.7	3.6	3.2	3.5	2.5	3.5	2.5	3.4	3.1	3.3	3.6	3.4	3.6	3.1	2.8	3.7	1.5	1.7	2.0	3.5
Zn (ICP-MS)	385.9	58.1	54.0	45.6	100.3	23.7	33.5	53.8	562.2	67.2	38.0	194.1	24.5	56.5	64.2	35.3	286.3	49.7	85.6	125.6	21.7
Zr	45.1	42.1	179	160	678	334	382	197	216	161	414	213	162	193	459	138	180	29.4	155	54.8	203
Ti/Zr	122.4	128.4	8.0	6.2	9.5	5.3	6.0	12.5	6.6	13.1	5.5	17.6	7.0	8.5	6.9	8.3	9.1	100.8	88.2	22.6	7.8
P_2O_5/TiO_2	0.2	0.2	0.2	0.2	0.2	0.2	0.2	0.2	0.2	0.2	0.2	0.2	0.1	0.3	0.2	0.2	0.2	0.2	0.2	0.8	0.1

L.O.I. = loss on ignition

[1] Rqp = coherent quartz-poor rhyolite sub-facies; Rqr = coherent quartz-rich rhyolite sub-facies; Rf = coherent feldspar-phyric rhyolite facies; Df = coherent feldspar-phyric dacite facies; Mfp = coherent feldspar-pyroxene-phyric mafic facies; PfS = polymictic felsic sandstone facies

[2] Polymictic sandstone

See Appendix D - *Anaytical methods and data*

3.3 Facies associations and interpretations

3.3.1 Rhyolite facies association

The rhyolite facies association comprises eight facies: 1) coherent feldspar-quartz-phyric rhyolite, 2) coherent feldspar-phyric rhyolite, 3) monomictic rhyolite breccia, 4) monomictic mud-matrix rhyolite breccia, 5) monomictic fiamme-rich rhyolite breccia, 6) polymictic rhyolite breccia, 7) polymictic mud-matrix rhyolite breccia, and 8) polymictic rhyolite sandstone. The location of the diamond drill holes intersecting facies of the rhyolite facies association is shown in Figures 3.2 and 3.3. The characteristics of the facies comprising the rhyolite facies association are summarized in Table 3.3.

3.3.1.1 Coherent feldspar-quartz-phyric rhyolite facies (Rfq)

The coherent feldspar-quartz-phyric rhyolite facies occurs from Sock Creek to Burns Peak, and in the White Spur and Howards Road areas (Figures 3.2 and 3.3). This facies comprises two sub-facies: 1) coherent quartz-rich rhyolite and 2) coherent quartz-poor rhyolite.

Coherent quartz-rich rhyolite sub-facies (Rqr)

The coherent quartz-rich rhyolite sub-facies occurs in the Sock Creek-Sock Creek South and Burns Peak areas, and on Boco Road, W of the Murchison Highway (Figure 3.2). It also occurs locally in the White Spur area (Figure 3.3). This sub-facies is spatially associated with coherent feldspar-phyric rhyolite, monomictic rhyolite breccia and monomictic mud-matrix rhyolite breccia facies (Table 3.3). Its lateral extent is 3 km in the Sock Creek-Sock Creek South area and 150 m in the Burns Peak area. Coherent quartz-rich rhyolite intervals range from 2 to 102 m thick. The coherent quartz-rich rhyolite sub-facies occurs as single units, and in combination with monomictic rhyolite breccia facies (Figures 3.4 and 3.5). Upper and lower contacts with monomictic rhyolite breccia and monomictic mud-matrix rhyolite breccia facies are typically gradational or locally faulted (Figure 3.5).

Coherent quartz-rich rhyolites (Figure 3.5 - A to G) are strongly porphyritic, typically pale to dark green and grey, massive or flow-banded and locally perlitic. Quartz phenocrysts (5-15%, 1-10 mm) are typically pale grey and round to elongate, and are commonly less abundant and on average slightly larger than feldspar phenocrysts (5-25%, 1-8 mm) (Figure 3.5 - D; Figure 3.6 - A and F). Quartz phenocrysts are represented by typically embayed, clear, unaltered and commonly fractured, euhedral to anhedral crystals with hexagonal to irregular and amoeboid shapes (Figure 3.6 - B, D and F). Feldspar is white, cream to pale and dark yellow, orange or green, tabular or irregular, and occurs both as single phenocrysts or glomerocrysts (Figure 3.5 - D; Figure 3.6 - A, C and F). Feldspar phenocrysts are commonly zoned and have a thin, less-altered rim surrounding a broad, more-altered core. Feldspar is commonly twinned and weakly to moderately sericite-altered (Figure 3.6 - C and F).

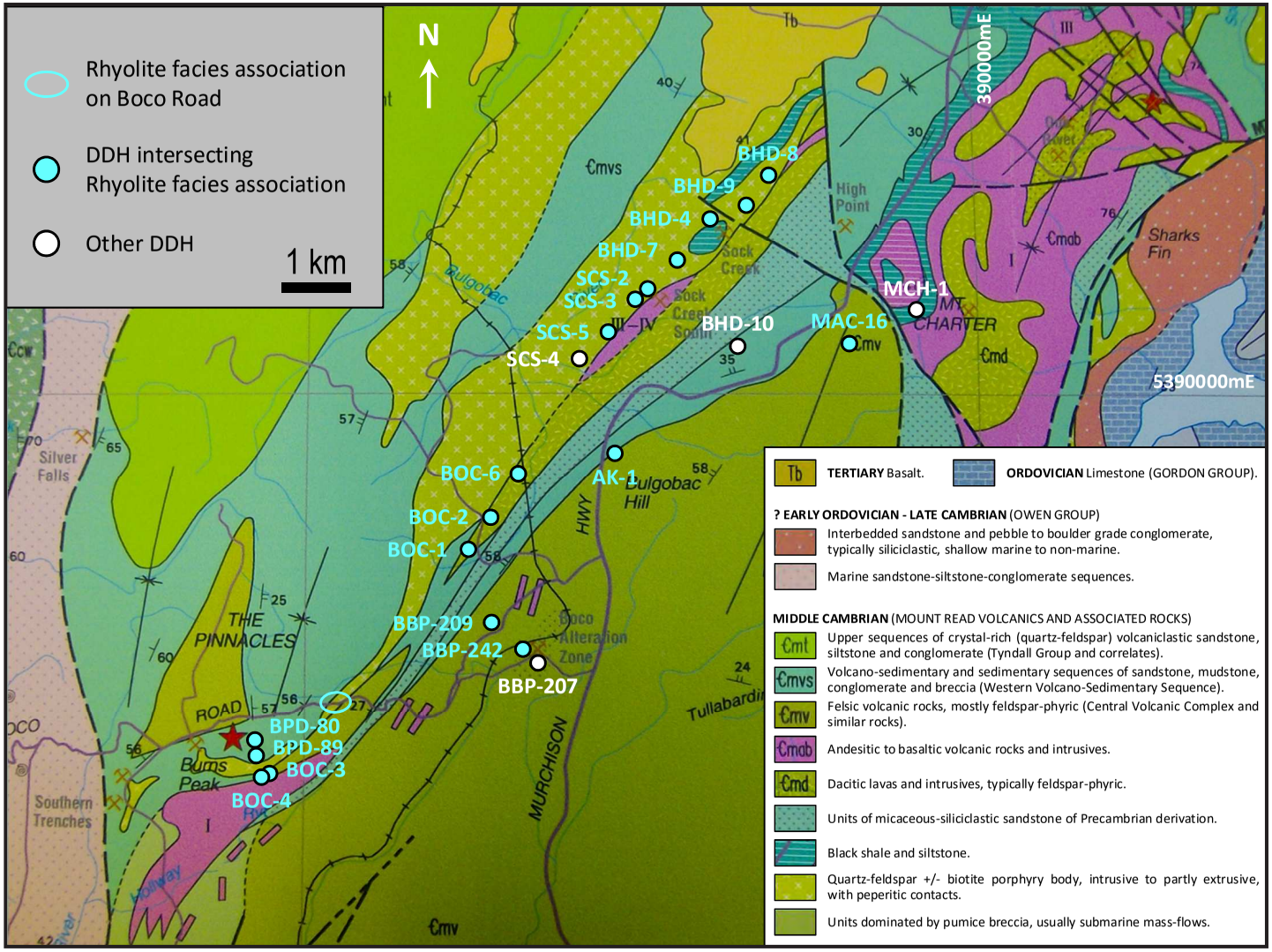

Figure 3.2: Geology of the Que River-Burns Peak area showing the location of the diamond drill holes (DDH) in this study, after Corbett (2002a). Facies of the rhyolite facies association occur at Boco Road and are intersected by DDH AK-1 (Bulgobac Hill area), BBP-209 and BBP-242 (Boco Alteration Zone area), BHD-4, BHD-7, BHD-8 and BHD-9 (Sock Creek area), BOC-1, BOC-2 and BOC-6 (Boco area), BOC-3, BOC-4, BPD-80 and BPD-89 (Burns Peak area), MAC-16 (Mackintosh area), and SCS-2, SCS-3 and SCS-5 (Sock Creek South area).

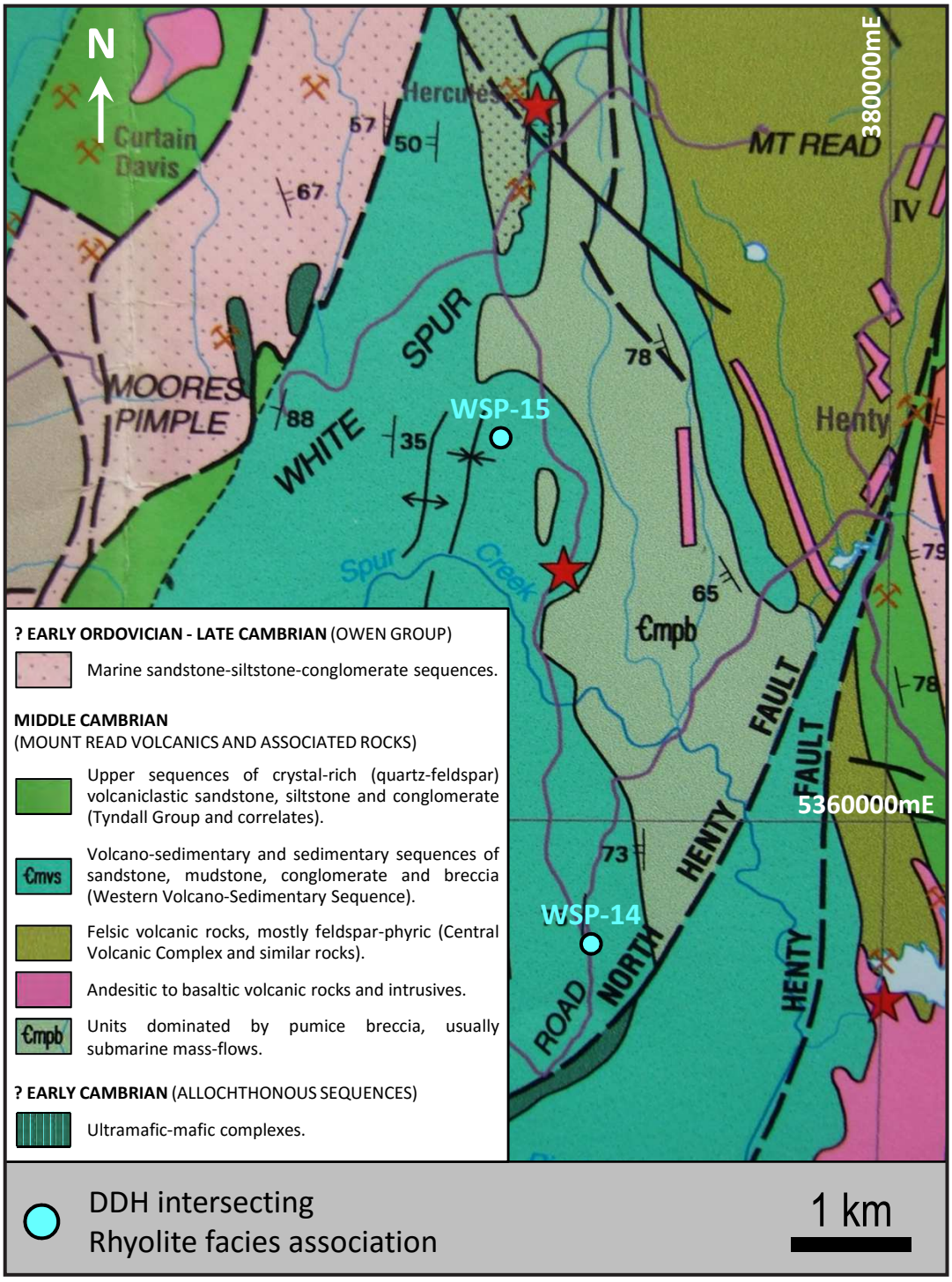

Figure 3.3: Geology of the White Spur-Howards Road area showing the location of the diamond drill holes (DDH) in this study, after Corbett (2002a). Facies of the rhyolite facies association (R) are intersected by DDH WSP-14 (Howards Road) and WSP-15 (White Spur area).

Table 3.3: Characteristics, location and interpretation of the facies comprising the rhyolite facies association.

Facies association, facies and sub-facies			Lithofacies characteristics	Thickness x lateral extent	Mineralogy/Components	Textures	Associated facies	Location and diamond drill holes	Interpretation
Rhyolite facies association (R)	*Coherent feldspar-quartz-phyric rhyolite facies* ***(Rfq)***	*Coherent quartz-rich rhyolite sub-facies* ***(Rqr)***	Massive; flow-banded; locally fractured and brecciated	2-102 m x 0.2-3 km	Feldspar phenocrysts and glomerocrysts (5-25%, 1-8 mm); quartz phenocrysts (5-15%, 1-10 mm)	Strongly porphyritic and glomeroporphyritic; perlitic	Rf; RmB; RmmB; (Mud)	Sock Creek: **BHD-4, BHD-7, BHD-8, BHD-9**; Burns Peak: **BPD-80, BPD-89**; Sock Creek South: **SCS-2, SCS-3, SCS-5**; White Spur: **WSP-15**; Boco Road	Coherent facies of syn-volcanic sills and cryptodomes
		Coherent quartz-poor rhyolite sub-facies ***(Rqp)***	Massive; flow-banded; locally fractured and brecciated	1-97 m x <12 km (discontinuously)	Feldspar phenocrysts and glomerocrysts (5-15%, 1-8 mm); quartz phenocrysts (<1-5%, 1-2 mm) and	Weakly to strongly porphyritic and glomeroporphyritic; perlitic	Rf; RmB; RmfrB; (Mud)	Bulgobac Hill: **AK-1**; Boco Alteration Zone: **BBP-209, BBP-242**; Sock Creek: **BHD-4**; Boco: **BOC-1, BOC-6**; Burns Peak: **BOC-3, BOC-4**; Mackintosh: **MAC-16;** Howards Road: **WSP-14**	Coherent facies of lavas and domes, and syn-volcanic sills and/or cryptodomes
	Coherent feldspar-phyric rhyolite facies ***(Rf)***		Massive; flow-banded; locally fractured and brecciated	15-77 m x ? km	Feldspar phenocrysts and glomerocrysts (<3-15%, 0.4-5 mm)	Weakly to moderately porphyritic and glomeroporphyritic; perlitic	Rfq; RmB; (Mud)	Boco: **BOC-2**; Burns Peak: **BOC-3, BOC-4**; Sock Creek: **BHD-7, BHD-9**; White Spur: **WSP-15**	Coherent facies of lavas and domes, and syn-volcanic sills and/or cryptodomes
	Monomictic rhyolite breccia facies ***(RmB)***		Massive to locally graded; poorly sorted; matrix-supported (clast-rotated) to clast-supported (jigsaw-fit)	<1-72 m x <12 km (discontinuously)	Irregular-shaped to blocky rhyolite clasts with planar and curviplanar margins; feldspar and quartz crystals and crystal fragments; fiamme (<5-35%)	Rhyolite clasts are massive, feldspar-quartz-phyric, feldspar-phyric and/or aphyric, non to weakly amygdaloidal, flow-banded or perlitic	Rfq; Rf; RmmB; RmfrB; (Mud)	Bulgobac Hill: **AK-1**; Boco Alteration Zone: **BBP-242**; Sock Creek: **BHD-4, BHD-7, BHD-9**; Boco: **BOC-1**; Burns Peak: **BOC-3, BOC-4, BPD-80, BPD-89**; Mackintosh: **MAC-16**	In situ and clast-rotated autoclastic breccia
	Monomictic mud-matrix rhyolite breccia facies ***(RmmB)***		Massive; poorly sorted; mud matrix-supported	<1-5 m x 1.3 km?	Irregular-shaped to blocky rhyolite clasts; feldspar and quartz crystals and crystal fragments; fiamme	Irregular feldspar-quartz-phyric, feldspar-phyric and/or aphyric rhyolite clasts; some rhyolite clasts are perlitic	Rfq; Rf; RmB; (Mud)	Sock Creek: **BHD-4, BHD-7, BHD-9**; Burns Peak: **BPD-80**	Peperite
	Monomictic fiamme-rich rhyolite breccia facies ***(RmfrB)***		Massive; poorly sorted; clast- to matrix-supported	47 m x ?	Abundant feldspar-phyric to apparently aphyric fiamme (up to 90%, 0.2-80 mm); rhyolite clasts and chloritic fragments (<30%)	Sub-parallel, aligned fiamme; some rhyolite clasts are flow-banded or perlitic	Rf	Burns Peak: **BOC-3**	Diagenetically compacted autoclastic breccia
	Polymictic rhyolite breccia facies ***(RpB)***		Massive; normally graded; clast-supported to matrix-supported; irregular lower contacts	<1-80 m x <12 km?	Abundant feldspar-quartz-phyric rhyolite clasts and feldspar and quartz crystal fragments; variable amounts of sandstone, mudstone and lithic clasts and fiamme	Blocky fragments and wispy and irregular fiamme; porphyritic to aphyric, massive, flow-banded, perlitic and spherulitic fragments	RpmmB; RpS; Rfq; RmB; RmfrB; RmfrS; (Mud)	Sock Creek: **BHD-4**; Burns Peak: **BPD-80**; Howards Road: **WSP-14**; White Spur: **WSP-15**	Submarine high-concentration density current deposits
	Polymictic mud-matrix rhyolite breccia facies ***(RpmmB)***		Massive; normally graded; mud matrix-supported; irregular lower contacts	<1-13 m x ?	Abundant feldspar-quartz-phyric rhyolite clasts and feldspar and quartz crystal fragments; variable amounts of sandstone, mudstone and lithic clasts and fiamme	Blocky fragments and wispy and irregular fiamme; porphyritic to aphyric, massive, flow-banded, perlitic and spherulitic fragments	RpB; RpS; (Mud)	Burns Peak: **BPD-80**; Howards Road: **WSP-14**	Submarine muddy high-concentration density current deposits
	Polymictic rhyolite sandstone facies ***(RpS)***		Massive to laminated; weakly bedded; well to very poorly sorted; very fine to very coarse-grained; normally graded	<0.1-33 m x <12 km?	Fragments identical to RpfrB, but < 2 mm; sporadic > 2 mm (up to 20 mm in diameter) rhyolite, lithic and mudstone fragments and fiamme	Blocky fragments and wispy and irregular fiamme; porphyritic to aphyric, massive, flow-banded, perlitic and spherulitic fragments; flame structures	RmfrB; RpB; RpmmB; (Mud)	Sock Creek: **BHD-4**; Burns Peak: **BPD-80**; Howards Road: **WSP-14**; White Spur: **WSP-15**	Submarine high-concentration density current deposits

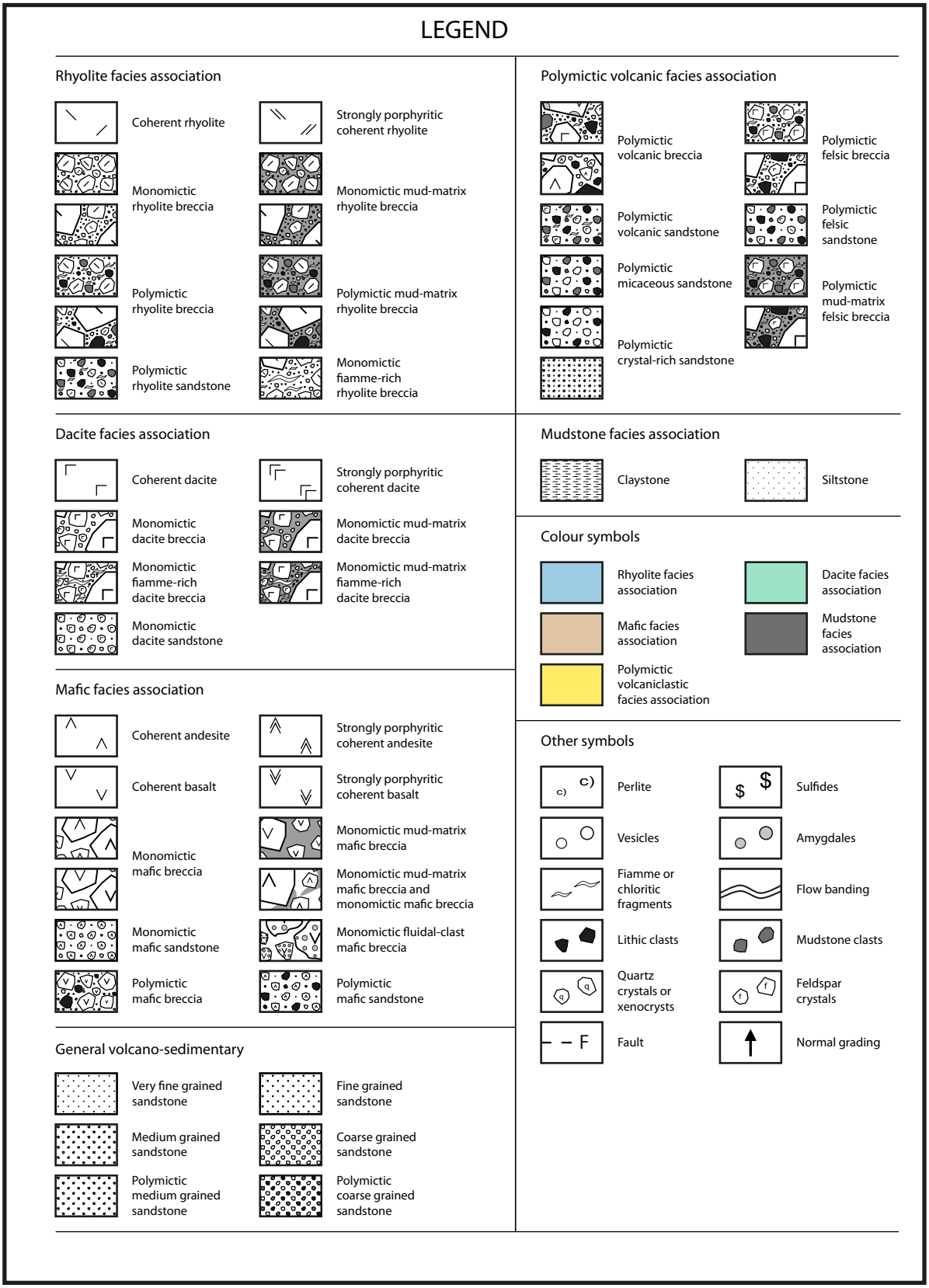

Figure 3.4: Symbols for graphic logs in Chapter 3.

Figure 3.5: Graphic log of part of diamond drill hole BHD-4 (Sock Creek area) through facies of the rhyolite facies association. See Figure 3.4 for legend to graphic log. The lower rhyolite interval (153.2-213.4 m) comprises coherent quartz-rich rhyolite sub-facies (Rqr) and monomictic rhyolite breccia (RmB) and monomictic mud-matrix rhyolite breccia (RmmB) facies, and has lower and upper mingled contacts with sulfide-bearing black mudstone facies (BMud) (section 3.3.5). The middle rhyolite interval (136.0-152.0 m) comprises coherent quartz-rich rhyolite sub-facies and monomictic rhyolite breccia and minor monomictic mud-matrix rhyolite breccia at the top, and has upper and lower mingled contacts with black mudstone facies. The upper rhyolite interval (60.5-135.2 m) includes a relatively thick (>40 m) part comprising monomictic rhyolite breccia overlying coherent quartz-rich rhyolite sub-facies, and has an upper irregular contact with polymictic rhyolite breccia (RpB) and sandstone (RpS) facies at 60.5 m. The rhyolite facies association and black mudstone facies (section 3.3.5) from 60.5 to 213.4 m is interpreted as a partly extrusive rhyolite cryptodome (section 3.3.1.9). Intervals of monomictic mud-matrix rhyolite breccia are interpreted as peperite and indicate local intrusion of the rhyolite cryptodome (section 3.3.1.9). The lower and middle rhyolite intervals are interpreted as intrusions. The upper rhyolite interval (60.5-135.2 m) represents extrusion of the rhyolite cryptodome (section 3.3.1.9). The upper interval (7.0-60.5 m) comprises normally graded units of polymictic rhyolite breccia (RpB) and sandstone (RpS) at the base and black mudstone facies (BMud) at the top interpreted as multiple high-concentration density current deposits (section 3.3.1.9).

A: BHD-4 (52.8 m) - Clast-supported, feldspar crystal-rich polymictic rhyolite breccia. Rhyolite clasts are strongly feldspar-quartz-phyric. Part of a large chloritic rhyolite clast (lower right) occurs. Dark green, aphyric and feldspar-quartz-phyric chloritic fragments, and mudstone and lithic clasts also occur.

B: BHD-4 (60.0 m) - Polymictic rhyolite sandstone. The sandstone is weakly bedded (parallel to the white two-headed arrow) and composed of fine grained (<2 mm) rhyolite and chloritic clasts, feldspar and quartz crystal fragments and lithic fragments.

C: BHD-4 (102.4 m) - Matrix-supported monomictic rhyolite breccia. Rhyolite clasts are feldspar-quartz-phyric, and separated by finer-grained (<2 mm) rhyolite fragments and feldspar and quartz crystals and crystal fragments.

D: BHD-4 (112.8 m) - Coherent quartz-rich rhyolite. Feldspar phenocrysts are commonly smaller and more abundant than quartz phenocrysts.

E: BHD-4 (165.4 m) - Monomictic mud-matrix rhyolite breccia. Porphyritic rhyolite clasts are locally surrounded by pale to dark grey and black mud. Uphole and younging directions: A, B, C and E - right to left; D - left to right.

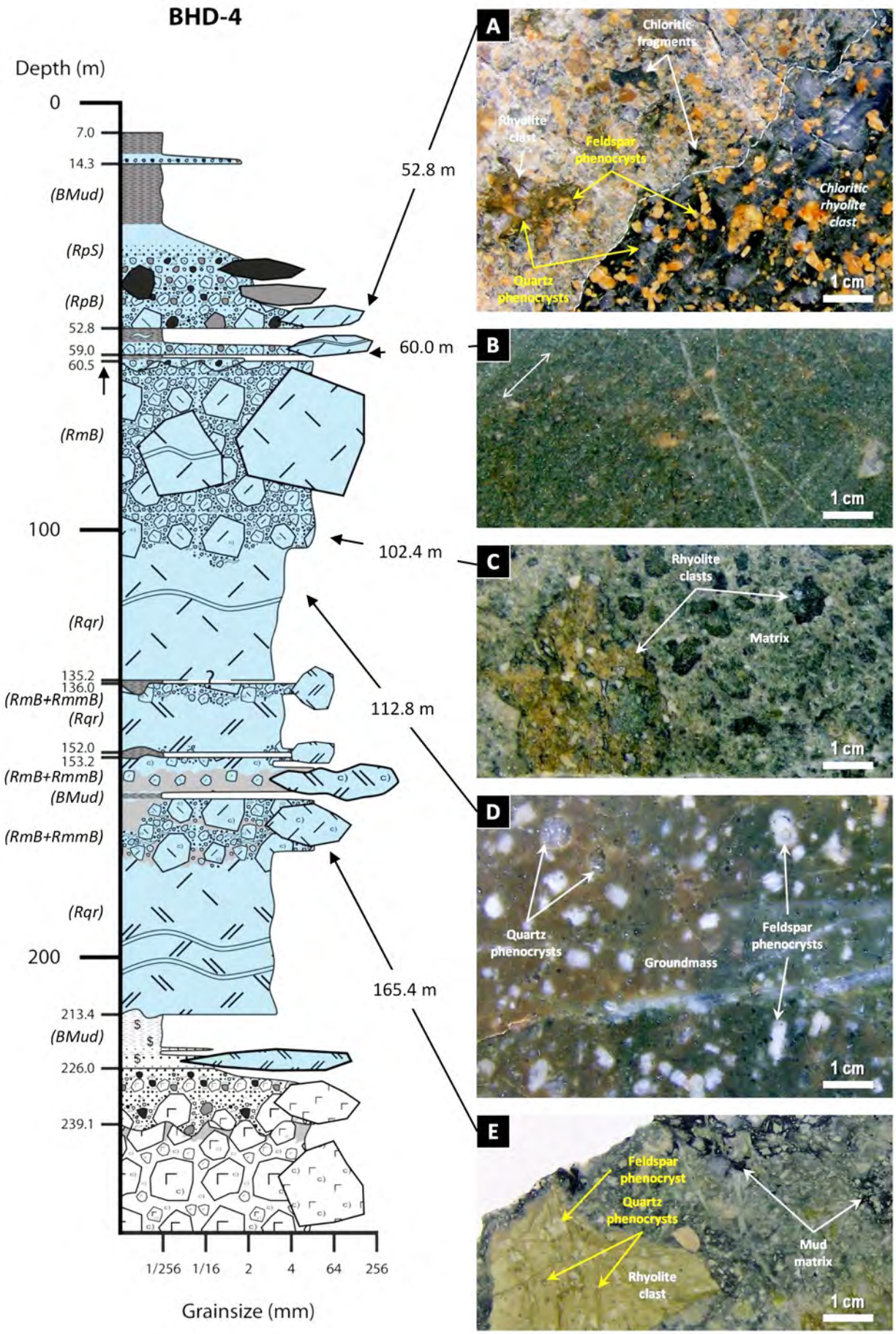
BHD-4
Depth (m)
0
7.0
14.3
(BMud)
(RpS)
(RpB)
52.8
59.0
60.5
(RmB)
100
(Rqr)
135.2
136.0
(RmB+RmmB)
(Rqr)
152.0
153.2
(RmB+RmmB)
(BMud)
(RmB+RmmB)
(Rqr)
200
213.4
(BMud)
226.0
239.1
1/256 1/16 2 4 64 256
Grainsize (mm)
52.8 m
60.0 m
102.4 m
112.8 m
165.4 m
A
Chloritic fragments
Rhyolite clast
Feldspar phenocrysts
Chloritic rhyolite clast
Quartz phenocrysts
1 cm
B
1 cm
C
Rhyolite clasts
Matrix
1 cm
D
Quartz phenocrysts
Groundmass
Feldspar phenocrysts
1 cm
E
Feldspar phenocryst
Quartz phenocrysts
Rhyolite clast
Mud matrix
1 cm

Figure 3.6: Coherent feldspar-quartz-phyric rhyolite facies. A and B: BHD-7 (40.7 m); C: SCS-5 (20.4 m); D: BPD-80 (377.0 m); E: WSP-15 (205.4 m); F and G: WSP-15 (227.2 m); H to J: BBP-209 (152.4 m); K: MAC-16 (166.9 m); L to N: WSP-14 (456.3 m).

A: Handspecimen photograph of the coherent quartz-rich rhyolite sub-facies (uphole and younging direction: left to right). Feldspar phenocrysts are commonly more abundant and on average, slightly smaller than quartz phenocrysts.

B to D: Photomicrographs of the coherent quartz-rich rhyolite sub-facies (B - transmitted, cross polarised light; C and D - transmitted, plane polarised light). The groundmass comprises very fine-grained feldspar and quartz.

B: Subhedral and embayed quartz phenocryst with amoeboid shape due to the presence of multiple embayments.

C: Moderately sericitic feldspar phenocrysts.

D: Hexagonal quartz phenocryst.

E: Handspecimen photograph of a sharp, wavy contact between coherent quartz-rich rhyolite sub-facies (Rqr) and black mudstone facies (BMud; section 3.3.5). The mudstone is dark brown close to the contact with the rhyolite and grey away from the contact with the rhyolite.

F and G: Photomicrographs of the coherent quartz-rich rhyolite sub-facies (transmitted, plane polarised light).

F: Embayed quartz and feldspar phenocrysts surrounded by strongly-altered, fine-grained, quartz-feldspar-chlorite-sericite-rich groundmass.

G: Altered perlitic groundmass.

H and L: Handspecimen photographs of the coherent quartz-poor rhyolite sub-facies (uphole and younging direction: right to left).

I to K, M and N: Photomicrographs of the coherent quartz-poor rhyolite sub-facies (transmitted, plane polarised light).

H: Flow-banded coherent quartz-poor rhyolite. Flow bands are represented by wavy, irregular, sub-parallel, cream and pale orange feldspar-bearing bands. Feldspar phenocrysts occur both within the flow bands and as isolated crystals surrounded by microgranular greyish green groundmass. Quartz phenocrysts are rarely visible in drill core.

I: Flow-banded coherent quartz-poor rhyolite. Flow bands are wavy, irregular, sub-parallel, dark green chlorite- and sericite-rich bands. Feldspar phenocrysts occur between the flow bands as isolated crystals surrounded by feldspar-quartz-rich groundmass.

J: Anhedral, embayed quartz phenocryst in a very fine-grained feldspar-quartz-rich groundmass.

K: Perlitic groundmass. Perlitic fractures are delineated by very fine-grained phyllosilicates and opaque phases (Fe oxides) (dark brown); the fractures surround round to irregular cores of intact rhyolite (former glass).

L and M: Coherent quartz-poor rhyolite sub-facies with false clastic texture represented by dark green (chlorite-rich) domains (L). Abundant feldspar phenocrysts are evenly distributed and occur both within the chlorite-rich domains and as isolated crystals surrounded by strongly altered groundmass.

N: Quartz phenocryst surrounded by chlorite-sericite-rich groundmass.

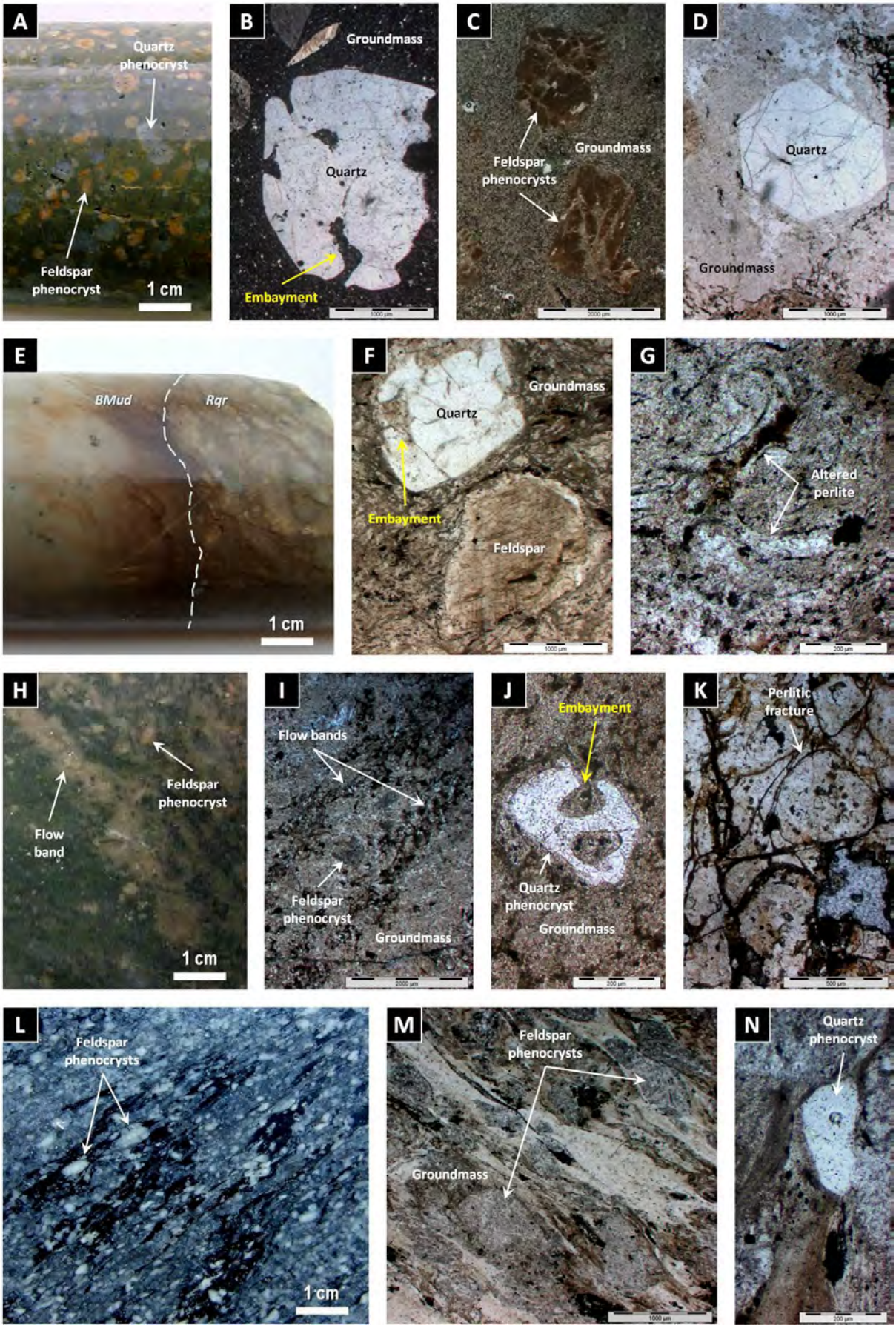
A
Quartz phenocryst
Feldspar phenocryst
1 cm
B
Groundmass
Quartz
Embayment
C
Feldspar phenocrysts
Groundmass
D
Quartz
Groundmass
E
BMud
Rqr
1 cm
F
Groundmass
Quartz
Embayment
Feldspar
G
Altered perlite
H
Feldspar phenocryst
Flow band
1 cm
I
Flow bands
Feldspar phenocryst
Groundmass
J
Embayment
Quartz phenocryst
Groundmass
K
Perlitic fracture
L
Feldspar phenocrysts
1 cm
M
Feldspar phenocrysts
Groundmass
N
Quartz phenocryst

The groundmass is composed of a polycrystalline mosaic of feldspar and quartz with minor amounts of sericite, chlorite and carbonate (Figure 3.6 - B, C, D and F). Rare (up to 1%) pyrite and sphalerite occur as disseminated grains and clusters or in veins and fractures. Zircon and apatite occur sporadically.

Coherent quartz-poor rhyolite sub-facies (Rqp)

The coherent quartz-poor rhyolite sub-facies occurs from Sock Creek to Burns Peak, and in the Howards Road area (Figures 3.2 and 3.3). In the Sock Creek-Burns Peak area, it extends laterally for about 12 km discontinuously. This sub-facies is spatially associated with coherent feldspar-phyric rhyolite and monomictic rhyolite breccia facies (Table 3.3). Coherent quartz-poor rhyolite intervals range from 1 to 97 m thick. The coherent quartz-poor rhyolite sub-facies occurs as single units, and in combination with monomictic rhyolite breccia facies (Figure 3.7 - BOC-1). Upper and lower contacts with coherent feldspar-phyric rhyolite and monomictic rhyolite breccia are typically gradational or locally sharp and planar (Figure 3.7 - BOC-1).

The coherent quartz-poor rhyolite sub-facies (Figure 3.6 - H to N) is weakly to strongly porphyritic, massive or flow-banded, commonly perlitic, locally amygdaloidal and pink, pale to dark green, brown, grey or orange. Flow-banded quartz-poor rhyolite intervals are represented by wavy, irregular and sub-parallel, green to pale brown and variably thick (2 to 10 mm) feldspar phenocryst-bearing bands (Figure 3.6 - H and I). Coherent quartz-poor rhyolite sub-facies with false clastic textures occur in the Howards Road area. The false clastic texture is represented by sub-parallel, irregular, wispy, chlorite-rich, dark green domains (Figure 3.6 - L and M).

Feldspar phenocrysts and glomerocrysts (5-10%, <15%; 1-3 mm, <8 mm) are evenly distributed, typically euhedral to anhedral, tabular or irregular, commonly twinned, and of variable colour (white, cream, pink, orange, green) due to various degrees of alteration (Figure 3.6 - H, I and M). Quartz phenocrysts are less abundant and commonly smaller (average <1-2%, but up to 5%; average 1-2 mm) than feldspar phenocrysts. They are typically subhedral to anhedral, round and irregular, embayed and fractured (Figure 3.6 - J and N). Quartz phenocrysts are rarely visible in drill core.

The groundmass is microgranular and comprises a polycrystalline mosaic of feldspar and quartz with sericite, carbonate, and minor chlorite (Figure 3.6 - I, J and M). Common perlitic textures are represented by classical perlite cracks (Figure 3.6 - K). Sphalerite occurs as disseminated (<1%) grains. Rare apatite and zircon crystals occur.

3.3.1.2 Coherent feldspar-phyric rhyolite facies (Rf)

The coherent feldspar-phyric rhyolite facies was identified based on whole-rock compositional data (Table 3.2) acquired from six samples in the Sock Creek, Boco, Burns Peak and White Spur areas (Figures 3.2 and 3.3). This facies is closely associated with coherent feldspar-quartz-phyric rhyolite and monomictic rhyolite breccia facies (Table 3.3). Coherent feldspar-phyric rhyolite intervals range from 15 to 77 m thick. This facies occurs as single units, and in combination with monomictic rhyolite breccia facies (Figure 3.7 -

BOC-2, BOC-4 and BHD-7). Upper and lower contacts with coherent feldspar-quartz-phyric rhyolite and monomictic rhyolite breccia facies are typically gradational or sharp and planar.

Coherent feldspar-phyric rhyolites are weakly to moderately porphyritic, massive or flow-banded, locally perlitic and/or amygdaloidal, and typically pink, pale to dark green or brown (Figure 3.8). Coherent feldspar-phyric rhyolite facies with false clastic textures occur in the White Spur area. The false clastic texture is represented by irregular, chlorite-rich, dark green domains (Figure 3.8 - K and L).

Flow-banded coherent feldspar-phyric rhyolite intervals are represented by wavy, irregular and sub-parallel, green to brown and variably thick (2 to 10 mm) feldspar phenocryst-bearing bands (Figure 3.8 - A, D, E and I). In some examples (Figure 3.8 - D and E), flow-bands are defined by alternating pale brown-pink feldspar phenocryst-rich and amygdale-bearing bands and pale to dark green and grey feldspar-chlorite-sericite-rich bands. The pale brown-pink bands contain fine-grained (0.3-0.8 mm) feldspar phenocrysts and oval-shaped, dark green and concentrically zoned chlorite-carbonate (green-cream) or quartz-carbonate (white-cream) amygdales aligned parallel to the flow-bands. The pale to dark green and grey bands typically contain larger carbonate amygdales and coarser-grained (0.5-2 mm) feldspar phenocrysts and/or glomerocrysts which define the flow foliation.

Feldspar phenocrysts (<3-15%, 0.4-5 mm) are typically euhedral to anhedral, weakly to moderately sericite-altered, commonly twinned, and have variable colours (white, cream, pink, orange, green) due to different alteration mineralogy (Figure 3.8 - B, D, F, H to M). Feldspar glomerocrysts are common (Figure 3.8 - E). The groundmass is composed of fine-grained feldspar, quartz, chlorite, sericite and carbonate (Figure 3.8 - B, E, F, I, K and M). Pyrite and sphalerite occur as disseminated (up to 1%) grains and clusters or in veins and fractures.

3.3.1.3 Monomictic rhyolite breccia facies (RmB)

The monomictic rhyolite breccia facies occurs from Sock Creek to Burns Peak (Figure 3.2) and extends laterally for about 12 km discontinuously. This facies is spatially associated with coherent feldspar-quartz-phyric rhyolite, coherent feldspar-phyric rhyolite and monomictic mud-matrix rhyolite breccia facies (Table 3.3). Monomictic rhyolite breccia intervals range from 1 to 72 m thick. Monomictic rhyolite breccias occur as single units and in combination with coherent rhyolite (Figures 3.5 and 3.7). Upper and lower contacts with coherent feldspar-quartz-phyric and feldspar-phyric rhyolite, and monomictic mud-matrix rhyolite breccia facies are typically gradational or sharp and planar (Figures 3.5 and 3.7). Intervals of monomictic rhyolite breccia are locally normally graded and grade into finer-grained monomictic rhyolite breccia (Figures 3.5 - BHD-4; Figure 3.7 - BOC-1).

The monomictic rhyolite breccia facies is typically poorly sorted and matrix-supported (clast-rotated texture) to clast-supported (jigsaw-fit texture) (Figure 3.9 - A, E, H, J and K). In jigsaw-fit domains, the rhyolite clasts are angular to sub-angular and have blocky to splintery shapes and planar to curviplanar edges (Figure

Figure 3.7: Four graphic logs of parts of diamond drill holes BOC-1 and BOC-2 (Boco area), BOC-4 (Burns Peak area) and BHD-7 (Sock Creek area) through facies of the rhyolite facies association. See Figure 3.4 for legend to graphic logs.

BOC-1: The close spatial association of, and gradational contact between, coherent quartz-poor rhyolite sub-facies (Rqp) and monomictic rhyolite breccia facies (RmB), and the top gradational contact with polymictic felsic breccia (PfB) and sandstone (PfS) facies (section 3.3.4) are all consistent with the interpretation of this rhyolite facies association as a rhyolite dome or lava. The rhyolite clasts in the polymictic felsic breccia are similar to the lower coherent rhyolite and clasts in the monomictic rhyolite breccia, supporting the interpretation of an extrusive emplacement for this rhyolite interval (491.3-551.5 m).

BOC-2: The coherent feldspar-phyric rhyolite (Rf) (158.9-177.9 m) has an upper mingled contact and a lower sharp planar contact with two black mudstone intervals (BMud). The presence of large (up to 14 cm in diameter) rhyolite apophyses within the upper sulfide-bearing mudstone interval close to the upper contact with the coherent rhyolite, the spatial distribution and the upper mingled contact between the coherent feldspar-phyric rhyolite and the mudstone intervals are all consistent with the interpretation of this rhyolite as a syn-volcanic sill.

BHD-7: The close spatial association and gradational contacts between coherent feldspar-phyric rhyolite (Rf), monomictic rhyolite breccia (RmB) and monomictic mud-matrix rhyolite breccia (RmmB) facies, the presence of monomictic mud-matrix rhyolite breccia (interpreted as peperite) at the top contact of the rhyolite facies association, upper and lower sharp planar contacts with micaceous mudstone facies (MMud) (section 3.3.5) at 241.6 m and 335.1 m, and the presence of relatively large (up to 10 cm in diameter) rhyolite apophyses within the lower mudstone-sandstone unit (335.1-361.7 m) close to the contact with coherent rhyolite are all consistent with the interpretation of this rhyolite interval (241.6-335.1 m) as a syn-volcanic sill.

BOC-4: Intervals of monomictic rhyolite breccia (RmB) occur in the middle and at the base of a lower rhyolite interval (487.0-545.7 m) that separates two intervals of coherent feldspar-phyric mafic facies (Mf). The upper rhyolite interval (436.8-485.2 m) comprises flow-banded feldspar-phyric rhyolite (Rf) and monomictic rhyolite breccia (RmB) at the top. The presence of flow-bands in the coherent feldspar-phyric rhyolite (Rf), flow-banded rhyolite clasts within the monomictic rhyolite breccia (RmB), the spatial distribution of the rhyolite facies association and the sharp and planar upper and lower contacts are all consistent with the interpretation of the two rhyolite intervals as one rhyolite unit (436.8-545.7 m). However, this is a case where no interpretations can be made regarding the nature (extrusive vs. intrusive) of this rhyolite unit. The coherent feldspar-phyric mafic unit (485.2-487.0 m) is interpreted as a dyke or sill (section 3.3.3).

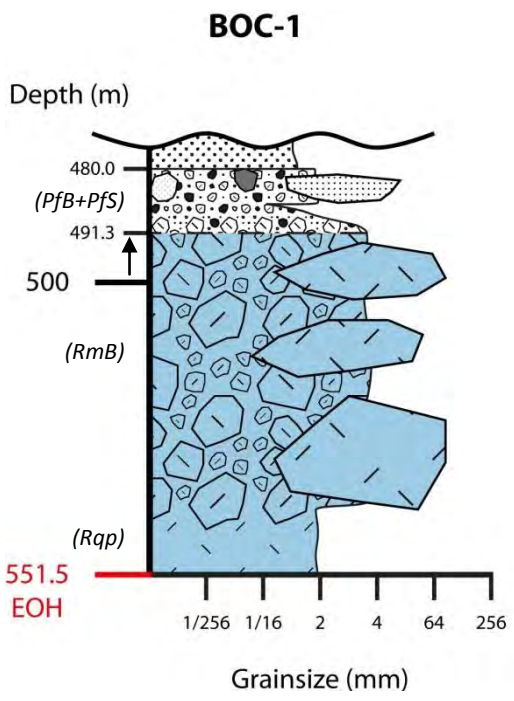
BOC-1
Depth (m)
480.0
(PfB+PfS)
491.3
500
(RmB)
(Rqp)
551.5
EOH
1/256 1/16 2 4 64 256
Grainsize (mm)

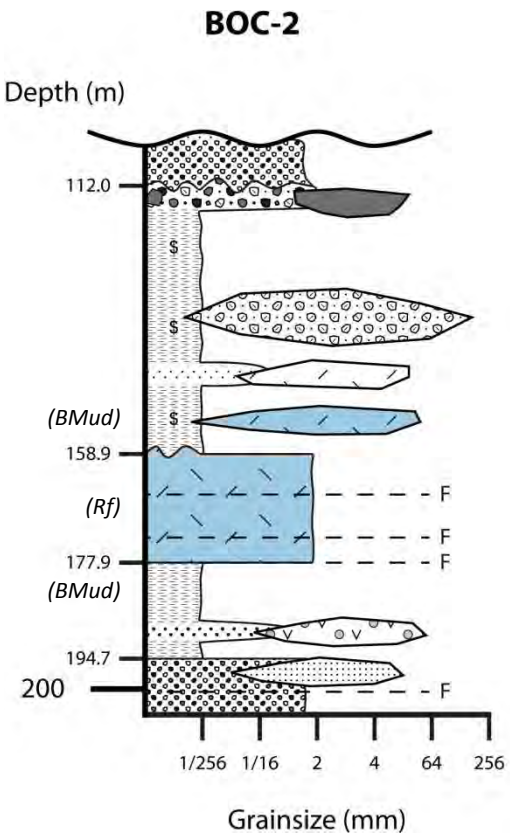
BOC-2
Depth (m)
112.0
(BMud)
158.9
(Rf)
F
177.9
(BMud)
194.7
200
1/256 1/16 2 4 64 256
Grainsize (mm)

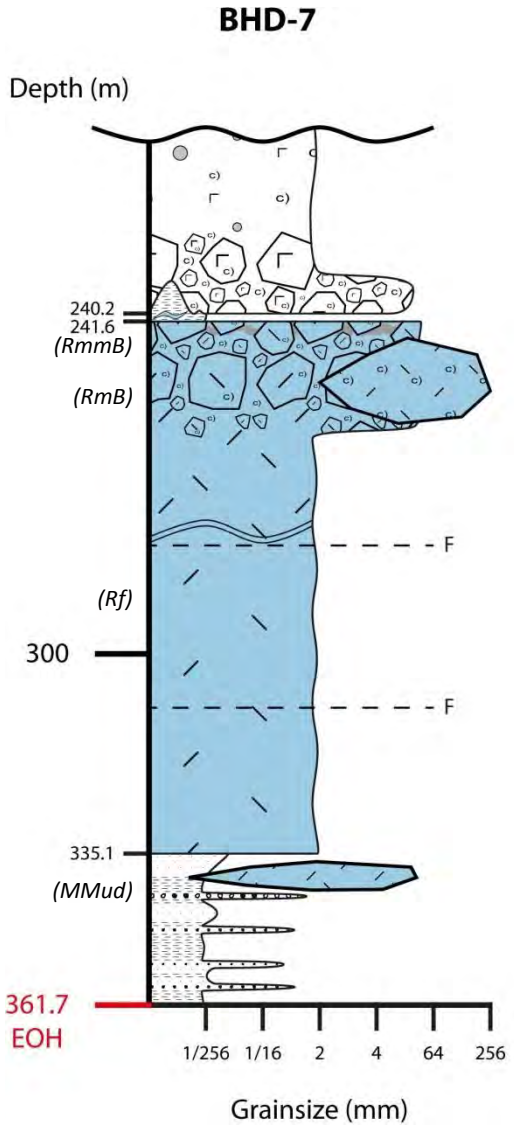
BHD-7
Depth (m)
240.2
241.6
(RmmB)
(RmB)
F
(Rf)
300
335.1
(MMud)
361.7
EOH
1/256 1/16 2 4 64 256
Grainsize (mm)

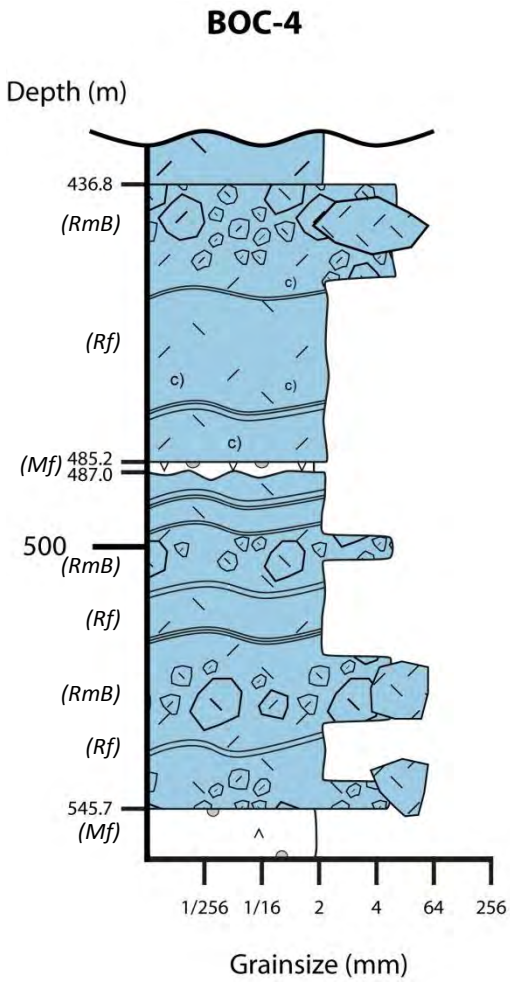
BOC-4
Depth (m)
436.8
(RmB)
(Rf)
(Mf)
485.2
487.0
500
(RmB)
(Rf)
(RmB)
(Rf)
545.7
(Mf)
1/256 1/16 2 4 64 256
Grainsize (mm)

Figure 3.8: Coherent feldspar-phyric rhyolite facies. A and B: BHD-7 (277.5 m); C: BHD-9 (290.0 m); D to G: BHD-9 (351.1 m); H and I: BOC-2 (160.7 m); J: BOC-4 (382.6 m); K and L: WSP-15 (248.7 m); M: WSP-15 (388.8 m). A, C, D, H, J and K: Handspecimen photographs of the coherent feldspar-phyric rhyolite facies (uphole and younging direction: A - left to right; D, K and N - right to left; C and H - not recorded). B, E to G, I, L and M: Photomicrographs of the coherent feldspar-phyric rhyolite facies (B, E, G, I, and L - transmitted, plane polarised light; F and M - transmitted, cross polarised light). The groundmass is fine-grained and feldspar-quartz-rich. A and B: Flow-banded, amygdaloidal coherent feldspar-phyric rhyolite.

A: Flow bands and chlorite amygdales are sub-parallel.

B: Subhedral feldspar phenocryst and sub-parallel quartz amygdales.

C: Perlitic, amygdaloidal coherent feldspar-phyric rhyolite. Amygdales are predominantly chlorite-filled (dark green), elongate and aligned. Rare, elongate quartz-carbonate amygdales (white-pale grey) occur. Classical perlite is present throughout.

D and E: Flow-banded coherent feldspar-phyric rhyolite. Flow bands are wavy, irregular, sub-parallel, and chlorite-rich.

F: Euhedral, twinned, zoned feldspar phenocryst in a carbonate-phyllosilicate-rich groundmass.

G: Carbonate amygdale. A few euhedral (hexagonal) apatite crystals also occur.

H: Coherent feldspar-phyric rhyolite.

I: Flow-banded coherent feldspar-phyric rhyolite. Flow bands are wavy, irregular, sub-parallel, and chlorite-rich.

J: Coherent feldspar-phyric rhyolite. Feldspar phenocrysts are abundant and evenly distributed.

K and L: Coherent strongly feldspar-phyric rhyolite with false clastic texture represented by irregular, chlorite-rich, dark green domains. Abundant feldspar phenocrysts are evenly distributed and typically more distinct within the altered (chlorite-rich) domains.

M: Strongly altered, coherent feldspar-phyric rhyolite. Abundant feldspar phenocrysts are surrounded by strongly altered, feldspar-quartz-chlorite-sericite-rich groundmass.

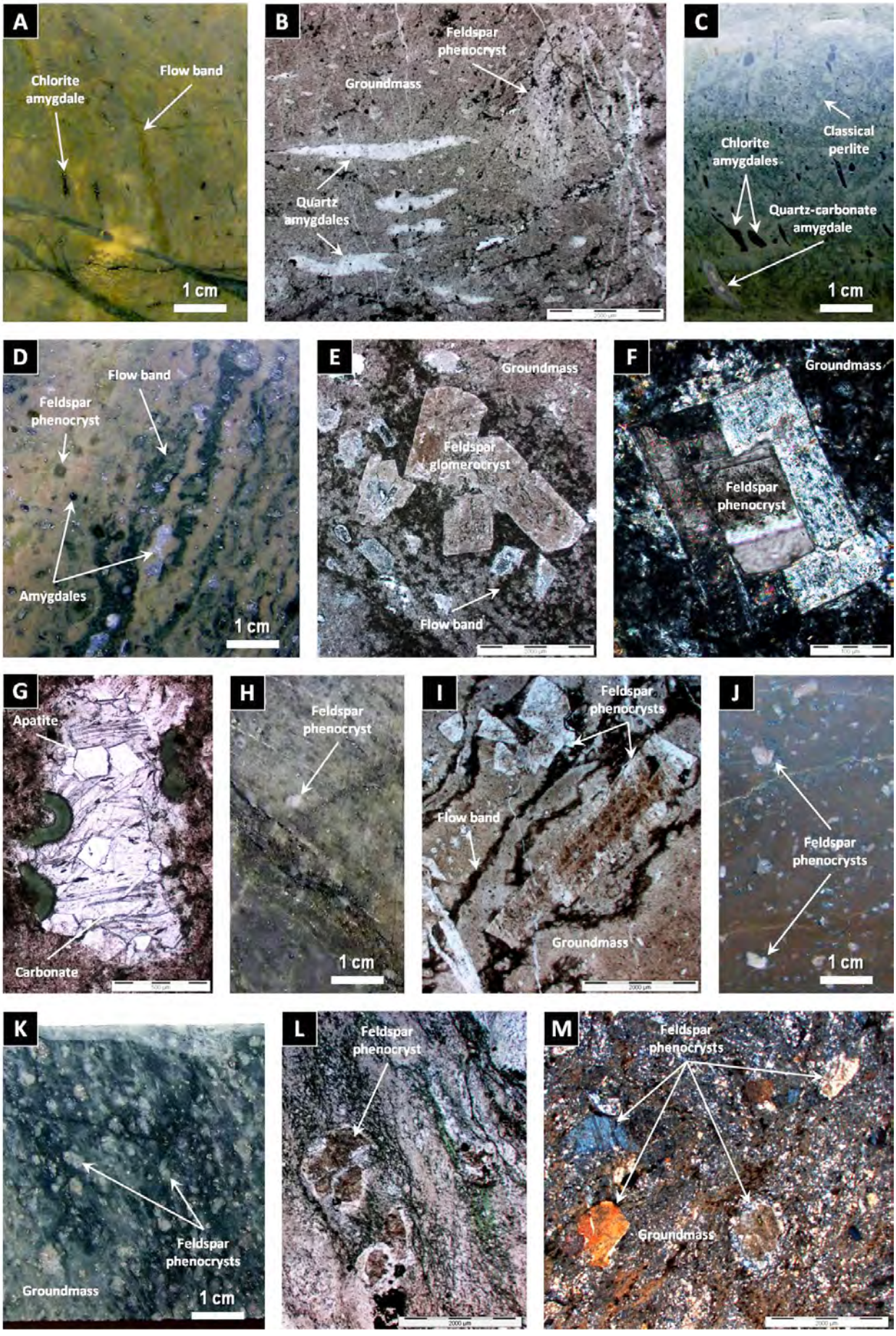
A
Chlorite amygdale
Flow band
1 cm
B
Feldspar phenocryst
Groundmass
Quartz amygdales
C
Chlorite amygdales
Classical perlite
Quartz-carbonate amygdale
1 cm
D
Flow band
Feldspar phenocryst
Amygdales
1 cm
E
Groundmass
Feldspar glomerocryst
Flow band
F
Groundmass
Feldspar phenocryst
G
Apatite
Carbonate
H
Feldspar phenocryst
1 cm
I
Feldspar phenocrysts
Flow band
Groundmass
J
Feldspar phenocrysts
1 cm
K
Feldspar phenocrysts
Groundmass
1 cm
L
Feldspar phenocryst
M
Feldspar phenocrysts
Groundmass

Figure 3.9: Monomictic rhyolite breccia and monomictic mud-matrix rhyolite breccia facies. A to D: BHD-4 (93.4 m); E: BHD-4 (167.8 m); F: BHD-4 (153.4 m); G: BHD-4 (382.4 m); H: BHD-9 (192.4 m); I: BHD-4 (382.7 m); J: BPD-80 (300.0 m); K: BPD-89 (49.8 m). A, E, H, J and K: Handspecimen photographs of the monomictic rhyolite breccia facies (uphole and younging direction: A - right to left; K - left to right; E - not recorded). F to J: Handspecimen photographs of the monomictic mud-matrix rhyolite breccia facies (uphole and younging direction: F - not recorded; I - left to right; G - right to left). H and J: Handspecimen photographs of contacts between monomictic rhyolite breccia and monomictic mud-matrix rhyolite breccia facies (uphole and younging direction: H - right to left; J - left to right). B to D: Photomicrographs of the monomictic rhyolite breccia facies (transmitted, plane polarised light). The matrix is composed of fine (<2 mm) rhyolite clasts, fiamme, and feldspar and quartz crystals and crystal fragments embedded in microcrystalline quartz, feldspar, chlorite and minor sericite.

A: Poorly sorted monomictic rhyolite breccia composed of orange and dark green (chloritic), strongly feldspar-quartz-phyric rhyolite clasts and abundant dark green chloritic fragments. Feldspar phenocrysts and crystal fragments are orange. Quartz phenocrysts are pale grey.

B: Irregular, chloritic, feldspar-quartz-phyric rhyolite clasts.

C: Quartz and feldspar crystal fragments and chloritic fragments in very fine-grained matrix.

D: Subhedral quartz crystals with amoeboid shapes and embayments.

E: Feldspar-quartz-phyric rhyolite clast embedded in very fine-grained matrix.

F: Contact between mudstone and monomictic rhyolite breccia. Feldspar-quartz-phyric rhyolite clasts and are separated by black mudstone matrix.

G: Coarse, feldspar-phyric, orange (top right) and dark green (chloritic) (bottom left) rhyolite clasts separated by homogeneous black mudstone matrix. Feldspar phenocrysts are rectangular and pink.

H: Sharp contact between monomictic rhyolite breccia (RmB) and monomictic mud-matrix rhyolite breccia (RmmB) facies. Strongly feldspar-phyric rhyolite clasts occur in both facies.

I: Feldspar-phyric, blocky and sub-round rhyolite clasts are separated by scarce amounts of black mudstone matrix. Jigsaw-fit texture occurs.

J: Gradational contact between monomictic rhyolite breccia (RmB) and monomictic mud-matrix rhyolite breccia (RmmB) facies. Rhyolite clasts are surrounded by a bluish dark grey mud matrix and contain relatively large (up to 10 mm) quartz phenocrysts.

K: Gradation from coherent feldspar-phyric rhyolite (right) to monomictic rhyolite breccia with jigsaw-fit texture.

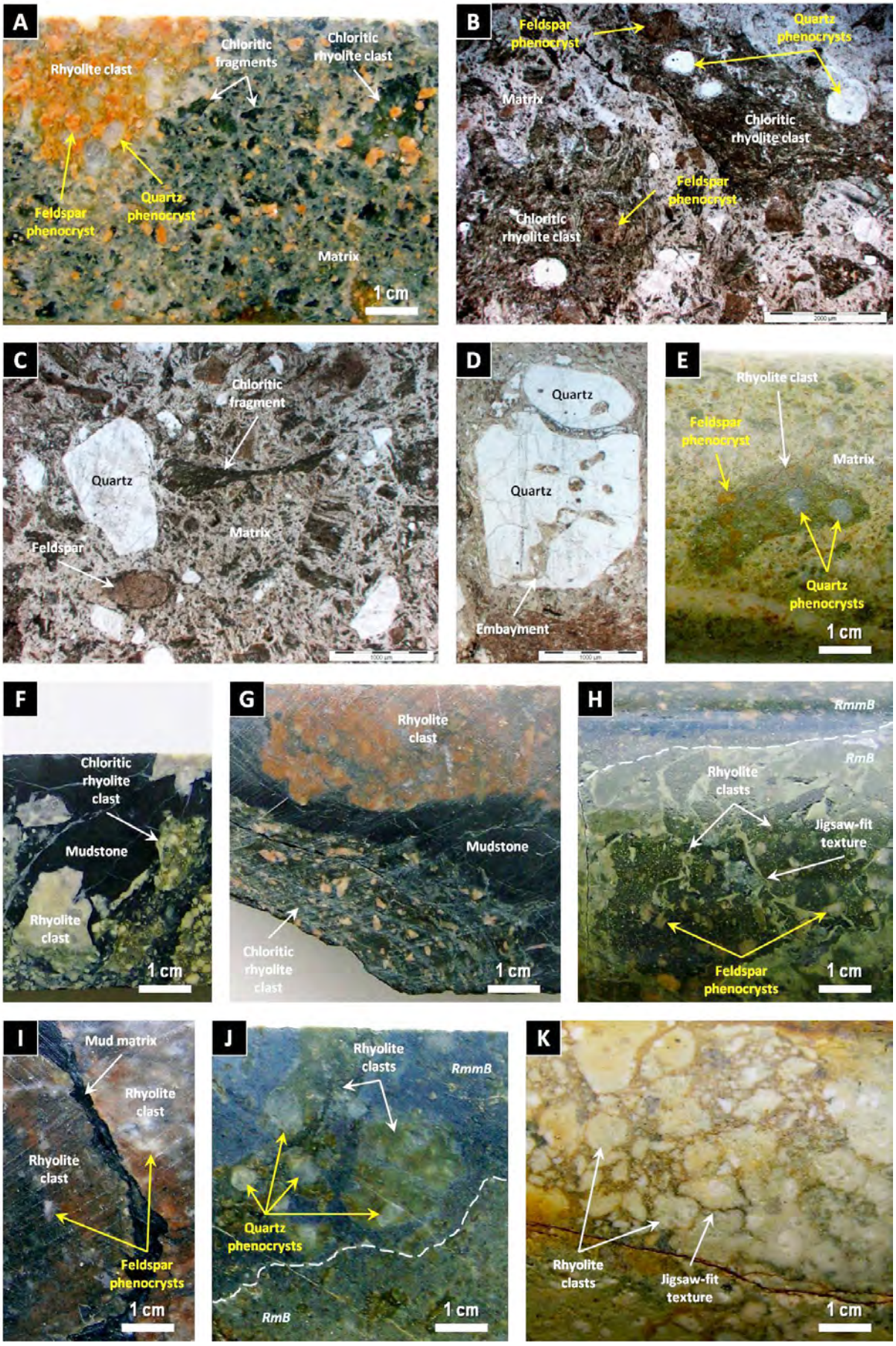
A
Rhyolite clast
Chloritic fragments
Chloritic rhyolite clast
Feldspar phenocryst
Quartz phenocryst
Matrix
1 cm
B
Feldspar phenocryst
Quartz phenocrysts
Matrix
Chloritic rhyolite clast
Feldspar phenocryst
Chloritic rhyolite clast
C
Chloritic fragment
Quartz
Matrix
Feldspar
D
Quartz
Quartz
Embayment
E
Rhyolite clast
Feldspar phenocryst
Matrix
Quartz phenocrysts
1 cm
F
Chloritic rhyolite clast
Mudstone
Rhyolite clast
1 cm
G
Rhyolite clast
Mudstone
Chloritic rhyolite clast
1 cm
H
RmmB
RmB
Rhyolite clasts
Jigsaw-fit texture
Feldspar phenocrysts
1 cm
I
Mud matrix
Rhyolite clast
Rhyolite clast
Feldspar phenocrysts
1 cm
J
Rhyolite clasts
RmmB
Quartz phenocrysts
RmB
1 cm
K
Rhyolite clasts
Jigsaw-fit texture
1 cm

3.9 - H and K). Spaces between clasts are scarce and are commonly filled with finer-grained (<2 mm) rhyolite clasts. In clast-rotated domains, rhyolite clasts are sub-angular to sub-round and have irregular and amoeboid shapes. They are surrounded by finer-grained (<2 mm) rhyolite clasts, feldspar and quartz crystals and crystal fragments, and fine carbonate-rich cement (Figure 3.9 - A and E). Quartz crystals and crystal fragments are commonly subhedral to irregular with amoeboid shapes (Figure 3.9 - C and D). Feldspar crystals and crystal fragments are sub-round to sub-angular (Figure 3.9 - C).

The rhyolite clasts are weakly to strongly porphyritic, pale grey, orange or dark green (chloritic), and range from 2 mm up to approximately 120 mm in diameter (Figure 3.9 - A, B, E, H and K). The phenocryst population of most rhyolite clasts is identical to the coherent feldspar-quartz-phyric (section 3.3.1.1) or feldspar-phyric (section 3.3.1.2) rhyolite facies in terms of abundance and distribution. Some rhyolite clasts are apparently aphyric, weakly amygdaloidal, flow-banded and/or perlitic. Irregular carbonate and quartz veins, leucoxene and disseminated sulfides occur locally.

The monomictic rhyolite breccia facies may contain variable amounts (<5-35%) of chloritic fragments (Figure 3.9 - A and C). They are elongate to lenticular, dark green to pale brown, moderately to strongly chloritic, and have irregular to bow-tie shapes and curved margins (Figure 3.9 - A and C). The chloritic fragments are aphyric (Figure 3.9 - C) to strongly porphyritic and typically smaller than the rhyolite clasts. The phenocryst population of the porphyritic chloritic fragments is identical to the rhyolite clasts. The chloritic fragments are commonly randomly oriented or very locally aligned.

3.3.1.4 Monomictic mud-matrix rhyolite breccia facies (RmmB)

The monomictic mud-matrix rhyolite breccia facies occurs in the Sock Creek and Burns Peak areas, W of the Murchison Highway (Figure 3.2). Its lateral extent may be in the order of 1.3 km in the Sock Creek area. The monomictic mud-matrix rhyolite breccia facies is spatially associated with monomictic rhyolite breccia and coherent feldspar-quartz-phyric or feldspar-phyric rhyolite facies (Table 3.3). Monomictic mud-matrix rhyolite breccia intervals range from <1 to 5 m thick. This facies occurs typically at the top margins of coherent rhyolite and rhyolite breccia units that may be associated with mudstone facies (section 3.3.5). Upper and lower contacts with monomictic rhyolite breccia and coherent feldspar-quartz-phyric and feldspar-phyric rhyolite facies are typically gradational (Figure 3.5; Figure 3.7 - BHD-7).

The monomictic mud-matrix rhyolite breccia facies is similar to the monomictic rhyolite breccia facies (section 3.3.1.3) in terms of rhyolite clast characteristics, abundances and distribution, but it is commonly matrix-supported and the matrix is composed of massive, variably silicified, homogeneous, pale to dark grey or black mudstone (Figure 3.9 - F to J). Domains of dark grey and black mud matrix are locally contorted and/or disrupted. In some examples, the mud matrix is pale grey and silicified immediately adjacent to the rhyolite clasts, whereas away from the rhyolite clasts it is dark grey to black.

3.3.1.5 Monomictic fiamme-rich rhyolite breccia facies (RmfrB)

The monomictic fiamme-rich rhyolite breccia facies occurs exclusively in the Burns Peak area (DDH BOC-3) (Figures 3.2 and 3.10) as a 47 m thick massive to locally faulted interval. This facies is spatially associated with coherent feldspar-phyric rhyolite facies (Table 3.3).

The monomictic fiamme-rich rhyolite breccia facies is poorly sorted, and clast- to matrix-supported (Figure 3.10). This facies is characterised by abundant (up to 90%) feldspar-phyric to apparently aphyric fiamme (Figure 3.10 - A, B and C). The fiamme (0.2-80 mm) are lensoidal, wispy and irregular-shaped with wavy and irregular margins and flame-like ends. They are pale to dark green (moderately to strongly chloritic) or pale brown. The fiamme are strongly aligned and sub-parallel (Figure 3.10 - A and B), or else they are sub-parallel but bent around blocky rhyolite clasts (Figure 3.10 - C).

Blocky, sub-angular and irregular rhyolite clasts and chloritic fragments (<30%) also occur (Figure 3.10 - C). Some rhyolite clasts are flow-banded or perlitic. Clusters of rhyolite clasts locally have jigsaw-fit texture, but most rhyolite clasts have clast-rotated texture. The phenocryst population of the porphyritic fiamme, rhyolite clasts and chloritic fragments are very similar to the coherent feldspar-phyric rhyolite facies (section 3.3.1.2) in terms of abundance and distribution. The matrix is composed of variable amounts of finer-grained (<2 mm) fiamme, rhyolite clasts, and feldspar crystals and crystal fragments embedded in fine carbonate (Figure 3.10 - B).

3.3.1.6 Polymictic rhyolite breccia facies (RpB)

The polymictic rhyolite breccia facies occurs at Sock Creek, Burns Peak, White Spur and Howards Road areas (Figures 3.2 and 3.3). Its lateral extent may be in the order of 12 km in the Sock Creek-Burns Peak area and 5 km in the White Spur-Howards Road area. This facies is closely spatially associated with polymictic mud-matrix rhyolite breccia and polymictic rhyolite sandstone facies (Table 3.3). It is also spatially associated with monomictic fiamme-rich rhyolite breccia, monomictic rhyolite breccia and coherent feldspar-quartz-phyric rhyolite facies. Polymictic rhyolite breccia intervals range from 1 to 80 m thick.

The polymictic rhyolite breccia facies typically occurs at the base of normally graded units comprising polymictic rhyolite breccia at the base and polymictic rhyolite sandstone (and mudstone) at the top (Figures 3.11 and 3.12). Upper and lower contacts between adjacent normally graded units are typically sharp and planar, but some lower contacts are irregular or faulted (Figure 3.12). Upper contacts with polymictic rhyolite sandstone are typically gradational and lower contacts with polymictic mud-matrix rhyolite breccia are irregular and wavy (Figures 3.11 and 3.12).

The polymictic rhyolite breccia facies is poorly sorted, matrix- to clast-supported, and weakly to moderately sericitic and chloritic (Figure 3.13 - A to F). It comprises rhyolite clasts (5-35%, 2-250 mm), chloritic fragments (<5-25%, 2-100 mm), quartz (2-20%, <4 mm) and feldspar (15-30%, <5 mm) crystal fragments, lithic (non-juvenile) clasts (5-20%, <120 mm), sandstone clasts (1-5%, <60 mm) and mudstone clasts (1-10%, <500 mm).

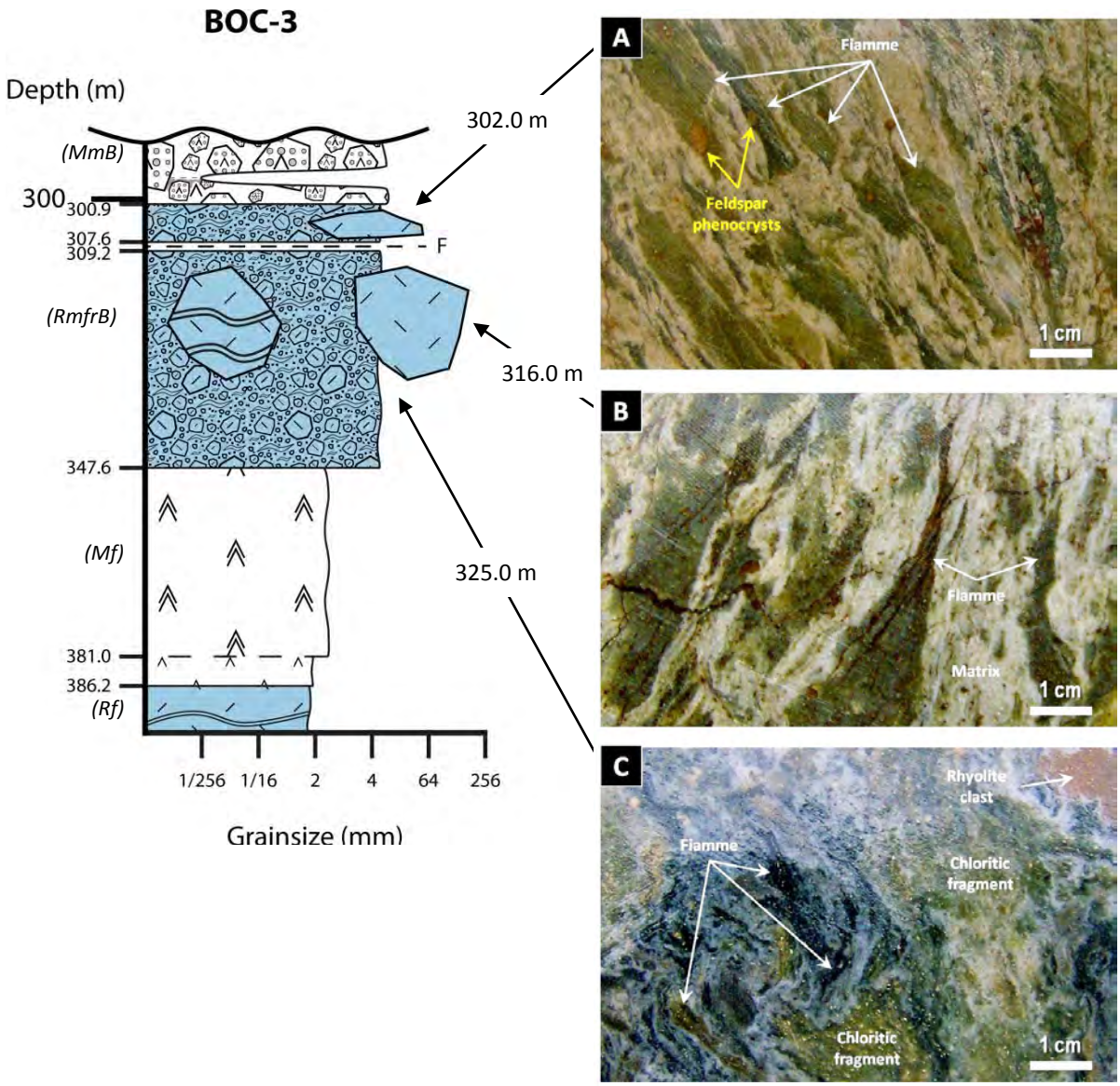

Figure 3.10: Graphic log of part of diamond drill hole BOC-3 (Burns Peak area) through facies of the rhyolite facies association. See Figure 3.4 for legend to graphic log. The monomictic fiamme-rich rhyolite breccia (RmfrB) (300.9-347.6 m) occurs between a lower, strongly feldspar-phyric mafic interval (Mf) (347.6-381.0 m) and an upper monomictic mafic breccia unit (MmB) (above 300.9 m). The monomictic fiamme-rich rhyolite breccia is massive, locally faulted (307.6-309.2 m) and comprises massive and flow-banded rhyolite clasts and abundant fiamme. These features are consistent with the interpretation of this monomictic fiamme-rich rhyolite breccia as in situ autobreccia related to a nearby lava or dome, probably the flow-banded feldspar-phyric rhyolite (Rf) (section 3.3.1.9).

A: BOC-3 (302.0 m) - Strongly aligned, aphyric to feldspar-phyric fiamme.

B: BOC-3 (316.0 m) - Strongly aligned, dark green fiamme. The matrix is mainly composed of finer-grained (<2 mm) fiamme.

C: BOC-3 (325.0 m) - The fiamme are locally bent around the rhyolite clasts.

Uphole and younging directions: A and B - right to left; C - left to right.

Polymictic rhyolite breccias from the northern (Sock Creek and Burns Peak) and southern (White Spur and Howards Road) areas differ slightly in colour, phenocryst size and abundance of the rhyolite clasts. In the southern area (Figure 3.11; Figure 3.13 - C and H), the rhyolite fragments are white, cream, grey and green, feldspar-quartz-phyric, feldspar-phyric or aphyric, and locally perlitic (Figure 3.14 - H). The feldspar phenocrysts (2-30%, 0.2-4 mm) are more abundant and larger than the quartz phenocrysts (1-5%, 0.1-3 mm).

In the northern area (Figure 3.5; Figure 3.12; Figure 3.13 - A, B, D to F), the rhyolite fragments are typically grey to green and orange, feldspar-quartz-phyric, angular to sub-round, blocky and irregular, non- to weakly amygdaloidal (<5% amygdales), sporadically flow-banded, and locally spherulitic (Figure 3.12 - C; Figure 3.14 - D). In weakly amygdaloidal examples, amygdales are typically pale to dark yellow, round to elongate, and filled with carbonate. The rhyolite fragments are similar to the coherent quartz-rich rhyolite sub-facies (section 3.3.1) and the rhyolite clasts of the monomictic rhyolite breccia facies (section 3.3.3) occurring in the Sock Creek and Burns Peak areas (Figures 3.5 and 3.12). Feldspar phenocrysts (10-20%, 0.1-8 mm) are typically more abundant but smaller than quartz phenocrysts (5-15%, 0.1-10 mm). Feldspar phenocrysts are weakly to moderately sericite-altered, twinned, rectangular and subhedral. Quartz phenocrysts are round to sub-round, commonly embayed and fractured crystals with irregularly wavy margins (Figure 3.14 - E).

The chloritic fragments are similar to the blocky rhyolite clasts in terms of phenocryst abundances and distribution, but are commonly wispy and irregular with wavy margins and flame-like ends. Chloritic fragments range from aphyric to feldspar-quartz-phyric (Figure 3.13 - A, C, D and F; Figure 3.14 - C and E) and are typically smaller and locally more abundant than blocky rhyolite fragments, constituting an important part of the matrix in matrix-supported domains. Chloritic fragments are dark green to pale brown and moderately to strongly chloritic. Quartz and feldspar phenocrysts within porphyritic chloritic fragments are similar to phenocrysts in the blocky, porphyritic rhyolite fragments.

The feldspar and quartz crystals and crystal fragments are very abundant, similar to the phenocrysts, and form the bulk of the matrix (Figure 3.13 - A to D; Figure 3.14 - A to H). Quartz is represented by sub-round to very angular, pale grey crystals and crystal fragments that are commonly smaller and less abundant than feldspar. Feldspar is typically rectangular, tabular, and white, cream or pale orange.

The lithic fragments are homogeneously cream to brown or grey, round and sub-round to irregular, and variably silicified (Figure 3.12 - B). They are very fine-grained and lack internal structure, which prevents identification (Figure 3.14 - F). Sandstone clasts are massive or diffusely bedded, very fine to medium-grained, cream to pale brown fragments that occur sporadically in the middle or typically at the base of polymictic rhyolite breccia units or intervals.

The mudstone clasts are very common in the polymictic rhyolite breccia facies, and their abundance, distribution, shape and size vary widely (Figure 3.12 - D; Figure 3.13 - E and G). Most mudstone clasts are massive, black to dark grey and round, elongate or irregular and wispy. They occur in the middle or

Figure 3.11: Two graphic logs of parts of diamond drill holes WSP-14 (Howards Road area) and WSP-15 (White Spur area) through facies of the rhyolite facies association. See Figure 3.4 for legend to graphic log.

WSP-14: The lowest part of WSP-14 (454.2-494.6 m) comprises coherent quartz-poor rhyolite (Rqp) and has an upper sharp planar contact with black mudstone (BMud) (452.5-454.2 m). The top of the rhyolite includes abundant massive to disseminated sulfides. The rhyolite is interpreted as an intrusion (section 3.3.1.9). The mudstone is overlain by a relatively thin interval of locally brecciated coherent quartz-poor rhyolite (447.9-452.5 m), which is very similar to the lower rhyolite interval. This relatively thin rhyolitic interval is interpreted as an apophysis of the rhyolite intrusion (section 3.3.1.9). The normally graded units of polymictic mud-matrix rhyolite breccia (RpmmB), and polymictic rhyolite breccia (RpB) and sandstone (RpS) facies (above 447.9 m) contain volcanic quartz and are interpreted as submarine density current deposits (section 3.3.1.9). The black mudstone (BMud) formed via settling of suspended, very fine grained particles through the water column during the waning stages of density currents. In some cases, the submarine density currents incorporated mud from the substrate (e.g. 341.3-447.9 m).

WSP-15: The normally graded polymictic rhyolite breccia (RpB) and sandstone (RpS) unit (above 180.0 m) contains volcanic quartz and is interpreted as a submarine density current deposit. The black mudstone (BMud) at the top is interpreted as a settling by suspension deposit (section 3.3.5.4). The coherent quartz-rich rhyolite (Rqr) (205.4-232.0 m) has an upper sharp planar contact with black mudstone (BMud) (180.0-205.4 m). The mudstone is brown (baked) close to the contact with the rhyolite (just above 205.4 m) (See Figure 3.6 - E). The coherent quartz-rich rhyolite is interpreted as an intrusion. Intervals of coherent feldspar-phyric rhyolite (Rf) (e.g. 315.2-355.3 m) have upper sharp contacts with massive, well sorted, polymictic rhyolite sandstone (RpS) (e.g. 285.4-287.5 m; 312.1-315.2 m), which do not contain volcanic quartz; these polymictic rhyolite sandstone units are interpreted as high-concentration density current deposits probably produced by slope failure. The sharp to locally irregular (285.4 m) contacts between the coherent feldspar-phyric rhyolite and the polymictic rhyolite sandstone units could not be interpreted due to alteration and false clastic textures (Figure 3.8 - K to M) in the coherent rhyolite. The close spatial association of these two facies suggests that the coherent rhyolite (Rf) intervals could be lavas, but these parts of the section are too strongly altered and the nature (intrusive vs. extrusive) of the rhyolite (Rf) intervals remains ambiguous. The polymictic rhyolite sandstone intervals probably represent distal products of resedimented autoclastic facies. Intervals of coherent aphyric mafic facies (Ma) have upper sharp planar (e.g. 273.7-280.1 m) or mingled (e.g. 355.3-356.2 m) contacts, and are interpreted as intrusions (section 3.3.3).

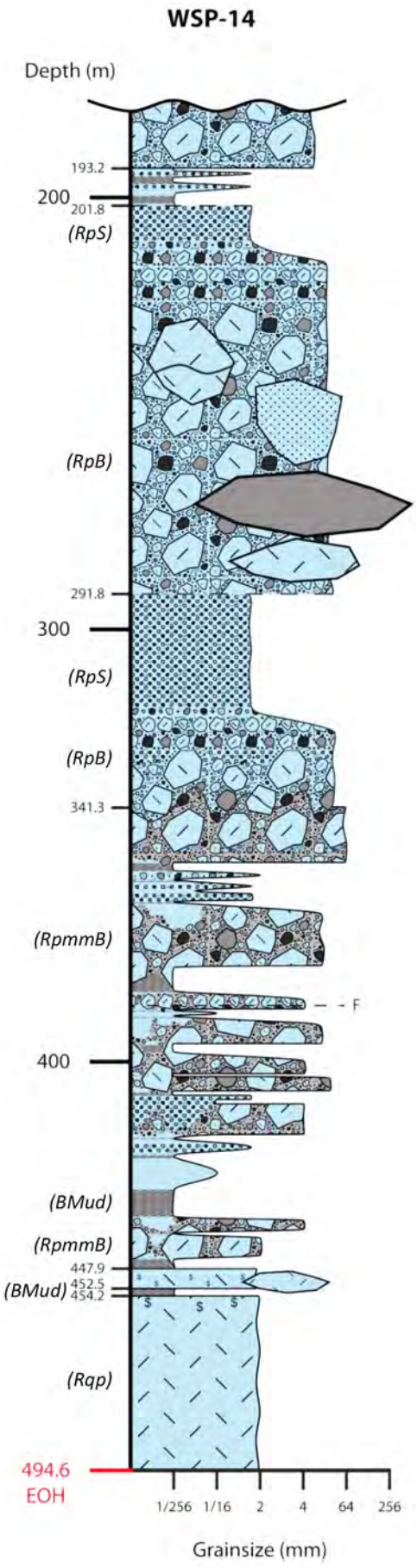
WSP-14
Depth (m)
193.2
200
201.8
(RpS)
(RpB)
291.8
300
(RpS)
(RpB)
341.3
(RpmmB)
F
400
(BMud)
(RpmmB)
447.9
(BMud) 452.5
454.2
(Rqp)
494.6
EOH
1/256 1/16 2 4 64 256
Grainsize (mm)

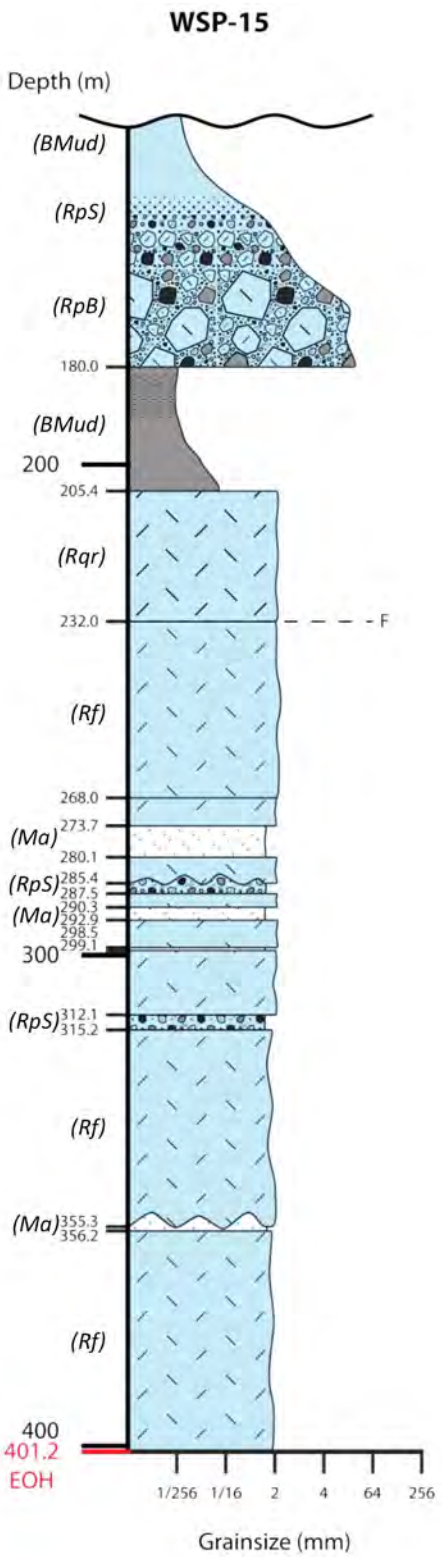
WSP-15
Depth (m)
(BMud)
(RpS)
(RpB)
180.0
(BMud)
200
205.4
(Rqr)
232.0
F
(Rf)
268.0
(Ma) 273.7
280.1
(RpS) 285.4
287.5
(Ma) 290.3
292.9
298.5
299.1
300
(RpS) 312.1
315.2
(Rf)
(Ma) 355.3
356.2
(Rf)
400
401.2
EOH
1/256 1/16 2 4 64 256
Grainsize (mm)

Figure 3.12: Graphic log of part of diamond drill hole BPD-80 (Burns Peak area) through facies of the rhyolite facies association. See Figure 3.4 for legend to graphic log. The lower rhyolite facies association (297.0-391.8 m) comprises coherent quartz-rich feldspar-quartz-phyric rhyolite sub-facies (Rqr), monomictic rhyolite breccia (RmB) and monomictic mud-matrix rhyolite breccia (RmmB; peperite) facies. It has a lower mingled contact and an upper gradational contact with two black mudstone (BMud) intervals (section 3.3.5), and is interpreted as an extrusion (probably a lava). The upper rhyolite facies association (above 297.0 m) comprises massive to normally graded units of polymictic mud-matrix rhyolite breccia (RpmmB), polymictic rhyolite breccia (RpB) and sandstone (RpS) are all consistent interpreted as submarine density current deposits (section 3.3.1.9). The polymictic mud-matrix rhyolite breccia intervals (e.g. 218.0-227.7 m) are interpreted as deposits of submarine density currents that incorporated mud from the substrate. Relatively thick (up to 6 m) intervals of laminated black mudstone (e.g. between 283.8 m and 297.0 m) represent muddy density current and/or hemipelagic deposits.

A: BPD-80 (148.7 m) - Interbedded polymictic rhyolite sandstone (RpS) and black mudstone (BMud).

B: BPD-80 (169.7 m) - Polymictic rhyolite breccia comprising relatively abundant chloritic fragments intermixed with feldspar and quartz crystals and crystal fragments. Sporadic massive grey lithic clasts are sub-angular to sub-round and irregular.

C: BPD-80 (247.2 m) - Polymictic mud-matrix rhyolite breccia comprising massive and flow-banded rhyolite clasts. The matrix includes domains of black mudstone (upper right) and is mainly composed of rhyolite, lithic and mudstone clasts, and feldspar and quartz crystals and crystal fragments.

D: BPD-80 (272.0 m) - Polymictic mud-matrix rhyolite breccia. Clasts include mudstone and greenish brown rhyolite. The matrix includes domains of dark grey to black mudstone (upper right) containing abundant crystal fragments (most likely feldspar and quartz).

E: BPD-80 (290.8 m) - Flame structures at the lower contact between overlying polymictic rhyolite sandstone (RpS) and underlying black mudstone (BMud).

F: BPD-80 (345.5 m) - Matrix-supported monomictic rhyolite breccia. Sporadic feldspar-quartz-phyric rhyolite clasts (middle right) are surrounded by matrix mainly composed of <2 mm feldspar and quartz crystals and crystal fragments.

Uphole and younging directions: A and B - left to right; C, D, E and F - right to left.

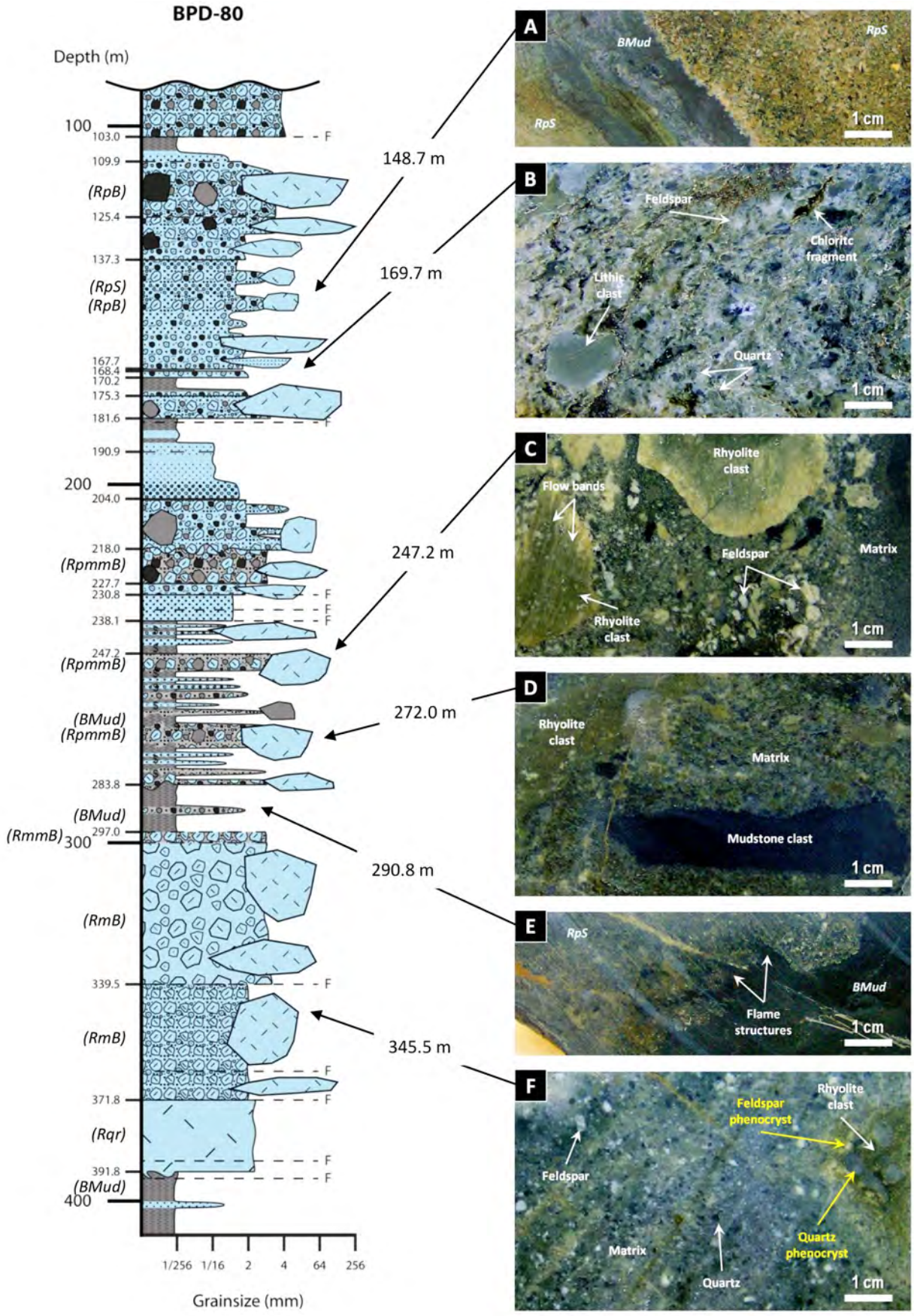
BPD-80
Depth (m)
100
103.0
109.9
(RpB)
125.4
137.3
(RpS)
(RpB)
167.7
168.4
170.2
175.3
181.6
190.9
200
204.0
218.0
(RpmmB)
227.7
230.8
238.1
247.2
(RpmmB)
(BMud)
(RpmmB)
283.8
(BMud)
(RmmB)
297.0
300
(RmB)
339.5
(RmB)
371.8
(Rqr)
391.8
(BMud)
400
F
1/256 1/16 2 4 64 256
Grainsize (mm)
148.7 m
169.7 m
247.2 m
272.0 m
290.8 m
345.5 m
A
BMud
RpS
RpS
1 cm
B
Feldspar
Chloritc fragment
Lithic clast
Quartz
1 cm
C
Rhyolite clast
Flow bands
Feldspar
Matrix
Rhyolite clast
1 cm
D
Rhyolite clast
Matrix
Mudstone clast
1 cm
E
RpS
BMud
Flame structures
1 cm
F
Feldspar phenocryst
Rhyolite clast
Feldspar
Matrix
Quartz phenocryst
Quartz
1 cm

Figure 3.13: Polymictic rhyolite breccia and polymictic mud-matrix rhyolite breccia facies. A: BHD-4 (57.5 m); B: BHD-4 (58.8 m); C: WSP-14 (188.0 m); D: BPD-80 (120.7 m); E: BPD-80 (165.3 m); F: BPD-80 (218.0 m); G: BPD-80 (250.0 m); H: WSP-14 (350.8 m). A to E: Handspecimen photographs of the polymictic rhyolite breccia facies (uphole and younging direction: A and C - not recorded; B and E - right to left; D - left to right).

A: Feldspar-quartz-phyric rhyolite clasts in a poorly sorted matrix composed of abundant feldspar and quartz crystals and crystal fragments. Relatively abundant aphyric and porphyritic felsic and chloritic fragments also occur.

B: Irregular sharp contact between polymictic rhyolite breccia (RpB) and black mudstone (BMud) facies. The polymictic rhyolite breccia is feldspar and quartz crystal-rich. Orange feldspar-phyric felsic fragments occur.

C: Clast-supported, feldspar and quartz crystal-rich polymictic rhyolite breccia. Aphyric to porphyritic chloritic fragments occur.

D: Clast-supported, silicified, feldspar crystal-rich polymictic rhyolite breccia. Abundant rhyolite clasts and aphyric to porphyritic dark green chloritic fragments are embedded in a feldspar crystal-rich matrix.

E: Internally massive, dark grey mudstone clasts in polymictic rhyolite breccia.

F: Irregular sharp contact between the polymictic rhyolite breccia (RpB) and polymictic mud-matrix rhyolite breccia (RpmmB) facies (uphole and younging direction: right to left).

G and H: Handspecimen photographs of the polymictic mud-matrix rhyolite breccia facies (uphole and younging direction: G - not recorded; H - left to right).

G: Strongly feldspar-quartz-phyric rhyolite clasts embedded in volcanic mud and sand matrix containing feldspar crystal fragments. The mud and sand matrix are variably silicified and locally diffusely bedded and contorted.

H: Feldspar-phyric rhyolite clasts and dark green chloritic fragments embedded in matrix comprising mud and abundant feldspar crystal fragments. The mud matrix is locally diffusely bedded. The rhyolite clasts and chloritic fragments are aligned.

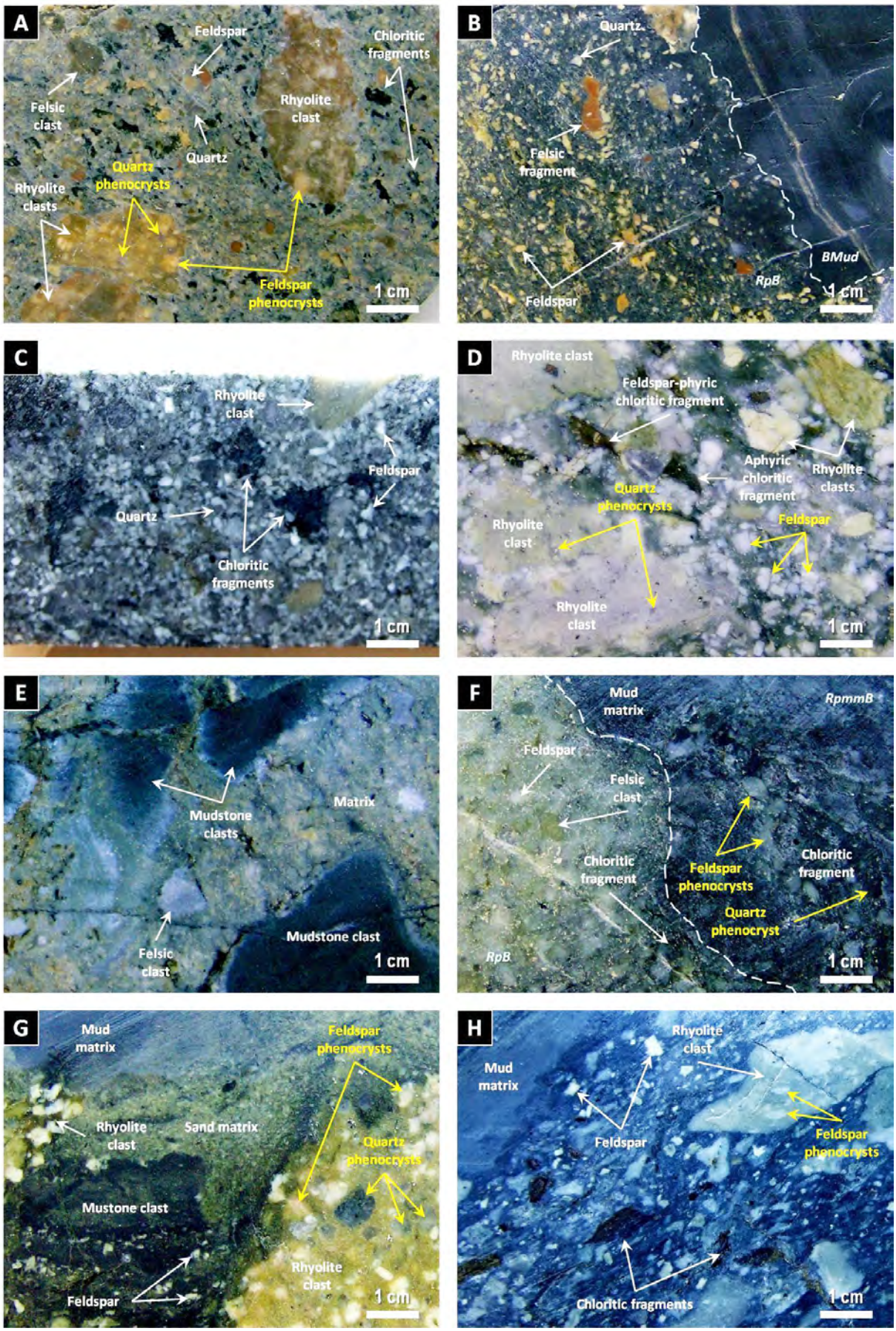
A
Feldspar
Chloritic fragments
Felsic clast
Rhyolite clast
Quartz
Quartz phenocrysts
Rhyolite clasts
Feldspar phenocrysts
1 cm
B
Quartz
Felsic fragment
BMud
RpB
Feldspar
1 cm
C
Rhyolite clast
Feldspar
Quartz
Chloritic fragments
1 cm
D
Rhyolite clast
Feldspar-phyric chloritic fragment
Aphyric chloritic fragment
Rhyolite clasts
Quartz phenocrysts
Feldspar
Rhyolite clast
Rhyolite clast
1 cm
E
Mudstone clasts
Matrix
Mudstone clast
Felsic clast
1 cm
F
Mud matrix
RpmmB
Feldspar
Felsic clast
Chloritic fragment
Feldspar phenocrysts
Chloritic fragment
Quartz phenocryst
RpB
1 cm
G
Mud matrix
Feldspar phenocrysts
Rhyolite clast
Sand matrix
Quartz phenocrysts
Mustone clast
Rhyolite clast
Feldspar
1 cm
H
Rhyolite clast
Mud matrix
Feldspar
Feldspar phenocrysts
Chloritic fragments
1 cm

Figure 3.14: Photomicrographs of the polymictic rhyolite breccia facies (A to H - transmitted, plane polarised light; I - Transmitted, cross polarised light). A to D: BHD-4 (58.8 m); E to I: WSP-14 (188.0 m).

A: Felsic clast and feldspar and quartz crystal fragments surrounded by very fine-grained carbonate-sericite-rich matrix.

B: Feldspar-quartz-phyric felsic clast (most likely rhyolite), and quartz and feldspar crystal fragments.

C: Feldspar-quartz-phyric chloritic fragment, and feldspar and quartz crystal fragments surrounded by very fine-grained carbonate-sericite-rich matrix.

D: Feldspar-quartz-phyric felsic clast (most likely rhyolite) surrounded by quartz crystal fragments and very fine-grained carbonate-sericite-rich matrix. The internal structure is locally apparently spherulitic.

E: Feldspar-quartz-phyric chloritic fragment, and quartz and feldspar crystals and crystal fragments surrounded by very fine-grained carbonate-sericite-rich matrix. The quartz crystal fragment is partly surrounded by pyrite. Feldspar crystals and crystal fragments are moderately to strongly altered to sericite.

F: Quartzite and very fine-grained lithic clasts surrounded by feldspar crystal-rich and carbonate-sericite-rich matrix.

G: Feldspar-quartz-phyric chloritic felsic clast (most likely rhyolite), and quartz and feldspar crystal fragments surrounded by very fine-grained carbonate-sericite-rich matrix.

H: Perlitic felsic clast surrounded by quartz and feldspar crystals and crystal fragments.

I: Sub-angular quartzite clast composed of intergrown polycrystalline quartz.

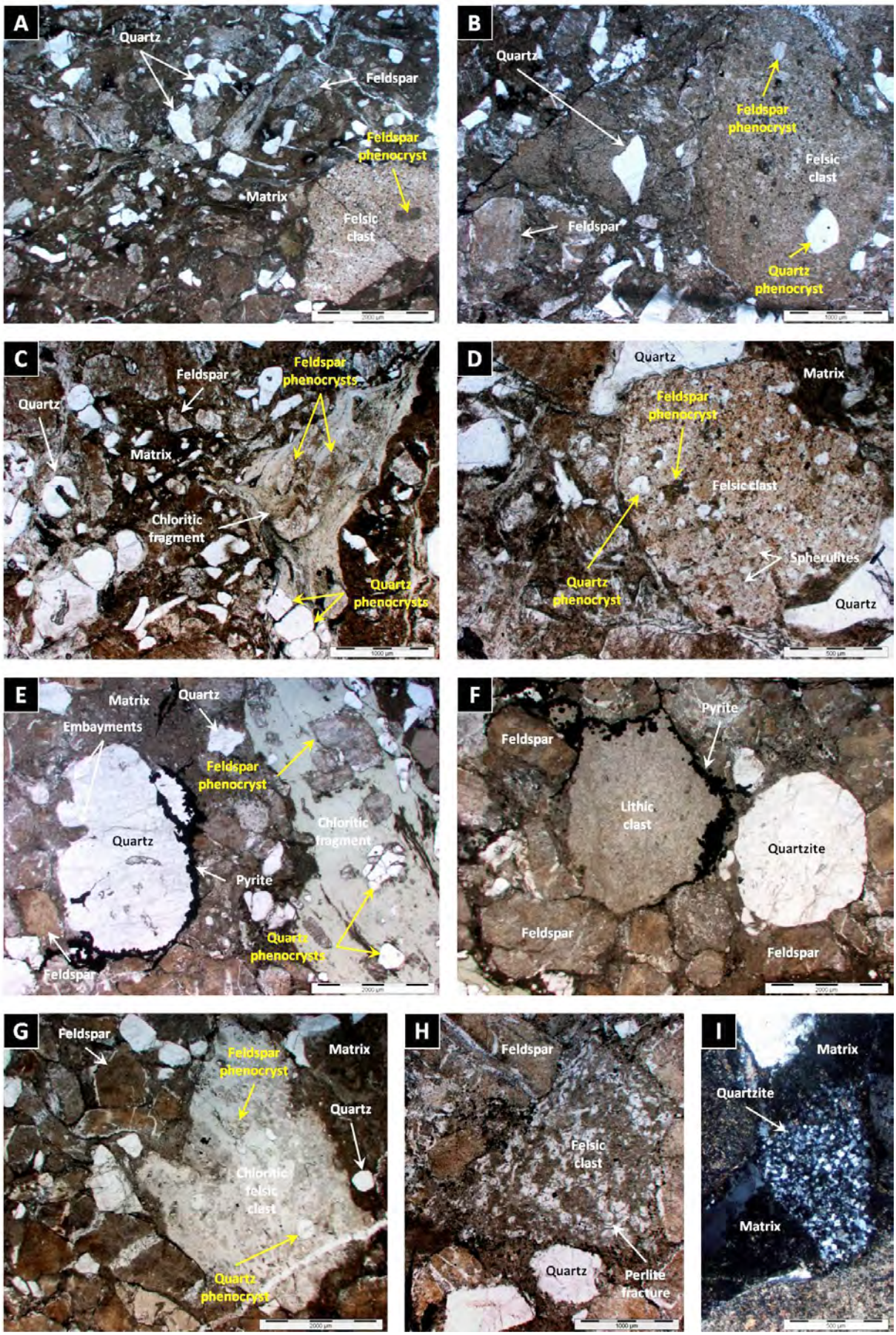
A
Quartz
Feldspar
Feldspar phenocryst
Matrix
Felsic clast
B
Quartz
Feldspar phenocryst
Felsic clast
Feldspar
Quartz phenocryst
C
Feldspar
Feldspar phenocrysts
Quartz
Matrix
Chloritic fragment
Quartz phenocrysts
D
Quartz
Matrix
Feldspar phenocryst
Felsic clast
Spherulites
Quartz phenocryst
Quartz
E
Matrix
Quartz
Embayments
Feldspar phenocryst
Chloritic fragment
Quartz
Pyrite
Quartz phenocrysts
Feldspar
F
Pyrite
Feldspar
Lithic clast
Quartzite
Feldspar
Feldspar
G
Feldspar
Feldspar phenocryst
Matrix
Quartz
Chloritic felsic clast
Quartz phenocryst
H
Feldspar
Felsic clast
Quartz
Perlite fracture
I
Matrix
Quartzite
Matrix

commonly at the base of single, massive polymictic rhyolite breccia units, or intervals of normally graded polymictic rhyolite breccia and sandstone.

In both matrix-supported and clast-supported intervals, the matrix is mainly composed of <2 mm feldspar and quartz crystals and crystal fragments with variable amounts of carbonate, chlorite and sericite (Figure 3.13 - A to E; Figure 3.14 - A, C, D, E, G and I). Aphyric to porphyritic felsic and chloritic fragments, and mudstone clasts <2 mm also occur. Quartzite clasts are variably abundant (Figure 3.14 - F and I). Zones of microgranular (<0.1 mm) quartz, feldspar, carbonate, sericite and chlorite also occur. Zircon grains occur locally. Pyrite and sphalerite (<1-5%) typically occur as disseminated grains, in clusters or commonly surrounding fragment margins (Figure 3.15 - E and F).

3.3.1.7 Polymictic mud-matrix rhyolite breccia facies (RpmmB)

The polymictic mud-matrix rhyolite breccia facies occurs in the Burns Peak and Howards Road areas (Figures 3.2 and 3.3). This facies is spatially associated with polymictic rhyolite breccia and sandstone facies (Table 3.3). Polymictic mud-matrix rhyolite breccia intervals range from <1 to 13 m thick and occur as single massive units or intercalated with intervals of mudstone and minor polymictic rhyolite sandstone (Figures 3.11 - WSP-14; Figure 3.12). Upper and lower contacts with polymictic rhyolite sandstone are typically gradational, locally irregular or sharp and planar.

This facies is very similar to the polymictic rhyolite breccia facies (section 3.3.1.6) but the matrix is composed of massive, variably silicified, pale to dark grey or black mudstone (Figure 3.12 - C; Figure 3.13 - F to H). Intervals of polymictic mud-matrix rhyolite breccia are internally massive to weakly bedded, and may contain massive, relatively large (up to 60 mm across) sub-round mudstone clasts and/or domains (Figure 3.12 - D; Figure 3.13 - G). Flame structures are common at lower contacts between polymictic mud-matrix rhyolite breccia with mudstone.

3.3.1.8 Polymictic rhyolite sandstone facies (RpS)

The polymictic rhyolite sandstone facies occurs at Sock Creek, Burns Peak, White Spur and Howards Road areas (Figures 3.2 and 3.3). Its lateral extent may be in the order of 12 km in the Sock Creek-Burns Peak area and 5 km in the White Spur-Howards Road area. This facies is spatially associated with polymictic rhyolite breccia, polymictic mud-matrix rhyolite breccia and monomictic fiamme-rich rhyolite breccia facies (Table 3.3). Polymictic rhyolite sandstone intervals range from <0.1 to 33 m thick.

This facies typically occurs at the base of normally graded units of polymictic rhyolite sandstone and mudstone, or in the middle of normally graded units comprising polymictic rhyolite breccia at the base and mudstone at the top (Figures 3.5, 3.11 and 3.12). It also occurs as single massive units, in units comprising intercalated mudstone and polymictic mud-matrix rhyolite breccia (Figure 3.12), and also intercalated with coherent feldspar-phyric rhyolite (section 3.3.1.2) (Figures 3.11 - WSP-15).

The polymictic rhyolite sandstone facies is massive to laminated, locally normally graded, weakly bedded, well to very poorly sorted, very fine to very coarse grained, and weakly to moderately sericitic and chloritic (Figure 3.15 - A to H). This facies is very similar to the polymictic rhyolite breccia facies (the abundances of its components are very similar with local minor variations) (section 3.3.1.6), but it is finer grained (Figure 3.12 - A). The majority of the feldspar and quartz crystals and crystal fragments, chloritic, rhyolite, quartzite, sandstone, mudstone, and fine-grained lithic fragments are <2 mm in diameter, but some chloritic, rhyolite, lithic and mudstone fragments >2 mm (up to 20 mm) in diameter occur (Figure 3.15 - H). Bubble-wall shards are locally abundant (Figure 3.15 - L and M). Muscovite flakes occur sporadically (Figure 3.15 - K).

Shard-rich zones (Figure 3.15 - L and M) and zones of microgranular (<0.1 mm) quartz, feldspar, muscovite, carbonate, sericite and chlorite with local zircon and tourmaline grains also occur. Chloritic fragments are locally abundant (Figure 3.15 - I). Silicified, round to oval-shaped sections of sponge spicules and variably-shaped shell and other organic fragments (<1%, 0.05-0.2 mm) were also observed (Figure 3.15 - N to S). Flame structures occur at lower contacts between polymictic rhyolite sandstone with mudstone (Figure 3.12 - E). Pyrite and sphalerite (<1-2%) typically occur as disseminated grains or in clusters. Framboidal pyrite occurs (Figure 3.15 - J).

3.3.1.9 Interpretation

Coherent feldspar-quartz-phyric and feldspar-phyric rhyolite, monomictic rhyolite breccia and monomictic mud-matrix rhyolite breccia facies

The coherent feldspar-quartz-phyric and feldspar-phyric rhyolite facies are commonly spatially associated with monomictic rhyolite breccia and monomictic mud-matrix rhyolite breccia facies. Most intervals of coherent quartz-feldspar-phyric and feldspar-phyric rhyolite have gradational contacts with monomictic rhyolite breccia and monomictic mud-matrix rhyolite breccia (Figure 3.5; Figure 3.7 - BOC-1, BOC-4, BHD-7; Figure 3.12), and the rhyolite clasts within monomictic rhyolite breccia and monomictic mud-matrix rhyolite breccia are both mineralogically and texturally very similar to the coherent feldspar-quartz-phyric or feldspar-phyric rhyolite facies. These observations suggest that the monomictic rhyolite breccia and monomictic mud-matrix rhyolite breccia facies are genetically related to the coherent feldspar-quartz-phyric or feldspar-phyric rhyolite facies. The spatial association and similar mineralogy suggest that these facies may be products of the same eruptive and/or depositional event.

Gradational contacts, textural and mineralogical similarities and spatial relationships among intervals of monomictic rhyolite breccia, monomictic mud-matrix rhyolite breccia and coherent feldspar-quartz-phyric or feldspar-phyric rhyolite facies are consistent with the generation of rhyolite clasts within monomictic rhyolite breccia and monomictic mud-matrix rhyolite breccia from fragmentation of coherent feldspar-quartz-phyric or feldspar-phyric rhyolite. The presence of jigsaw-fit texture in domains of clast-supported monomictic rhyolite breccia (Figure 3.9 - H and K) and most intervals of monomictic mud-matrix rhyolite breccia indicates that fragmentation was at least locally in situ (cf. Pichler, 1965; Scutter et al., 1998).

Figure 3.15: Polymictic rhyolite sandstone facies. A, E, I and L: WSP-14 (216.2 m); B, F, J, P and Q: WSP-14 (325.3 m); C and G: WSP-15 (51.8 m); D, H and M: WSP-15 (163.4 m); K: WSP-15 (314.2 m); N: WSP-14 (99.0 m); O: WSP-14 (193.3 m); R: WSP-14 (420.2 m); S: WSP-15 (286.6 m).

A to D: Handspecimen photographs of the polymictic rhyolite sandstone facies (uphole and younging direction: A - right to left; B - left to right; C and D - not recorded). A and D: Fragments are randomly distributed and not aligned. B and C: Most fragments are elongate and aligned (direction: B - upper left-lower right; C - lower left-upper right). E to S: Photomicrographs of the polymictic rhyolite sandstone facies (E to I, L to N, and P to S - transmitted, plane polarised light; J - transmitted, reflected light; K and O - transmitted, cross polarised light).

E: Perlitic clast and quartz crystal fragment surrounded by very fine-grained carbonate-sericite-altered matrix.

F: Aligned aphyric chloritic fragments (direction: lower left-upper right) and quartzite and quartz crystal fragments. The quartzite fragment is elongate and composed of intergrown polycrystalline quartz.

G: Aligned quartz, mudstone and fine-grained lithic clasts.

H: Feldspar-quartz-phyric chloritic fragment, and quartz and feldspar crystals and crystal fragments surrounded by very fine-grained carbonate-sericite-altered matrix. The feldspar crystal fragments and phenocrysts are moderately to strongly altered to sericite. I: Chloritic fragment surrounded by very fine-grained carbonate-sericite-altered matrix.

J: Framboidal pyrite.

K: Muscovite fragment.

L: Formerly glassy shards.

M: Y-shaped shard.

N: Circular section of sponge spicule and triangular quartz crystal fragment.

O: Circular section of sponge spicule with core.

P: Oval-shaped organic fragment with radial internal structure.

Q: Linear organic fragment (probably shell fragment).

R: Gently curved shell fragment.

S: Oval section of organic fragment (probably sponge spicule) with core. Professor Patrick Quilty assisted in the identification of sponge spicules and organic fragments (N to S).

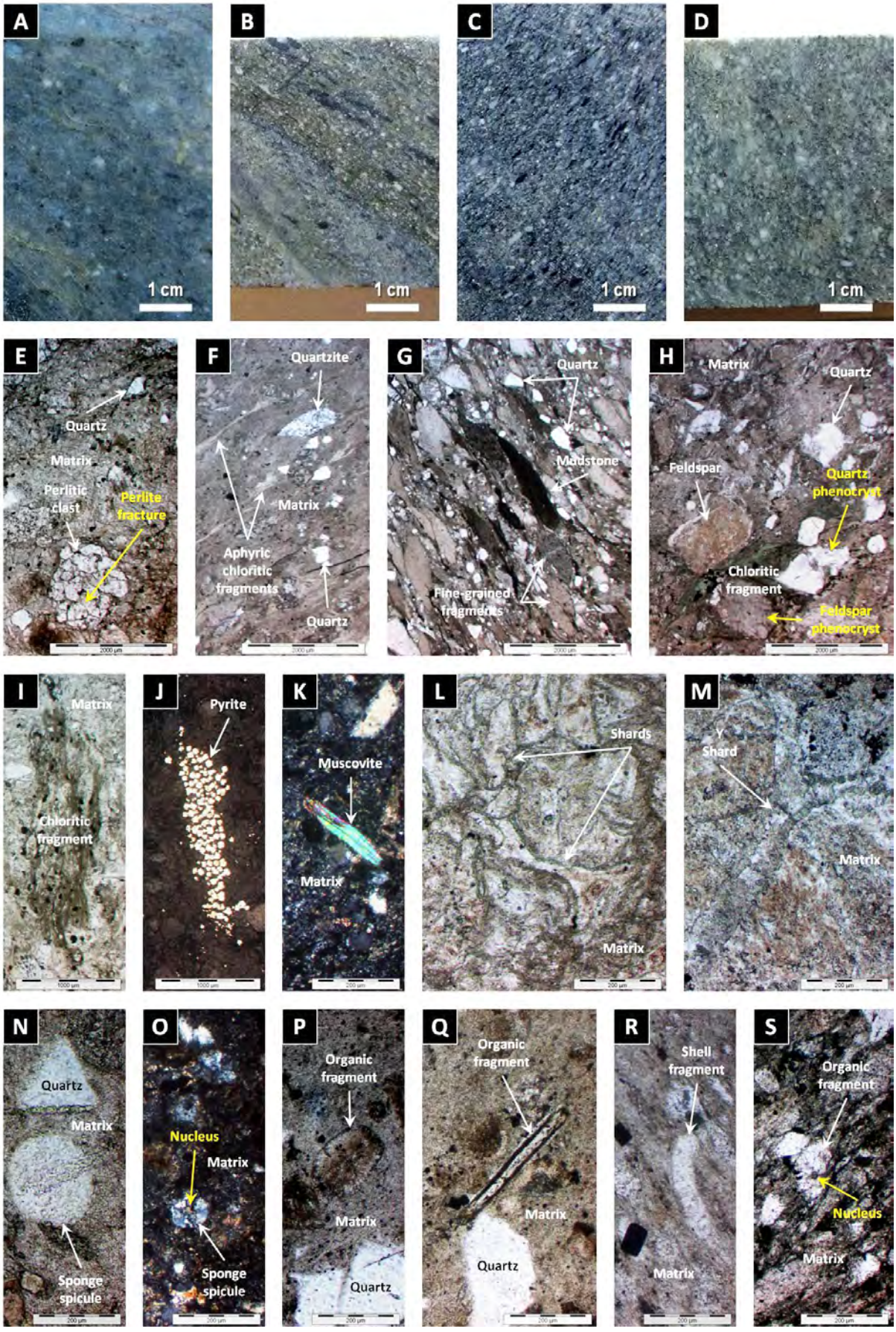
A
1 cm
B
1 cm
C
1 cm
D
1 cm
E
Quartz
Matrix
Perlitic clast
Perlite fracture
F
Quartzite
Matrix
Aphyric chloritic fragments
Quartz
G
Quartz
Mudstone
Fine-grained fragments
H
Matrix
Quartz
Feldspar
Quartz phenocryst
Chloritic fragment
Feldspar phenocryst
I
Matrix
Chloritic fragment
J
Pyrite
K
Muscovite
Matrix
L
Shards
Matrix
M
Y Shard
Matrix
N
Quartz
Matrix
Sponge spicule
O
Nucleus
Matrix
Sponge spicule
P
Organic fragment
Matrix
Quartz
Q
Organic fragment
Matrix
Quartz
R
Shell fragment
Matrix
S
Organic fragment
Nucleus
Matrix

Jigsaw-fit monomictic rhyolite breccia intervals comprise blocky and splintery rhyolite clasts with planar and curviplanar edges identical to clasts produced by quench fragmentation (cf. Pichler, 1965), and are interpreted as in situ hyaloclastite (cf. Pichler, 1965). Jigsaw-fit monomictic mud-matrix rhyolite breccia is interpreted as in situ intrusive hyaloclastite (Cas et al, 1990).

Some intervals of monomictic rhyolite breccia and domains of monomictic mud-matrix rhyolite breccia have clast-rotated texture, are internally massive, and do not show jigsaw-fit texture (Figure 3.5 - C; Figure 3.9 - A and E). The dominant rhyolite clasts within clast-rotated monomictic rhyolite breccia intervals are sub-angular to sub-round, massive to flow-banded and/or perlitic, and have blocky, elongate, irregular and amoeboid shapes (Figure 3.9 - A and B). Gradational contacts, identical phenocryst populations and the spatial association between massive to flow-banded and/or perlitic, irregular- to amoeboid-shaped rhyolite clasts within monomictic rhyolite breccia and adjacent, flow-banded coherent feldspar-quartz-phyric or feldspar-phyric rhyolite facies are consistent with rhyolite clasts within the monomictic rhyolite breccia being at least partly derived from autoclastic (non-explosive) fragmentation of coherent feldspar-quartz-phyric or feldspar-phyric rhyolite (cf. Fisher, 1960).

Local intervals of monomictic rhyolite breccia with clast-rotated texture and flow-banded rhyolite clasts (Figure 3.5) are interpreted as autobreccia (cf. Fisher, 1960). Intervals of clast-rotated monomictic rhyolite breccia that are locally graded and grade into finer-grained monomictic rhyolite breccia (Figure 3.5 - BHD-4; Figure 3.7 - BOC-1) are consistent with extrusion of the rhyolite and suggest that some quench-fragmented and/or autobrecciated rhyolite was resedimented down slope, possibly contemporaneous with growth of the associated feldspar-quartz-phyric rhyolite dome or lava flow (Kano et al., 1991).

Perlitic fractures in some rhyolite clasts within both jigsaw-fit and clast-rotated monomictic rhyolite breccia and monomictic mud-matrix rhyolite breccia reflect the original glassy nature of these clasts (Ross and Smith, 1955); the glassy nature suggests rapid cooling on contact with water or wet sediment in a subaqueous environment. Rhyolite clasts that are perlitic, angular to sub-angular with blocky to splintery shapes and planar to curviplanar edges were probably produced by quench fragmentation (Pichler, 1965).

Local gradation from jigsaw-fit to clast-rotated monomictic rhyolite breccia and monomictic mud-matrix rhyolite breccia associated with intervals of coherent feldspar-quartz-phyric or feldspar-phyric rhyolite (Figure 3.9 - K) suggests that rotation of the rhyolite clasts may have resulted from endogenous growth of the adjacent feldspar-quartz-phyric or feldspar-phyric rhyolite. Local jigsaw-fit textures within intervals of clast-rotated monomictic rhyolite breccia record the progressive fragmentation of larger rhyolite clasts.

Many intervals of clast-rotated monomictic rhyolite breccia contain variable amounts (<5-35%) of elongate, dark green, aphyric to porphyritic chloritic fragments. The chloritic fragments are commonly randomly oriented and mineralogically identical to the associated rhyolite clasts. The spatial association and distribution, and identical mineralogy between the chloritic fragments and rhyolite clasts within intervals of clast-rotated monomictic rhyolite breccia suggest that the chloritic fragments and the rhyolite clasts are related, and that

the chloritic fragments were also produced by autoclastic fragmentation of adjacent intervals of coherent feldspar-quartz-phyric or feldspar-phyric rhyolite.

The elongate to lenticular shapes of the chloritic fragments are probably the result of locally higher shear stress during flowage of rhyolite lava/magma. The elongate, irregular and amoeboid shapes of some dark green, chlorite-rich, porphyritic rhyolite clasts within clast-rotated monomictic rhyolite breccia were probably produced by the same process.

The monomictic mud-matrix rhyolite breccia facies typically occurs at the top margins of coherent rhyolite and rhyolite breccia units (Figure 3.5; Figure 3.7 - BHD-7). Domains of dark grey and black mud matrix are locally contorted and/or disrupted close to the contact with monomictic rhyolite breccia or coherent feldspar-quartz-phyric or feldspar-phyric rhyolite facies. Away from the contact, the mud matrix grades into massive or laminated mudstone. These features indicate that the mud matrix was unconsolidated at the time of mingling. The occurrence of silicified mud matrix immediately adjacent to the rhyolite clasts is consistent with induration of the mud on contact with hot rhyolite clasts (e.g., Gifkins et al., 2002). These observations, together with the presence of rhyolite apophyses within the adjacent mudstone units close to the upper and/or lower contacts with the rhyolite (Figure 3.5; Figure 3.7 - BHD-7, BOC-2), are all consistent with the interpretation of the monomictic mud-matrix rhyolite breccia facies as peperite (e.g., White et al., 2000).

Peperite is a rock formed essentially in situ by disintegration of magma intruding and mingling with unconsolidated or poorly consolidated sediments (White et al., 2000). It commonly occurs at the contacts between shallow intrusions and wet unconsolidated sediment, and along the basal contacts of lavas with underlying sediment (McPhie et al., 1993; Skilling et al. 2002).

Very similar internal textures and mineralogy, and spatial associations of coherent feldspar-quartz-phyric or feldspar-phyric rhyolite, and monomictic rhyolite breccia can be present in lavas or domes (extrusive) versus cryptodomes or syn-volcanic sills (intrusive; Cas et al., 1990; Kano et al., 1991; Goto and McPhie, 1998; Gifkins et al., 2002). The association of abundant, internally massive to locally normally graded monomictic rhyolite breccia facies (in situ and locally resedimented autobreccia and hyaloclastite) at the top of coherent feldspar-quartz-phyric or feldspar-phyric rhyolite facies is consistent with extrusion of the rhyolite lava (Figure 3.7 - BOC-1 and BOC-4). In contrast, the occurrence of peperite (monomictic mud-matrix rhyolite breccia facies) typically at the top margins of coherent and brecciated rhyolite units, commonly closely associated with mudstone, is consistent with the interpretation of shallow intrusion of coherent feldspar-quartz-phyric or feldspar-phyric rhyolite as syn-volcanic sills or cryptodomes (Figure 3.5; Figure 3.7 - BHD-7, BOC-2).

Monomictic fiamme-rich rhyolite breccia

The monomictic fiamme-rich rhyolite breccia facies (Figure 3.10) is spatially associated with coherent feldspar-phyric rhyolite facies. The fiamme are texturally and mineralogically identical to the blocky rhyolite clasts within the monomictic fiamme-rich rhyolite breccia facies and the coherent feldspar-phyric rhyolite.

The spatial association and similar phenocryst mineralogy suggest that these facies are genetically related and may be products of the same eruptive and/or depositional event.

The presence of both fiamme and massive to flow-banded, blocky, perlitic rhyolite clasts and the apparent lack of fine (<2 mm, ash) components within the monomictic fiamme-rich rhyolite breccia facies are consistent with the fiamme within monomictic fiamme-rich rhyolite breccia facies being generated from autoclastic (non-explosive) fragmentation and resedimentation of feldspar-phyric rhyolite lava (cf. Fisher, 1960). The fiamme are feldspar-phyric to apparently aphyric and, in contrast to the blocky rhyolite clasts, they are moderately to strongly chloritic (Figure 3.10 - A and B). The fiamme were probably originally texturally different from the rhyolite clasts, probably due to variations in vesicularity (pumiceous versus dense) or crystallinity (crystalline versus glassy) of the groundmass in feldspar-phyric rhyolite lava (e.g., Bull and McPhie, 2007). The texture, shape and strong alignment of the fiamme suggest that they were probably originally vesicular rhyolite lava fragments that have been compacted during diagenesis (e.g., Peterson, 1979; Allen, 1988; Branney and Sparks et al., 1990). In contrast, the blocky rhyolite clasts represent non-vesicular parts of feldspar-phyric rhyolite lava that resisted diagenetic compaction.

Polymictic rhyolite breccia and sandstone, and polymictic mud-matrix rhyolite breccia facies

The polymictic rhyolite breccia and sandstone, and polymictic mud-matrix rhyolite breccia facies are closely spatially associated and typically occur associated with monomictic fiamme-rich rhyolite breccia and sandstone, or monomictic rhyolite breccia and coherent feldspar-quartz-phyric rhyolite facies. The rhyolite clasts and porphyritic chloritic fragments within all of these facies are very similar, suggesting that these facies are genetically related.

The thick (up to approximately 80 m thick), normally graded, polymictic, and poorly sorted nature of the polymictic rhyolite breccia facies, gradational contacts between polymictic rhyolite breccia and sandstone facies, and the presence of angular to sub-round rhyolite fragments, and feldspar and quartz crystals and crystal fragments are all consistent with deposition of polymictic rhyolite breccia from submarine density currents, most probably high-concentration density currents (cf. Lowe, 1982).

Intervals of well sorted, massive to locally normally graded polymictic rhyolite sandstone at the top of normally graded intervals of polymictic rhyolite breccia and sandstone are consistent with deposition from lower-concentration density currents (cf. Lowe, 1976; Lowe, 1982). Intervals of mudstone at the top of normally graded units of polymictic rhyolite breccia and sandstone were probably deposited by settling of suspended very fine grained particles through the water column during the waning stages of the density currents.

The massive to normally graded units of polymictic rhyolite breccia and sandstone (many with mudstone tops) are up to >90 m thick (Howards Road area; Figure 3.11 - WSP-14), and may be laterally extensive for >3 km in the White Spur-Howards Road area (Figures 3.3 and 3.11) or >12 km in the Sock Creek-Burns Peak area (Figures 3.2, 3.5 and 3.12). Furthermore, the polymictic rhyolite breccia facies comprises

relatively abundant chloritic fragments that may have originally been glassy. The locally abundant bubble-wall shards within the polymictic rhyolite sandstone facies (Figure 3.15 - L and M) were produced by explosive fragmentation of highly vesicular felsic magma (Niem, 1977; Cas and Wright, 1991). The shards are undeformed, suggesting they were cool and solid at deposition and no welding compaction has occurred (e.g., McPhie et al., 1993). The components, thickness and extent of units of the polymictic rhyolite breccia and sandstone facies are consistent with submarine explosive eruption-fed deposits (e.g., McPhie et al., 1993; White, 2000; McPhie and Allen, 2003; Jutzeler et al., 2014). The chloritic fragments, bubble-wall shards, and many quartz and feldspar crystals and crystal fragments within the polymictic rhyolite breccia and sandstone are most likely juvenile pyroclasts.

The presence of sponge spicules, shell fragments and other organic fragments within the polymictic rhyolite sandstone facies (Figure 3.15 - N to S) confirms the subaqueous environment of deposition (Quilty, 1971, 1972b; Quilty and Telfer, 1994; Quilty and Seymour, 2010), and might indicate that the submarine density currents were not strictly eruption-fed. However, the sponge spicules and shell fragments could have been collected en route and incorporated into the submarine density currents along with larger fragments. The presence of large mudstone (up to 50 cm) and sandstone (up to 6 cm) clasts typically at the base of normally graded units of polymictic breccia and sandstone units (Figure 3.11 - WSP-14) is consistent with this interpretation.

Some black mudstone clasts are homogeneous and have irregular margins, suggesting they are intraclasts (Figure 3.12 - D, Figure 3.13 - E and G). Rare, sub-rounded quartzite fragments are not foliated (Figure 3.14 - F and I), suggesting they are not basement-derived. Instead, they have probably been recycled from the loose sediment substrate (along with the mudstone and sandstone clasts, and the sponge spicules and shell fragments) and are intrabasinal. The abundant rhyolite clasts are non-vesicular/non-amygdaloidal and most probably represent dense, non-juvenile pyroclasts. Some of the fine-grained volcanic and lithic fragments may represent a different volcanogenic source.

The polymictic rhyolite breccia and sandstone facies were most likely produced by intrabasinal, submarine explosive eruption-fed density currents. Where these currents overrode a mud substrate, the polymictic mud-matrix rhyolite breccia facies was formed. The local occurrence of irregular lower contacts between overlying polymictic mud-matrix rhyolite breccia and underlying mudstone intervals indicate that the mud-supported density currents were erosive (Figure 3.12 - 283.8 m). The rhyolite clasts within polymictic rhyolite breccia and polymictic mud-matrix rhyolite breccia facies were incorporated by excavation of underlying, pre-existing monomictic rhyolite breccia (interpreted as autobreccia) (Figure 3.12), or else they could be non-juvenile pyroclasts indicating that the explosive eruptions were seated in nearby domes or lavas.

3.3.2 Dacite facies association

The dacite facies association comprises six facies: 1) coherent feldspar-phyric dacite, 2) monomictic dacite breccia, 3) monomictic mud-matrix dacite breccia, 4) monomictic fiamme-rich dacite breccia, 5) monomictic mud-matrix fiamme-rich dacite breccia, and 6) monomictic dacite sandstone. The location of the diamond

drill holes intersecting facies of the dacite facies association is shown in Figure 3.16. The characteristics of the facies comprising the dacite facies association are summarized in Table 3.4.

3.3.2.1 Coherent feldspar-phyric dacite facies (Df)

The coherent feldspar-phyric dacite facies occurs from Sock Creek to Boco Road, W of the Murchison Highway, and in the Bulgobac Hill, Mackintosh and Mount Charter areas, E of the Murchison Highway (Figure 3.16). It extends laterally for about 10 km discontinuously. This facies is spatially associated with monomictic dacite breccia and monomictic mud-matrix dacite breccia facies, and locally with monomictic fiamme-rich dacite breccia and monomictic dacite sandstone facies (Table 3.4). Coherent feldspar-phyric dacite intervals range from 1 to 206 m thick.

The coherent feldspar-phyric dacite facies occurs as single coherent units, and in combination with monomictic dacite breccia facies (Figures 3.17 and 3.18). Upper and lower contacts with monomictic dacite breccia, monomictic mud-matrix dacite breccia and monomictic fiamme-rich dacite breccia facies are typically gradational or locally sharp and planar or irregular (Figures 3.17 and 3.18).

The coherent feldspar-phyric dacite facies is weakly to locally strongly porphyritic, non- to weakly amygdaloidal, massive or flow-banded, and typically pale to dark green, brown or pink (Figure 3.19). Feldspar phenocrysts (1-30%; 0.3-5 mm) are typically euhedral to anhedral, tabular or irregular, and commonly twinned. Feldspar phenocrysts are commonly zoned and have a narrow, less-altered rim surrounding a broad, more-altered core (Figure 3.19 - H). Feldspar phenocrysts are moderately to strongly altered to sericite, carbonate and chlorite. They have variable colours (white, cream, pink, orange, green) due to various degrees of alteration, and are commonly too altered to distinguish the original feldspar type (plagioclase versus K-feldspar). Feldspar glomerocrysts are common.

The groundmass (70-99 %) of the coherent feldspar-phyric dacite facies is predominantly composed of fine-grained feldspar and quartz (Figure 3.19 - B, D, F to H) and typically weakly to strongly altered to any combination of sericite, chlorite, carbonate and quartz. Zircon, sphene, apatite, and biotite occur locally. Pyrite and sphalerite occur as disseminated (up to 1%) grains and clusters or associated with veins and fractures. In many examples, patchy alteration has created false clastic textures. Relict perlite, mainly classical perlite, is very common (Figure 3.17 - B; Figure 3.19 - D to G and I); rare banded perlite also occurs (Figure 3.19 - J). Classical perlitic fractures commonly enclose or intersect concentrically zoned amygdales (Figure 3.19 - F and G).

In amygdaloidal dacite intervals (Figure 3.19 - E to G), amygdales (<5-10%, 0.1-5 mm) are typically concentrically zoned and filled with any combination of quartz, carbonate, chlorite, and sericite in radial and concentric arrays. Chlorite amygdales are commonly dark to pale green and round to elongate (Figure 3.19 - E). Sporadic chlorite amygdale-rich massive dacite intervals occur, and in many examples amygdales are highly elongate. Quartz-carbonate amygdales (2-3%, up to 5 mm in diameter) are typically white to pale yellow, round, elongate or very rarely multi-globular and irregular-shaped due to vesicle coalescence (Figure

3.19 - G). They are typically larger and commonly more abundant than carbonate-chlorite amygdales (1-2%, 1-2 mm). Round to elongate and oval to irregular-shaped quartz-chlorite and quartz-chlorite-carbonate amygdales also occur.

In flow-banded coherent feldspar-phyric dacite intervals (Figure 3.17 - D; Figure 3.18 - B; Figure 3.19 - A, B, K and L), flow-bands are represented by wavy, sub-parallel, green versus brown, and variably thick (2-10 mm thick), feldspar phenocryst-bearing, chlorite-rich bands. Flow-bands occur both throughout coherent feldspar-phyric dacite intervals and near the margins of units; rare flow-folds are present (Figure 3.19 - L).

3.3.2.2 Monomictic dacite breccia facies (DmB)

The monomictic dacite breccia facies occurs from Sock Creek to Boco Road, W of the Murchison Highway, and in the Bulgobac Hill, Mackintosh and Mount Charter areas, E of the Murchison Highway (Figure 3.16). It extends laterally for about 10 km discontinuously. This facies is spatially associated with coherent feldspar-phyric dacite, monomictic mud-matrix dacite breccia, monomictic fiamme-rich dacite breccia and monomictic dacite sandstone facies (Table 3.4). Monomictic dacite breccia intervals range from 1 to 56 m thick.

Monomictic dacite breccias occur as single units, and in combination with coherent feldspar-phyric dacite facies (Figures 3.17 and 3.18). Upper and lower contacts with coherent feldspar-phyric dacite, monomictic mud-matrix dacite breccia and monomictic dacite sandstone facies are typically gradational or locally sharp, and planar or irregular (Figures 3.17 and 3.18). Local intervals of monomictic dacite breccia are weakly normally graded and grade into monomictic dacite sandstone (Figure 3.18 - SCS-4).

The monomictic dacite breccia facies is typically poorly sorted, clast-supported (jigsaw-fit texture) to locally matrix-supported (clast-rotated texture) massive to locally normally graded, weakly to moderately sericitic and chloritic, and variably silicified (Figure 3.20). In clast-supported jigsaw-fit monomictic dacite breccia intervals (Figure 3.17 - A; Figure 3.20 - A to F, and J), dacite clasts are angular to sub-angular and have blocky and splintery shapes, and planar and curviplanar edges. Spaces between clasts are scarce and are commonly filled with finer-grained (<2 mm) dacite clasts. In matrix-supported clast-rotated domains (Figure 3.18 - A; Figure 3.20 - G and H), dacite clasts are blocky, angular to sub-round and have curviplanar and irregular edges. They are surrounded by finer-grained (<2 mm) dacite clasts.

The dacite clasts vary widely in size (up to 50 cm in diameter). The dominant clasts are feldspar-phyric to apparently aphyric, non- to weakly amygdaloidal, massive to flow-banded and/or perlitic. The phenocryst and amygdale abundances and distributions are very similar to the phenocryst and amygdale populations of the associated coherent feldspar-phyric dacite facies (section 3.3.2.1). In many examples, larger dacite clasts have thin, partly fragmented and/or perlitic, pale grey or green margins surrounding broad, intact, dark green cores (Figure 3.20 - F).

The matrix (<2 mm) is composed dominantly of dacite clasts and minor amounts (<3%) of feldspar crystals

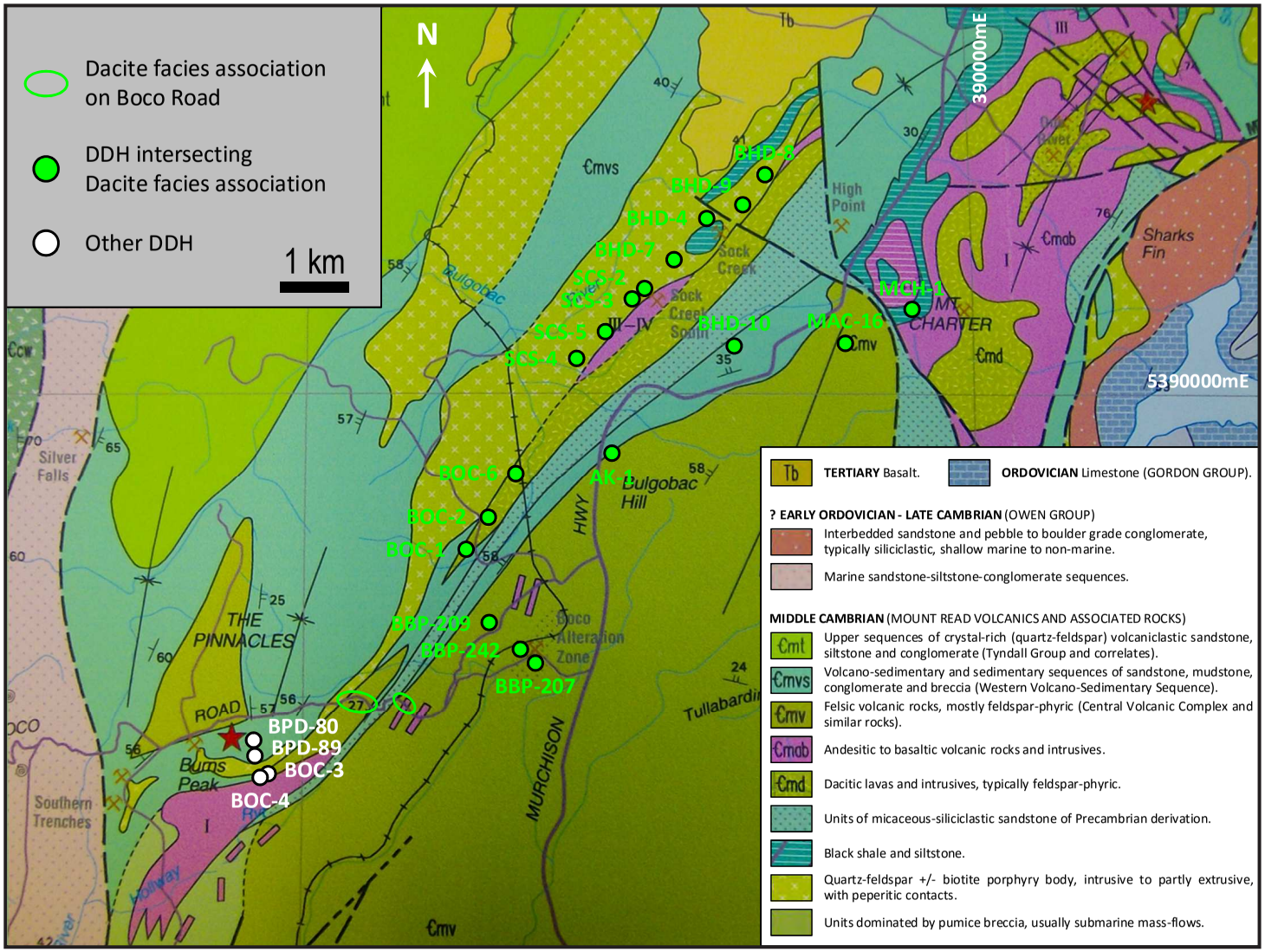

Figure 3.16: Geology of the Que River-Burns Peak area showing the location of the diamond drill holes (DDH) in this study, after Corbett (2002a). Facies of the dacite facies association (D) occur at Boco Road and are intersected by DDH AK-1 (Bulgobac Hill area), BBP-207, BBP 209 and BBP-242 (Boco Alteration Zone area), BHD-4, BHD-7, BHD-8 and BHD-9 (Sock Creek area), BOC-1, BOC-2 and BOC-6 (Boco area), MAC-16 (Mackintosh area), MCH-1 (Mount Charter area), and SCS-2, SCS-3, SCS-4 and SCS-5 (Sock Creek South area).

Table 3.4: Characteristics, location and interpretation of the facies comprising the dacite facies association.

Facies association, facies and sub-facies		Lithofacies characteristics	Thickness x lateral extent	Mineralogy/Components	Textures	Associated facies	Location and diamond drill holes	Interpretation
Dacite facies association (D)	*Coherent feldspar-phyric dacite facies* ***(Df)***	Massive; flow-banded; locally fractured and brecciated	1-208 m x 10 km (discontinuously)	Feldspar phenocrysts and glomerocrysts (1-30%, 0.3-5 mm)	Weakly to strongly porphyritic and glomeroporphyritic; perlitic; amygdaloidal.	DmB; DmmB; DmfrB; DmS; (Mud)	Bulgobac Hill: **AK-1**; Boco Alteration Zone: **BBP-207, BBP-209, BBP-242**; Sock Creek: **BHD-4, BHD-7, BHD-8, BHD-9**; Sock Creek South: **BHD-10, SCS-2, SCS-3, SCS-4, SCS-5**; Boco: **BOC-1, BOC-2, BOC-6**; Mackintosh: **MAC-16**; Mount Charter: **MCH-1**; Boco Road	Coherent facies of lavas, domes and/or syn-volcanic sills
	Monomictic dacite breccia facies ***(DmB)***	Massive to locally normally graded; poorly sorted; clast-supported (jigsaw-fit) to matrix-supported (clast-rotated)	1-56 m x 10 km (discontinuously)	Blocky, angular to sub-angular dacite clasts with planar and curviplanar margins; minor amounts (<3 %) of feldspar crystals and crystal fragments and chloritic fragments	Feldspar-phyric to apparently aphyric, non to weakly amygdaloidal, massive to flow-banded and/or perlitic dacite clasts; aphyric to feldspar-phyric chloritic fragments	Df; DmmB; DmfrB; DmmfrB; DmS; (Mud)	Bulgobac Hill: **AK-1**; Sock Creek: **BHD-4, BHD-7, BHD-8, BHD-9**; Boco: **BOC-1, BOC-2, BOC-6**; Mackintosh: **MAC-16**; Mount Charter: **MCH-1**; Sock Creek South: **SCS-2, SCS-3, SCS-4, SCS-5**; Boco Road	In situ and clast-rotated autoclastic breccia
	Monomictic mud-matrix dacite breccia facies ***(DmmB)***	Massive; poorly sorted; mud matrix-supported	<1-7 m x 5 km? (discontinuously)	Blocky, angular to sub-angular dacite clasts with planar and curviplanar margins; minor amounts (<3 %) of feldspar crystals and crystal fragments and fiamme	Feldspar-phyric to apparently aphyric, non to weakly amygdaloidal, massive to flow-banded and/or perlitic dacite clasts	Df; DmB; DmfrB; DmS; (Mud)	Sock Creek: **BHD-4, BHD-8, BHD-9**; Boco: **BOC-6**; Mackintosh: **MAC-16**; Sock Creek South: **SCS-2, SCS-3, SCS-4, SCS-5**	Peperite
	Monomictic fiamme-rich dacite breccia facies ***(DmfrB)***	Massive to locally normally graded; poorly sorted; clast-supported to localy matrix-supported	1-15 m x 5 km? (discontinuously)	Abundant aphyric to feldspar-phyric fiamme (up to 80%); blocky dacite clasts (up to 25%)	Aligned fiamme; some dacite clasts are flow-banded or perlitic	Df; DmB; DmmB; DmmfrB; DmS	Bulgobac Hill: **AK-1**; Sock Creek: **BHD-4**; Boco: **BOC-6**; Sock Creek South: **SCS-2, SCS-3, SCS-4, SCS-5**	Diagenetically compacted autoclastic breccia
	Monomictic mud-matrix fiamme-rich dacite breccia facies ***(DmmfrB)***	Massive; poorly-sorted; mud matrix-supported	<1-2 m x ?	Abundant aphyric to feldspar-phyric fiamme (up to 80%); blocky dacite clasts (up to 25%)	Aligned fiamme; some dacite clasts are flow-banded or perlitic	DmB; DmfrB; (Mud)	Bulgobac Hill: **AK-1**; Sock Creek: **BHD-8**; Sock Creek South: **SCS-5**	Pumiceous peperite or intrusive hyaloclastite
	Monomictic dacite sandstone facies ***(DmS)***	Massive or weakly bedded (locally laminated); commonly normally graded; well to moderately sorted	<1-5 m x 1.2 km? (Sock Creek South)	Dacite fragments identical to DmB but <2 mm; sporadic >2 mm (<10 mm in diameter) dacite fragments; feldspar crystals and crystal fragments (5-25 %, 0.2-2-5 mm); may contain chloritic fragments (<10%, <30 mm)	Feldspar-phyric to apparently aphyric, non to weakly amygdaloidal, massive to flow-banded and/or perlitic dacite clasts; aphyric to feldspar-phyric chloritic fragments	Df; DmB; DmmB; DmfrB; (Mud)	Bulgobac Hill: **AK-1**; Boco: **BOC-2**; Mount Charter: **MCH-1**; Sock Creek South: **SCS-3, SCS-4**	Distal resedimented autoclastic deposits

Figure 3.17: Graphic log of part of diamond drill hole BHD-8 (Sock Creek area) through facies of the dacite facies association. See Figure 3.4 for legend to graphic log. The lower dacite unit (245.4-303.6 m) comprises coherent feldspar-phyric dacite (Df) and monomictic mud-matrix dacite breccia (DmmB) facies, and occurs between two mudstone intervals. Although the upper contact is not exposed in drill core, the occurrence of monomictic mud-matrix dacite breccia at the top of this dacite unit and the mingled lower contact are consistent with the interpretation of this dacite unit as a syn-volcanic sill (section 3.3.2.7). The fiamme within the underlying monomictic mud-matrix fiamme-rich dacite breccia facies (DmmfrB) (E) are interpreted as former vesicular dacite clasts that have been diagenetically compacted. The upper dacite unit (75.9-230.4 m) includes coherent feldspar-phyric dacite (Df) and monomictic dacite breccia (DmB) facies, and has a lower sharp, planar contact. The upper contact is not exposed in drill core. The upper and lower monomictic dacite breccia shows jigsaw-fit texture, and the middle coherent feldspar-phyric dacite interval is massive, perlitic and amygdaloidal. The textures within the facies of this dacite facies association are consistent with the interpretation of this unit as a dacitic lava (section 3.3.2.7). The dacite clasts present in the polymictic breccia (above 75.9 m) are very similar to the dacite clasts within the monomictic dacite breccia facies (below 75.9 m), and further support this interpretation.

A: BHD-8 (79.9 m) - Poorly sorted, clast-supported monomictic dacite breccia. The dacite clasts are blocky, angular to sub-angular and have planar, curviplanar and ragged margins. Jigsaw-fit texture occurs.

B: BHD-8 (133.3 m) - Strongly perlitic coherent feldspar-phyric dacite.

C: BHD-8 (245.4 m) - Monomictic mud-matrix dacite breccia. The dacite clasts are blocky, very angular to sub-angular and have planar, curviplanar and ragged margins. They are partly surrounded by massive, black mud matrix. Jigsaw-fit texture occurs.

D: BHD-8 (274.4 m) - Flow-banded coherent feldspar-phyric dacite. Flow bands are wavy, sub-parallel, and pale and dark green.

E: BHD-8 (305.5 m) - Monomictic mud-matrix fiamme-rich dacite breccia. Abundant, strongly aligned, feldspar-phyric fiamme are surrounded by dark grey to black mudstone.

Uphole and younging directions: A and E - left to right; C and D - right to left; B - not recorded.

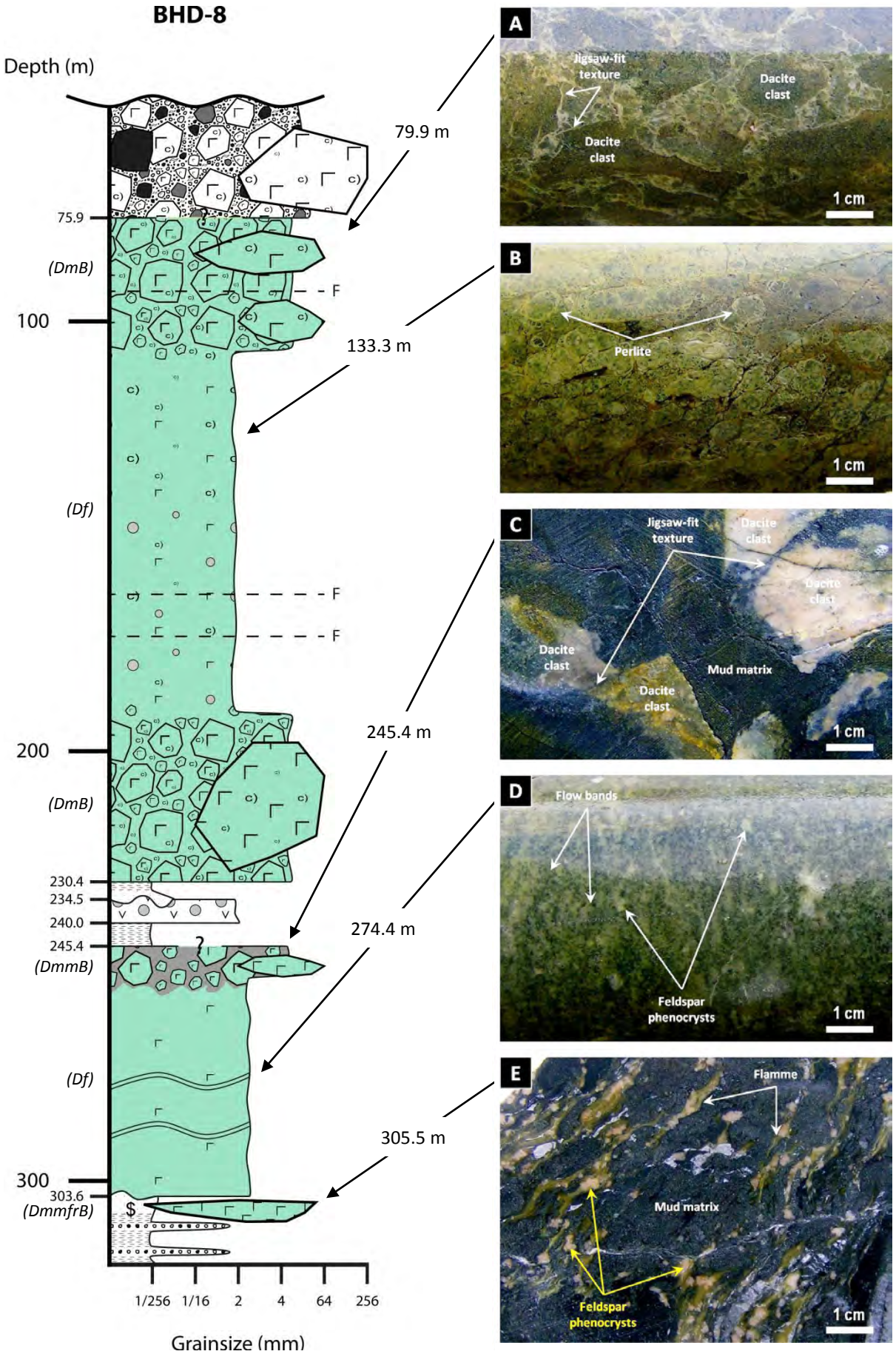
BHD-8
Depth (m)
75.9
(DmB)
100
(Df)
200
(DmB)
230.4
234.5
240.0
245.4
(DmmB)
(Df)
300
303.6
(DmmfrB)
1/256 1/16 2 4 64 256
Grainsize (mm)
79.9 m
133.3 m
245.4 m
274.4 m
305.5 m
A
Jigsaw-fit texture
Dacite clast
Dacite clast
1 cm
B
Perlite
1 cm
C
Jigsaw-fit texture
Dacite clast
Dacite clast
Dacite clast
Mud matrix
Dacite clast
1 cm
D
Flow bands
Feldspar phenocrysts
1 cm
E
Flamme
Mud matrix
Feldspar phenocrysts
1 cm

Figure 3.18: Graphic logs of parts of diamond drill holes SCS-2 and SCS-4 (Sock Creek South area) through facies of the dacite facies association. See Figure 3.4 for legend to graphic log.

SCS-2: The lower part of SCS-2 (123.5-148.5 m) comprises poorly sorted, clast-supported monomictic fiamme-rich dacite breccia (DmfrB), interpreted as autoclastic facies derived from a dacite lava or dome (section 3.3.2.7). Some fiamme have tube vesicle texture. The fiamme were most likely pumice clasts derived from the pumiceous carapace of the lava or dome, and the blocky dacite clasts possibly represent non-vesicular parts of the dacite dome or lava. The mixing of clast types indicates that local transport occurred. The upper part of SCS-2 (89.5-121.5 m) includes monomictic mud-matrix dacite breccia (DmmB) (interpreted as peperite - section 3.3.2.7) overlain by massive to flow-banded coherent feldspar-phyric dacite (Df) intercalated with monomictic dacite breccia (DmB). This interval is interpreted as an extrusive lava or dome (section 3.3.2.7) on the basis of the lower mingled contact, and the weakly normally graded nature of the upper interval of monomictic dacite breccia.

SCS-4: The lower dacite unit (178.6-195.2 m) comprises an upper interval (178.6-181.5 m) of monomictic mud-matrix dacite breccia (DmmB) (interpreted as peperite - section 3.3.2.7) and a lower interval (181.5-195.2 m) of monomictic dacite breccia (DmB) (at the top) and coherent feldspar-phyric dacite (Df) (at the bottom). The spatial association and distribution and the gradational contacts among these facies are consistent with the interpretation of a syn-volcanic intrusion (section 3.3.2.7), probably a sill or a cryptodome. The association of monomictic mud-matrix dacite breccia (DmmB; interpreted as peperite - section 3.3.2.7) and coherent feldspar-phyric dacite (Df) (153.2-157.2 m) and upper mingled contact with mudstone (153.2 m) are consistent with another syn-volcanic intrusion, probably a small dacite lobe related to but separate from the lower intrusive dacite (178.6-195.2 m). The normally graded units of polymictic felsic breccia and sandstone facies (PfB + PfS) (157.2-178.6 m) are interpreted as submarine density current deposits (section 3.2.4.9). They include dacite clasts similar to the underlying and overlying dacitic intrusions, suggesting that the dacite was partly extrusive nearby, and the dacite clasts within the polymictic facies were probably derived from the extrusive lava or dome. The upper dacite interval (128.0-142.8 m) comprises monomictic mud-matrix dacite breccia (DmmB) (at the bottom) overlain by normally graded units of monomictic dacite breccia (DmB) and sandstone (DmS). The presence of monomictic mud-matrix dacite breccia above the lower contact with mudstone is interpreted as resedimented autoclastic dacite breccia emplaced over mud, whereas the overlying normally graded units of monomictic dacite breccia and sandstone are interpreted as resedimented autoclastic facies derived from the upper part of a dacitic lava.

A: SCS-2 (94.6 m) - Matrix-supported monomictic dacite breccia. The matrix comprises finer-grained dacite clasts and feldspar crystals and crystal fragments.

B: SCS-2 (111.0 m) - Feldspar-phyric dacite. Feldspar phenocrysts are conspicuous in the flow-banded domain.

C: SCS-2 (119.0 m) - Poorly sorted monomictic mud-matrix dacite breccia. Dacite clasts are dark green or pink, feldspar-phyric and have curviplanar and irregular margins.

D: SCS-2 (127.2 m) - Monomictic fiamme-rich dacite breccia. Strongly aligned fiamme surround sporadic blocky dacite clasts and include relict tube pumice.

E: SCS-3 (180.7 m) - Monomictic mud-matrix dacite breccia. Jigsaw-fit texture and relict tube pumice occur. Uphole and younging directions: A and E - left to right; B, C and D - right to left.

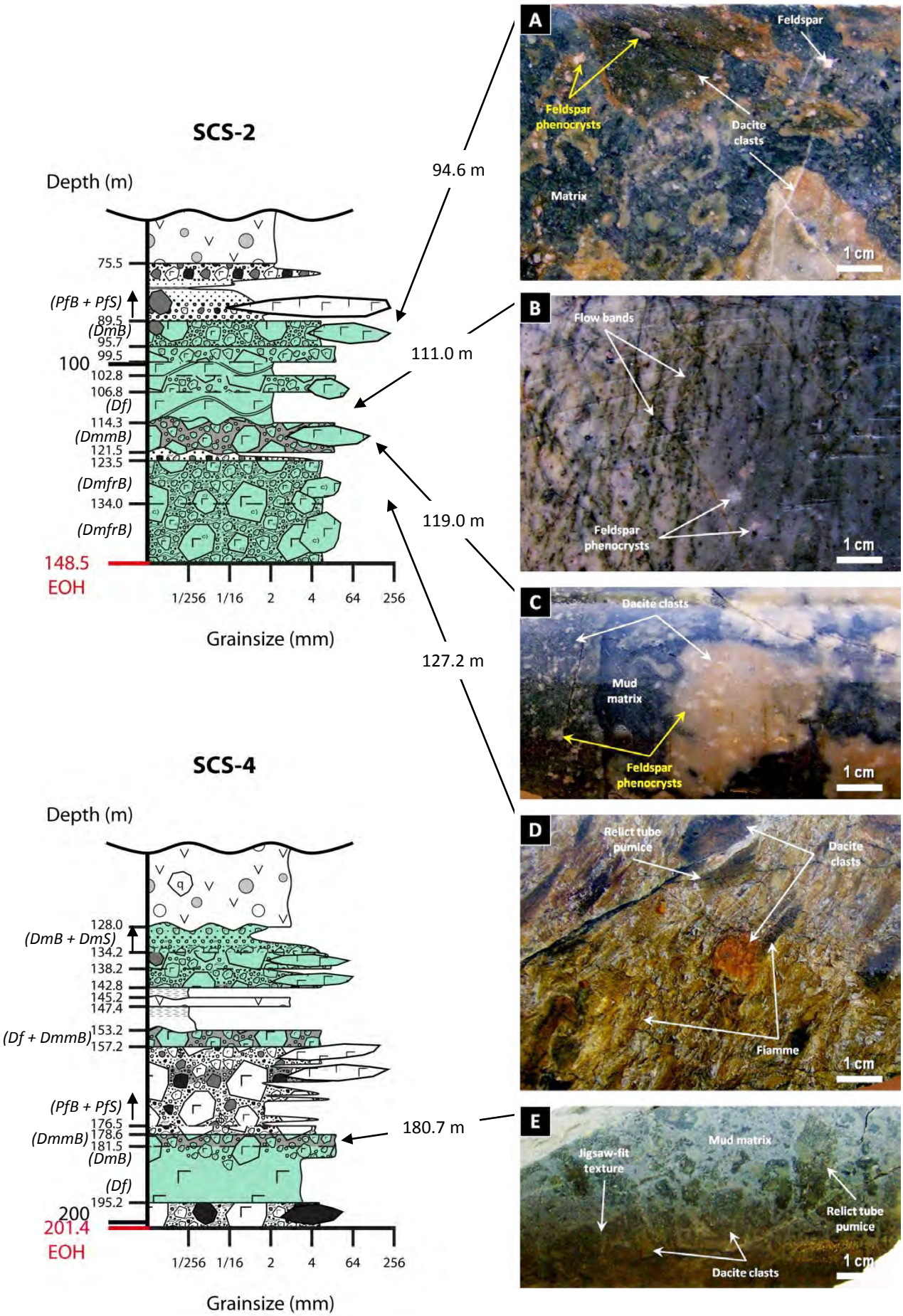
SCS-2
Depth (m)
75.5
(PfB + PfS)
89.5
(DmB)
95.7
99.5
100
102.8
106.8
(Df)
114.3
(DmmB)
121.5
123.5
(DmfrB)
134.0
(DmfrB)
148.5
EOH
1/256 1/16 2 4 64 256
Grainsize (mm)
94.6 m
111.0 m
119.0 m
127.2 m
A
Feldspar
Feldspar phenocrysts
Dacite clasts
Matrix
1 cm
B
Flow bands
Feldspar phenocrysts
1 cm
C
Dacite clasts
Mud matrix
Feldspar phenocrysts
1 cm
SCS-4
Depth (m)
128.0
(DmB + DmS)
134.2
138.2
142.8
145.2
147.4
(Df + DmmB)
153.2
157.2
(PfB + PfS)
176.5
(DmmB)
178.6
181.5
(DmB)
(Df)
195.2
200
201.4
EOH
1/256 1/16 2 4 64 256
Grainsize (mm)
180.7 m
D
Relict tube pumice
Dacite clasts
Flamme
1 cm
E
Jigsaw-fit texture
Mud matrix
Relict tube pumice
Dacite clasts
1 cm

Figure 3.19: Coherent feldspar-phyric dacite facies. A and B: AK-1 (291.6 m); C and D: AK-1 (346.6 m); E to G: BHD-7 (121.2 m); H: SCS-5 (262.7 m); I: BHD-4 (363.5 m); J: BHD-7 (141.9 m); K: SCS-2 (102.3 m); L: SCS-5 (285.9 m). A, C, E, I to L: Handspecimen photographs (uphole and younging direction: A and C - right to left; E and J - left to right; I, K and L - not recorded). B, D, F to H: Photomicrographs (transmitted, plane polarised light).

A and B - Flow-banded coherent feldspar-phyric dacite. Flow bands are represented by wavy, sub-parallel, alternating dark green and pale brown bands. Feldspar phenocrysts are evenly distributed in the groundmass.

C and D: Perlitic coherent feldspar-phyric dacite. Feldspar phenocrysts are evenly distributed and randomly oriented.

E to G: Strongly perlitic, amygdaloidal coherent feldspar-phyric dacite.

E: Elongate, round or irregular, chlorite-filled (dark green) amygdales in perlitic groundmass.

F: Concentrically zoned amygdale (chlorite core and carbonate rim) embedded in a strongly perlitic (classical perlite) groundmass.

G: Quartz-carbonate amygdale.

H: Concentrically zoned feldspar phenocryst (more-altered core and less-altered rim).

I and J: Strongly perlitic, amygdaloidal, coherent weakly feldspar-phyric dacite. I: Classical perlite is > 1 cm in diameter. Amygdales are chlorite-filled (dark green) and quartz-carbonate-filled (white).

J: Banded perlitic fractures are characterized by a roughly rectilinear fracture network (direction: lower left-upper right).

K and L: Flow-banded coherent feldspar-phyric dacite. Intricately folded flow-bands occur (L).

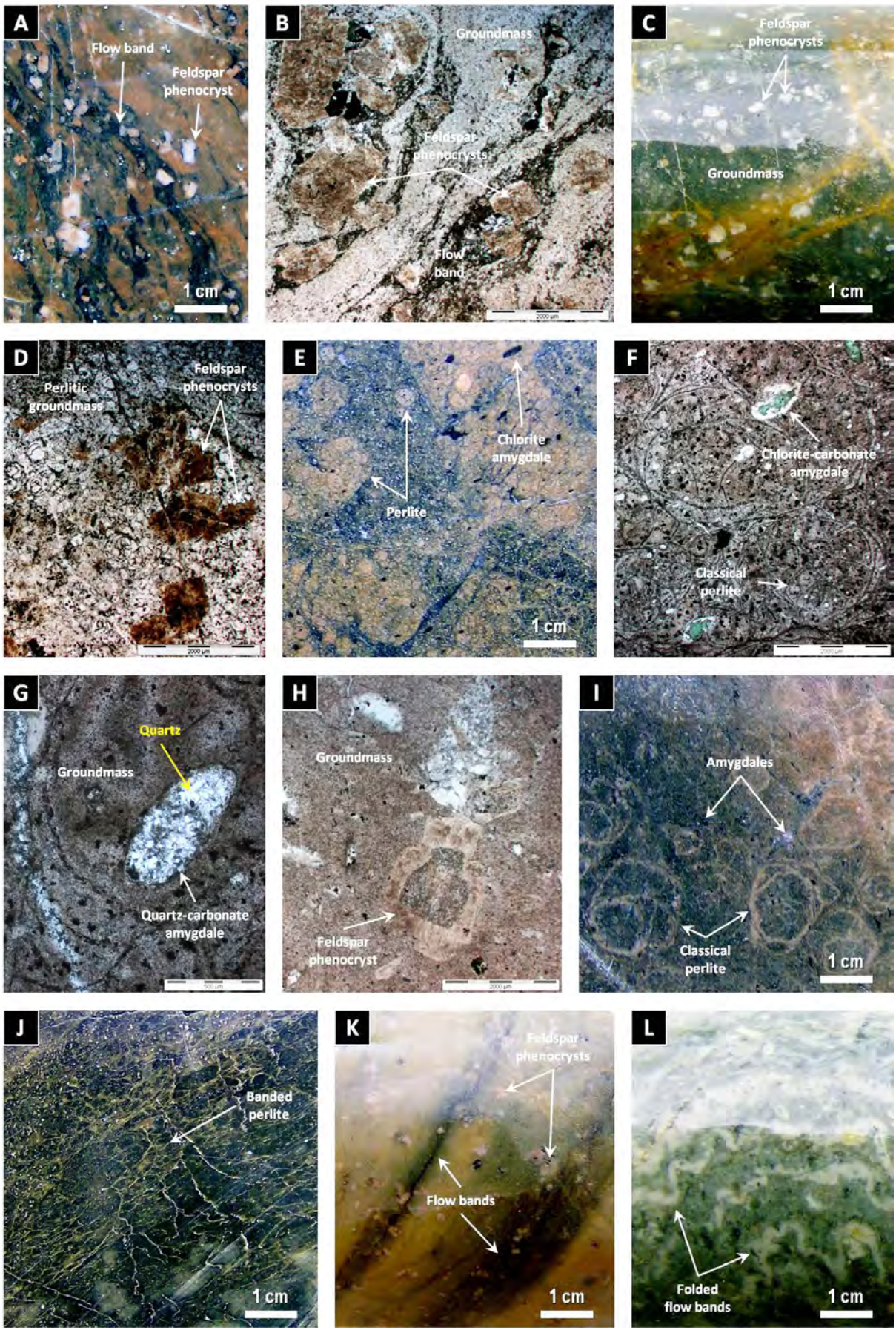
A
Flow band
Feldspar phenocryst
1 cm
B
Groundmass
Feldspar phenocrysts
Flow band
C
Feldspar phenocrysts
Groundmass
1 cm
D
Perlitic groundmass
Feldspar phenocrysts
E
Chlorite amygdale
Perlite
1 cm
F
Chlorite-carbonate amygdale
Classical perlite
G
Quartz
Groundmass
Quartz-carbonate amygdale
H
Groundmass
Feldspar phenocryst
I
Amygdales
Classical perlite
1 cm
J
Banded perlite
1 cm
K
Feldspar phenocrysts
Flow bands
1 cm
L
Folded flow bands
1 cm

Figure 3.20: Monomictic dacite breccia facies. A to E: BHD-9 (181.2 m); F: BHD-8 (105.0 m); G: BHD-4 (288.4 m); H: BOC-6 (59.0 m); I: BOC-6 (196.0 m); J: Boco road (BR vertical section). A, F to J: Handspecimen photographs (uphole and younging direction: A and I - left to right; F and G - right to left; H and J - not recorded). B to E: Photomicrographs (B to D - transmitted, plane polarised light; E - reflected, plane polarised light).

A: Poorly sorted, clast-supported monomictic dacite breccia. Jigsaw-fit texture is visible locally. Dacite clasts are strongly perlitic, and blocky or splintery with curviplanar and irregular edges. The matrix is mainly composed of finer-grained dacite clasts.

B: Aphyric, strongly perlitic dacite clasts in quartz-rich matrix. Dacite clasts have blocky and splintery shapes and curviplanar edges. The matrix is composed of finer-grained dacite clasts (some splintery clasts occur) cemented by quartz, carbonate cement, and chlorite.

C: Perlitic texture (classical perlite) in aphyric dacite clast. Perlitic fractures are filled with very fine-grained phyllosilicates.

D: Feldspar phenocryst in strongly perlitic dacite clast. The feldspar phenocryst is altered to very fine-grained phyllosilicates. A fracture crosscuts dacite clast and the matrix. The matrix contains finer-grained dacite clasts. Local jigsaw-fit texture is visible.

E: Jigsaw-fit and perlitic textures observed in reflected light.

F: Clast-supported monomictic dacite breccia. Jigsaw-fit texture is visible locally. Dacite clasts are predominantly aphyric to weakly feldspar-phyric, non- to weakly amygdaloidal, and typically blocky, elongate and sub-round with curviplanar and irregular margins. The matrix is mainly composed of fine-grained dacite clasts, phyllosilicates and carbonate.

G: Matrix-supported monomictic dacite breccia. The matrix comprises abundant chloritic fragments.

H: Matrix-supported monomictic dacite breccia. The matrix is composed of finer grained dacite clasts and feldspar crystals and crystal fragments. Local clusters of dacite clasts show jigsaw-fit texture.

I: Clast-supported monomictic dacite breccia. Dacite clasts are flow-banded, feldspar-phyric, blocky and sub-round with curviplanar edges. The flow-bands are defined by alternating pale grey and dark green bands.

J: Clast-supported monomictic dacite breccia with jigsaw-fit texture. The dacite clasts have planar and curviplanar margins.

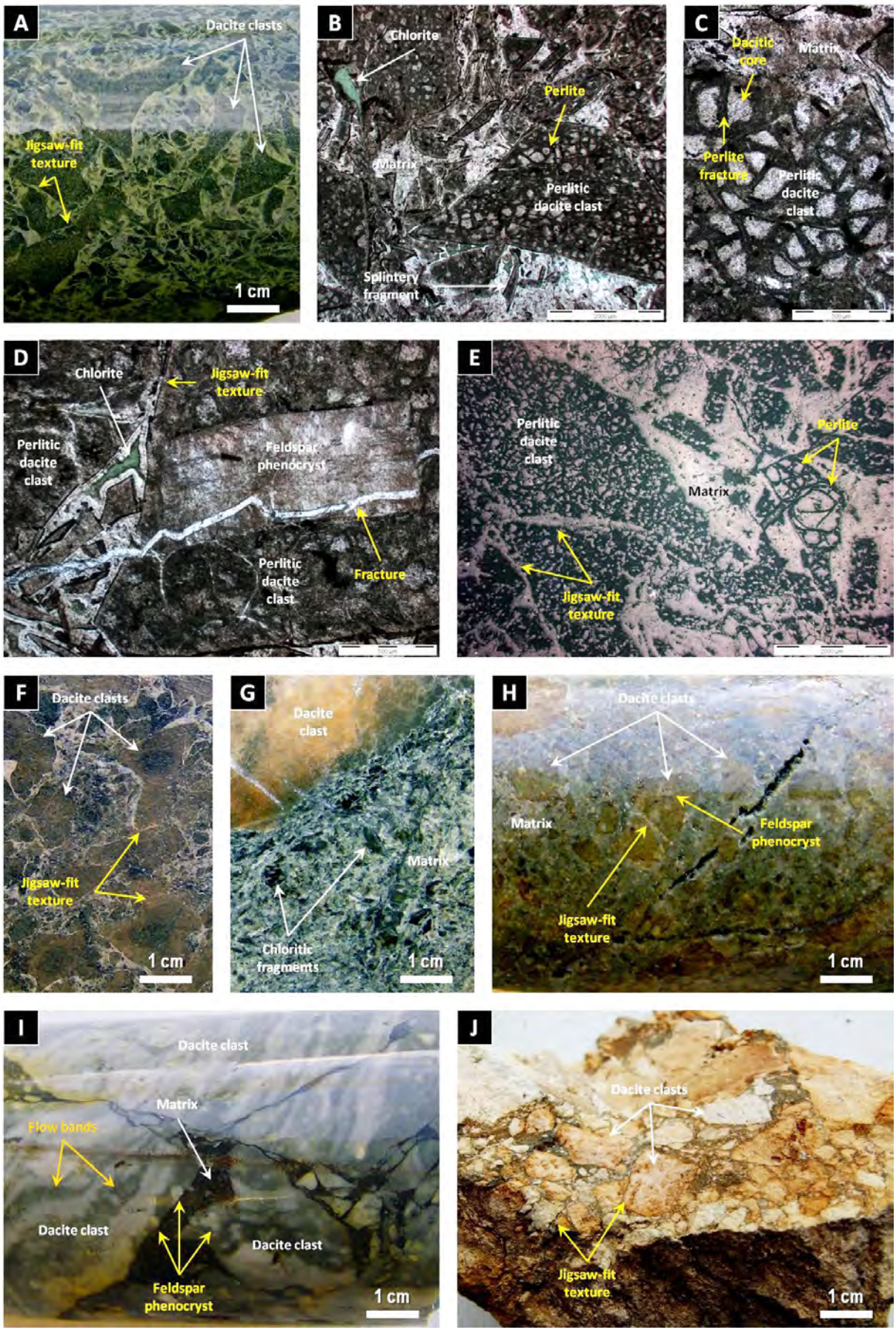
A
Dacite clasts
Jigsaw-fit texture
1 cm
B
Chlorite
Perlite
Matrix
Perlitic dacite clast
Splintery fragment
C
Dacitic core
Matrix
Perlite fracture
Perlitic dacite clast
D
Chlorite
Jigsaw-fit texture
Perlitic dacite clast
Feldspar phenocryst
Perlitic dacite clast
Fracture
E
Perlitic dacite clast
Perlite
Matrix
Jigsaw-fit texture
F
Dacite clasts
Jigsaw-fit texture
1 cm
G
Dacite clast
Matrix
Chloritic fragments
1 cm
H
Dacite clasts
Matrix
Feldspar phenocryst
Jigsaw-fit texture
1 cm
I
Dacite clast
Matrix
Flow bands
Dacite clast
Dacite clast
Feldspar phenocryst
1 cm
J
Dacite clasts
Jigsaw-fit texture
1 cm

and crystal fragments embedded in a very fine-grained cement comprising variable amounts of quartz, carbonate, chlorite, and sericite (Figure 3.20 - B, C, E, H and I). Locally abundant chloritic fragments (up to 20%) are dark green (strongly chloritic), elongate to lenticular, and mainly aphyric to weakly feldspar-phyric. They comprise an important part of the matrix in matrix-supported monomictic dacite breccia domains (Figure 3.20 - G). The phenocryst population of porphyritic chloritic fragments is identical to the dacite clasts. The chloritic fragments are commonly randomly oriented or very locally aligned. Irregular carbonate and quartz veins, leucoxene and disseminated sulfides also occur.

3.3.2.3 Monomictic mud-matrix dacite breccia facies (DmmB)

The monomictic mud-matrix dacite breccia facies occurs from Sock Creek to W of Bulgobac Hill, W of the Murchison Highway, and in the Mackintosh area, E of the Murchison Highway (Figure 3.16). It extends laterally for possibly 5 km discontinuously. This facies is spatially associated with coherent feldspar-phyric dacite, monomictic dacite breccia, monomictic fiamme-rich dacite breccia and monomictic dacite sandstone facies (Table 3.4). Monomictic mud-matrix dacite breccia intervals range from <1 to 7 m thick.

The monomictic mud-matrix dacite breccia facies occurs as single units, and at the margins of intervals or units of monomictic dacite breccia or coherent feldspar-phyric dacite, or interfingered with mudstone and monomictic dacite sandstone and breccia units (Figures 3.17 and 3.18). Within units, upper and lower contacts with coherent feldspar-phyric dacite, monomictic dacite breccia and/or sandstone facies are typically gradational (Figure 3.17; Figure 3.18 - SCS-4). Upper and lower contacts with enclosing units are commonly mingled, sharp and planar or irregular (Figure 3.18 - SCS-2 and SCS-4).

The monomictic mud-matrix dacite breccia facies is similar to the monomictic dacite breccia facies (section 3.3.2.2) in terms of dacite clast characteristics, abundances and distribution, but it is typically matrix-supported and the matrix is composed of massive, variably silicified, homogeneous dark grey to black mudstone (Figure 3.21 - A and B). Domains of dark grey and black mud matrix are locally contorted and/or disrupted. In local clast-supported intervals, the matrix occurs as irregular, wispy, silicified domains of mudstone between dacite clasts. In some intervals of matrix-supported monomictic mud-matrix dacite breccia, isolated or jigsaw-fit clusters of dacite clasts are scattered in the mud matrix (Figure 3.17 - C).

The dacite clasts are blocky to irregular, angular to sub-round and have planar to curviplanar and ragged margins, and are texturally and mineralogically identical to the coherent feldspar-phyric dacite facies (section 3.3.2.1) and dacite clasts within the monomictic dacite breccia facies (section 3.3.2.2). Sporadic chloritic fragments with relict tube vesicle texture (relict tube pumice) occur (Figure 3.18 - E).

3.3.2.4 Monomictic fiamme-rich dacite breccia facies (DmfrB)

The monomictic fiamme-rich dacite breccia facies occurs from Sock Creek to W of Bulgobac Hill, W of the Murchison Highway, and in the Bulgobac Hill area, just E of the Murchison Highway (Figure 3.16). It

extends laterally for possibly 5 km discontinuously. This facies is spatially associated with coherent feldspar-phyric dacite, monomictic dacite breccia, monomictic mud-matrix dacite breccia, monomictic mud-matrix fiamme-rich dacite breccia and monomictic dacite sandstone facies (Table 3.4). Monomictic fiamme-rich dacite breccia intervals range from 1 to 15 m thick.

The monomictic fiamme-rich dacite breccia facies typically occurs as single massive units, or locally at the upper and/or lower margins of coherent feldspar-phyric dacite and monomictic dacite breccia units (Figure 3.18 - SCS-2). Upper and lower contacts with adjacent units are typically sharp and planar or locally gradational.

The monomictic fiamme-rich dacite breccia facies is massive to locally weakly graded, poorly sorted and clast-supported to locally matrix-supported. This facies is similar to the monomictic dacite breccia facies (section 3.3.2.2), but contains abundant (25-80%) aphyric to feldspar-phyric, pale to dark green or brown, strongly chloritised fiamme (Figure 3.18 - D; Figure 3.21 - C to E). Fiamme (2-55 mm) are lensoidal, wispy and irregular-shaped with wavy and irregular margins and flame-like ends (Figure 3.21 - C to E). They form an important part of matrix-supported monomictic fiamme-rich dacite breccia domains. Some intervals of monomictic fiamme-rich dacite breccia facies locally grade into monomictic dacite sandstone facies comprising abundant finer fiamme.

Variable amounts of blocky, sub-angular to sub-round dacite clasts (up to 25%) also occur (Figure 3.21 - D and E), and some are flow-banded or perlitic. Fiamme are commonly smaller than the blocky dacite clasts and preferentially aligned. In many cases, abundant fiamme are strongly aligned but bent around the larger, blocky rhyolite clasts (Figure 3.21 - E). The phenocryst population of the feldspar-phyric fiamme and dacite clasts are very similar to the coherent feldspar-phyric dacite facies (section 3.3.2.1) in terms of abundance and distribution. Sporadic fiamme with relict tube vesicle texture (relict tube pumice) occur (Figure 3.18 - D). Scarce leucoxene, pyritic and feldspar crystal-rich zones occur.

3.3.2.5 Monomictic mud-matrix fiamme-rich dacite breccia facies (DmmfrB)

The monomictic mud-matrix fiamme-rich dacite breccia facies occurs locally at Sock Creek (DDH BHD-8), Sock Creek South (DDH SCS-5) and Bulgobac Hill (DDH AK-1) (Figure 3.16). This facies is spatially associated with monomictic dacite breccia and monomictic fiamme-rich dacite breccia facies (Table 3.4). Intervals of monomictic mud-matrix fiamme-rich dacite breccia range from <1 to 2 m thick. They occur at the margins of monomictic dacite breccia or monomictic fiamme-rich dacite breccia facies, or close to the lower contact of coherent feldspar-phyric dacite facies (Figure 3.17 - E).

The monomictic mud-matrix fiamme-rich dacite breccia facies is similar to the monomictic fiamme-rich dacite breccia facies (section 3.3.2.4) in terms of fiamme characteristics, abundances and distribution, but it is commonly matrix-supported and the matrix is composed of massive, variably silicified, homogeneous, dark grey or black mudstone (Figure 3.21 - F and G). Domains of dark grey and black mud matrix are laminated and laminae are contorted and/or disrupted.

Figure 3.21: A and B: Handspecimen photographs of the monomictic mud-matrix dacite breccia facies.

A: Gradation from fractured coherent feldspar-phyric dacite (Df) to monomictic mud-matrix dacite breccia (DmmB) facies.

B: Dacite clasts are aphyric, perlitic, blocky and sub-angular with curviplanar edges. Clasts are separated by homogeneous black mudstone matrix containing finer-grained aphyric dacite clasts which are variably silicified. Larger dacite clasts have dark green cores and fractured, pale margins. C to E: Handspecimen photographs of the monomictic fiamme-rich dacite breccia facies.

C: Strongly chloritic fiamme.

D: Clast-supported monomictic fiamme-rich dacite breccia. The dacite clasts are perlitic and have pink cores and pale green to dark brown margins. They are separated by abundant pale to dark brown fiamme.

E: Very poorly sorted, clast-supported monomictic fiamme-rich dacite breccia. Dacite clasts are aphyric to weakly feldspar-phyric and typically blocky, elongate, and locally wispy. They are separated by very abundant dacitic fiamme that are bent around the dacite clasts.

F and G: Handspecimen photographs of the monomictic mud-matrix fiamme-rich dacite breccia facies.

F and G: Monomictic mud-matrix fiamme-rich dacite breccia. Dacitic fiamme are chlorite-rich (pale to dark green) and range from aphyric to moderately feldspar-phyric. The mud-matrix is pale to dark grey. Mud-matrix domains typically have wavy outlines and are massive to internally laminated and laminae are contorted.

A: BHD-4 (241.0 m); B: BHD-8 (251.9 m); C: BOC-6 (150.7 m); D: SCS-3 (143.0 m); E: SCS-5 (162.3 m); F: AK-1 (442.9 m); G: SCS-5 (166.8 m). Uphole and younging direction: A, B, E to G - left to right; C and D - right to left.

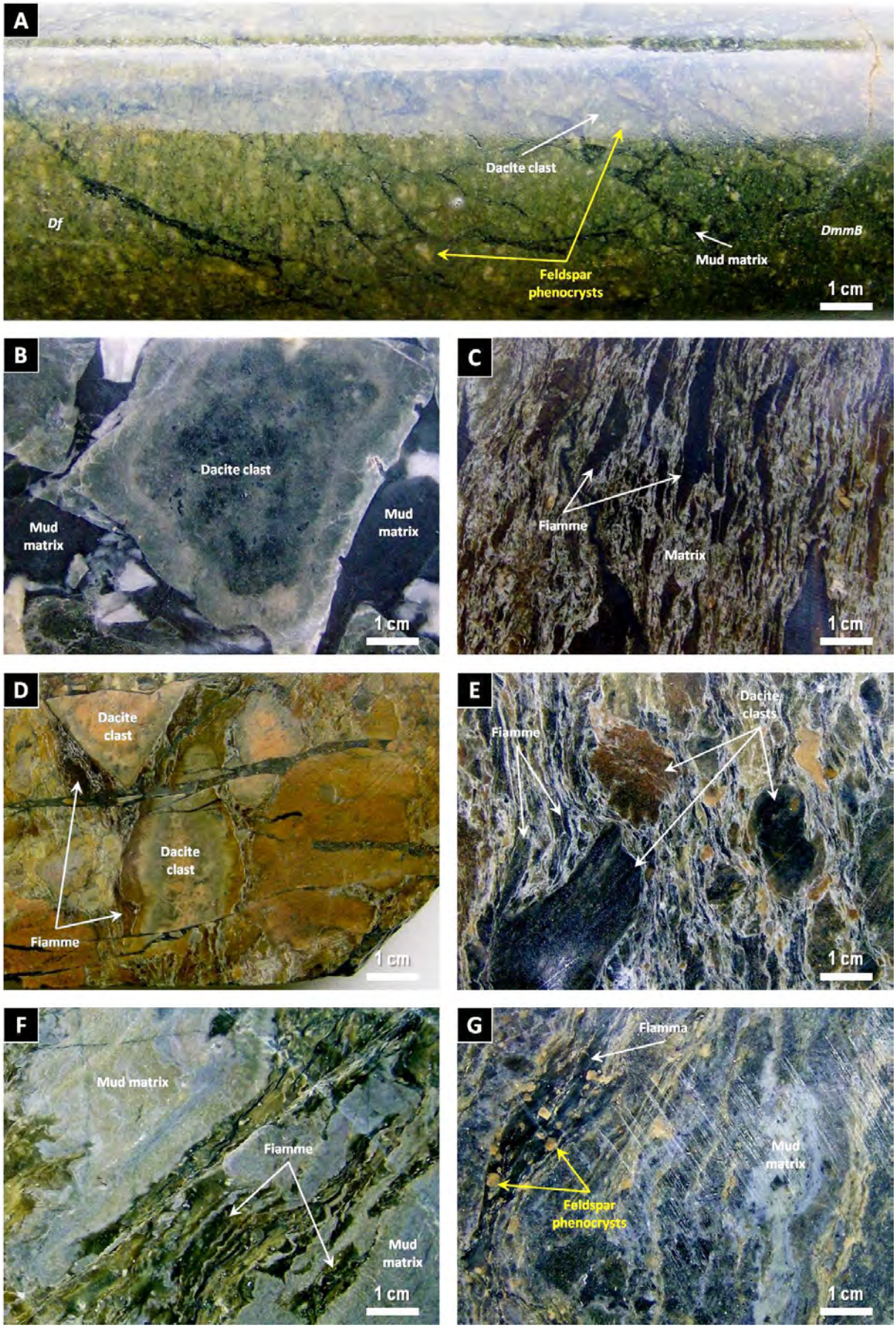
A
Dacite clast
Df
DmmB
Mud matrix
Feldspar phenocrysts
1 cm
B
Dacite clast
Mud matrix
Mud matrix
1 cm
C
Fiamme
Matrix
1 cm
D
Dacite clast
Dacite clast
Fiamme
1 cm
E
Fiamme
Dacite clasts
1 cm
F
Mud matrix
Fiamme
Mud matrix
1 cm
G
Flamma
Mud matrix
Feldspar phenocrysts
1 cm

3.3.2.6 Monomictic dacite sandstone facies (DmS)

The monomictic dacite sandstone facies occurs locally in the Bulgobac Hill, Boco, Mount Charter and Sock Creek South areas (Figure 3.16). Its lateral extent may be in the order of 1.2 km in the Sock Creek South area. This facies is spatially associated with coherent feldspar-phyric dacite, monomictic dacite breccia, monomictic mud-matrix dacite breccia and monomictic fiamme-rich dacite breccia facies (Table 3.4). Intervals of monomictic dacite sandstone range from <1 to 5 m thick.

This facies occurs in normally graded intervals comprising monomictic dacite sandstone at the base and mudstone at the top, in the middle of normally graded units comprising monomictic dacite breccia at the base and mudstone at the top (Figure 3.18 - SCS-4), and locally as single massive units of monomictic dacite sandstone. This facies also occurs at the base of units comprising monomictic dacite breccia and sandstone at the base, monomictic fiamme-rich dacite breccia in the middle and monomictic mud-matrix fiamme-rich dacite breccia at the top. Contacts with adjacent intervals of monomictic dacite breccia, monomictic mud-matrix dacite breccia or monomictic fiamme-rich dacite breccia facies are gradational (Figure 3.18 - SCS-4), and contacts with adjacent units are sharp and planar.

The monomictic dacite sandstone facies is massive or weakly bedded (locally laminated), commonly normally graded and well to moderately sorted. This facies is very similar to the monomictic dacite breccia facies (section 3.3.2.2), but it is finer grained. It may contain chloritic fragments (<10%, <30 mm), which are identical to the chloritic fragments within monomictic dacite breccia facies (Figure 3.20 - G). It also comprises feldspar crystals and crystal fragments (5-25%, 0.2-2.5 mm). Monomictic dacite sandstone intervals may include disseminated sulfides.

3.3.2.7 Interpretation

Most facies of the dacite facies association are very similar to the facies of the rhyolite facies association (section 3.3.1) and are interpreted in the same way. Intervals of monomictic dacite breccia comprising blocky dacite clasts with planar and curviplanar edges and jigsaw-fit texture (Figure 3.17 - A) are interpreted as in situ hyaloclastite produced by quench fragmentation of coherent feldspar-phyric dacite (cf. Pichler, 1965). Local intervals of monomictic dacite breccia that do not show jigsaw-fit texture and comprise flow-banded, angular to sub-round dacite clasts are interpreted as autobreccia (cf. Fisher, 1960). The elongate to lenticular shapes of locally abundant chloritic fragments in domains on matrix-supported monomictic dacite breccia (Figure 3.20 - G) are probably the result of locally higher shear stress during flowage of dacite lava.

Local intervals of clast-rotated and normally graded monomictic dacite breccia that grade into monomictic dacite sandstone (Figure 3.18 - SCS-4) are consistent with extrusion of the dacite and suggest that some quench-fragmented and/or autobrecciated dacite was resedimented down slope, possibly contemporaneous with growth of the associated feldspar-phyric dacite dome or lava flow. The monomictic dacite sandstone facies is interpreted as a distal product of resedimentation of autoclastic facies (Figure 3.18 - SCS-4).

The monomictic mud-matrix dacite breccia facies (Figures 3.17 and 3.18) is interpreted as peperite (White et al., 2000). Perlitic fractures in some dacite clasts within both jigsaw-fit and clast-rotated monomictic dacite breccia and monomictic mud-matrix dacite breccia reflect the original glassy nature of these clasts (Ross and Smith, 1955), and suggest rapid cooling by contact with water or wet sediment in a subaqueous environment. Larger dacite clasts have partly fragmented, perlitic, pale grey or green margins and broad, intact, dark green cores (Figure 3.18 - A; Figure 3.20 - F) were possibly chilled when in contact with water or wet unconsolidated mud.

The monomictic fiamme-rich dacite breccia is very similar to the monomictic fiamme-rich rhyolite breccia in the Burns Peak area (section 3.3.1.9), and is interpreted in the same way. Strongly aligned fiamme within the monomictic fiamme-rich dacite breccia facies (Figure 3.18 - D; Figure 3.21 - C) are interpreted as former vesicular dacite fragments (pumice) that have been mechanically compacted during diagenesis (Peterson, 1979; Allen, 1988; Branney and Sparks et al., 1990). Sporadic, blocky dacite clasts within the monomictic fiamme-rich dacite breccia facies (Figure 3.18 - D; Figure 3.21 - D and E) most likely represent non-vesicular fragments of feldspar-phyric dacite that resisted diagenetic compaction. Local intervals of massive to weakly normally graded monomictic fiamme-rich dacite breccia (Figure 3.18 - SCS-2) are consistent with local resedimentation of pumiceous autobreccia and/or hyaloclastite forming the pumiceous carapace of an emergent dome or lava.

The monomictic mud-matrix fiamme-rich dacite breccia facies (Figure 3.17 - E; Figure 3.21 - F and G) comprises characteristics of both monomictic fiamme-rich dacite breccia and monomictic mud-matrix dacite breccia facies. It typically occurs at irregular, mingled upper or lower contacts of coherent dacite and/or monomictic dacite breccia intervals associated with intervals of mudstone (Figure 3.17). The mud matrix is massive and the fiamme are commonly strongly aligned and sub-parallel. These features are all consistent with the interpretation of the monomictic mud-matrix fiamme-rich dacite breccia facies as pumiceous peperite or intrusive hyaloclastite (e.g., Gifkins et al., 2002) formed where pumiceous coherent feldspar-phyric dacite locally encountered unconsolidated, possibly wet mud. The pumice clasts were later mechanically compacted during diagenesis.

3.3.3 Mafic facies association

The mafic facies association comprises nine facies: 1) coherent feldspar-pyroxene-phyric mafic facies, 2) coherent feldspar-phyric mafic facies, 3) coherent aphyric mafic facies, 4) monomictic mafic breccia, 5) monomictic mud-matrix mafic breccia, 6) monomictic fluidal-clast mafic breccia, 7) monomictic mafic sandstone, 8) polymictic mafic breccia, and 9) polymictic mafic sandstone. The location of the diamond drill holes intersecting facies of the mafic facies association is shown in Figures 3.22 and 3.23. The characteristics of the facies comprising the mafic facies association are summarized in Table 3.5.

The term “mafic” is used here for basalts and andesites for simplicity. A colour criterion was used to discriminate basalts from andesites when logging drill core; darker colours (e.g., grey or dark green) were logged as basalt, whereas paler colours (e.g., pale grey or green) were logged as andesite. The symbols used in

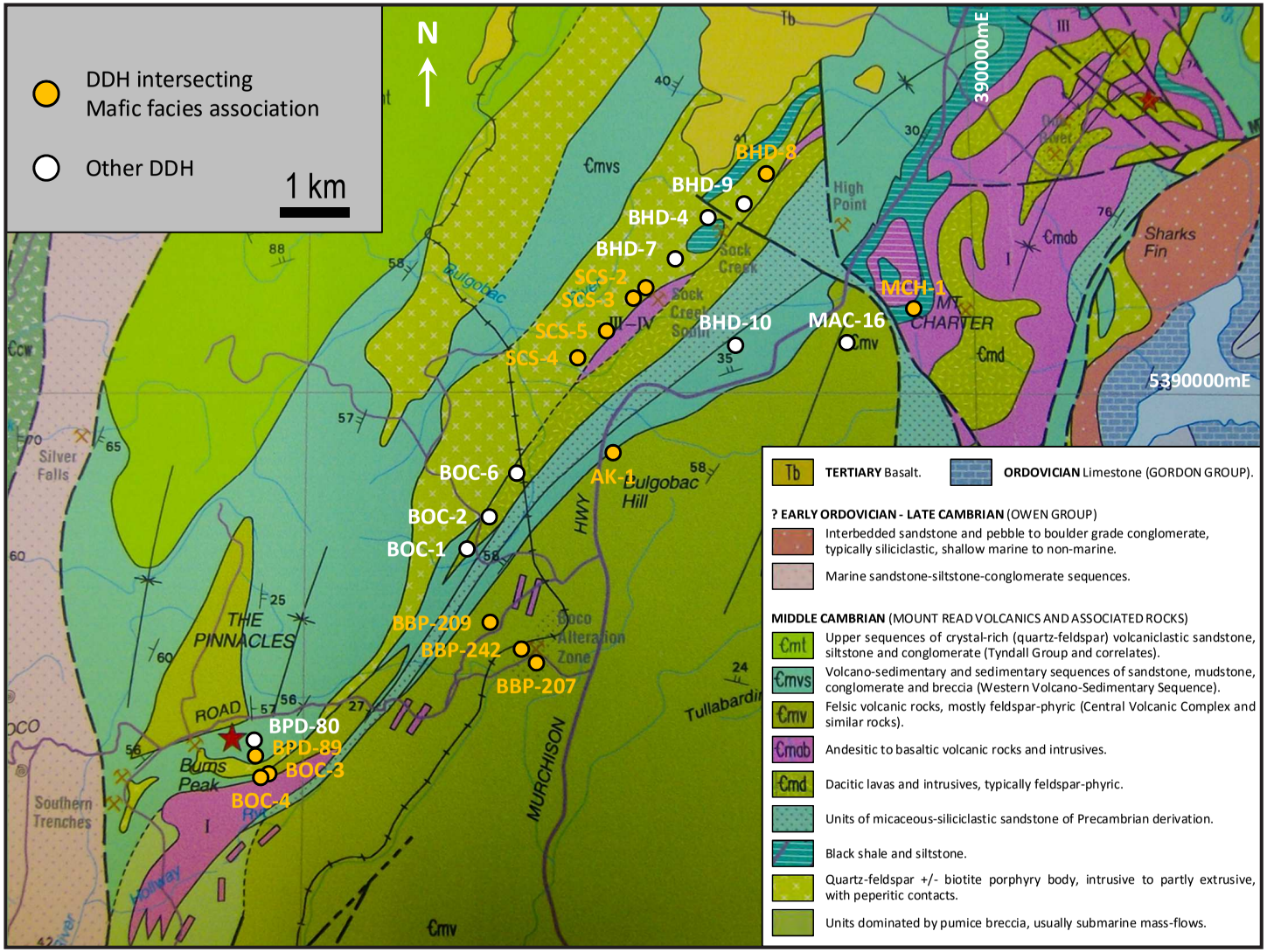

Figure 3.22: Geology of the Que River-Burns Peak area showing the location of the diamond drill holes (DDH) in this study, after Corbett (2002a). Facies of the mafic facies association (M) are intersected by DDH AK-1 (Bulgobac Hill area), BBP-207, BBP 209 and BBP-242 (Boco Alteration Zone area), BHD-8 (Sock Creek area), BOC-3, BOC-4 and BPD-89 (Burns Peak area), MCH-1 (Mount Charter area), and SCS-2, SCS-3, SCS-4 and SCS-5 (Sock Creek South area).

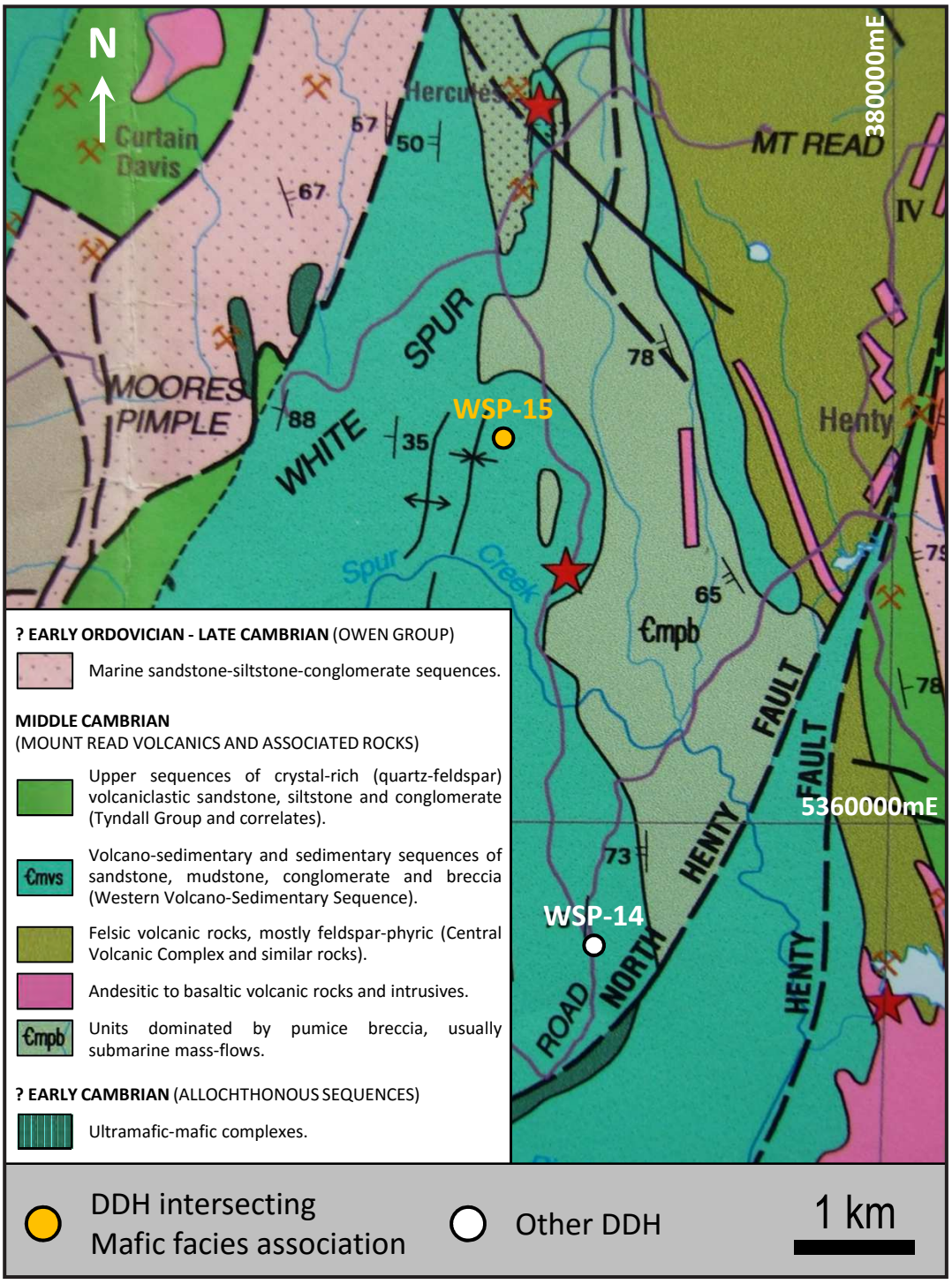

Figure 3.23: Geology of the White Spur-Howards Road area showing the location of the diamond drill holes (DDH) in this study, after Corbett (2002a). Facies of the mafic facies association (M) are intersected by DDH WSP-15 (White Spur area).

Table 3.5: Characteristics, location and interpretation of the facies comprising the mafic facies association.

Facies association, facies and sub-facies		Lithofacies characteristics	Thickness x lateral extent	Mineralogy/Components	Textures	Associated facies	Location and diamond drill holes	Interpretation
Mafic facies association (M)	*Coherent feldspar-pyroxene-phyric mafic facies* ***(Mfp)***	Massive; locally fractured	1-52 m x 1325 m (continuously) (Sock Creek South area)	Feldspar phenocrysts and glomerocrysts (2-10%; 0.2-6 mm); pyroxene phenocrysts (3-15%; 0.2-2 mm)	Weakly to moderately porphyritic and glomeroporphyritic; amygdaloidal; locally vesicular	MmB; MmmB; (Mud)	Bulgobac Hill: **AK-1**; Boco Alteration Zone: **BBP-209, BBP-242**; Burns Peak: **BOC-3, BOC-4**; Sock Creek South: **SCS-2, SCS-3, SCS-4, SCS-5**	Coherent facies of lavas; dykes and/or sills
	Coherent feldspar-phyric mafic facies ***(Mf)***	Massive; locally fractured	<1-58 m x 100 m (continuously) (Burns Peak area)	Feldspar phenocrysts and glomerocrysts (<1-30%; 0.7-5 mm)	Weakly to strongly porphyritic and glomeroporphyritic; amygdaloidal; locally vesicular	MmB; MmmB; MmfcB; MpB; (Mud)	Bulgobac Hill: **AK-1**; Boco Alteration Zone: **BBP-207, BBP-242**; Sock Creek: **BHD-8**; Burns Peak: **BOC-3, BOC-4, BPD-89**; Mount Charter: **MCH-1**	Coherent facies of lavas; dykes and/or sills
	Coherent aphyric mafic facies ***(Ma)***	Massive; locally fractured	<1-44 m x ? m	Feldspar (20-35%; <0.1-0.8 mm), pyroxene (15-40%; <0.1-0.5 mm), chlorite (10-35%; <0.1-0.2 mm), sericite (10-15%; <0.1 mm), and carbonate (3-15%; <0.1 mm).	Aphyric; amygdaloidal; locally vesicular	MmB; MpS; (Mud)	Bulgobac Hill: **AK-1**; Boco Alteration Zone: **BBP-209, BBP-242**; Burns Peak: **BOC-4**; Mount Charter: **MCH-1**; White Spur: **WSP-15**	Coherent facies of lavas; dykes and/or sills
	Monomictic mafic breccia facies ***(MmB)***	Massive to locally normally graded. Poorly sorted, clast-supported (jigsaw-fit) to matrix-supported (clast-rotated)	<1-20 m x 100 m (continuously) (Burns Peak area)	Angular to sub-angular or sub-round, blocky to splintery mafic clasts with planar and curviplanar or irregular margins. Feldspar (and pyroxene) crystal fragments. Carbonate-, sericite- and chlorite-bearing cement.	Feldspar-pyroxene-phyric, feldspar phyric or aphyric, and massive to strongly amygdaloidal mafic clasts. Some mafic clasts are zoned.	Mfp; Mf; Ma; MmmB; MmfcB; MmS; MpB; MpS; (Mud)	Boco Alteration Zone: **BBP-242**; Burns Peak: **BOC-3, BOC-4, BPD-89**; Mount Charter: **MCH-1**	In situ and clast-rotated hyaloclastite
	Monomictic mud-matrix mafic breccia facies ***(MmmB)***	Massive; poorly sorted, clast-supported (jigsaw-fit) to locally matrix-supported (clast-rotated). Black to dark grey mud matrix	<1-26m x ? m	Angular to sub-angular, blocky to splintery mafic clasts with planar and curviplanar margins. Feldspar (and pyroxene) crystal fragments.	Feldspar-pyroxene-phyric or feldspar-phyric, and massive to amygdaloidal mafic clasts. Some mafic clasts are zoned.	Mfp; Mf; MmB; MmfcB; MmS; (Mud)	Sock Creek South: **SCS-5**; Burns Peak: **BOC-3, BPD-89**; Mount Charter: **MCH-1**	Peperite
	Monomictic fluidal-clast mafic breccia facies ***(MmfcB)***	Poorly sorted, clast-supported; internally massive	8-74 m x 100 m (continuously) (Burns Peak area)	Ovoid, amoeboid and highly contorted fluidal mafic clasts (<20%, 2-25 cm) and blocky, splintery, angular to sub-angular mafic clasts (<80%, <1-5 cm).	Aphyric, non- to strongly amygdaloidal mafic clasts. Amygdale grading in fluidal clasts.	Mf; MmB; MmmB; MpB	Burns Peak: **BOC-3, BOC-4**	Subaqueous lava fountaning
	Monomictic mafic sandstone facies ***(MmS)***	Massive to locally laminated and weakly bedded; normally graded; well to moderately sorted	<1-28 m x ? m	Sub-angular or round, blocky mafic clasts. Feldspar crystals and crystal fragments. Carbonate-, sericite- and chlorite-bearing cement.	Feldspar-phyric and aphyric, massive to amygdaloidal mafic clasts.	Mf; MmB; MmmB; (Mud)	Burns Peak: **BOC-3, BPD-89**; Mount Charter: **MCH-1**	Distal resedimented autoclastic deposits
	Polymictic mafic breccia facies ***(MpB)***	Massive to normally graded; poorly sorted; clast- to matrix-supported	<1-2 m x ? m	Sub-angular to round mafic clasts. Sub-round, massive, homogeneous, pink to cream lithic clasts (1-3%; <5 cm). Feldspar crystals and crystal fragments	Feldspar-phyric and aphyric, non- to moderately amygdaloidal mafic clasts	Mf; MmB; MmfcB; MpS	Burns Peak: **BOC-4**	Submarine high-concentration density current deposits
	Polymictic mafic sandstone facies ***(MpS)***	Massive to locally laminated and weakly bedded; normally graded; well to moderately sorted	<1-5 m x ? m	Sub-angular to round mafic clasts. Sub-round, massive, homogeneous, pink to cream lithic clasts (1-3%; <2 mm). Feldspar crystal-rich domains (<10 %). Micaceous.	Feldspar-phyric and aphyric, non- to moderately amygdaloidal mafic clasts	Mf; MmB; MpB	Burns Peak: **BOC-4**; Mount Charter: **MCH-1**	Submarine high-concentration density current deposits

drill core logs (Figure 3.4) follow this criterion. Discriminating between basalt and andesite in handspecimen and thin-section is difficult, and using colour alone as a criterion may be unreliable, but it was not possible to analyse all the relevant samples. The terms "basalt" and "andesite" are used where whole-rock compositional data are available (Figure 3.1; Table 3.2).

3.3.3.1 Coherent feldspar-pyroxene-phyric mafic facies (Mfp)

The coherent feldspar-pyroxene-phyric mafic facies occurs from Sock Creek South to Burns Peak (Figure 3.22). In the Sock Creek South area, it extends laterally for at least 1325 m continuously. This facies is spatially associated with monomictic mafic breccia and monomictic mud-matrix mafic breccia facies (Table 3.5). Coherent feldspar-pyroxene-phyric mafic intervals range from 1 to 52 m thick.

This facies occurs as single coherent units, and in combination with monomictic mafic breccia facies (Figure 3.24). Upper and lower contacts with monomictic mafic breccia and monomictic mud-matrix mafic breccia are gradational. Upper and lower contacts with adjacent units are typically sharp. Single coherent units have tabular geometry and cross-cut stratigraphy (Figure 3.24).

The coherent feldspar-pyroxene-phyric mafic facies (Figure 3.25) is weakly to moderately porphyritic, typically massive and amygdaloidal, and dark green, brown or grey. Feldspar phenocrysts (2-10%; 0.2-6 mm) are euhedral to subhedral, tabular or irregular and elongate, typically twinned, commonly zoned with more-altered cores and less-altered rims, and weakly to strongly altered to sericite, chlorite and/or carbonate (Figure 3.25 - F). Feldspar glomerocrysts are common. Pyroxene phenocrysts (3-15%; 0.2-2 mm) are euhedral to subhedral, prismatic, typically twinned, fractured, commonly zoned and weakly to strongly altered to chlorite or any combination of chlorite, sericite and carbonate (Figure 3.25 - C, G, J and K). They may contain chromite inclusions (1-3%, <0.2 mm).

Olivine phenocrysts (2-5%; 0.2-2.5 mm) may occur (Figure 3.25 - J). They typically preserve original subhedral, six-sided, diamond or prismatic shapes and a single pointy edge. Olivine phenocrysts are typically extremely altered to any combination of chlorite, sericite and carbonate; some have chloritic rims and sericite-carbonate-rich cores. They may also contain chromite inclusions.

In amygdaloidal mafic intervals, amygdales (5-15%, 0.1-30 mm) are circular, oval, elongate, and irregular to amoeboid or multi-globular due to vesicle coalescence (Figure 3.25 - C, E, and H). Amygdales are typically polycrystalline, concentrically zoned, and filled by combinations of quartz, carbonate, chlorite and sericite in radial and concentric arrays. Carbonate amygdales (3-15%, 0.2-30 mm) are white to pale yellow, larger and more abundant than quartz (8%, 0.1-10 mm), chlorite (1-5%, 0.1-10 mm) or sericite (2%, 0.1-1.5 mm) amygdales (Figure 3.25 - E).

The groundmass (60-85%) is predominantly composed of interlocking, fine-grained feldspar and pyroxene with variable amounts of chlorite, sericite, carbonate and quartz (Figure 3.25 - D, F to H, and J). Feldspar is commonly more abundant than pyroxene. Feldspar and pyroxene crystals are very similar to phenocrysts, but

Figure 3.24: Two graphic logs of diamond drill hole SCS-3 and part of diamond drill hole SCS-5 (Sock Creek South area) through facies of the mafic facies association. See Figure 3.4 for legend to graphic log. The distance between diamond drill holes is approximately 625 m.

SCS-5: The upper (53.4-105.8 m; basalt; Figure 3.1; Table 3.2) and middle (147.2-153.2 m; andesite or basalt; Figure 3.1; Table 3.2) mafic units comprise amygdaloidal coherent feldspar-pyroxene-phyric mafic facies (Mfp), have sharp upper contacts and tabular geometry, and occur between unrelated volcaniclastic units. These mafic units are interpreted as sills. The lower mafic unit (379.4-402.7 m; andesite or basalt; Figure 3.1; Table 3.2) occurs between mudstone intervals, and comprises a lower, thicker interval of coherent feldspar-pyroxene-phyric mafic facies (Mfp) and an upper, thinner interval of monomictic mud-matrix mafic breccia (MmmB), which is interpreted as peperite (section 3.3.3.10). The top contact is mingled. These observations are consistent with the interpretation of the lower mafic unit as a syn-volcanic intrusion, probably a sill.

SCS-3: The amygdaloidal and vesicular coherent feldspar-pyroxene-phyric mafic (Mfp) unit (49.9-85.7 m) is very similar to the upper mafic unit in SCS-5. It occurs between volcaniclastic units, and has tabular geometry and an upper sharp and planar contact. This mafic unit is interpreted as a sill. It includes mudstone clasts near the lower contact, possibly included in the mafic facies during intrusion.

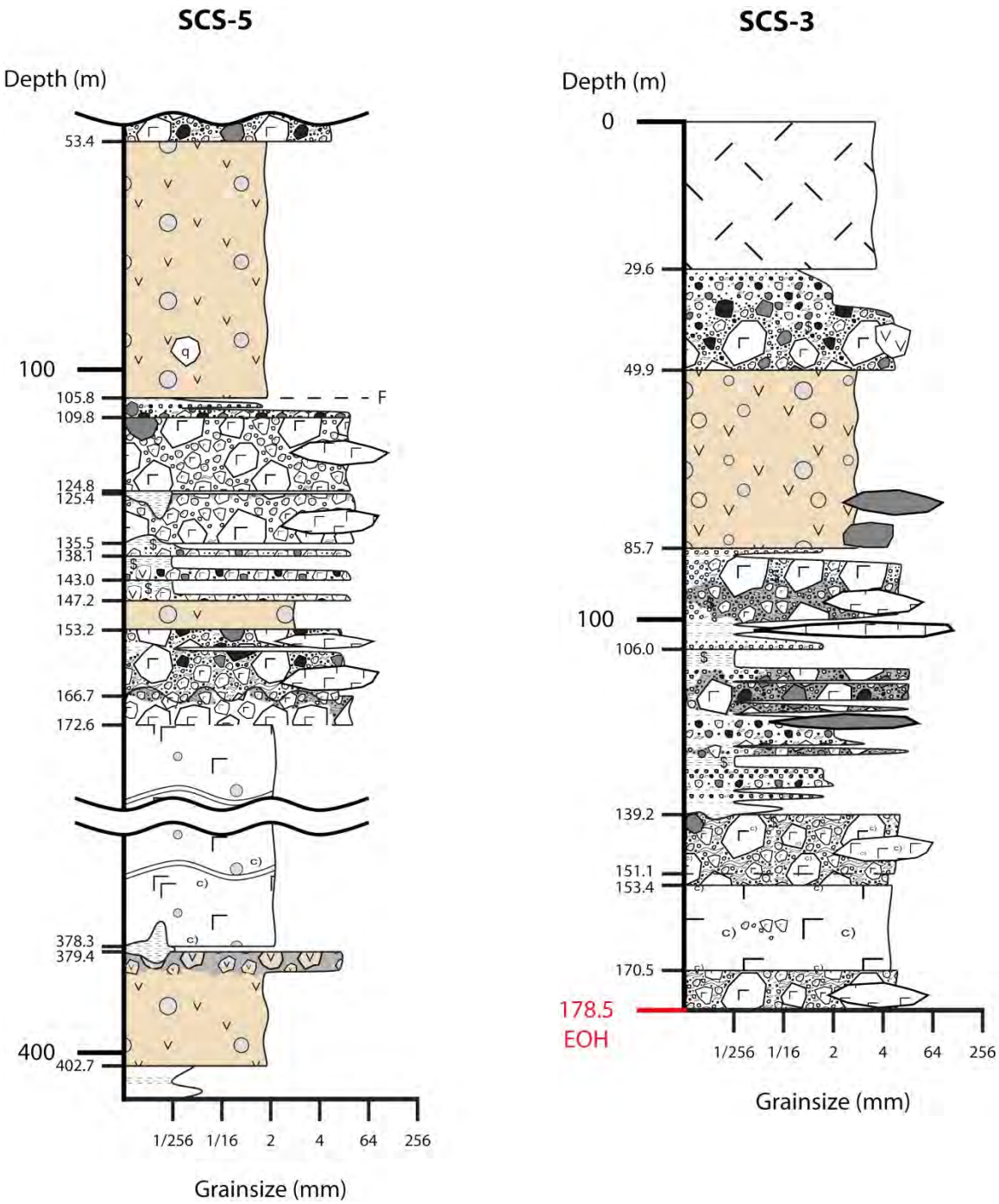
SCS-5
Depth (m)
53.4
100
105.8
109.8
F
124.8
125.4
135.5
138.1
143.0
147.2
153.2
166.7
172.6
378.3
379.4
400
402.7
1/256 1/16 2 4 64 256
Grainsize (mm)
SCS-3
Depth (m)
0
29.6
49.9
85.7
100
106.0
139.2
151.1
153.4
170.5
178.5
EOH
1/256 1/16 2 4 64 256
Grainsize (mm)

Figure 3.25: Coherent feldspar-pyroxene-phyric mafic facies. A and E: Handspecimen photographs (uphole and younging directions: A - right to left; E - not recorded). B to D, F to K: Photomicrographs (B to D, and G - transmitted, cross polarised light; F, H to K - transmitted, plane polarised light). A to D: SCS-5 (96.3 m); E to H: SCS-3 (84.4 m); I and J: SCS-4 (117.5 m); K: SCS-5 (397.0 m).

A to D: Coherent feldspar-pyroxene-phyric basalt (Figure 3.1; Table 3.2).

A: A large quartz xenocryst occurs.

B: Fractured, embayed quartz xenocryst surrounded by a thin rim of very fine-grained pyroxene.

C: Abundant pyroxene phenocrysts are commonly twinned. Feldspar phenocrysts (centre left) and carbonate amygdales (upper left) occur.

D: Feldspar lath-rich groundmass.

E: Strongly amygdaloidal feldspar-pyroxene-phyric mafic facies. Carbonate (white-cream) amygdales are larger and more abundant than chlorite (dark green) amygdales.

F: Subhedral, zoned feldspar phenocryst surrounded by feldspar-rich groundmass.

G: Twinned, fractured, euhedral pyroxene phenocryst.

H: Chlorite amygdales. Some chlorite amygdales (lower left) have multi-globular shapes due to vesicle coalescence.

I: Embayed quartz xenocrysts and pyroxene phenocrysts.

J: Pseudomorphs of olivine and pyroxene phenocrysts.

K: Euhedral (octagonal) pyroxene phenocryst.

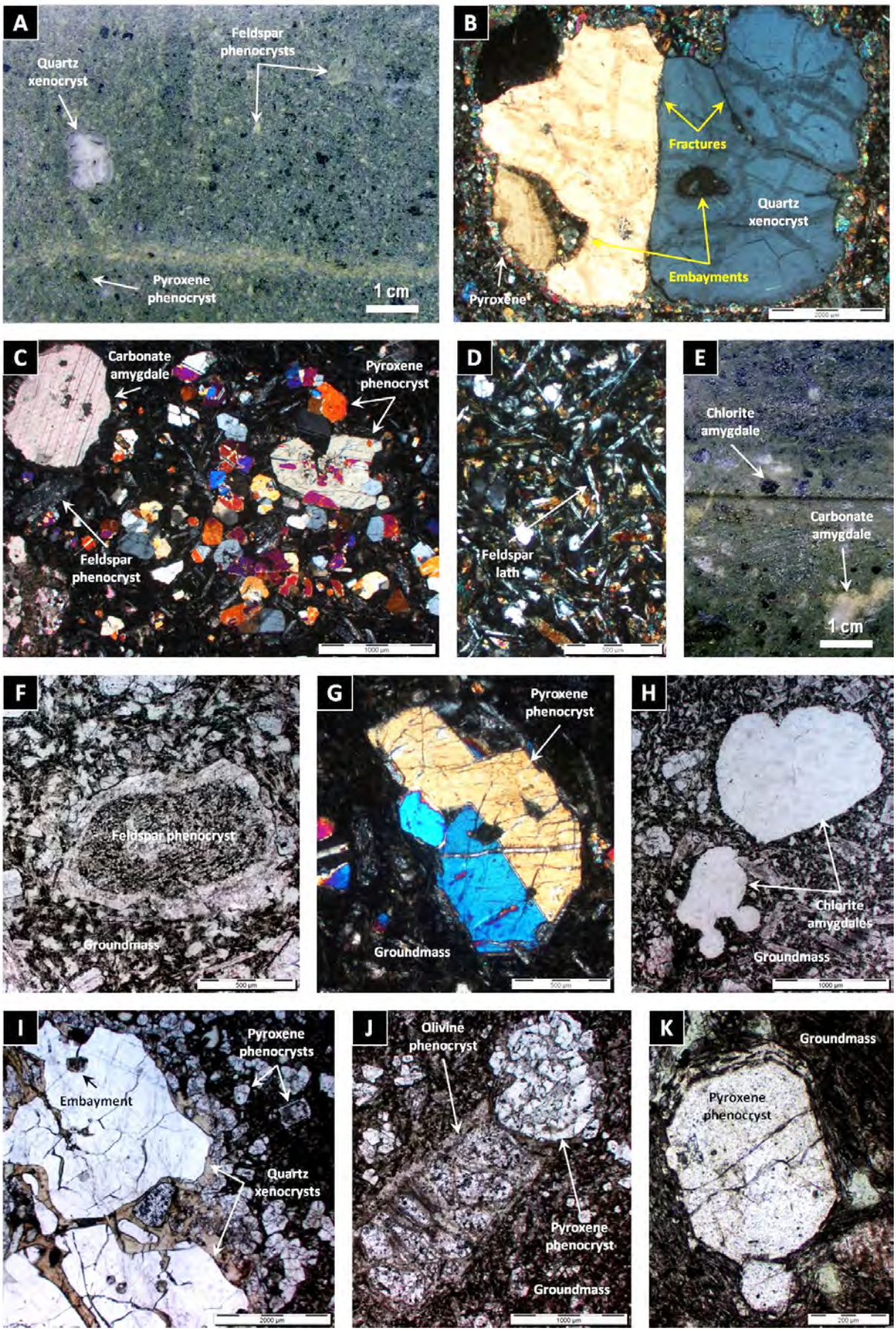
A
Quartz xenocryst
Feldspar phenocrysts
Pyroxene phenocryst
1 cm
B
Fractures
Quartz xenocryst
Embayments
Pyroxene
C
Carbonate amygdale
Pyroxene phenocryst
Feldspar phenocryst
D
Feldspar lath
E
Chlorite amygdale
Carbonate amygdale
1 cm
F
Feldspar phenocryst
Groundmass
G
Pyroxene phenocryst
Groundmass
H
Chlorite amygdales
Groundmass
I
Pyroxene phenocrysts
Embayment
Quartz xenocrysts
J
Olivine phenocryst
Pyroxene phenocryst
Groundmass
K
Groundmass
Pyroxene phenocryst

much finer-grained (<0.2 mm). Feldspar is sporadically swallow-tailed and commonly oriented around large pyroxene phenocrysts. Pyroxene may occur as fine-grained rims surrounding quartz xenocrysts (Figure 3.25 - B and I). Fine-grained amphibole or olivine may also occur. Opaque minerals are very scarce. Carbonate and quartz veins are common and some contain disseminated pyrite and sphalerite.

3.3.3.2 Coherent feldspar-phyric mafic facies (Mf)

The coherent feldspar-phyric mafic facies occurs from Sock Creek to Burns Peak, and in the Mount Charter area (Figure 3.22). In the Burns Peak area, it extends laterally for at least 100 m continuously. This facies is spatially associated with monomictic mafic breccia, monomictic mud-matrix mafic breccia, monomictic fluidal-clast mafic breccia, and polymictic mafic breccia facies (Table 3.5). Coherent feldspar-phyric mafic intervals range from <1 to 58 m thick.

This facies occurs as single coherent units, and in combination with monomictic mafic breccia facies (Figure 3.26). Upper and lower contacts with monomictic mafic breccia, monomictic mud-matrix mafic breccia, monomictic fluidal-clast mafic breccia and polymictic mafic breccia are typically gradational or sharp and planar. Upper and lower contacts with adjacent units are sharp and planar or mingled. Single coherent units have tabular geometry and cross-cut stratigraphy (Figure 3.26).

The coherent feldspar-phyric mafic facies (Figure 3.27 - A to F) is texturally very similar to the coherent feldspar-pyroxene-phyric mafic facies (section 3.3.3.1), but pyroxene (and olivine) phenocrysts are absent, and the feldspar phenocrysts differ in size and abundances. Feldspar phenocrysts (<1-40%; 0.7-5 mm) are otherwise texturally very similar to the feldspar phenocrysts of the coherent feldspar-pyroxene-phyric mafic facies (section 3.3.3.1). Feldspar glomerocrysts are very common in strongly feldspar-phyric mafic intervals (Figure 3.27 - C). Amygdaloidal (and vesicular) feldspar-phyric mafic facies is very similar to amygdaloidal feldspar-pyroxene-phyric mafic facies (section 3.3.3.1).

The groundmass (70-99%) is composed of feldspar laths and variable amounts of chlorite, sericite, and carbonate (Figure 3.27 - B). Some feldspar laths are swallow-tailed. Pyrite, chalcopyrite and sphalerite occur as disseminated grains or commonly around amygdales.

3.3.3.3 Coherent aphyric mafic facies (Ma)

The coherent aphyric mafic facies occurs from Bulgobac Hill to Burns Peak, and in the Mount Charter area (Figure 3.22). It also occurs in the White Spur area (Figure 3.23). This facies is spatially associated with monomictic mafic breccia and polymictic mafic sandstone facies (Table 3.5). Coherent aphyric mafic intervals range from <1 to 44 m thick.

This facies occurs as single coherent units, and in combination with monomictic mafic breccia facies (Figure 3.26). Upper and lower contacts with monomictic mafic breccia are gradational. Upper and lower contacts

with adjacent units and polymictic mafic sandstone facies are typically sharp and planar. Lower mingled contacts occur locally. Single coherent units have tabular geometry and cross-cut stratigraphy (Figure 3.26).

The coherent aphyric mafic facies (Figure 3.27 - G to M) is mineralogically very similar to the coherent feldspar-pyroxene-phyric mafic facies (section 3.3.3.1), but phenocrysts are absent. This facies predominantly comprises feldspar (20-35%; <0.1-0.8 mm) and pyroxene (15-40%; <0.1-0.5 mm) and variable amounts of chlorite (10-35%; <0.1-0.2 mm), sericite (10-15%; <0.1 mm) and carbonate (3-15%; <0.1 mm) (Figure 3.27 - H and K).

The coherent aphyric mafic facies is massive to amygdaloidal and weakly to strongly altered to chlorite, sericite and carbonate. Amygdales are mineralogically and texturally very similar to amygdales in the coherent feldspar-pyroxene-phyric mafic facies (section 3.3.3.1). Epidote- and carbonate-rich veins occur (Figure 3.27 - J and L). Pyrite and rare (<1%) sphalerite occur typically in veins or as disseminated grains (Figure 3.27 - L and M).

3.3.3.4 Monomictic mafic breccia facies (MmB)

The monomictic mafic breccia facies occurs in the Boco Alteration Zone, Burns Peak and Mount Charter areas (Figure 3.22). In the Burns Peak area, it extends laterally for at least 100 m continuously. This facies is spatially associated with coherent feldspar-pyroxene-phyric, feldspar-phyric and aphyric mafic facies, monomictic mud-matrix mafic breccia, monomictic fluidal-clast mafic breccia, monomictic mafic sandstone, and polymictic mafic breccia and sandstone facies (Table 3.5). Monomictic mafic breccia intervals range from <1 to 20 m thick.

Monomictic mafic breccias occur as single units, and in combination with coherent mafic intervals (Figure 3.26 - MCH-1). Upper and lower contacts with coherent feldspar-pyroxene-phyric, feldspar-phyric and aphyric mafic facies, monomictic mud-matrix mafic breccia and monomictic mafic sandstone facies are gradational. Upper and lower contacts with adjacent units and polymictic mafic breccia and sandstone facies are typically sharp and planar (Figure 3.26 - MCH-1).

The monomictic mafic breccia facies is typically poorly sorted and clast-supported (jigsaw-fit texture) or locally matrix-supported (clast-rotated texture; Figure 3.28 - A to D). It is massive to locally normally or reversely graded, and grades into monomictic mafic sandstone facies (section 3.3.3.5). In clast-supported jigsaw-fit monomictic mafic breccia intervals, the mafic (andesite or basalt) clasts are angular to sub-angular and have blocky and splintery shapes, and planar and curviplanar edges (Figure 3.28 - A and B). Local matrix-supported, clast-rotated domains comprise blocky, angular to sub-round mafic clasts with curviplanar and irregular margins surrounded by finer-grained (<2 mm) mafic clasts (Figure 3.28 - C and D).

The mafic clasts (up to 20 cm in diameter) are feldspar-pyroxene-phyric, feldspar-phyric or aphyric, and massive to strongly amygdaloidal (Figure 3.28 - A to D). The phenocryst and amygdale abundances and

Figure 3.26: Two graphic logs of parts of diamond drill holes MCH-1 (Mount Charter area) and AK-1 (Bulgobac Hill area) through facies of the mafic facies association. See Figure 3.4 for legend to graphic log.

MCH-1: The upper interval (196.0-354.5 m) of intercalated amygdaloidal coherent aphyric mafic facies (Ma) and monomictic mafic breccia facies (MmB) has an irregular upper contact (probably erosional) with a polymictic volcaniclastic unit that contains mafic clasts similar to the underlying mafic unit (196.0-354.5 m), consistent with the interpretation of this mafic interval as lava (section 3.3.3.10). The massive to normally graded polymictic mafic sandstone (MpS) at 354.5-359.6 m is interpreted as a high-concentration density current deposit. The middle interval (359.6-491.4 m) of coherent feldspar-phyric mafic facies (Mf), monomictic mafic breccia (MmB) and monomictic mud-matrix breccia (MmmB) facies is interpreted as a lava. The monomictic mud-matrix mafic breccia is interpreted as peperite (section 3.3.3.10), and its location in the middle of monomictic mafic breccia and coherent feldspar-phyric mafic facies suggests that a lobe of lava locally mingled with unconsolidated mud. The close spatial association and intercalation of monomictic mafic breccia and coherent feldspar-phyric mafic facies, and the gradational contact at 407.5 m are consistent with an extrusive origin. The lower interval (491.4-561.6 m) comprises a thin (<3 m) interval of coherent feldspar-phyric mafic facies (Mf) overlying monomictic mafic breccia and monomictic mud-matrix mafic breccia (497.2-518.2 m), and massive to normally graded units of monomictic mafic breccia (MmB) and sandstone (MmS) facies (491.4-497.2 m and 518.2-561.6 m). The monomictic mud-matrix mafic breccia is interpreted as peperite (section 3.3.3.10). The upper sharp, planar contact (497.2 m), the presence of peperite and the occurrence of similar facies above (491.4-497.2 m) and below (518.2-561.6 m) are consistent with the interpretation of the mafic interval at 497.2-518.2 m as an intrusion. The normally graded intervals of monomictic mafic breccia and sandstone are interpreted as resedimented autoclastic deposits, probably derived from non-explosive fragmentation of the adjacent or nearby mafic lava (coherent feldspar-phyric mafic facies).

AK-1: The massive to amygdaloidal, aphyric (Ma) to feldspar-phyric (Mf) mafic intervals are relatively thin (<15 m), cross-cut stratigraphy, and have tabular geometry and sharp and planar upper contacts with the surrounding rhyolite or dacite units. The thickness, geometry and spatial distribution of these mafic intervals are all consistent with the interpretation that they represent dykes or sills (section 3.3.3.10).

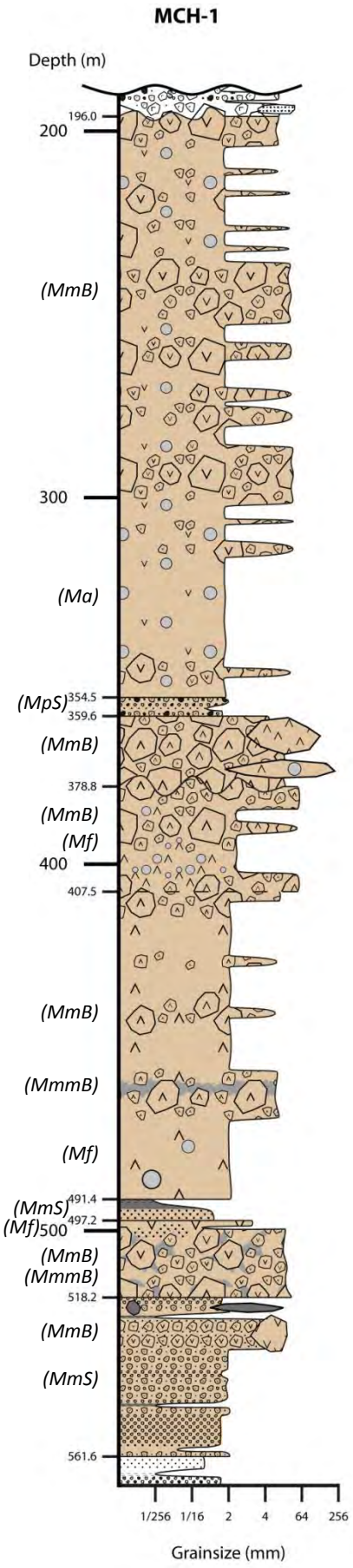
MCH-1
Depth (m)
196.0
200
(MmB)
300
(Ma)
354.5
(MpS)
359.6
(MmB)
378.8
(MmB)
(Mf)
400
407.5
(MmB)
(MmmB)
(Mf)
491.4
(MmS)
497.2
(Mf)500
(MmB)
(MmmB)
518.2
(MmB)
(MmS)
561.6
1/256 1/16 2 4 64 256
Grainsize (mm)

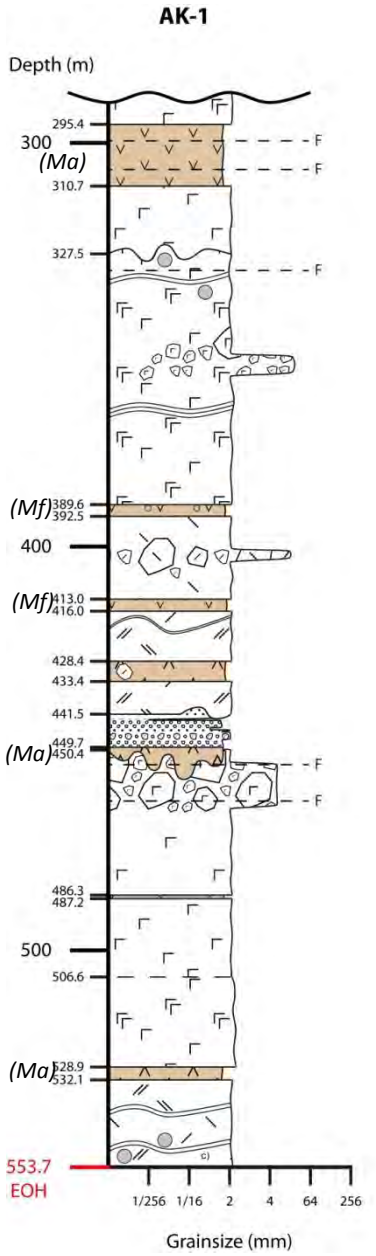
AK-1
Depth (m)
295.4
300
(Ma)
310.7
327.5
(Mf)389.6
392.5
400
(Mf)413.0
416.0
428.4
433.4
441.5
(Ma)449.7
450.4
486.3
487.2
500
506.6
(Ma)528.9
532.1
553.7
EOH
1/256 1/16 2 4 64 256
Grainsize (mm)

Figure 3.27: Coherent feldspar-phyric mafic facies. A, C to F: Handspecimen photographs (uphole and younging directions: A and E - left to right; C, D and F - not recorded). B: Photomicrograph (B - transmitted, plane polarised light). A and B: BHD-8 (236.3 m); C: BBP-242 (265.2 m); D: BOC-4 (610.4 m); E: MCH-1 (27.0 m); F: MCH-1 (118.0 m). Coherent aphyric mafic facies. G and J: Handspecimen photographs (uphole and younging directions: G - not recorded; J - left to right). H, I, K to M: Photomicrographs (H, K and L - transmitted, cross polarised light; I - transmitted, plane polarised light; M - reflected, plane polarised light). G to I: BBP-209 (102.8 m); J to M: AK-1 (304.7 m).

A: Amygdaloidal weakly feldspar-phyric mafic facies.

B: Amygdaloidal, weakly feldspar-phyric mafic facies. Rare feldspar phenocrysts and chlorite amygdales are surrounded by interlocking feldspar and a ferromagnesian phase replaced by chlorite. Feldspar phenocrysts are commonly concentrically zoned. The feldspar crystals in the groundmass are typically elongate, narrow, and commonly swallow-tailed.

C: Strongly feldspar-phyric mafic facies. Abundant (up to 40%) feldspar phenocrysts and glomerocrysts occur.

D: Weakly amygdaloidal, feldspar-phyric mafic facies. Rare carbonate amygdales occur.

E: Coherent feldspar-phyric mafic facies. Patchy pale and dark green domains impart a false clastic texture. Feldspar phenocrysts are abundant and equally distributed in both pale and dark green domains.

F: Strongly vesicular, weakly feldspar-phyric mafic facies. Vesicles are elongate to oval-shaped and up to 3 cm across.

G: Massive, aphyric basalt (Figure 3.1; Table 3.2).

H: Coherent aphyric basalt (Figure 3.1; Table 3.2) composed of abundant pyroxene and feldspar crystals <4 mm across.

I: Subhedral feldspar and euhedral pyroxene crystals surrounded by very fine-grained feldspar, pyroxene, chlorite.

J: Massive, aphyric basalt (Figure 3.1; Table 3.2) cross-cut by a carbonate-epidote-rich vein.

K: Coherent aphyric basalt (Figure 3.1; Table 3.2) comprising abundant pyroxene and feldspar crystals, and chlorite.

L: Carbonate-epidote-pyrite vein. M: Cluster of euhedral to irregular pyrite grains.

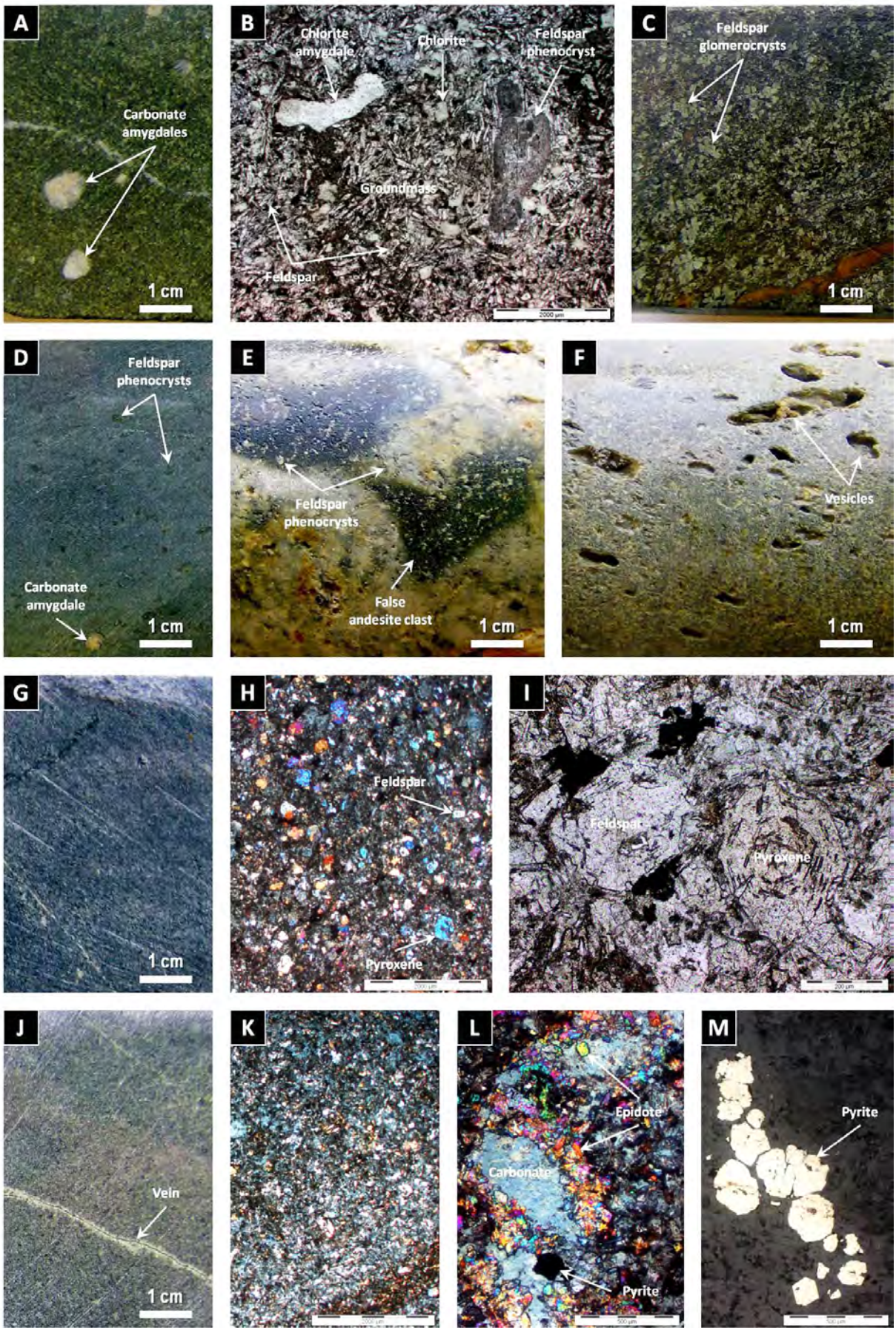
A
Carbonate amygdales
1 cm
B
Chlorite amygdale
Chlorite
Feldspar phenocryst
Groundmass
Feldspar
C
Feldspar glomerocrysts
1 cm
D
Feldspar phenocrysts
Carbonate amygdale
1 cm
E
Feldspar phenocrysts
False andesite clast
1 cm
F
Vesicles
1 cm
G
1 cm
H
Feldspar
Pyroxene
I
Feldspar
Pyroxene
J
Vein
1 cm
K
L
Epidote
Carbonate
Pyrite
M
Pyrite

Figure 3.28: A to D: Handspecimen photographs of the monomictic mafic breccia facies.
A: Clast- to matrix-supported monomictic mafic breccia. Mafic clasts are blocky and angular to sub-angular with planar and curviplanar margins. The matrix is mainly composed of finer-grained mafic clasts, feldspar and fine-grained carbonate. Jigsaw-fit texture occurs (arrow).

B: Clast-supported monomictic mafic breccia. Mafic clasts are non- to strongly amygdaloidal, blocky and mainly angular to sub-angular with planar and curviplanar margins. Mafic clasts with irregular margins also occur (upper middle). Amygdales in mafic clasts (right) are narrow and elongate. Jigsaw-fit texture occurs (arrow).

C: Matrix-supported monomictic mafic breccia. Mafic clasts are blocky, sub-angular to sub-round and partly to completely surrounded by matrix composed of finer-grained (<2 mm) mafic clasts.

D: Matrix-supported monomictic mafic breccia. The triangular mafic clast has a thin, pale green margin and a broad, dark green core.

E and F: Handspecimen photographs of the monomictic mafic sandstone facies. E: Coarse-grained, well sorted, monomictic mafic sandstone. F: Wavy, contorted, grey monomictic mafic sandstone beds intercalated with dark grey to black mudstone.

G: Contact between monomictic mafic breccia and mudstone (uphole and younging direction: not recorded). Sub-parallel, wavy, contorted, orange to black laminations occur in the mudstone (white arrows). Large mafic clasts are blocky and have sharp, curviplanar to irregular margins.

H and I: Handspecimen photographs of the monomictic mud-matrix mafic breccia facies.

H: Mafic clasts are vesicular, blocky to sub-round, and separated by scarce amounts of black mud matrix. Jigsaw-fit texture occurs (arrow).

I: Mafic (andesite or basalt; Figure 3.1; Table 3.2) clasts are blocky, angular and irregular, and have planar and curviplanar margins. They are surrounded by mud matrix, which is darker (black) away from the basalt clasts and paler (grey) close to the margins of the mafic clasts. Some mafic clasts (right) are strongly fractured.

A: MCH-1 (279.5 m); B: BOC-3 (263.3 m); C: BOC-3 (173.2 m); D: BOC-4 (194.0 m); E: BOC-3 (176.0 m); F: MCH-1 (552.0 m); G: BOC-3 (297.6 m); H: MCH-1 (65.6 m); I: SCS-5 (381.0 m). Uphole and younging directions: A, F, H and I - right to left; B to E - not recorded.

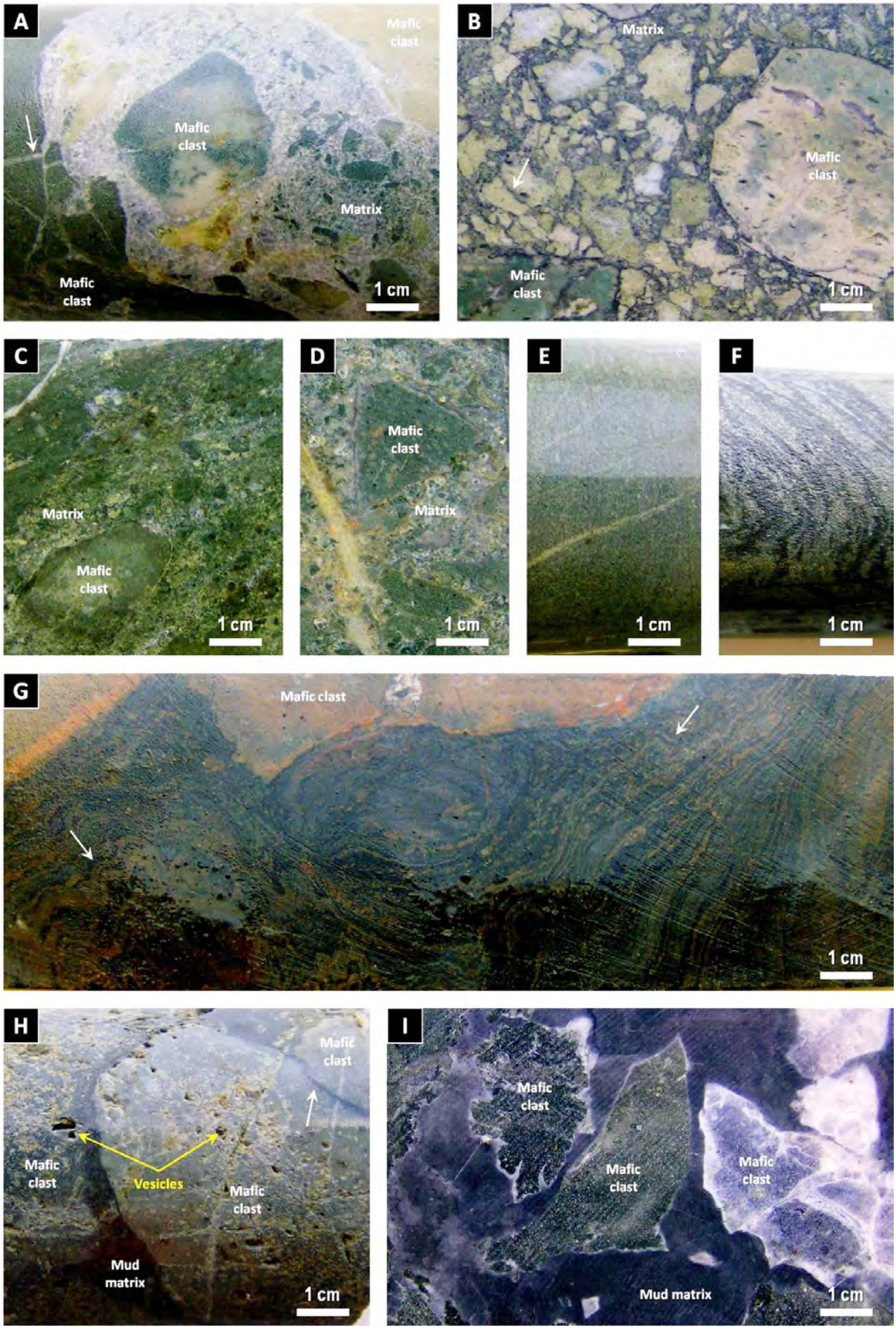
A
Mafic clast
Mafic clast
Matrix
Mafic clast
1 cm
B
Matrix
Mafic clast
Mafic clast
1 cm
C
Matrix
Mafic clast
1 cm
D
Mafic clast
Matrix
1 cm
E
1 cm
F
1 cm
G
Mafic clast
1 cm
H
Mafic clast
Mafic clast
Vesicles
Mafic clast
Mud matrix
1 cm
I
Mafic clast
Mafic clast
Mafic clast
Mud matrix
1 cm

distributions are very similar to the phenocryst and amygdale populations of the associated coherent feldspar-pyroxene-phyric, feldspar-phyric or aphyric mafic facies (sections 3.3.3.1, 3.3.3.2 and 3.3.3.3). In some examples, larger mafic clasts are zoned and have thin, fragmented, pale green to grey margins and broad, intact to fragmented, dark green to grey cores (Figure 3.28 - D).

The matrix is composed predominantly of finer-grained (<2 mm) mafic clasts and minor amounts (<2%) of feldspar (and pyroxene) crystals and crystal fragments embedded in a very fine-grained cement comprising variable amounts of carbonate, chlorite and sericite (Figure 3.28 - A to D).

3.3.3.5 Monomictic mud-matrix mafic breccia facies (MmmB)

The monomictic mud-matrix mafic breccia facies occurs in the Sock Creek South, Burns Peak and Mount Charter areas (Figure 3.22). This facies is spatially associated with coherent feldspar-pyroxene-phyric and feldspar-phyric mafic facies, monomictic mafic breccia and sandstone, and monomictic fluidal-clast mafic breccia facies (Table 3.5). Monomictic mud-matrix mafic breccia intervals range from <1 to 26 m thick.

This facies occurs intercalated with monomictic mafic breccia and coherent feldspar-pyroxene-phyric or feldspar-phyric mafic intervals (Figure 3.26 - MCH-1; Figure 3.29), or at the top contact of coherent feldspar-pyroxene-phyric mafic facies (Figure 3.24 - SCS-5). Within units, upper and lower contacts with associated facies are gradational. Upper and lower contacts with adjacent units are typically mingled, sharp and planar or gradational.

The monomictic mud-matrix mafic breccia facies is texturally and mineralogically very similar to the monomictic mafic breccia facies (section 3.3.3.4), but it is massive, the mafic clasts are feldspar-pyroxene-phyric or feldspar-phyric, and the matrix is composed of massive, variably silicified, homogeneous, dark grey to black mudstone (Figure 3.28 - H and I). Domains of dark grey and black mudstone are laminated and laminae are locally contorted. In clast-supported intervals, the mud matrix is represented by irregular, wispy, and silicified domains between mafic clasts (Figure 3.28 - H). Matrix-supported monomictic mud-matrix mafic breccia intervals contain isolated or jigsaw-fit clusters of mafic clasts that are scattered in the mud matrix (Figure 3.28 - I). In some examples, the mud matrix is pale grey and silicified immediately adjacent to the mafic clasts, whereas away from the mafic clasts it is dark grey to black (Figure 3.28 - I).

3.3.3.6 Monomictic fluidal-clast mafic breccia facies (MmfcB)

The monomictic fluidal-clast mafic breccia facies occurs exclusively in the Burns Peak area (DDH BOC-3 and BOC-4) (Figure 3.22), and extends laterally for at least 100 m continuously. This facies is spatially associated with coherent feldspar-phyric mafic facies, monomictic mafic breccia, monomictic mud-matrix mafic breccia and polymictic mafic breccia facies (Table 3.5). Monomictic fluidal-clast mafic breccia intervals range from 8 to 74 m thick.

This facies occurs as single massive units (Figure 3.29). Upper contacts with coherent feldspar-phyric mafic facies, monomictic mafic breccia and monomictic mud-matrix breccia facies are gradational. Lower contacts with coherent feldspar-phyric mafic facies and polymictic mafic breccia facies are sharp and planar.

The monomictic fluidal-clast mafic breccia is poorly sorted, clast-supported and internally massive (Figure 3.30 - A to D). This facies comprises aphyric mafic clasts that are either fluidally shaped and strongly amygdaloidal, or blocky, splintery and non- to strongly amygdaloidal (Figure 3.30 - A). The fluidal mafic clasts range from approximately 2 to 25 cm in diameter and comprise up to 20% of the monomictic fluidal-clast mafic breccia facies. Fluidal mafic clasts have ovoid, amoeboid and highly contorted shapes and irregular to smoothly curved margins that show local, narrow (<2 cm across), elongate protrusions (Figure 3.30 - A).

Fluidal mafic clasts are strongly amygdaloidal and locally show amygdale grading from amygdale-rich cores to amygdale-poor or amygdale-absent margins (Figure 3.30 - B). Amygdales are round to elongate and highly irregular, either dark green (chlorite-rich) or white to pale yellow (quartz- and/or carbonate-rich), and up to 2 cm in diameter. Amygdales may form up to 60% of fluidal clasts and are commonly interconnected (Figure 3.30 - B and D).

The blocky mafic clasts form an important component of the monomictic fluidal-clast mafic breccia facies, comprising up to 80% and dominating the <2-cm-size fraction of this facies (Figure 3.30 - C). Two sub-types of blocky mafic clasts occur. The sub-type 1 clasts form up to 50% of the monomictic fluidal-clast mafic breccia facies. They are commonly <1 to 2 cm in diameter, non-to weakly amygdaloidal (<5% amygdales), and have angular, blocky and splintery shapes and curviplanar margins (Figure 3.30 - C). Amygdales range from 0.1 to 0.2 mm in diameter. Sub-type 1 clasts are generally more intensely altered to chlorite than the sub-type 2 and fluidal clasts.

The sub-type 2 clasts form up to 30% of the monomictic fluidal-clast mafic breccia facies. They are typically 2 to 5 cm in diameter, moderately to strongly amygdaloidal, and the amygdale shape, size and abundance are similar to those in the cores of the fluidal mafic clasts (Figure 3.30 - C). The sub-type 2 clasts have angular to sub-angular and blocky shapes, and curviplanar margins that locally cross-cut amygdales.

3.3.3.7 Monomictic mafic sandstone facies (MmS)

The monomictic mafic sandstone facies occurs in the Burns Peak and Mount Charter areas (Figure 3.22). This facies is spatially associated with coherent feldspar-phyric mafic facies, monomictic mafic breccia, and monomictic mud-matrix mafic breccia facies (Table 3.5). Monomictic mafic sandstone intervals range from <1 to 28 m thick.

This facies occurs as single massive or normally graded units, or in normally or locally reversely graded units comprising monomictic mafic breccia and sandstone facies (Figure 3.26 - MCH-1; Figure 3.29 - BOC-3). Lower contacts with monomictic mafic breccia are gradational. Upper and lower contacts with coherent feldspar-phyric mafic facies and monomictic mud-matrix mafic breccia facies are typically sharp and planar.

Figure 3.29: Two graphic logs of parts of adjacent diamond drill holes BOC-3 and BOC-4 (Burns Peak area) through facies of the mafic facies association. See Figure 3.4 for legend to graphic log. The distance between diamond drill holes is approximately 100 m.

BOC-3 and BOC-4: The monomictic fluidal-clast mafic breccia facies (MmfcB) is interpreted as subaqueous lava fountain deposits (section 3.3.3.10). The spatial association of monomictic mafic breccia (MmB) and coherent feldspar-phyric mafic (Mf) facies with monomictic fluidal-clast mafic breccia is consistent with extrusion of the mafic facies. The coherent feldspar-phyric mafic facies (Mf) are interpreted as coherent facies of lavas, whereas the associated monomictic mafic breccia facies (MmB) is interpreted as the autoclastic domains of the lavas.

BOC-3: The association of monomictic mafic breccia (MmB) and monomictic mud-matrix mafic breccia (MmmB) (68.4-94.0 m) has a gradational upper contact with monomictic mafic breccia (62.8-68.4 m), and the facies association (62.8-94.0 m) is interpreted as a lava. The monomictic mud-matrix mafic breccia is interpreted as peperite (section 3.3.3.10) and suggests that lava lobes locally mingled with unconsolidated, probably wet mud. At the base (just above 300 m), a thin (<1 m) interval of mudstone is associated and locally interfingered with monomictic mafic breccia. The mudstone is laminated, and the laminae are well defined and highly contorted (see Figure 3.28 - G), indicative of ductile deformation having occurred. The deformed laminae in the mudstone were probably generated by the passive emplacement of the mafic facies or mud without mingling. The association of normally graded monomictic mafic breccia (MmB) and sandstone (MmS) facies (171.2-176.5 m) is interpreted as resedimented autoclastic breccia and sandstone (section 3.3.3.10).

BOC-4: Relatively thin intervals of polymictic mafic breccia (MpB) and sandstone (MpS) facies are massive to normally graded, and closely spatially associated with monomictic mafic breccia (MmB) and coherent feldspar-phyric mafic (Mf) facies. They are interpreted as high-concentration density current deposits (section 3.3.3.10). The monomictic mud-matrix mafic breccia facies (MmmB) is interpreted in the same way as in BOC-3.

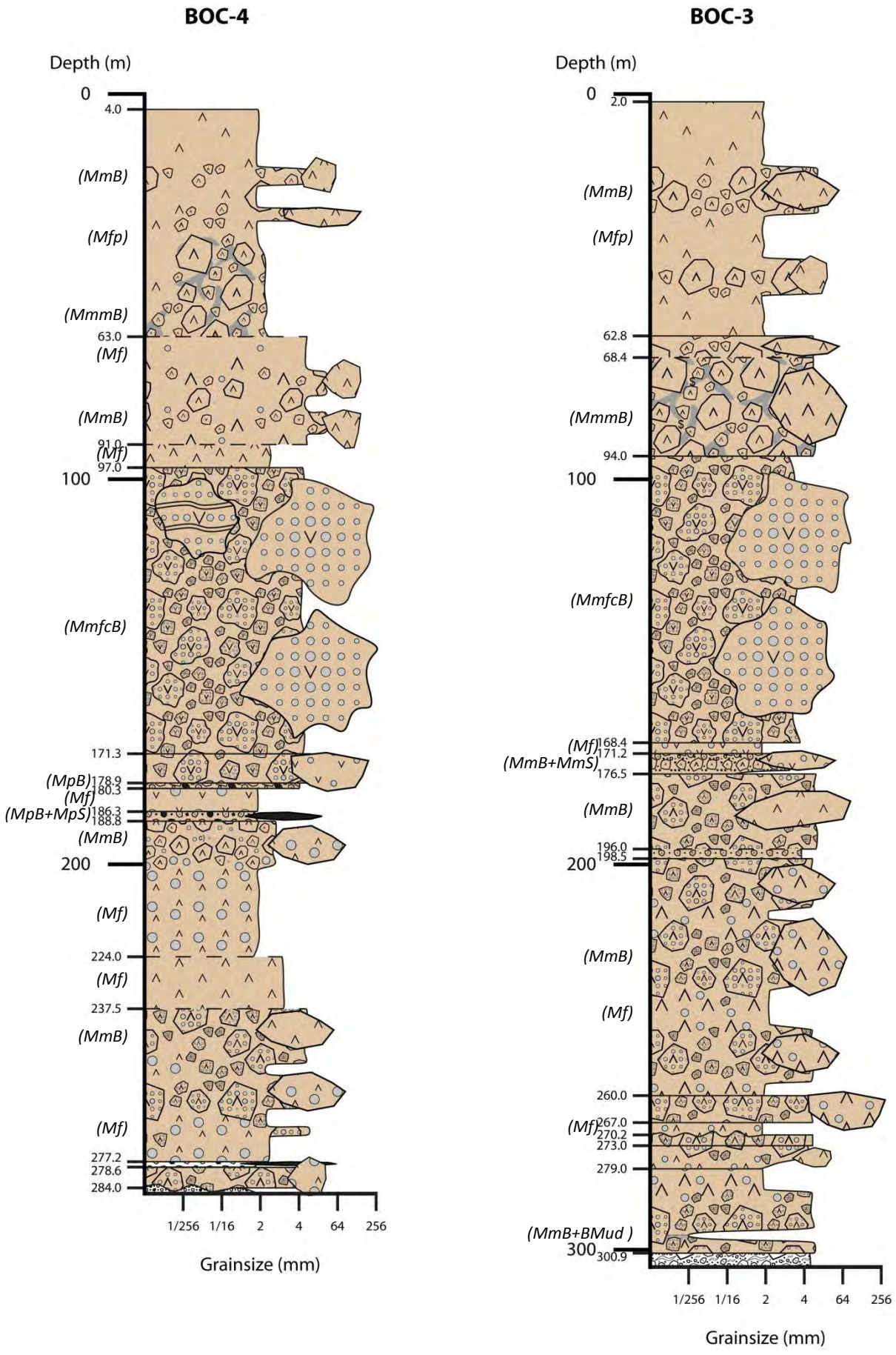
BOC-4
Depth (m)
0
4.0
(MmB)
(Mfp)
(MmmB)
63.0
(Mf)
(MmB)
91.0
(Mf)
97.0
100
(MmfcB)
171.3
(MpB)
178.9
180.3
(Mf)
(MpB+MpS)
186.3
188.8
(MmB)
200
(Mf)
224.0
(Mf)
237.5
(MmB)
(Mf)
277.2
278.6
284.0
1/256 1/16 2 4 64 256
Grainsize (mm)
BOC-3
Depth (m)
0
2.0
(MmB)
(Mfp)
62.8
68.4
(MmmB)
94.0
100
(MmfcB)
(Mf)
168.4
171.2
(MmB+MmS)
176.5
(MmB)
196.0
198.5
200
(MmB)
(Mf)
260.0
(Mf)
267.0
270.2
273.0
279.0
(MmB+BMud)
300
300.9
1/256 1/16 2 4 64 256
Grainsize (mm)

Figure 3.30: Handspecimen photographs of the monomictic fluidal-clast mafic breccia, and polymictic mafic breccia and sandstone facies (uphole and younging directions: A and F - not recorded; B, C, E - right to left; D - left to right).

A to D: Monomictic fluidal-clast mafic breccia facies.

E: Polymictic mafic breccia facies.

F: Polymictic mafic sandstone facies.

A: BOC-3 (94.8 m); B: BOC-3 (107.3 m); C: BOC-4 (113.0 m); D: BOC-4 (119.0 m); E: BOC-4 (186.5 m); F: MCH-1 (355.5 m).

A: The fluidal mafic clasts are larger, grey to pale cream and have globular and irregular margins. Blocky mafic clasts are smaller and show a thin, pale grey margin and a broad dark grey core.

B: Large (up to 8 cm across) fluidal mafic clast with amygdale size grading. Larger (up to 1 cm in diameter) and more abundant amygdales occur in the interior and smaller and less abundant (to locally absent) amygdales occur at the margins of the fluidal mafic clast. Carbonate amygdales are larger and less abundant than chlorite amygdales.

C: Monomictic fluidal-clast mafic breccia with abundant blocky mafic clasts. The sub-type 1 blocky mafic clasts are non-amygdaloidal, smaller and more abundant that the sub-type 2 blocky mafic clasts. Most sub-type 2 blocky mafic clasts are moderately to strongly amygdaloidal (lower left).

D: Monomictic fluidal-clast mafic breccia with abundant fluidal mafic clasts. A fluidal mafic clast fragment (upper right) contains large carbonate amygdales that are cross-cut by curviplanar margins.

E: Matrix-supported polymictic mafic breccia. Relatively large (lower middle) and small (upper left) lithic clasts are surrounded by matrix composed of finer-grained (<2 mm) mafic and lithic clasts, and feldspar crystals and crystal fragments.

F: Moderately sorted, pyrite-bearing polymictic mafic sandstone.

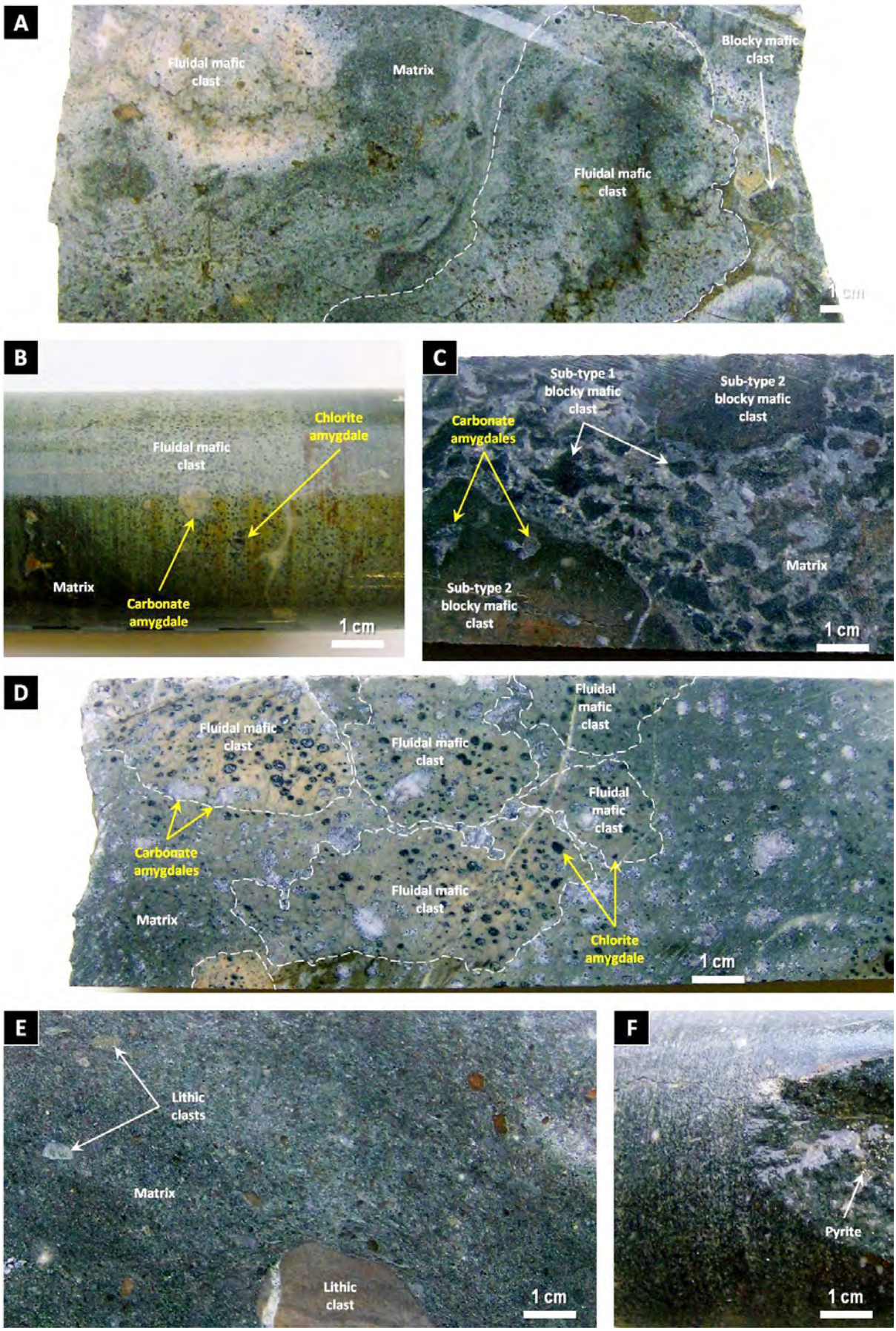
A
Fluidal mafic clast
Matrix
Blocky mafic clast
Fluidal mafic clast
1 cm
B
Chlorite amygdale
Fluidal mafic clast
Matrix
Carbonate amygdale
1 cm
C
Sub-type 1 blocky mafic clast
Sub-type 2 blocky mafic clast
Carbonate amygdales
Matrix
Sub-type 2 blocky mafic clast
1 cm
D
Fluidal mafic clast
Fluidal mafic clast
Fluidal mafic clast
Fluidal mafic clast
Carbonate amygdales
Fluidal mafic clast
Matrix
Chlorite amygdale
1 cm
E
Lithic clasts
Matrix
Lithic clast
1 cm
F
Pyrite
1 cm

The monomictic mafic sandstone facies is massive or weakly bedded (locally laminated), commonly normally graded, and well to moderately sorted (Figure 3.28 - E and F). Sandstone beds are commonly intercalated with mudstone beds, and domains of sandstone-mudstone are locally disrupted and/or contorted (Figure 3.28 - F). This facies is very similar to the monomictic mafic breccia facies (section 3.3.3.4), but it is finer grained and the mafic clasts are feldspar-phyric or aphyric and apparently non-amygdaloidal. Local intervals of monomictic mafic sandstone are feldspar crystal-rich (up to 10%), and may contain disseminated (<1%) sulfides.

3.3.3.8 Polymictic mafic breccia facies (MpB)

The polymictic mafic breccia facies occurs exclusively in the Burns Peak area (DDH BOC-4) (Figure 3.22). This facies is spatially associated with coherent feldspar-phyric mafic facies, monomictic mafic breccia, monomictic fluidal-clast mafic breccia, and polymictic mafic sandstone facies (Table 3.5). Polymictic mafic breccia intervals range from <1 to 2 m thick.

This facies occurs as single massive units, or normally graded units comprising polymictic mafic breccia at the bottom and polymictic mafic sandstone at the top (Figure 3.29 - BOC-4). Upper contacts with polymictic mafic sandstone are gradational. Upper and lower contacts with adjacent units are sharp and planar (Figure 3.29 - BOC-4).

The polymictic mafic breccia facies is poorly sorted, typically matrix-supported to locally clast-supported, and internally massive or normally graded (Figure 3.30 - E). This facies is similar to the monomictic mafic breccia facies (3.3.3.4), but it includes minor amounts of lithic clasts (1-3%; <5 cm). Lithic clasts are sub-round, massive, homogeneous, and pink to cream (Figure 3.30 - E). Mafic clasts are feldspar-phyric and aphyric, sub-angular to round, and non- to moderately amygdaloidal.

3.3.3.9 Polymictic mafic sandstone facies (MpS)

The polymictic mafic sandstone facies occurs exclusively in the Burns Peak and Mount Charter areas (DDH BOC-4 and MCH-1) (Figure 3.22). This facies is spatially associated with coherent feldspar-phyric mafic facies, monomictic mafic breccia, and polymictic mafic breccia facies (Table 3.5). Polymictic mafic sandstone intervals range from <1 to 5 m thick.

This facies occurs as massive to normally graded units comprising exclusively polymictic mafic sandstone (Figure 3.26 - MCH-1), or polymictic mafic sandstone at the top and polymictic mafic breccia at the bottom (Figure 3.29 - BOC-4). Lower contacts with polymictic mafic breccia are gradational. Upper and lower contacts with adjacent units are sharp and planar.

The polymictic mafic sandstone facies is massive or weakly bedded (locally laminated), commonly normally graded, and well to moderately sorted (Figure 3.30 - F). This facies is similar to the polymictic mafic breccia facies (section 3.3.3.8), but it is finer grained, the lithic clasts are pink or grey, and may be locally micaceous.

Intervals of polymictic mafic sandstone are locally feldspar crystal-rich (up to 10%) and/or pyrite-bearing (Figure 3.30 - F).

3.3.3.10 Interpretation

Coherent feldspar-pyroxene-phyric, feldspar-phyric and aphyric mafic facies, monomictic mafic breccia, monomictic mud-matrix mafic breccia, and monomictic mafic sandstone facies

Many single units of coherent feldspar-pyroxene-phyric, feldspar-phyric or aphyric mafic facies range from <1 to 52 m thick, have tabular geometries and sharp planar upper contacts with adjacent units, and cross-cut stratigraphy (Figure 3.24; Figure 3.26 - AK-1). They occur intercalated with mudstone, coherent rhyolite or dacite, or polymictic volcaniclastic units. The geometry, thickness, spatial distribution and sharp planar upper contacts of these single coherent feldspar-pyroxene-phyric, feldspar-phyric or aphyric mafic units suggest that they are dykes and sills.

The coherent feldspar-pyroxene-phyric, feldspar-phyric and/or aphyric mafic facies may be spatially associated with monomictic mafic breccia facies and locally with monomictic mud-matrix mafic breccia facies. Coherent feldspar-pyroxene-phyric, feldspar-phyric and/or aphyric mafic intervals have gradational contacts with monomictic mafic breccia and monomictic mud-matrix mafic breccia (Figure 3.24 - SCS-5; Figure 3.26 - MCH-1; Figure 3.29), and the mafic (andesite or basalt) clasts within monomictic mafic breccia and monomictic mud-matrix mafic breccia are texturally and mineralogically very similar to the coherent mafic facies. These observations suggest that the monomictic mafic breccia and monomictic mud-matrix mafic breccia facies are genetically related to the coherent feldspar-pyroxene-phyric, feldspar-phyric and/or aphyric mafic facies. The spatial association and similar texture and mineralogy suggest that these facies may be products of the same eruptive event.

Gradational contacts, textural and mineralogical similarities and spatial relationships between intervals of monomictic mafic breccia, monomictic mud-matrix mafic breccia and coherent feldspar-pyroxene-phyric, feldspar-phyric or aphyric mafic facies are consistent with the generation of mafic clasts within monomictic mafic breccia and monomictic mud-matrix mafic breccia by fragmentation of coherent mafic intervals. Blocky and splintery mafic clasts with planar and curviplanar margins within jigsaw-fit monomictic mafic breccia and monomictic mud-matrix mafic breccia facies (Figure 3.28 - A, B, H and I) are identical to clasts produced by in situ quench fragmentation, and are interpreted as in situ hyaloclastite (cf. Yamagishi, 1987, 1991).

The association of coherent mafic intervals and clast-rotated, massive to normally or locally reversely graded monomictic mafic breccia (hyaloclastite) that comprises blocky, angular to sub-round mafic clasts, and grades into monomictic mafic sandstone (Figure 3.26 - MCH-1; Figure 3.28 - C and E; Figure 3.29 - BOC-3) are consistent with extrusion of the mafic facies, and suggest that some quench-fragmented mafic intervals were resedimented down slope, possibly in response to growth of the associated mafic facies. The mafic clasts still

have curviplanar edges, which indicate transport distance was short. The monomictic mafic sandstone facies is interpreted as fine-grained resedimented hyaloclastite.

The monomictic mud-matrix mafic breccia facies occurs locally at the top margin of coherent feldspar-pyroxene-phyric mafic facies (Figure 3.24 - SCS-5), comprises angular to sub-angular, blocky and splintery mafic clasts (Figure 3.28 - I) with local jigsaw-fit texture, and in places the mud matrix is locally contorted and/or disrupted. These features are consistent with the interpretation of the monomictic mud-matrix mafic breccia facies as peperite (White et al., 2000). The occurrence of silicified mud matrix immediately adjacent to mafic clasts (Figure 3.28 - I) is consistent with induration of the mud on contact with hot mafic clasts (Gifkins et al., 2002). Larger mafic clasts in this facies that have thin, fragmented, pale green to grey or white margins, and broad, intact to fragmented, dark green to grey cores (Figure 3.28 - D and I) were possibly chilled on contact with wet, unconsolidated mud.

Monomictic mud-matrix mafic breccia facies also occurs intercalated with monomictic mafic breccia and coherent feldspar-pyroxene-phyric or feldspar-phyric mafic facies in units that have mingled upper contacts with adjacent units. These features are also consistent with the interpretation of the monomictic mud-matrix mafic breccia as peperite, and indicate intrusion of the associated coherent mafic facies. In other cases, where the upper contacts of units comprising monomictic mud-matrix mafic breccia in the middle and/or at the base of monomictic mafic breccia and coherent mafic facies are irregular or gradational (Figure 3.26 - MCH-1; Figure 3.29 - BOC-3), the monomictic mud-matrix mafic breccia facies is interpreted as peperite where lava lobes and/or the basal margin of lava locally mingled with unconsolidated, possibly wet mud.

Monomictic fluidal-clast mafic breccia facies

The monomictic fluidal clast mafic breccia facies is a distinctive monomictic volcanic breccia formed by subaqueous lava fountains (e.g., Simpson and McPhie, 2001) (Figure 3.31). The association, distribution, and relative sizes and abundances of strongly amygdaloidal fluidal mafic clasts and non- to strongly amygdaloidal blocky and splintery mafic clasts, and amygdale size grading (Figure 3.30 - B) in fluidal mafic clasts are all consistent with this interpretation.

The fluidal mafic clasts were most likely produced by tearing apart of relatively low-viscosity lava during subaqueous lava fountaining eruptions (Simpson and McPhie, 2001). Surface tension and hydrodynamic forces on hot lava fragments partly controlled the fluidal and highly contorted shapes of the fluidal mafic clasts. The amygdale-poor to amygdale-absent margins of the fluidal mafic clasts were probably formed by quenching on contact with water.

Following Simpson and McPhie (2001), it is inferred that post-vesiculation brittle fragmentation (clast-to-clast collision and quench fragmentation) of fluidal clasts during transport and deposition generated the two sub-types of blocky, splintery mafic clasts. The smaller, non- to weakly amygdaloidal blocky mafic clasts (sub-type 1) were probably derived from the non- to weakly amygdaloidal chilled margins of larger fluidal mafic clasts, whereas the larger, moderately to strongly amygdaloidal blocky mafic clasts (sub-type 2)

were generated by fragmentation of the moderately to strongly amygdaloidal interiors of fluidal mafic clasts (Figure 3.30 - C). The fact that the smaller sub-type 1 mafic clasts are typically more intensely altered than the sub-type 2 and fluidal mafic clasts could indicate they were glassy or partly glassy.

The occurrence of fluidal-clast breccia facies is commonly interpreted to represent near-vent settings (tens of m), although fluidal-clast breccia units may have wider lateral extents (Simpson and McPhie, 2001). The thickness (up to 74 m) of the monomictic fluidal clast breccia facies within adjacent diamond drill holes (DDH BOC-3 and BOC-4, approximately 100 m apart) at Burns Peak (Figures 3.23 and 3.29) probably indicates a near-vent setting, suggesting the presence of a localized mafic eruptive centre at, or near (tens of m) Burns Peak.

Polymictic mafic breccia and sandstone facies

The polymictic mafic breccia and sandstone facies are closely spatially associated, have gradational contacts, and occur in massive to normally graded units closely associated with coherent feldspar-phyric mafic facies and monomictic mafic breccia facies (Figures 3.26 - MCH-1; Figure 3.29 - BOC-4). The clasts within polymictic mafic breccia and sandstone facies are very similar to the coherent feldspar-phyric mafic facies and mafic clasts within monomictic mafic breccia facies. Textural and mineralogical similarities, gradational contacts and the spatial association between polymictic mafic breccia and sandstone, monomictic mafic breccia and coherent feldspar-phyric mafic facies suggest that these facies are genetically related.

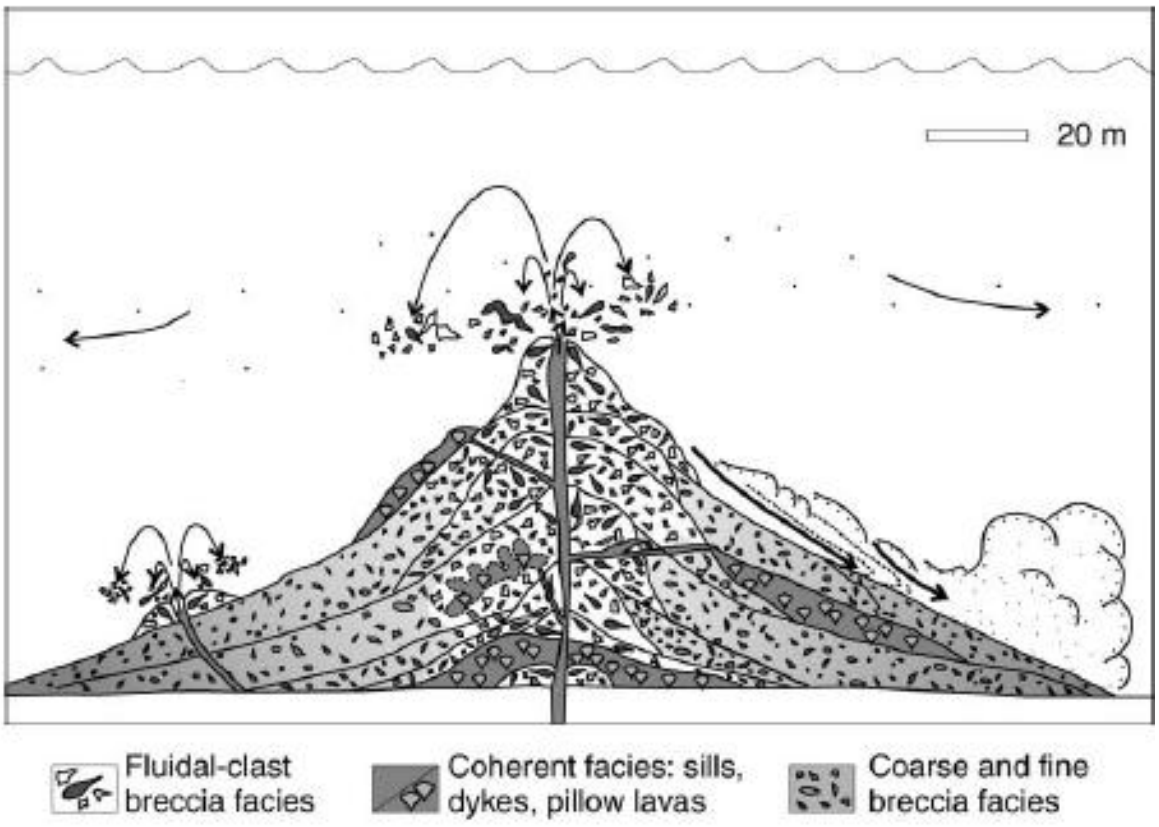

Figure 3.31: Schematic model for the monomictic fluidal-clast mafic breccia facies (after Simpson and McPhie, 2001).

The normally graded, polymictic and poorly sorted nature of the polymictic mafic breccia facies, and upper gradational contacts with polymictic mafic sandstone are consistent with deposition from submarine high-concentration density currents (cf. Lowe, 1982). The polymictic mafic breccia intervals were probably generated by localized resedimentation of unstable monomictic mafic breccia piles. Minor amounts of lithic clasts (1-3%) that possibly represent a different volcanogenic source were probably picked up during transport. Intervals of well to moderately sorted, locally normally graded polymictic mafic sandstone at the top of polymictic mafic breccia intervals (Figure 3.29 - BOC-4), and massive to normally graded units of polymictic mafic sandstone (Figures 3.26 - MCH-1) are consistent with deposition from high-concentration density currents (cf. Lowe, 1976; Lowe, 1982).

The thickness (up to 5 m) and very localized occurrence of the polymictic mafic breccia and/or sandstone units are inconsistent with eruption-fed density currents (e.g., McPhie et al., 1993; White, 2000; McPhie and Allen, 2003; Jutzeler et al., 2014). The density currents that produced the polymictic mafic breccia and sandstone facies were probably generated by local slope instability associated with volcano-tectonic earthquakes or continued emplacement of mafic lava during subaqueous eruptions.

3.3.4 Polymictic volcaniclastic facies association

The polymictic volcaniclastic facies association comprises seven facies: 1) polymictic volcanic breccia, 2) polymictic volcanic sandstone, 3) polymictic felsic breccia, 4) polymictic mud-matrix felsic breccia, 5) polymictic felsic sandstone, 6) polymictic micaceous sandstone, and 7) polymictic crystal-rich sandstone. The location of the diamond drill holes intersecting facies of the polymictic volcaniclastic facies association is shown in Figure 3.32. The characteristics of the facies comprising the polymictic volcaniclastic facies association are summarized in Table 3.6.

3.3.4.1 Polymictic volcanic breccia facies (PvB)

The polymictic volcanic breccia facies occurs in the Mount Charter, Sock Creek, Sock Creek South, Boco and Burns Peak areas (Figure 3.32). In the Sock Creek-Sock Creek South area, it extends laterally for at least 3 km continuously. This facies is closely spatially associated with polymictic volcanic sandstone and polymictic felsic breccia and sandstone facies (Table 3.6). It is also spatially associated with monomictic rhyolite (section 3.3.1.3) and dacite (section 3.3.2.2) breccia, monomictic mud-matrix dacite breccia (section 3.3.2.3), and coherent feldspar-pyroxene-phyric (section 3.3.3.1) and feldspar-phyric (section 3.3.3.2) mafic facies. Polymictic volcanic breccia intervals range from 1 to 32 m thick.

This facies occurs typically in normally graded units comprising polymictic volcanic breccia and sandstone, or in massive units of polymictic volcanic breccia (Figure 3.33). Upper contacts with polymictic volcanic sandstone are gradational. Upper contacts with adjacent units are sharp and planar. Lower contacts with adjacent units are either sharp and planar or irregular (Figure 3.33).

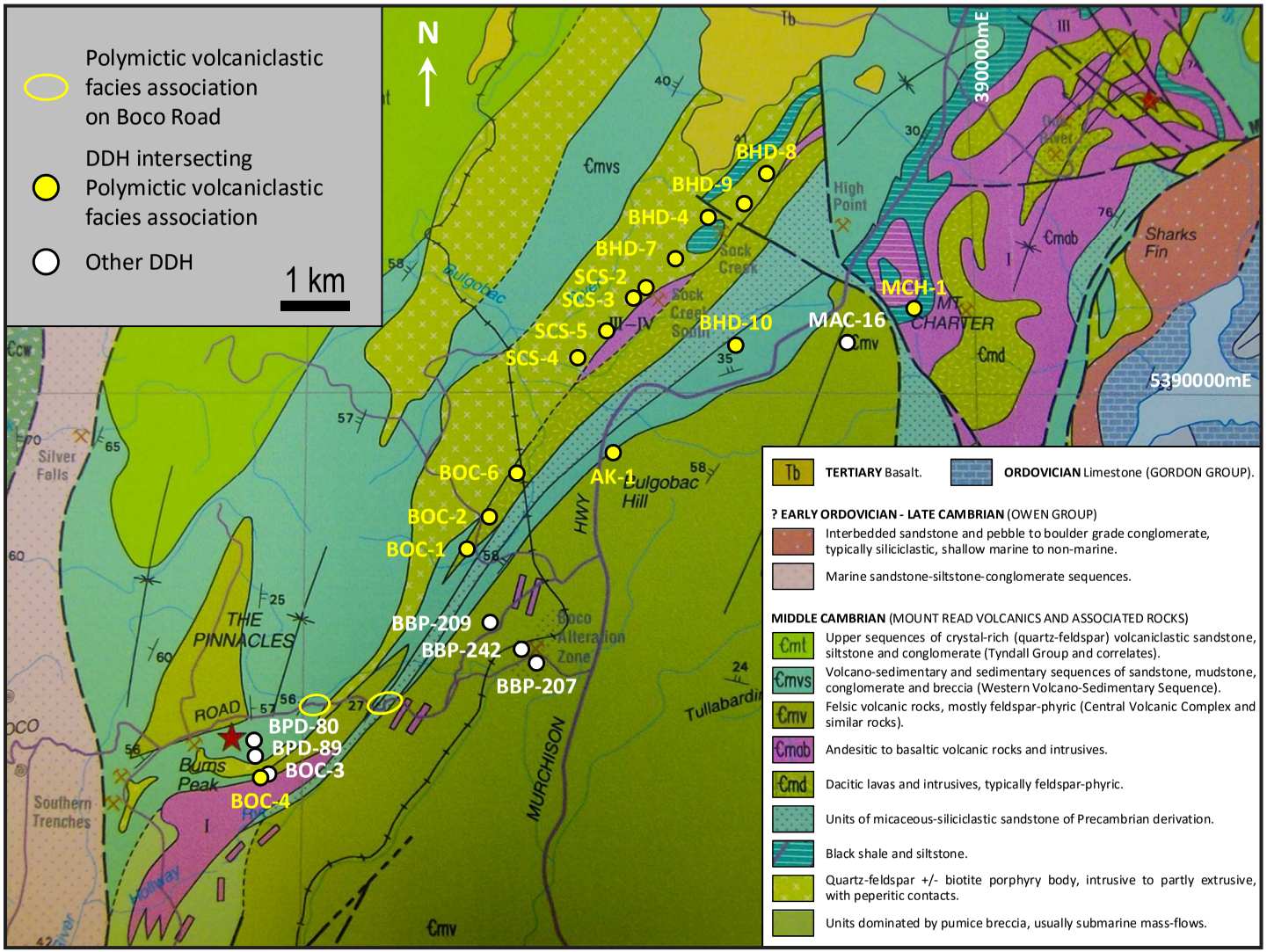

Figure 3.32: Geology of the Que River-Burns Peak area showing the location of the diamond drill holes (DDH) in this study, after Corbett (2002a). Facies of the polymictic volcaniclastic facies association (P) occur at Boco Road and are intersected by DDH AK-1 (Bulgobac Hill area), BHD-4, BHD-7, BHD-8 and BHD-9 (Sock Creek area), BHD-10, SCS-2, SCS-3, SCS-4 and SCS-5 (Sock Creek South area), BOC-1, BOC-2 and BOC-6 (Boco area); BOC-4 (Burns Peak area), and MCH-1 (Mount Charter area).

blank

Table 3.6: Characteristics, location and interpretation of the facies comprising the polymictic volcaniclastic facies association.

Facies association, facies and sub-facies		Lithofacies characteristics	Thickness x lateral extent	Mineralogy/Components	Textures	Associated facies	Location and diamond drill holes	Interpretation
Polymictic volcaniclastic facies association (P)	*Polymictic volcanic breccia facies* ***(PvB)***	Moderately to very poorly sorted; clast- to matrix-supported. Massive to normally graded	5-32 m x 3 km (continuously) (Sock Creek-Sock Creek South area)	Felsic (2-35%, 2-300 mm), mafic (3-40%, 2-550 mm), lithic (1-10%, 5-15 mm), and quartzite (1-2%, 2-3 mm) fragments. Mudstone intraclasts (1-10%, 15-90 mm). Feldspar (1-5%, 2-8 mm) and quartz (1-5%, 2-3 mm) crystal fragments. Fiamme (1-2%, 2-50 mm).	Perlitic, aphyric, feldspar-phyric and feldspar-quartz-phyric felsic fragments. Aphyric, amygdaloidal and/or vesicular and weakly feldspar-phyric mafic fragments. Shard-rich (10-15%, <1.5 mm) domains.	PvS; PfB; PfS; (RmB; DmB; DmmB; MmB; Mfp; Mf)	Boco: **BOC-2**; Burns Peak: **BOC-4**; Sock Creek: **BHD-4, BHD-7, BHD-8, BHD-9**; Mount Charter: **MCH-1**; Sock Creek South: **SCS-2, SCS-3, SCS-5**	Submarine high-concentration density current deposits
	Polymictic volcanic sandstone facies ***(PvS)***	Well to very poorly sorted; very fine- to very coarse-grained. Massive to normally graded. Locally laminated to weakly bedded	<1-15 m x 3 km (continuously)	Fragments and abundances very similar to PVfmB, but <2 mm. Common (up to 10%) >2 mm fragments.	Textures identical to PVfmB	PvB; (Rfq; Mud)	Sock Creek: **BHD-4, BHD-7, BHD-8, BHD-9**; Mount Charter: **MCH-1**; Sock Creek South: **SCS-2, SCS-3, SCS-5**	Submarine lower-concentration density current deposits
	Polymictic felsic breccia facies ***(PfB)***	Moderately to very poorly sorted; clast- to matrix-supported. Massive to normally graded	<1-10 m x 1.5 km (continuously) (Boco area)	Felsic (5-60%, 2-100 mm), lithic (1-5%, 2-8 mm), quartzite (1-30%, 2-5 mm), and schist and phyllite (0-7%, 2-3 mm) fragments. Mudstone clasts (1-10%, 2-60 mm). Feldspar (1-30%, 2-4 mm) and quartz (1-10%, 2-5 mm) crystal fragments. Fiamme (<30 %, <40 mm).	Locally amygdaloidal, aphyric, feldspar-phyric and feldspar-quartz-phyric felsic fragments. Shard-bearing (up to 10%, <1.5 mm) domains. Locally aphyric to feldspar-phyric, sub-parallel, strongly aligned fiamme.	PmmfB; PfB; PfS; PvB; PmS; (Rf; RmB; Df; DmB; Mfp; MmB; Mud)	Bulgobac Hill: **AK-1**; Boco: **BOC-1, BOC-2, BOC-6**; Sock Creek South: **BHD-10, SCS-2, SCS-3, SCS-4, SCS-5**	Submarine high-concentration density current deposits
	Polymictic mud-matrix felsic breccia facies ***(PmmfB)***	Moderately to very poorly sorted; clast- to matrix-supported. Massive to normally graded. Black to dark grey mud matrix	3-9 m x 1.2 km (discontinuously) (Sock Creek South area)	Fragments and abundances very similar to PVfB.	Textures identical to PVfB	PfB; PfS; (Mud)	Boco: **BOC-6**; Sock Creek South: **BHD-10**, **SCS-3, SCS-4**	Submarine muddy high-concentration density current deposits
	Polymictic felsic sandstone facies ***(PfS)***	Well to very poorly sorted. Massive to normally graded, or laminated to bedded; very fine- to very coarse-grained. Beds range from <10 mm up to >10 m	<1-92 m x 1.5 km (continuously) (Boco area)	Fragments and abundances very similar to PVfB, but <2 mm. Common (up to 10%) >2 mm fragments.	Textures identical to PVfB	PfB; PmmfB; PvB; PmS; (RmB; Df; DmB; Mfp; MmB; (Mud)	Boco: **BOC-1, BOC-2, BOC-6**; Sock Creek South: **BHD-10, SCS-2, SCS-3, SCS-4, SCS-5**	Submarine lower-concentration density current deposits
	Polymictic micaceous sandstone facies ***(PmS)***	Well to poorly sorted. Massive to normally graded or bedded to laminated; very fine- to very coarse-grained; micaceous. Beds range from <10 mm up to >10 m	<1-45 m x 10 km (continuously) (Sock Creek to Boco Road)	Fine-grained lithic fragments (1-10%, 0.1-2 mm); quartzite and schist (4-30%, 0.1-2 mm); quartz (3-45%, 0.1-0.8 mm) and feldspar (1-30%, 0.2-0.8 mm) crystal fragments; muscovite (1-10%, 0.2-0.8 mm) and biotite (1-5%, 0.1-0.4 mm); rare tourmaline and zircon	Soft-sediment deformation; aphyric to feldspar-phyric fiamme; kinked and ragged muscovite and biotite flakes; framboisal pyrite clusters (up to 3 cm)	PfB; PfS; (Mud)	Boco: **BOC-1, BOC-2, BOC-6**; Burns Peak: **BOC-4**; Sock Creek: **BHD-4, BHD-7, BHD-8 and BHD-9**; Sock Creek South: **SCS-5**; Mount Charter: **MCH-1**; **Boco Road**	Submarine lower-concentration density current deposits
	Polymictic crystal-rich sandstone facies ***(PcrS)***	Moderately to poorly sorted. Massive or bedded to locally laminated. Coarse- to very coarse-grained	4-139 m x ? M	Feldspar (up to 20%, <2 mm) and quartz (up to 15%, <2 mm) crystals and crystal fragments; lithic fragments (5%, <20 mm)	Orange lithic clasts; round and irregular quartz crystal fragments; tabular and irregular feldspar crystal fragments	(Mud)	**Boco Road**	Submarine high-concentration density current deposits

Figure 3.33: Four graphic logs of parts of diamond drill holes SCS-3 (Sock Creek South area), BHD-7 (Sock Creek area), BOC-2 (Boco area) and BOC-4 (Burns Peak area) through facies of the polymictic volcaniclastic facies association. See Figure 3.4 for legend to graphic log.

SCS-3: The polymictic volcanic breccia (PvB) and sandstone (PvS) unit (29.6-49.9 m) occurs between amygdaloidal coherent feldspar-pyroxene-phyric mafic facies (Mfp) (below) and coherent feldspar-quartz-phyric rhyolite (Rfq) (above), and is interpreted as a high-concentration density current deposit. The mafic clasts within the polymictic volcanic breccia and sandstone are aphyric to weakly feldspar-phyric, and texturally and mineralogical different from the underlying coherent feldspar-pyroxene-phyric mafic interval, which has been interpreted as an intrusion (section 3.3.3.10). These features suggest that the mafic clasts within the polymictic volcanic breccia and sandstone facies were derived from a different source, possibly from a nearby, coeval mafic lava and associated autoclastic deposits.

BHD-7: The polymictic volcanic breccia (PvB) and sandstone (PvS) unit (46.5-73.9 m) occurs between monomictic dacite breccia (DmB) (below) and coherent feldspar-quartz-phyric rhyolite (Rfq) (above), and is interpreted as a high-concentration density current deposit. Many felsic clasts within the polymictic volcanic breccia facies are perlitic and/or feldspar-phyric, and texturally and mineralogically similar to the dacite clasts within the underlying monomictic dacite breccia, suggesting that the felsic clasts within the polymictic volcanic breccia facies were sourced from the monomictic dacite breccia.

BOC-2: Two massive to locally normally-graded units (546.7-552.2 m and 570.4-575.8 m) of polymictic volcanic breccia (PvB) occur intercalated with polymictic felsic breccia (PfB) and sandstone (PfS) intervals. The polymictic volcanic and felsic breccia facies (PvB and PfB) are interpreted as high-concentration density current deposits; the polymictic volcanic and felsic sandstone intervals are interpreted as lower-concentration density current deposits.

BOC-4: The polymictic volcanic breccia (PvB) unit (603.7-609.8 m) occurs between amygdaloidal, weakly feldspar-phyric mafic intervals (Mf) (interpreted as syn-volcanic intrusions - section 3.3.3.10), and above monomictic rhyolite breccia (RmB) and coherent feldspar-quartz-phyric rhyolite (Rfq) facies. The polymictic volcanic breccia unit is interpreted as a high-concentration density current deposit. It contains rhyolitic clasts similar to the clasts within the monomictic rhyolite breccia and the coherent feldspar-quartz-phyric rhyolite. They are interpreted to have been sourced from the coherent and monomictic rhyolite breccia unit.

A and B: BOC-2 (549.7 m) - Poorly sorted, clast-supported polymictic volcanic breccia. The mafic clasts are strongly amygdaloidal. Many amygdales are commonly multi-globular due to vesicle coalescence (B).

C and D: BOC-4 (605.0 m) - Massive, poorly sorted, clast-supported polymictic volcanic breccia. The felsic clasts are orange. The mafic clasts are dark green. Larger mafic clasts have thin, pale green margins (probably chilled) and broad, fine-grained, dark green cores (D). Uphole and younging directions: right to left.

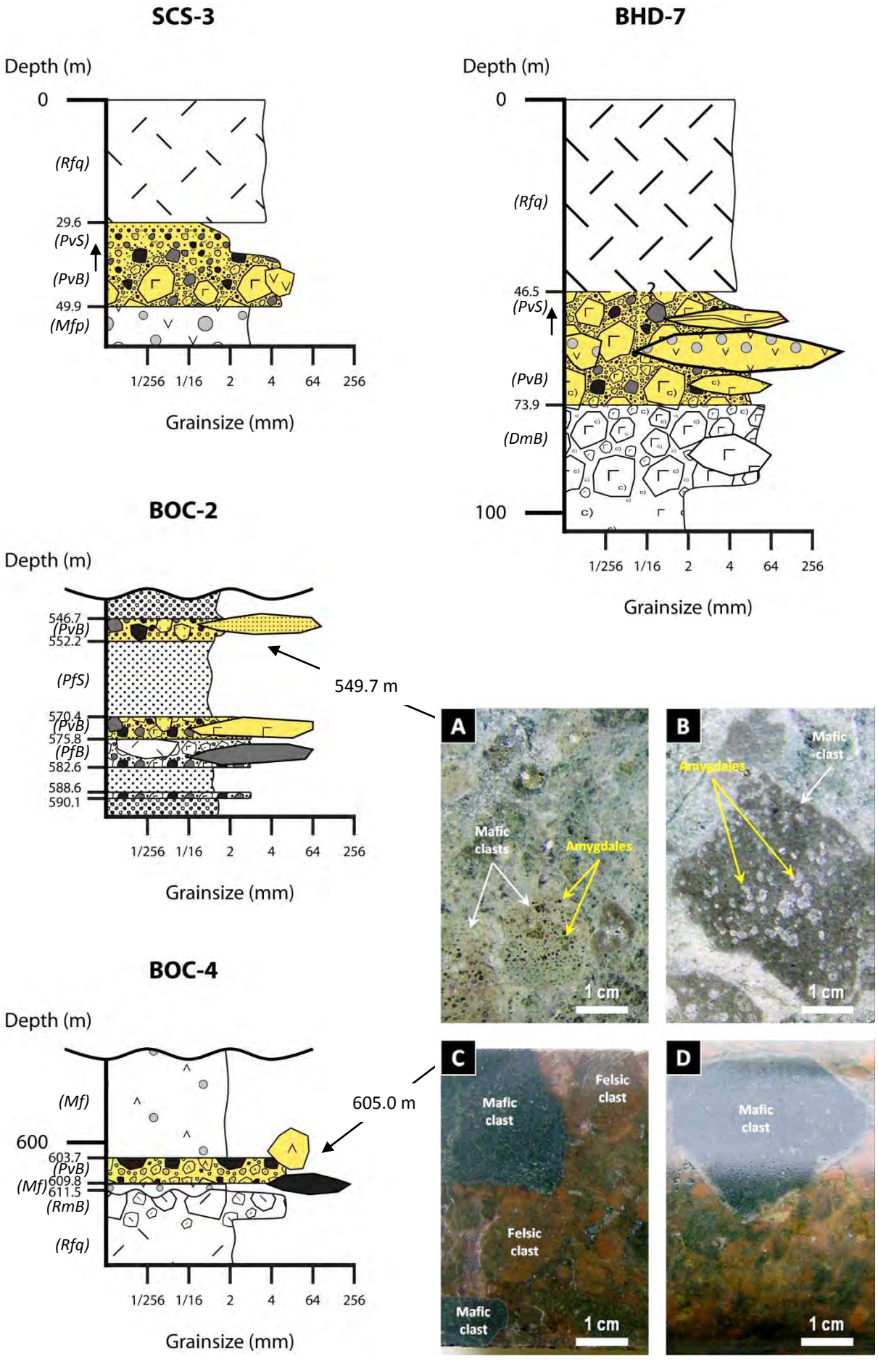
SCS-3
Depth (m)
0
(Rfq)
29.6
(PvS)
(PvB)
49.9
(Mfp)
1/256 1/16 2 4 64 256
Grainsize (mm)
BHD-7
Depth (m)
0
(Rfq)
46.5
(PvS)
(PvB)
73.9
(DmB)
100
1/256 1/16 2 4 64 256
Grainsize (mm)
BOC-2
Depth (m)
546.7
(PvB)
552.2
(PfS)
570.4
(PvB)
575.8
(PfB)
582.6
588.6
590.1
549.7 m
1/256 1/16 2 4 64 256
Grainsize (mm)
BOC-4
Depth (m)
(Mf)
600
603.7
(PvB)
609.8
(Mf)
611.5
(RmB)
(Rfq)
605.0 m
1/256 1/16 2 4 64 256
Grainsize (mm)
A
Mafic clasts
Amygdales
1 cm
B
Amygdales
Mafic clast
1 cm
C
Mafic clast
Felsic clast
Felsic clast
Mafic clast
1 cm
D
Mafic clast
1 cm

The polymictic volcanic breccia facies (Figures 3.34 and 3.35) is moderately to very poorly sorted, clast- to matrix-supported, and massive to normally graded. The clasts are randomly oriented and distributed, and clusters of variable clast types occur locally. This facies is composed of felsic (2-35%, 2-300 mm), mafic (3-40%, 2-550 mm), lithic (1-15%, <2-15 mm), mudstone (1-10%, 15-90 mm), and quartzite and schist (1-2%, 2-3 mm) clasts. It also comprises feldspar (1-20%, <2-8 mm) and quartz (1-10%, <1.5-3 mm) crystals and crystals fragments. Pale green and brown, aphyric to weakly feldspar-phyric, chloritic fragments also occur (1-2%, 2-50 mm) (Figure 3.35 - A and F), some of which are flattened and aligned.

The felsic clasts are aphyric, feldspar-phyric or feldspar-quartz-phyric, sub-angular to rounded, elongate and irregular, commonly strongly perlitic, and rarely flow-banded and amygdaloidal (Figure 3.34 - A and B; Figure 3.35 - A and B). In feldspar-quartz-phyric felsic clasts, feldspar phenocrysts (1-5%, 1-3 mm) are commonly larger and more abundant than quartz phenocrysts (0-1%, 1-2 mm).

The mafic clasts are aphyric or weakly feldspar-phyric, sub-rounded to elongate or irregular, and weakly to strongly amygdaloidal and/or vesicular (Figure 3.34 - A, C and G; Figure 3.35 - B). The feldspar phenocrysts are euhedral to subhedral, and weakly altered to chlorite and sericite (Figure 3.34 - H; Figure 3.35 - B). Feldspar glomerocrysts occur (Figure 3.34 - I). The groundmass comprises abundant, randomly oriented, evenly distributed feldspar laths (Figure 3.34 - H to J). The amygdales and vesicles are round, oval-shaped, elongate and irregular, and some are multi-globular due vesicle coalescence (Figure 3.33 - B; Figure 3.34 - G and H). The amygdales are typically filled by chlorite (Figure 3.33 - A; Figure 3.34 - J), or by carbonate and quartz (Figure 3.33 - B; Figure 3.34 - G). In some examples, coarse mafic clasts are blocky, angular and zoned, and have thin, pale green margins and broad, intact, fine-grained, dark green cores (Figure 3.33 - D).

The lithic clasts are fine-grained, homogeneous, and siliceous (Figure 3.35 - C and D). In rare examples, the lithic fragments present a network of perlitic fractures, and an array of jigsaw-fit, intact, smaller, microgranular cores (Figure 3.35 - C). The mudstone clasts are dark grey to black, elongate or irregular, mainly composed of very fine-grained sericite with minor quartz and feldspar (Figure 3.35 - A). They typically occur close to the lower contact of normally graded units of polymictic volcanic breccia and sandstone units. The quartzite and schist clasts are sub-angular and irregular and weakly foliated (Figure 3.34 - D and F; Figure 3.35 - E).

The feldspar crystal fragments are euhedral and subhedral, commonly twinned, and variably altered to sericite and/or chlorite (Figure 3.34 - D and E; Figure 3.35 - B and D). The quartz crystal fragments include euhedral (square/rectangular) to anhedral, embayed, angular to round, elongate, clear volcanic quartz, and metasedimentary quartz (Figure 3.34 - D and F; Figure 3.35 - D, I to K) characterized by undulose extinction and subgrains.

The matrix (30-75%) is moderately to very poorly sorted, commonly shard-rich and mainly composed of rock and crystal fragments, and minor amounts of carbonate, chlorite (2%, <0.2 mm), zircon (<<1%, <0.05 mm), sphene (<<1%, <0.1 mm), and pyrite and sphalerite (<2%, <0.3 mm) (Figure 3.34 - B, C and D; Figure 3.35 - B to E, and H). Pyrite and sphalerite are euhedral to anhedral and disseminated, or locally

accumulated around fragment margins. Green, aphyric to weakly feldspar-phyric, chloritic fragments (up to 5%, <1.5 mm) are also present.

The shards (10-15%, <1.5 mm) have curved margins, pointy edges and cuspate, platy, C, Y and X shapes, and are pale to dark brown, undeformed, typically altered to secondary feldspar, and locally very abundant (Figure 3.35 - H). The rock and crystal fragments in the matrix are identical to their coarser (>2 mm) counterparts. The rock fragments include aphyric, feldspar-phyric and feldspar-quartz-phyric fragments (probably felsic and mafic), and lithic fragments. Sponge spicules and circular to ovoid organic fragments are also present (Figure 3.35 - G).

3.3.4.2 Polymictic volcanic sandstone facies (PvS)

The polymictic volcanic sandstone facies occurs in the Mount Charter, Sock Creek and Sock Creek South areas (Figure 3.32), and extends laterally for at least 3 km continuously. This facies is closely spatially associated with polymictic volcanic breccia facies (Table 3.6). It is also spatially associated with coherent feldspar-quartz-phyric rhyolite (section 3.3.1.1) and mudstone (section 3.3.5) facies. Polymictic volcanic sandstone intervals range from <1 to 15 m thick. This facies occurs typically in normally graded units comprising polymictic volcanic sandstone and breccia (Figure 3.33 - SCS-3 and BHD-7) that locally have mudstone beds at the top. Lower contacts with polymictic volcanic breccia and upper contacts with mudstone beds are gradational. Upper contacts with adjacent units are sharp and planar.

The polymictic volcanic sandstone facies (Figure 3.36) is well to very poorly sorted, massive to normally graded, or weakly bedded (locally laminated). This facies is very similar to the polymictic volcanic breccia facies (section 3.3.4.1), but it is finer grained (most fragments are <2 mm). The polymictic volcanic sandstone facies commonly includes variable amounts (up to 10%) of coarser (>2 mm) fragments (Figure 3.36 - A to C, and G).

3.3.4.3 Polymictic felsic breccia facies (PfB)

The polymictic felsic breccia facies occurs in the Mount Charter, Sock Creek South, Boco and Bulgobac Hill areas (Figure 3.32). It extends laterally for at least 1325 m continuously in the Sock Creek South area and 1500 m continuously in the Boco area. This facies is closely spatially associated with polymictic felsic sandstone, polymictic mud-matrix felsic breccia, polymictic volcanic breccia, and polymictic micaceous sandstone facies. It is also spatially associated with coherent feldspar-phyric rhyolite (section 3.3.1.2) and dacite (section 3.3.2.1), coherent feldspar-pyroxene-phyric mafic facies (section 3.3.3.1), and monomictic rhyolite (section 3.3.1.3), dacite (section 3.3.2.2) and mafic (section 3.3.3.4) breccia facies (Table 3.6). Polymictic felsic breccia intervals range from <1 to 10 m thick.

Figure 3.34: Polymictic volcanic breccia facies. A and G: Handspecimen photographs (uphole and younging directions: left to right). B to F, H to J: Photomicrographs (B to E, H and I - transmitted, plane polarised light; F and J - transmitted, cross polarised light). A to F: BHD-7 (60.3 m); G to J: BHD-7 (61.9 m).

A: Poorly sorted, clast-supported polymictic felsic-mafic breccia. Felsic and mafic clasts are partly surrounded by feldspar- and quartz-bearing matrix. Abundant perlitic felsic clasts occur.

B: Strongly perlitic felsic clasts partly surrounded by feldspar- and quartz-bearing matrix.

C: Amygdaloidal, weakly feldspar-phyric, irregular mafic clast partly surrounded by feldspar- and quartz-bearing matrix.

D: Quartzite clast, and quartz and feldspar crystal fragments in very fine-grained, silicified matrix. The quartzite clast is sub-angular and composed of polycrystalline quartz. The quartz crystal fragments are sub-angular and have undulose extinction, suggesting they are metamorphic. The feldspar is moderately altered to sericite.

E: Strongly sericite-altered, euhedral (rectangular) feldspar crystal surrounded by very fine-grained, silicified matrix.

F: Quartzite clast and round quartz crystal fragment (metamorphic) in a very fine-grained, silicified matrix.

G to J: Vesicular and amygdaloidal, feldspar-phyric mafic clasts in the polymictic volcanic breccia facies.

G: Chlorite-filled (dark green) amygdales are generally smaller than carbonate- or quartz-filled (cream) amygdales.

H: Feldspar phenocrysts are subhedral, rectangular and elongate. The groundmass comprises abundant and evenly distributed feldspar laths.

I: Heart-shaped feldspar glomerocryst.

J: Chlorite-filled amygdale surrounded by feldspar-rich groundmass.

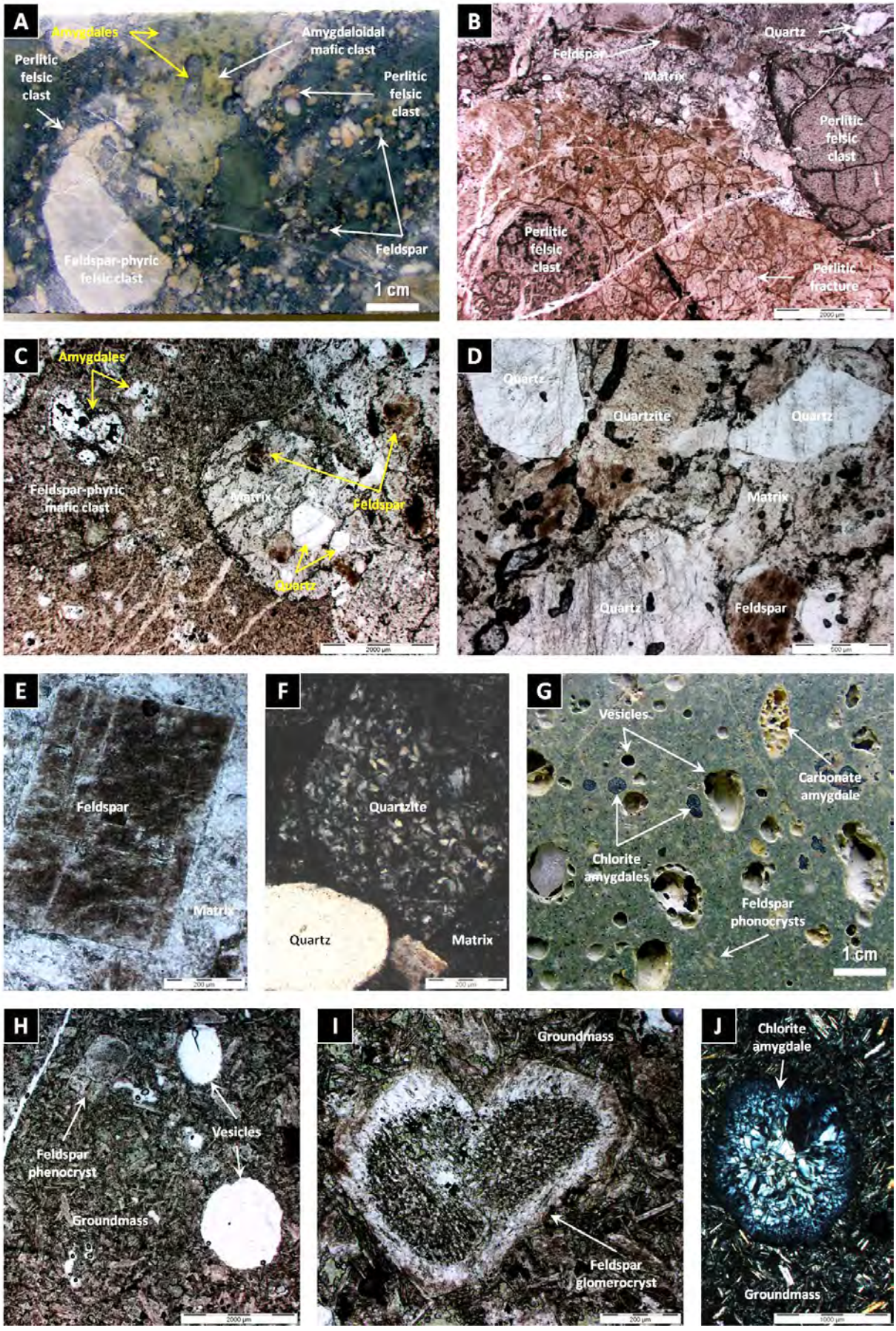
A
Amygdales
Amygdaloidal mafic clast
Perlitic felsic clast
Perlitic felsic clast
Feldspar
Feldspar-phyric felsic clast
1 cm
B
Quartz
Feldspar
Matrix
Perlitic felsic clast
Perlitic felsic clast
Perlitic fracture
C
Amygdales
Feldspar-phyric mafic clast
Matrix
Feldspar
Quartz
D
Quartz
Quartzite
Quartz
Matrix
Quartz
Feldspar
E
Feldspar
Matrix
F
Quartzite
Quartz
Matrix
G
Vesicles
Carbonate amygdale
Chlorite amygdales
Feldspar phenocrysts
1 cm
H
Vesicles
Feldspar phenocryst
Groundmass
I
Groundmass
Feldspar glomerocryst
J
Chlorite amygdale
Groundmass

Figure 3.35: Polymictic volcanic breccia facies. A: Handspecimen photograph (uphole and younging directions: left to right). B to k: Photomicrographs (B to I, and K - transmitted, plane polarised light; J - transmitted, cross polarized light). A to K: SCS-3 (44.8 m).

A: Poorly sorted, clast-supported, polymictic volcanic breccia. Feldspar-phyric felsic clasts, mudstone clasts and chloritic fragments are aligned and mixed with feldspar-, quartz- and lithic-bearing matrix.

B: Weakly feldspar-phyric mafic and felsic clasts, and fine-grained feldspar- and metasedimentary quartz-bearing matrix.

C: Perlitic, fine-grained lithic clast. Abundant, secondary feldspar-altered, blocky and pointy-edged shards (similar to I) with curviplanar margins occur.

D: Fine-grained lithic clast, and feldspar and metasedimentary quartz crystal fragments. Secondary feldspar-altered shards occur.

E: Schist clast in feldspar-bearing matrix. The schist clast is composed of very fine-grained quartz, feldspar and phyllosilicates.

F: Chloritic fragment in very fine-grained quartz-bearing matrix.

G: Ovoid fragment (probably organic) and circular section of a sponge spicule. Professor Patrick Quilty assisted in the identification of sponge spicules and organic fragments.

H: Secondary feldspar-altered, X-shaped, bubble-wall shard.

I to K: Quartz crystal fragments.

I: Hexagonal volcanic quartz crystal with straight extinction.

J: Embayed, subhedral metamorphic quartz crystal fragment.

K: Round metamorphic quartz.

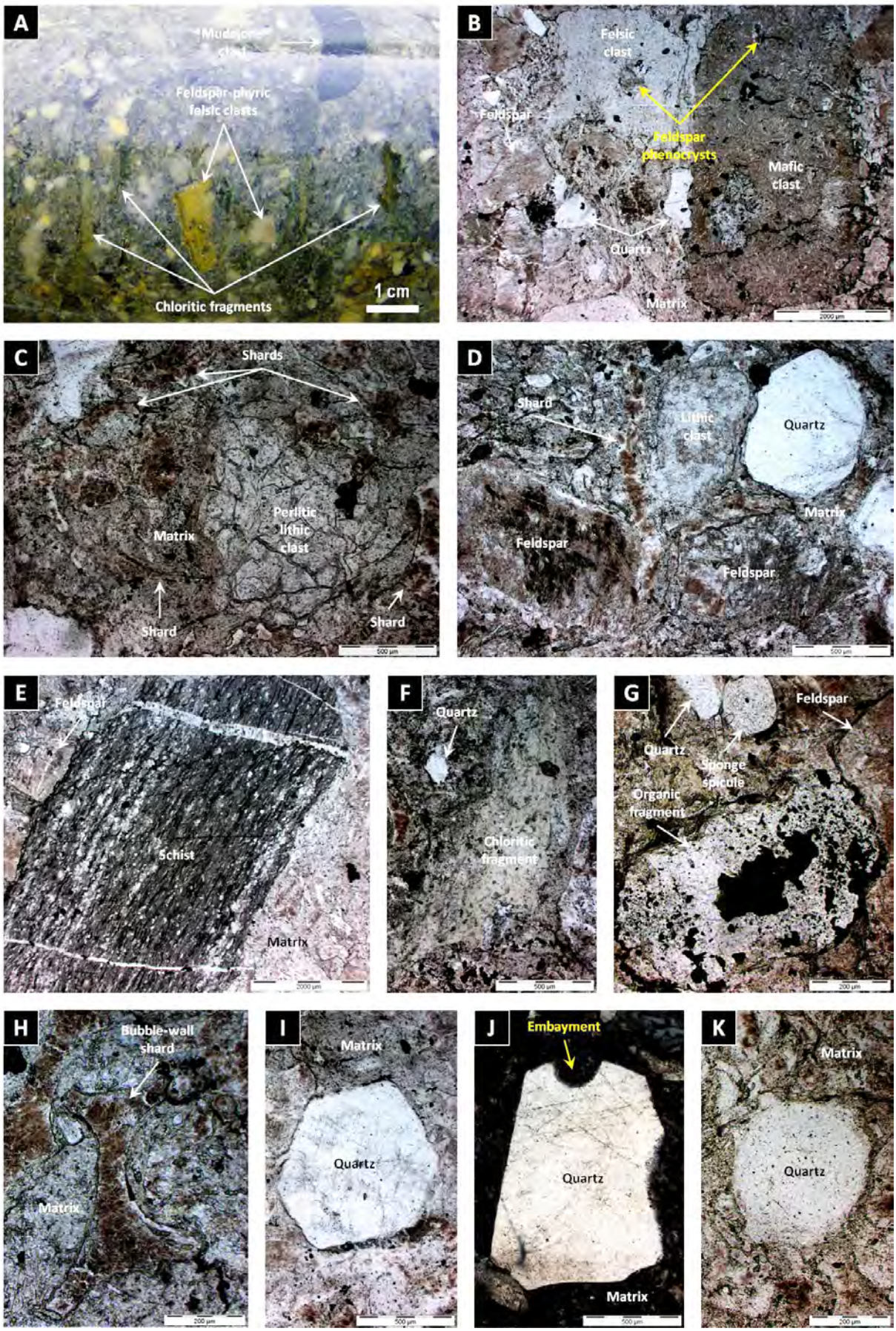
A
Mudstone clast
Feldspar-phyric felsic clasts
Chloritic fragments
1 cm
B
Felsic clast
Feldspar
Feldspar phenocrysts
Mafic clast
Quartz
Matrix
C
Shards
Matrix
Perlitic lithic clast
Shard
Shard
D
Shard
Lithic clast
Quartz
Matrix
Feldspar
Feldspar
E
Feldspar
Schist
Matrix
F
Quartz
Chloritic fragment
G
Feldspar
Quartz
Sponge spicule
Organic fragment
H
Bubble-wall shard
Matrix
I
Matrix
Quartz
J
Embayment
Quartz
Matrix
K
Matrix
Quartz

Figure 3.36: Polymictic volcanic sandstone facies. A: Handspecimen photograph (uphole and younging directions: right to left). B to L: Photomicrographs (B, C, E to G, J to L - transmitted, plane polarised light; D, H and I - transmitted, cross polarised light). A to L: BHD-8 (54.8 m).

A: Poorly sorted polymictic volcanic sandstone. Scarce, large (>2 mm), feldspar-phyric felsic clasts and mudstone clasts are surrounded by feldspar-bearing matrix.

B: Large (>1 cm in diameter), weakly feldspar-phyric mafic clast, and feldspar and quartz crystal fragments.

C: Schist clast, chloritic fragment, and feldspar and quartz crystal fragments. The schist clast is foliated. The chloritic fragment is irregular, wispy and strongly chloritic. The quartz crystal fragments are less abundant than the feldspar crystal fragments and commonly have embayed margins.

D: Rectangular, twinned feldspar crystal fragment altered to sericite and minor chlorite.

E: Euhedral (square) quartz crystal fragments in a very fine-grained shard-rich matrix.

F: Perlitic felsic clast, and quartz crystal fragments.

G: Chloritic fragment surrounded by fine-grained shard-rich matrix.

H: Sub-round quartzite fragment.

I: Elongate muscovite flake.

J: Mudstone clast.

K. Secondary feldspar-altered shards. L: Silicified, circular section of an organic fragment. Professor Patrick Quilty assisted in the identification of organic fragments.

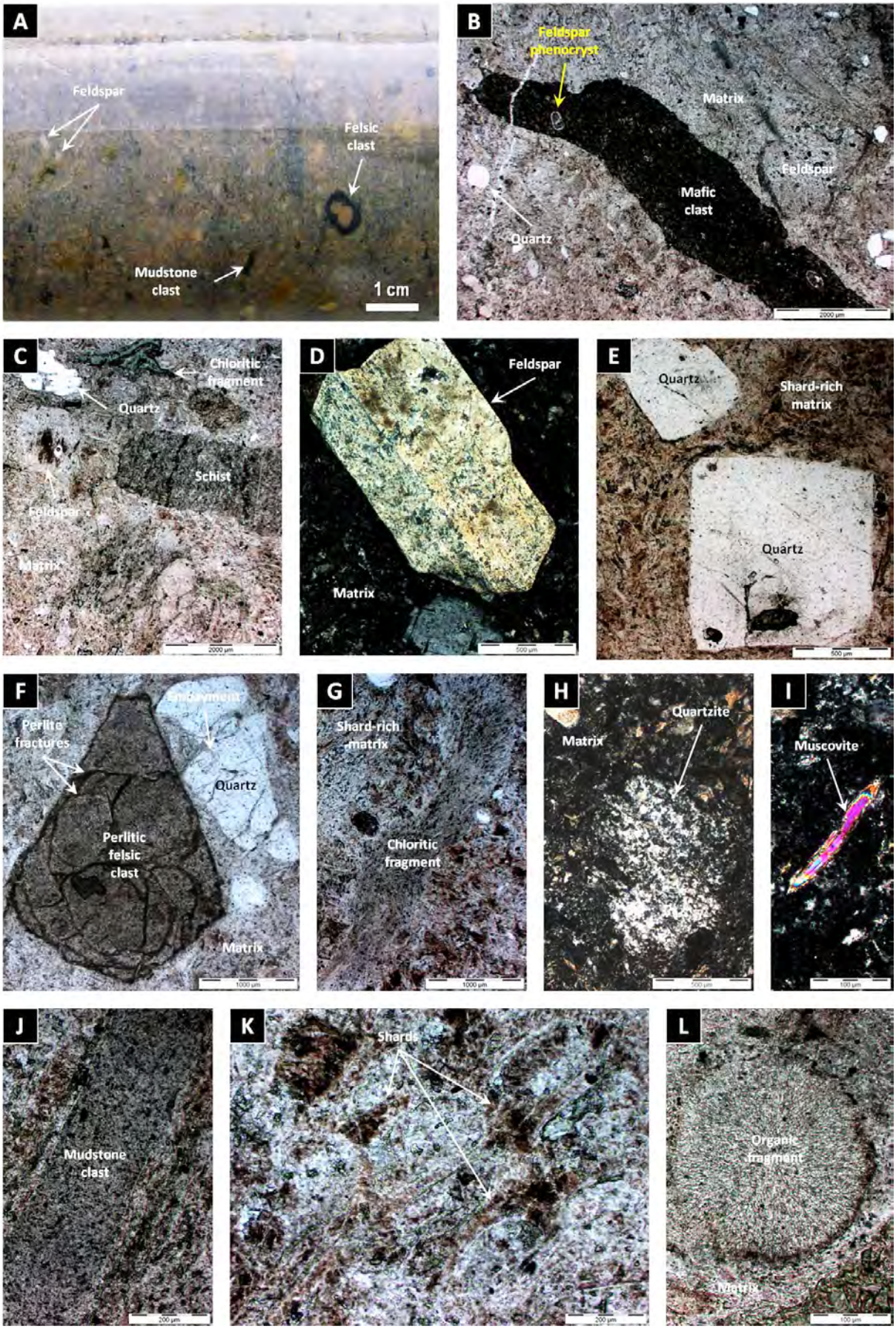
A
Feldspar
Felsic clast
Mudstone clast
1 cm
B
Feldspar phenocryst
Matrix
Feldspar
Mafic clast
Quartz
C
Chloritic fragment
Quartz
Schist
Feldspar
Matrix
D
Feldspar
Matrix
E
Quartz
Shard-rich matrix
Quartz
F
Perlite fractures
Quartz
Perlitic felsic clast
Matrix
G
Shard-rich matrix
Chloritic fragment
H
Quartzite
Matrix
I
Muscovite
J
Mudstone clast
K
Shards
L
Organic fragment
Matrix

This facies occurs typically in normally graded units or intervals comprising polymictic felsic breccia and sandstone with or without mudstone tops (Figure 3.37), in massive units of polymictic felsic breccia, or interbedded with intervals of polymictic felsic sandstone. Upper and lower contacts with polymictic felsic sandstone are gradational. Upper contacts with adjacent units are sharp and planar. Lower contacts with adjacent units are sharp and planar, gradational, irregular or faulted (Figure 3.37).

The polymictic felsic breccia facies (Figure 3.38 - A to D; Figure 3.39) is moderately to very poorly sorted, clast- to matrix-supported, massive to normally graded, and locally silicified. This facies is similar to the polymictic volcanic breccia facies (3.2.4.1), but it lacks mafic clasts and the abundances of its components are different. The polymictic felsic breccia facies comprises felsic (5-60%, 2-100 mm), lithic (1-5%, 2-3 mm), quartzite (1-30%, 2-5 mm), schist (0-5%, 2-3 mm), phyllite (0-2%, 2-3 mm), and mudstone (1-10%, 2-60 mm) clasts. Pale green, aphyric to feldspar-phyric, chloritic fragments (5-10%, 2-80 mm) are present (Figure 3.39 - B). This facies also includes feldspar (1-30%, 2-4 mm) and quartz (1-10%, 2-5 mm) crystals and crystal fragments.

In the Boco area (DDH BOC-6), a 1.2 m thick massive to weakly bedded interval of polymictic felsic breccia comprises abundant (up to 30%), sub-parallel, strongly aligned, aphyric to feldspar-phyric, pale to dark green, grey or brown, chloritic fiamme up to 4 cm in diameter (Figure 3.38 - F). This interval is clast-supported and finer-grained (most clasts are <1 cm across). Narrow, elongate, strongly aligned, homogeneous, dark grey to black mudstone clasts are common (Figure 3.38 - F).

The felsic clasts are aphyric, feldspar-phyric or feldspar-quartz-phyric, sub-round to elongate, and locally weakly amygdaloidal (Figure 3.38 - A and C). The lithic clasts are fine-grained, homogeneous, sub-rounded to rounded, equant or elongate, pale grey or brown, and commonly silicified (Figure 3.38 - A, B and D; Figure 3.39 - J). The quartzite (metamorphic, intergrown, polycrystalline quartz with or without muscovite) clasts are sub-angular to sub-rounded (Figure 3.39 - C to E). The schist (polycrystalline metamorphic quartz with intergrown, foliated muscovite and/or biotite) and phyllite (very fine-grained, foliated, intergrown muscovite with minor amounts of polycrystalline quartz) clasts are rounded to sub-rounded and elongate, and typically quartz- and muscovite- or biotite-rich (Figure 3.39 - E, G and H). The mudstone clasts are dark grey to black, round to elongate and irregular, and composed of very fine-grained quartz, feldspar, sericite and chlorite (Figure 3.38 - C).

The feldspar crystal fragments are euhedral and subhedral, commonly twinned, and typically strongly altered to sericite and/or chlorite (Figure 3.38 - A, B and D; Figure 3.39 - F and H). The quartz crystal fragments include euhedral to anhedral, very angular to rounded, embayed, clear volcanic quartz, and metasedimentary quartz with undulose extinction (Figure 3.39 - D, E and H).

The matrix (15-75%) (Figure 3.38 - A to D; Figure 3.39 - B to E, and J) is moderately to very poorly sorted, and mainly comprises rock (up to 20%, 0.1-2 mm) and crystal (up to 40%, 0.08-2 mm) fragments that are identical to their coarser (>2 mm) counterparts. Rock fragments include felsic (up to 5%, 0.1-1.6 mm), lithic (1%, 0.1-1 mm), quartzite (up to 10%, 0.1-1.8 mm), schist (2%, 0.1-1.7 mm), phyllite (1%, 0.1-0.9

mm), and mudstone fragments (2%, 0.1-1.6 mm). Crystal fragments include feldspar (up to 30%, 0.1-2 mm), and quartz (up to 10%, 0.1-1.6 mm). Biotite (2%, 0.08-0.6 mm), and muscovite (1%, 0.08-0.3 mm) occur as narrow and elongate flakes that are commonly kinked (Figure 3.39 - L). Aphyric to feldspar-phyric, chloritic fragments (5%, 0.1-2 mm) occur.

The matrix also comprises variable amounts (up to 20%) of sericite, chlorite, and carbonate. Shard-bearing domains also occur. The shards have curved margins, pointy edges, and C, Y and X shapes, and are undeformed and locally abundant (up to 10%, <1.5 mm). Sub-round chromite grains or clusters (1%, 0.1-0.2 mm) (Figure 3.39 - J), and rare apatite (<<1%, 0.1-0.2 mm) and tourmaline (<<1%, 0.08-0.1 mm) may also occur. Rare (<1%) opaque minerals include pyrite, chalcopyrite and sphalerite. Sponge spicules and circular to ovoid organic fragments are also present (Figure 3.39 - L).

3.3.4.4 Polymictic mud-matrix felsic breccia facies (PmmfB)

The polymictic mud-matrix felsic breccia facies occurs in the Sock Creek South and Boco areas (Figure 3.32). In the Sock Creek South area, it extends laterally for approximately 1175 m discontinuously. This facies is closely spatially associated with polymictic felsic breccia and sandstone, and mudstone (section 3.3.5) facies (Table 3.6). Polymictic mud-matrix felsic breccia intervals range from 3 to 9 m thick.

This facies occurs as single massive units of polymictic mud-matrix felsic breccia (Figure 3.37), in rare normally graded units comprising polymictic mud-matrix felsic breccia and mudstone, and intercalated with polymictic felsic breccia and sandstone intervals. Upper and lower contacts with adjacent, associated facies are gradational. Upper and lower contacts with adjacent units are sharp and planar, or locally irregular (Figure 3.37).

The polymictic mud-matrix felsic breccia facies is very similar to the polymictic felsic breccia facies (section 3.3.4.3), but it is typically massive (or locally normally graded) and the matrix is predominantly composed of massive, dark grey to black mudstone (Figure 3.37 - C; Figure 3.38 - E). In clast-supported domains, the mud matrix is distributed between clasts and may be scarce, whereas in matrix-supported domains, the mud matrix is abundant and partly to completely surrounds the clasts (Figure 3.37 - C).

3.3.4.5 Polymictic felsic sandstone facies (PfS)

The polymictic felsic sandstone facies occurs in the Mount Charter, Sock Creek South, and Boco areas (Figure 3.32). It extends laterally for at least 1325 m continuously in the Sock Creek South area and 1500 m continuously in the Boco area. This facies is closely spatially associated with polymictic felsic breccia, polymictic mud-matrix felsic breccia, polymictic volcanic breccia, and polymictic micaceous sandstone facies. It is also spatially associated with coherent feldspar-phyric dacite (section 3.3.2.1), coherent feldspar-pyroxene-phyric mafic facies (section 3.3.3.1), monomictic rhyolite (section 3.3.1.3), dacite (section 3.3.2.2) and mafic (section 3.3.3.4) breccia, and mudstone (section 3.3.5) facies (Table 3.6). Polymictic felsic sandstone intervals range from <1 to 92 m thick.

Figure 3.37: Graphic log of part of diamond drill hole BHD-10 (Sock Creek South area) through facies of the polymictic volcaniclastic facies association. See Figure 3.4 for legend to graphic log. BHD-10: Normally graded intervals comprising polymictic felsic breccia (PfB) and sandstone (PfS) with shard-rich mudstone (SMud) tops (e.g. 113.7-119.5 m), and normally graded intervals of polymictic felsic sandstone with shard-rich mudstone tops (e.g. 119.5-202.2 m) are interpreted as high-concentration density current and suspension deposits. The interval of polymictic mud-matrix felsic breccia (PmmfB) (88.0-97.4 m) is interpreted as a muddy high-concentration density current deposit.

A: BHD-10 (25.0 m) - Bedded to laminated polymictic felsic sandstone. Sandstone beds and laminae are pale to dark grey.

B: BHD-10 (30.8 m) - Sharp irregular contact between shard-rich mudstone (SMud; section 3.3.5) and polymictic felsic sandstone (PfS) facies marked by the presence of flame structures.

C: BHD-10 (89.5 m) - Matrix-supported polymictic mud-matrix felsic breccia. Feldspar crystals and crystal fragments are embedded by abundant, black mud matrix.

D: BHD-10 (119.5 m) - Sharp irregular contact between shard-rich mudstone (SMud; section 3.3.5) and polymictic felsic sandstone (PfS), and polymictic felsic breccia (PfB) facies. The mudstone and polymictic felsic sandstone are massive to finely laminated, and the beds are locally contorted.

E: BHD-10 (235.2 m) - Poorly sorted polymictic felsic breccia. Chloritic (dark green) fragments are aphyric to feldspar-phyric. Feldspar crystals and crystal fragments are abundant.

Uphole and younging directions: A and C - not recorded; D and E - right to left; B - left to right.

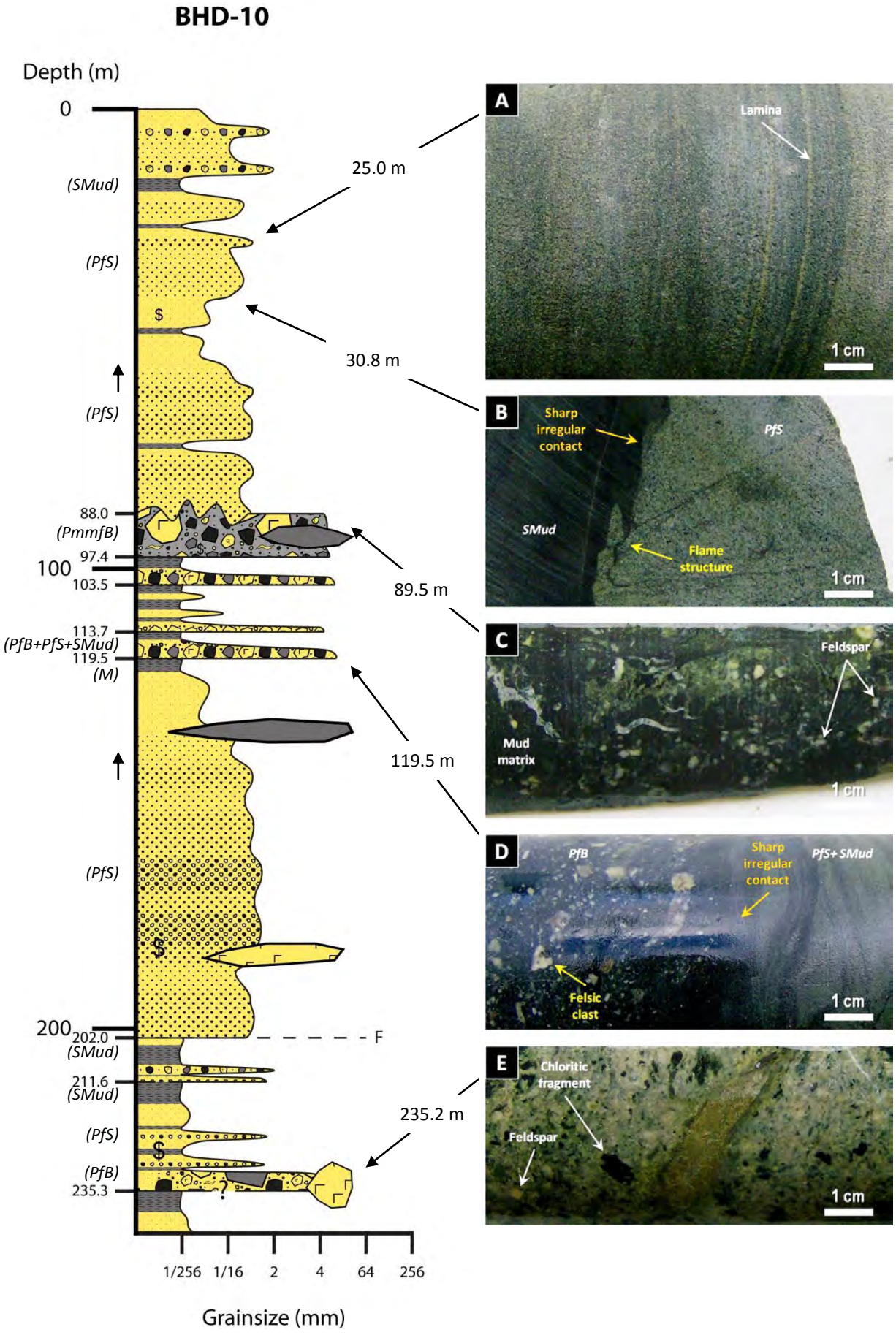
BHD-10
Depth (m)
0
(SMud)
(PfS)
$
(PfS)
88.0
(PmmfB)
97.4
100
103.5
113.7
(PfB+PfS+SMud)
119.5
(M)
(PfS)
$
200
202.0
(SMud)
211.6
(SMud)
(PfS)
$
(PfB)
235.3
F
1/256 1/16 2 4 64 256
Grainsize (mm)
25.0 m
30.8 m
89.5 m
119.5 m
235.2 m
A
Lamina
1 cm
B
Sharp irregular contact
PfS
SMud
Flame structure
1 cm
C
Feldspar
Mud matrix
1 cm
D
PfB
Sharp irregular contact
PfS+SMud
Felsic clast
1 cm
E
Chloritic fragment
Feldspar
1 cm

Figure 3.38: Polymictic felsic breccia (A to D, and F), polymictic mud-matrix felsic breccia (E), and polymictic felsic sandstone (G and H) facies (uphole and younging directions: A, F, and G - right to left; B to D, and H - left to right; E - not recorded). A: BOC-1 (466.8 m); B: BOC-2 (580.0 m); C: BOC-2 (617.7 m); D: BOC-6 (644.8 m); E: SCS-3 (113.3 m); F: BOC-6 (580.0 m); G: BOC-2 (498.8 m); H: BOC-2 (546.7 m).

A: Very poorly sorted, clast-supported polymictic felsic breccia. Large (up to 4 cm across) felsic and lithic clasts are mixed with scarce, feldspar-bearing matrix.

B: Poorly sorted, clast-supported, feldspar crystal-rich polymictic felsic breccia.

C: Very poorly sorted, clast-supported polymictic felsic breccia.

D: Poorly sorted, matrix-supported, feldspar crystal-rich polymictic felsic breccia. The lithic clasts are surrounded by silicified, feldspar crystal-rich matrix.

E: Poorly sorted polymictic mud-matrix felsic breccia. Felsic clasts, chloritic fragments and feldspar crystals and crystal fragments are surrounded by black mud matrix.

F: Sharp wavy contact between polymictic felsic breccia (PfB) and sandstone and mudstone. The polymictic felsic breccia comprises abundant, sub-parallel, aligned fiamme.

G: Massive polymictic felsic sandstone. Large (up to 2 cm across) fiamme occur and are aligned parallel to bedding (yellow two-headed arrow).

H: Weak normal grading (white arrow) in polymictic felsic sandstone.

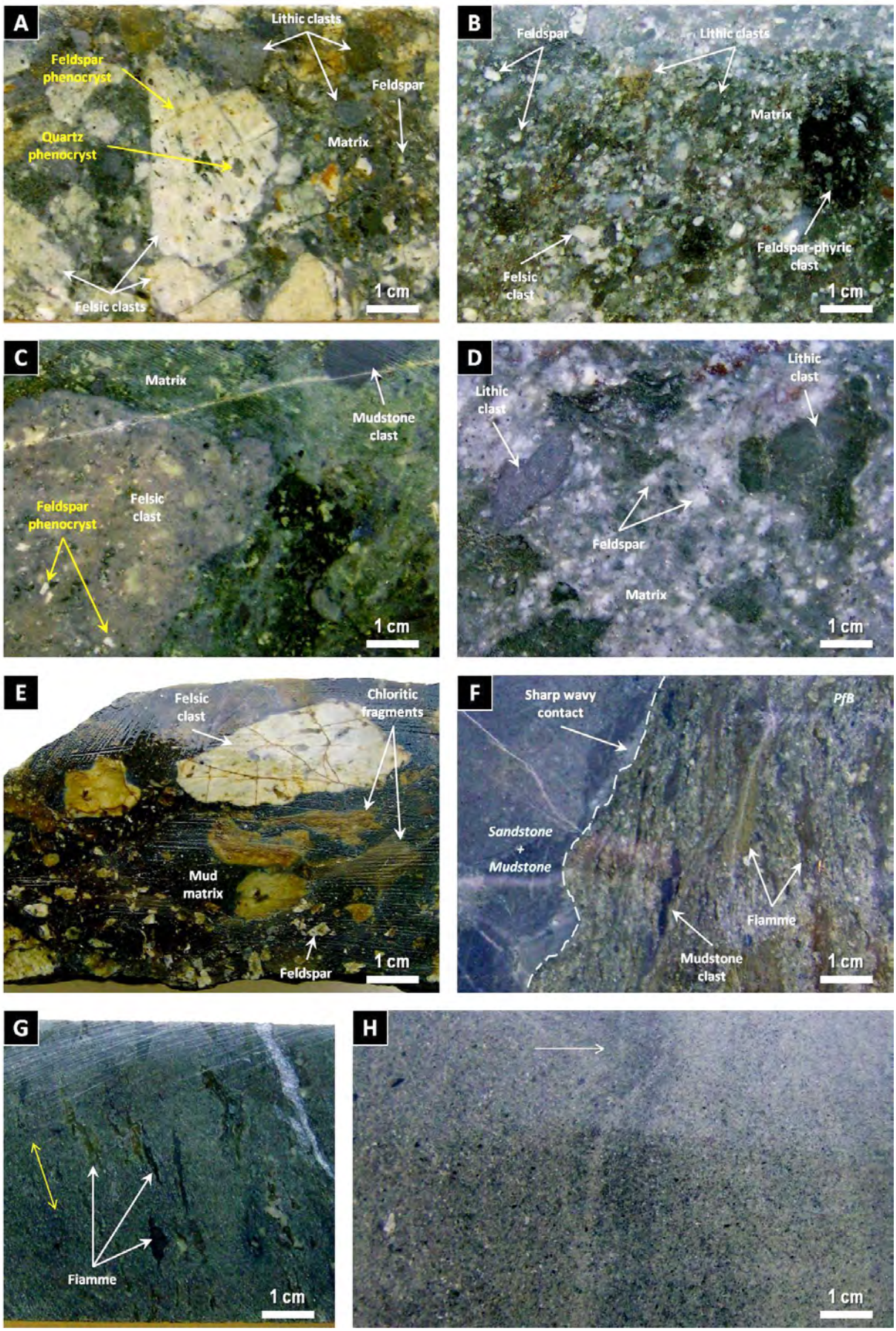
A
Lithic clasts
Feldspar phenocryst
Feldspar
Quartz phenocryst
Matrix
Felsic clasts
1 cm
B
Feldspar
Lithic clasts
Matrix
Feldspar-phyric clast
Felsic clast
1 cm
C
Matrix
Mudstone clast
Feldspar phenocryst
Felsic clast
1 cm
D
Lithic clast
Lithic clast
Feldspar
Matrix
1 cm
E
Felsic clast
Chloritic fragments
Mud matrix
Feldspar
1 cm
F
Sharp wavy contact
PfB
Sandstone + Mudstone
Fiamme
Mudstone clast
1 cm
G
Fiamme
1 cm
H
1 cm

Figure 3.39: Polymictic felsic breccia facies (A, B, F to H, J, K and M - transmitted, plane polarised light; C to E, and L - transmitted, cross polarised light; I - transmitted, reflected light). A to M: BHD-10 (119.5 m).

A: Sharp irregular contact between mudstone (lower left) and polymictic felsic breccia (upper right) facies. A large quartz crystal fragment occurs within the mudstone domain.

B: Strongly chloritic fragment partly surrounded by poorly sorted, feldspar- and quartz-bearing matrix.

C: Sub-angular quartzite fragment.

D: Quartzite fragments and embayed volcanic quartz crystal fragment.

E: Round volcanic quartz, quartzite and schist fragments.

F: Rectangular feldspar.

G: Kinked biotite-rich schist fragment.

H: Angular metamorphic quartz, rectangular feldspar and elongate schist fragments.

I: Sphalerite-chalcopyrite-rich fragment. The sphalerite has chalcopyrite disease.

J: Chromite and fine-grained lithic fragments in sericite- and carbonate-rich matrix.

K: Phyllite fragment.

L: Muscovite flake and circular section of sponge spicule. Professor Patrick Quilty assisted in the identification of sponge spicules.

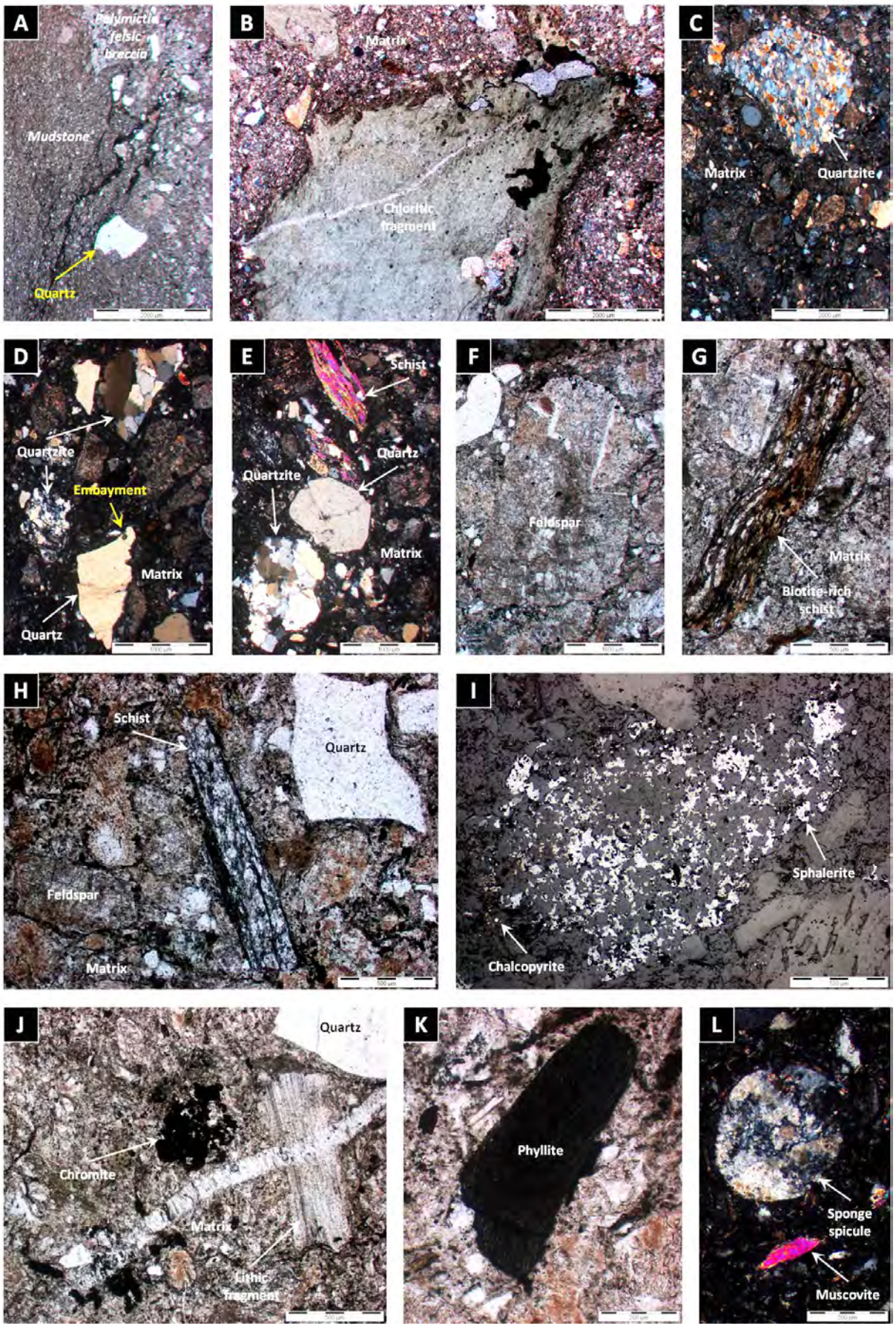
A
Polymictic felsic breccia
Mudstone
Quartz
B
Matrix
Chloritic fragment
C
Matrix
Quartzite
D
Quartzite
Embayment
Matrix
Quartz
E
Schist
Quartz
Quartzite
Matrix
F
Feldspar
G
Matrix
Biotite-rich schist
H
Schist
Quartz
Feldspar
Matrix
I
Sphalerite
Chalcopyrite
J
Quartz
Chromite
Matrix
Lithic fragment
K
Phyllite
L
Sponge spicule
Muscovite

blank

This facies occurs typically in normally graded units comprising polymictic felsic sandstone and breccia with or without mudstone tops (Figure 3.37), in massive units of polymictic felsic sandstone, or intercalated with intervals of polymictic felsic breccia. Many sandstone beds are interbedded with and grade into mudstone beds. Lower and upper contacts with polymictic felsic breccia and mudstone (section 3.3.5), respectively, are gradational. Upper contacts with adjacent units are sharp and planar. Lower contacts with adjacent units are sharp and planar, gradational or irregular (Figure 3.37).

The polymictic felsic sandstone facies (Figure 3.38 - G and H; Figures 3.40 and 3.41) is well to very poorly sorted, massive to normally graded, or bedded (locally laminated). This facies is very similar to the polymictic felsic breccia facies (section 3.3.4.3), but it is finer grained (most fragments are <2 mm). It commonly includes variable amounts (up to 20%) of coarser (>2 mm) fragments, including mudstone clasts up to 8 cm in diameter, chloritic fragments up to 8 cm long, fiamme up to 4 cm long (Figures 3.38 - G; Figure 3.40 - J), fine-grained lithic clasts up to 2 cm in diameter, and aphyric, feldspar-phyric and/or feldspar-quartz-phyric felsic clasts up to 2 cm in diameter.

Single sandstone beds range from less than 10 mm (laminated) up to more than 10 m thick, and are locally silicified and/or disrupted (Figures 3.37 - A). Local feldspar crystal-rich (30-45%, 1-2 mm) domains occur (Figure 3.40 - C). Soft-sediment deformation structures, including mudstone lenses, flame and load structures at the base of single sandstone beds, and sand dykes at the top of single sandstone beds, are common (Figures 3.37 - B; Figures 3.40 - A).

Local shard-rich domains occur (Figure 3.41 - F). The shards are undeformed, composed of polycrystalline quartz, and have cuspate, platy, C, X, Y and irregular, angular shapes (Figure 3.40 - E). Sponge spicules and other organic fragments are also present (Figure 3.40 - F). Rare (<1%) apatite, tourmaline, zircon, rutile, chromite, sphene, and opaque minerals (pyrite, chalcopyrite and sphalerite) also occur (Figure 3.41 - E).

3.3.4.6 Polymictic micaceous sandstone facies (PmS)

The polymictic micaceous sandstone facies occurs from Sock Creek to Burns Peak, and in the Mount Charter area (Figure 3.32). It extends laterally for at least 10 km from Sock Creek to Boco Road. This facies is closely spatially associated with polymictic felsic breccia and sandstone, and mudstone (section 3.3.5) facies (Table 3.6). Polymictic micaceous sandstone intervals range from <1 to 45 m thick.

This facies occurs typically in normally graded intervals or units comprising polymictic micaceous sandstone with mudstone tops, or as massive intervals intercalated with mudstone beds (Figure 3.42). Within normally graded intervals, upper contacts with mudstone beds (section 3.3.5) are gradational. Upper and lower contacts with adjacent units are sharp and planar, or irregular to locally faulted (Figure 3.42).

The polymictic micaceous sandstone facies (Figure 3.43) is well to moderately sorted, massive to normally graded (Figure 3.42 - A and B), or bedded (locally laminated). Polymictic micaceous sandstone beds range

Figure 3.40: Polymictic felsic sandstone facies (A, B, E to H, and J - transmitted, plane polarised light; C, D, and I - transmitted, cross polarised light). A: BHD-10 (30.8 m); B and C: BOC-1 (319.0 m); D: BOC-1 (344.8 m); E to G: BOC-1 (384.5 m); H and I: BOC-2 (286.0 m); J and K: BOC-2 (498.8 m).

A: Sharp irregular contact between shard-rich mudstone (SMud; section 3.3.5) and polymictic felsic sandstone (PfS) facies marked by a flame structure (soft-sediment deformation) of shard-rich mudstone in the polymictic felsic sandstone.

B: Chloritic fragment.

C: Feldspar crystal-rich polymictic felsic sandstone. Abundant feldspar crystals and crystal fragments are strongly sericite-altered.

D: Quartz crystal-rich polymictic felsic sandstone.

E: Delicate and spiky bubble-wall shard.

F: Circular section of sponge spicule with chloritic core. Professor Patrick Quilty assisted in the identification of sponge spicules.

G: Sub-round volcanic quartz fragment with multiple embayments.

H: Sub-angular perlitic felsic fragment.

I: Narrow, elongate muscovite flake.

J: Feldspar-phyric fiamma in quartz-bearing, fine-grained matrix (See Figure 3.37 - G). K: Schist fragment.

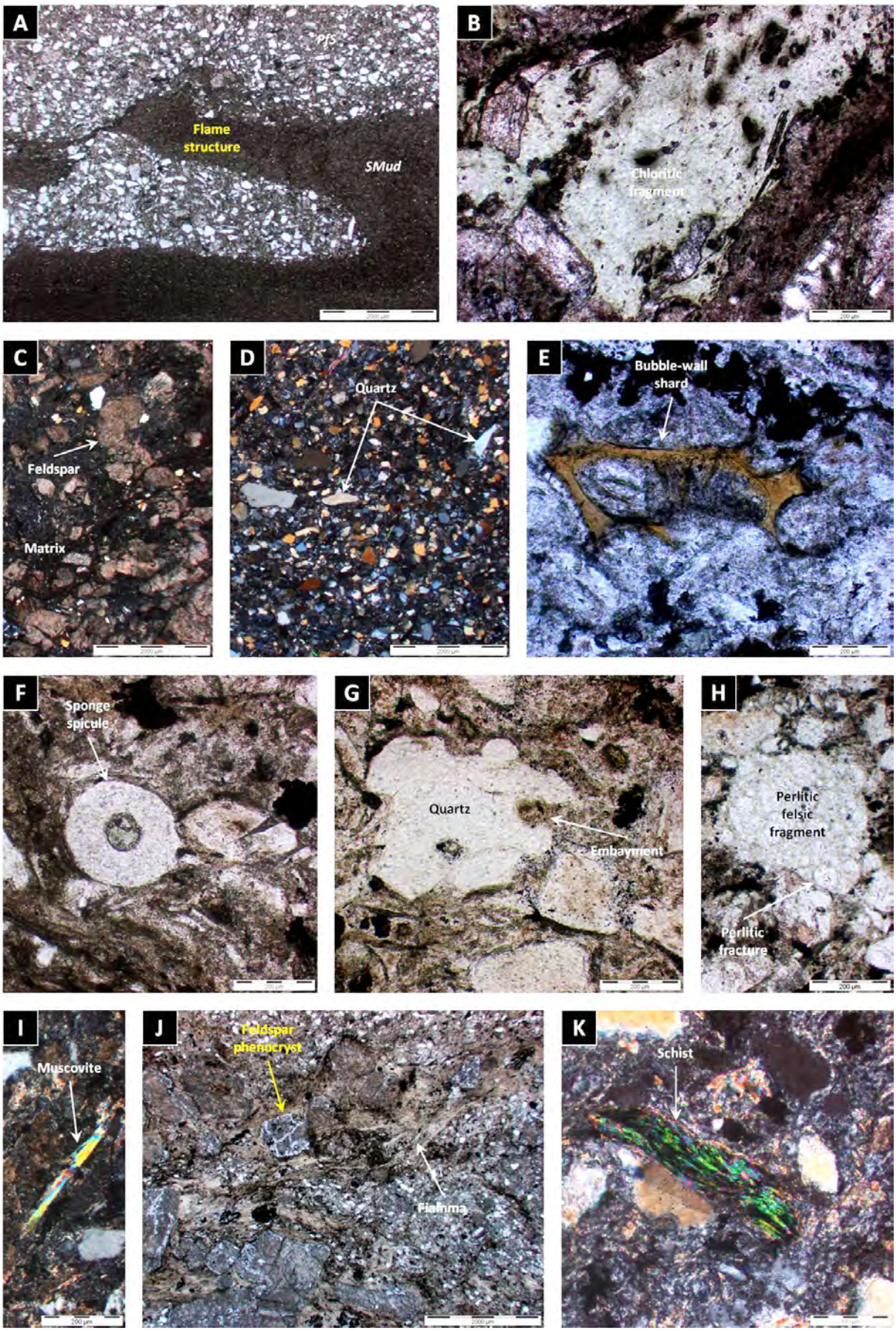
A
pfs
Flame structure
SMud
B
Chloritic fragment
C
Feldspar
Matrix
D
Quartz
E
Bubble-wall shard
F
Sponge spicule
G
Quartz
Embayment
H
Perlitic felsic fragment
Perlitic fracture
I
Muscovite
J
Feldspar phenocryst
Fiamma
K
Schist

Figure 3.41: Polymictic felsic sandstone facies (A, B, D, F, G, and J - transmitted, plane polarised light; C, H, and I - transmitted, cross polarised light; E - transmitted, reflected light). A to F: BOC-6 (459.9 m); G to J: BOC-6 (468.1 m).

A: Quartz-, feldspar-rich polymictic felsic sandstone.
B: Very angular volcanic quartz fragment.
C: Round metasedimentary quartz fragment.
D: Tube pumice fragment surrounded by quartz- and zircon-bearing matrix.
E: Pyrite-chalcopyrite-rich fragment.
F: Quartzite and feldspar fragments in shard-bearing matrix.
G: Fine-grained lithic fragment, and quartz crystals and crystal fragments.
H: Quartzite and feldspar fragments. The feldspar is strongly sericite-altered.
I: Micaceous quartzite fragment. Quartzite fragments range from mica-free to moderately micaceous.
J: Aphyric chloritic fragment surrounded by quartz crystals and crystal fragments.

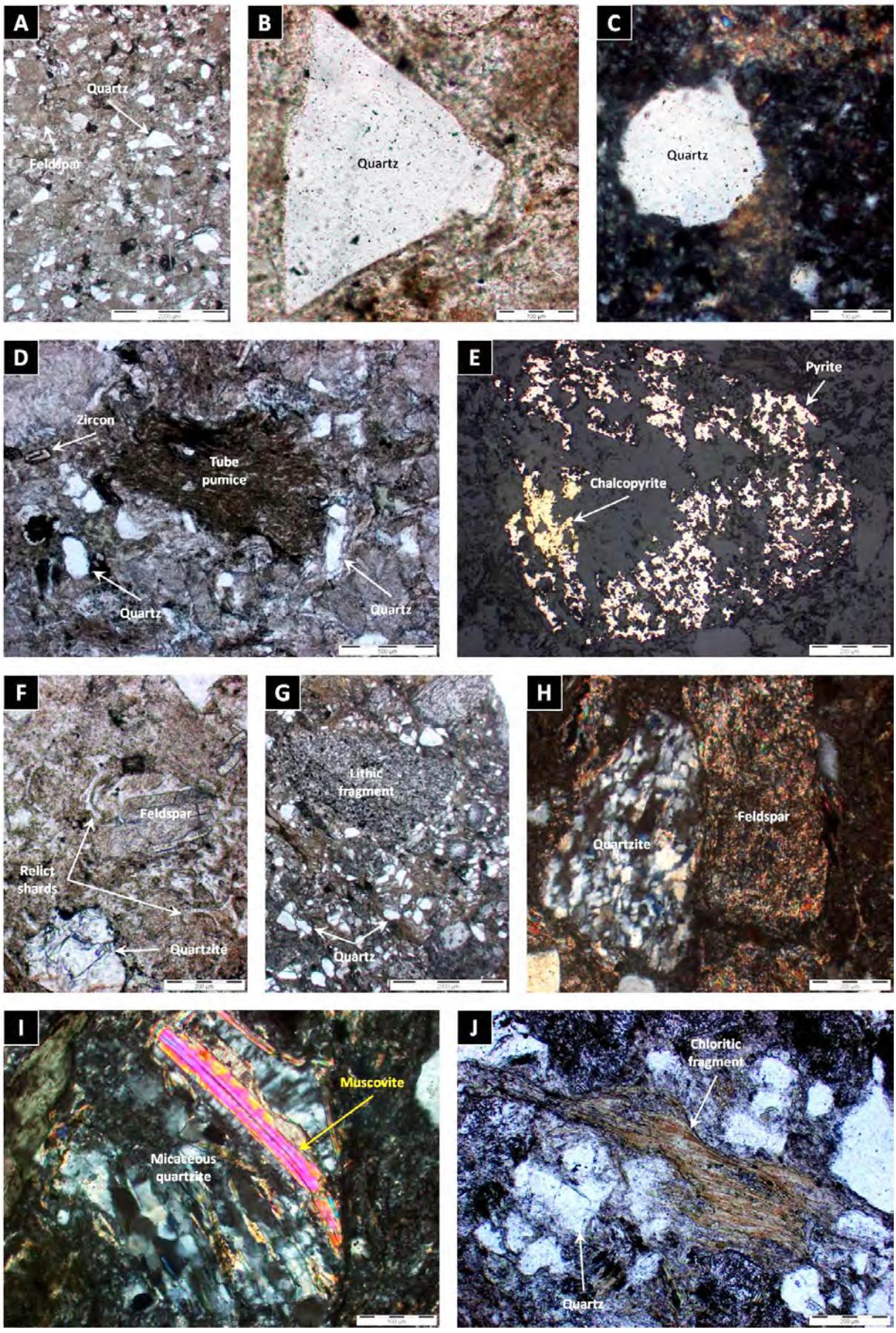
A
Quartz
Feldspar
B
Quartz
C
Quartz
D
Zircon
Tube pumice
Quartz
Quartz
E
Pyrite
Chalcopyrite
F
Feldspar
Relict shards
Quartzite
G
Lithic fragment
Quartz
H
Feldspar
Quartzite
I
Muscovite
Micaceous quartzite
J
Chloritic fragment
Quartz

blank

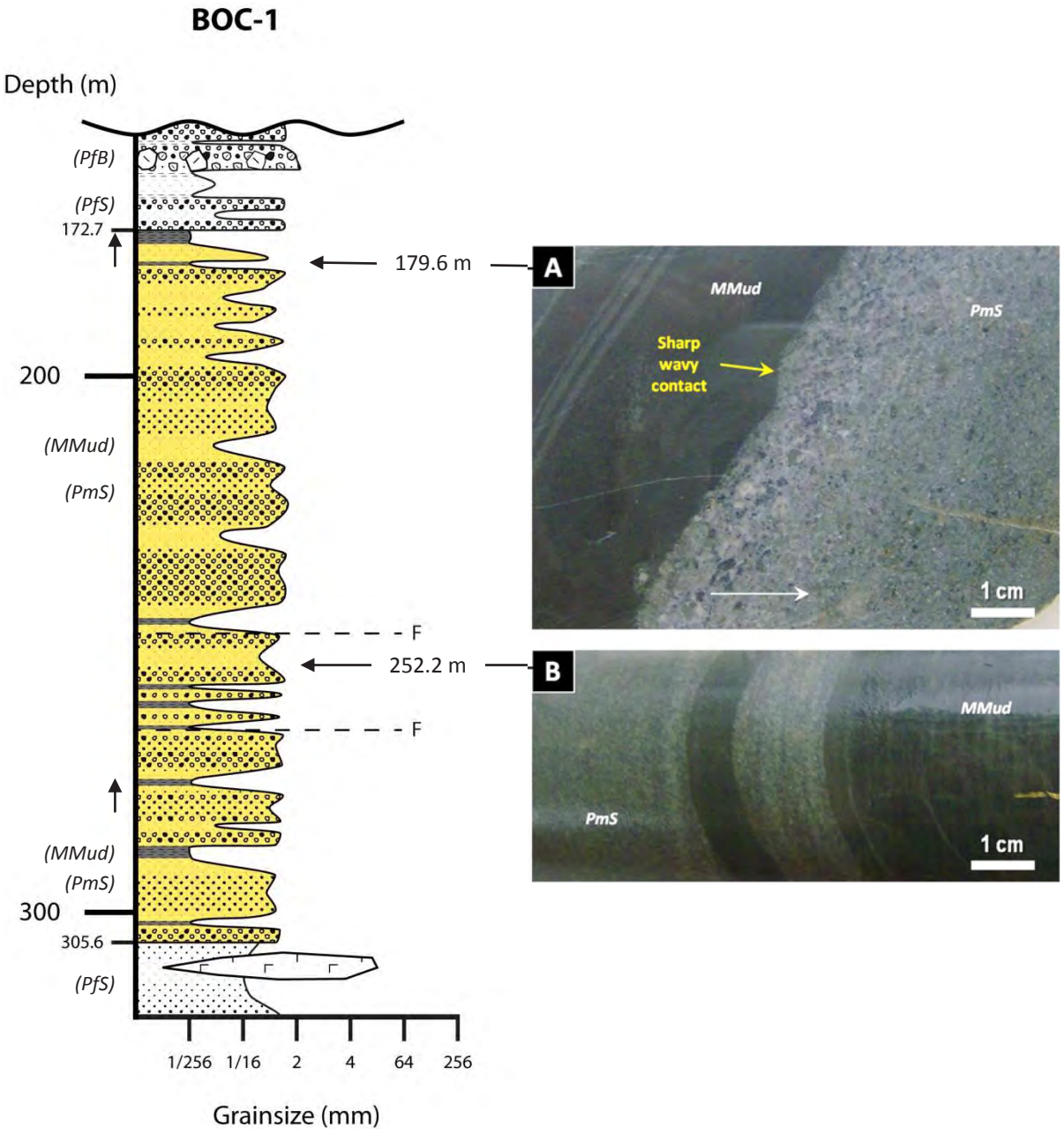

Figure 3.42: Graphic log of part of diamond drill hole BOC-1 (Boco area) through facies of the polymictic volcaniclastic facies association. See Figure 3.4 for legend to graphic log. BOC-1: Normally graded intervals comprising polymictic micaceous sandstone (PmS) with micaceous mudstone (MMud) tops (172.7-305.6 m) occur between polymictic felsic breccia (PfB) and sandstone (PfS) intervals, and are interpreted as density currents and suspension deposits (section 3.3.4.8).

A: BOC-1 (179.6 m) - Sharp wavy contact between laminated micaceous mudstone (MMud) and normally graded (white arrow) polymictic micaceous sandstone (PmS) facies.

B: BOC-1 (252.2 m) - Sharp contacts between laminated micaceous mudstone (MMud) and massive to normally graded polymictic micaceous sandstone (PmS) facies. Uphole and younging directions: A - left to right; B - right to left.

Figure 3.43: Polymictic micaceous sandstone facies. A to C: Handspecimen photographs (uphole and younging directions: A and B - left to right; C - right to left). D to L: Photomicrographs (D, E, H to K - transmitted, plane polarised light; F, G, and L - transmitted, cross polarised light). A: BHD-7 (343.0 m); B and H: BHD-8 (349.0 m); C: BOC-6 (407.8 m); D to G: BHD-4 (564.3 m); I to K: BOC-6 (438.0 m); L: BOC-1 (179.6 m).

A: Sharp, irregular contact between micaceous mudstone (MMud) and polymictic micaceous sandstone (PmS) facies. B: Sharp planar contacts between micaceous mudstone (black) and polymictic micaceous sandstone (grey) beds.

C: Micaceous mudstone (MMud) lenses and dykelets in polymictic micaceous sandstone (PmS).

D: Metamorphic quartz-rich polymictic micaceous sandstone. Abundant metamorphic quartz crystals and crystal fragments surround muscovite flakes and sporadic lithic fragments.

E: Sub-angular metamorphic quartz crystal fragments.

F: Metamorphic quartz crystal fragment and quartzite fragment.

G: Kinked muscovite flake and metamorphic quartz crystal fragment.

H: Muscovite- and biotite-rich polymictic micaceous sandstone. Abundant muscovite and biotite flakes are narrow, elongate, and sub-parallel. Some muscovite and biotite flakes are kinked.

I: Mudstone clast in quartz-rich polymictic micaceous sandstone. Mudstone clasts are composed of very fine grained sericite, chlorite and quartz.

J: Sharp wavy contact between micaceous mudstone (MMud) and polymictic micaceous sandstone (PmS) facies. The mudstone domain (lower left) comprises abundant phyllosilicates (including muscovite and chlorite) and quartz. The polymictic micaceous sandstone domain (upper right) comprises abundant quartz (including volcanic quartz crystal fragments with embayments - top left), and narrow, elongate muscovite flakes.

K: Micaceous quartzite, quartz, biotite and metamorphic quartz fragments.

L: Strongly sericite-altered feldspar crystal fragments.

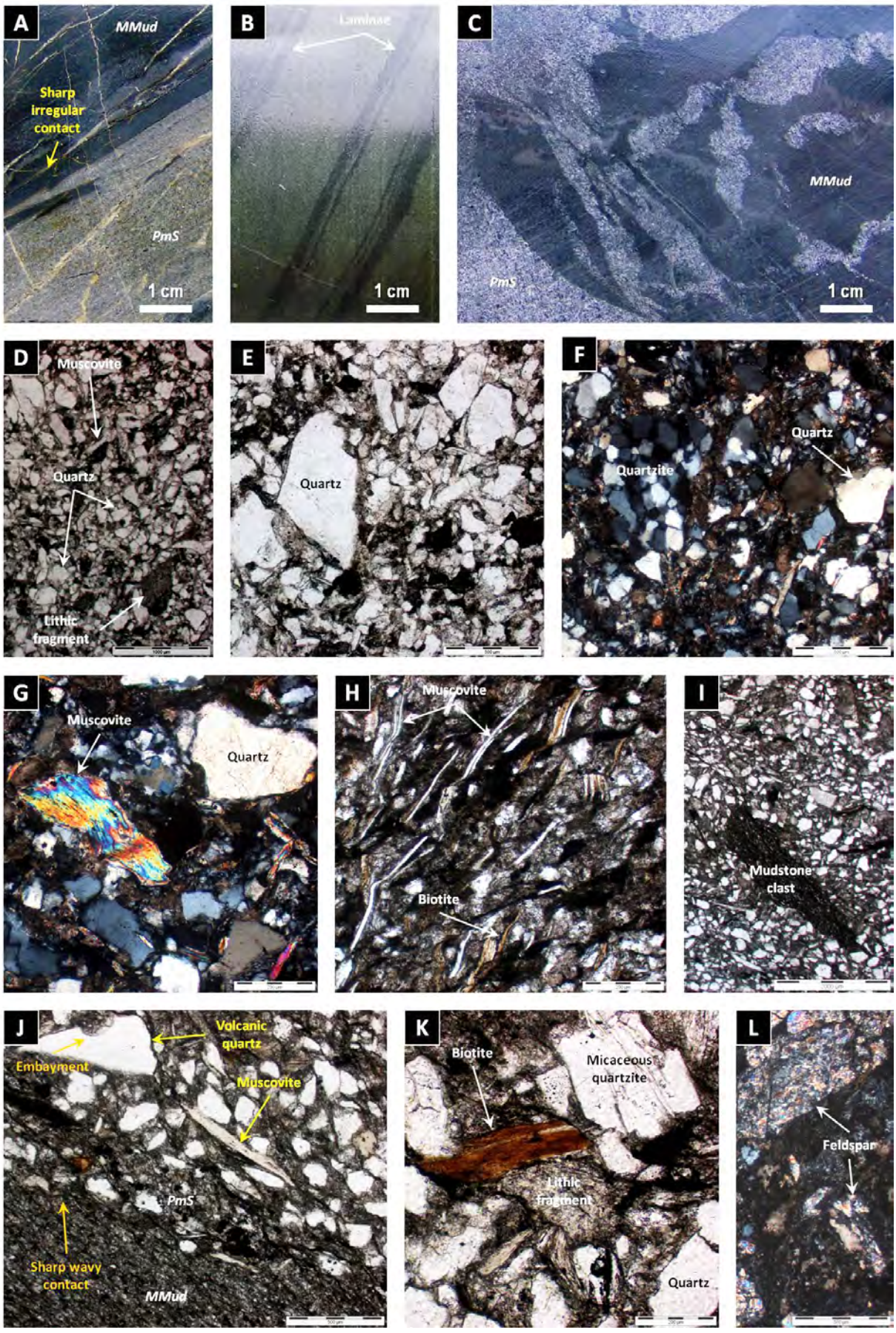
A
MMud
Sharp irregular contact
PmS
1 cm
B
Laminae
1 cm
C
MMud
PmS
1 cm
D
Muscovite
Quartz
Lithic fragment
E
Quartz
F
Quartz
Quartzite
G
Muscovite
Quartz
H
Muscovite
Biotite
I
Mudstone clast
J
Volcanic quartz
Embayment
Muscovite
PmS
Sharp wavy contact
MMud
K
Biotite
Micaceous quartzite
Lithic fragment
Quartz
L
Feldspar

from less than 10 mm (laminated) (Figure 3.43 - B) up to more than 10 m thick (Figure 3.42 - BOC-1), and are locally silicified. Common soft-sediment deformation structures occur at the base of single micaceous sandstone beds, and include mudstone lenses and dykelets (Figure 3.43 - C), and flame and load structures. Local sand dykes occur at the top of single sandstone beds.

The polymictic micaceous sandstone facies is mainly composed of rock (5-40 %, 0.1-2 mm) and crystal fragments (40-70 %, 0.1-1 mm). The rock fragments include fine-grained lithic fragments (1-10%, 0.1-2 mm) and polycrystalline quartz-rich fragments (4-30%, 0.1-2 mm), including quartzite and schist that may contain muscovite (Figure 3.43 - F and K). The crystal fragments include quartz (3-45%, 0.1-0.8 mm) and feldspar (1-30%, 0.1-0.8 mm). The quartz crystals and crystal fragments comprise sub-angular to sub-rounded metasedimentary quartz, and very angular to sub-rounded, clear volcanic quartz with embayed margins (Figure 3.43 - D to G, J and K). Feldspar occurs as sub-angular to sub-rounded, commonly twinned, strongly sericite-altered crystals and crystal fragments (Figure 3.43 - L).

The polymictic micaceous sandstone is characterised by relatively abundant muscovite (1-10%, 0.2-0.8 mm) and biotite (1-5%, 0.1-0.4 mm) crystals and crystal fragments (Figure 3.43 - H). Muscovite and biotite are represented by narrow, elongate flakes that are commonly kinked or ragged (Figure 3.43 - G, J and K). Biotite is commonly altered to chlorite.

This facies also contains variable amounts (up to 15%) of coarser (>2 mm) fragments, including mudstone clasts up to 25 cm in diameter (Figure 3.43 - I), aphyric to feldspar-phyric chloritic fragments up to 2 cm long, fine-grained lithic clasts up to 1 cm in diameter, and aphyric and/or feldspar-phyric felsic clasts up to 8 cm in diameter.

The polymictic micaceous sandstone facies also includes tourmaline (<1%, 0.05-0.1 mm), zircon (<1%, 0.05-0.1 mm), chromite (<1%, 0.05-0.1 mm), and very rare (<<1%) sphene, rutile and apatite. Euhedral to framboidal pyrite also occurs as disseminated grains or clusters up to 3 cm in diameter. Rare sponge spicules and other organic fragments similar to the ones found within the polymictic felsic sandstone facies (section 3.3.4.6) also occur.

3.3.4.7 Polymictic crystal-rich sandstone facies (PcrS)

The polymictic crystal-rich sandstone facies occurs exclusively on Boco Road (Figure 3.32) as massive or bedded (locally laminated) units that are closely spatially associated with mudstone facies (section 3.3.5) (Table 3.6), and may be spatially associated with coherent feldspar-quartz-phyric rhyolite and polymictic rhyolite breccia and sandstone facies (section 3.3.1). Polymictic crystal-rich sandstone intervals range from 4 to 139 m thick. Upper and lower contacts with adjacent units are not exposed at Boco Road.

The polymictic crystal-rich sandstone facies (Figure 3.44) is massive or bedded (locally laminated), moderately to very poorly sorted, and coarse- to very coarse-grained (most fragments are 0.5-2 mm). It is composed of feldspar (<20%, <2 mm) and quartz (<15%, <2 mm) crystals and crystal fragments, and lithic fragments

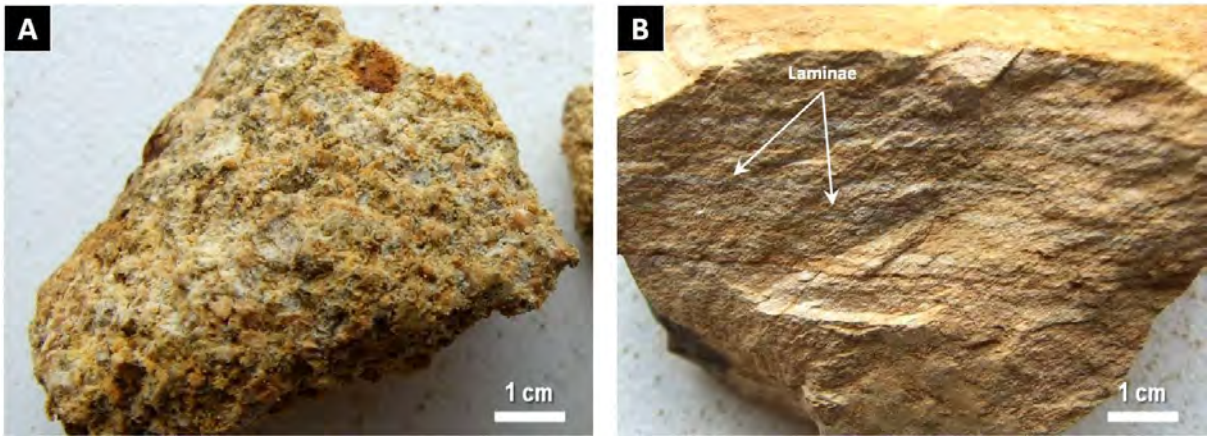

Figure 3.44: Polymictic crystal-rich sandstone facies. A and B: Boco Road (BR vertical section) (uphole and younging directions: not recorded). A: Massive polymictic crystal-rich sandstone. B: Laminated polymictic crystal-rich sandstone.

(<5%, <20 mm). The quartz crystals and crystal fragments are rounded to sub-rounded and irregular. The feldspar crystals and crystal fragments are white to yellow, tabular and irregular. The lithic fragments are orange, tabular and irregular.

3.3.4.8 Interpretation

Polymictic volcanic breccia and sandstone facies

The polymictic volcanic breccia and sandstone facies are closely spatially associated, and clasts types and abundances within these two facies are very similar. Intervals of polymictic volcanic breccia typically grade into polymictic volcanic sandstone (Figure 3.33 - SCS-3 and BHD-7). Textural and mineralogical similarities, gradational contacts, and the spatial association between these two facies suggest that they are genetically related.

The poorly sorted, thickly bedded, and normally graded (to locally massive) natures of the polymictic volcanic breccia and sandstone facies are consistent with deposition of the polymictic volcanic breccia and sandstone from submarine density currents (cf. Lowe, 1982). The polymictic volcanic breccia intervals are probably derived from high-concentration density currents (perhaps debris flows), whereas the polymictic volcanic sandstone intervals are consistent with deposition from lower concentration density currents (cf. Lowe, 1982). Mudstone beds at the top of normally graded units of polymictic volcanic breccia and sandstone were probably the result of settling by suspension of very fine-grained particles through the water column during the waning stages of the density currents.

The locally abundant cuspate and bubble-wall shards in the polymictic volcanic breccia and sandstone facies (Figure 3.35 - H; Figure 3.36 - K) indicates that the source magma or lava was significantly vesicular; the shards were most likely produced by explosive fragmentation of a vesicular, probably felsic magma (e.g.,

Niem, 1977; Cas and Wright, 1991). The shards are undeformed, suggesting that they were cool and solid at deposition and no welding compaction has occurred (e.g., McPhie et al., 1993). The presence of sponge spicules and other organic fragments in the polymictic volcanic breccia and sandstone facies (Figure 3.35 - G; Figure 3.36 - L) is consistent with a subaqueous environment of deposition (Quilty, 1971, 1972b; Quilty and Telfer, 1994; Quilty and Seymour, 2010). The chloritic fragments in the polymictic volcanic breccia and sandstone facies may have been originally glassy; some chloritic fragments that are flattened and aligned (Figure 3.35 - A and F) were probably originally vesicular, juvenile pyroclasts (possibly former pumice).

The massive to normally graded units of polymictic volcanic breccia and sandstone (many with mudstone beds at the top) are up to 50 m thick (Sock Creek area), spatially associated with relatively thick (tens of metres up to approximately 200 m) intervals of coherent feldspar-phyric dacite and monomictic dacite breccia, and laterally extensive for at least 3 km in the Sock Creek-Sock Creek South area (Figures 3.33 – BHD-7 and SCS-3). Furthermore, the polymictic volcanic breccia and sandstone facies comprises some chloritic fragments, locally abundant shards, and relatively abundant (up to 30%) feldspar and quartz crystals and crystal fragments that are most likely juvenile pyroclasts. These features are consistent with submarine, felsic explosive eruption-fed deposits (e.g., McPhie et al., 1993; White, 2000; McPhie and Allen, 2003; Jutzeler et al., 2014).

The locally abundant mafic clasts in the polymictic volcanic breccia and sandstone facies are either non-juvenile pyroclasts or accidental clasts collected from the substrate during transport. The abundant aphyric, feldspar-phyric, and feldspar-quartz-phyric felsic volcanic clasts in the polymictic volcanic breccia and sandstone facies were derived from aphyric, feldspar-phyric and feldspar-quartz-phyric sources (most likely dacitic and rhyolitic). The aphyric and feldspar-phyric felsic clasts could be juvenile pyroclasts because they have the same phenocryst population as the chloritic fragments interpreted to be juvenile. The feldspar-quartz-phyric felsic clasts are non-juvenile fragments and could be non-juvenile pyroclasts or accidental clasts excavated from underlying, pre-existing monomictic felsic (rhyolite and/or dacite) breccia. The sponge spicules, organic fragments and black mudstone clasts were probably collected en route from the substrate. The high abundance of perlitic felsic fragments suggests that the explosive eruption(s) were seated in glassy or partly glassy felsic domes or lavas.

The rare quartzite and schist clasts have a metamorphic basement origin. The nearest in situ basement outcrops are presently 5-10 km from the northern Mount Read Volcanics (Figure 2.2). These components are difficult to explain but three possibilities exist: (1) they could be extrabasinal clasts originally transported into the basin by turbidity currents and then recycled from the unconsolidated substrate into the volcaniclastic density currents, or (2) they could be non-juvenile pyroclasts sampled from the deep conduit by explosive eruptions at an intrabasinal vent, or (3) they could be non-juvenile pyroclasts or accidental clasts incorporated in pyroclastic density currents that originated at the basin margin and then crossed the shoreline, becoming water-supported density currents.

Polymictic felsic breccia and sandstone facies

The polymictic felsic breccia and sandstone facies (Figure 3.37 - BHD-10) are similar to the polymictic volcanic breccia and sandstone facies, respectively, and are interpreted in a similar way. The main difference is the lack of mafic clasts within the polymictic felsic breccia and sandstone facies.

Sand dykes at the top of single polymictic felsic sandstone beds indicate that upward intergranular flow occurred locally, typical of a fluidized flow (cf. Lowe, 1982). Other soft-sediment deformation structures, such as mudstone lenses, flame and load structures at the base of single polymictic felsic sandstone beds (Figure 3.37 - B) may have been produced during decelerating density currents. Soft-sediment deformation structures are characteristic of high-accumulation rate environments.

The locally abundant shards, chloritic fragments, at least some quartz and feldspar crystals and crystal fragments, and possibly some of the amygdaloidal felsic clasts are most likely juvenile pyroclasts, and suggest that the density currents were probably at least partly felsic explosive-eruption-fed (e.g., McPhie et al., 1993; White, 2000; McPhie and Allen, 2003; Jutzeler et al., 2014). The thickness (up to approximately 100 m) of normally graded intervals of polymictic felsic breccia and sandstone is also consistent with this interpretation.

The schist, phyllite, and relatively abundant quartzite clasts have a metamorphic basement origin, and present the same challenges for interpretation as they do for the polymictic volcanic breccia and sandstone facies. However, in these facies, the metamorphic clasts are associated with rare detrital chromite. The detrital chromite was sourced from the mafic-ultramafic complexes (Crawford et al., 1992), indicating that these complexes had already been emplaced and were being eroded when the polymictic felsic breccia and sandstone facies were accumulating. Hence, the metamorphic clasts were most likely derived from deformed, metamorphic basement exposed at the basin margin, indicating that the eruption-fed density currents originated from basin-margin, rather than intrabasinal, vents.

The locally abundant fiamme within the thin interval (1.2 m thick) of polymictic felsic breccia facies in the Boco area (DDH BOC-6) (Figure 3.38 - F) were probably pumice clasts originally sourced from a felsic explosive eruption. This interval could be explosive-eruption-fed but resedimentation of a pre-existing pyroclastic deposit is also plausible. The narrow, elongate, strongly aligned mudstone clasts (Figure 3.38 - F) were probably derived from the mud substrate across which the density currents moved.

Polymictic mud-matrix felsic breccia facies

The dark grey to black mudstone in the polymictic mud-matrix felsic breccia facies (Figure 3.37 - BHD-10 and C) is interpreted to have been incorporated by mixing of pre-existing mud sediment with the other components during submarine density current episodes. Local interbedding of polymictic mud-matrix felsic breccia and mudstone intervals with gradational contacts supports this interpretation.

Polymictic micaceous sandstone facies

The polymictic micaceous sandstone facies (Figure 3.42 - BOC-1) is spatially associated with and similar to the polymictic felsic sandstone facies, and is also interpreted to comprise deposits from submarine density currents. The abundant muscovite and biotite flakes (Figure 3.43 - G, H and are commonly kinked and ragged, and are probably detrital. The presence of rare detrital chromite (sourced from the mafic-ultramafic complexes; Crawford et al., 1992) in the polymictic micaceous sandstone facies suggests that the metamorphic clasts (quartzite and schist) and possibly some muscovite and biotite flakes were derived from deformed, metamorphic basement exposed at the basin margin. Some of the muscovite and biotite crystals and crystal fragments could be non-juvenile pyroclasts collected en route from the substrate by the density currents.

The density currents that produced the polymictic micaceous sandstone facies carried a substantial amount of non-volcanic, metamorphic debris, and most likely originated from the basin margin. The density currents were probably generated by slope failure associated with tectonic earthquakes or movement along syn-depositional faults.

Polymictic crystal-rich sandstone facies

The polymictic crystal-rich sandstone facies (Figure 3.44) has bed forms consistent with deposition from high- and low-concentration density currents (cf. Lowe, 1982). This facies may be spatially associated with coherent feldspar-quartz-phyric rhyolite and polymictic rhyolite breccia and sandstone facies, from where at least some of the quartz and feldspar crystals and crystal fragments may have been derived. The lack of data prevents the complete interpretation of this facies.

3.3.5 Mudstone facies association

The mudstone facies association comprises three facies: 1) black mudstone, 2) micaceous mudstone, and 3) shard-rich mudstone. The location of the diamond drill holes intersecting facies of the polymictic volcaniclastic facies association is shown in Figures 3.45 and 3.46. The characteristics of the facies comprising the mudstone facies association are summarized in Table 3.7.

3.3.5.1 Black mudstone facies (BMud)

The black mudstone facies occurs from Sock Creek to Burns Peak, on Boco Road, and in the Bulgobac Hill and Mount Charter areas (Figure 3.45). It also occurs in the White Spur and Howards Road areas (Figure 3.46). Intervals of dark grey and black mudstone intersected by diamond drill holes in this study range from <0.1 to 36 m thick (the thickest interval was intersected in the Burns Peak area), and are massive or laminated (Table 3.7). Single mudstone beds range from <2 mm (finely laminated) up to approximately 1 m. Laminated mudstone is commonly deformed and/or disrupted by minor faults. Sharp, planar and wavy contacts typically separate single mudstone beds. This facies commonly occurs interbedded with

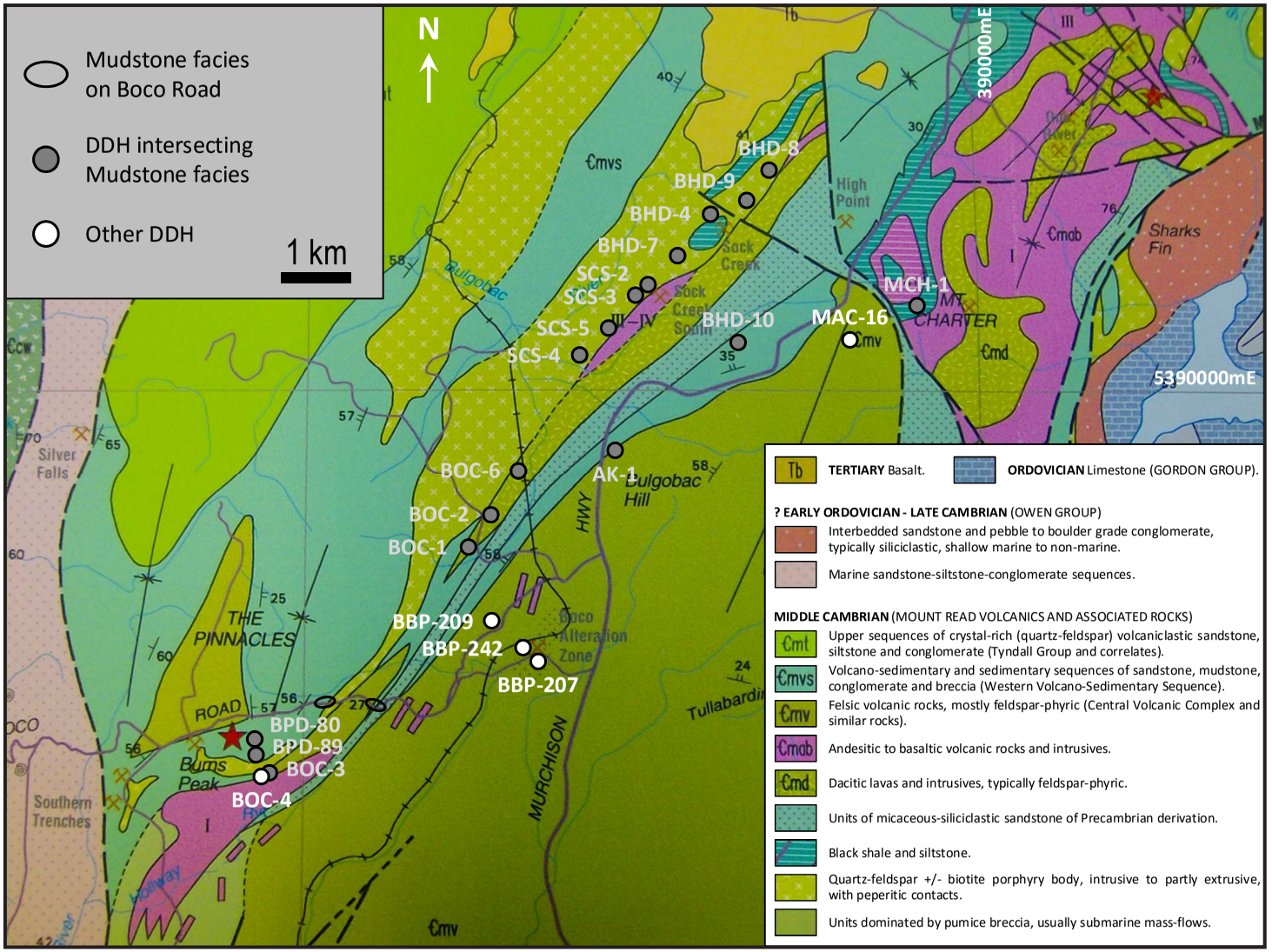

Figure 3.45: Geology of the Que River-Burns Peak area showing the location of the diamond drill holes (DDH) in this study, after Corbett (2002a). Facies of the mudstone facies association (Mud) occur at Boco Road and are intersected by DDH AK-1 (Bulgobac Hill area), BHD-4, BHD-7, BHD-8 and BHD-9 (Sock Creek area), BHD-10, SCS-2, SCS-3, SCS-4 and SCS-5 (Sock Creek South area), BOC-1, BOC-2 and BOC-6 (Boco area); BOC-3, BPD-80 and BPD-89 (Burns Peak area), and MCH-1 (Mount Charter area).

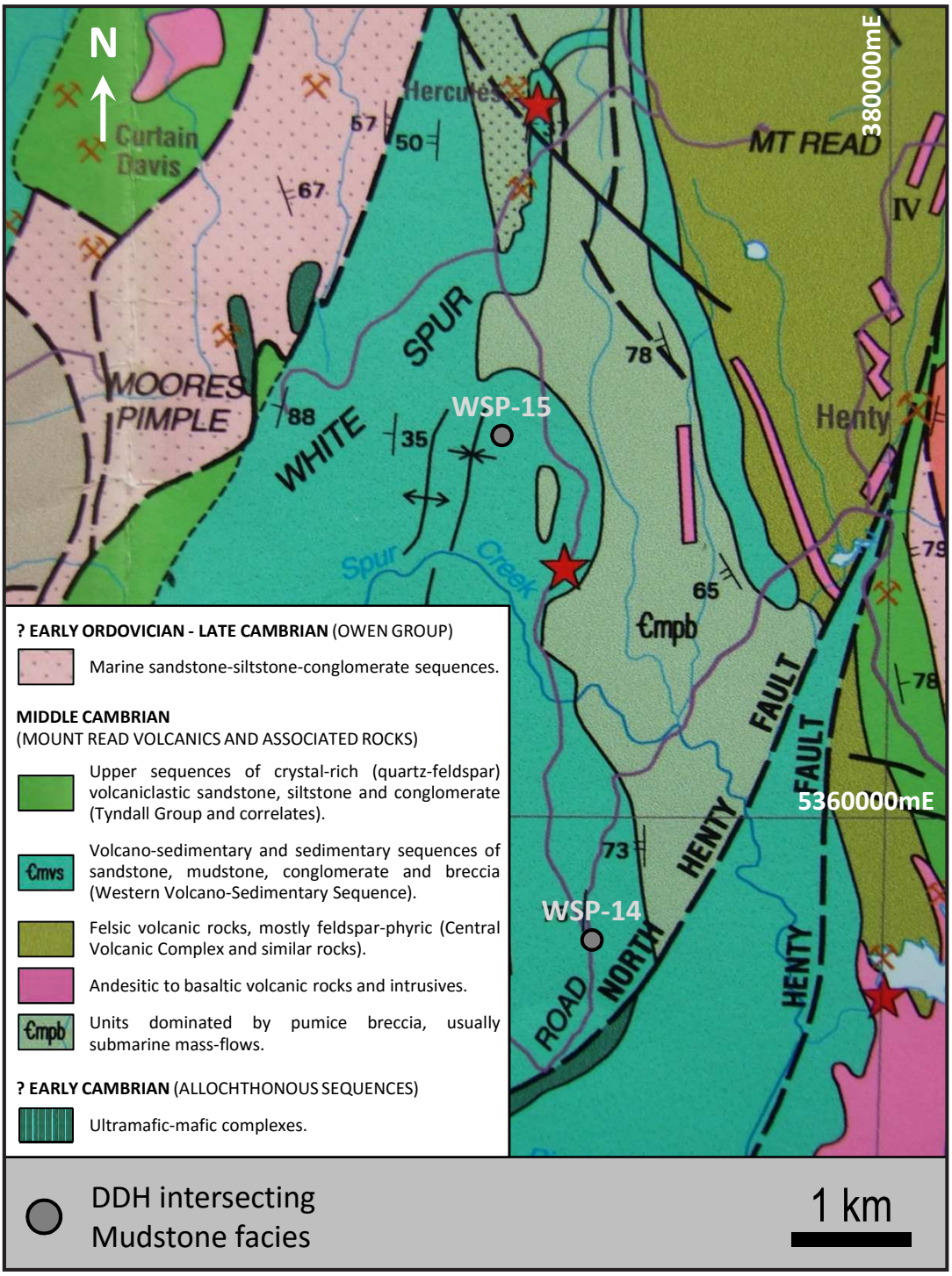

Figure 3.46: Geology of the White Spur-Howards Road area showing the location of the diamond drill holes (DDH) in this study, after Corbett (2002a). Facies of the mudstone facies association (Mud) are intersected by DDH WSP-14 (Howards Road) and WSP-15 (White Spur area).

Table 3.7: Characteristics, location and interpretation of the facies comprising the mudstone facies association.

Facies association, facies and sub-facies		Lithofacies characteristics	Thickness x lateral extent	Mineralogy/Components	Textures	Associated facies	Location and diamond drill holes	Interpretation
Mudstone facies association (Mud)	*Black mudstone facies* ***(BMud)***	Massive, bedded to laminated; abundant lamina; dark grey to black	<0.1-36 m x 12 km? (Sock Creek to Burns Peak)	Muscovite, chlorite, carbonate, iron oxides, carbon; minor (<1%) quartz (volcanic and metamorphic), quartzite, micaceous quartzite, and lithic fragments; rare feldspar, apatite, zircon, and sponge spicules; pyrite, chalcopyrite, sphalerite, pyrrhotite	Soft-sediment deformation structures (mudstone lenses and dykelets, flame and load structures)	Polymictic rhyolite sandstone; polymictic volcanic sandstone	Bulgobac Hill: **AK-1**; Sock Creek: **BHD-4, BHD-7, BHD-8, BHD-9**; Sock Creek South: **SCS-2, SCS-3, SCS-4, SCS-5**; Boco: **BOC-1, BOC-2, BOC-6**; Burns Peak: **BOC-3, BPD-80, BPD-89**; Mount Charter: **MCH-1**; Howards Road: **WSP-14**; White Spur: **WSP-15**; Boco Road	Suspension deposits in subaqueous environments; muddy density currents
	Micaceous mudstone facies ***(MMud)***	Massive, bedded to laminated; abundant lamina; pale to dark grey and black	<0.1-8 m x 12 km? (Sock Creek to Burns Peak)	Muscovite (<30%), chlorite, carbonate, iron oxides, and quartz; coarser (<20%, <2 mm) fragments, including quartzite, schist, lithic fragments, quartz, feldspar and muscovite fragments; rare apatite, zircon, and sponge spicules; pyrite, chalcopyrite, and sphalerite	Soft-sediment deformation structures (mudstone lenses and dykelets, flame and load structures); bedding parallel foliation (muscovite flakes)	Polymictic micaceous sandstone	Sock Creek: **BHD-4, BHD-7, BHD-8, BHD-9**; Sock Creek South: **SCS-5**; Boco: **BOC-1, BOC-2, BOC-6**; Burns Peak: **BOC-4**; Mount Charter: **MCH-1**; Boco Road	Suspension deposits in subaqueous environments; muddy density currents
	Shard-rich mudstone facies ***(SMud)***	Massive, bedded to laminated; abundant lamina; pale grey/greenish	<0.1-15 m x 4 km? (Sock Creek South to Boco)	Muscovite (<15%), chlorite, carbonate, iron oxides, and quartz; coarser (<2 mm) fragments similar to Mmud; shard-rich (<30%, <0.8 mm); rare apatite, zircon, and sponge spicules; pyrite, chalcopyrite, and sphalerite	Soft-sediment deformation structures (mudstone lenses and dykelets, flame and load structures); shards with cuspate, platy, C, Y, and irregular, splintery shapes; bedding parallel foliation (muscovite flakes)	Polymictic felsic sandstone	Sock Creek South: **BHD-10**; Boco: **BOC-1, BOC-2, BOC-6**	Suspension deposits in subaqueous environments; muddy density currents

or typically at the top of normally graded intervals of polymictic rhyolite sandstone (section 3.3.1) and polymictic volcanic sandstone (section 3.3.4). Soft-sediment deformation structures occur in places and include mudstone lenses and dykelets, and flame and load structures.

The black mudstone facies (Figure 3.47 - A) is carbonaceous and dominantly composed of muscovite, chlorite, carbonate and iron oxides, and minor amounts (<1%) of quartz, quartzite, micaceous quartzite and fine-grained lithic fragments. The quartz crystal fragments are mainly of metamorphic origin, but minor, apparently volcanic quartz may also occur. Rare apatite, zircon and feldspar crystal fragments, and sponge spicules are also present. Pyrite, sphalerite, chalcopyrite, and pyrrhotite also occur. Pyrite occurs as <2 cm lenticular nodules and lenses <1 cm thick parallel to bedding, as fillings in bedding surfaces and small fractures and faults, and as disseminated, anhedral to euhedral (cubes) spots (Figure 3.47 - A). Framboidal pyrite is common. The black mudstone facies may comprise rare, coarser (<12 cm) feldspar-quartz-phyric rhyolite and chloritic fragments.

3.3.5.2 Micaceous mudstone facies (MMud)

The micaceous mudstone facies occurs from Sock Creek to Burns Peak, and in the Mount Charter area (Figure 3.45). Intervals of micaceous mudstone range from <0.1 to 8 m thick, and are massive or commonly laminated (Table 3.7). Intervals of micaceous mudstone occur intercalated with or typically at the top of normally graded units comprising polymictic micaceous sandstone (section 3.3.4).

The micaceous mudstone facies (Figure 3.47 - B to I) is similar to the black mudstone facies, but it is pale to dark grey or black, strongly micaceous (<30% muscovite), and commonly comprises coarser (<20%, <2 mm) fragments, including rock and crystal fragments (Figure 3.47 - D). Rock fragments include quartzite, micaceous quartzite and schist fragments, and fine-grained lithic fragments. The crystal fragments include quartz, feldspar, and muscovite. The quartz crystal fragments include metamorphic quartz and clear, embayed volcanic quartz (Figure 3.47 - D, G and H). The feldspar is typically strongly sericite-altered (Figure 3.47 - D). Abundant muscovite typically occurs as narrow, elongate, locally arcuate flakes that are commonly aligned defining a bedding-parallel foliation (Figure 3.47 - E). The micaceous mudstone facies typically comprises strongly altered domains composed of any combination of carbonate, sericite and chlorite.

3.3.5.3 Shard-rich mudstone facies (SMud)

The shard-rich mudstone facies occurs from Sock Creek South to the Boco area (Figure 3.45). Intervals of shard-rich mudstone range from <0.1 to 15 m thick, and are massive or laminated (Table 3.7). This facies occurs intercalated with or typically at the top of normally graded units comprising polymictic felsic sandstone (section 3.3.4) (Figure 3.37 - BHD-10, B and D).

The shard-rich mudstone facies is similar to the micaceous mudstone facies, but it is pale grey/greenish, and comprises abundant (<30%, <0.8 mm) devitrified glass shards (Figure 3.47 - L). The shards are typically composed of polycrystalline and cryptocrystalline quartz, and include undeformed, bubble-wall shards with

cuspate, platy, C, X, Y and irregular shapes. Coarse (<2 mm) quartz fragments are angular to sub-angular and mainly of volcanic origin. Coarse (<2 mm) feldspar crystal fragments and sponge spicules occur (Figure 3.47 - J and K).

3.3.5.4 Interpretation

The facies of the mudstone facies association are interpreted to have settled from suspension. Intervals of thick, massive, black, micaceous or shard-rich mudstone probably also include deposits from muddy density currents. The presence of sponge spicules (Figure 3.47 - K) is consistent with a subaqueous environment of deposition (Quilty, 1971, 1972b; Quilty and Telfer, 1994; Quilty and Seymour, 2010). Intervals of laminated, pyritic, carbonaceous black mudstone (Figure 3.47 - A) are consistent with relatively deep (below wave base) subaqueous environments with quiet, reducing conditions.

The abundant muscovite in the micaceous mudstone facies (Figure 3.47 - E) is probably detrital and sourced from deformed, locally exposed metamorphic basement at the basin margin. The close spatial association between micaceous mudstone and polymictic micaceous sandstone (sections 3.3.4.6 and 3.3.4.8) facies, and the occurrence of coarse (<2 mm) metamorphic quartz with undulose extinction, quartzite, micaceous quartzite and schist fragments (Figure 3.47 - D) within the micaceous mudstone facies are consistent with this interpretation.

The presence of abundant bubble-wall shards in the shard-rich mudstone facies (Figure 3.47) indicates that the source magma was significantly vesicular. The shards are undeformed, suggesting that they were cool and solid at deposition and no welding compaction has occurred (e.g., McPhie et al., 1993). The shards were originally produced by explosive fragmentation of a probably felsic magma (Niem, 1977; Cas and Wright, 1991).

The presence of volcanic quartz crystal fragments (Figure 3.47 - H) in the micaceous and shard-rich mudstone facies indicates a volcanic origin. The fine-grained lithic fragments (Figure 3.47 - D) may represent a different volcanogenic source.

3.4 Summary

Five different facies associations have been identified in the Sock Creek-Burns Peak, White Spur-Howards Road and Mount Charter areas of the northern Mount Read Volcanics. Three distinct facies of the mudstone facies association (black, micaceous and shard-rich mudstone) are intercalated with the different volcanic facies, and constrain the depositional setting to below-wave-base. The spatial distribution, bedforms and textural and mineralogical characteristic of the seven different facies of the polymictic volcaniclastic facies associations are consistent with high- and low- concentration density currents, some of which were explosive eruption-fed, and further support a below-wave-base setting.

Figure 3.47: Black (A), micaceous (B to I) and shard-rich (B, J to L) mudstone facies. A, B and F: Handspecimen photographs (uphole and younging directions: right to left). C to E, G to L: Photomicrographs (C, I and L - transmitted, reflected light; D, E, G, J and K - transmitted, cross polarised light; H - transmitted, plane polarised light). A: BHD-4 (595.8 m); B and C: BOC-1 (172.7 m); D: BHD-7 (343.0 m); E: BHD-10 (30.8 m); F to I: BHD-10 (64.5 m); J to L: BOC-6 (570.2 m).

A: Pyrite nodule in black mudstone facies.

B: Planar sharp and sharp irregular contacts between shard-rich mudstone (SMud) and micaceous mudstone (MMud), respectively, with normally graded (white arrow) polymictic felsic sandstone facies (PfS). The shard-rich mudstone is pale grey/greenish and the micaceous mudstone is pale and dark grey and laminated.

C: Disseminated to locally massive pyrite.

D: Sandy micaceous mudstone. Crystal fragments include metamorphic and volcanic quartz, feldspar, and muscovite. Rock fragments include schist and fine-grained lithic fragments.

E: Bedding-parallel foliation defined by the alignment of abundant, narrow, elongate muscovite flakes.

F: Laminated micaceous mudstone. Mudstone laminae are pale to dark grey and black.

G: Micaceous quartzite and metamorphic quartz fragments in micaceous mudstone.

H: Embayed volcanic quartz fragment and narrow, elongate muscovite flakes. The muscovite flake is arcuate.

I: Sphalerite with chalcopyrite disease.

J: Strongly sericite-altered feldspar crystal fragment.

K: Silicified circular section of sponge spicule. Professor Patrick Quilty assisted in the identification of sponge spicules.

L: Shard-rich mudstone. Abundant, undeformed, devitrified bubble-wall glass shards have cuspate, platy, C, Y, and irregular shapes.

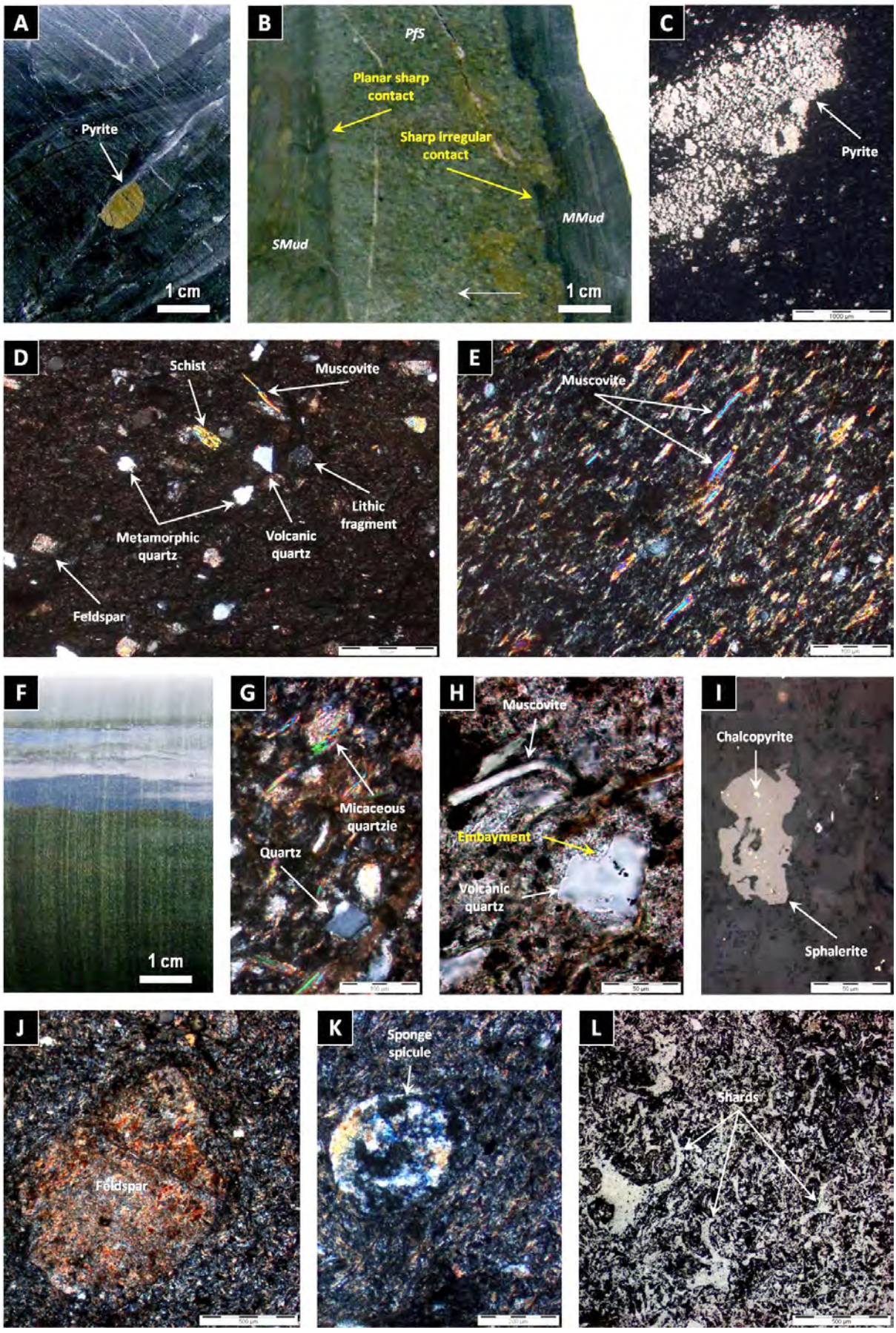
A
Pyrite
1 cm
B
PfS
Planar sharp contact
Sharp irregular contact
MMud
SMud
1 cm
C
Pyrite
D
Schist
Muscovite
Lithic fragment
Metamorphic quartz
Volcanic quartz
Feldspar
E
Muscovite
F
1 cm
G
Micaceous quartzie
Quartz
H
Muscovite
Embayment
Volcanic quartz
I
Chalcopyrite
Sphalerite
J
Feldspar
K
Sponge spicule
L
Shards

Coherent facies of the rhyolite, dacite and mafic (andesite and basalt) facies associations are interpreted as lavas, domes, syn-volcanic sills, dykes and/or cryptodomes, and are typically associated with monomictic rhyolite, dacite and mafic breccia facies, respectively, which represent proximal autoclastic (autobreccia and hyaloclastite) facies. Normally graded intervals of monomictic rhyolite, dacite and mafic breccia and sandstone spatially associated with coherent rhyolite, dacite and mafic facies, respectively, are consistent with extrusion of the coherent facies, whereas the presence of peperitic upper contacts (monomictic mud-matrix rhyolite, dacite and mafic breccia facies) indicates intrusion of the associated coherent facies. Monomictic rhyolite and dacite breccia comprising abundant fiamme (monomictic fiamme-rich rhyolite and dacite breccia facies) are interpreted as resedimented, diagenetically compacted autoclastic deposits.

Very thick successions of rhyolitic and dacitic coherent facies and associated monomictic breccia facies indicate the presence of multiple, mainly effusive to shallow intrusive, felsic intrabasinal volcanic centres. The presence of monomictic fluidal-clast mafic breccia facies locally in the Burns Peak area, a distinctive monomictic volcanic breccia facies, indicates subaqueous mafic lava fountaining, and suggests a mafic eruptive centre was active at, or near (tens of m) Burns Peak.

CHAPTER 4

Stratigraphy, correlations and facies architecture in the Sock Creek-Burns Peak area

4.1 Introduction

This chapter focuses on the stratigraphy, correlations and facies architecture of the Sock Creek-Burns Peak area in the northern Mount Read Volcanics (MRV). It is divided into three parts. The first part (section 4.2) introduces the local geology and stratigraphy of the Sock Creek-Burns Peak area. The second part (section 4.3) deals with the major identified stratigraphic units and correlations in the Sock Creek-Burns Peak area. Connections between the major identified stratigraphic units and the formal regional stratigraphy are discussed. The third part (section 4.5) discusses the facies architecture in the Sock Creek-Burns Peak area.

Correlations in the Sock Creek-Burns Peak area are presented as stratigraphic fence diagrams constructed from detailed logging of twenty one DDH (appendix A) and mapping of an approximately 2-km-section along Boco Road, roughly midway between the Boco Alteration Zone and the Pinnacles (Figure 4.1). The stratigraphy and regional correlations of the Sock Creek-Burns Peak area with the areas to the NE (Hellyer-Mount Charter) and SSW (Rosebery-Howards Road) are discussed in Chapter 5.

Correlations are based on: (1) the lithofacies characteristics (composition, textures, structures and internal organization), (2) the contact relationships and spatial distribution of the separate facies and facies associations, and (3) the relative stratigraphic position of the major identified stratigraphic units. The reliability of correlations depends on: the proximity between diamond drill holes (DDH) and whether or not the facies grouped into each stratigraphic unit are distinctive. In many cases, direct correlations are questionable, and inferred correlations are considered instead due to: (1) the distance between DDH, (2) the variability in the lithofacies characteristics of the facies grouped into each stratigraphic unit, and (3) the absence (unexposed) of upper and lower contacts of stratigraphic units.

4.2 Local geology and stratigraphy of the Sock Creek-Burns Peak area

4.2.1 Introduction

The Mount Charter Fault separates the Sock Creek-Burns Peak area from the Hellyer-Mount Charter area in the NE (Figure 4.1). Splays of the Mount Black and Rosebery Faults in the Mount Kershaw area, S of Burns Peak, separate the Sock Creek-Burns Peak area from the Rosebery-Hercules area to the SSW (Corbett and McNeill, 1986; Corbett, 2007). The Burns Peak Shear Zone is a NE-striking, sub-vertical to steeply

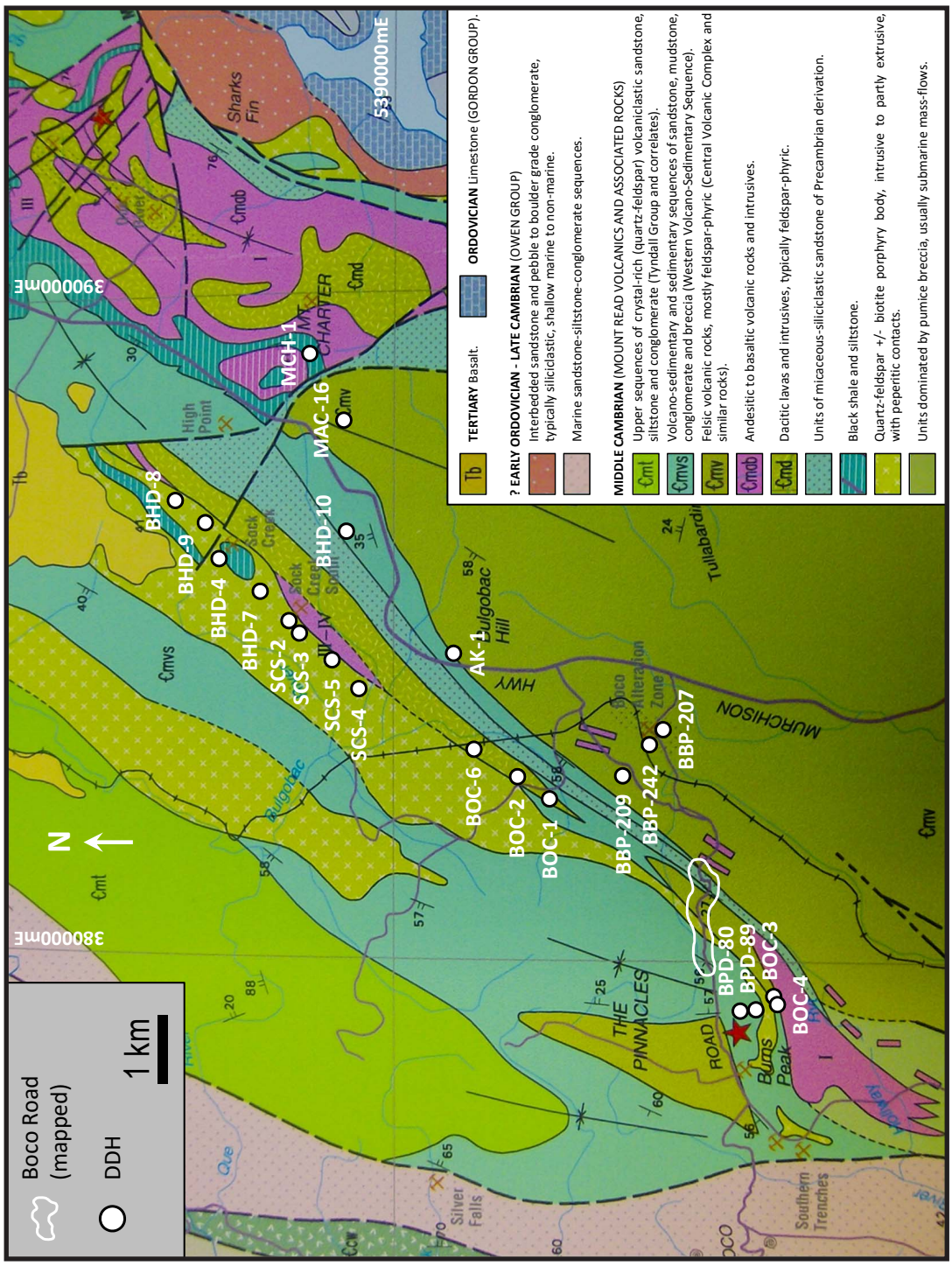

Figure 4.1: Geology of the Que River-Burns Peak area showing the location of the diamond drill holes (DDH) and mapped Boco Road section in this study, after Corbett (2002a).

E-dipping fault structure occurring E of Burns Peak and extending to the SW, N of Cone Hill, where it can no longer be recognised in the Kershaw Pumice Formation (Gifkins, 2001).

No economically significant mineral deposits have been noted in the Sock Creek-Burns Peak area (McNeill, 2001). Zinc-dominated and gold/silver-poor sulfide prospects at Sock Creek and Sock Creek South (Purvis, 1993; McNeill, 2002a), the large "barren" sericite-pyrite Boco Alteration Zone (Skirka and McNeill, 2006; Herrmann et al., 2009) and minor base metals at the Hollway prospect (Skirka and McNeill, 2006) have been extensively explored.

The Sock Creek-Burns Peak area comprises the Central Volcanic Complex (CVC) (McNeill and Corbett, 1989) and the Mount Charter Group (Corbett, 1992) (Chapter 2). The Mount Charter Group is partly unconformably covered by Tertiary basalts, N of Sock Creek (Skirka and McNeill, 2006). Extensive, unconsolidated Quaternary glacial and fluvioglacial deposits obscure much of the Palaeozoic geology W of Mount Block.

4.2.2 Central Volcanic Complex (CVC)

The CVC (Corbett and McNeill, 1986; Corbett and Solomon, 1989) outcrops in the SE part of the Sock Creek-Burns Peak area, extending from N of Lake Rosebery to SW of Mount Charter (Corbett, 2002a), and comprises the Mount Black Formation (Gifkins, 2001; Gifkins and Allen, 2001). It includes a thick succession of dominantly massive to flow-banded, feldspar-phyric dacite and feldspar-quartz-phyric rhyolite, and monomictic rhyolite and dacite breccia (Corbett, 2002a; this thesis). Abundant, relatively thin (<10 m thick) mafic dykes intrude the CVC from Bulgobac Hill southwestward to the Boco Alteration Zone (McNeill and Corbett, 1989; this thesis).

The CVC is bound to the SE by the NE-striking and NW-dipping Henty Fault (Berry, 1989), and appears to form a regional antiform that is N-plunging in the Mount Block area (McNeill and Corbett, 1989). To the E and NE, the CVC is in fault contact (Mount Charter Fault) with the basal units of the Mount Charter Group (Animal Creek Greywacke W and SW of Mount Charter and Black Harry Beds E of Mount Block) (Corbett and McNeill, 1986; Komyshan, 1986a; Corbett and Komyshan, 1989). From High Point to Burns Peak, much of the contact between the CVC and the Mount Charter Group appears to be disconformable (McNeill and Corbett, 1989; this thesis).

4.2.3 Mount Charter Group

The Mount Charter Group (Figure 4.2) was first defined by Corbett (1992) as the volcano-sedimentary sequence containing the Hellyer and Que River VHMS deposits, and occurring between the CVC below and the Owen Group above. Stratigraphic equivalents of the Mount Charter Group overlie the CVC in the northwestern part of the Sock Creek-Burns Peak area and are described below.

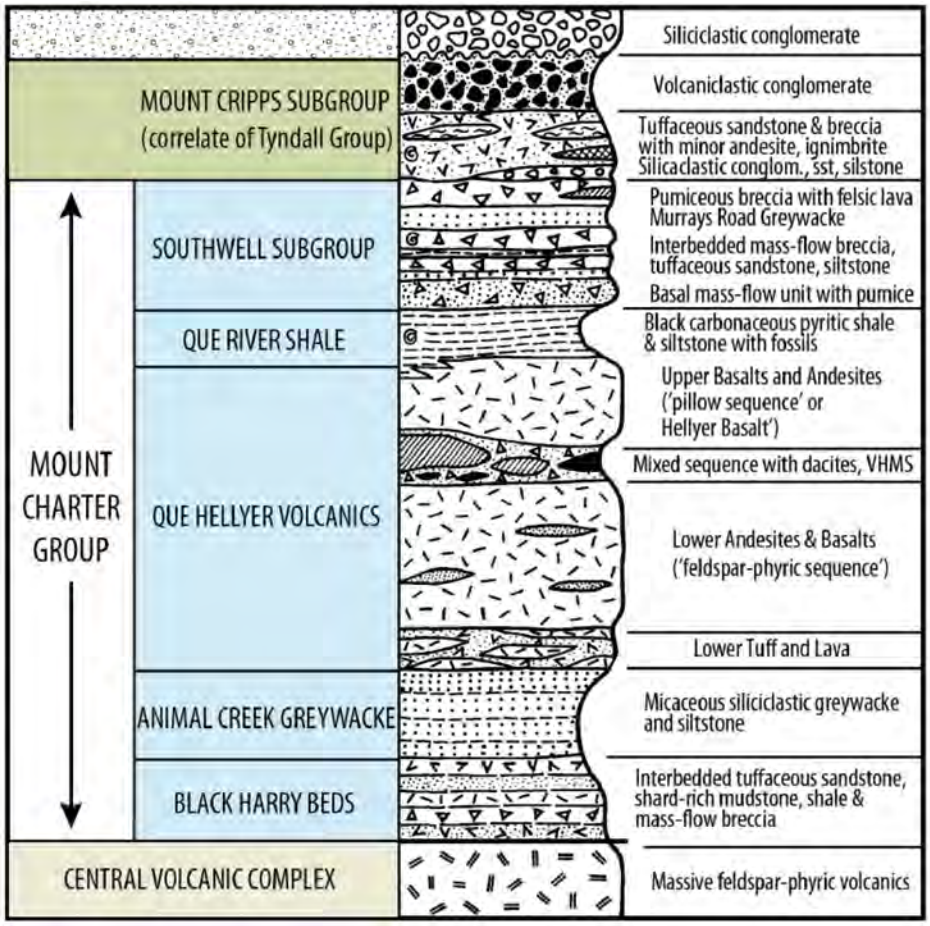

Figure 4.2: Stratigraphic column for the Mount Charter Group in the Hellyer-Que River area, after Corbett (1992).

4.2.3.1 Black Harry Beds

The term "Black Harry Beds" was first used by Corbett (1992) to refer to an approximately 300-m-thick sequence of interbedded marine shard-rich mudstone, tuffaceous sandstone, volcaniclastic mass-flow breccia, and green to black shale overlying or in faulted contact with the CVC on the Murchison Highway, NW of Mount Block. Before Corbett (1992), the Black Harry Beds were referred to as the "lower tuffaceous part" of the Animal Creek Greywacke (Corbett and Komyshan, 1989) and to the "lower vitric tuff sequence" of Pemberton et al. (1991). Pemberton et al. (1991) described the "lower vitric tuff sequence" as a probably 600-m-thick widespread unit of vitric tuff, tuffaceous siltstone, sandstone and shale, intercalated with quartz-phyric tuffs and coarse mass flow units. The Black Harry Beds are considered in this thesis to be the oldest formation of the Mount Charter Group (Corbett, 1992).

Stratigraphically, the Black Harry Beds gradationally underlie the Animal Creek Greywacke and overlie the CVC (Figure 4.2). The contact with the CVC has been described by other authors to be poorly defined (Corbett, 1992), a faulted unconformity (Komyshan, 1986a, 1986b), or a fault dipping 30º NE (Corbett and Komyshan, 1989). Corbett (1992) pointed out the occurrence of intercalated units essentially identical

to the Black Harry Beds with the CVC and suggested the possibility of an original interfingering relationship between the Black Harry Beds and the CVC.

Field relationships and observations based on several diamond drill holes (DDH BOC-1, BOC-2 and BOC-6; this thesis) show that to the NW of the Boco Alteration Zone, W of Mount Block, the Black Harry Beds conformably underlie (DDH BOC-1 and BOC-2) or are in faulted contact (DDH BOC- 6) with the equivalents of the Animal Creek Greywacke. The fault contact seems to be a localized occurrence. In DDH BHD-10 (this thesis), SE of Sock Creek South, the contact between the Black Harry Beds and the CVC has been logged as a fault. In the Boco area (DDH BOC-1; this thesis), this contact has been logged as conformable and gradational, but in DDH BOC-2 and BOC-6 the nature of this contact is unknown due to broken or missing core. The Black Harry Beds thin out just N of Boco Road, W of the Boco Alteration Zone, where they pass laterally into the Animal Creek Greywacke. The Boco Road was mapped (this thesis), but neither this contact nor the contact between the Animal Creek Greywacke and the underlying CVC are exposed.

The Black Harry Beds are also known to extend from E of Mount Block, S of Mount Charter, to the Two Hummocks area, NW of Hellyer (Pemberton et al., 1991). At Black Harry Road, NW of Hellyer, several feldspar-porphyritic dacitic units occur within the Black Harry Beds and have been interpreted by Pemberton et al. (1991) as dacitic intrusions and possible lavas compositionally similar to the Que-Hellyer Volcanics. In the Two Hummocks area, the Black Harry Beds are NW-SE striking and dip moderately to the NE, but W of the Mount Charter-Mount Block area they are NE-SW striking and generally dip and young to the NW (Pemberton et al., 1991).

4.2.3.2 Animal Creek Greywacke

The Animal Creek Greywacke was first described by Collins (in Collins et. al, 1981) as an approximately 500-m-thick unit of pale to dark grey greywacke, siltstone, mudstone and very fine grained vitric tuff that cropped out along the Murchison Highway for about 4 km north of Animal Creek. Corbett and Komyshan (1989) further subdivided the Animal Creek Greywacke into an upper micaceous greywacke, siltstone and mudstone sequence, and a “lower tuffaceous part” which corresponds to the “lower vitric tuff sequence” of Pemberton et al. (1991), and was later called the Black Harry Beds by Corbett (1992).

The Animal Creek Greywacke is part of the Mount Charter Group of Corbett (1992) (Figure 4.2). Stratigraphically, the Animal Creek Greywacke gradationally and conformably overlies the Black Harry Beds, and is conformably overlain by the Que-Hellyer Volcanics (Corbett and McNeill, 1986; Pemberton et al., 1991). The Animal Creek Greywacke is composed predominantly of elongate, kinked and ragged muscovite flakes and Precambrian-derived polycrystalline quartzite and schist clasts and quartz grains with undulose extinction, and minor chromite and tourmaline grains and volcanic fragments (Pemberton et al., 1991; this thesis).

Field relationships and observations based on several diamond drill holes (e.g., DDH MCH-1; Corbett and Komyshan, 1989; this thesis) show that to the N of the Mount Charter Fault, in the Mount Charter and Que River areas, the Animal Creek Greywacke is conformably overlain by the Que-Hellyer Volcanics, or is separated from the overlying Que River Shale by a deformed contact partly of tectonic origin (Corbett and Komyshan, 1989; Pemberton et al., 1991). It is also known to extend further N to the western end of the Cradle Mountain Link Road where it is well exposed and is conformably separated from the overlying Que River Shale by only a very thin unit of basalt (10 m or less) representing the Que-Hellyer Volcanics (Corbett and Komyshan, 1989). The Animal Creek Greywacke extends at least 30 km from S of Mount Charter to the Two Hummocks area, and is of the order of 350 m thick (Pemberton et al., 1991).

To the S of the Mount Charter Fault, the Animal Creek Greywacke is bounded to the NW by coherent rhyolite and dacite and monomictic rhyolite and dacite breccia on the eastern side of Bulgobac Plain (Corbett and Komyshan, 1989; Corbett, 2002a; this thesis) and is separated from the CVC to the SE by the underlying Black Harry Beds. The Animal Creek Greywacke can be traced along strike for >12 km from the Mount Charter Fault to the Boco Road area, and probably S of Burns Peak (DDH BOC-4; this thesis); it is known to wedge out near the Hollway Rivulet (Corbett, 2007). In the Burns Peak-Boco Road area, the Animal Creek Greywacke interfingers with small lenses of Boco Road Dacite and Hollway Andesite (section 4.4.2.3; McIntyre, 2006). Within the Henty Fault Zone, the Animal Creek Greywacke is highly deformed and strongly altered (Corbett and Komyshan, 1989).

The Animal Creek Greywacke is NE-SW striking and generally dips and youngs to the NW in the Sock Creek-Burns Peak area (Pemberton et al., 1991), but youngs and dips fairly uniformly W in the Murchison Highway-Sock Creek area, and in the Sharks Fin area, SE of the Que River mine (Corbett and Komyshan, 1989; Corbett, 2002a).

4.2.3.3 Que-Hellyer Volcanics equivalents

Sock Creek Dacites

The Sock Creek Dacites were first called the "Sock Creek lava" by Corbett and Solomon (1989), a unit of felsic lava with intercalations of siltstone, sandstone and breccia. The Sock Creek Dacites occur at Sock Creek and Sock Creek South (Wilde and Kerr, 1989; Lorrigan, 1991; DDH SCS-5; Skirka and McNeill, 2006; this thesis), and are part of the Sock Creek Volcanics described by McNeill (2002a) as a complex of shales, intrusive quartz-feldspar porphyries and dacitic to basaltic lavas with minor volcaniclastic facies, geochemically distinct from the Que-Hellyer Volcanics (Crawford et al., 1992), but considered to be their time equivalents S and W of the Mount Charter Fault (McNeill, 2002a; this thesis). The Sock Creek Dacites overlie the Animal Creek Greywacke. The Sock Creek Volcanics are overlain by equivalents of the Southwell Subgroup (McNeill, 2002a).

Boco Road Dacite

The Boco Road Dacite is part of the Burns Peak Subgroup (Corbett, 2005a, 2005b) and comprises lens-shaped, weakly amygdaloidal, variably flow banded, feldspar-phyric dacite and monomictic dacite breccia that cross Boco Road (Corbett, 2005a, 2005b; McIntyre, 2006; this thesis), and appears to be an along-strike correlate of the dacites at Sock Creek (Sock Creek Dacites) and Que-Hellyer (McNeill, 2002b; this thesis). The Boco Road Dacite is westwards-thinning (Corbett, 2005a) and interfingered with the Hollway Andesite (McNeill, 2002b; McIntyre, 2006). On Boco Road, the Boco Road Dacite overlies the Animal Creek Greywacke, but the contact is not exposed (this thesis).

Hollway Andesite

The Hollway Andesite is also part of the Burns Peak Subgroup (Corbett, 2005a, 2005b) and comprises a sequence of feldspar-pyroxene-phyric andesitic to feldspar-phyric basaltic lavas, monomictic fluidal-clast mafic breccia, and minor siltstone and mudstone S of Burns Peak (Corbett and McNeill, 1986; McIntyre, 2006; this thesis). It overlies the Animal Creek Greywacke and is overlain by equivalents of the Que River Shale and Southwell Subgroup (Corbett, 2005a, 2005b; McIntyre, 2006; this thesis). To the SE of Burns Peak, the Hollway Andesite overlies the CVC and interfingers with the Boco Road Dacite (Corbett, 2005a, 2005b; McIntyre, 2006; this thesis). The Hollway Andesite is compositionally and petrologically similar to the Hellyer Basalt (Que-Hellyer Volcanics; Coutts, 1990), which lies immediately above the Hellyer and Que River VHMS deposits.

4.2.3.4 Que River Shale and equivalents

The Que River Shale was first described by Gee et al. (1970) as the Que River Beds, based on exposures along the Murchison Highway, N and S of the Que River Bridge. It consists dominantly of black to dark grey, weakly carbonaceous and strongly siliceous, fossiliferous, pyritic mudstone and siltstone (Gee et al., 1970; Corbett and Komyshan, 1989) with minor fine- to medium-grained sandstone beds that generally occur towards the base of the unit (Waters and Wallace, 1992). The Que River Shale conformably overlies the Que-Hellyer Volcanics (Figure 4.2) and is conformably and gradationally overlain by felsic rocks of the Southwell Subgroup in the area between the Murchison Highway and Hellyer mine (Corbett and Komyshan, 1989; Corbett, 1992).

The average thickness of the Que River Shale is approximately 100 m, but the formation is of the order of 150 m thick in the Murchison Highway and thins eastwards and may wedge out completely in the Southwell River area, SE of Hellyer (Corbett and Komyshan, 1989). The Que River Shale contains an important and diverse fossil fauna that indicates a late Middle Cambrian Floran-Undillan age (E. opimus Zone to P. punctuosus Zone) and marine depositional conditions (Gee et al., 1970; Quilty, 1971, 1972a; Jago, 1973, 1977; Waters and Wallace, 1992; Laurie et al., 1995). The Que River Shale is intruded by a 499.3 ± 0.9 Ma rhyolite sill (Mortensen et al., 2015).

To the NW of Hellyer, towards the Cradle Mountain Link Road, the Que River Shale conformably overlies a thin lens of Que-Hellyer Volcanics (Corbett and Komyshan, 1989), which in turn overlies the Animal Creek Greywacke. Near the western end of the Cradle Mountain Link Road, the Que River Shale dips gently to the SE. In this area, the lower contact with the Que-Hellyer Volcanics is highly variable and is well exposed in a drainage canal, W of which the Que River Shale is highly deformed and in direct contact with the Animal Creek Greywacke (Pemberton et al., 1991).

In the Hellyer-Haulage Road area, the top of the Que River Shale is interbedded with coarse, graded units of the Southwell Subgroup, and the base is mingled with the Hellyer Basalt (Corbett and Komyshan, 1989; Tomes, 2011). The Que River Shale also occurs in the Black Marsh syncline area, where it is approximately 50 m thick and is separated from underlying coherent mafic rocks of the Que-Hellyer Volcanics by a 3-m-thick unit of polymictic volcaniclastic breccia similar to that reported in the Hellyer area, and containing both felsic and mafic volcanic clasts in a very fine-grained matrix (Corbett and Komyshan, 1989; Pemberton et al., 1991).

In the Mount Charter area, E of the Mount Charter Fault (DDH MCH-1; Corbett and Komyshan, 1989; this thesis), the Que River Shale overlies the Hellyer Basalt. The contact is mingled, interpenetrating and peperitic, and large-scale interdigitation of lava lobes and mudstone occurs in places (Corbett, 1992; Tomes, 2011; this thesis).

In the Sock Creek area, W of the Mount Charter Fault (DDH BHD-4, BHD-8 and BHD-9; this thesis), several units of black mudstone (possible equivalents of the Que River Shale; section 4.3.5.5) are intercalated with sub-concordant feldspar-quartz-phyric rhyolite. The lowermost black mudstone unit sits directly and conformably on a laterally extensive (>3.5 km), graded polymictic volcanic breccia and sandstone unit (probably laterally equivalent to the mixed sequence of the Que-Hellyer Volcanics; section 5.4), which is part of the Sock Creek Volcanics (Lorrigan, 1991; McNeill, 2002a).

In the Burns Peak-Boco Road area, a relatively thick (locally up to 42 m) black mudstone unit has been correlated with the Que River Shale (Reid, 1990; this thesis) and is overlain by equivalents of the Southwell Subgroup (Corbett and Komyshan, 1989; Corbett, 1992; Bold 2009; this thesis), underlain by the Hollway Andesite (Corbett and McNeill, 1986; McIntyre, 2006; this thesis), and intruded by quartz-feldspar rhyolite porphyries (Corbett and Komyshan, 1989; McNeill, 2002a; Corbett, 2005a; this thesis).

4.2.3.5 Quartz-feldspar rhyolite porphyries

Two sub-concordant, intrusive-extrusive, quartz-feldspar-phyric rhyolite porphyries occur in the Sock Creek and Burns Peak areas (Corbett and Komyshan, 1989; McNeill, 2002a; Corbett, 2005a; this thesis). The rhyolite porphyry at Sock Creek has been termed the Sock Creek Porphyry by Wilde and Kerr (1989). The rhyolite porphyries intrude the Que River Shale and Southwell Subgroup equivalents (Corbett and Komyshan, 1989; Corbett, 2005a; this thesis). The rhyolite porphyries are locally flow banded and comprise embayed quartz phenocrysts and glomerocrysts 5-10 mm across, and twinned, zoned feldspar phenocrysts

and glomerocrysts up to 4 mm across (Corbett and Komyshan, 1989; Corbett, 2005a; this thesis). The groundmass is composed of quartz, feldspar, sericite and chlorite, with minor apatite and zircon (Corbett and Komyshan, 1989; this thesis). Peperitic contacts are common and indicate emplacement of the rhyolite porphyries into unconsolidated mud (Corbett, 2005a; this thesis).

Several similar quartz-feldspar-phyric rhyolite porphyries occur in the bed of the Que River and on the South Charter track (Corbett and Komyshan, 1989), and in the Browns Tunnel-Southern Trenches area (Corbett, 2005a).

4.2.3.6 Southwell Subgroup and equivalents

The Southwell Subgroup was defined by Corbett and Komyshan (1989), and comprises quartz-feldspar-porphyritic pumiceous mass flow breccia and sandstone interbedded with greywacke sandstone, siltstone, shale, and minor felsic lava (Corbett, 1992; Bold 2009). It conformably overlies the Que River Shale (Figure 4.2) in the vicinity of the Hellyer mine (Corbett and Komyshan, 1989), and is overlain by the Mount Cripps Subgroup, a correlate of the Tyndall Group (Corbett, 1992; White and McPhie, 1996).

The Southwell Subgroup is in the order of 1000 m thick (Corbett, 1992), and is exposed W of the Pinnacles Ridge, and along the Boco Road, E and W of Burns Peak (Corbett, 2005a, 2005b). An equivalent of the Southwell Subgroup occurs in the Sock Creek-Burns Peak area (Corbett and Komyshan, 1989; Corbett, 2002a, 2005a, 2005b; Bold, 2009). The age of the Southwell Subgroup has been assigned to the late Middle Cambrian from fossils within rare shallow-water limestone clasts (Jago and McNeill, 1997). The lowermost unit of the Southwell Subgroup is intruded by a 499.3 ± 0.9 Ma rhyolite sill (Mortensen et al., 2015). The lower part of the Southwell Subgroup corresponds to the upper rhyolitic sequence of Hellyer mine terminology (McArthur, 1996).

Pemberton et al. (1991) divided the Southwell Subgroup into four units. The basal unit (lower tuff unit; Corbett and Komyshan, 1989) is of the order of 300 m thick, and includes graded quartz-feldspar-phyric crystal-vitric-lithic mass-flow sandstone and breccia units up to 20 m thick with minor interbeds of shale, siltstone and greywacke (Pemberton et al., 1991). This unit contains large (> 1 m long) mudstone and quartz-phyric relict pumice clasts (Corbett and Komyshan, 1989; Corbett, 1992).

The second lowest unit is >250 m thick and comprises quartz-feldspar crystal-rich sandstone and lithic-rich pumiceous mass-flow breccia-sandstone interbedded with graded tuffaceous greywacke and minor siltstone and shale (Pemberton et al., 1991). This unit includes fossiliferous limestone clasts.

The third lowest unit is the Murrays Road Greywacke, which comprises well-bedded, fine to coarse-grained turbidites, granule conglomerate and micaceous siltstone. This unit contains Precambrian detrital components and volcanic components, including sericitic relict pumice, rhyolite and rare andesite clasts, and sub-angular volcanic quartz grains (Pemberton et al., 1991; Corbett, 1992).

The uppermost unit of the Southwell Subgroup is a sequence of pumice-bearing crystal and crystal-lithic sandstone-breccia with minor lithic breccia, vitric sandstone, greywacke and flow-banded quartz-feldspar-phyric lava. This unit contains chloritic relict pumice and pink rhyolite clasts (Pemberton et al., 1991).

McPhie and Allen (1992) identified three key facies associations within the Southwell Subgroup. Facies A is a volcaniclastic facies ranging from a few tens of metres to greater than 100 m comprising bluish-grey, pumiceous sandstone and pumice breccia characterised by wispy, sparsely feldspar-bearing relic pumice (now composed of sericite or chlorite) with a variably minor component of quartz fragments (McPhie and Allen, 1992). Facies A is made up of thinner intervals of a single-graded unit, and thicker intervals of a small number of graded units (McPhie and Allen, 1992). Facies A most likely correlates with the lower tuff unit defined by Corbett and Komyshan (1989).

Facies B is volcaniclastic and comprises crystal-rich volcaniclastic sandstone and mudstone, characterised by coarse (1 cm commonly), round, fractured quartz and more abundant, prismatic feldspar (2-4 mm), formerly glassy (now sericite) coarsely quartz-feldspar-phyric lenses and wisps of relic pumice, and minor lithic clasts. Facies B includes a complex mixture of juvenile volcanic particles and non-volcanic mud, and some sections of this facies include apparently coherent, coarse quartz-feldspar porphyry that is locally flow banded or brecciated (McPhie and Allen, 1992). Facies B most likely correlates with the second lowest unit of Pemberton et al. (1991).

Facies C is a sedimentary facies comprising black, laminated or massive, commonly pyritic mudstone. Facies C appears below, between, within (as intraclasts) and above Facies A and B, and is considered a continuation of the Que River Shale (McPhie and Allen, 1992).

Corbett (2005a, 2005b) identified three major lithotypes within the Southwell Subgroup: (i) interbedded sandstone and siltstone in beds 5 cm-1 m thick, commonly graded; (ii) sandstone-dominated units with 20-40% siltstone; (iii) siltstone-shale-dominated units ranging from grey-green siltstone to black-grey shale, typically with interbedded thin sandstone layers.

The sandstone is typically volcaniclastic and felsic, and dominated by feldspar crystals, quartz crystals (sparse to abundant and up to 8 mm across as “quartz eyes”), pumice and felsic lava clasts, shards, and sedimentary clasts (mostly shale-siltstone and cherty ash). Graded mass-flow sandstone units up to 10 m thick, with lithic-rich bases and fine-grained tops are common. Coarse quartz-feldspar crystal-rich sandstone with a fine-grained matrix and large “quartz-eyes”, and a variable percentage of lithic clasts, occur locally. Pumice-rich sandstone with abundant pumice clasts up to 10 cm across also occur (Corbett, 2005a, 2005b).

4.3 Stratigraphic units and correlations in the Sock Creek-Burns Peak area

4.3.1 Introduction

Descriptions and interpretations of the facies identified in the Sock Creek-Burns Peak area are presented in Chapter 3. The geological setting and stratigraphy of the Sock Creek-Burns Peak area were presented in the previous section. In this section, stratigraphic units and correlations in the Sock Creek-Burns Peak area are discussed.

For matters of clarity and simplicity, and due to the scale of this research, correlations in the Sock Creek-Burns Peak area (SB) are sub-divided into three sub-areas (Figure 4.3), from NE to SW: 1) Sock Creek-Sock Creek South and Mackintosh (SB-North), 2) Bulgobac Hill-Boco-Boco Alteration Zone (SB-Central) and 3) Boco Road-Burns Peak (SB-South). For each sub-area, local stratigraphic units (USB-N, USB-C and USB-S, respectively) have been assigned to assist local correlations and help recognize laterally equivalent stratigraphic levels. Each local stratigraphic unit includes at least one facies (Chapter 3), but most include multiple facies and multiple intervals of the same facies are present in parts of the succession.

Local correlations within each sub-area are mostly lithological (or facies) correlations, based on similarity of the facies and facies associations in the different DDH. In many cases, these correlations are strongly supported by the relatively close proximity of the DDH within each sub-area.

In cases involing partly extrusive and partly intrusive units (interpreted as partly extrusive cryptodomes, Chapter 3), the relationship between the intrusive part and the adjacent stratigraphy may be intrinsically complex and as a result, some of the named stratigraphic units do not obey the normal principles of stratigraphy (Figure 4.3; DDH BHD-4, USB-N5 is intercalated with USB-N6; DDH BHD-7, BHD-8 and BHD-9, USB-N3 is intercalated with USB-N4a). In these cases, the nature of the partly extrusive and partly intrusive units is considered and the intruded stratigraphic units have been divided into sub-units in order to facilitate correlations.

Mafic and felsic intrusions have been identified in the Sock Creek-Burns Peak area and are considered separately from the local stratigraphic units within each sub-area. Mafic intrusions comprise coherent feldspar-pyroxene-phyric, feldspar-phyric and aphyric mafic facies, and minor monomictic mud-matrix mafic breccia facies (section 3.3.3). Felsic intrusions include coherent feldspar-phyric rhyolite and dacite and monomictic dacite breccia facies (sections 3.3.1 and 3.3.2). Intrusions occur practically everywhere from Sock Creek, in the NE, to Burns Peak, in the SW, and at all stratigraphic levels. They are discussed within each sub-area from lowest to highest stratigraphic position of the succession they intrude into.

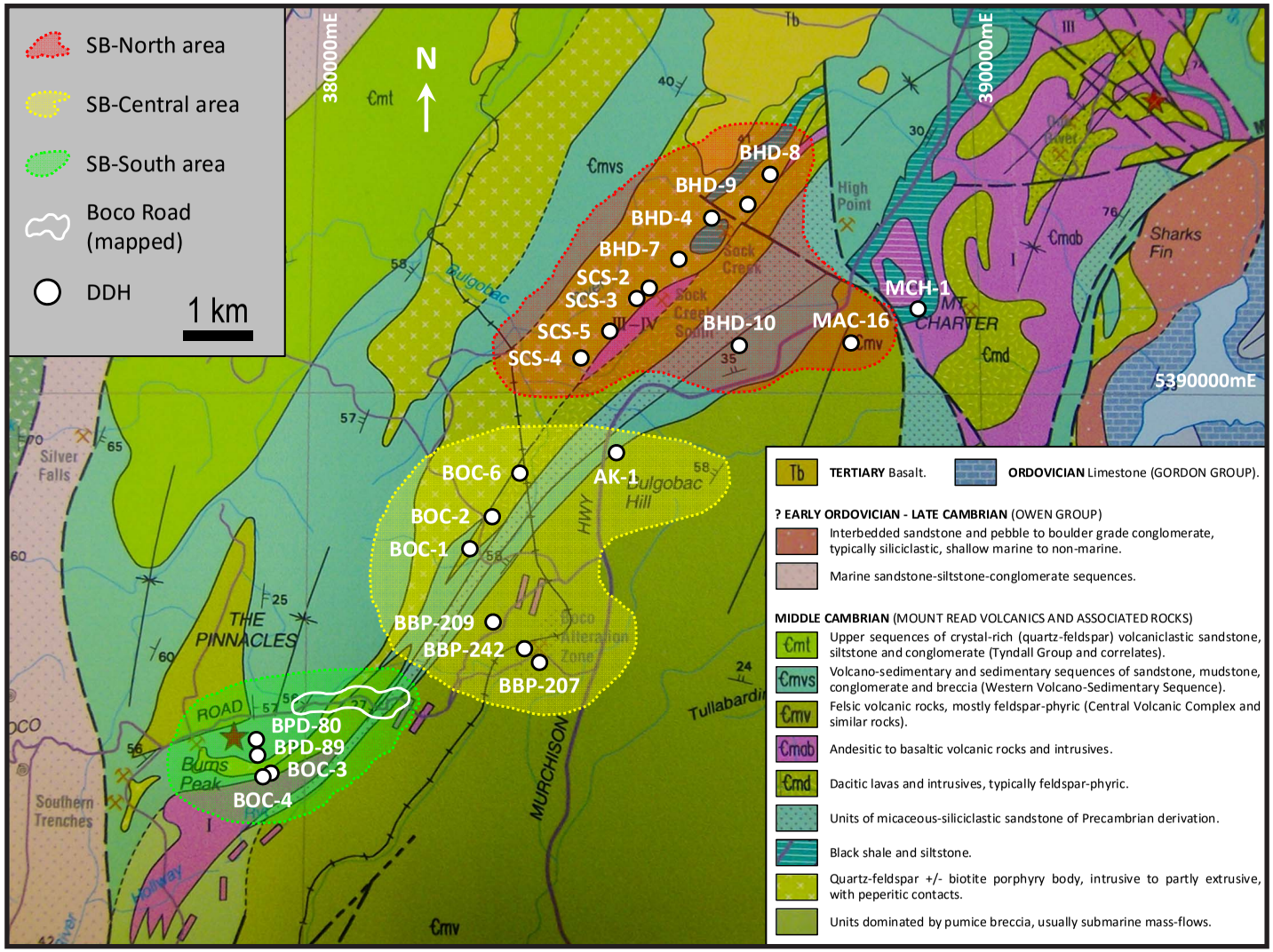

Figure 4.3: Geology of the Que River-Burns Peak area showing the three sub-areas of the Sock Creek-Burns Peak area with the location of the diamond drill holes (DDH) and mapped Boco Road section in this study, after Corbett (2002a).

4.3.2 Correlations in the Sock Creek-Sock Creek South and Mackintosh areas (SB-North)

In the Sock Creek-Sock Creek South and Mackintosh areas (SB-North), seven local stratigraphic units (USB-N; unit, Sock Creek-Burns Peak, northern area) were identified. The facies and sub-facies of each USB-N are presented in Table 4.1. Correlations of the USB-N are presented in Figure 4.4 and discussed below.

4.3.2.1 USB-N1

USB-N1 occurs in two DDH and includes four facies and one sub-facies (Table 4.1; coherent feldspar-phyric dacite, monomictic dacite and rhyolite breccia, and monomictic mud-matrix dacite breccia facies, and coherent quartz-poor rhyolite sub-facies). This unit extends laterally for at least 1.7 km from DDH BHD-10 (SE of Sock Creek South) to DDH MAC-16 (Mackintosh area) (Figure 4.4). The upper faulted contact with USB-N2 was intersected in DDH BHD-10 (Figure 4.4). The lower contact of USB-N1 was not intersected in this DDH. Both the upper and lower contacts of USB-N1 were not intersected in DDH MAC-16, preventing any direct correlations with DDH BHD-10.

4.3.2.2 USB-N2

USB-N2 includes three facies (Table 4.1; polymictic felsic breccia and sandstone, and shard-rich mudstone facies) and occurs exclusively in DDH BHD-10, preventing any correlations in the SB-North area (Figure 4.4). This unit will be considered in section 4.3.5 for larger scale correlations in the Sock Creek-Burns Peak area.

4.3.2.3 USB-N3

USB-N3 occurs in five DDH and includes polymictic micaceous sandstone and micaceous mudstone facies (Table 4.1). This unit extends laterally for at least 3.5 km from DDH SCS-5, in the SW, to DDH BHD-8 in the NE. USB-N3 is distinctive and simple to correlate in the SB-North area, and provides an excellent stratigraphic marker for the correlation of adjacent, laterally-equivalent stratigraphic units (Figure 4.4). The lower contact of USB-N3 was not intersected by any of the DDH in the SB-North area (Figure 4.4), but the upper contact with USB-N4a is correlated in the Sock Creek area and between Sock Creek and DDH SCS-5 (Sock Creek South area) (Figure 4.4). In DDH SCS-5, USB-N3 is cross cut by coherent feldspar-pyroxene-phyric mafic facies (interpreted as intrusive; Chapter 3; section 4.3.2.8).

In the Sock Creek area, USB-N3 includes two sub-units: USB-N3a (DDH BHD-7, 335.1-361.7 m; DDH BHD-8, 303.6-398.4 m; DDH BHD-9, 392.3-419.0 m) and USB-N3b (DDH BHD-7, 240.2-241.6 m; DDH BHD-8, 230.4-234.5 m and 240.0-245.4 m; DDH BHD-9, 365.0-369.5 m) (Figure 4.4).

4.3.2.4 USB-N4

USB-N4 includes two sub-units: USB-N4a and USB-N4b. USB-N4a occurs in eight DDH and includes twelve facies (Table 4.1; coherent feldspar-phyric rhyolite and dacite, monomictic rhyolite and dacite breccia,

Table 4.1: Stratigraphic units and associated facies and sub-facies in the Sock Creek-Sock Creek South and Mackintosh areas (SB-North). See Chapter 3 for details on each facies.

Local stratigraphic units		Facies and sub-facies	Location and diamond drill holes	Extention (km)
USB-N7		Polymictic rhyolite breccia (**RpB**) and sandstone (**RpS**), and black mudstone (**BMud**) facies	Sock Creek: **BHD-4**	?
USB-N6		Monomictic rhyolite breccia (**RmB**) and monomictic mud-matrix rhyolite breccia (**RmmB**) facies, and coherent quartz-rich rhyolite sub-facies (**Rqr**)	Sock Creek: **BHD-4, BHD-7, BHD-8 and BHD-9**; Sock Creek South: **SCS-2, SCS-3 and SCS-5**	>3.5 km
USB-N5		Black mudstone (**BMud**) facies	Sock Creek: **BHD-4, BHD-8 and BHD-9**	>1 km
USB-N4	*USB-N4b*	Polymictic volcanic breccia (**PvB**) and sandstone (**PvS**) facies	Sock Creek: **BHD-4, BHD-7, BHD-8 and BHD-9**; Sock Creek South: **SCS-2, SCS-3 and SCS-5**	>3.5 km
	USB-N4a	Coherent feldspar-phyric rhyolite (**Rf**) and dacite (**Df**), monomictic rhyolite (**RmB**) and dacite (**DmB**) breccia, monomictic mud-matrix rhyolite (**RmmB**) and dacite (**DmmB**) breccia, monomictic fiamme-rich dacite breccia (**DmfrB**), polymictic mud-matrix felsic breccia (**PmmfB**), polymictic felsic breccia (**PfB**) and sandstone (**PfS**), and black (**BMud**) and micaceous (**MMud**) mudstone facies	Sock Creek: **BHD-4, BHD-7, BHD-8 and BHD-9**; Sock Creek South: **SCS-2, SCS-3, SCS-4 and SCS-5**	>4 km
USB-N3		Polymictic micaceous sandstone (**PmS**), and micaceous mudstone (**MMud**) facies	Sock Creek: **BHD-4, BHD-7, BHD-8 and BHD-9**; Sock Creek South: **SCS-5**	>3.5 km
USB-N2		Polymictic felsic breccia (**PfB**) and sandstone (**PfS**), and shard-rich mudstone (**SMud**) facies	Sock Creek South: **BHD-10**	?
USB-N1		Monomictic rhyolite breccia (**RmB**), coherent feldspar-phyric dacite (**Df**), monomictic dacite breccia (**DmB**), and monomictic mud-matrix dacite breccia (**DmmB**) facies, and coherent quartz-poor rhyolite sub-facies (**Rqp**)	Sock Creek South: **BHD-10**; Mackintosh: **MAC-16**	>1.7 km

CORRELATION DIAGRAM

Sock Creek-Sock Creek South and Mackintosh areas

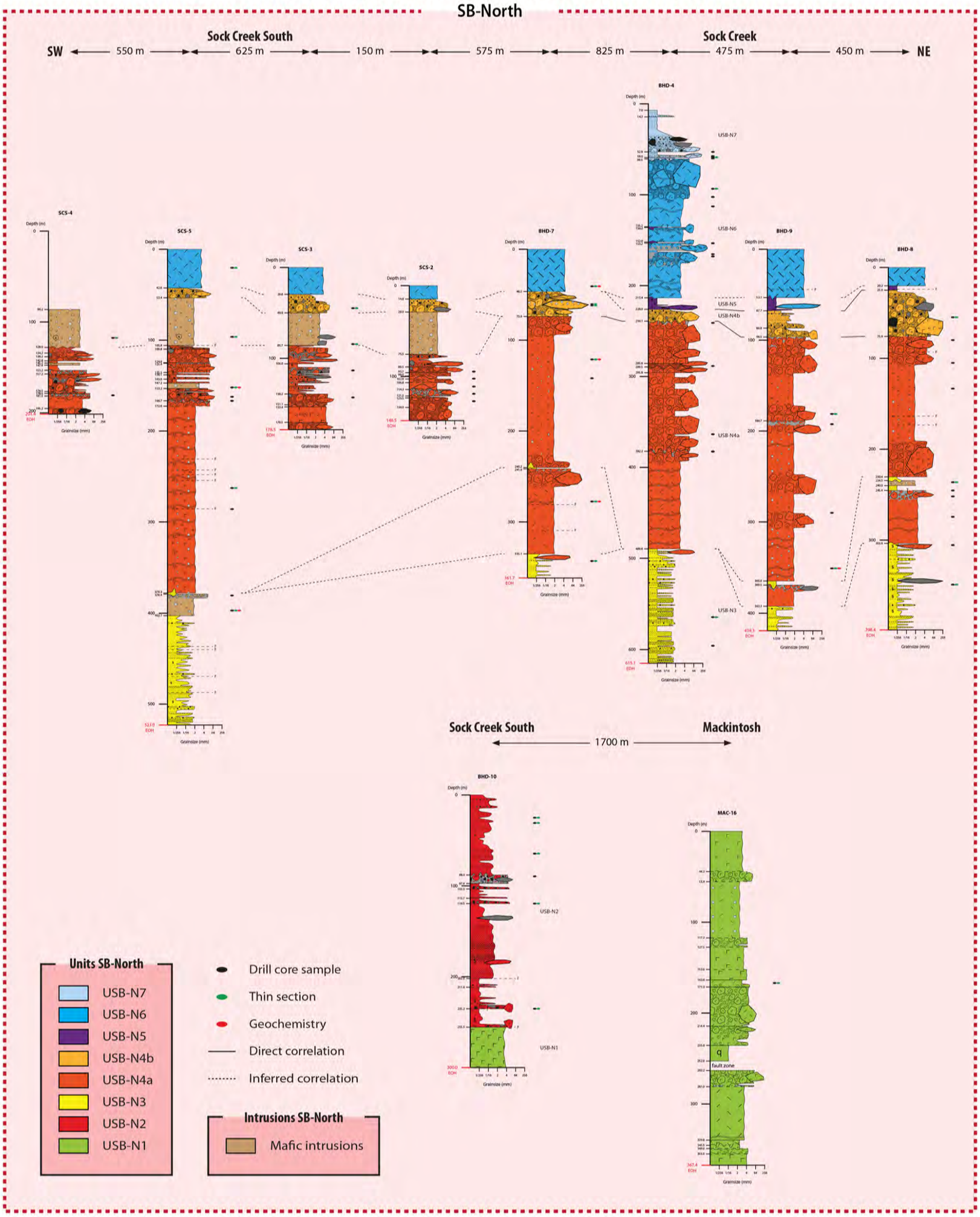

Figure 4.4: Correlation diagram of the local stratigraphic units (USB-N) identified in the Sock Creek-South and Mackintosh areas (SB-North). Unit labels are given on the right of the logs of DDH BHD-4 and BHD-10. See Figure 3.4 for legend to graphic logs.

monomictic mud-matrix rhyolite and dacite breccia, monomictic fiamme-rich dacite breccia, polymictic mud-matrix felsic breccia, polymictic felsic breccia and sandstone, and black and micaceous mudstone facies). This sub-unit extends laterally for at least 4 km from DDH SCS-4, in the SW, to DDH BHD-8, in the NE (Figure 4.4), and has been interpreted as partly intrusive (lower part) and partly extrusive (upper part). The upper and lower contacts of USB-N4a are simple to correlate due to its stratigraphic position. In the Sock Creek area (Figure 4.4), USB-N4a is overlain by USB-N4b, but in the Sock Creek South area, USB-N4a is overlain by coherent feldspar-pyroxene-phyric mafic facies, which is interpreted as a basaltic sill (Chapter 3; Figure 3.1; Table 3.2; section 4.3.2.8). In DDH BHD-7, BHD-8 and BHD-9 (Sock Creek area), the lower part of USB-N4a (interpreted as intrusive; Chapter 3) is intercalated with USB-N3 (USB-N3a and USB-N3b; section 4.3.2.3). USB-N4a will be considered in section 4.3.5 for larger scale correlations in the Sock Creek-Burns Peak area.

USB-N4b occurs in seven DDH and includes normally graded units of polymictic volcanic breccia and sandstone facies (section 3.3.4; Table 4.1). This sub-unit is an excellent stratigraphic marker in the SB-North area, extending for at least 3.5 km from DDH SCS-5, in the SW, to DDH BHD-8, in the NE (Figure 4.4). In the Sock Creek area (except in DDH BHD-7), USB-N4b underlies USB-N5 (black mudstone facies; section 3.3.5; Table 4.1) and overlies USB-N4a, but in the Sock Creek South area, USB-N4b directly overlies coherent feldspar-pyroxene-phyric mafic facies (interpreted as a basaltic sill, Chapter 3; Figure 3.1; Table 3.2; section 4.3.2.8) and is directly overlain by USB-N6 (coherent quartz-rich rhyolite sub-facies, section 3.3.1; Table 4.1) (Figure 4.4). In DDH BHD-7, USB-N4b occurs between USB-N6 above and USB-N4a below (Figure 4.4).

USB-N4b is polymictic, including relic shards, chloritic fragments, and felsic, mafic, lithic and mudstone clasts. The lithofacies characteristics, stratigraphic position and the close proximity of the DDH where it occurs, allow a simple correlation of this sub-unit in the SB-North area (Figure 4.4). A basaltic sill occurs between USB-N4a and USB-N4b in the Sock Creek South area (Chapter 3; Figure 3.1; Table 3.2; section 4.3.2.8).

4.3.2.5 USB-N5

USB-N5 is present in three DDH and comprises black mudstone facies (section 3.3.5; Table 4.1). In DDH BHD-4 (Sock Creek area), USB-N5 includes three sub-units: USB-N5a (213.4-226.0 m), USB-N5b (152.0-153.2 m) and USB-N5c (135.2-136.0 m) (Figure 4.4). USB-N5a extends for at least 1 km and is simple to correlate in the Sock Creek area due to its stratigraphic position (above USB-N4 and below USB-N6) and the close proximity of the DDH where it occurs (Figure 4.4).

4.3.2.6 USB-N6

USB-N6 occurs in seven DDH and includes two facies and one sub-facies (Table 4.1; monomictic rhyolite breccia and monomictic mud-matrix rhyolite breccia facies, and coherent quartz-rich rhyolite sub-facies).

This unit extends laterally for at least 3.5 km from DDH SCS-5, in the SW, to DDH BHD-8, in the NE (Figure 4.4).

USB-N6 is thickest (approximately 150 m) in DDH BHD-4 at Sock Creek (Figure 4.4). Exclusively in DDH BHD-4, coherent quartz-rich rhyolite sub-facies is associated with monomictic rhyolite breccia and monomictic mud-matrix rhyolite breccia facies (Chapter 3; Table 4.1; Figure 4.4), and these facies interfinger with USB-N5 (black mudstone facies, section 3.3.5; Table 4.1). To the NE and SW of DDH BHD-4, USB-N6 includes coherent quartz-rich rhyolite sub-facies only (Figure 4.4). To the NE (DDH BHD-9 and BHD-8), USB-N6 overlies USB-N5 (black mudstone facies, section 3.3.5; Table 4.1), but in DDH BHD-7 and further SW in the Sock Creek South area, USB-N6 directly overlies USB-N4b (polymictic volcanic breccia and sandstone facies, section 3.3.4; section 4.3.2.4) (Figure 4.4).

The interfingering relationship of USB-N6 with USB-N5 (black mudstone facies, section 3.3.5; Table 4.1; Figure 4.4) and the occurrence of USB-N7 (polymictic rhyolite breccia and sandstone facies, section 3.3.1) overlying USB-N6 suggest that the full thickness of USB-N6 is intersected in DDH BHD-4 (Figure 4.4). The presence of peperite (monomictic mud-matrix rhyolite breccia, section 3.3.1) involving USB-N6 in DDH BHD-4 (Figure 4.4) suggests that USB-N6 is syn-depositional and contemporaneous with USB-N5. The upper contact of USB-N6 was not intersected in the DDH NE and SW of DDH BHD-4 (Figure 4.4).

The feldspar and quartz phenocryst population of the coherent quartz-rich rhyolite sub-facies (section 3.3.1) of USB-N6 is very similar in all DDH of the SB-North area intersecting USB-N6 (Figure 4.4). Combined with the stratigraphic position and lateral extent of USB-N6, and the proximity of the different DDH, there is good evidence for correlation of the lower contact of USB-N6 in the Sock Creek-Sock Creek South area (Figure 4.4).

4.3.2.7 USB-N7

USB-N7 occurs at the top of DDH BHD-4 and includes three facies (Table 4.1; polymictic rhyolite breccia and sandstone, and black mudstone facies). This unit cannot be correlated with others in the SB-North area (Figure 4.4), but will be considered again in section 4.3.5 for possible larger scale correlations in the Sock Creek-Burns Peak area.

4.3.2.8 Intrusions

A relatively thick (<52 m) interval comprising coherent feldspar-pyroxene-phyric mafic facies occurs in all DDH in the Sock Creek South area (Figure 4.4) between USB-N4a (dominantly coherent rhyolite and dacite and monomictic rhyolite and dacite breccia facies, sections 3.3.1 and 3.3.2; Table 4.1) and USB-N4b (polymictic volcanic breccia and sandstone facies, section 3.3.4; Table 4.1). This unit extends laterally for at least 1.5 km (Figure 4.4), and has been interpreted as a basaltic sill (Chapter 3; Figure 3.1; Table 3.2). The stratigraphic position of this sill (above USB-N4a and below USB-N4b), its tabular geometry, distinct lithofacies characteristics and spatial distribution, and the proximity of the DDH where it occurs, provide a

simple correlation in the Sock Creek South area (Figure 4.4). Thinner (<6 m) intervals of coherent feldspar-pyroxene-phyric mafic facies, possibly lobes or apophyses associated with the sill, intrude USB-N4a in DDH SCS-4 and SCS-5 (Sock Creek South area, Figure 4.4).

In DDH SCS-5 (Sock Creek South area, Figure 4.4), an approximately 23-m-thick mafic intrusion comprising coherent feldspar-pyroxene-phyric mafic facies and peperite (monomictic mud-matrix mafic breccia facies, section 3.3.3) occurs near the top of USB-N3. In DDH BHD-8 (Sock Creek area, Figure 4.4), a 6-m-thick interval of coherent feldspar-phyric mafic facies (section 3.3.3) intrudes part of USB-N3 (USB-N3b; section 4.3.2.3).

4.3.3 Correlations in the Bulgobac Hill-Boco-Boco Alteration Zone area (SB-Central)

In the Bulgobac Hill-Boco-Boco Alteration Zone area (SB-Central), four local stratigraphic units (USB-C; unit, Sock Creek-Burns Peak, central area) were identified. The facies and sub-facies of each USB-C are presented in Table 4.2. Correlations of the USB-C are presented in Figure 4.5 and discussed below.

4.3.3.1 USB-C1

USB-C1 includes two sub-units: USB-C1a and USB-C1b. USB-C1a occurs in four DDH and includes nine facies (Table 4.2; coherent feldspar-quartz-phyric rhyolite, coherent feldspar-phyric rhyolite and dacite, monomictic rhyolite and dacite breccia, monomictic fiamme-rich dacite breccia, monomictic mud-matrix fiamme-rich dacite breccia, monomictic dacite sandstone and polymictic felsic breccia facies). This sub-unit extends laterally for at least 3.5 km from DDH BBP-207, in the SSW, to DDH AK-1, in the NNE (Figure 4.5). USB-C1a is intruded by abundant mafic dykes (Chapter 3; section 4.3.3.5).

The predominance of massive and flow-banded facies and the lack of distinctive, laterally extensive volcaniclastic facies, together with the distance between DDH (DDH AK-1 at Bulgobac Hill is located > 3 km to the NE of DDH BBP-209 in the Boco Alteration Zone area), prevent any direct correlation within USB-C1a (Figure 4.5). However, similar composition, textures, and specially the phenocryst population within the dacite and rhyolite comprising USB-C1a, suggest that these thick successions may occur at the same stratigraphic level.

USB-C1b occurs in three DDH and includes eight facies and one sub-facies (Table 4.2; coherent feldspar-phyric dacite, monomictic rhyolite and dacite breccia, monomictic dacite sandstone, polymictic mud-matrix felsic breccia, polymictic felsic breccia and sandstone, and black mudstone facies, and coherent quartz-rich rhyolite sub-facies). This sub-unit is overlain by USB-C2, and extends laterally for at least 1.5 km from DDH BOC-1, in the SW, to DDH BOC-6, in the NE (Figure 4.5). In DDH BOC-1 and BOC-2, USB-C1b comprises coherent rhyolite and dacite, monomictic rhyolite and dacite breccia, and monomictic dacite sandstone facies (sections 3.3.1 and 3.3.2), which is overlain by USB-C2, but in DDH BOC-6, coherent and monomictic facies are minor and USB-C1b consists dominantly of polymictic felsic breccia and sandstone (Figure 4.5).

Table 4.2: Stratigraphic units and associated facies and sub-facies in the Bulbobac Hill-Boco-Boco Alteration Zone area (SB-Central). See Chapter 3 for details on each facies.

Local stratigraphic units		Facies and sub-facies	Location and diamond drill holes	Extention (km)
USB-C4		Coherent feldspar-phyric rhyolite (**Rf**) and dacite (**Df**), monomictic rhyolite (**RmB**) and dacite (**DmB**) breccia, monomictic mud-matrix dacite breccia (**DmmB**), polymictic felsic breccia (**PfB**) and sandstone (**PfS**), and black (**BMud**) and shard-rich (**SMud**) mudstone facies	Boco: **BOC-1, BOC-2 and BOC-6**	>1.5 km
USB-C3		Polymictic micaceous sandstone (**PmS**) and micaceous mudstone (**MMud**) facies	Boco: **BOC-1, BOC-2 and BOC-6**	>1.5 km
USB-C2		Polymictic felsic breccia (**PfB**) and sandstone (**PfS**), and shard-rich mudstone (**SMud**) facies	Boco: **BOC-1, BOC-2 and BOC-6**	>1.5 km
USB-C1	*USB-C1b*	Coherent feldspar-phyric dacite (**Df**), monomictic rhyolite (**RmB**) and dacite (**DmB**) breccia, monomictic dacite sandstone (**DmS**), polymictic mud-matrix felsic breccia (**PmmfB**), polymictic felsic breccia (**PfB**) and sandstone (**PfS**), and black mudstone (**BMud**) facies, and coherent quartz-rich rhyolite sub-facies (**Rqr**)	Boco: **BOC-1, BOC-2 and BOC-6**	>1.5 km
	USB-C1a	Coherent feldspar-quartz-phyric rhyolite (**Rfq**), coherent feldspar-phyric rhyolite (**Rf**) and dacite (**Df**), monomictic rhyolite (**RmB**) and dacite (**DmB**) breccia, monomictic fiamme-rich dacite breccia (**DmfrB**), monomictic mud-matrix fiamme-rich dacite breccia (**DmmfrB**), monomictic dacite sandstone (**DmS**), and polymictic felsic breccia (**PfB**) facies	Bulgobac Hill: **AK-1**; Boco Alteration Zone: **BBP-207, BBP-209 and BBP-242**	>3.5 km

CORRELATION DIAGRAM

Bulgobac Hill-Boco-Boco Alteration Zone area

SB-Central

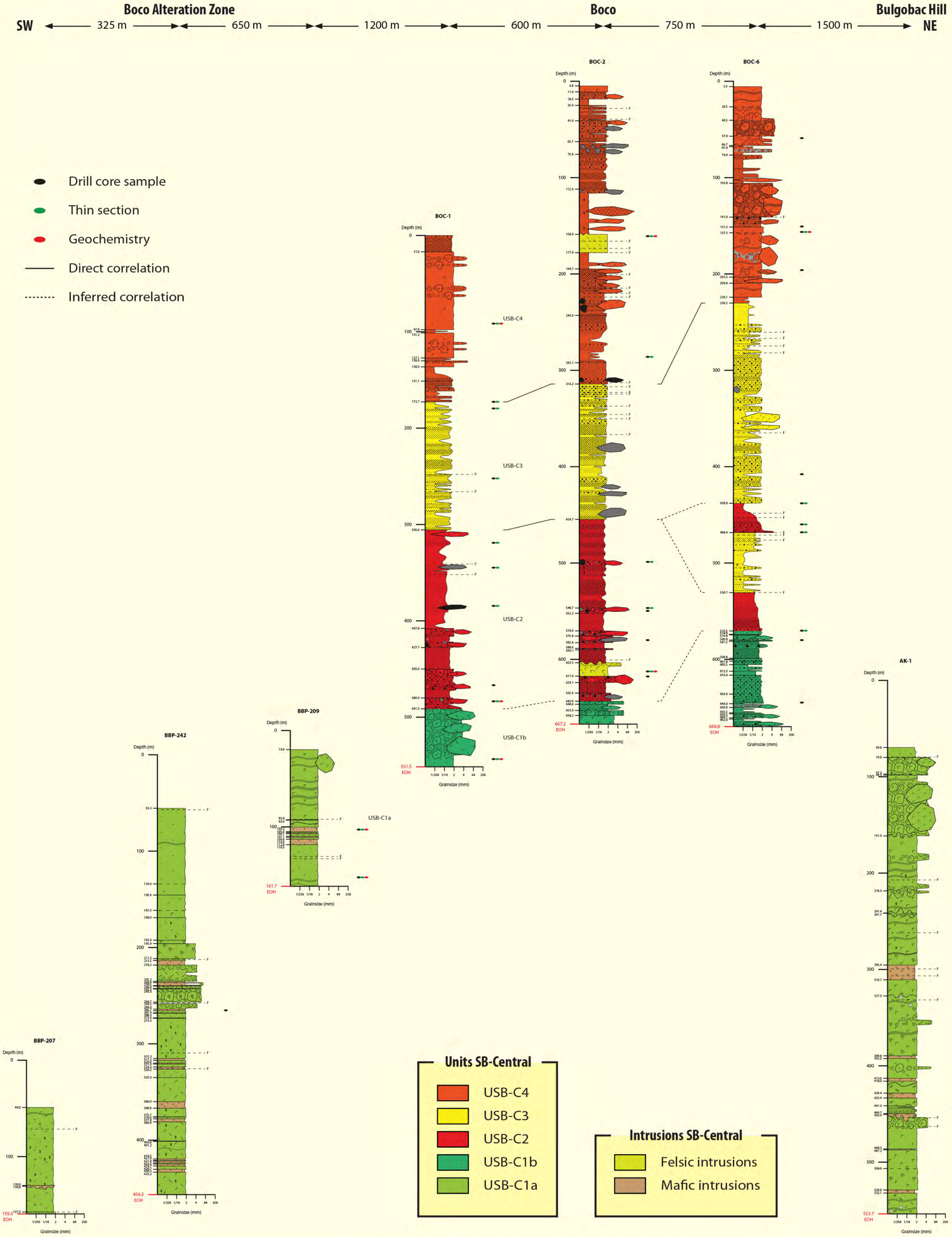

Figure 4.5: Correlation diagram of the local stratigraphic units (USB-C) identified in the Bulgobac Hill-Boco-Boco Alteration Zone area (SB-Central). Unit labels are given on the right of the logs of DDH BOC-1 and BBP-209. See Figure 3.4 for legend to graphic logs.

The proximity of the DDH and the stratigraphic position and lithofacies characteristics of the facies grouped into USB-C1b suggest that they are related, but direct correlations are difficult (Figure 4.5).

4.3.3.2 USB-C2

USB-C2 occurs in three DDH and includes three facies (Table 4.2; polymictic felsic breccia and sandstone and shard-rich mudstone facies). This unit extends laterally for at least 1.5 km from DDH BOC-1, in the SW, to DDH BOC-6, in the NE (Figure 4.5). The upper contact of USB-C2 is present in all DDH in this area and directly correlated, except in DDH BOC-6, where the upper part of USB-C2 (DDH BOC-6; 438.0-468.4 m) is repeated by a fault (Figure 4.5). The correlation of the lower contact is inferred because some of the contacts between USB-C2 and USB-C1 (coherent feldspar-quartz-phyric rhyolite and feldspar-phyric dacite, monomictic rhyolite and dacite breccia, monomictic dacite sandstone, polymictic felsic breccia and sandstone, and black mudstone facies; Chapter 3) appear to be disconformable (DDH BOC-2, Figure 4.5).

The lithofacies characteristics and stratigraphic position of USB-C2, and the close proximity of the DDH where it occurs suggest that USB-C2 is correlated in this area (Figure 4.5). USB-C2 will be considered again in section 4.3.5 for larger scale correlations between the SB-Central and SB-North areas.

4.3.3.3 USB-C3

USB-C3 occurs in three DDH and includes polymictic micaceous sandstone and micaceous mudstone facies (Table 4.2). This unit extends laterally for at least 1.5 km from DDH BOC-1, in the SW, to DDH BOC-6, in the NE (Figure 4.5). The full thickness of this unit was intersected in all DDH allowing a simple, direct correlation of both the upper and lower contacts in this area (Figure 4.5). The maximum thickness (207.8 m) is intersected in DDH BOC-6. Here, USB-C3 is represented by two sequences separated by a faulted repetition of USB-C2 (Figure 4.5). USB-C3 is a distinctive stratigraphic marker and easily correlated in the SB-Central area (Figure 4.5).

4.3.3.4 USB-C4

USB-C4 occurs in three DDH and includes nine facies (Table 4.2; coherent feldspar-phyric rhyolite and dacite, monomictic rhyolite and dacite breccia, monomictic mud-matrix dacite breccia, polymictic felsic breccia and sandstone, and black and shard-rich mudstone facies). This unit extends laterally for at least 1.5 km from DDH BOC-1, in the SW, to DDH BOC-6, in the NE (Figure 4.5). The upper contact of USB-C4 was not intersected by any of the DDH, but a direct correlation of the lower contact with USB-C3 is possible in the SB-Central area (Figure 4.5).

The stratigraphic position of USB-C4 (above USB-C3), its distinctive succession of facies (Table 4.2) and the close proximity of the DDH where it occurs (Figure 4.5) allow correlation of USB-C4 in the SB-Central area. This unit will be considered in section 4.3.5 for larger scale correlations in the Sock Creek-Burns Peak area.

4.3.3.5 Intrusions

Relatively thin (<10 m), abundant mafic dykes (coherent feldspar-pyroxene-phyric, feldspar-phyric and aphyric mafic facies; section 3.3.3) intrude USB-C1a (dominantly coherent rhyolite and dacite, and monomictic rhyolite and dacite breccia facies; sections 3.3.1 and 3.3.2) (Figure 4.5). Some of these intrusions might be related, but the different lithofacies characteristics and the distance between DDH prevent any correlations of these intrusions.

In DDH BOC-2, an approximately 14-m-thick interval comprising coherent feldspar-phyric dacite and monomictic dacite breccia facies (section 3.3.2) intrudes USB-C2 (polymictic felsic breccia and sandstone, and shard-rich mudstone facies; sections 3.3.4 and 3.3.5) (Figure 4.5). Also in DDH BOC-2, a 19-m-thick interval comprising coherent feldspar-phyric rhyolite facies (section 3.3.1) intrudes black mudstone of USB-C4 (coherent feldspar-phyric rhyolite and dacite, monomictic rhyolite and dacite breccia, monomictic mud-matrix dacite breccia, polymictic felsic breccia and sandstone, black and shard-rich mudstone facies; Chapter 3) (Figure 4.5). No similar intrusions have been identified in adjacent DDH (DDH BOC-1 and BOC-6) at the same stratigraphic levels, and no correlations can be made.

4.3.4 Correlations in the Boco Road-Burns Peak area (SB-South)

In the Boco Road-Burns Peak area (SB-South), eight local stratigraphic units (USB-S; unit, Sock Creek-Burns Peak, southern area) were identified. The facies and sub-facies of each USB-S are presented in Table 4.3. Correlations of the USB-S are presented in Figure 4.6 and discussed below.

4.3.4.1 USB-S1

USB-S1 occurs in two DDH and on Boco Road, and includes six facies (Table 4.3; coherent feldspar-quartz-phyric rhyolite, coherent feldspar-phyric rhyolite and dacite, monomictic rhyolite breccia, monomictic fiamme-rich rhyolite breccia, and polymictic volcanic breccia facies). This unit extends laterally for at least 2 km. On Boco Road, USB-S1 was observed at the far E end of the mapped area (Figure 4.3), occurring stratigraphically beneath USB-S2 (polymictic micaceous sandstone and micaceous mudstone facies; sections 3.3.4 and 3.3.5; Table 4.3) (Figure 4.6). The contact between USB-S1 and USB-S2 is not exposed on Boco Road (Figure 4.6).

Correlation of the upper contact of USB-S1 can only be inferred between DDH BOC-3 and DDH BOC-4, because USB-S1 occurs below USB-S2 (polymictic micaceous sandstone and micaceous mudstone facies; sections 3.3.4 and 3.3.5; Table 4.3) in DDH BOC-4 and below USB-S3 (dominantly coherent dacite and mafic facies, and monomictic dacite and mafic breccia facies; sections 3.3.2 and 3.3.3; Table 4.3) in DDH BOC-3 (Figure 4.6). The lower contact of USB-S1 was not intersected in these DDH. Correlation of the upper contact of USB-S1 can also be inferred from DDH BOC-3 to Boco Road, where it occurs somewhere between the mapped feldspar-phyric dacite (USB-S1) and USB-S2 (Figure 4.6). This unit may allow a larger scale correlation in the Sock Creek-Burns Peak area (section 4.3.5).

4.3.4.2 USB-S2

USB-S2 occurs on Boco Road and possibly in DDH BOC-4, and includes polymictic micaceous sandstone and micaceous mudstone facies (Table 4.3). In DDH BOC-4, a 3.4-m-thick unit comprising polymictic micaceous sandstone and micaceous mudstone facies (sections 3.3.4 and 3.3.5) occurs between USB-S1 and USB-S3, and is very similar to USB-S2 on Boco Road, suggesting a possible correlation (Figure 4.6). If correct, USB-S2 extends laterally for at least 2 km in the SB-South area and represents an excellent stratigraphic marker, constraining the stratigraphic position of USB-S3.

4.3.4.3 USB-S3

USB-S3 occurs in three DDH and on Boco Road, and includes ten facies (Table 4.3; coherent feldspar-pyroxene-phyric mafic facies, coherent feldspar-phyric dacite and mafic facies, monomictic dacite and mafic breccia, monomictic mafic sandstone, monomictic mud-matrix mafic breccia, monomictic fluidal-clast mafic breccia, and polymictic mafic breccia and sandstone facies). This unit extends for at least 2 km, from DDH BOC-4, in the SW, to Boco Road, in the NE (Figure 4.6). In DDH BPD-89, USB-S3 occurs below USB-S4, but the lower contact of USB-S3 was not intersected (Figure 4.6). In DDH BOC-3, USB-S3 occurs above USB-S1 (coherent rhyolite and dacite, and monomictic rhyolite breccia; sections 3.3.1 and 3.3.2; Table 4.3), but in DDH BOC-4 USB-S3 occurs above USB-S2 (polymictic micaceous sandstone and micaceous mudstone; sections 3.3.4 and 3.3.5; Table 4.3), thus correlation of the lower contact of USB-S3 between DDH BOC-3 and BOC-4 can only be inferred (Figure 4.6). Within USB-S3, the monomictic fluidal-clast mafic breccia facies (section 3.3.3) occurs between coherent feldspar-phyric mafic facies, monomictic mafic breccia and monomictic mud-matrix mafic breccia facies (DDH BOC-3 and BOC-4; Figure 4.6). This distinctive facies is easily correlated between DDH BOC-3 and BOC-4 because of the proximity (approximately 150 m) of these DDH (Figure 4.6).

Although the facies comprising USB-S3 on Boco Road (coherent feldspar-phyric dacite and monomictic dacite breccia) are different from those in DDH BOC-3, BOC-4 and BPD-89 (Burns Peak area), correlation of USB-S3 in the Burns Peak area and in Boco Road is possible because it occurs at the same stratigraphic position (below USB-S4 and above USB-S1 and USB-S2) in both locations (Figure 4.6). USB-S3 will be considered in section 4.3.5 for larger scale correlations in the Sock Creek-Burns Peak area.

4.3.4.4 USB-S4

USB-S4 occurs in two DDH and on Boco Road, and includes three facies (Table 4.3; black mudstone and polymictic rhyolite breccia and sandstone facies). This unit extends laterally for at least 1.3 km in the SB-South area. In DDH BPD-80 (Burns Peak area), USB-S4 includes two sub-units: USB-S4a (391.8-469.7 m) and USB-S4b (283.8-297.0 m) (Figure 4.6).

Similar lithofacies characteristics and the close proximity (approximately 300 m) of DDH BPD-80 to DDH BPD-89 suggest that USB-S4 corresponds to the same unit in the two DDH (Figure 4.6). Similar lithofacies

Table 4.3: Stratigraphic units and associated facies and sub-facies in the Boco Road-Burns Peak area (SB-South). See Chapter 3 for details on each facies.

Local stratigraphic units		Facies and sub-facies	Location and diamond drill holes	Extention (km)
USB-S6	*USB-S6b*	Polymictic crystal-rich sandstone (**PcrS**) facies	Boco Road	?
	USB-S6a	Polymictic rhyolite breccia (**RpB**) and sandstone (**RpS**), polymictic mud-matrix rhyolite breccia (**RpmmB**), and black mudstone (**BMud**) facies	Burns Peak: **BPD-80**	?
USB-S5		Monomictic rhyolite breccia (**RmB**) and monomictic mud-matrix rhyolite breccia (**RmmB**) facies, and coherent quartz-rich rhyolite sub-facies (**Rqr**)	Burns Peak: **BPD-80 and BPD-89**; Boco Road	>1.3 km
USB-S4		Black mudstone (**BMud**) and polymictic rhyolite breccia (**RpB**) and sandstone (**RpS**) facies	Burns Peak: **BPD-80 and BPD-89**; Boco Road	>1.3 km
USB-S3		Coherent feldspar-pyroxene-phyric mafic facies (**Mfp**), coherent feldspar-phyric dacite (**Df**) and mafic (**Mf**) facies, monomictic dacite (**DmB**) and mafic (**MmB**) breccia, monomictic mafic sandstone (**MmS**), monomictic mud-matrix mafic breccia (**MmmB**), monomictic fluidal-clast mafic breccia (**MmfcB**), and polymictic mafic breccia (**MpB**) and sandstone (**MpS**) facies	Burns Peak: **BOC-3, BOC-4 and BPD-89**; Boco Road	>2 km
USB-S2		Polymictic micaceous sandstone (**PmS**) and micaceous mudstone (**MMud**) facies	Burns Peak: **BOC-4**; Boco Road	>2 km?
USB-S1		Coherent feldspar-quartz-phyric rhyolite (**Rfq**), coherent feldspar-phyric rhyolite (**Rf**) and dacite (**Df**), monomictic rhyolite breccia (**RmB**), monomictic fiamme-rich rhyolite breccia (**RmfrB**), and polymictic volcanic breccia (**PvB**) facies	Burns Peak: **BOC-3 and BOC-4**; Boco Road	>2 km

CORRELATION DIAGRAM

Boco Road-Burns Peak area

SB-South

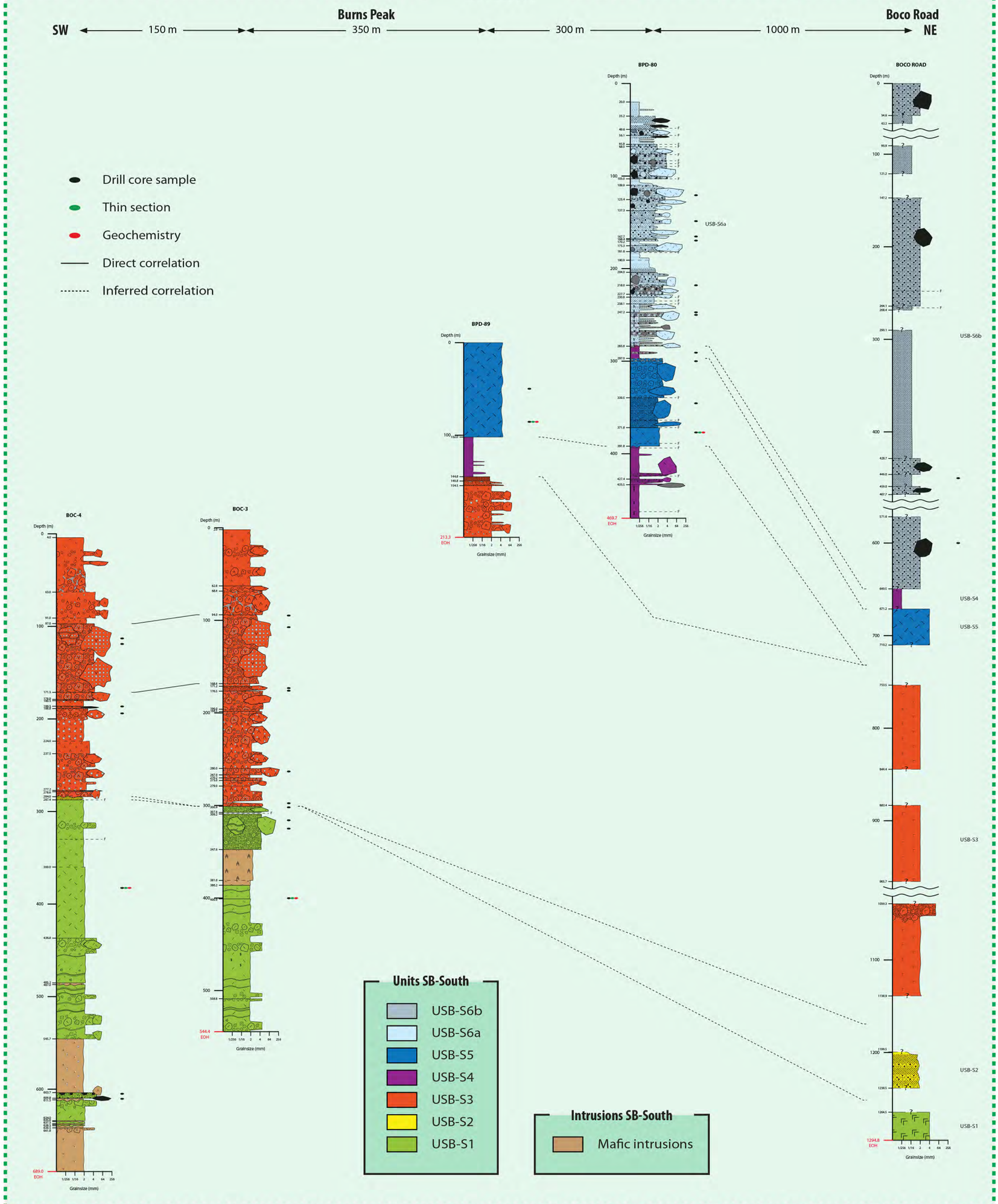

Figure 4.6: Correlation diagram of the local stratigraphic units (USB-S) identified in the Boco Road-Burns Peak area (SB-South). Unit labels are given on the right of the logs of DDH BPD-80 and Boco Road. See Figure 3.4 for legend to graphic logs.

characteristics and stratigraphic position of USB-S4b in DDH BPD-80 and USB-S4 on Boco Road suggest that these units are related (Figure 4.6). The stratigraphic position of USB-S4 and the relationship between USB-S4 and USB-S5 (coherent quartz-rich rhyolite sub-facies and monomictic rhyolite breccia and monomictic mud-matrix rhyolite breccia facies; section 3.3.1; interpreted as a partly extrusive rhyolite cryptodome, Chapter 3) hampers the direct correlation of both the upper and lower contacts (Figure 4.6).

4.3.4.5 USB-S5

USB-S5 occurs in two DDH and on Boco Road, and includes two facies and one sub-facies (Table 4.3; monomictic rhyolite breccia and monomictic mud-matrix rhyolite breccia facies, and coherent quartz-rich rhyolite sub-facies). This unit extends laterally for at least 1.3 km, and has been interpreted as a partly extrusive rhyolite cryptodome (Chapter 3). Its full thickness (94.8 m) is intersected in DDH BPD-80 (Figure 4.6). In DDH BPD-89, USB-S5 occurs above USB-S4 (black mudstone and minor polymictic rhyolite breccia and sandstone facies; sections 3.3.1 and 3.3.5; Table 4.3), but the upper contact was not intersected (Figure 4.6). On Boco Road, the lower and upper contacts of USB-S5 are not exposed (Figure 4.6). The presence of peperite (monomictic mud-matrix rhyolite breccia, section 3.3.1) involving USB-S5 in DDH BPD-80 (Figure 4.6) suggests that USB-S5 is syn-depositional and contemporaneous with USB-S4.

The close proximity (approximately 300 m) of DDH BPD-80 to DDH BPD-89 and the lithofacies characteristics of USB-S5, including identical phenocryst populations, are good evidence for correlation of the lower contact of USB-S5 in the Burns Peak area (Figure 4.6). However, the nature of this unit (partly extrusive cryptodome) and the distance between DDH BPD-80 and Boco Road make direct correlation of both the upper and lower contacts of USB-S5 unreliable. Correlation of the lower and upper contacts between DDH BPD-80 and Boco Road can only be inferred (Figure 4.6).

4.3.4.6 USB-S6

USB-S6 includes two sub-units: USB-S6a and USB-S6b (Table 4.3; Figure 4.6). USB-S6a occurs exclusively in DDH BPD-80 and includes four facies (Table 4.3; polymictic rhyolite breccia and sandstone, polymictic mud-matrix rhyolite breccia, and black mudstone facies). USB-S6b occurs exclusively on Boco Road and comprises polymictic crystal-rich sandstone facies (Table 4.3). USB-S6a and USB-S6b have different lithofacies characteristics, but they occur at the same stratigraphic level (above USB-S4 and USB-S5; Figure 4.6); correlation of the lower contact of USB-S6a and USB-S6b is inferred (Figure 4.6). USB-S6 will be considered again in section 4.3.5 for possible larger scale correlations in the Sock Creek-Burns Peak area.

4.3.4.7 Intrusions

In DDH BOC-3 and DDH BOC-4 (Burns Peak area), USB-S1 is intruded by relatively thick (<58 m) mafic dykes/sills (coherent feldspar-phyric and aphyric mafic facies, and monomictic mafic breccia facies; section 3.3.3) (Figure 4.6). The different lithofacies characteristics and the absence of whole-rock compositional data prevent any correlations of these intrusions, despite the close proximity of the DDH.

4.3.5 Regional correlations in the Sock Creek-Burns Peak area

In the Sock Creek-Burns Peak area (SB), seven regional stratigraphic units (USB; unit, Sock Creek-Burns Peak) were identified (Table 4.4; Figure 4.7). Each USB corresponds to a stratigraphic level identified from correlations of local stratigraphic units (USB-N, USB-C and USB-S, respectively) in the SB-North, SB-Central and SB-South areas (previous sections), and includes one or more local stratigraphic units and at least one facies (Chapter 3) (Table 4.4; Figure 4.7). Correlations in the Sock Creek-Burns Peak area are presented in Figure 4.7 and discussed below.

4.3.5.1 USB1

USB1 comprises four local stratigraphic units occurring in the SB-North (USB-N1), SB-Central (USB-C1a and USB-C1b) and SB-South (USB-S1) areas, and includes fifteen facies (Table 4.4; dominantly coherent feldspar-quartz-phyric rhyolite, coherent feldspar-phyric rhyolite and dacite and monomictic rhyolite and dacite breccia facies). USB1 is sub-divided into two sub-units: USB1a and USB1b. The equivalents of these sub-units and their associated facies are presented in Table 4.4. USB1b is equivalent to USB-C1b (SB-Central; Figure 4.7), and local correlations regarding this sub-unit have been discussed earlier (section 4.3.3.1). USB-N1, USB-C1a and USB-S1 (USB1a) can be correlated based on their stratigraphic positions and similar lithofacies characteristics.

In the SB-North area, USB-N1 occurs stratigraphically below USB-N2 and the contact between USB-N1 and USB-N2 has been interpreted as a fault (DDH BHD-10; Figures 4.4 and 4.7), but in the SB-Central area, USB-C1 is overlain by USB-C2, although the upper contact of USB-C1a is not intersected (Figures 4.5 and 4.7). USB-N1 and USB-C1a comprise very similar coherent rhyolite and dacite and monomictic rhyolite and dacite breccia (interpreted as coherent and autoclastic facies of lavas and domes, and possibly syn-volcanic intrusions; sections 3.3.1 and 3.3.2). Although these units do not comprise laterally extensive volcaniclastic facies, the facies similarities and stratigraphic position suggest that USB-N1 and USB-C1a occur roughly at the same stratigraphic position, and correlation of the upper contact of these sub-units can be inferred between SB-north and SB-Central (Figure 4.7).

The same criteria are used to correlate USB-C1 (SB-Central) and USB-S1 (SB-South). These units comprise very similar facies and occur roughly at the same stratigraphic level (Figure 4.7).

The lithofacies characteristics and stratigraphic position of USB1a and USB1b (USB1; Figure 4.7) are very similar to those of the CVC (section 4.2.2) (Corbett, 1979, 1981, 1992, 2002a; Corbett and McNeill, 1986; Corbett and Komyshan, 1989; Corbett and Solomon, 1989; McNeill and Corbett, 1989). The CVC has been mapped from N of Lake Rosebery to SW of Mount Charter (Corbett, 2002a), and comprises the Mount Black Formation, the Kershaw Pumice Formation and the Hercules Pumice Formation (section 2.5.3) (Gifkins; 2001). USB1a comprises dominantly feldspar-quartz-phyric rhyolite, feldspar-phyric dacite and monomictic rhyolite and dacite breccia facies that are very similar to those described in the Mount Black Formation (Gifkins, 2001). This correlation implies that the equivalents of the Kershaw Pumice Formation

and the Hercules Pumice Formation, which contains the Footwall Member and Host-rock Member of the Rosebery and Hercules VHMS deposits, are not present in the Sock Creek-Burns Peak area. The consequences of this correlation are considered in the following chapters.

In the Boco area, USB1b occurs stratigraphically below USB2 (interpreted to correspond to the Black Harry Beds; next section), and the nature of the contact has been logged as conformable and gradational (DDH BOC-1) or could not be described due to broken or missing core (DDH BOC-2 and BOC-6), and was not resolved. (Figure 4.7; Appendix A); the contact between the CVC and the Mount Charter Group (Black Harry Beds) has been described by other authors to be a faulted unconformity (Komyshan, 1986a, 1986b), a fault dipping 30º NE (Corbett and Komyshan, 1989), disconformable from High Point to Burns Peak (McNeill and Corbett, 1989), and poorly defined (Corbett, 1992).

These observations support the interpretation that USB1 corresponds to the Mount Black Formation (CVC; Gifkins, 2001).

4.3.5.2 USB2

USB2 comprises two local stratigraphic units occurring in the SB-North (USB-N2) and SB-Central (USB-C2) areas, and includes three facies (Table 4.4; polymictic felsic breccia and sandstone and shard-rich mudstone facies).

Stratigraphic correlation of USB-C2 and USB-N2 is supported by very similar lithofacies characteristics and the stratigraphic position of these units (Table 4.4; Figure 4.7). Although the upper contact of USB-N2 is not intersected in DDH BHD-10 (SB-North; Figures 4.4 and 4.7), this unit occurs stratigraphically below USB-N3. In the Boco area (SB-Central), USB-C2 is directly underlain by USB-C3, which is stratigraphically equivalent to USB-N3 (section 4.3.5.3) in the SB-North area (Table 4.4; Figure 4.7).

The lower contact of USB-N2 is intersected in DDH BHD-10 (SB-North; Figure 4.4 and 4.7) and has been logged as a fault. Correlation of same contact can only be inferred in the Boco area (SB-Central; Figures 4.5 and 4.7); here, the nature of the contact between USB-C2 and USB-C1 was not resolved. Thus, an inferred correlation of the lower contact of USB2 is suggested between the SB-Central and SB-North areas (Figure 4.7).

The lithofacies characteristics, stratigraphic position and, to some degree, thickness and lateral extent of USB2 are very similar to those of the Black Harry Beds (section 4.2.3.1) (Corbett, 1992; Corbett and Komyshan, 1989; Pemberton et al., 1991). In the Boco area, USB2 conformably and gradationally underlies USB3 (Figures 4.5 and 4.7), interpreted to correspond to the Animal Creek Greywacke (next section), and the Black Harry Beds are known to conformably and gradationally underlie the Animal Creek Greywacke from SW of Mount Charter to NE of Boco Road (Corbett and McNeill, 1986; Pemberton et al., 1991; Corbett, 1992; Corbett, 2002a; this thesis).

Table 4.4: Stratigraphic units, location, associated facies and sub-facies, and equivalent formal stratigraphic units in the Sock Creek-Burns Peak (SB) area.

Regional stratigraphic units		Location and local stratigraphic units	Facies and sub-facies	Location and diamond drill holes	Extention (km)	Equivalents (stratigraphic units)
USB7	***USB7c***	SB-South: **USB-S6b**	Polymictic crystal-rich sandstone (**PcrS**) facies	Boco Road	>12 km? (if correlated)	**Southwell Subgroup**
	USB7b	SB-South: **USB-S6a**	Polymictic rhyolite breccia (**RpB**) and sandstone (**RpS**), polymictic mud-matrix rhyolite breccia (**RpmmB**), and black mudstone (**Bmud**) facies	Burns Peak: **BPD-80**		
	USB7a	SB-North: **USB-N7**	Polymictic rhyolite breccia (**RpB**) and sandstone (**RpS**), and black mudstone (**BMud**) facies	Sock Creek: **BHD-4**		
USB6	***USB6b***	SB-South: **USB-S5**	Monomictic rhyolite breccia (**RmB**) and monomictic mud-matrix rhyolite breccia (**RmmB**) facies, and coherent quartz-rich rhyolite sub-facies (**Rqr**)	Burns Peak: **BPD-80, BPD-89**; Boco Road	>12 km? (if correlated)	**Quartz-feldspar rhyolite porphyries**
	USB6a	SB-North: **USB-N6**		Sock Creek: **BHD-4, BHD-7, BHD-8 and BHD-9**; Sock Creek South: **SCS-2, SCS-3 and SCS-5**		
USB5	***USB5b***	SB-South: **USB-S4**	Black mudstone (**BMud**), and polymictic rhyolite breccia (**RpB**) and sandstone (**RpS**) facies	Burns Peak: **BPD-80, BPD-89**; Boco Road	>12 km? (if correlated)	**Que River Shale equivalent**
	USB5a	SB-North: **USB-N5**	Black mudstone facies (**BMud**)	Sock Creek: **BHD-4, BHD-8 and BHD-9**		
USB4	***USB4b***	SB-North: **USB-N4b**	Polymictic volcanic breccia (**PvB**) and sandstone (**PvS**) facies	Sock Creek: **BHD-4, BHD-7, BHD-8 and BHD-9**; Sock Creek South: **SCS-2, SCS-3 and SCS-5**	>3.5 km	***Mixed sequence*** **(Que-Hellyer Volcanics) equivalent**
	USB4a	SB-North: **USB-N4a**; SB-Central: **USB-C4**; SB-South: **USB-S3**	Coherent feldspar-pyroxene-phyric mafic facies (**Mfp**), coherent feldspar-phyric rhyolite (**Rf**), dacite (**Df**) and mafic (**Mf**) facies, monomictic rhyolite (**RmB**), dacite (**DmB**) and mafic (**MmB**) breccia, monomictic mafic sandstone (**MmS**), monomictic mud-matrix rhyolite (**RmmB**), dacite (**DmmB**) and mafic (**MmmB**) breccia, monomictic fiamme-rich dacite breccia (**DmfrB**), monomictic fluidal-clast mafic breccia (**MmfcB**), polymictic mafic breccia (**MpB**) and sandstone (**MpS**), polymictic mud-matrix felsic breccia (**PmmfB**), polymictic felsic breccia (**PfB**) and sandstone (**PfS**), and black (**BMud**), micaceous (**MMud**) and shard-rich (**SMud**) mudstone facies	Sock Creek: **BHD-4, BHD-7, BHD-8 and BHD-9**; Sock Creek South: **SCS-2, SCS-3, SCS-4 and SCS-5**; Boco: **BOC-1, BOC-2 and BOC-6**; Burns Peak: **BOC-3, BOC-4, and BPD-89**; Boco Road	>12 km	**Que-Hellyer Volcanics equivalents (include Sock Creek Dacites, Boco Road Dacite and Hollway Andesite)**
USB3		SB-North: **USB-N3**; SB-Central: **USB-C3**; SB-South: **USB-S2**	Polymictic micaceous sandstone (**PmS**) and micaceous mudstone (**MMud**) facies	Sock Creek: **BHD-4, BHD-7, BHD-8 and BHD-9**; Sock Creek South: **SCS-5**; Boco: **BOC-1, BOC-2 and BOC-6**; Burns Peak: **BOC-4**; Boco Road	>12 km	**Animal Creek Greywacke**
USB2		SB-North: **USB-N2**; SB-Central: **USB-C2**	Polymictic felsic breccia (**PfB**) and sandstone (**PfS**), and shard-rich mudstone (**SMud**) facies	Sock Creek South: **BHD-10**; Boco: **BOC-1, BOC-2 and BOC-6**	>4.5 km	**Black Harry Beds**
USB1	***USB1b***	SB-Central: **USB-C1b**	Coherent quartz-rich rhyolite sub-facies (**Rqr**); coherent feldspar-phyric dacite (**Df**), monomictic rhyolite (**RmB**) and dacite (**DmB**) breccia, monomictic dacite sandstone (**DmS**), polymictic felsic breccia (**PfB**) and sandstone (**PfS**), polymictic mud-matrix felsic breccia (**PmmfB**), and black mudstone (**BMud**) facies	Boco: **BOC-1, BOC-2 and BOC-6**	>1.5 km	**Central Volcanic Complex (Mount Black Formation)**
	USB1a	SB-North: **USB-N1**; SB-Central: **USB-C1a**; SB-South: **USB-S1**	Coherent feldspar-quartz-phyric rhyolite (**Rfq**), coherent feldspar-phyric rhyolite (**Rf**) and dacite (**Df**), monomictic rhyolite (**RmB**) and dacite (**DmB**) breccia, monomictic mud-matrix dacite breccia (**DmmB**), monomictic fiamme-rich rhyolite (**RmfrB**) and dacite (**DmfrB**) breccia, monomictic mud-matrix fiamme-rich dacite breccia (**DmmfrB**), monomictic dacite sandstone (**DmS**), polymictic volcanic breccia (**PvB**), and polymictic felsic breccia (**PfB**) facies	Mackintosh: **AK-1**; Sock Creek South: **BHD-10**; Boco Alteration Zone: **BBP-207, BBP-209 and BBP-242**; Burns Peak: **BOC-3 and BOC-4**; Boco Road	>12 km	

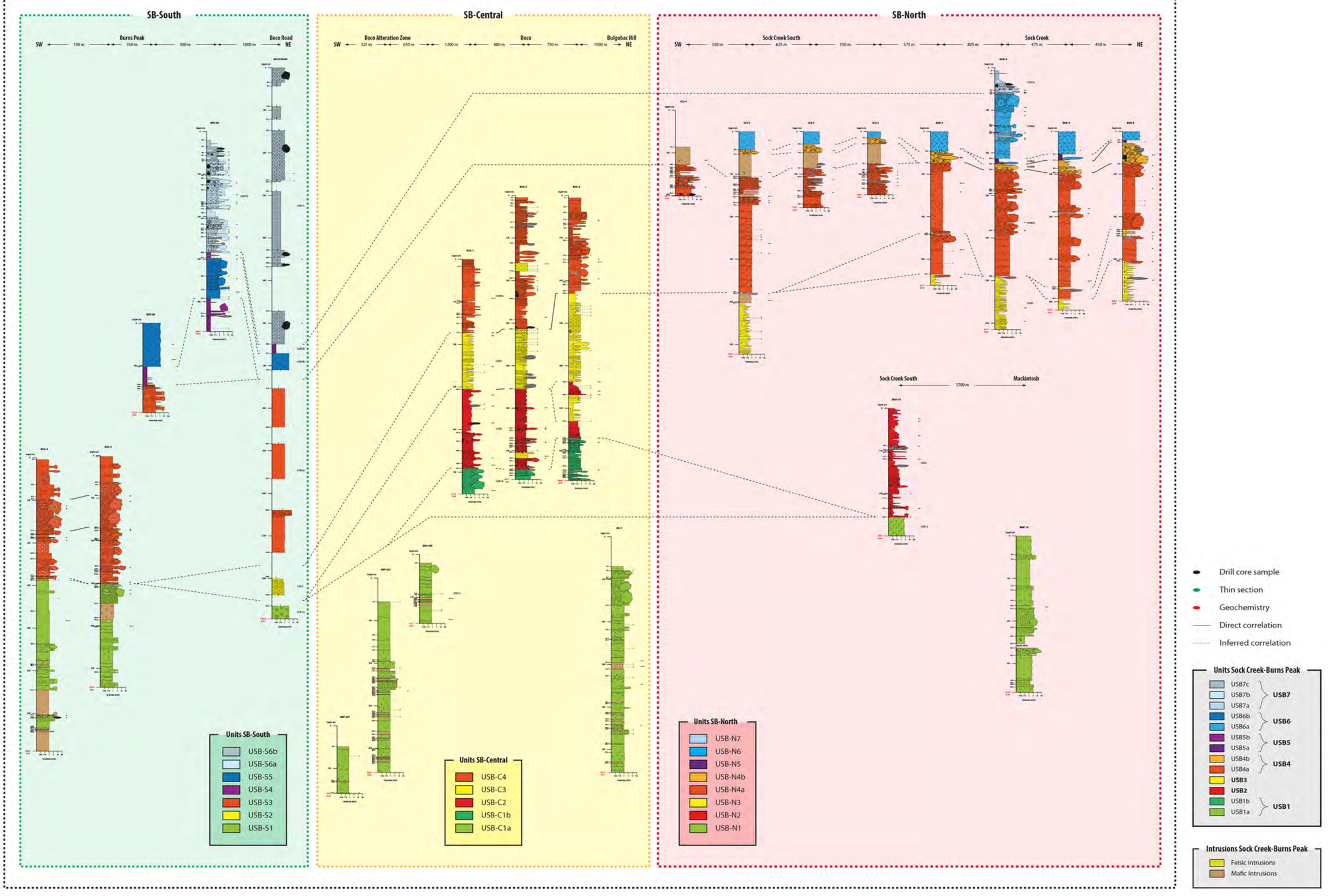

Figure 4.7: Correlation diagram of the regional stratigraphic units (USB) identified in the Sock Creek-Burns Peak area (SB). Unit labels are given on the right of the logs of DDH BHD-4 and BHD-10 (SB-North), BBP-209 and BOC-1 (SB-Central), and BPD-80 and Boco Road (SB-South). See Figure 3.4 for legend to graphic logs.

These observations are consistent with the interpretation of USB2 being equivalent to the Black Harry Beds.

4.3.5.3 USB3

USB3 comprises three local stratigraphic units occurring in the SB-North (USB-N3), SB-Central (USB-C3) and SB-South (USB-S2) areas, and includes polymictic micaceous sandstone and micaceous mudstone facies (Table 4.4).

USB-N3, USB-C3a and USB-S2 comprise very similar successions of polymictic micaceous sandstone and micaceous mudstone facies with very similar bedforms, supporting the interpretation that these units are laterally equivalent (USB3; Figure 4.7). Furthermore, the relatively close proximity (<3 km; Figure 4.1) between DDH SCS-5 (SB-North) and DDH BOC-6 (SB-Central), DDH BOC-1 (SB-Central) and Boco Road (SB-South), and Boco Road and possibly DDH BOC-4 (SB-South) also support the correlation of these units (Figure 4.7).

The lithofacies characteristics, thickness, lateral extent, and stratigraphic position of USB3 are very similar to those of the Animal Creek Greywacke (section 4.2.3.2) (Corbett and McNeill, 1986; Pemberton et al., 1991; Corbett, 2002a). USB3 comprises polymictic micaceous sandstone facies (section 3.3.4), which includes abundant muscovite and metamorphic, basement-derived fragments, similar to those described in the Animal Creek Greywacke (Corbett and McNeill, 1986; Pemberton et al., 1991). Similarly to the Animal Creek Greywacke, USB3 extends laterally for >12 km in the Sock Creek-Burns Peak area, and wedges out to the SW in the Burns Peak-Boco Road area. Furthermore, USB3 conformably and gradationally overlies USB2, interpreted to correspond to the Black Harry Beds (previous section), in the Sock Creek-Boco area (Figure 4.7), and the Animal Creek Greywacke is known to conformably and gradationally overlie the Black Harry Beds from the Mount Charter Fault to NE of Boco Road (Corbett and McNeill, 1986; Pemberton et al., 1991; Corbett, 1992; Corbett, 2002a).

These similarities are consistent with the interpretation of USB3 being equivalent to the Animal Creek Greywacke.

4.3.5.4 USB4

USB4 comprises four local stratigraphic units occurring in the SB-North (USB-N4a and USB-N4b), SB-Central (USB-C4) and SB-South (USB-S3) areas, and includes twenty-three facies (Table 4.4; dominantly coherent feldspar-pyroxene-phyric mafic facies, coherent feldspar-phyric rhyolite, dacite and mafic facies, monomictic rhyolite, dacite and mafic breccia, monomictic mud-matrix rhyolite, dacite and mafic breccia, monomictic fluidal-clast mafic breccia, and polymictic volcanic breccia and sandstone facies). USB4 is sub-divided into two sub-units: USB4a and USB4b. The equivalents of these sub-units and their associated facies are presented in Table 4.4. USB4b (polymictic volcanic breccia and sandstone facies, section 3.3.4) is equivalent to USB-N4b (Figure 4.7), and has been considered to be part of USB-N4 (section 4.3.2.4). USB-N4a, USB-C4 and USB-S3 (USB4a) can be correlated based on their stratigraphic positions and lithofacies characteristics.

Correlation of USB-N4a with USB-C4 (SB-North and SB-Central areas, respectively) is supported by their similar succession of facies, but specially their stratigraphic position (Table 4.4; Figure 4.7). These units are underlain by USB-N3 and USB-C3 (polymictic micaceous sandstone and micaceous mudstone facies; sections 3.3.4 and 3.3.5) respectively, which are considered to occur at the same stratigraphic level (USB3; previous section; Figure 4.7). Although the upper contact of USB-C4 is not intersected in the SB-Central area, correlation of the lower contact of USB-C4 and USB-N4a is possible between the SB-Central and SB-North areas (Figure 4.7). This relationship is supported by the relatively close proximity (approximately 2.5 km) between DDH BOC-6 (SB-Central area) and SCS-5 (SB-North area) (Figure 4.7).

The same criteria support the correlation of USB-C4 with USB-S3 (between the SB-Central and SB-South areas, Figure 4.7). These units occur above USB-C3 and USB-S2 (polymictic micaceous sandstone and micaceous mudstone facies; sections 3.3.4 and 3.3.5) respectively, which are considered to occur at the same stratigraphic level (USB3; previous section). An inferred correlation of the lower contact of these units is thus suggested due to their stratigraphic position and the relatively close proximity (approximately 3 km) of DDH BOC-1 to Boco Road (Figure 4.7).

On Boco Road (SB-South area), the upper contact of USB-S3 is not exposed, but in the Burns Peak area (SB-South area), USB-S3 is overlain by USB-S4 (black mudstone facies; DDH BPD-89; Figures 4.6 and 4.7). A similar relationship occurs in the Sock Creek area (DDH BHD-4, BHD-8 and BHD-9; Figures 4.4 and 4.7), where USB-N4 is overlain by USB-N5 (black mudstone facies; section 3.3.5). USB-N5 and USB-S4 (dominantly black mudstone facies) are interpreted to occur at the same stratigraphic level (USB5; next section; Figure 4.7), which support the interpretation that USB-S3 (SB-South area) and USB-N4a (SB-North area) are lateral stratigraphic equivalents.

In DDH BOC-4, the 3.4-m-thick unit of polymictic micaceous sandstone and micaceous mudstone occurring underneath USB-S3 may correlate with USB-S2 in Boco Road (polymictic micaceous sandstone and micaceous mudstone facies; sections 3.3.4 and 3.3.5) (Figure 4.7). If correct, then a direct correlation of USB-S2 is possible between DDH BOC-4 and the Boco Road (previous section) (Figure 4.7), which supports the interpretation that USB-S3 in Boco Road and USB-S3 at Burns Peak (DDH BOC-3, BOC-4 and BPD-89) are lateral stratigraphic equivalents (USB-S3).

The previous observations support the interpretation that USB-N4a, USB-C4 and USB-S3 occur roughly at the same stratigraphic level (USB4a; Figure 4.7).

The lithofacies characteristics and stratigraphic position of USB4a in the SB-North area (USB-N4a; Figures 4.4 and 4.7) are very similar to those of the Sock Creek Dacites (section 4.2.3.3) (Wilde and Kerr, 1989; McNeill, 2002a; DDH SCS-5; Skirka and McNeill, 2006). USB4a overlies USB3, correlated with the Animal Creek Greywacke (previous section), and the Sock Creek Dacites overlie the Animal Creek Greywacke. Hence, USB4a in the SB-North area is interpreted to correspond to the Sock Creek Dacites. The facies comprising USB4a in the Sock Creek South area (SB-North) seem to extend to the SB-Central area (USB-C4; Figure 4.7).

The stratigraphic position of USB4a in the Boco Road area (USB-S3; Boco Road vertical section; Figures 4.6 and 4.7) is identical to that of the Boco Road Dacite (section 4.2.3.3) (McNeill, 2002b; Corbett, 2005a, 2005b; McIntyre, 2006). The Boco Road Dacite overlies the Animal Creek Greywacke (McIntyre, 2006), and USB4a in the Boco Road area overlies USB-S2, interpreted to correspond to an equivalent of the Animal Creek Greywacke (previous section). Furthermore, USB4a in the Boco Road area comprise coherent feldspar-phyric dacite and monomictic dacite breccia facies (section 3.3.2) that are very similar to those of the Boco Road Dacite (e.g., McIntyre, 2006), hence USB4a in the Boco Road area is interpreted to correspond to the Boco Road Dacite.

The stratigraphic position of USB4a in the Burns Peak area (USB-S3; DDH BOC-3, BOC-4 and BPD-89; Figures 4.6 and 4.7) is identical to that of the Hollway Andesite (section 4.2.3.3) (McNeill, 2002b; Corbett, 2005a, 2005b), and both the Hollway Andesite and USB4a in the Burns Peak area comprise a sequence of feldspar-pyroxene-phyric and feldspar-phyric mafic (andesites and basalts) facies, and include monomictic fluidal-clast mafic breccia facies (section 3.3.3; McIntyre, 2006). Hence, USB4a in the Burns Peak area is interpreted to correspond to the Hollway Andesite.

4.3.5.5 USB5

USB5 includes two local stratigraphic units occurring in the SB-North (USB-N5) and SB-South (USB-S4) areas, and comprises three facies (Table 4.4; black mudstone and polymictic rhyolite breccia and sandstone facies).

USB5 is sub-divided into two sub-units: USB5a and USB5b. The equivalents of these sub-units and their associated facies are presented in Table 4.4. These sub-units are interpreted to belong to the same stratigraphic level (USB5, Figure 4.7) because they comprise black mudstone facies with very similar lithofacies characteristics that occur at the same stratigraphic level. However, the lack of similar mudstone facies in the SB-Central and Sock Creek South (SB-North) areas, and the distance between DDH comprising this facies in the SB-North and SB-South areas (the distance separating DDH BHD-4 at SB-North from Boco Road at SB-South is approximately 9 km) make direct correlations difficult (Figure 4.7).

The lithofacies characteristics and stratigraphic position of USB5 (USB5a and USB5b) are very similar to those of the Que River Shale (section 4.2.3.4) (Gee et al., 1970; Corbett and Komyshan, 1989). USB5a and USB5b comprise black mudstone facies (section 3.3.5) that is very similar to the Que River Shale (section 4.2.3.4). Also, the Que River Shale overlies the Que Hellyer Volcanics and is overlain by the Southwell Subgroup (Corbett and Komyshan, 1989; Corbett, 1992); in the Sock Creek, Boco Road and Burns Peak areas (Figure 4.7), USB5a and USB5b overlie USB4a and USB4b respectively, interpreted as possible equivalents of the Que-Hellyer Volcanics (previous section), and underlie USB7a, USB7b and USB7c, interpreted as possibly equivalents of the Southwell Subgroup (section 4.3.5.7). Furthermore, mapping in the Boco-Pinnacles area (Corbett and McNeill, 1986; Reid, 1990; Corbett, 2002a) has identified possible stratigraphic equivalents of the Que River Shale from the Hellyer-Mount Charter areas (Corbett and Komyshan, 1989).

These observations suggest that USB5a and USB5b (USB5) are equivalents of the Que River Shale.

4.3.5.6 USB6

USB6 comprises two local stratigraphic units occurring in the SB-North (USB-N6) and SB-South (USB-S5) areas, and includes two facies and one sub-facies (Table 4.4; monomictic rhyolite breccia and monomictic mud-matrix rhyolite breccia facies, and coherent quartz-rich rhyolite sub-facies). The spatial association and distribution of the facies comprising these local stratigraphic units have been interpreted to represent partly extrusive rhyolite cryptodomes (Chapter 3).

USB6 can be sub-divided into two sub-units: USB6a and USB6b. The equivalents of these sub-units and their associated facies are presented in Table 4.4. These sub-units are interpreted to occur roughly at the same stratigraphic level (USB6, Table 4.4; Figure 4.7).

USB6a and USB6b are partly extrusive (Chapter 3), have very similar lithofacies characteristics (phenocryst population, textures and internal structures) and the facies association is identical (coherent quartz-rich rhyolite sub-facies associated with monomictic rhyolite breccia and monomictic mud-matrix rhyolite breccia facies; Table 4.4; Figure 4.7). Furthermore, and because these units are partly intrusive, they have an intricate stratigraphic relationship with USB5a and USB5b (black mudstone facies; section 3.3.5; Figure 4.7), which have been interpreted to occur at the same stratigraphic level (USB5; previous section; Figure 4.7). These observations suggest that USB6a and USB6b occur roughly at the same stratigraphic level (USB6; Figure 4.7).

However, the absence of similar rhyolite facies in the SB-Central area and the distance between DDH displaying these facies in the SB-North and SB-South areas (the distance separating DDH SCS-5 at SB-North from Boco Road at SB-South is approximately 7 km; Figure 4.1) make direct correlations difficult (Figure 4.7). USB6a and USB6b may or may not belong to the same rhyolite body, but it is suggested in this thesis that a stratigraphic relationship exists between USB6a and USB6b, based on whole-rock compositional data (samples 179356, 179441 and 179443; Figure 3.1; Table 3.2).

The lithofacies characteristics and stratigraphic position of USB6 (USB6a and USB6b) are very similar to those of the quartz-feldspar rhyolite porphyries identified by Corbett and Komyshan (1989), McNeill (2002a, 2002b) and Corbett (2005a) (section 4.2.3.5). USB6a, USB6b and the rhyolite porphyries comprise coarse (<1 cm in diameter) embayed quartz and twinned feldspar phenocrysts, and are locally flow banded (section 3.3.1). Furthermore, the rhyolite porphyries occur within the Que River Shale and Southwell Subgroup equivalents (Corbett and Komyshan, 1989; Corbett, 2005a); USB6a and USB6b occur above and intercalated with USB5a and USB5b (interpreted as possible equivalents of the Que River Shale; previous section) respectively, and USB6a occurs below USB7a (interpreted to be a possible equivalent of the Southwell Subgroup; next section).

These features suggest that USB6a and USB6b (USB6) are related to the quartz-feldspar rhyolite porphyries identified by Corbett and Komyshan (1989), McNeill (2002a, 2002b) and Corbett (2005a).

4.3.5.7 USB7

USB7 includes two local stratigraphic units occurring in the SB-North (USB-N7) and SB-South (USB-S6) areas, and comprises five facies (Table 4.4; polymictic rhyolite breccia and sandstone, polymictic mud-matrix rhyolite breccia, polymictic crystal-rich sandstone and black mudstone facies).

USB7 is sub-divided into three sub-units: USB7a, USB7b and USB7c. The equivalents of these sub-units and their associated facies are presented in Table 4.4. These sub-units are interpreted to correspond to the same stratigraphic level (USB7, Figure 4.7). Criteria supporting this hypothesis are the stratigraphic positions of USB-N7 (above USB-N6), USB-S6a and USB-S6b (above USB-S4 and USB-S5, respectively), and the facies similarities between USB-N7 and USB-S6a (Table 4.4; Figure 4.7). However, direct correlations are difficult due to the distance between DDH (Figures 4.1 and 4.7). The lithofacies characteristics of USB-S6a and USB-S6b are distinct, but these sub-units have been grouped into USB-S6 (section 4.3.4.6) and interpreted to occur at the same stratigraphic level (USB7; Figure 4.7).

The lithofacies characteristics and stratigraphic position of USB7 are very similar to those of the Southwell Subgroup (section 4.2.3.6) (Corbett and Komyshan, 1989; McPhie and Allen, 1992; Corbett, 1992, 2005a, 2005b; Bold 2009). USB7a, USB7b, and the Southwell Subgroup contain large (>25 cm long) feldspar-quartz-phyric rhyolite clasts that are similar to the feldspar-quartz-phyric rhyolite units occurring in the Sock Creek and Burns Peak areas (USB-N6 and USB-S5, respectively). The basal unit of the Southwell Subgroup (lower tuff unit; Corbett and Komyshan, 1989) contains large (< 50 cm long) mudstone clasts, and conformably overlies the Que River Shale in the Hellyer area; the contact is irregular and erosional in the Haulage Road area (Corbett and Komyshan, 1989). USB7a and USB7b also contain large (< 50 cm long) mudstone clasts near the base of normally graded intervals of polymictic rhyolite breccia and sandstone (Figure 4.7), and USB7b overlies USB-S4 (possible correlate of the Que River Shale) in the SB-South area, and the contact has been logged as irregular and erosional in DDH BPD-80 (Figures 4.6 and 4.7). Furthermore, mapping in the Boco Road-Burns Peak area (Reid, 1990; McNeill, 2002a, 2002b) has identified stratigraphic equivalents of the Southwell Subgroup from the Sock Creek and Hellyer-Que River areas (Corbett, 2002b).

These observations support the interpretation that USB7a, USB7b and USB7c (USB7) are equivalents of the lower part of the Southwell Subgroup.

4.4 Facies architecture in the Sock Creek-Burns Peak area

4.4.1 Introduction

The interpretation of the facies and facies associations identified in this thesis (Chapter 3), combined with studies of emplacement processes and textures of facies present in the northern MRV (e.g., McPhie and Allen, 1992; McPhie et al. 1993; Gifkins, 2001), has confirmed that the texturally diverse coherent and volcaniclastic facies of parts of the northern MRV (Chapter 3) were emplaced in a below-wave-base submarine environment. The occurrence of sponge spicules, shell fragments and other organic fragments within distinct mudstone and polymictic volcaniclastic facies (Chapter 3) constrains the depositional setting to below-wave-base (Gee et al., 1970; Quilty, 1971, 1972a). Perlitic fractures in coherent rhyolite and dacite facies (Chapter 3), and in rhyolite and dacite clasts within associated autoclastic facies (monomictic rhyolite and dacite breccia facies; Chapter 3) suggest rapid cooling on contact with water or wet sediment in a subaqueous environment. Background suspension sedimentation of mudstone facies (Chapter 3) was episodically interrupted by deposition of high- and low-concentration turbidites, some of which were explosive eruption-fed, and emplacement of rhyolite to basalt lavas, domes, syn-volcanic sills, dykes and cryptodomes, and associated autoclastic (autobreccia and hyaloclastite) facies.

In this section, the regional facies architecture in the Sock Creek-Burns Peak area is reconstructed based on the characteristics and interpretations of the facies and facies associations (Chapter 3), and on the local and regional stratigraphic units and correlations discussed previously (section 4.3; Figure 4.7). The reconstruction of the regional facies architecture in the Sock Creek-Burns Peak area is discussed in terms of the local facies architecture of each of the three adjacent sub-areas considered in the SB area (Figure 4.3), and supported by the regional correlation diagram of the diamond drill holes (DDH) logged in this study (Figure 4.7). Syn-volcanic intrusions (e.g., sills/dykes and cryptodomes associated with peperite) and partly extrusive cryptodomes have been included in the seven-stage reconstruction of the facies architecture in the Sock Creek-Burns Peak area, which is presented in Figure 4.8 and discussed below. Post-volcanic intrusions are considered at the end of this section.

4.4.2 Reconstruction of the facies architecture in the Sock Creek-Burns Peak area

Stage 1: Felsic dome and lava complexes

The lowest part of the Sock Creek-Burns Peak succession consists of USB1 (USB1a and USB1b; correlated with the Mount Black Formation of the CVC - section 4.3.5.1) (Figures 4.7 and 4.8). USB1a (Figure 4.7 - USB-N1, USB-C1 and USB-S1) comprises a thick (<500 m) succession of dominantly massive to flow-banded and/or locally amygdaloidal and perlitic, feldspar-quartz-phyric rhyolite and feldspar-phyric rhyolite and dacite, and monomictic rhyolite and dacite breccia facies (sections 3.3.1 and 3.3.2; Table 4.4). The top of USB1a in DDH BOC-3 (Figure 4.7 - SB-South) also includes monomictic fiamme-rich rhyolite breccia facies (section 3.3.1.5).

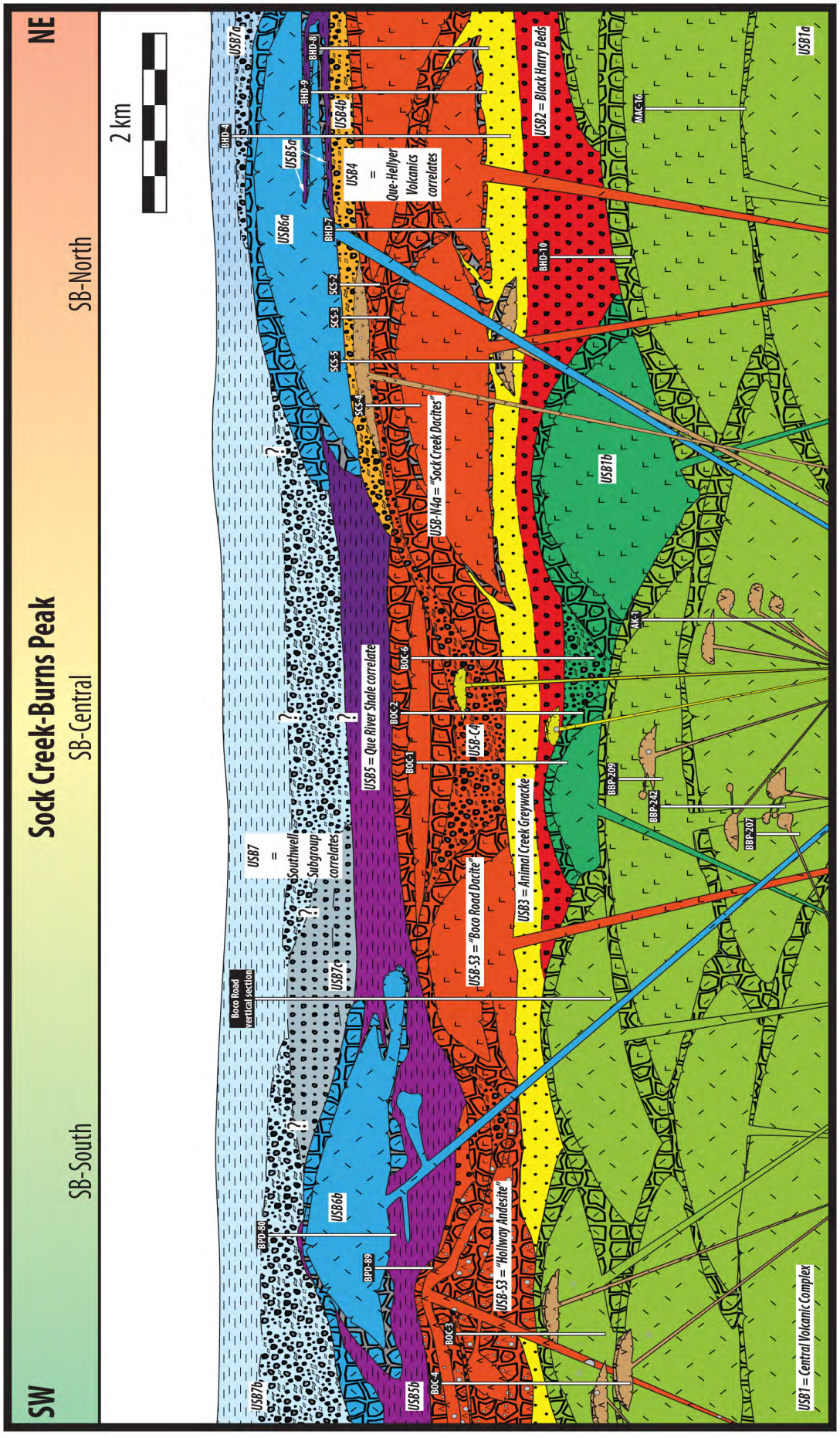

Figure 4.8: Schematic diagram depicting the facies architecture in the Sock Creek-Burns Peak area and the approximate position of the diamond drill holes (vertical lines) in this study.

Stage 1 involved the growing of a large volcanic complex comprising overlapping feldspar-quartz-phyric rhyolitic and feldspar-phyric rhyolitic and dacitic lavas and domes, and minor cryptodomes in the SB area. In the Burns Peak area (DDH BOC-3, SB-South), autoclastic (non-explosive) fragmentation, resedimentation and diagenetic compaction of feldspar-phyric rhyolitic pumiceous lava fragments, produced monomictic fiamme-rich rhyolite breccia facies (Figure 4.8).

Later in stage 1, feldspar-quartz-phyric rhyolite and feldspar-phyric dacite lavas and domes erupted in the SB-Central area (Figures 4.7 and 4.8 - USB1b; Table 4.4), and the associated autobreccia and hyaloclastite were resedimented down slope. Syn- to post-eruptive polymictic felsic breccia and sandstone (Figures 4.7 and 4.8 - USB1b; Table 4.4) were deposited from density currents derived from the rhyolitic to dacitic volcanic complex.

The intrusive versus extrusive nature of many rhyolites and dacites within USB1a in the Sock Creek-Burns Peak area (Figure 4.7) has not been resolved because the textures and contact relationships are commonly ambiguous in drill core. The paucity of volcano-sedimentary units (e.g., black mudstone, polymictic volcanic sandstone) and the thickness (<500 m) of rhyolite and dacite units imply that the rhyolite and dacite units were either erupted rapidly from adjacent vents or fissures, or that they constructed significant topography, which strongly limited post-eruptive sedimentation.

Stage 2: Syn- to post-eruptive density currents

Stage 2 marks the deposition of USB2 (USB-N2 and USB-C2; correlated with the Black Harry Beds - section 4.3.5.2) from density currents in the SB-North and SB-Central areas (Figures 4.7 and 4.8). USB2 comprises normally graded units of polymictic felsic breccia and sandstone bases and shard-rich mudstone tops (sections 3.3.4 and 3.3.5; Table 4.4). The density currents were probably partly explosive eruption-fed because the deposits contain abundant shards. The presence of basement-derived fragments (schist, phyllite and quartzite) suggests that the currents originated within exposed metamorphic basement at the basin margin. The rhyolite and dacite clasts within the polymictic felsic breccia facies (Figure 4.7 - USB2; Table 4.4) are similar to the underlying rhyolite and dacite units (Figure 4.7 - USB1a and USB1b; Table 4.4) and could have had a local source.

Stage 3: Uplift and basement-derived density currents

Stage 3 involves the deposition of USB3 (USB-N3, USB-C3 and USB-S2; correlated with the Animal Creek Greywacke - section 4.3.5.3) in the SB area (Figures 4.7 and 4.8). USB3 consists of normally graded units of polymictic micaceous sandstone and micaceous mudstone facies (sections 3.3.4 and 3.3.5; Table 4.4), and comprises abundant metamorphic fragments (muscovite, biotite, quartzite and schist) interpreted to have been derived from erosion of exposed basement at the basin margin. Detrital chromite within USB3 indicates that obduction of the mafic-ultramafic complexes (Berry and Crawford, 1988; Crawford and Berry, 1992) had occurred and that one or more of these complexes were being eroded. The density currents that deposited USB3 originated at the basin margin and were probably generated by slope failure associated with

tectonic earthquakes or movement along syn-depositional faults.

At the end of stage 3, USB3 was intruded by a feldspar-pyroxene-phyric mafic sill/dyke in the Sock Creek South area (Figure 4.7 - SB-North; DDH SCS-5; 379.4 to 402.7 m). The presence of monomictic mud-matrix mafic breccia facies (interpreted as peperite - section 3.3.3.10) at the top contact indicates that USB3 was unlithified when intruded.

Stage 4: Intrabasinal rhyolitic to basaltic effusive volcanism

Stage 4 encompasses the emplacement of USB4 (USB4a and USB4b; correlated with equivalents of the Que-Hellyer Volcanics - section 4.3.5.4) in the SB area (Figures 4.7 and 4.8). The facies comprising USB4a (Figure 4.7 - USB-N4a, USB-C4 and USB-S3) are presented in Table 4.4. During stage 4, partly extrusive feldspar-phyric rhyolitic to dacitic cryptodomes, andesitic lavas and domes, and minor basaltic facies were emplaced on the seafloor in the Sock Creek-Burns Peak area (Figures 4.7 and 4.8).

In the SB-North area, major felsic effusive volcanic activity occurred associated with the emplacement of USB-N4a (correlated with the Sock Creek Dacites - section 4.3.5.4; Table 4.1; Figures 4.7 and 4.8). USB-N4a is dominated by massive to flow-banded, amygdaloidal and/or perlitic feldspar-phyric rhyolite and dacite, and monomictic rhyolite and dacite breccia with local monomictic mud-matrix rhyolite and dacite breccia facies (Table 4.1). The emplacement of USB-N4a began with the intrusion of rhyolitic and dacitic cryptodomes into USB-N3 (polymictic micaceous sandstone and micaceous mudstone facies - Table 4.1; Figure 4.7) which eventually breached through the sea-floor surface and emerged as extrusive dome complexes and lava flows (up to approximately 200 m thick) at probably multiple vents. The occurrence of monomictic mud-matrix rhyolite and dacite breccia facies (interpreted as peperite - sections 3.3.1.9 and 3.3.2.7) at the tops of single coherent rhyolite and dacite units lower in the stratigraphy (Figures 4.7 and 4.8) support an early intrusive phase for USB-N6. This relationship is evident in DDH BHD-4, BHD-7 and BHD-8 (Figure 4.7 - Sock Creek area). The later extrusive phase is dominated by monomictic rhyolite and dacite breccia facies (sections 3.3.1 and 3.3.2), and represented by the upper feldspar-phyric dacite (section 3.3.2.1) units in the Sock Creek area (Figure 4.7 - SB-North) and polymictic felsic breccia and minor sandstone facies (section 3.3.4) in the Sock Creek South area (Figure 4.7 - SB-North).

In the SB-Central area, the emplacement of USB-C4 (Table 4.2; Figures 4.7 and 4.8) began with the deposition of polymictic felsic breccia and sandstone facies (sections 3.3.4.3 and 3.3.4.5) that were probably resedimented from local sources. Extrusion of rhyolitic to dacitic lavas and/or domes followed. The rhyolite and dacite lavas and/or domes were the source of monomictic rhyolite and dacite breccia and polymictic felsic breccia and sandstone (Figures 4.7 and 4.8).

In the SB-South area, dome complexes and lava flows were erupted associated with the emplacement of USB-S3 (correlated with the Boco Road Dacite, at Boco Road, and the Hollway Andesite, SW of Burns Peak - section 4.3.5.4; Table 4.3; Figures 4.7 and 4.8). Coherent feldspar-phyric dacite and minor monomictic dacite breccia facies (USB-S3; Table 4.3) were erupted at Boco Road (Boco Road Dacite).

Massive to amygdaloidal and vesicular andesite and basalt, and monomictic mafic breccia facies (USB-S3; Table 4.3) were erupted SE and S of Burns Peak (Hollway Andesite), and monomictic fluidal-clast mafic breccia facies was produced by local lava fountains. Eruption of the Boco Road Dacite and Hollway Andesite was contemporaneous, because they have an interfingering relationship between Boco Road and the Hollway area (McNeill, 2002b; McIntyre, 2006).

Stage 5: Partly explosive eruption-fed density currents and deposition of black mudstone

In the beginning of stage 5, normally graded, volcanic quartz-bearing, polymictic volcanic breccia and sandstone facies (Table 4.4 - USB-N4b; Figures 4.7 and 4.8 - USB-N4b) were emplaced exclusively in the SB-North area above USB-N4a (Table 4.1; Figure 4.7 - SB-North). USB-N4b derived from partly explosive eruption-fed density currents because the deposits contain locally abundant shards. USB-N4b also incorporates felsic fragments most likely derived from USB-N4a (Table 4.4; Figures 4.7 and 4.8). Mafic fragments are also present but the mafic source has not been identified. Fine-grained lithic clasts may be basement-derived. USB-N4b is thickest (50 m) in DDH BHD-8 (Figure 4.7 - Sock Creek area) and appears to thin out towards the SW (USB-N4b is only 11 m thick in DDH SCS-5; Figure 4.7), which suggests that the source of the density currents was roughly located to the NE of DDH BHD-8 (Figure 4.1 - Sock Creek area).

During stage 5, black mudstone of USB5 (USB-N5 and USB-S4; interpreted to be correlates of the Que River Shale - section 4.3.5.5) was deposited in the SB-North and SB-South areas, and probably in the SB-Central area (Figures 4.7 and 4.8). The black mudstone was deposited in a relatively deep (below-wave-base) submarine environment with quiet, reducing conditions.

Stage 6: Partly extrusive rhyolite cryptodomes

Stage 6 involves the emplacement of USB6 (USB-N6 and USB-S5) in the SB-North and SB-South area (Table 4.4; Figures 4.7 and 4.8), interpreted as two partly extrusive feldspar-quartz-phyric rhyolite cryptodomes possibly related to quartz-feldspar rhyolite porphyries identified by Corbett and Komyshan (1989), McNeill (2002a, 2002b) and Corbett (2005a) (section 4.3.5.4). USB6 comprises coherent quartz-rich rhyolite sub-facies, monomictic rhyolite breccia and monomictic mud-matrix rhyolite breccia facies (Table 4.4; Figures 4.7 and 4.8). The partly extrusive rhyolite cryptodomes were emplaced into and onto black mudstone (Figures 4.7 and 4.8 - USB5); they contain peperite (monomictic mud-matrix rhyolite breccia facies; section 3.3.1.9), which indicates that the black mudstone (Figures 4.7 and 4.8 - USB5) was still unconsolidated when intruded. Extrusion of feldspar-quartz-phyric rhyolite occurred in the Sock Creek and Burns Peak areas (Figures 4.7 and 4.8 - SB-North and SB-South; DDH BHD-4 and BPD-80) because the overlying polymictic rhyolite breccia facies (Figures 4.7 and 4.8 - USB7a and USB7b) contains rhyolite clasts that are very similar to the underlying feldspar-quartz-phyric rhyolite (Figures 4.7 - USB6). Whole-rock compositional data from two samples of the rhyolite in the Burns Peak area, one from DDH BPD-80

(377.4 m) and one from DDH BPD-89 (85.5 m) (Figure 3.1; Table 3.2) indicate that they match suite I (calc-alkaline) of Crawford et al. (1992), and suggest they could be related.

Stage 7: Syn- to post-eruptive density currents and suspension sedimentation

Stage 7 matches the emplacement of USB7 (USB7a, USB7b and USB7c; interpreted to be correlates of the lower part of the Southwell Subgroup - section 4.3.5.7) in the Sock Creek, Boco Road and Burns Peak areas (Figures 4.7 and 4.8 - SB-North and SB-South; DDH BHD-4 and BPD-80, and Boco Road). USB7a and USB7b comprise dominantly thick (>90 m), normally graded, volcanic quartz-bearing, polymictic rhyolite breccia and sandstone units with mudstone tops (Table 4.4). These units were derived from explosive eruption-fed density currents because the deposits contain locally abundant shards. The density currents were most likely generated by intrabasinal rhyolitic explosive eruptions because USB7a and USB7b lack basement-derived fragments. These units were at least partly sourced from the two partly extrusive feldspar-quartz-phyric rhyolite cryptodomes (USB6a and USB6b) considered in the previous stage because both are volcanic quartz-bearing and comprise very similar rhyolite clasts, and USB7a and USB7b are directly underlain by USB6a and USB6b, respectively. Suspension sedimentation produced mudstone intervals.

4.4.3 Post-volcanic intrusions

Several post-volcanic mafic to felsic intrusions have been identified in the Sock Creek-Burns Peak area in this study (Figures 4.7 and 4.8). Post-volcanic mafic intrusions include dominantly coherent feldspar-pyroxene-phyric, feldspar-phyric and aphyric mafic facies (section 3.3.3). Post-volcanic felsic intrusions comprise coherent feldspar-quartz-phyric rhyolite and feldspar-phyric dacite, and associated monomictic rhyolite and dacite breccia facies (sections 3.3.1 and 3.3.2). Intrusions occur practically everywhere from Sock Creek in the NE to Burns Peak in the SW and at all stratigraphic levels (Figures 4.7 and 4.8). The following post-volcanic intrusions identified in the Sock Creek-Burns Peak area are considered from lowest to highest stratigraphic position of the successions they intrude into.

Mafic intrusions in USB1a (correlate of the upper Central Volcanic Complex)

Abundant mafic dykes (coherent feldspar-phyric to aphyric mafic facies, and minor monomictic mafic breccia facies - section 3.3.3) are intercalated at various levels within the rhyolitic to dacitic succession comprising USB1a (Table 4.4; correlated with the upper Central Volcanic Complex - section 4.3.5.1) from Bulgobac Hill to Burns Peak in the SB-Central and SB-South areas (Figures 4.7 and 4.8). Most of these mafic dykes are relatively thin (< 7 m thick) relative to the enclosing felsic succession, which can be up to hundreds of meters thick (e.g., DDH AK-1 at Bulgobac Hill; Figure 4.7).

The P_2O_5/TiO_2 and Ti/Zr values from analysis of two basalt dyke samples (Figure 3.1; Table 3.2; DDH AK-1, 304.7 m; DDH BBP-209, 102.8 m) indicate that these basalts fall into suite V of Crawford et al. (1992), but the TiO_2 values are consistent with suite IV.

Dacite intrusion in USB2 (correlate of the Black Harry Beds)

The coherent feldspar-phyric dacite and monomictic dacite breccia facies in DDH BOC-2 (603.5 to 617.4 m; Figure 4.7) intrudes polymictic felsic breccia and sandstone facies of USB2 (correlated with the Black Harry Beds - section 4.3.5.2) (Figures 4.7 and 4.8). The absence of peperitic margins suggests that either USB2 was lithified when intruded, or that USB2 was unlithified but peperite did not develop at the location where intersected DDH BOC-2.

The P_2O_5/TiO_2 and TiO_2 values from analysis of a feldspar-phyric dacite sample in DDH BOC-2 (612.5 m; Figure 3.1; Table 3.2) indicates an affinity with the calc-alkaline suite I of Crawford et al. (1992), but the Ti/Zr value is consistent with both suites I and II. Since suite II rocks are only known to occur S of the Henty Fault (Crawford et al., 1992), the dacite sampled from DDH BOC-2 is considered in this study to belong to suite I of Crawford et al. (1992).

Intrusions in USB4a (correlate of the Que-Hellyer Volcanics)

In DDH BOC-2 (Figures 4.7 and 4.8 - SB-Central), massive feldspar-phyric rhyolite (158.9 to 177.9 m) has a mingled upper contact with black mudstone. One sample of the rhyolite from DDH BOC-2 (160.9 m; Figure 3.1; Table 3.2) falls in the calc-alkaline suite I field of Crawford et al. (1992).

In the Sock Creek South area (Figures 4.7 and 4.8 - SB-North), intervals of coherent feldspar-pyroxene-phyric basalt facies occurring in DDH SCS-2, SCS-3, SCS-4 and SCS-5 have been interpreted to represent a sill based on the sharp or mingled upper contacts, their tabular and conformable nature, and the absence of associated autoclastic facies (section 4.3.2.8). The basalt sill can be correlated for approximately 1.5 km in adjacent DDH. The basalt intrudes USB-N4a (dacite units correlated with the Que-Hellyer Volcanics - section 4.3) and the contact between USB-N4a and USB-N4b (polymictic volcanic breccia and sandstone facies - sections 3.3.4.1 and 3.3.4.2; correlated with the mixed sequence of the Que-Hellyer Volcanics) (Figure 4.7).

Geochemical analyses of two samples of basalt from DDH SCS-5 (96.3 m, 152.0 m; Figure 3.1; Table 3.2) indicate that they match both suites III (calc-alkaline and shoshonitic) and IV (tholeiitic) of Crawford et al. (1992). The shallower sample is characteristic of the Sock Creek basalts (Crawford et al, 1992), which are petrographically identical to but compositionally distinct from the Hellyer Basalt (Crawford et al, 1992).

4.5 Summary

Seven regional stratigraphic units (USB) have been identified in the Sock Creek-Burns Peak area (Figure 4.7). Each USB comprises one or more local stratigraphic units identified in the three sub-areas of the Sock Creek-Burns Peak area (SB-North, SB-Central and SB-South), and corresponds to a stratigraphic level, which can be correlated as follows:

1. USB1 comprises dominantly massive to flow-banded rhyolite and dacite and includes three sub-units: USB-N1 (SB-North), USB-C1 (SB-Central), and USB-S1 (SB-South) (Table 4.4; Figure 4.7). These sub-units occur at the same stratigraphic level (USB1), which has been correlated with the Mount Black Formation (CVC, Corbett, 1979, 1981, 1992, 2002a; Corbett and McNeill, 1986; Corbett and Komyshan, 1989; Corbett and Solomon, 1989; McNeill and Corbett, 1989; Gifkins, 2001; Gifkins and Allen, 2001). The CVC lavas and extrusive dome complexes (Chapter 3) correspond to the first stage of the interpreted evolution of the regional facies architecture in the Sock Creek-Burns Peak area (Figure 4.8).
2. USB4 comprises mostly massive to flow-banded feldspar-phyric rhyolite, dacite and mafic facies and monomictic rhyolite, dacite and mafic breccia, and includes three sub-units: USB-N4 (SB-North), USB-C4 (SB-Central), and USB-S3 (SB-South) (Table 4.4; Figure 4.7). These sub-units, although composed of different lithofacies, occur at the same stratigraphic level (USB4), which is interpreted to correlate with the Que-Hellyer Volcanics (Corbett and Komyshan, 1989; Corbett, 1992). Partly extrusive rhyolitic to dacitic cryptodomes and lavas (SB-North and SB-Central), and andesitic to basaltic lavas and domes (SB-South) (Chapter 3) of USB4 correspond to the fifth stage of the interpreted evolution of the regional facies architecture in the Sock Creek-Burns Peak area (Figure 4.8).

3. USB7 includes intercalated mudstone, feldspar-quartz polymictic rhyolite breccia and sandstone and polymictic crystal-rich sandstone of USB-N7 (SB-North) and USB-S6 (SB-South) (Table 4.4; Figure 4.7). These sub-units occur at the same stratigraphic level (USB7), which is interpreted to correlate with the lower Southwell Subgroup (Corbett and Komyshan, 1989; McPhie and Allen, 1992; Corbett, 1992, 2005a, 2005b; Bold 2009). The emplacement of volcanic quartz-bearing, explosive eruption-fed density current deposits (Chapter 3) of the lower Southwell Subgroup corresponds to the seventh stage of the evolution of the regional facies architecture in the Sock Creek-Burns Peak area (Figure 4.8).

4. Correlations of the USB help constrain the stratigraphic position of potentially mineralised units in the Sock Creek-Burns Peak area. This topic is dealt with at length and in more detail in Chapters 5 and 6.

CHAPTER 5

Stratigraphy and correlations in the northern Mount Read Volcanics

5.1 Introduction

Descriptions and interpretations of the facies identified in the Sock Creek-Burns Peak, Mount Charter and White Spur-Howards Road areas were presented in Chapter 3. The stratigraphy, correlations and facies architecture in the Sock Creek-Burns Peak area were presented in Chapter 4. This chapter focuses on the stratigraphy and correlations of the Mount Read Volcanics (MRV) in the Sock Creek-Burns Peak area with the areas to the NE (Hellyer-Mount Charter) and SSW (Rosebery-Howards Road) (Figure 5.1).

This chapter is divided into three parts. The first part (sections 5.2 to 5.4) introduces the geology of the Hellyer-Mount Charter area and discusses potential correlations between the Hellyer-Mount Charter and Sock Creek-Burns Peak areas. The second part (sections 5.5 to 5.7) introduces the geology of the Rosebery-Howards Road area and the stratigraphy of the Rosebery-Hercules host sequences. Correlations between the Sock Creek-Burns Peak, Rosebery-Hercules and White Spur-Howards Road areas are discussed. The third part (section 5.8) summarizes the stratigraphy and regional correlations between all three areas and the implications in terms of mineralisation and paleogeography for the northern MRV.

5.2 Geology of the Hellyer-Mount Charter area

The Hellyer-Mount Charter area is located N of Lake Mackintosh, approximately midway between Mount Block, in the SSW, and Mount Cripps, in the ENE (Figure 5.1). The area is covered by the 1:25 000 Charter geological map sheet (Corbett, 1995). The Hellyer-Mount Charter area is transected by the Murchison Highway to the W, and bounded by the Cradle Mountain Link Road to the N and the Southwell River to the E (Figure 5.1). The Murchison Highway provides main road access to the Hellyer-Mount Charter undulating plateau, which sits at an average elevation of approximately 700 m and falls steeply to the Southwell River and Lake Mackintosh valley in the E. The area is remote and covered by dense rainforest vegetation, but the development of the Hellyer, Que River and Mount Charter mines and related exploration led to the construction of forestry roads and tracks, which significantly improved access and rock exposure (Corbett and Komyshan, 1989; Murphy, 2007).

The Hellyer-Mount Charter area covers an approximately 9 km long, NE-striking section of the northern MRV (Waters, 1995). It is separated from the Sock Creek-Burns Peak area to the SW by the Mount Charter Fault, and is bound to the SE by the northern termination of the NE-striking and NW-dipping Henty Fault (Figure 5.1) (Corbett and McNeill, 1986; Komyshan, 1986).

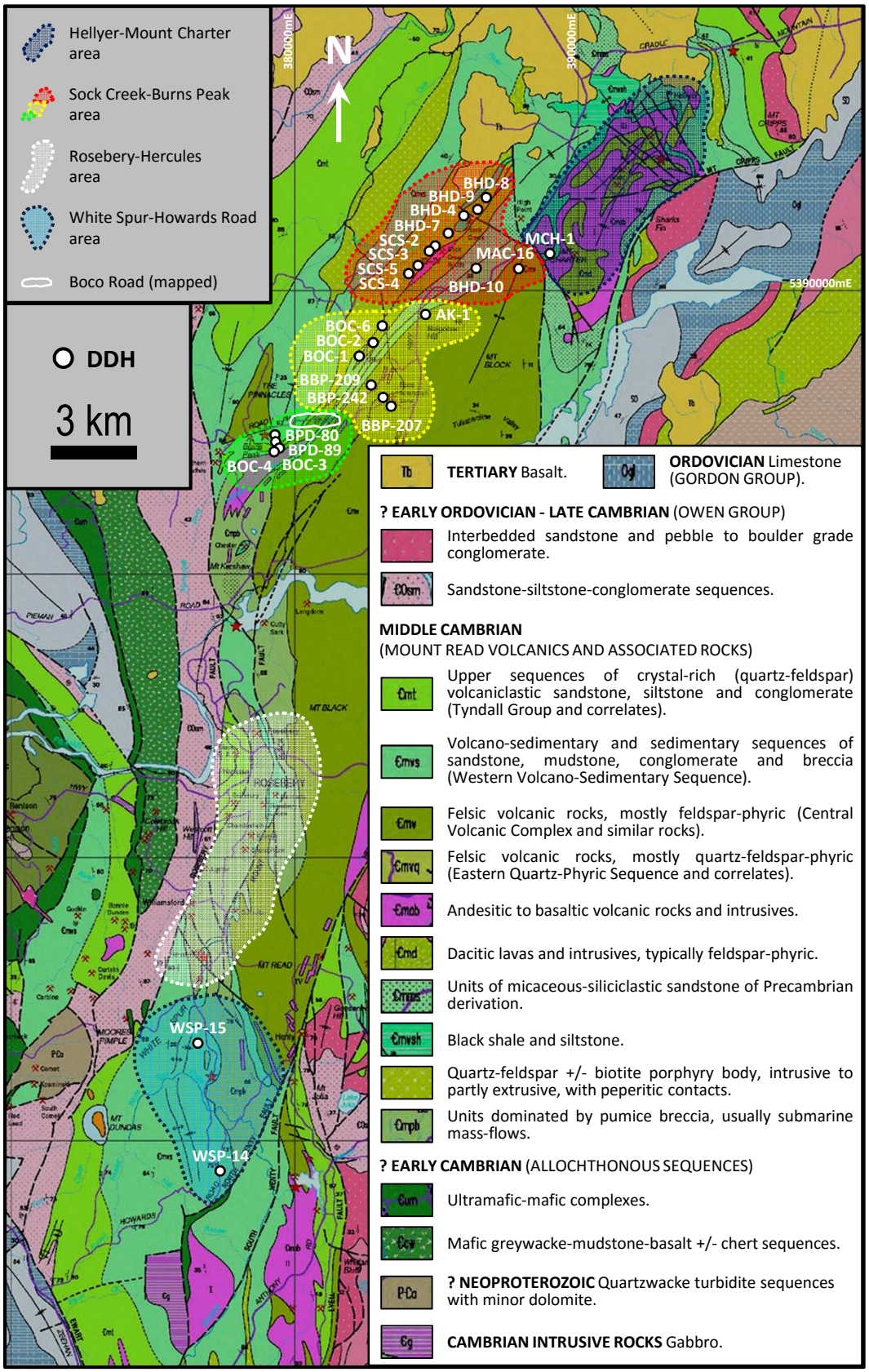

Figure 5.1: Bedrock geological map of the northern Mount Read Volcanics, showing the areas with the location of the diamond drill holes (DDH) and mapped Boco Road section in this study, after Corbett (2002a).

The Hellyer, Fossey, Que River and Mount Charter VHMS deposits (Chapter 2) occur over a strike length of 6 km in the Hellyer-Mount Charter area (Figure 5.1), and are hosted by the mixed sequence of the Que-Hellyer Volcanics (QHV), which is part of the Mount Charter Group (Corbett, 1992; Waters and Wallace; 1992; Corbett et al., 2014). The mixed sequence consists of dominantly dacitic domes and lavas, andesitic to basaltic lavas, monomictic dacitic to basaltic breccia, polymictic breccia and sandstone, and minor mudstone (Corbett and Komyshan, 1989; Waters and Wallace; 1992; Waters, 1995). The QHV (next section) conformably overlies the Animal Creek Greywacke (section 4.2.3.2) and is conformably overlain by the Que River Shale (section 4.2.3.4), which in turn is conformably and gradationally overlain by the Southwell Subgroup (section 4.2.3.6) (Corbett and Komyshan, 1989). The age of the Hellyer and Que River VHMS deposits is enclosed between the 500.4 ± 0.9 Ma age for an andesite breccia sample from approximately 100 m below the mixed sequence, and the 499.3 ± 0.9 Ma age of a rhyolite sill intruding the Que River Shale and Southwell Subgroup (Mortensen et al., 2015). The stratigraphy of the QHV is presented in detail in the following section. A small Zn prospect occurs at High Point NW of Mount Charter, between the Mount Charter Fault and the Murchison Highway (Purvis, 1993).

A few Cambrian dykes and sub-concordant bodies of fine-grained spherulitic quartz porphyry intrude the volcano-sedimentary succession in the vicinity of the Hellyer and Que River mines. Post-Cambrian rocks in the area include siliciclastic conglomerate and sandstone of the Owen Conglomerate (Late Cambrian to Early Ordovician), the Gordon Group Limestone (Ordovician) and sandstone and siltstone of the Eldon Group (Silurian to Devonian). The Mount Charter Dolerite (Devonian) intrudes the Que River Shale between Mount Charter and the Murchison Highway (Corbett and Komyshan, 1989). Tertiary basalt covers large areas to the N, NW and W of the Hellyer-Que River area, and NE of Mount Cripps. Abundant patches of Quaternary glacial and fluvioglacial deposits blanket much of the Paleozoic geology in the Hellyer-Mount Charter area (Corbett and Komyshan, 1989).

5.3 Stratigraphy of the Que-Hellyer Volcanics

The QHV were first described by Corbett and Komyshan (1989) using the complete intersection in diamond drill hole (DDH) MCH-1 (Corbett and Komyshan, 1989; this thesis) (Figure 5.2). The QHV are a submarine sequence of calc-alkaline, dominantly intermediate to mafic and minor felsic coherent and volcaniclastic rocks within the Mount Charter Group (Corbett and Komyshan, 1989; Corbett, 1992; Waters and Wallace, 1992; Waters, 1995; McNeill, 1999) lying conformably between the micaceous Animal Creek Greywacke below and the carbonaceous, fossiliferous Que River Shale above (Gee et al., 1970; Corbett and Komyshan, 1989; Corbett, 1992). The QHV are exposed in the Hellyer-Mount Charter area and host the Hellyer and Que River high-grade polymetallic volcanic-hosted massive sulfide (VHMS) deposits, the massive barite and high-grade base metal sulfide (BMS) deposits at Fossey, and the Mount Charter Au-Ag-(Zn)-(Ba) deposit.

The QHV extend 10 km NE of the Hellyer mine in the Black Marsh syncline (Pemberton et al., 1991). To

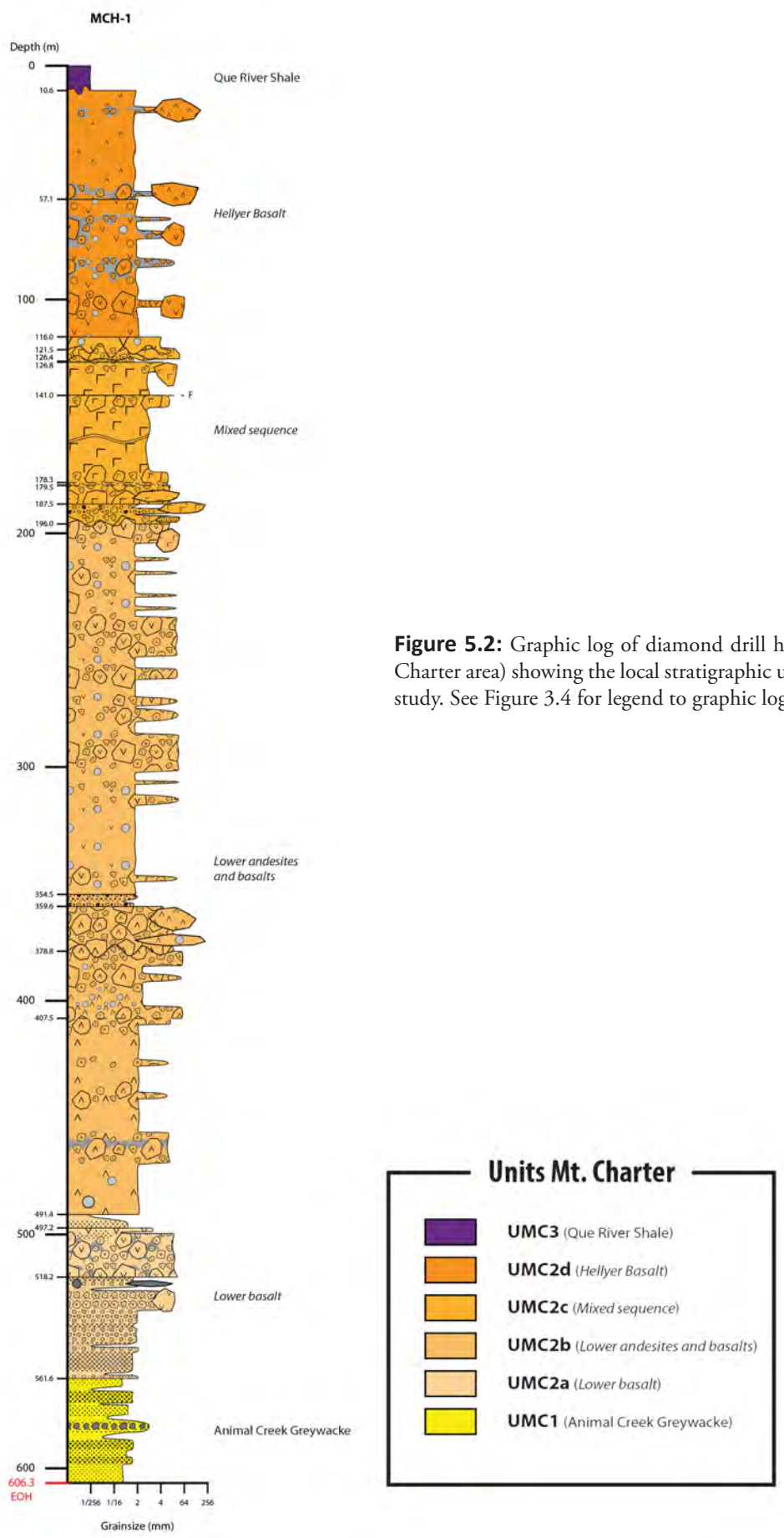

Figure 5.2: Graphic log of diamond drill hole MCH-1 (Mount Charter area) showing the local stratigraphic units identified in this study. See Figure 3.4 for legend to graphic logs.

the SW of the Mount Charter Fault, stratigraphic equivalents of the QHV occur from Sock Creek to Burns Peak and include the Sock Creek Dacites, Boco Road Dacite and Hollway Andesite (section 4.2) (Corbett and McNeill, 1986; Corbett and Komyshan, 1989; Wilde and Kerr, 1989; Crawford et al., 1992; McNeill, 2002a, 2002b, Corbett, 2005a, 2005b; McIntyre, 2006; this thesis), and tholeiitic basalts (Sock Creek basalts) with a different geochemical signature to the QHV (Crawford et al., 1992). In the Que River mine area, the QHV have a maximum thickness of about 1 km, but the unit thins dramatically to the W, SW and NW (Pemberton et al., 1991). To the W of Mount Charter, the QHV are approximately 480 m thick (DDH MCH-1; Corbett and Komyshan, 1989) (Figure 5.2).

The QHV have been informally subdivided into four units (Corbett and Komyshan, 1989; Waters and Wallace, 1992): (1) lower basalt, (2) lower andesites and basalts, (3) mixed sequence, and (4) Hellyer Basalt, which are described in detail below.

5.3.1 Lower basalt

The lower basalt is the oldest unit of the QHV and corresponds to the "lower tuff and lavas" of Corbett and Komyshan (1989) and Corbett (1992). It consists of massive to locally pillowed and amygdaloidal basalt and monomictic basalt breccia interbedded with volcaniclastic rocks and volcanic sandstone and siltstone (Corbett and Komyshan, 1989; Waters and Wallace, 1992; Corbett et al., 2014). The thickness of this unit is extremely variable and poorly constrained due to the paucity of drilling intersecting the QHV, but the lower basalt appears to be thickest (200-300 m) SE of the Que River VHMS deposit (Corbett and Komyshan, 1989). The lower basalt is poorly exposed and extends only to the SE of Mount Charter where it occupies the core of a large N-plunging syncline. In DDH MCH-1 (Mount Charter) (Figure 5.2), the lower basalt is only about 60 m thick (Corbett and Komyshan, 1989). The lower basalt has a lower conformable, interfingering contact with the Animal Creek Greywacke.

5.3.2 Lower andesites and basalts

The lower andesites and basalts (feldspar-phyric sequence or feldspar-phyric andesite) conformably overlie the lower basalt, and comprise up to 800 m of dominantly coherent, locally amygdaloidal andesite; basaltic to dacitic lavas and monomictic basaltic to dacitic breccia, and minor epiclastic rocks (Corbett and Komyshan, 1989; Waters and Wallace, 1992; Corbett et al., 2014) are also present. The thickness of the lower andesites and basalts is highly variable, reaching about 400-500 m at Que River, but thinning to only a few metres at the western margins of the QHV. In DDH MCH-1 (Mount Charter) (Figure 5.2), this unit is approximately 260 m thick (Corbett and Komyshan, 1989). The lower andesites and basalts represent the footwall to the VHMS deposits in the Hellyer-Mount Charter area (Corbett and Komyshan, 1989; Waters and Wallace, 1992).

5.3.3 Mixed sequence

The mixed sequence or mine sequence conformably overlies the lower andesites and basalts and hosts the Hellyer, Fossey, Que River and Mount Charter deposits (Corbett and Komyshan, 1989; Waters and Wallace, 1992; Corbett et al., 2014). It consists dominantly of coherent dacite, andesitic to basaltic facies, monomictic dacitic to basaltic breccia, and massive to normally graded polymictic volcanic breccia and sandstone comprising locally derived dacitic to basaltic clasts similar to the coherent facies (Corbett and Komyshan, 1989; Waters and Wallace, 1992; Waters, 1995). The thickness of the mixed sequence is highly variable, ranging up to approximately 250 m in the Portal road area, about 2 km NE of the Que River mine (Corbett and Komyshan, 1989). At Hellyer, the mixed sequence is only 10 m thick and comprises polymictic volcanic breccia and sandstone and minor mudstone that partly overly the Hellyer VHMS deposit (Wu, 2014). In DDH MCH-1 (Mount Charter) (Figure 5.2), the mixed sequence is approximately 80 m thick (Corbett and Komyshan, 1989).

The mixed sequence has been subdivided by Waters and Wallace (1992) into two subunits: mixed sequence volcaniclastics and mixed sequence dacites. The mixed sequence volcaniclastics are on the order of 120 m thick and dominantly comprise polymictic basaltic to dacitic volcanic breccia and coarse-grained sandstone with minor laminated mudstone in the vicinity of the ore deposits. The mixed sequence dacites are locally very thick. They show intense hydrothermal alteration and are closely associated with the Fossey, Que River and Mount Charter deposits.

5.3.4 Hellyer Basalt

The Hellyer Basalt or Upper Basalt is the uppermost unit in the QHV and corresponds to the "upper basalts and andesites" of Corbett and Komyshan (1989) and Corbett (1992). It comprises a sequence of massive to pillowed, generally amygdaloidal, pyroxene-phyric basalt, monomictic basalt breccia and peperite, and minor interbedded fine-grained sedimentary units. The Hellyer Basalt conformably overlies or interfingers with the mixed sequence and its thickness ranges up to a maximum of 350 m just NE of the Hellyer VHMS deposit and W of Mount Charter (Waters and Wallace, 1992; Corbett et al., 2014). In DDH MCH-1 (Mount Charter) (Figure 5.2), the Hellyer Basalt is about 90 m thick (Corbett and Komyshan, 1989). The presence of abundant peperite within the Hellyer Basalt provides evidence that it was emplaced as shallow sills into the unconsolidated mud of the Que River Shale (Waters and Wallace, 1992; Tomes, 2011).

5.4 Correlations between the Hellyer-Mount Charter and Sock Creek-Burns Peak areas

5.4.1 Introduction

The geology and stratigraphy of the Hellyer-Mount Charter area were presented in previous sections. In this section, correlations between the Hellyer-Mount Charter and Sock Creek-Burns Peak areas are discussed.

Correlations between the Hellyer-Mount Charter and Sock Creek-Burns Peak areas were produced from the construction of a fence diagram (Figure 5.3) using the stratigraphic data obtained from detailed logging

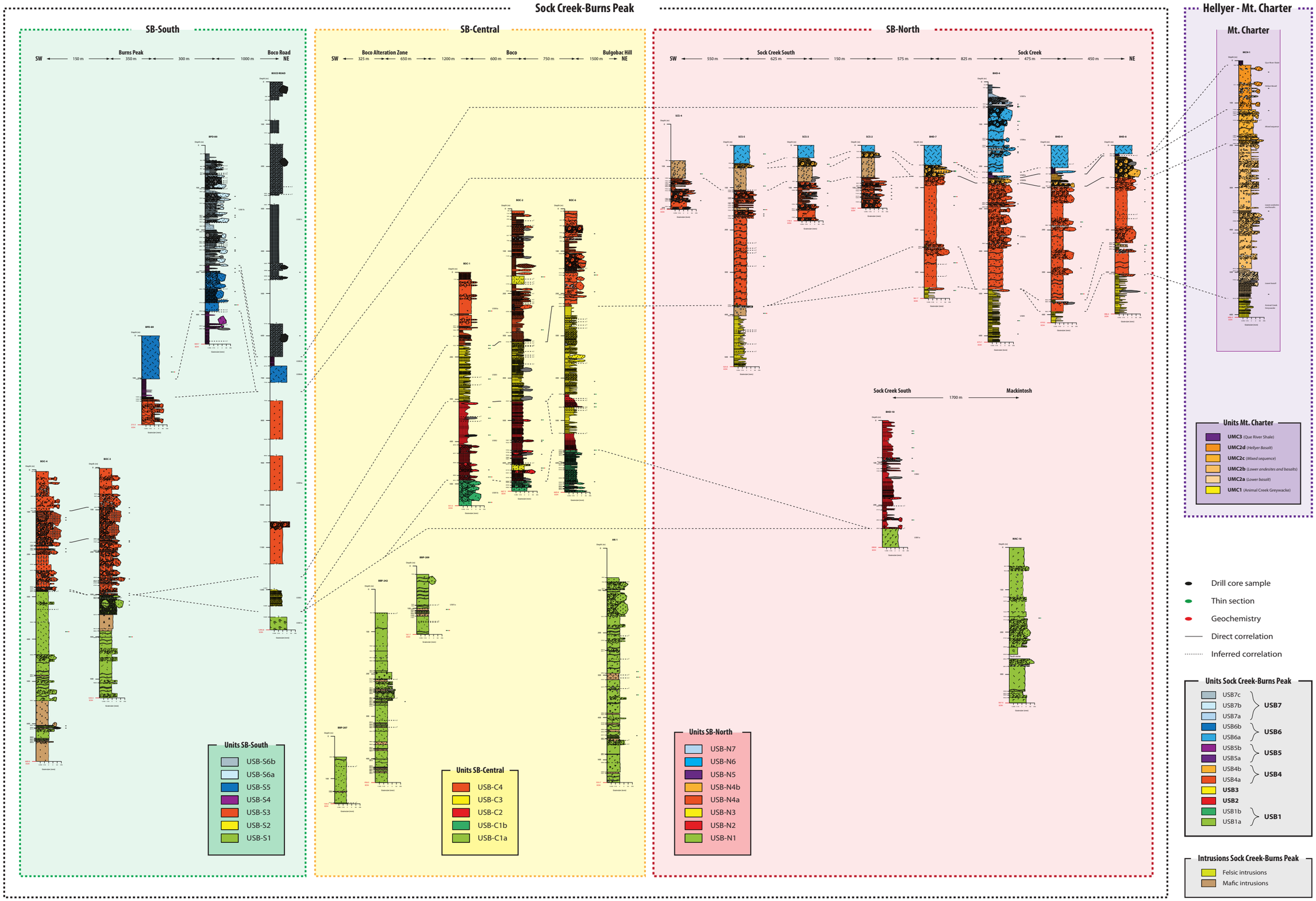

Figure 5.3: Correlation diagram of the regional stratigraphic units (USB) identified in the Sock Creek-Burns Peak area and the local stratigraphic units (UMC) identified in the Mount Charter area. Unit labels are given on the right of the logs of DDH BHD-4 and BHD-10 (SB-North), BBP-209 and BOC-1 (SB-Central), BPD-80 and Boco Road (SB-South), and MCH-1 (Mount Charter). See Figure 3.4 for legend to graphic logs.

of DDH MCH-1 (Figure 5.2), located in the Mount Charter area (Figure 5.1), and the twenty one DDH in the Sock Creek-Burns Peak area (Chapter 4) (appendix A). Correlations were supported by stratigraphic data from the Hellyer-Mount Charter area (Figure 5.1) obtained from Corbett and Komyshan (1989) and Waters and Wallace (1992). Published fossil and absolute ages are also considered in the correlations below.

5.4.2 Correlations between the Mount Charter and Sock Creek-Burns Peak areas

In DDH MCH-1 (Mount Charter area), three local stratigraphic units (UMC; unit, Mount Charter) were identified (Figure 5.2). The facies of each UMC and equivalent formal stratigraphic units are presented in Table 5.1. Correlations between the local stratigraphic units in the Mount Charter (UMC) and Sock Creek-Burns Peak (USB; Chapter 4) areas are presented in Figure 5.3 and discussed below.

5.4.2.1 UMC1 (Animal Creek Greywacke correlate)

UMC1 is at least 44.7 m thick and is represented by polymictic micaceous sandstone and micaceous mudstone facies (Table 5.1). This unit has very similar lithofacies characteristics to, and occurs at the same stratigraphic position as, the Animal Creek Greywacke defined by Corbett and Komyshan (1989). UMC1 is distinctive and simple to correlate with USB-N3 (SB-North area) due to their identical lithofacies characteristics and stratigraphic position (Figure 5.3). USB3 identified in the Sock Creek-Burns Peak area (Chapter 4) includes USB-N3 (SB-North area), USB-C3 (SB-Central area) and USB-S2 (SB-South area).

The distinctive lithofacies characteristics of both UMC1 and USB3 provide an excellent stratigraphic marker from Mount Charter to Boco Road (and possibly further SW to Burns Peak) and help constrain the stratigraphic position and correlation of adjacent, laterally equivalent stratigraphic units (most significantly UMC2 and USB4) from Sock Creek-Burns Peak to Mount Charter.

5.4.2.2 UMC2 (Que-Hellyer Volcanics correlate)

UMC2 was intersected in DDH MCH-1 from 10.6 to 561.6 m depth (551 m thick) and includes twelve facies (Table 5.1; coherent feldspar-phyric dacite and mafic facies, coherent aphyric mafic facies, monomictic dacite and mafic breccia and sandstone, monomictic mud-matrix mafic breccia, polymictic volcanic breccia and sandstone, polymictic mafic sandstone and micaceous sandstone facies). UMC2 corresponds to the QHV defined by Corbett and Komyshan (1989). UMC2 can be sub-divided into four sub-units: UMC2a, UMC2b, UMC2c and UMC2d, each of which corresponds to one of the four components of the QHV (section 5.3) as presented in Table 5.1. Correlation of each of the UMC2 sub-units with one of the four components of the QHV was based on the comparison between the facies, position and thickness of each of the UMC2 sub-units with each of the four components of the QHV identified by Corbett and Komyshan (1989) and described by Waters and Wallace (1992).

UMC2 and USB-N4 (SB-North area; coherent feldspar-phyric rhyolite and dacite, monomictic rhyolite and dacite breccia, monomictic mud-matrix rhyolite and dacite breccia, monomictic fiamme-rich dacite

Table 5.1: Local stratigraphic units, associated facies and equivalent stratigraphic units in DDH MCH-1 (Mount Charter area). See Chapter 3 for details on each facies.

Local stratigraphic units		Facies	Depth interval and thickness (m)	Equivalents (stratigraphic units)
UMC3		Black mudstone (**BMud**) facies	**0-10.6 m** (10.6 m thick)	**Que River Shale**
UMC2	***UMC2d***	Coherent feldspar-phyric mafic (**Mf**) facies, monomictic mafic breccia (**MmB**) and monomictic mud-matrix mafic breccia (**MmmB**) facies	**10.6-116.0 m** (105.4 m thick)	***Hellyer Basalt*** **(QHV)**
	UMC2c	Coherent feldspar-phyric dacite (**Df**) and mafic (**Mf**) facies, monomictic dacite (**DmB**) and mafic (**MmB**) breccia, monomictic dacite sandstone (**DmS**), polymictic volcanic breccia (**PvB**) and sandstone (**PvS**) facies	**116.0-196.0 m** (80.0 m thick)	***Mixed sequence*** **(QHV)**
	UMC2b	Coherent feldspar-phyric (**Mf**) and aphyric (**Ma**) mafic facies, monomictic mafic breccia (**MmB**), monomictic mud-matrix mafic breccia (**MmmB**), polymictic mafic sandstone (**MpS**) and micaceous mudstone (**Mmud**) facies	**196.0-491.4 m** (295.4 m thick)	***Lower andesites and basalts*** **(QHV)**
	UMC2a	Coherent feldspar-phyric mafic (**Mf**) facies, monomictic mafic breccia (**MmB**) and sandstone (**MmS**), monomictic mud-matrix mafic breccia (**MmmB**), polymictic mafic sandstone (**MpS**) and micaceous mudstone (**Mmud**) facies	**491.4-561.6 m** (70.2 m thick)	***Lower Basalt*** **(QHV)**
UMC1		Polymictic micaceous sandstone (**PmS**) and micaceous mudstone (**MMud**) facies	**561.6-606.3 m** (44.7 m thick)	**Animal Creek Greywacke**

breccia, polymictic volcanic breccia and sandstone, polymictic mud-matrix felsic breccia, polymictic felsic breccia and sandstone, black and micaceous mudstone facies; Table 4.1) are interpreted to occur at the same stratigraphic level even though the compositions and proportions of the facies present in each unit are different. The correlation of the upper and lower contacts of UMC2 and USB-N4 is inferred from Mount Charter to the SB-North area (Figure 5.3) because these units occur at the same stratigraphic position but approximately 1.5 km apart. UMC2 and USB-N4 occur below black mudstone facies of, respectively, UMC3 (Que River Shale) and USB-N5 (interpreted to occur at the same stratigraphic level; next section), and above polymictic micaceous sandstone and micaceous mudstone facies of, respectively, UMC1 (Animal Creek Greywacke) and USB-N3, which are interpreted to occur at the same stratigraphic level (previous section) (Figure 5.3). This correlation of units above and below suggests that UMC2 and USB4 occur at the same stratigraphic level (Figure 5.3). Furthermore, USB4 identified in the Sock Creek-Burns Peak area (Figure 5.3) includes USB-N4 (SB-North area), USB-C4 (SB-Central area), and USB-S3 (SB-South area), which have been interpreted to occur at the same stratigraphic level (Chapter 4).

The dominantly intermediate to mafic succession (with only one relatively minor felsic interval from 121.5 m to 196.0 m depth) within UMC2 differs from the exclusively felsic successions observed in USB-N4 (SB-North area) and USB-C4 (SB-Central area) (Figure 5.3). However, the intermediate to mafic successions within USB-S3 at Burns Peak (SB-South area) suggest that similarities between USB-S3 and UMC2 may exist. A direct correlation between UMC2 and USB-S3 is difficult due to the distance (>10 km) between the Mount Charter and the Burns Peak areas (Figures 5.1 and 5.3), but these two dominantly intermediate to mafic units appear to be at the same stratigraphic position.

UMC2c (coherent feldspar-phyric dacite and mafic facies, monomictic dacite and mafic breccia, monomictic dacite sandstone, polymictic volcanic breccia and sandstone facies) at Mount Charter and USB4b (polymictic volcanic breccia and sandstone facies; equivalent to USB-N4b) in the SB-North area are interpreted to occur at the same stratigraphic position (Figure 5.3). UMC2c comprises a normally graded interval of polymictic volcanic breccia and sandstone that is similar to the normally graded units of polymictic volcanic breccia and sandstone of USB4b. Furthermore, dacitic and mafic clasts within UMC2c at Mount Charter and USB4b in the SB-North area are also very similar. These features support the correlation of UMC2c and USB4b between Mount Charter and the SB-North area (Figure 5.3), and suggest that USB4b might extend laterally for 4.5 km from Sock Creek South to Mount Charter. However, the distance between DDH MCH-1 at Mount Charter and the DDH in the SB-North area and the lack of whole-rock compositional data mean that the correlation of UMC2c and USB4b is tentative. No correlate of UMC2d (Hellyer Basalt equivalent) has been identified in the Sock Creek-Burns Peak area.

5.4.2.3 UMC3 (Que River Shale correlate)

UMC3 is at least 10.6 m thick and is exclusively represented by the black mudstone facies (Table 5.1). This unit is equivalent to the Que River Shale defined by Corbett and Komyshan (1989) (section 4.2.3.4). Fossil data within the Que River Shale indicate a late Middle Cambrian Floran-Undillan age (E. opimus Zone to P. punctuosus Zone) (Gee et al., 1970; Jago, 1977; Laurie et al., 1995).

The upper contact of UMC3 was not intersected in DDH MCH-1 (Figure 5.2). The correlation between the lower contact of UMC3 and the base of USB-N5 (SB-North area; black mudstone facies; Table 4.1) is inferred (Figure 5.3) because UMC3 and USB-N5 have similar lithofacies characteristics and stratigraphic position but they occur at approximately 1.5 km apart, and the absence of fossil and absolute age data in USB-N5 prevents a firm correlation between these two black mudstone intervals. If the correlation is correct, this black mudstone unit extends for at least 2.5 km from Sock Creek to Mount Charter.

UMC3 (Mount Charter area) and USB5 (Sock Creek-Burns Peak area) occur at the same stratigraphic level (Figure 5.3). USB5 (black mudstone and minor polymictic rhyolite breccia and sandstone facies) identified in the Sock Creek-Burns Peak area (Chapter 4) includes USB-N5 (SB-North area) and USB-S4 (SB-South area) (Figure 5.3; Table 4.4). The correlation between UMC3, USB-N5 and USB-S4 is, however, uncertain due to the distance between these units, the absence of black mudstone facies intersected by DDH in the SB-Central area (Figure 5.3), and the lack of fossil and absolute age data in USB-N5 and USB-S4. However, if this correlation is correct, the black mudstone comprising UMC3 and USB5 extends laterally for at least 15 km from Mount Charter to Burns Peak.

5.4.3 Implications in the Hellyer-Mount Charter and Sock Creek-Burns Peak areas

The stratigraphy of the QHV, which host the VHMS deposits in the Hellyer-Mount Charter area (section 5.3) is well represented in DDH MCH-1 at Mount Charter (Figure 5.2). The dominantly intermediate to mafic and minor felsic coherent and volcaniclastic facies of the QHV are underlain by the micaceous Animal Creek Greywacke and overlain by the black, pyritic, fossiliferous, carbonaceous Que River Shale (Gee et al., 1970; Corbett and Komyshan, 1989).

Considering that DDH MCH-1 is representative of the stratigraphy in the Hellyer-Mount Charter area, correlations between DDH MCH-1 (Mount Charter) and the DDH in the Sock Creek-Burns Peak area can be extended to the Hellyer-Que River area with the following major stratigraphic implications:

1. UMC1 identified in DDH MCH-1 can be correlated with the Animal Creek Greywacke defined by Corbett and Komyshan (1989). UMC1 can be traced from Mount Charter to Boco Road (and possibly as far as Burns Peak), providing an excellent stratigraphic marker between the Hellyer-Mount Charter and Sock Creek-Burns Peak areas.

2. UMC2 identified in DDH MCH-1 (Mount Charter area) is equivalent to the QHV identified by Corbett and Komyshan (1989). UMC2 can be correlated with USB4 (dominantly dacitic to rhyolitic and intermediate to mafic coherent and volcaniclastic facies) in the Sock Creek-Burns Peak area because these units occur at the same stratigraphic position, indicating that USB4 is a correlate of the QHV. USB4 includes the Sock Creek Dacites in the Sock Creek-Sock Creek South area, the Boco Road Dacite at Boco Road, and the Hollway Andesite S of Burns Peak (Chapter 4).

3. At the top of USB4 in the Sock Creek-Burns Peak North area, USB4b (polymictic volcanic breccia and sandstone facies - section 3.3.4) has been tentatively correlated with UMC2c (dominantly

coherent dacitic to mafic facies, monomictic dacitic to mafic breccia and polymictic volcanic breccia and sandstone facies - section 3.3) in the Mount Charter area, which is equivalent to the VHMS-hosting mixed sequence of the QHV in the Hellyer-Mount Charter area (Corbett and Komyshan, 1989). These units comprise normally graded intervals of polymictic volcanic breccia and sandstone that include very similar dacitic and mafic clasts, suggesting that the polymictic volcanic breccia and sandstone facies of USB4b are equivalents of the facies that host the VHMS deposits in the Hellyer-Mount Charter area.

4. UMC3 (black mudstone facies - section 3.3.5) identified in DDH MCH-1 (Mount Charter area) can be correlated with the Que River Shale identified by Corbett and Komyshan (1989). This unit is potentially correlated with similar black mudstone facies of USB5 in the Sock Creek (USB-N5) and Burns Peak (USB-S4) areas (SW of Mount Charter). If correct, black mudstone facies of UMC3 and USB5 may extend laterally for at least 15 km from Mount Charter in the NE to Burns Peak in the SW.

5. Potentially prospective, laterally equivalent stratigraphic units in the Hellyer-Mount Charter and Sock Creek-Burns Peak areas, are USB4, a correlate of the QHV in the Sock Creek-Burns Peak area, and USB4b, a correlate of the VHMS-hosting mixed sequence of the QHV in the Sock Creek-Sock Creek South area.

5.5 Geology and stratigraphy of the Rosebery-Howards Road area

The Rosebery-Howards Road area is an approximately 15-km-long, N- to NE-striking section of the northern MRV, covered by the 1:25 000 Rosebery, Dundas and Oceana geological map sheets (Seymour and McClenaghan, 2003; McClenaghan, 2003). The Rosebery-Howards Road area is located SSW of Lake Rosebery, extending from W of Mount Black southwards to Howards Road, immediately N of the Henty Fault wedge (Figure 5.1). The Rosebery-Howards Road area is transected by the Murchison Highway to the N, and is surrounded by Mount Black, NE of Rosebery, Mount Read, E of Hercules, and Mount Dundas, SW of White Spur (Figure 5.1).

The area is mountainous and heavily forested. Road access is mainly via the Murchison Highway, Williamsford Road, Howards Road and a network of forestry and logging tracks extending from W of Mount Black to the western slope of Mount Read (Briggs and McNeill, 2001; Vicary, 1998). A Hydro Electric Commission road that follows the Hall Rivulet canal provides access to the southernmost part of the area. The Stitt River bisects the Rosebery-Hercules area S of Rosebery, flowing from N of Mount Read to Lake Pieman, W of Rosebery. Tributaries of the Ring River occur in the Williamsford and Hercules area, N and W of Mount Hamilton. The White Spur Creek and Hall Rivulet cross cut the White Spur-Howards Road area, E of Mount Dundas (Corbett, 2002a).

Rosebery-Hercules area

The Rosebery-Hercules area encompasses a structurally complex, approximately 10-km-long, NNE-striking section of the northern MRV (Corbett and Lees, 1987; Berry and Keele, 1997; Gifkins, 2001). It includes two major E-dipping (approximately 45º) faults: the Rosebery Fault to the W and the Mount Black Fault to the E (Corbett et al., 2014). The Rosebery Fault extends for more than 35 km, from NW of Mount Dundas to NE of Silver Falls. It passes through the White Spur Formation (WSF) between Williamsford and Moores Pimple, W and SW or Hercules, following the contact between the northern Central Volcanic Complex (CVC) and the Dundas Group (WSF) between Hercules and Rosebery (Corbett and Lees, 1987). A "window" of WSF is exposed beneath the Rosebery Fault immediately W of Rosebery (Corbett and Lees, 1987), and units correlated with the WSF have been mapped from S of Lake Bull to the western margin of Lake Rosebery (Gifkins, 2001). To the NNW of Rosebery, the Rosebery Fault intersects the Dundas Group W and NW of the Pinnacles-Burns Peak area (Corbett and McNeill, 1986). The Mount Black Fault has a strike length of at least 10 km and has been mapped from SE of Hercules to Bastyan Dam (Corbett and McNeill, 1986). The Rosebery and Mount Black faults are sub-parallel and bound an approximately 1 to 1.5 km-wide and N- to NNE-trending structural corridor that hosts the Rosebery and Hercules VHMS deposits.

The Rosebery, Hercules and South Hercules VHMS deposits (Chapter 2) occur at the same stratigraphic level and are hosted by the upper part of the northern CVC (Corbett and Lees, 1987; Gifkins, 2001). In the Rosebery-Hercules area, the northern CVC is bound to the W by the Rosebery Fault and to the E and S by the Henty Fault. The northern CVC has been subdivided from base to top into four formations (Chapter 2): 1) Sterling Valley Volcanics, 2) Mount Black Formation, 3) Kershaw Pumice Formation, and 4) Hercules Pumice Formation (Gifkins, 2001; Gifkins and Allen, 2001). The Mount Black Formation is gradationally and conformably underlain by the Sterling Valley Volcanics on the Murchison Highway E of Rosebery and is conformably overlain by the Kershaw Pumice Formation between Mount Read and Dallwitz. The Kershaw Pumice Formation is laterally equivalent to the Hercules Pumice Formation (Gifkins, 2001). The upper member (Host-rock Member) of the Hercules Pumice Formation is the host to the Rosebery and Hercules VHMS deposits (Gifkins, 2001; Gifkins and Allen, 2001), and consists of stratified, thinly bedded, felsic, crystal-pumice-lithic sandstone and siltstone (Large et al., 2001a). The stratigraphy of the Rosebery-Hercules host sequence is described in detail in the following section. A large number of old workings and smaller prospects occur between Rosebery and Hercules, including Grand Centre, Jupiter, Chamberlain, Salisbury and Black P. A. (Green et al., 1981).

White Spur-Howards Road area

The White Spur Howards Road area, S of Hercules, is an approximately 5-km-long, N-striking section of the northern MRV (Corbett and Lees, 1987; Berry and Keele, 1997; Gifkins, 2001). The area comprises the CVC and the WSF (Dundas Group) (Corbett and Lees, 1987; Vicary, 1998). In this area, the CVC consists of extensive feldspar-phyric pumice breccia and rhyolitic and dacitic lavas, sills and cryptodomes (Corbett,

1981, 1992; Corbett and Lees, 1987; Dugdale, 1992; Corbett et al., 2014). At Hercules, the pumice breccia normally grades into stratified, pumiceous, crystal-rich sandstone which is overlain by black mudstone and feldspar-quartz-phyric volcaniclastic units of the WSF (Jago, 2005). The WSF dips and youngs W (Corbett and Lees, 1987; McPhie and Allen, 2003; Jago, 2005). The CVC and WSF extend S to the North Henty Fault.

The contact between the CVC and the WSF is an important marker for exploration of Rosebery-Hercules-like VHMS deposits (Allen, 1998). The contact has been interpreted to be conformable in some areas (Gifkins, 2001), whereas in other areas it is believed to be a folded, low-angle unconformity or disconformity (Gifkins, 2001), a paraconformity (Allen, 1991, 1994a) or an erosional angular unconformity (Corbett, 1984; Lees, 1987; Corbett and Lees, 1987). At Hercules, the contact is complicated by folding of the CVC about an anticline (Corbett, 1992; Dugdale, 1992), but S of White Spur, the contact dips W (Corbett and Lees, 1987; Dugdale, 1992). The contact between the CVC and the WSF is very similar to the contact between the footwall and hangingwall successions of the Rosebery and Hercules VHMS deposits in the Rosebery-Hercules area (Allen, 1998).

5.6 Stratigraphy of the Rosebery-Hercules host sequence

The host sequence to the Rosebery and Hercules VHMS deposits has been described in detail by Brathwaite (1969, 1974), Green et al. (1981), Corbett and Lees (1987), Lees (1987), Corbett and Solomon (1989), Allen (1990b, 1991, 1992b, 1993, 1994a, 1994b), Allen and Cas (1990), Gifkins (2001), and Martin (2004). It is divided into four principal units (Figure 5.4) (Green et al., 1981; Corbett and Lees, 1987; Large et al., 2001a), informally named from base to top: 1) *Footwall Pyroclastics*, comprising feldspar-phyric pumice breccia with minor coherent and brecciated rhyolite and dacite, 2) *Host Rocks*, composed of bedded siltstone, and crystal-rich and tuffaceous sandstone, 3) *black mudstone* (also called "black slate" or "shale"), including grey and black pyritic mudstone and minor crystal-rich and mixed-provenance sandstone, and 4) *Hangingwall Volcaniclastics*, dominated by massive, very thick-bedded, quartz and feldspar crystal-, lithic- and pumice-rich volcanic sandstone and breccia, interbedded with black mudstone. These units are structurally overlain by the Mount Black Formation (Gifkins, 2001; Gifkins and Allen, 2001), which extends from Mount Read to Mount Block between the Mount Black Fault to the W, and the Henty Fault to the E (Gifkins, 2001) (Figure 5.4).

Gifkins (2001) subdivided the Rosebery-Hercules host sequence into the Hercules Pumice Formation (CVC) and the *Hangingwall Volcaniclastics* (Dundas Group; including the black mudstone). The Hercules Pumice Formation was further subdivided into a lower *Footwall Member* (*Footwall Pyroclastics*) and an upper *Host-rock Member* (*Host Rocks*). The northern CVC was originally considered to unconformably underlie the W-younging middle Middle Cambrian WSF at the base of the Dundas Group (Corbett and Lees, 1987). McPhie and Allen (1992) suggested an interfingering relationship between the upper CVC and the WSF. Gifkins (2001) proposed that the *Hangingwall Volcaniclastics* lie at the base of the Dundas Group, suggesting

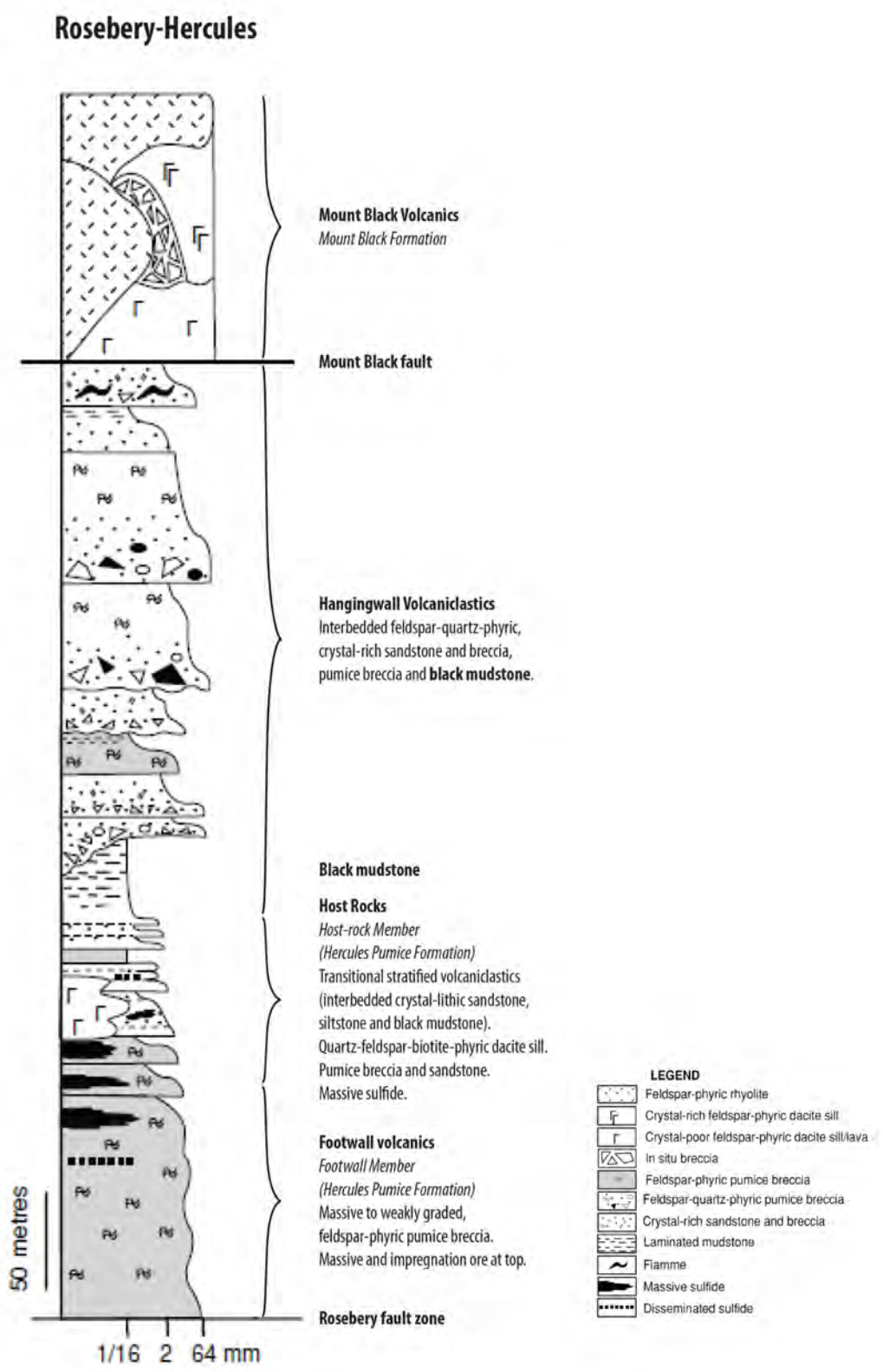

Figure 5.4: Simplified stratigraphic log of the host volcanic succession to the Rosebery-Hercules VHMS deposits (from Allen, 1997 and Large et al., 2001). Total illustrated thickness is approximately 600 m.

a correlation between the *Hangingwall Volcaniclastics* and the WSF after Allen (1994a). For the purposes of this thesis, both nomenclatures of Green et al. (1981) and Gifkins (2001) are considered in the stratigraphy of the host sequence to the Rosebery-Hercules VHMS deposits.

5.6.1 Footwall Pyroclastics (Footwall Member of the Hercules Pumice Formation)

The *Footwall Pyroclastics* correspond to the *Footwall Member* of the Hercules Pumice Formation of Gifkins (2001) and comprise a thick (up to 500 m), massive to weakly graded, poorly stratified succession of feldspar-phyric, rhyolitic to dacitic pumice breccia intercalated with rhyolitic to dacitic sills (Lees, 1987; Allen, 1990b, 1994b). The originally glassy pumice clasts are completely replaced by fine-grained quartz-feldspar-phyllosilicate-carbonate assemblages, but locally well-preserved clast shapes and tube-pumice texture occur. The tops of single pumice breccia beds are fine-grained and stratified (Lees, 1987; Allen, 1991). At the base, sparse lithic clasts occur and include feldspar-phyric, spherulitic and amygdaloidal rhyolite and dacite, basalt and crystal-rich sandstone (Lees, 1987; Allen, 1991). This unit lacks quartz-phyric pumice and quartz crystals and crystal fragments.

The *Footwall Pyroclastics* relic pumice breccias were originally interpreted as both welded and non-welded ignimbrites based on the presence of relic pumice clasts, shards, and flattened fiamme phyllosilicate-rich lenses which define a bedding-parallel foliation (Corbett, 1981; Green et al., 1981). Allen and Cas (1990) attributed the bedding-parallel foliation to diagenetic alteration and compaction of pumice clasts, and interpreted the pumice breccia units to be non-welded. The *Footwall Pyroclastics* were interpreted to comprise the deposits from volcaniclastic density currents and suspension generated by a large, felsic explosive eruption in a submarine, below-wave-base environment (Allen, 1990b, 1991, 1994a; Large et al., 2001a; McPhie and Allen, 2003).

The base of the *Footwall Pyroclastics* is the Rosebery Fault (Corbett and Lees, 1987). In the Rosebery-Hercules area, the *Footwall Pyroclastics* are conformably overlain by the Host Rocks (Host-rock Member) or the *Hangingwall Volcaniclastics* (Lees, 1987; Gifkins, 2001).

5.6.2 Host Rocks (*Host-rock Member* of the Hercules Pumice Formation)

The *Host Rocks* are equivalent to the *Host-rock Member* of the Hercules Pumice Formation of Gifkins (2001) and consist of a 5- to 60-m-thick, discontinuous layer at the top of the *Footwall Pyroclastics (Footwall Member*; Gifkins, 2001) comprising thinly bedded, pumice-crystal-shard-rich and lithic-bearing rhyolitic sandstone and siltstone, pumice breccia and black mudstone (Lees, 1987; Allen, 1994b; Gifkins, 2001). The sandstone and siltstone are composed of relic pumice clasts, relic shards and feldspar and minor quartz crystal fragments; minor pyrite and carbonate, and accessory sphene, rutile, zircon and tourmaline are also present (Eastoe, 1973; Lees, 1987; Allen, 1991).

The contact between the *Host Rocks* (*Host-rock Member*; Gifkins, 2001) and the *Footwall Pyroclastics* (*Footwall Member*; Gifkins, 2001) is gradational and, at Rosebery, is intruded by a quartz-feldspar-phyric rhyolite sill (Allen, 1990b, 1991; Large et al., 2001a; Gifkins, 2001). The *Host Rocks* are interpreted to represent

sedimentation from water-settled suspension or local reworking and redeposition of freshly erupted local pyroclastic debris, and quartz-bearing volcaniclastic turbidity currents derived from distal rhyolitic volcanic centres (Allen, 1990b, 1991, 1994a; Large et al., 2001a). The age of the *Host-rock Member* at Rosebery is inferred to be approximately 500 Ma (Mortensen et al., 2015).

5.6.3 Black mudstone

Lenses of finely laminated, dark grey to black mudstone about 5- to 20-m-thick occur locally above the *Host Rocks* (*Host-rock Member*; Gifkins, 2001). The black mudstone includes thin bands of framboidal pyrite and is interbedded with volcanic quartz-feldspar-bearing siltstone and sandstone containing basement-derived quartzite, phyllite and quartz-mica schist clasts (Green et al., 1981). The black mudstone represents a period of non-volcanic, low-energy sedimentation (Green et al., 1981; Large et al., 2001a). The black mudstone sharply overlies the *Host Rocks* (*Host-rock Member*; Gifkins, 2001) and the *Footwall Pyroclastics* (Green et al., 1981; *Footwall Member*; Gifkins, 2001) and is overlain by the *Hangingwall Volcaniclastics* (Lees, 1987; Allen, 1991).

5.6.4 Hangingwall Volcaniclastics

The *Hangingwall Volcaniclastics* are a 5- to 400-m-thick, volcaniclastic succession comprising pumice breccia, quartz-feldspar-phyric and crystal-rich volcanic breccia and sandstone, and interbedded black mudstone lenses (Brathwaite, 1969; Lees, 1987; Allen, 1990b, 1991; Gifkins, 2001). The volcanic quartz-bearing and pumice-rich breccia units are polymictic and contain abundant quartz- and/or feldspar-phyric rhyolite, spherulitic and amygdaloidal dacite, and pumice clasts, and minor schist, sandstone, siltstone and black mudstone clasts (Lees, 1987). The basal part of the *Hangingwall Volcaniclastics* is black-grey, laminated, pyritic mudstone and graded quartz-feldspar-phyric rhyolite breccia-sandstone with locally abundant black mudstone intraclasts, distinctive, coarse, round quartz and prismatic feldspar crystals, and rare massive sulfide clasts (Lees, 1987; Corbett and Solomon, 1989; Allen, 1991; McPhie and Allen, 1992; Williams, 2009). The *Hangingwall Volcaniclastics* have been subdivided into five 0.1- to 100-m-thick units by Allen, 1991 and six units (including sub-units) by Williams (2009).

The *Hangingwall Volcaniclastics* are the youngest exposed portion of the Rosebery-Hercules host sequence (Gifkins, 2001). The contact between the *Hangingwall Volcaniclastics* and the underlying black mudstone is conformable and locally erosional (Corbett and Solomon, 1989), so that locally the *Hangingwall Volcaniclastics* disconformably overlie the *Footwall Pyroclastics*. In the Hercules-Mount Read area the contact is repeated by a series of E-dipping thrust faults (Gifkins, 2001). The *Hangingwall Volcaniclastics* are interpreted as submarine, below-wave-base, non-welded, pyroclastic turbidity current and suspension deposits comprising medial to distal facies of one or multiple felsic volcanic centre(s) (Allen, 1991, 1994a; McPhie and Allen, 2002, 2003).

Lithological similarities and structural interpretations suggest that the *Hangingwall Volcaniclastics* are equivalent to the WSF at the base of the Dundas Group (Corbett and Lees, 1987; Allen, 1990b, 1994a, 1998; McPhie and Allen, 1992; Gifkins, 2001; Williams, 2009).

5.7 Correlations between the Rosebery-Howards Road and Sock Creek-Burns Peak areas

5.7.1 Introduction

The geology and stratigraphy of the Rosebery-Howards Road area and the stratigraphy of the Rosebery-Hercules host sequences were presented in previous sections. In this section, correlations between the Rosebery-Howards Road and Sock Creek-Burns Peak areas are discussed.

Correlations between the Rosebery-Howards Road and Sock Creek-Burns Peak areas were produced from the construction of a fence diagram (Figure 5.5) using the stratigraphic data and correlations obtained from detailed logging of two representative DDH (Figure 5.6), located in the White Spur and Howards Road areas (Figure 5.1), and the twenty one DDH in the Sock Creek-Burns Peak area (Chapter 4) (appendix A). Stratigraphic data and the correlation of units in the Rosebery-Hercules area were presented by Allen (1990b, 1991, 1992b) and have been elaborated on by Nunn (1995) (Figure 5.4). Published fossil and absolute ages are also considered in the correlations below.

5.7.2 Stratigraphic units and correlations in the White Spur-Howards Road area

In the White Spur-Howards Road area, two regional stratigraphic units (UWH; unit, White Spur; Howards Road) were identified (Figure 5.6). Each UWH corresponds to a stratigraphic level probably extending for at least 5 km from White Spur to Howards Road, and includes one local stratigraphic unit identified only in the White Spur area (UWS; unit, White, Spur) and one local stratigraphic unit identified only in the Howards Road area (UHR; unit, Howards, Road) (Figure 5.6). The facies and lithofacies characteristics of each of the local stratigraphic units (UWS and UHR) occurring in the White Spur and Howards Road areas are presented in Tables 5.2 and 5.3, respectively. The facies of each UWH and correlated formal stratigraphic units are presented in Table 5.4. Correlations of the UWH are presented in Figure 5.6 and discussed below.

5.7.2.1 UWH1 (Central Volcanic Complex correlate)

UWS1 and UHR1 are interpreted to correspond to the same stratigraphic level (UWH1), which includes four facies (Table 5.4; coherent feldspar-quartz-phyric and feldspar-phyric rhyolite, polymictic rhyolite sandstone and black mudstone facies) (Chapter 3). Criteria supporting this hypothesis are (1) the stratigraphic position of UWS1 and UHR1 (below UWH2; next section) and (2) similar lithofacies characteristics in both UWS1 and UHR1. However, a detailed correlation between UWS1 and UHR1 is impossible due to the distance between drill holes (>5 km) and in WSP14, only about 40 m of UHR1 was intersected, compared with more than 200 m in WSP15 (Figure 5.6).

UWH1 is interpreted to be part of the CVC (Corbett, 1979). In the White Spur-Howards Road area, the CVC includes massive to weakly graded, feldspar-phyric fiamme breccia and rhyolitic and dacitic lavas, sills and cryptodomes (Corbett, 1981, 1992; Corbett and Lees, 1987; Dugdale, 1992; Corbett et al., 2014). UWS1 and UHR1 comprise dominantly coherent feldspar-quartz-phyric and feldspar-phyric rhyolite facies

Table 5.2: Local stratigraphic units and associated facies and sub-facies in DDH WSP-15 (White Spur area). See Chapter 3 for details on each facies.

Local stratigraphic units	Facies and sub-facies	Depth interval (m)	Thickness (m)
UWS2	Polymictic rhyolite breccia (**RpB**) and sandstone (**RpS**) and black mudstone (**BMud**) facies	6.0-232.0 m	≥ 226.0 m
UWS1	Coherent quartz-rich rhyolite sub-facies (**Rqp**); coherent feldspar-phyric rhyolite (**Rf**), polymictic rhyolite sandstone (**RpS**) and black mudstone (**BMud**) facies	180.0-401.2 m	≥ 221.2 m

Table 5.3: Local stratigraphic units and associated facies and sub-facies in DDH WSP-14 (Howards Road area). See Chapter 3 for details on each facies.

Local stratigraphic units	Facies and sub-facies	Depth interval (m)	Thickness (m)
UHR2	Polymictic mud-matrix rhyolite breccia (**RpmmB**), polymictic rhyolite breccia (**RpB**) and sandstone (**RpS**) and black mudstone (**BMud**) facies	0-447.9 m	≥ 447.9 m
UHR1	Coherent quartz-poor rhyolite sub-facies (**Rqp**) and black mudstone facies (**BMud**)	447.9-494.6 m	≥ 46.7 m

Table 5.4: Stratigraphic units, location, associated facies and sub-facies, and equivalent formal stratigraphic units in the White Spur-Howards Road area. See Chapter 3 for details on each facies.

Stratigraphic units and location		Facies and sub-facies	Equivalents (stratigraphic units)
UWH2	White Spur: **UWS2**; Howards Road: **UHR2**	Polymictic mud-matrix rhyolite breccia (**RpmmB**), polymictic rhyolite breccia (**RpB**) and sandstone (**RpS**) and black mudstone (**BMud**) facies	**White Spur Formation**
UWH1	White Spur: **UWS1**; Howards Road: **UHR1**	Coherent feldspar-quartz-phyric (**Rfq**) and feldspar-phyric (**Rf**) rhyolite, polymictic rhyolite sandstone (**RpS**) and black mudstone (**BMud**) facies	***Hercules Pumice Formation*** **(CVC)**

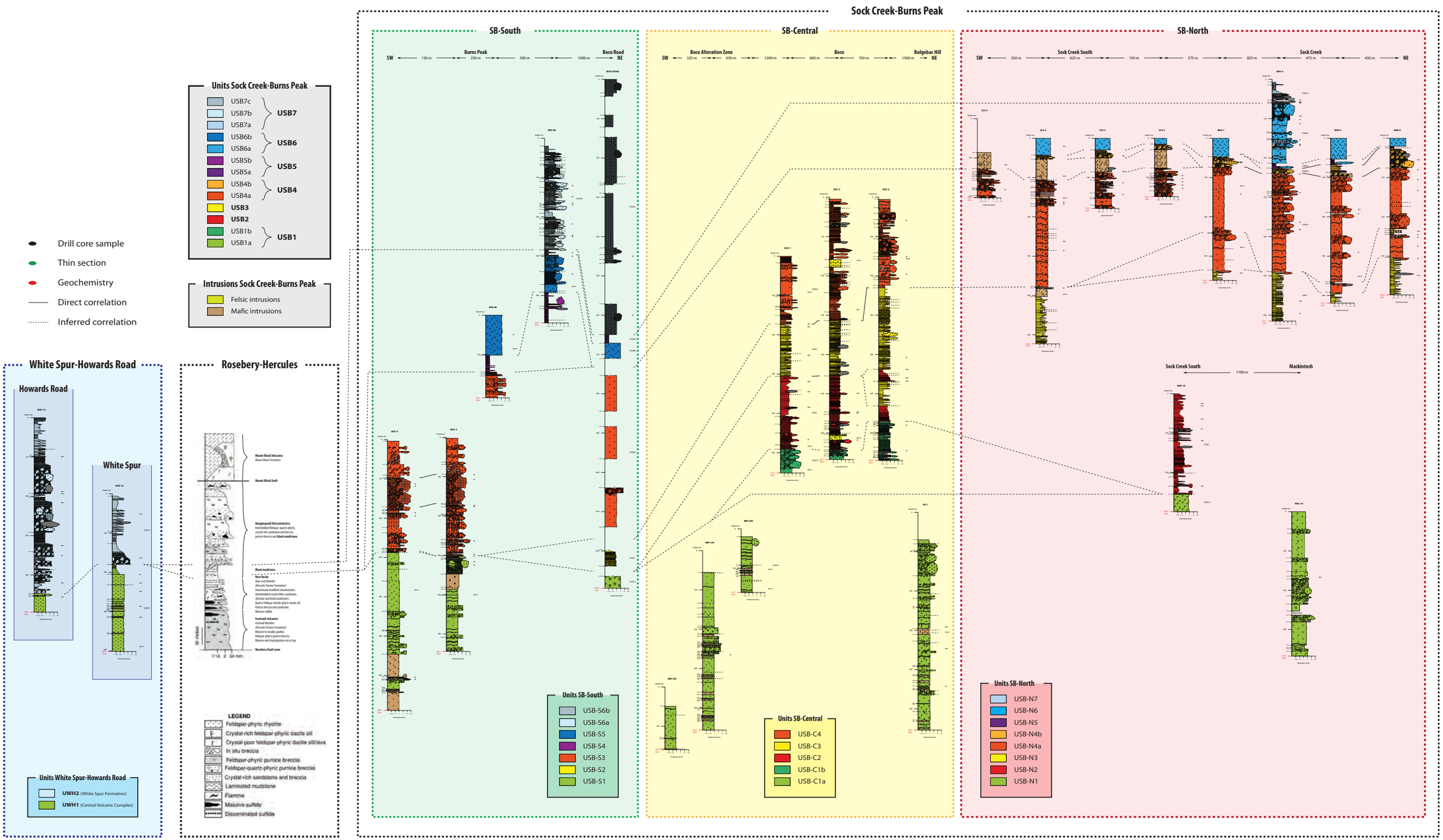

Figure 5.5: Correlation diagram of the regional stratigraphic units (USB) identified in the Sock Creek-Burns Peak area and the local stratigraphic units (UWH) identified in the White Spur-Howards Road area. Stratigraphic data and the correlation of units in the Rosebery-Hercules area has been compiled into a representative and simplified stratigraphic log after the work of Allen (1990b, 1991, 1992b, 1997), Nunn (1995) and Large et al. (2001). Unit labels are given on the right of the logs of DDH BHD-4 and BHD-10 (SB-North), BBP-209 and BOC-1(SB-Central), BPD-80 and Boco Road (SB-South), and WSP-15 (White Spur). See Figure 3.4 for legend to graphic logs.

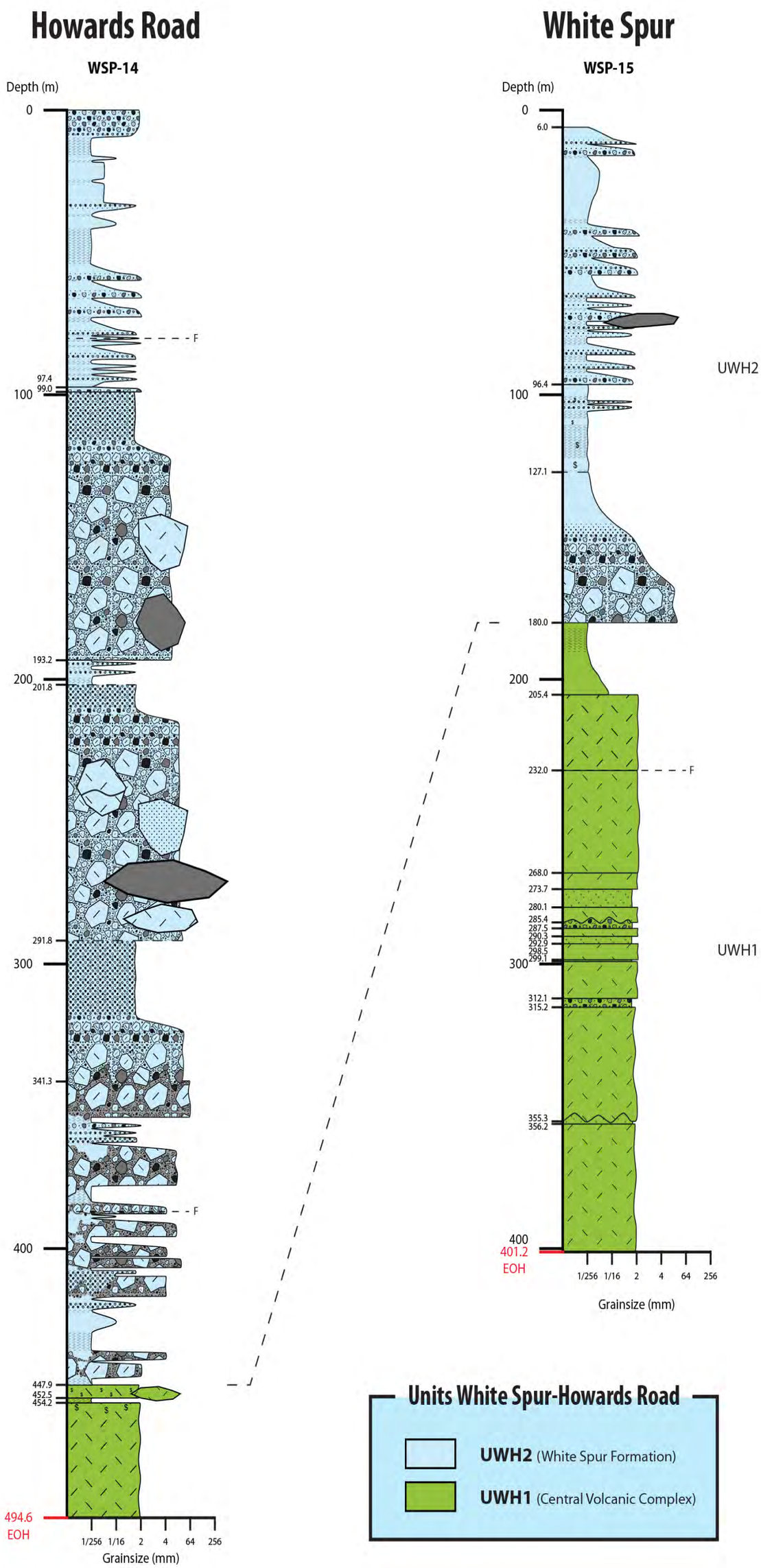

Figure 5.6: Correlation diagram of the local stratigraphic units (UWH) identified in the White Spur and Howards Road areas. See Figure 3.4 for legend to graphic logs.

(Figure 5.6) with fiamme texture (Figure 3.6 - L and M; Figure 3.8 - K and L). These rhyolitic facies are extremely altered and the fiamme texture is interpreted to be the product of alteration because it occurs together with an evenly porphyritic texture (e.g., Allen, 1988; Gifkins et al., 2005). Some of the coherent rhyolite facies have been interpreted as intrusions (Chapter 3). Furthermore, the CVC in the White Spur-Howards Road area is overlain by polymictic, volcanic quartz-feldspar-bearing crystal-rich pumiceous volcaniclastic rocks of the WSF (Corbett, 1981, 1985, 1992; Corbett and Lees, 1987; Dugdale, 1992; Nunn, 1995; Gifkins, 2001; Corbett et al., 2014) and both UWS1 and UHR1 are overlain by similar graded units of volcanic quartz-bearing polymictic rhyolite breccia and sandstone (Figure 5.6).

5.7.2.2 UWH2 (White Spur Formation correlate)

UWS2 and UHR2 are interpreted to correspond to the same stratigraphic level (UWH2), which includes four facies (Table 5.4; polymictic rhyolite breccia and sandstone, polymictic mud-matrix rhyolite breccia and black mudstone facies) (Chapter 3). The stratigraphic position of UWH2 (above UWH1) and similar facies and bedforms in both UWS2 and UHR2 support this hypothesis (Figure 5.6). However, the distance between DDH WSP-15 and DDH WSP-14 (>5 km) prevents direct correlation of subdivisions within UW2 and UHR2 (Figure 5.6).

UWH2 is interpreted to be part of the lower WSF (Corbett and Lees, 1987). In the White Spur-Howards Road area, the WSF comprises normally graded units of polymictic, volcanic quartz-feldspar-bearing, crystal-rich, pumiceous volcanic sandstone and breccia, which may grade into mudstone (Corbett, 1981, 1985, 1992; Corbett and Lees, 1987; McPhie and Allen, 1992; Dugdale, 1992; Nunn, 1995; Corbett et al., 2014). Both UWS2 and UHR2 include very similar lithofacies, interbedded with pyritic black mudstone (Figure 5.6). In addition, the WSF overlies the CVC in the White Spur-Howards Road area (Corbett, 1981, 1985, 1992; Corbett and Lees, 1987; Dugdale, 1992; Nunn, 1995; Corbett et al., 2014) and UWH2 overlies UWH1 (Figure 5.6), which has been interpreted to be part of the CVC (previous section).

5.7.3 Correlations between the White Spur-Howards Road and Rosebery-Hercules areas

Correlations between the local stratigraphic units identified in the White Spur-Howards Road (UWH; Figure 5.6) and Rosebery-Hercules (section 5.6; Figure 5.4) areas are presented in Figure 5.7 and discussed below.

In the White Spur-Howards Road area, UWH1 and UWH2 have been interpreted to correspond to the CVC and the lower part of the WSF, respectively (previous section). UWH1 in the White Spur-Howards Road area (Figure 5.7) comprises dominantly coherent feldspar-quartz-phyric and feldspar-phyric rhyolite. In addition, the top of UHR1 (447.9 to 454.2 m) in DDH WSP-14 (Howards Road area) includes strongly pyritic black mudstone and sulfide-bearing coherent quartz-poor rhyolite facies similar to parts of the Host-rock Member (Gifkins, 2001; Gifkins and Allen, 2001). The textures and the stratigraphic position of UWH1 support the interpretation that UWH1 and the CVC occur at the same stratigraphic level.

The dominant facies in UWH1 are similar to those in the Mount Black Formation, which is inferred to be present beneath the Hercules Pumice Formation in the Rosebery-Hercules area (Gifkins, 2001). Correlation of UWH1 with the Mount Black Formation requires explaining the absence of the Hercules Pumice Formation, which is the uppermost subdivision of the CVC mapped in the Rosebery-Hercules area, and which regional maps show as continuing S towards the White Spur-Howards Road area (e.g., Corbett, 2002a; Seymour and McClenaghan, 2003; McClenaghan, 2003). Possibilities include the Hercules Pumice Formation having locally lensed out, or having been removed by erosion. It is equally plausible that UWH1 represents a local variation in facies in the Hercules Pumice Formation. The data are too limited to resolve a more precise correlation, and UWH1 is correlated broadly with the CVC.

UWH2 (Figure 5.7) and the Hangingwall Volcaniclastics (Gifkins, 2001; Gifkins and Allen, 2001) comprise normally graded, volcanic quartz-feldspar-rich, polymictic rhyolite breccia and sandstone, interbedded with black mudstone, and are very similar to the WSF (Corbett, 1981, 1985, 1992; Corbett and Lees, 1987; McPhie and Allen, 1992; Dugdale, 1992; Nunn, 1995; Gifkins, 2001; Corbett et al., 2014). The presence of volcanic quartz in UWH2 differentiates it from UWH1. The same lithofacies difference occurs between the quartz-feldspar-rich WSF and the feldspar-rich CVC, which contains no quartz-phyric pumice and essentially no volcanic quartz crystals. The lithofacies characteristics and the stratigraphic position of UWH2 support the interpretation that UWH2 and the Hangingwall Volcaniclastics occur at the same stratigraphic level.

5.7.4 Implications in the Rosebery-Howards Road and Sock Creek-Burns Peak areas

Considering that DDH WSP-15 and DDH WSP-14 provide a limited representation of the stratigraphy in the White Spur-Howards Road area (Figure 5.6), and that the stratigraphy of the Rosebery-Hercules host sequence is represented by the simplified graphic log in Figure 5.4 (Allen, 1990b, 1991, 1992b, 1997), the local and regional stratigraphic units identified in these areas and in the Sock Creek-Burns Peak area (Chapter 4) may be correlated as follows (Figure 5.7):

1. In the Sock Creek-Burns Peak area, coherent feldspar-quartz-phyric and feldspar-phyric rhyolite and dacite of USB1 have been interpreted to be part of the Mount Black Formation (Gifkins, 2001) of the CVC (section 4.3). Feldspar-quartz-phyric and feldspar-phyric rhyolite facies with fiamme textures occur in the White Spur-Howards Road area (UWH1) and have been interpreted to be part of the CVC (Corbett, 1979) (section 5.7.2). In the Rosebery-Hercules area, the CVC is represented by feldspar-phyric fiamme breccia of the Hercules Pumice Formation and rhyolite and dacite facies of the Mount Black Formation (Gifkins, 2001; Gifkins and Allen, 2001) (Figure 5.4). The data are too limited to resolve a more precise correlation between UWH1 (correlated with the CVC in the White Spur-Howards Road area), USB1 (correlated with the Mount Black Formation in the Sock Creek-Burns Peak area), and the Hercules Pumice Formation in the Rosebery-Hercules area. UWH1 either (1) represents a local variation in facies in the Hercules Pumice Formation or (2) is part of the Mount Black Formation, and the Hercules Pumice Formation has locally lensed out, or has been removed by erosion.

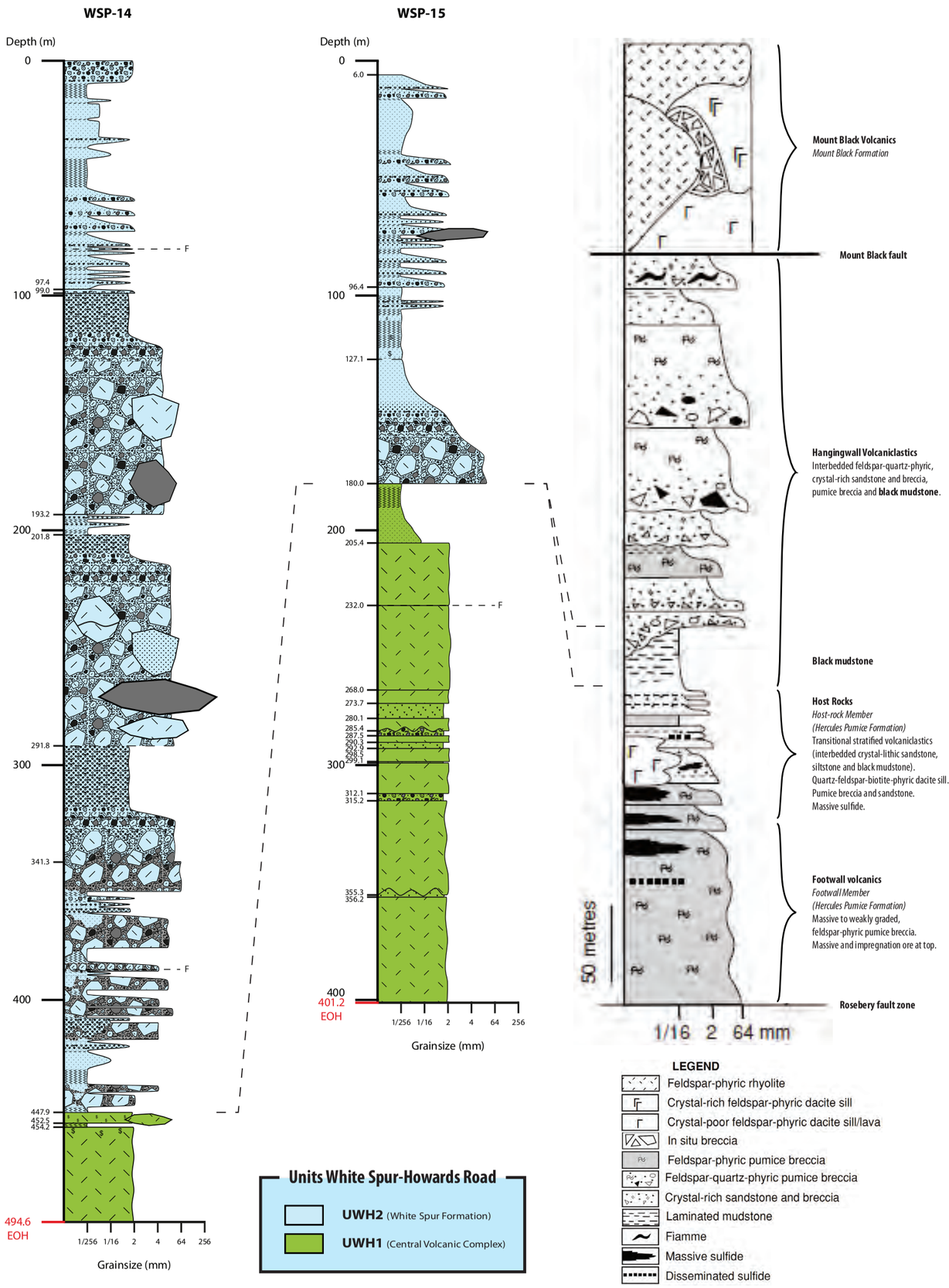

Figure 5.7: Correlation diagram of the local stratigraphic units (UWH) identified in the White Spur-Howards Road area and the stratigraphic units of the Rosebery-Hercules host succession. Stratigraphic data and the correlation of units in the Rosebery-Hercules area has been compiled into a representative and simplified stratigraphic log after the work of Allen (1990b, 1991, 1992b, 1997), Nunn (1995) and Large et al., (2001). See Figure 3.4 for legend to WSP-14 and WSP-15 graphic logs.

2. In the Sock Creek-Burns Peak area, normally graded units of volcanic quartz-bearing, polymictic rhyolite breccia and sandstone, and black mudstone of USB7 at the top of the succession have been interpreted to be part of the Southwell Subgroup (section 4.3). In the Rosebery-Hercules area, similar normally graded units of volcanic quartz-feldspar-rich polymictic sandstone and breccia are part of the WSF, which is equivalent to the Hangingwall Volcaniclastics (Corbett, 1981, 1985, 1992; Corbett and Lees, 1987; McPhie and Allen, 1992; Dugdale, 1992; Nunn, 1995; Gifkins, 2001; Gifkins and Allen, 2001). Very similar units in the White Spur-Howards Road area (UWH2) have been interpreted to be part of the lower WSF (section 5.7.2). These observations and interpretations suggest that USB7 (Sock Creek-Burns Peak area; Southwell Subgroup correlate), UWH2 (White Spur-Howards Road area), and the Hangingwall Volcaniclastics (Rosebery-Hercules area) occur at the same stratigraphic level (Figure 5.5); UWH2 and the Hangingwall Volcaniclastics are equivalent to the WSF in the Rosebery-Howards Road area and USB7 is equivalent to the Southwell Subgroup in the Sock Creek-Burns Peak area.

3. The Southwell Subgroup and correlates in the Hellyer-Mount Charter and Sock Creek-Burns Peak areas are lithologically similar to the WSF in the Rosebery-Howards Road area, and they are considered to be broadly stratigraphic equivalents occurring roughly at the same stratigraphic level (Corbett, 1992, 2002b, 2005a, 2005b; McPhie and Allen, 1992). The Southwell Subgroup differs from the WSF mainly in terms of the thicknesses of volcaniclastic versus non-volcanic or mixed provenance sedimentary facies: the Southwell Subgroup is dominated by non-volcanic or mixed provenance sedimentary facies whereas the WSF is dominated by volcaniclastic facies (McPhie and Allen, 1992). Radiometric and fossil age constraints support this correlation. The Southwell Subgroup contains trilobite fossils that indicate a late Middle Cambrian age (Jago and McNeill, 1997) and fossils found in the WSF provide an age range from Middle (Dundas area; Jago and Brown, 1989) to early Late Cambrian (Jago, 1986). The Southwell Subgroup (together with the Que River Shale) is intruded by a 499.3 ± 0.9 Ma rhyolitic sill (Mortensen et al., 2015) and the WSF is intruded by two rhyolite intrusions dated at 499.6 ± 0.8 Ma and 500.4 ± 0.8 Ma (Mortensen et al., 2015; Table 2.1). These observations suggest that USB7 (correlated with the Southwell Subgroup in Sock Creek-Burns Peak area), UWH2 (correlated with the WSF in the White Spur-Howards Road area), and the Hangingwall Volcaniclastics (equivalent to the WSF in the Rosebery-Hercules area) occur at the same stratigraphic level.

The stratigraphic unit represented by the Southwell Subgroup, USB7, UWH2, WSF and *Hangingwall Volcaniclastics* is probably diachronous (Figure 5.5). The Southwell Subgroup is approximately 1000 m thick in the Hellyer-Mount Charter area, whereas the WSF is only 300 to 400 m thick in the White Spur-Howards Road area. Assuming that sedimentation rates were comparable, the significantly greater thickness of the Southwell Subgroup in the Hellyer-Mount Charter area could reflect a longer duration. Similarly, the significantly greater thickness (<150 m) of the Que River Shale, which conformably underlies the Southwell Subgroup in the Hellyer-Mount Charter area, compared to the black mudstone (5 to 20 m thick) in the Rosebery-Hercules area, which immediately underlies the *Hangingwall Volcaniclastics* (Figure 5.4), could reflect a longer duration. Finally, there is a section up to approximately 1500 m thick above the CVC and below the Que River Shale in the Hellyer-Mount Charter area comprising the Black

Harry Beds, Animal Creek Greywacke and the QHV (Figure 5.3), and no equivalent section in the Rosebery-Hercules area (Figures 5.5).

4. The correlation of the local and regional stratigraphic units identified in the Sock Creek-Burns Peak (USB), White Spur-Howards Road (UWH), and Rosebery-Hercules (CVC and *Hangingwall Volcaniclastics*) areas help constrain the stratigraphic position of potentially mineralised units from Sock Creek-Burns Peak to White Spur-Howards Road (northern MRV). In this case, the top of USB1 (Sock Creek-Burns Peak area) and the top of UWH1 (White Spur-Howards Road area), both correlated with the CVC, represent the stratigraphic interval equivalent to the stratigraphy that hosts the VHMS deposits in the Rosebery-Hercules area, and are potentially prospective for sub-seafloor VHMS deposits (Figure 5.8). The correlation means that the WSF and equivalent units are post-mineralisation.

5.8 Regional correlations in the northern Mount Read Volcanics

5.8.1 Introduction

The regional geology and stratigraphy of the northern MRV were presented in Chapter 2. In this section, correlations within the northern MRV are discussed and summarized. Correlations in the northern MRV are based on the local and regional stratigraphic units identified in the: (1) Hellyer-Mount Charter (section 5.4), (2) Sock Creek-Burns Peak (Chapter 4), and (3) Rosebery-Howards Road (section 5.7) areas (Figure 5.9).

5.8.2 Stratigraphic units and correlations in the northern Mount Read Volcanics

In the northern MRV, seven regional stratigraphic units (UNMRV; Unit, Northern, Mount Read Volcanics) were identified (Figure 5.9), two of which occur in only one of the four areas previously considered (Figure 5.1) and five of which occur in at least two of the four areas (Figure 5.1). Each UNMRV corresponds to a stratigraphic level. The facies and sub-facies (Chapter 3) comprising each UNMRV and the associated formal stratigraphic units are presented in Table 5.5.

5.8.2.1 UNMRV1 (Central Volcanic Complex)

UNMRV1 groups fourteen facies (Table 5.5; dominantly coherent feldspar-quartz-phyric rhyolite, coherent feldspar-phyric rhyolite and dacite, and monomictic rhyolite and dacite breccia facies; Chapter 3) (Figure 5.9). UNMRV1 includes (1) USB1a and USB1b in the Sock Creek-Burns Peak area (correlated with the Mount Black Formation; Chapter 4), (2) the Hercules Pumice Formation (Footwall Member and Host-rock Member) (Gifkins, 2001) in the Rosebery-Hercules area (section 5.7), and (3) UWH1 in the White Spur-Howards Road area (correlated with the CVC; section 5.7) (Figure 5.9).

UNMRV1 comprises dominantly massive to flow-banded and/or locally amygdaloidal and perlitic feldspar-

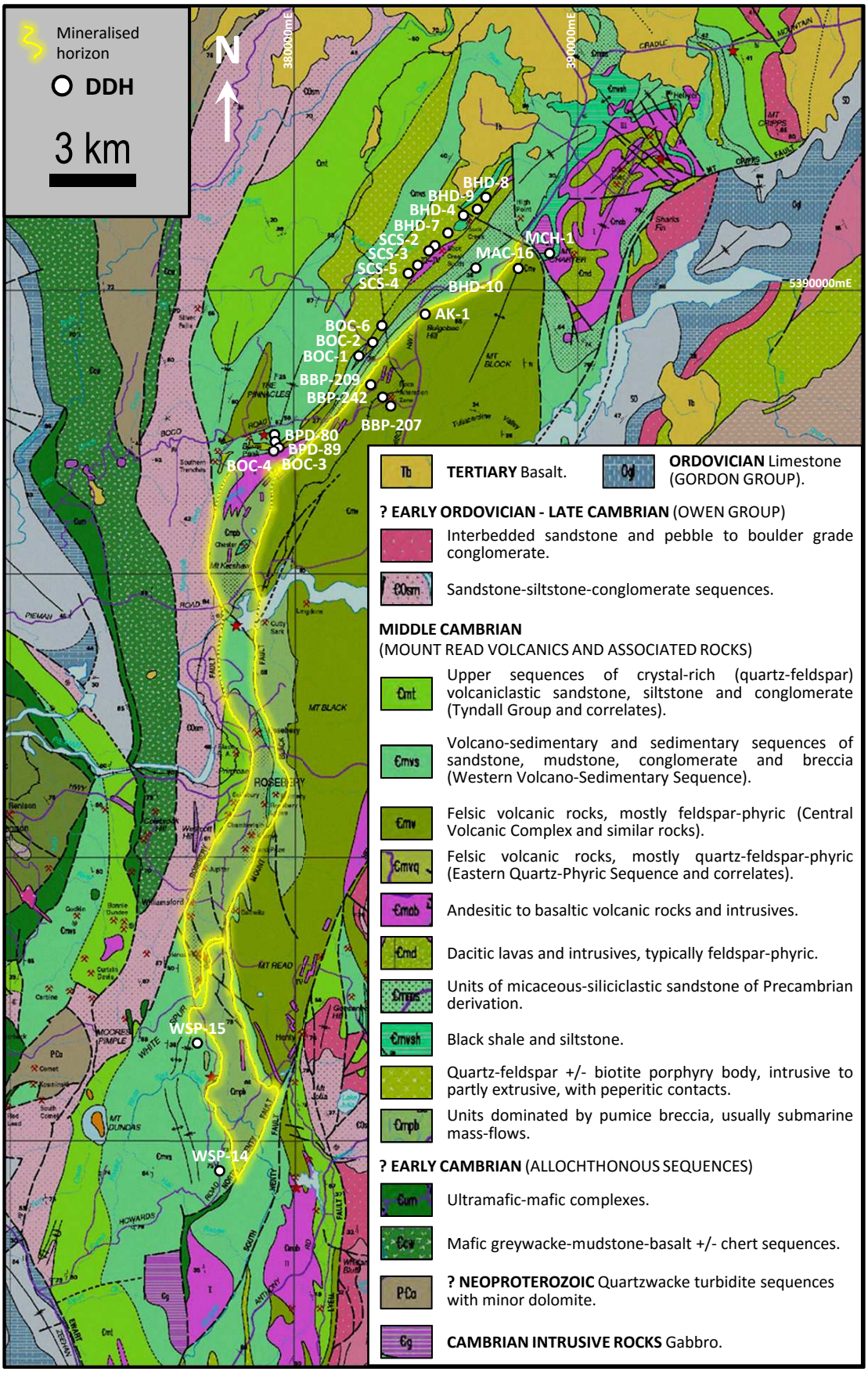

Figure 5.8: Bedrock geological map of the northern Mount Read Volcanics, showing the location of the diamond drill holes (DDH) in this study and the interpreted location of potential VHMS deposits (mineralised horizon) at the upper Central Volcanic Complex, after Corbett (2002).

quartz-phyric rhyolite and feldspar-phyric rhyolite and dacite, and monomictic rhyolite and dacite breccia, and minor monomictic fiamme-rich rhyolite breccia facies in the Sock Creek-Burns Peak and White Spur-Howards Road areas. It also comprises thick, extensive feldspar-phyric fiamme breccia in the Rosebery-Hercules area (Table 5.5; Figure 5.9). Coherent feldspar-quartz-phyric (quartz-rich) rhyolite and feldspar-phyric dacite, monomictic rhyolite and dacite breccia, polymictic felsic breccia and sandstone, and minor monomictic dacite sandstone, polymictic mud-matrix felsic breccia and black mudstone facies (USB1b) are restricted to the SB-Central area (Table 5.5; Figure 5.9).

UNMRV1 extends for at least 34 km from Howards Road (DDH WSP-14) in the SSW to the Mackintosh area (DDH MAC-16) in the NNE (Figures 5.1 and 5.9). The upper contact of UNMRV1 can be traced from DDH WSP-14 to DDH BHD-10 (Figures 5.1 and 5.9) and is well constrained at least from White Spur to Rosebery (Corbett, 1981, 1992; Corbett and Lees, 1987; Dugdale, 1992; Corbett et al., 2014). The lower contact of UNMRV1 is not exposed in the studied area of the northern MRV (Figure 5.9).

5.8.2.2 UNMRV2 (Black Harry Beds)

UNMRV2 is limited to the Sock Creek-Burns Peak area and matches USB2 (Chapter 4; Figure 5.9). It comprises polymictic felsic breccia and sandstone and shard-rich mudstone facies (Table 5.5; Chapter 3) and has been previously defined as the Black Harry Beds (Corbett, 1992). UNMRV2 extends for at least 4.5 km from DDH BOC-1 (Boco area) in the SW to DDH BHD-10 (Sock Creek South area) in the NE (Figures 5.1 and 5.9).

The lower contact of UNMRV2 can be easily traced from DDH BOC-1 to BHD-10, but direct correlation of the upper contact is limited to the Boco area (Figure 5.9). The proximity of the DDH, the stratigraphic position of UNMRV2, and the lithofacies characteristics of the facies grouped into UNMRV2 suggest that they are related (Figure 5.9).

5.8.2.3 UNMRV3 (Animal Creek Greywacke)

UNMRV3 consists of polymictic micaceous sandstone and micaceous mudstone facies (Table 5.5; Chapter 3), and includes (1) USB3 in the Sock Creek-Burns Peak area (Chapter 4) and (2) UMC1 in the Mount Charter area (DDH MCH-1; section 5.4). USB3 has been interpreted in Chapter 4 to be equivalent to the Animal Creek Greywacke (Collins et al., 1981; Corbett and Komyshan, 1989; Pemberton et al., 1991; Corbett, 1992) (Figure 5.9).

UNMRV3 extends for at least 12 km from Burns Peak (DDH BOC-4) in the SW to Mount Charter (DDH MCH-1) in the NE (Figures 5.1 and 5.9), but does not occur S of Burns Peak. Direct correlation of the upper contact of UNMRV3 is reliable from DDH BOC-1 (Boco area) to DDH MCH-1 (Mount Charter), but direct correlation of the lower contact is limited to the Boco area (Figure 5.9). To the SW, correlations are mainly inferred and UNMRV3 decreases significantly in thickness, disappearing in DDH BOC-3 and re-appearing in DDH BOC-4 (Figure 5.9).

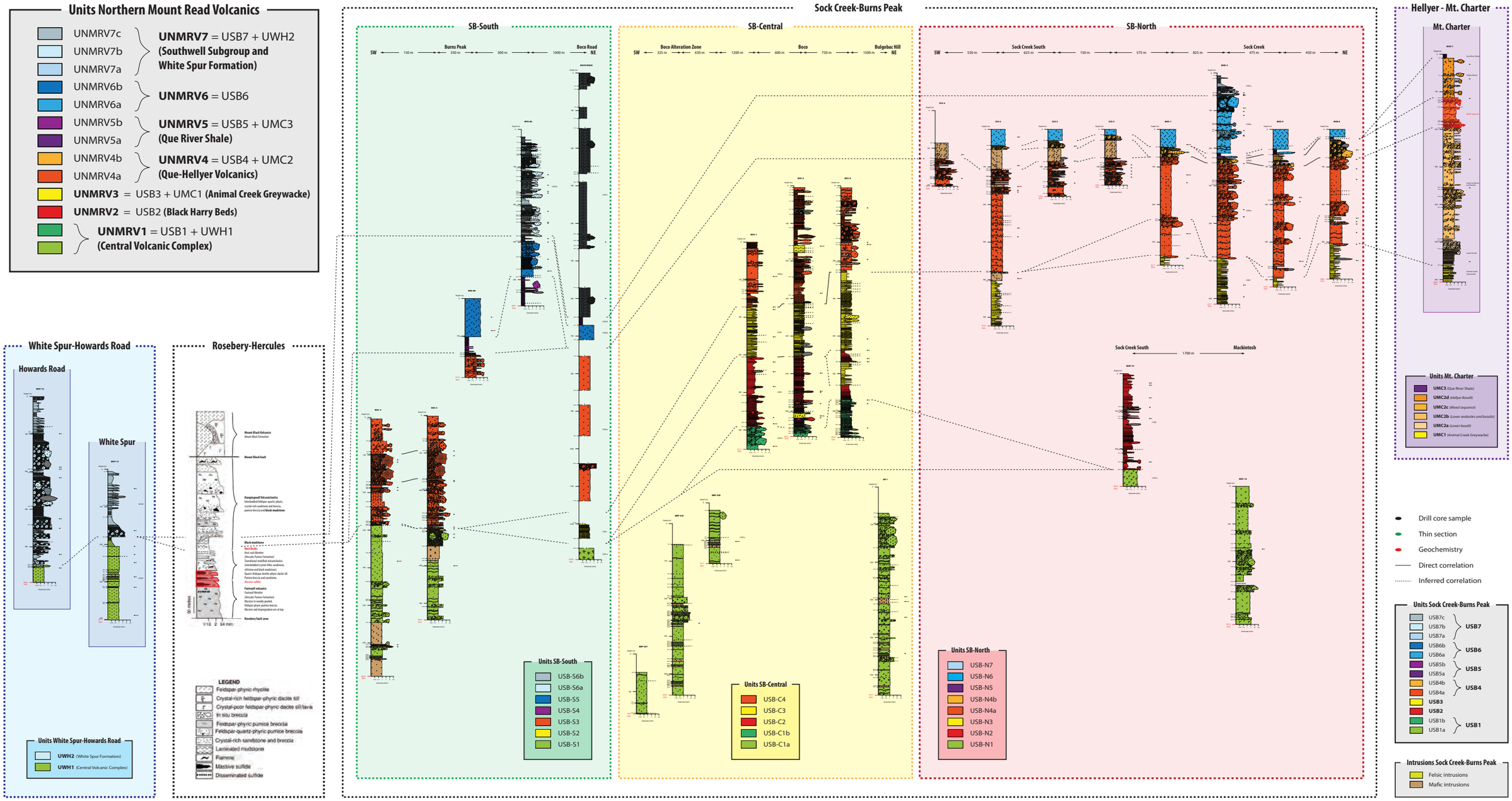

Figure 5.9: Correlation diagram of the regional stratigraphic units (UNMRV) identified in the northern Mount Read Volcanics showing the regional stratigraphic units identified in the Sock Creek-Burns Peak area (USB) and the local stratigraphic units identified in the Mount Charter (UMC) and White Spur-Howards Road (UWH) areas. Stratigraphic data and the correlation of units in the Rosebery-Hercules area has been compiled into a representative and simplified stratigraphic log after the work of Allen (1990b, 1991, 1992b, 1997), Nunn (1995) and Large et al., (2001). Unit labels are given on the right of the logs of DDH BHD-4 and BHD-10 (SB-North), BBP-209 and BOC-1 (SB-Central), BPD-80 and Boco Road (SB-South), MCH-1 (Mount Charter), and WSP-15 (White Spur). The position of the Rosebery-Hercules and Hellyer-Mount Charter VHMS deposits is highlighted in red in the Rosebery-Hercules and Mount Charter areas. See Figure 3.4 for legend to graphic logs.

Table 5.5: Stratigraphic units, location, associated facies and sub-facies, and equivalent formal stratigraphic units in the northern Mount Read Volcanics. See Chapter 3 for details on each facies.

Regional stratigraphic units		Location and local stratigraphic units	Facies and sub-facies	Location and diamond drill holes	Extention (km)	Equivalents (stratigraphic units)
UNMRV7	***UNMRV7c***	SB-South: **USB7c**	Polymictic crystal-rich sandstone (**PcrS**) facies	Boco Road	>12 km? (if correlated)	**Southwell Subgroup and White Spur Formation**
	UNMRV7b	SB-South: **USB7b**	Polymictic rhyolite breccia (**RpB**) and sandstone (**RpS**), polymictic mud-matrix rhyolite breccia (**RpmmB**), and black mudstone (**Bmud**) facies	Burns Peak: **BPD-80**		
	UNMRV7a	SB-North: **USB7a**	Polymictic rhyolite breccia (**RpB**) and sandstone (**RpS**), and black mudstone (**BMud**) facies	Sock Creek: **BHD-4**		
UNMRV6	***UNMRV6b***	SB-South: **USB6b**	Monomictic rhyolite breccia (**RmB**) and monomictic mud-matrix rhyolite breccia (**RmmB**) facies, and coherent quartz-rich rhyolite sub-facies (**Rqr**)	Burns Peak: **BPD-80, BPD-89**; Boco Road	>12 km? (if correlated)	**Quartz-feldspar rhyolite porphyries**
	UNMRV6a	SB-North: **USB6a**		Sock Creek: **BHD-4, BHD-7, BHD-8 and BHD-9**; Sock Creek South: **SCS-2, SCS-3 and SCS-5**		
UNMRV5	***UNMRV5b***	SB-South: **USB5b**	Black mudstone (**BMud**), and polymictic rhyolite breccia (**RpB**) and sandstone (**RpS**) facies	Burns Peak: **BPD-80, BPD-89**; Boco Road	>12 km? (if correlated)	**Que River Shale** (HMC area)**, black mudstone** (RH area) **and equivalents**
	UNMRV5a	SB-North: **USB5a**; HMC area: **UMC3**	Black mudstone facies (**BMud**)	Sock Creek: **BHD-4, BHD-8 and BHD-9**; Mount Charter: **MCH-1**		
UNMRV4	***UNMRV4b***	SB-North: **USB4b**; HMC area: **UMC2c**	Polymictic volcanic breccia (**PvB**) and sandstone (**PvS**) facies	Sock Creek: **BHD-4, BHD-7, BHD-8 and BHD-9**; Sock Creek South: **SCS-2, SCS-3 and SCS-5**; Mount Charter: **MCH-1**	>3.5 km	***Mixed sequence*** **(Que-Hellyer Volcanics) and equivalent**
	UNMRV4a	SB area: **USB4a**; HMC area: **UMC2a, UMC2b**	Coherent feldspar-pyroxene-phyric mafic facies (**Mfp**), coherent feldspar-phyric rhyolite (**Rf**), dacite (**Df**) and mafic (**Mf**) facies, monomictic rhyolite (**RmB**), dacite (**DmB**) and mafic (**MmB**) breccia, monomictic mafic sandstone (**MmS**), monomictic mud-matrix rhyolite (**RmmB**), dacite (**DmmB**) and mafic (**MmmB**) breccia, monomictic fiamme-rich dacite breccia (**DmfrB**), monomictic fluidal-clast mafic breccia (**MmfcB**), polymictic mafic breccia (**MpB**) and sandstone (**MpS**), polymictic mud-matrix felsic breccia (**PmmfB**), polymictic felsic breccia (**PfB**) and sandstone (**PfS**), and black (**BMud**), micaceous (**MMud**) and shard-rich (**SMud**) mudstone facies	Sock Creek: **BHD-4, BHD-7, BHD-8 and BHD-9**; Sock Creek South: **SCS-2, SCS-3, SCS-4 and SCS-5**; Boco: **BOC-1, BOC-2 and BOC-6**; Burns Peak: **BOC-3, BOC-4, and BPD-89**; Mount Charter: **MCH-1**; Boco Road	>12 km	**Que-Hellyer Volcanics and equivalents (Sock Creek Dacites, Boco Road Dacite and Hollway Andesite;** ***lower basalt*** **and** ***lower andesites and basalts*** **)**
UNMRV3		SB area: **USB3**; HMC area: **UMC1**	Polymictic micaceous sandstone (**PmS**) and micaceous mudstone (**MMud**) facies	Sock Creek: **BHD-4, BHD-7, BHD-8 and BHD-9**; Sock Creek South: **SCS-5**; Boco: **BOC-1, BOC-2 and BOC-6**; Burns Peak: **BOC-4**; Mount Charter: **MCH-1**; Boco Road	>12 km	**Animal Creek Greywacke**
UNMRV2		SB area: **USB2**	Polymictic felsic breccia (**PfB**) and sandstone (**PfS**), and shard-rich mudstone (**SMud**) facies	Sock Creek South: **BHD-10**; Boco: **BOC-1, BOC-2 and BOC-6**	>4.5 km	**Black Harry Beds**
UNMRV1	***UNMRV1b***	SB-Central: **USB1b**	Coherent quartz-rich rhyolite sub-facies (**Rqr**); coherent feldspar-phyric dacite (**Df**), monomictic rhyolite (**RmB**) and dacite (**DmB**) breccia, monomictic dacite sandstone (**DmS**), polymictic felsic breccia (**PfB**) and sandstone (**PfS**), polymictic mud-matrix felsic breccia (**PmmfB**), and black mudstone (**BMud**) facies	Boco: **BOC-1, BOC-2 and BOC-6**	>1.5 km	**Central Volcanic Complex (*Mount Black Formation* , *Hercules Pumice Formation*)**
	UNMRV1a	SB area: **USB1a**; WH area: **UWH1**; RH area: **Hercules Pumice Formation**	Coherent feldspar-quartz-phyric rhyolite (**Rfq**), coherent feldspar-phyric rhyolite (**Rf**) and dacite (**Df**), monomictic rhyolite (**RmB**) and dacite (**DmB**) breccia, monomictic mud-matrix dacite breccia (**DmmB**), monomictic fiamme-rich rhyolite (**RmfrB**) and dacite (**DmfrB**) breccia, monomictic mud-matrix fiamme-rich dacite breccia (**DmmfrB**), monomictic dacite sandstone (**DmS**), polymictic rhyolite sandstone (**RpS**), polymictic volcanic breccia (**PvB**), polymictic felsic breccia (**PfB**) and black mudstone (**BMud**) facies; **feldspar-phyric fiamme breccia** (*Hercules Pumice Formation*)	Mackintosh: **AK-1**; Sock Creek South: **BHD-10**; Boco Alteration Zone: **BBP-207, BBP-209 and BBP-242**; Burns Peak: **BOC-3 and BOC-4**; Boco Road; Howards Road: **WSP-14**; White Spur: **WSP-15**; Rosebery-Hercules	>34 km	

Abbreviations: SB = Sock Creek-Burns Peak; HMC = Hellyer-Mount Charter; WH = White Spur-Howards Road; RH = Rosebery-Hercules.

5.8.2.4 UNMRV4 (Que-Hellyer Volcanics)

UNMRV4 is limited to N of Burns Peak and consists of twenty three facies (Table 5.5; dominantly coherent feldspar-pyroxene-phyric mafic facies, coherent feldspar-phyric rhyolite, dacite and mafic facies, monomictic rhyolite, dacite and mafic breccia, and polymictic volcanic breccia and sandstone; Chapter 3) that have been grouped into two sub-units: UNMRV4a and UNMRV4b (Figure 5.9). UNMRV4a includes (1) USB4a in the Sock Creek-Burns Peak area (Chapter 4) and (2) UMC2a and UMC2b in the Mount Charter area (section 5.4), which have been identified as the lower basalt and lower andesites and basalts of the QHV (Corbett and Komyshan, 1989; Corbett, 1992), respectively by Corbett and Komyshan (1989) (Figure 5.9). UNMRV4b corresponds to USB4b in the Sock Creek-Burns Peak North area (Figure 5.9). USB4a has been interpreted in Chapter 4 to include lateral equivalents (Sock Creek Dacites, Boco Road Dacite and Hollway Andesite) of the QHV; USB4b has been interpreted in Chapter 4 as a likely correlate of the mixed sequence of the QHV.

USB4a consists of dominantly coherent mafic facies, massive to flow-banded and/or locally amygdaloidal and perlitic feldspar-phyric rhyolite and dacite, monomictic rhyolite, dacite and mafic breccia, and polymictic felsic breccia and sandstone facies (Table 5.5; Chapter 3; Figure 5.9). USB4b comprises normally graded units of polymictic volcanic breccia and sandstone facies (Table 5.5; Chapter 3; Figure 5.9).

UNMRV4a extends for at least 12 km from Burns Peak (DDH BOC-4) in the SW to Mount Charter (DDH MCH-1) in the NE (Figures 5.1 and 5.9). The upper contact of UNMRV4a can be traced from DDH BPD-89 (Burns Peak area) to DDH MCH-1 (Mount Charter), but direct correlation of this contact is reliable only from DDH SCS-4 (Sock Creek South) to Mount Charter (Figure 5.8.1). UNMRV4b is an excellent stratigraphic marker in the Sock Creek-Burns Peak area and extends for at least 3.5 km from DDH SCS-5 (Sock Creek South area) to DDH BHD-8 (Sock Creek area) (Figures 5.1 and 5.9). The upper and lower contacts of UNMRV4b can be correlated in the Sock Creek-Sock Creek South area (Figure 5.9).

5.8.2.5 UNMRV5 (Que River Shale)

UNMRV5 consists dominantly of black mudstone, and rare polymictic rhyolite breccia and sandstone facies (Table 5.5; Chapter 3) and matches (1) USB5 in the Sock Creek-Burns Peak area (Chapter 4) and (2) UMC3 in the Mount Charter area (section 5.4) (Figure 5.9), which has been identified as the Que River Shale (Corbett and Komyshan, 1989; Corbett, 1992) by Corbett and Komyshan (1989). UNMRV5 also probably includes most (except the lowest part) of the black mudstone (which overlies the Host-rock Member) in the Rosebery-Hercules area. USB5 was interpreted in Chapter 4 to be a possible correlate of the Que River Shale. UNMRV5 has been sub-divided into two sub-units: UNMRV5a (includes USB5a and UMC3) and UNMRV5b (equivalent to USB5b) (Table 5.5; Figure 5.9).

UNMRV5 occurs in two sub-areas (Mount Charter-Sock Creek and Boco Road-Burns Peak), discontinuously covering at least 12 km from Mount Charter (DDH MCH-1) in the NE to Burns Peak (DDH BPD-89) in the SW (Figures 5.1 and 5.9). In the Sock Creek area, the lower contact can be directly correlated; correlation

of the upper contact can only be inferred because this contact has been interpreted to be intrusive. In the Boco Road-Burns Peak area all correlations are inferred (Figure 5.9).

5.8.2.6 UNMRV6

UNMRV6 is limited to the Sock Creek and Burns Peak areas and matches USB6 (Chapter 4) (Figure 5.9). This unit comprises coherent quartz-rich rhyolite sub-facies, monomictic rhyolite breccia and monomictic mud-matrix rhyolite breccia facies (Table 5.5; Chapter 3). UNMRV6 can be sub-divided into two sub-units: UNMRV6a and UNMRV6b. UNMRV6 occurs in two sub-areas (Sock Creek-Sock Creek South and Boco Road-Burns Peak), extending discontinuously for at least 12 km from Sock Creek (DDH BHD-8) in the NE to Burns Peak (DDH BPD-89) in the SW (Figures 5.1 and 5.9). All correlations of the lower contact of UNMRV6 are inferred because this contact has been interpreted as intrusive; the correlation of the upper contact is also inferred due to the distance between DDH (Figures 5.1 and 5.9).

5.8.2.7 UNMRV7 (Southwell Subgroup and White Spur Formation)

UNMRV7 consists of volcanic quartz-bearing, polymictic rhyolite breccia and sandstone, polymictic mud-matrix rhyolite breccia, polymictic crystal-rich sandstone and black mudstone facies that extend throughout the northern MRV (Table 5.5; Chapter 3). UNMRV7 includes (1) USB7 in the Sock Creek-Burns Peak area (Chapter 4), (2) the Hangingwall Volcaniclastics in the Rosebery-Hercules area (section 5.7), and (3) UWH2 in the White Spur-Howards Road area (section 5.7) (Figure 5.9). The Hangingwall Volcaniclastics in the Rosebery-Hercules area is equivalent to the WSF (Corbett and Lees, 1987; McPhie and Allen, 1992; Allen, 1998; Jago, 2005; Gifkins, 2001; Williams, 2009). UWH2 has been interpreted in section 5.7 to be equivalent to the WSF. USB7 has been interpreted in Chapter 4 to be equivalent to the Southwell Subgroup.

UNMRV7 extends for at least 34 km from Howards Road (DDH WSP-14) in the SSW to the Sock Creek area (DDH BHD-4) in the NNE (Figures 5.1 and 5.9). The upper contact of UNMRV7 is not exposed in the studied area of the northern MRV (Figure 5.9). The lower contact of UNMRV7 can be traced from DDH WSP-14 (Howards Road area) to DDH BHD-4 (Sock Creek area), but direct correlations are unreliable. In the Rosebery-Howards Road area, UNMRV7 correlates with the WSF and the contact with the underlying CVC (UNMRV1) can be traced from Rosebery to Howards Road. In the Sock Creek-Burns Peak area, UNMRV7 correlates with the Southwell Subgroup and overlies UNMRV6.

5.8.3 Implications in the northern Mount Read Volcanics

Considering that (1) DDH MCH-1 is representative of the stratigraphy in the Hellyer-Que River area (Figure 5.2), (2) the stratigraphy of the Rosebery-Hercules host sequence is represented by a simplified graphic log (Figure 5.4) and (3) DDH WSP-15 and DDH WSP-14 provide a limited representation of the stratigraphy in the White Spur-Howards Road area (Figure 5.6), the regional stratigraphic units (UNMRV) identified in these areas and in the Sock Creek-Burns Peak area (Chapter 4 may be correlated as follows (Figure 5.9):

1. Massive to flow-banded feldspar-quartz-phyric and feldspar-phyric rhyolite and dacite of USB1 (Sock Creek-Burns Peak area) have been interpreted to be part of the Mount Black Formation (Gifkins, 2001; Gifkins and Allen, 2001) of the CVC (section 4.3). In the Rosebery-Hercules area, the CVC is represented by feldspar-phyric pumice breccia of the Hercules Pumice Formation and rhyolite and dacite facies of the Mount Black Formation (Gifkins, 2001; Gifkins and Allen, 2001) (Figure 5.4). In the White Spur-Howards Road area, feldspar-quartz-phyric and feldspar-phyric rhyolite facies with fiamme textures of UWH1 have been interpreted to correspond to the CVC (section 5.7.2), and a more precise correlation is not yet possible.

2. In the Sock Creek-Burns Peak area, massive to flow-banded feldspar-pyroxene-phyric mafic facies, feldspar-phyric rhyolite, dacite and mafic facies, monomictic rhyolite, dacite and mafic breccia facies and polymictic volcanic breccia and sandstone facies of USB4, and very similar lithofacies in UMC2 in DDH MCH-1 at Mount Charter, have been interpreted to correlate with the QHV(section 5.4). These observations and interpretations suggest that USB4 (Sock Creek-Burns Peak), UMC2 (Mount Charter area) and the QHV occur at the same regional stratigraphic level (UNMRV4) (Figure 5.9), but this level cannot be identified S of Burns Peak.

3. The Southwell Subgroup in the Hellyer-Mount Charter area and USB7 in the Sock Creek-Burns Peak area comprise normally graded units of volcanic quartz-bearing, polymictic rhyolite breccia and sandstone, and black mudstone that are lithologically similar to the WSF, Hangingwall Volcaniclastics and UWH2 in the Rosebery-Howards Road area, and they are all considered to be broadly stratigraphic equivalents occurring roughly at the same stratigraphic level (UNMRV7). Fossil and radiometric age determinations support the correlation between the Southwell Subgroup and the WSF (Jago, 1986; Jago and Brown, 1989; Jago and McNeill, 1997; Mortensen et al., 2015).

4. The correlation of the regional stratigraphic units (UNMRV) identified in the northern MRV help constrain the stratigraphic position of potentially mineralised units from the Hellyer-Mount Charter area in the NNE to the Rosebery-Howards Road area in the SSW, including the Sock Creek-Burns Peak area (Figures 5.1 and 5.9). In the Hellyer-Mount Charter area (NE of Sock Creek-Burns Peak), the Hellyer, Fossey, Que River and Mount Charter VHMS deposits occur within the mixed sequence of the QHV (Mount Charter Group), which has been correlated with USB4b in the Sock Creek-Burns Peak area. The Rosebery-Hercules VHMS deposits are hosted by the Host-rock Member of the Hercules Pumice Formation (Gifkins, 2001; Gifkins and Allen, 2001) of the upper CVC, which has been correlated with USB1 in the Sock Creek-Burns Peak area. The VHMS deposits in the Hellyer-Mount Charter and Rosebery-Hercules areas occur stratigraphically below black mudstone units (Que River Shale and black mudstone, respectively), which are correlated with USB5 in the Sock Creek-Burns Peak area. These correlations mean that UNMRV7 (USB7, Sock Creek-Burns Peak area; UWH2, White Spur-Howards Road area; Hangingwall Volcaniclastics, Rosebery-Hercules area), which is correlated with the WSF in the Rosebery-Howards Road area and the Southwell Subgroup and correlates in the Hellyer-Mount Charter and Sock Creek-Burns Peak areas, is post-mineralisation.

5.9 Summary

Seven regional stratigraphic units (UNMRV - Unit, Northern, Mount, Read, Volcanics) have been identified in four areas, from NNE to SSW: (1) Hellyer-Mount Charter (section 5.4), (2) Sock Creek-Burns Peak (Chapter 4), (3) Rosebery-Hercules (section 5.7), and (4) White Spur-Howards Road (section 5.7) (Figure 5.9). Each UNMRV corresponds to a stratigraphic level. The correlations of the UNMRV, together with published fossil and radiometric age data, help constrain the stratigraphic positions of mineralised units in the northern MRV: the VHMS deposits in the Rosebery-Hercules area occur at the top of UNMRV1 (correlated with the upper CVC) and the VHMS deposits in the Hellyer-Mount Charter area occur at the top of UNMRV4 (correlated with the QHV).

CHAPTER 6

Volcanic setting of mineralisation in the northern Mount Read Volcanics

6.1 Introduction

The stratigraphy, correlations and facies architecture of the Sock Creek-Burns Peak area were presented in Chapter 4. The regional correlations in the Sock Creek-Burns Peak area with the areas to the NE (Hellyer-Mount Charter) and SSW (Rosebery-Howards Road) were discussed in Chapter 5. This chapter focuses on the volcanic setting of mineralisation in the northern Mount Read Volcanics based on the local and regional correlations made in previous chapters.

This chapter is divided into four sections. The first (section 6.2) introduces the stratigraphic context of mineralization in the Hellyer-Mount Charter area (NE of Sock Creek-Burns Peak) and in the Rosebery-Hercules area (SSW of Sock Creek-Burns Peak). The regional correlations in the Sock Creek-Burns Peak area with the Hellyer-Mount Charter and Rosebery-Howards Road areas and the different genetic models for the formation of the Rosebery and Hercules VHMS deposits are summarized, and their implications for the timing and setting of VHMS formation in the northern Mount Read Volcanics are discussed.

The second (section 6.3) presents a paleogeography and mineralisation reconstruction of the northern Mount Read Volcanics before, during and after the formation of the Hellyer, Que River, Rosebery and Hercules VHMS deposits. It focuses on the paleogeography of the Sock Creek-Burns Peak area assuming the syn-volcanic, sub-seafloor replacement models for the formation of the Rosebery and Hercules VHMS deposits. The alternative scenario for the paleogeography and mineralisation reconstruction of the northern Mount Read Volcanics considering the formation of the Rosebery and Hercules VHMS deposits on the seafloor is also discussed.

The third section (section 6.4) presents the major implications and directions for VHMS exploration in both the Sock Creek-Burns Peak area and other parts of the Mount Read Volcanics. The fourth section (section 6.5) summarizes the major interpretations and conclusions.

6.2 Stratigraphic context of mineralisation in the northern Mount Read Volcanics

6.2.1 Introduction

The Pb-Zn-rich VHMS deposits in the northern Mount Read Volcanics (NMRV) occur at Hellyer and Que River in the NNE and at Rosebery and Hercules in the SSW. These major deposits occur at two stratigraphic

levels; the stratigraphically higher one (Hellyer and Que River) is associated with andesites and dacites of the Que-Hellyer Volcanics (QHV), and the other (Rosebery and Hercules) is associated with fiamme breccias in the upper part of the Central Volcanic Complex (CVC). The Sock Creek-Burns Peak area (Chapter 4), situated between the Hellyer-Mount Charter area in the NE and the Rosebery-Howards Road area in the SSW, includes these two stratigraphic levels.

6.2.2 Hellyer-Mount Charter area (NE of Sock Creek-Burns Peak)

The Hellyer-Mount Charter area includes the Hellyer and Que River high-grade polymetallic volcanic-hosted massive sulfide (VHMS) deposits, the massive barite and high-grade base metal sulfide (BMS) deposits at Fossey, and the Mount Charter Au-Ag-(Zn)-(Ba) deposit. These major deposits are hosted by the QHV (Corbett and Komyshan, 1989; Corbett and Solomon, 1989; Waters and Wallace, 1992), which is part of the Mount Charter Group (Corbett, 1992). The Hellyer and Que River VHMS deposits are considered to have formed at seafloor positions (Waters and Wallace, 1992; Gemmell and Fulton, 2001). The regional geology of the Hellyer-Mount Charter area has been presented in section 5.2.

The QHV comprise a late Middle Cambrian submarine succession of andesite, basalt and minor dacite which occurs conformably between the underlying micaceous Animal Creek Greywacke and the overlying carbonaceous Que River Shale (Corbett and Komyshan, 1989; Waters and Wallace, 1992). Both the QHV and the Animal Creek Greywacke are unfossiliferous, but the Que River Shale contains important and diverse fossil fauna that indicates a late Middle Cambrian Floran-Undillan age (E. opimus Zone to P. punctuosus Zone) and marine depositional conditions (Gee et al., 1970; Jago, 1977; Laurie et al., 1995). The age of the Hellyer and Que River VHMS deposits is enclosed between the 500.4 ± 0.9 Ma age for the footwall andesite, and the 499.3 ± 0.9 Ma age from a rhyolite sill intruding the Que River Shale (Mortensen et al., 2015). The QHV correspond to UMC2 identified in the Mount Charter area (section 5.4) (Figure 6.1 - DDH MCH-1). The stratigraphy of the QHV, including the Hellyer and Que River host sequences, has been presented in detail in section 5.3.

Within the QHV, the mixed sequence is host to VHMS deposits. It consists of a lithologically complex unit composed of two subunits - the mixed sequence volcaniclastics and the mixed sequence dacites (Waters and Wallace, 1992). In the vicinity of the ore deposits, the mixed sequence volcaniclastics dominantly comprise polymictic basaltic to dacitic, volcanic breccia and coarse-grained sandstone with minor laminated mudstone. A summary of the five different facies identified by Waters and Wallace (1992) within the mixed sequence volcaniclastics is presented in Table 6.1. In DDH MCH-1 (Mount Charter area) the mixed sequence is 80 m thick, occurring from 116.0 to 196.0 m depth (Figure 6.1).

The mixed sequence occurs stratigraphically between the underlying feldspar-phyric footwall andesites and basalts, and the overlying massive to pillow pyroxene-phyric hangingwall basalts (Hellyer Basalt; Waters and Wallace, 1992). The lower andesites and basalts (footwall to the massive sulfide deposit) overlie massive and pillow lavas of the lower basalt (QHV), which in turn overlies the

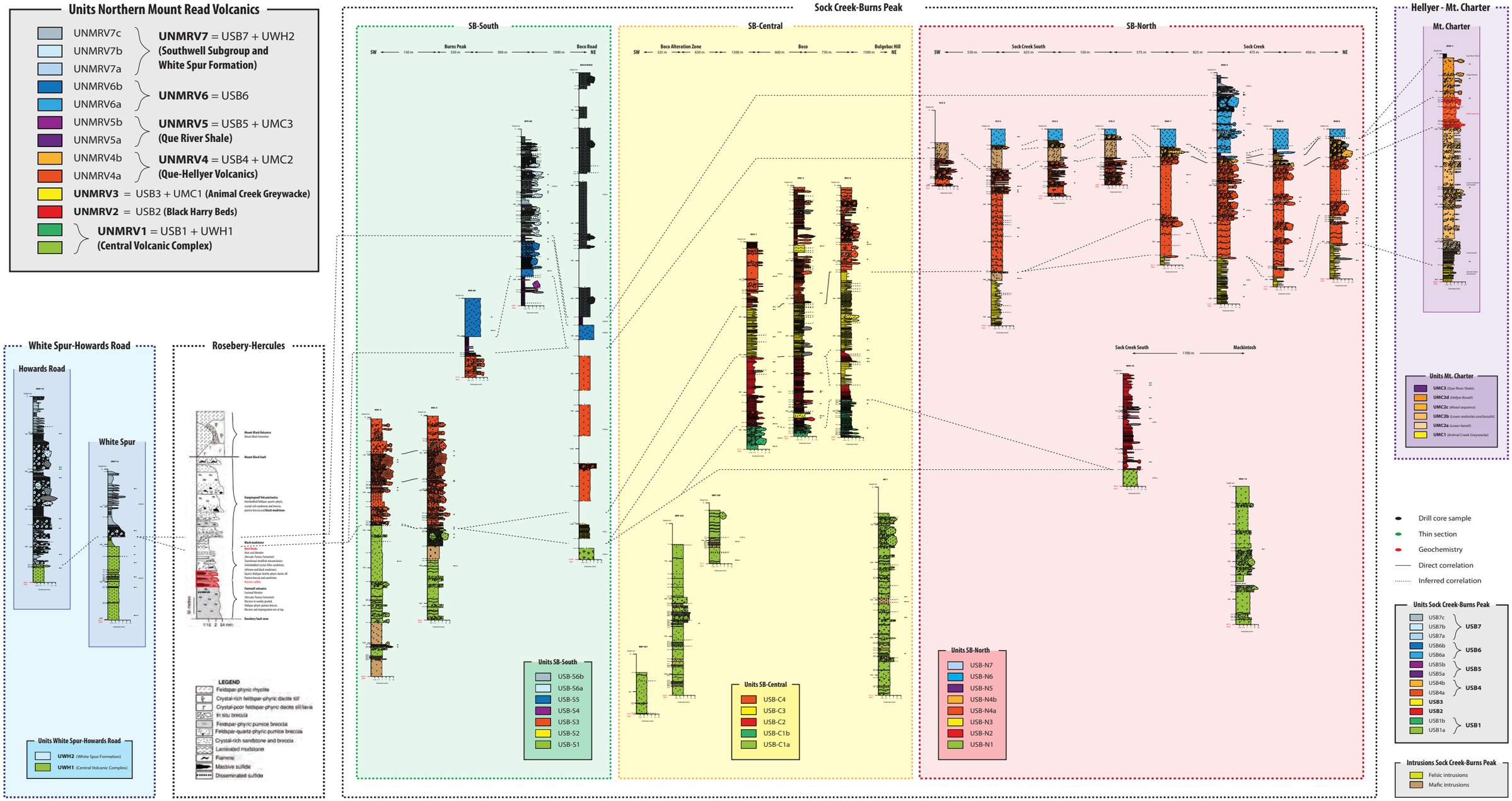

Figure 6.1: Correlation diagram of the regional stratigraphic units (UNMRV) identified in the northern Mount Read Volcanics showing the regional stratigraphic units identified in the Sock Creek-Burns Peak area (USB) and the local stratigraphic units identified in the Mount Charter (UMC) and White Spur-Howards Road (UWH) areas. Stratigraphic data and the correlation of units in the Rosebery-Hercules area has been compiled into a representative and simplified stratigraphic log after the work of Allen (1990b, 1991, 1992b, 1997), Nunn (1995) and Large et al., (2001). Unit labels are given on the right of the logs of DDH BHD-4 and BHD-10 (SB-North), BBP-209 and BOC-1 (SB-Central), BPD-80 and Boco Road (SB-South), MCH-1 (Mount Charter), and WSP-15 (White Spur). The position of the Rosebery-Hercules and Hellyer-Mount Charter VHMS deposits is highlighted in red in the Rosebery-Hercules and Mount Charter areas. See Figure 3.4 for legend to graphic logs.

Table 6.1: Summary of the facies present within the Mixed Sequence Volcaniclastics (adapted from Waters and Wallace, 1992).

Facies	Thickness	Grain size	Texture	Composition
Pvb lithotype A	1.5-8 m (beds: 1.5-8 m)	<30 cm	Open to closed framework breccias, minor grading, thickly bedded, angular to subangular framework	Framework: basaltic, dacitic, and basement derived greywacke lithics Matrix: muds (45-20%)
Pvb lithotype B				Framework: andesitic (footwall) lithics Matrix: muds (65-20%)
Ifc	0.35-1.40 m (beds: 0.5-30 cm)	<1-1.5 mm	Graded to massive, moderate to well sorted, angular framework	Framework: altered vitric fragments ± rare mafic lithics Matrix: muds (<70%)
Mvs	<15 m (beds: <4-5 m)	<2-3 mm	Massive, thickly bedded, poor to very poor sorting, subangular to angular framework, minor pebbly horizons	Framework: basaltic, andesitic, vitric, cherty lithics ± rare sulfide, and barite fragments Matrix: muds (20-25%)
Gvs	<6 m (beds: 5 cm-4 m)	<1-2 mm	Graded bedding, moderate to poor sorting, difusely laminated in places, subangular to angular framework	Framework: see Mvs Matrix: mud (5-20%)
Sh	<8 m (sst < 3-5 cm)	silt (sst <0.5 mm)	Thinly bedded, minor interbedded sandstones	Sandstones; framework: quartz

Abbreviations: Gvs = graded volcanic sandstone facies; Ifc = thinly interbedded fine and coarse volcaniclastic facies; Mvs = massive volcanic sandstone facies; Pvb = massive polymict volcanic breccia facies; Sh = thinly bedded to laminated shale facies; sst = sandstone.

Animal Creek Greywacke (Waters and Wallace, 1992). A hiatus in volcanic activity followed the emplacement of the footwall andesites and basalts and the mixed sequence volcaniclastics during which the massive sulfide mineralisation and associated hydrothermal alteration occurred. The stratigraphic position of the mixed sequence relative to the Hellyer and Que River VHMS deposits and the presence of sulfide clasts in the mixed sequence breccia indicate that the mixed sequence was deposited pre- and syn-mineralisation; weak hydrothermal alteration in the Hellyer Basalt above the Hellyer VHMS deposit indicates that the emplacement of the Hellyer Basalt occurred while the hydrothermal system was still active (Corbett and Komyshan, 1989; Gemmell and Fulton, 2001). The distribution and geometry of the mixed sequence volcaniclastics in relation to the massive sulfide deposits suggest they accumulated in possibly structurally controlled local topographic depressions. The uppermost volcaniclastic units of the mixed sequence comprise dacitic autoclastic facies resedimented from local sources, including dome-like dacitic bodies (Waters and Wallace, 1992).

Thin units of Que River Shale also accumulated during the hiatus following the QHV volcanism, burying the remaining parts of the massive sulfide mound not covered by the mixed sequence units. The presence of abundant peperite within the Hellyer Basalt provides evidence that it was emplaced as shallow sills into wet, Que River Shale-like sediment (Waters and Wallace, 1992; Tomes, 2011; this study). Deposition of the Que River Shale continued after the final phases of QHV volcanism (Waters and Wallace, 1992).

The VHMS deposits in the Hellyer-Mount Charter area are thus synchronous with the emplacement of the mixed sequence units and pre-date the deposition of the Que River Shale.

6.2.3 Rosebery-Hercules area (SSW of Sock Creek-Burns Peak)

The Rosebery-Hercules area includes VHMS deposits at Rosebery and Hercules, and a large number of small prospects, including Grand Center, Jupiter, Chamberlain, Salisbury and Black P.A. (Green et al., 1981). The Rosebery and Hercules VHMS deposits occur within the Hercules Pumice Formation (Gifkins, 2001; Gifkins and Allen, 2001), a regionally extensive unit with a strike length of at least 12 km, at the top of the CVC (Corbett, 1979, 1981, 1992). The regional geology of the Rosebery-Hercules area has been presented in section 5.5.

The Hercules Pumice Formation (Gifkins, 2001; Gifkins and Allen, 2001) comprises the lower Footwall Member (Footwall Pyroclastics), a poorly stratified succession of feldspar-phyric fiamme breccia up to 500 m thick intruded by rhyolitic and dacitic sills (Lees, 1987; Allen, 1990b; Allen 1994b; Gifkins, 2001), and the upper Host-rock Member (Host Rocks), composed of interbedded pumice-rich sandstone and siltstone approximately 5-60 m thick (Corbett and Solomon, 1989; Allen, 1991, 1994b; Gifkins, 2001). The age of the Footwall Member stands at approximately 503 Ma, whereas the age of the Host-rock Member is inferred to be approximately 500 Ma at Rosebery (Mortensen et al., 2015). The contact between the Footwall Member and the Host-rock Member is gradational from massive, monomictic feldspar-phyric fiamme breccia to stratified, locally volcanic quartz-bearing, polymictic crystal-lithic clast-rich sandstone and siltstone (Allen, 1993); at Rosebery, this facies is intruded by a rhyolitic quartz-feldspar-(biotite) porphyry sill with peperitic margins which is closely associated with the AB, P, K and PK ore lenses (Allen, 1990b, 1992, 1994a; Martin, 2004).

The Rosebery VHMS deposit includes at least twenty-one separate, broadly conformable, stratabound ore lenses that occur along a strike length of at least 3.2 km and a total vertical extent of more than 1.6 km (Large et al., 2001a; Corbett et al., 2014). The host succession to the Rosebery and Hercules VHMS deposits is presented in Figure 5.4. The stratigraphy of the Rosebery-Hercules host sequences has been presented in detail in section 5.6.

A basic subdivision of the Host-rock Member is possible based on the composition of the clastic components. The lower part of the Host-rock Member is feldspar-bearing and was formed by local re-working of the Footwall Member (Large et al., 2001a). In contrast, the upper part of the Host-rock Member is feldspar- and volcanic quartz-bearing and represents an influx of components of mixed provenance (Allen, 1991, 1992b, 1993; Martin, 2004). The Host-rock Member is conformably overlain by lenses of finely laminated black mudstone, which in turn are overlain by the Hangingwall Volcaniclastics. The Hangingwall Volcaniclastics are feldspar-quartz-phyric, and lithologically similar to and regionally correlated with the White Spur Formation (WSF; Allen, 1990b, 1991, 1994a; McPhie and Allen, 1992; Jago, 2005).

Genetic models

Several different genetic models have been proposed for the formation of the VHMS deposits in the Rosebery-Hercules area. These include: (1) exhalation of fluids and deposition on the seafloor (Brathwaite, 1974; Solomon and Walshe, 1979; Green et al., 1981; Huston and Large, 1988), (2) formation in a brine pool (Sainty, 1986; Solomon et al., 1990; Solomon and Groves, 1994), (3) epigenetic, syn-tectonic Devonian mineralisation (Aerden, 1990, 1991, 1992, 1993, 1994a, 1994b), and (4) syn-volcanic sub-seafloor replacement (Allen, 1994b; Martin, 2004).

The first and second models suggest that the ore formed from precipitation of sulfides from hot, dense, highly saline, metal-rich fluids venting at one to several closely spaced sites on the seafloor. The ore fluids gradually became denser than the surrounding seawater, allowing the rapid deposition of the suspended sulfides. Several arguments support these models, including (1) the stratiform, sheet-like nature of the ore lenses, (2) concordant, bedding parallel ore mineral bands, (3) the lack of significant hangingwall alteration, and (4) sulfur isotopes consistent with a seawater origin of the sulfur in the sulfides (Solomon et al., 1969; Brathwaite, 1974; Green et al., 1981).

The third model proposes that the ore was formed after pre-existing sulfides had been dissolved and re-precipitated in dilational zones resulting from the development of macro-scale structures during Devonian deformation and metamorphism (Aerden, 1990, 1991, 1992, 1993, 1994a, 1994b). The discordance between ore deposits and folds in the Host-rock Member at Rosebery, the discordant nature of the ore lenses at Hercules, overprinting of the regional cleavage by sulfides, replacement textures, undeformed sulfide minerals, and the apparent structural control of the position and texture of the ore on microscopic and macroscopic scales (Aerden, 1994) are all evidence that support this model.

It is intrinsic to the first and second models that the emplacement of most of the Host-rock Member occurred syn- to post-mineralisation; the third model suggests that deposition of the entire Host-rock Member pre-dated mineralisation. Allen (1994b) and Martin (2004) suggested that the Host-rock Member had been deposited prior to primary ore formation and that mineralisation occurred beneath the seafloor by a process of syn-volcanic sub-seafloor replacement. Preserved, uncompacted pumice clasts and shards in carbonate nodules associated with the ore deposits indicate that the hydrothermal system pre-dated diagenetic compaction and subsequent tectonic deformation (Allen, 1994b). Furthermore, massive sulfide clasts within the lowest unit of the Hangingwall Volcaniclastics 40 to 150 m stratigraphically above the Host-rock Member at and N of Rosebery (Bastyan Dam) and S of Hercules, and within the WSF SE of White Spur (Corbett, 1985) prove that sulfide deposits were in place prior to deposition of the Hangingwall Volcaniclastics; these clasts further suggest that mineralisation occurred close to the paleoseafloor and that the tops of the ore lenses were locally eroded (Allen, 1994b). Textural evidence from the South Hercules VHMS deposit also supports a sub-seafloor replacement origin (Khin Zaw and Large, 1992) for the Rosebery and Hercules VHMS deposits.

If the Rosebery and Hercules VHMS deposits formed at the seafloor, the emplacement of much of the Host-rock Member occurred after the deposition of the massive sulfides and before the deposition of the overlying black mudstone and Hangingwall Volcaniclastics. The alternate sub-seafloor replacement model of Allen (1994b) and Martin (2004) implies that the deposition of massive sulfides at Rosebery and Hercules post-dated the emplacement of the Host-rock Member and the quartz-feldspar-biotite-phyric rhyolitic porphyry sill. The formation of the Rosebery and Hercules VHMS deposits was probably synchronous with the deposition of most of the black mudstone and pre-dated the Hangingwall Volcaniclastics because these units contain sulfide clasts.

6.2.4 Regional correlations and implications

The Sock Creek-Burns Peak area includes the Hellyer-Que River and Rosebery-Hercules stratigraphic levels (Figure 6.1). Despite the occurrence of zinc-dominated and gold/silver-poor sulfide prospects at Sock Creek and Sock Creek South (Purvis, 1993; McNeill, 2002), the presence of the large "barren" sericite-pyrite Boco Alteration Zone (Skirka and McNeill, 2006), and minor base metals at the Hollway prospect (Skirka and McNeill, 2006), no economically significant mineral deposits have been noted in the Sock Creek-Burns Peak area (McNeill, 2001). The regional geology and stratigraphy of the Sock Creek-Burns Peak area was presented in detail in section 4.2.

6.2.4.1 Sock Creek-Burns Peak and Hellyer-Mount Charter areas

Black mudstone and minor sandstone of USB5 (Sock Creek-Burns Peak area) and UMC3 (DDH MCH-1 at Mount Charter) have been interpreted to represent the same stratigraphic level (UNMRV5) and correlate with the Que River Shale in the Hellyer-Mount Charter area (section 5.4) (Figure 6.1). The Que River Shale has been interpreted to have been deposited immediately after the formation of the seafloor VHMS deposits in the Hellyer-Mount Charter area. This constraint suggests that any potential VHMS mineralisation

(including seafloor deposition and sub-seafloor replacement) in the Sock Creek-Burns Peak area would have occurred prior to the deposition of USB5 (black mudstone facies; correlated with the Que River Shale) (Figure 6.1).

Coherent mafic facies, massive to flow-banded feldspar-phyric rhyolite and dacite, and monomictic rhyolite, dacite and mafic breccia of USB4a, and polymictic volcanic breccia and sandstone of USB4b (Sock Creek-Burns Peak area), and similar lithofacies of UMC2 (DDH MCH-1 at Mount Charter) have been interpreted to occur at the same stratigraphic level (UNMRV4) and correlate with the QHV in the Hellyer-Mount Charter area (section 5.8) (Figure 6.1). This correlation suggests that USB4 (USB4a and USB4b) in the Sock Creek-Burns Peak area is equivalent to the stratigraphy that hosts the Hellyer and Que River VHMS deposits in the Hellyer-Mount Charter area.

USB4b (exclusive in the SB-North area) consists of normally graded units of polymictic volcanic breccia and sandstone (section 3.3.4) that immediately underlie USB5 (black mudstone facies; correlated with the Que River Shale) (Figure 6.1) and have been correlated with the mixed sequence of the QHV in the Hellyer-Mount Charter area (section 5.4). This correlation suggests that the deposition of USB4b in the SB-North area (Figure 6.1) occurred immediately before to at the same time as the Hellyer and Que River VHMS deposits formed in the Hellyer-Mount Charter area. Furthermore, USB4 (Sock Creek-Burns Peak area) could potentially host VHMS deposits that formed by sub-seafloor replacement and seafloor deposition at the same time as the mixed sequence was emplaced and the Hellyer and Que River seafloor VHMS deposits formed. The deposition of USB5 (black mudstone) continued, covering USB4b and accumulating in the SB-North area (Figure 6.1).

6.2.4.2 Sock Creek-Burns Peak and Rosebery-Howards Road areas

Massive to flow-banded rhyolite and dacite and monomictic rhyolite and dacite breccia of USB1 (Sock Creek-Burns Peak area) and UWH1 (White Spur-Howards Road area), and feldspar-phyric fiamme breccia of the Hercules Pumice Formation (Gifkins, 2001) (Rosebery-Hercules area) have been interpreted to represent the same stratigraphic level (UNMRV1) and correlate with the upper part of the CVC (section 5.8) (Figure 6.1). The top of USB1 is therefore the stratigraphic level in the Sock Creek-Burns Peak area equivalent to the stratigraphic level at which the Rosebery and Hercules VHMS deposits occur.

Graded feldspar- and volcanic quartz-bearing polymictic rhyolite breccia and sandstone and crystal-rich sandstone units of USB7 (Sock Creek-Burns Peak area), and very similar graded units of the Hangingwall Volcaniclastics (Rosebery-Hercules area) and UWH2 (DDH WSP-14 and WSP-15 in the White Spur-Howards Road area) have been interpreted to represent the same stratigraphic level (UNMRV7) and correlate with the lower part of the WSF (section 5.8) (Figure 6.1). The emplacement of the Hangingwall Volcaniclastics (correlated with the WSF) has been interpreted to have been later than the formation of the Rosebery and Hercules VHMS deposits (section 6.2.3; Corbett, 1985; Allen, 1994b; Martin, 2004), suggesting that the deposition of USB7 (correlated with the WSF) in the Sock Creek-Burns Peak area post-dated the formation of the Rosebery and Hercules VHMS deposits.

6.2.4.3 Implications on the timing and setting of VHMS formation

Genetic models involving the exhalation of fluids and deposition on the seafloor, or formation in a brine pool for the formation of the Rosebery and Hercules VHMS deposits imply that massive sulfide precipitation occurred after the deposition of the Footwall Member (Footwall Pyroclastics) and before the deposition of much of the Host-rock Member. It has been interpreted that the emplacement of USB1 (coherent rhyolite and dacite, and monomictic rhyolite and dacite breccia facies; correlated with the upper CVC) in the Sock Creek-Burns Peak area (Figure 6.1) occurred more or less synchronously with the deposition of the Footwall Member. This interpretation leads to the conclusion that the Rosebery and Hercules VHMS deposits formed before the emplacement of USB4 (coherent mafic facies, coherent feldspar-phyric rhyolite and dacite, and monomictic rhyolite, dacite and mafic facies; correlated with the QHV) in the Sock Creek-Burns Peak area (Figure 6.1) and before the VHMS-hosting mixed sequence of the QHV in the Hellyer-Mount Charter area. In other words, the Rosebery and Hercules VHMS deposits are both stratigraphically lower and older than the VHMS deposits in the Hellyer-Mount Charter area.

In a syn-volcanic, sub-seafloor replacement model for the formation of the Rosebery and Hercules VHMS deposits, massive sulfide formation was synchronous with the deposition of the black mudstone, and pre-dated the deposition of the overlying Hangingwall Volcaniclastics (equivalent to the WSF) in the Rosebery-Hercules area. The formation of the Rosebery and Hercules VHMS deposits was also probably synchronous with the deposition of USB4b (polymictic volcanic breccia and sandstone facies; correlated with the mixed sequence of the QHV) and pre-dated the deposition of USB7 (polymictic rhyolite breccia and sandstone facies; correlated with the WSF) in the Sock Creek-Burns Peak area (Figure 6.1).

It has been interpreted that the deposition of USB5 (black mudstone facies; correlated with the Que River Shale) occurred immediately after the emplacement of USB4b (polymictic volcanic breccia and sandstone facies; correlated with the mixed sequence of the QHV) in the Sock Creek-Burns Peak area (Figure 6.1). This means that massive sulfide formation by syn-volcanic, sub-seafloor replacement within the Host-rock Member at Rosebery and Hercules would have occurred roughly at the same time as the deposition of USB4b in the Sock Creek-Burns Peak area and the VHMS-hosting mixed sequence of the QHV in the Hellyer-Mount Charter area (Figure 6.1).

The genetic models of Allen (1994b) and Martin (2004) for VHMS mineralisation by syn-volcanic, sub-seafloor replacement in the Rosebery-Hercules area, combined with the local and regional correlations established in this study, imply that the Rosebery, Hercules, Hellyer and Que River VHMS deposits are broadly contemporaneous and formed before the deposition of black mudstone (USB5 in the Sock Creek-Burns Peak area, Que River Shale in the Hellyer-Mount Charter area), but partly synchronous with black mudstone in the Rosebery-Hercules area. This mineralisation time interval coincided with the emplacement of USB4b (polymictic volcanic breccia and sandstone facies; correlated with the mixed sequence of the QHV; equivalent to USB-N4b in the SB-North area) in the Sock Creek-Burns Peak area (Figure 6.1). Fossil

(Gee et al., 1970; Jago, 1977; Laurie et al., 1995) and absolute (Mortensen et al., 2015) ages support these correlations and interpretations.

It is assumed in this thesis that the Rosebery and Hercules VHMS deposits formed by syn-volcanic, sub-seafloor replacement (Allen, 1194b; Martin, 2004).

6.2.5 Summary

Mineralisation in the Hellyer-Mount Charter area (NE of Sock Creek Burns Peak) occurs within the mixed sequence of the QHV (Mount Charter Group). The age of the Hellyer and Que River VHMS deposits stands between 500.4 ± 0.9 Ma (footwall andesite) and 499.3 ± 0.9 Ma (rhyolite sill intruding the Que River Shale) (Mortensen et al., 2015). Fossils within the Que River Shale, which overlies the QHV, indicate a late Middle Cambrian Floran-Undillan age (E. opimus Zone to P. punctuosus Zone) (Gee et al., 1970; Jago, 1977; Laurie et al., 1995). The Rosebery and Hercules VHMS deposits are hosted by the Host-rock Member of the Hercules Pumice Formation (upper CVC). The age of the Host-rock Member is inferred to be approximately 500 Ma at Rosebery (Mortensen et al., 2015). In both the Hellyer-Mount Charter and Rosebery-Hercules areas, VHMS deposits occur stratigraphically below black mudstone units (Que River Shale and black mudstone, respectively). These two black mudstone units have been correlated with USB5 (black mudstone facies; section 3.3.5) in the Sock Creek-Burns Peak area.

Correlations in the Sock Creek-Burns Peak area and the area to the NE (Hellyer-Mount Charter) suggest that USB4b (polymictic volcanic breccia and sandstone facies; correlated with the mixed sequence of the QHV) represents the stratigraphic level in the Sock Creek-Burns Peak area that could potentially host seafloor, Hellyer-Que River-like VHMS deposits (Figures 6.2 and 6.3). Correlations in the Sock Creek-Burns Peak area and the area to the SSW (Rosebery-Howards Road) suggest that the volcanic succession below the top of USB4b (polymictic volcanic breccia and sandstone facies; correlated with the mixed sequence of the QHV) represents the stratigraphic level in the Sock Creek-Burns Peak area that could potentially host sub-seafloor, Rosebery-Hercules-like VHMS deposits (Figures 6.2 and 6.3). The later interpretation is correct only if the mineralisation at Rosebery and Hercules occurred by sub-seafloor replacement (Allen, 1994b; Martin, 2004).

Assuming that a syn-volcanic, sub-seafloor replacement model (Allen, 1994b; Martin, 2004) best accounts for the formation of the Rosebery and Hercules VHMS deposits, the emplacement of USB4b (polymictic volcanic breccia and sandstone facies, correlated with the mixed sequence of the QHV) in the Sock Creek-Burns Peak North (SB-North) area is inferred to have occurred (1) partly at the same time as the deposition of black mudstone in the Rosebery-Howards Road area and (2) before the initial stage of deposition of black mudstone in the Sock Creek-Burns Peak (USB5) and Hellyer-Mount Charter (Que River Shale) areas. The emplacement of USB4b occurred immediately before, to at the same time as, the main mineralising event during which the Rosebery and Hercules sub-seafloor, and Hellyer and Que River seafloor VHMS deposits formed.

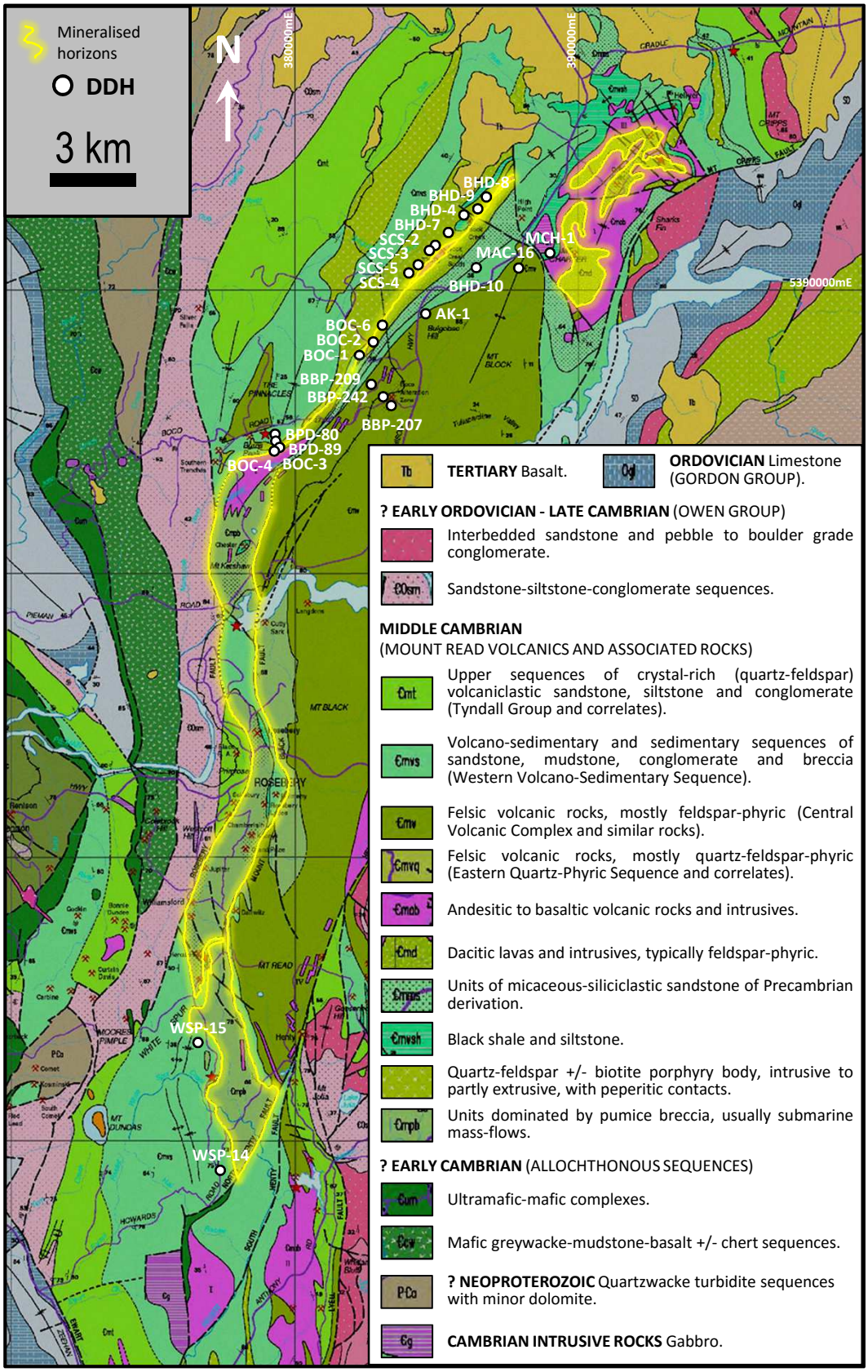

Figure 6.2: Bedrock geological map of the northern Mount Read Volcanics, showing the location of the diamond drill holes (DDH) and interpreted mineralised horizons in this study, after Corbett (2002).

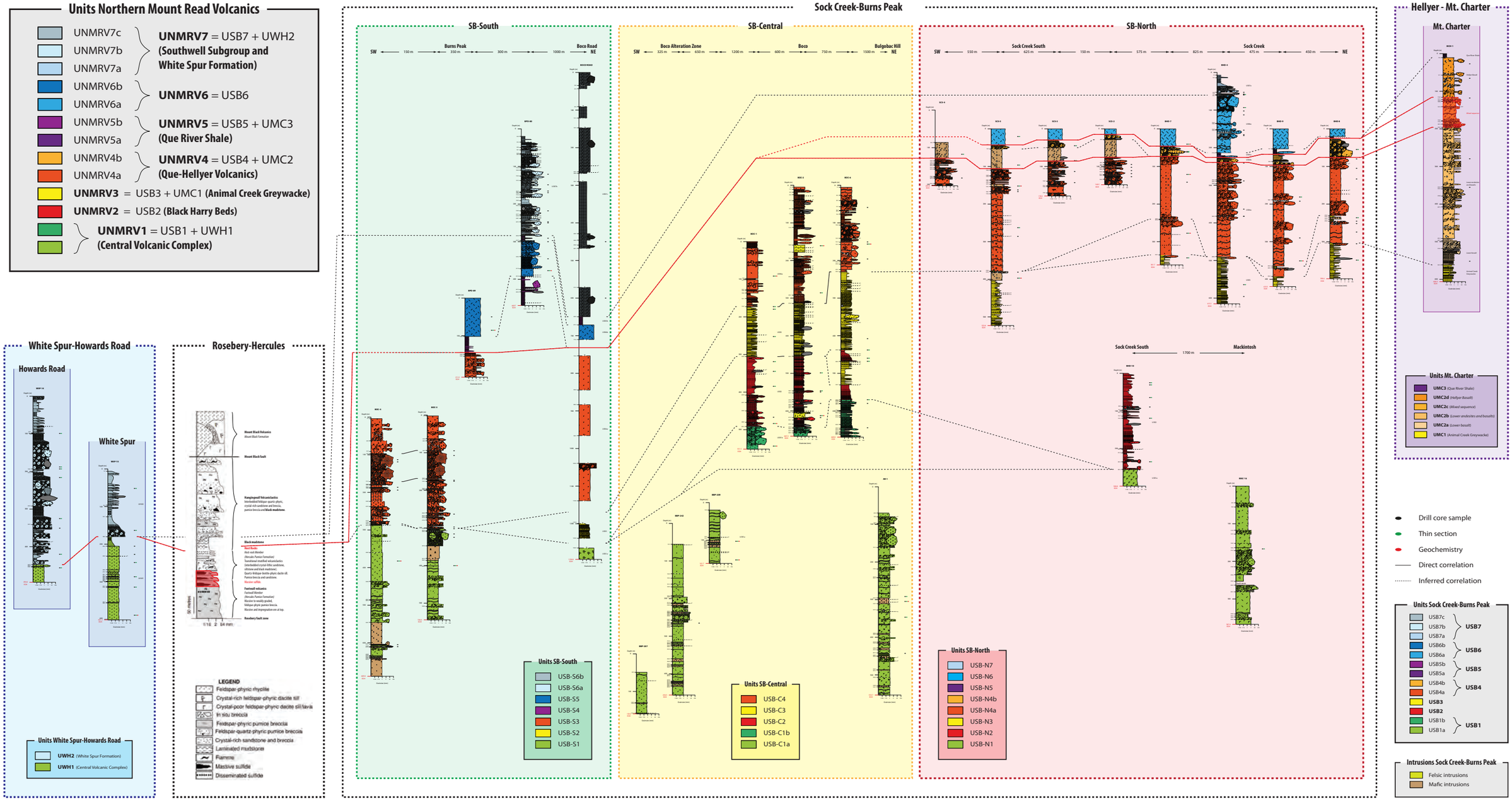

Figure 6.3: Correlation diagram of the regional stratigraphic units (UNMRV) identified in the northern Mount Read Volcanics showing the regional stratigraphic units identified in the Sock Creek-Burns Peak area (USB), the local stratigraphic units identified in the Mount Charter (UMC) and White Spur-Howards Road (UWH) areas, and the interpreted positions of the mineralised horizons. Stratigraphic data and the correlation of units in the Rosebery-Hercules area has been compiled into a representative and simplified stratigraphic log after the work of Allen (1990b, 1991, 1992b, 1997), Nunn (1995) and Large et al., (2001). Unit labels are given on the right of the logs of DDH BHD-4 and BHD-10 (SB-North), BBP-209 and BOC-1 (SB-Central), BPD-80 and Boco Road (SB-South), MCH-1 (Mount Charter), and WSP-15 (White Spur). The position of the Rosebery-Hercules and Hellyer-Mount Charter VHMS deposits is highlighted in red in the Rosebery-Hercules and Mount Charter areas. See Figure 3.4 for legend to graphic logs.

6.3 Paleogeography and mineralisation reconstruction of the northern Mount Read Volcanics

6.3.1 Introduction

The paleogeography and mineralisation reconstruction of the Sock Creek-Burns Peak area and the areas to the NE (Hellyer-Mount Charter) and SSW (Rosebery-Howards Road) are interpreted assuming the syn-volcanic, sub-seafloor replacement models of Allen (1994b) and Martin (2004) for the formation of the Rosebery and Hercules VHMS deposits. An alternative scenario for the paleogeography and mineralisation reconstruction of the northern Mount Read Volcanics based on the genetic models of Brathwaite (1974), Solomon and Walshe (1979), Green et al. (1981), Sainty (1986), Huston and Large (1988), Solomon et al. (1990), and Solomon and Groves (1990) for the formation of the Rosebery and Hercules VHMS deposits by exhalation of fluids and deposition on the seafloor is presented in section 6.3.5.

The paleogeography and mineralisation reconstruction proposed below are based on the characteristics and interpretations of the facies and facies associations (Chapter 3) and on the local and regional correlations (Chapters 4 and 5) discussed in previous chapters, and supported by cartoon diagrams and the regional correlation diagram of the DDH logged in this study (Figure 6.1). Syn-volcanic intrusions (e.g., sills/dykes and cryptodomes associated with peperite) and partly extrusive cryptodomes have been included in the eight-stage reconstruction discussed below. Post-volcanic intrusions occur in the Sock Creek-Burns Peak area and have been considered earlier (section 4.4).

6.3.2 Pre-mineralisation reconstruction of the northern Mount Read Volcanics

Stage 1: Major rhyolitic explosive eruption, felsic dome and lava complexes

Stage 1 (Figure 6.4) matches the emplacement of the CVC in the Sock Creek-Burns Peak (Figure 6.4 - B) and Rosebery-Howards Road areas (Figure 6.4 - A). In the Hellyer-Mount Charter area (Figure 6.4 - C), the CVC is only inferred to exist based on Pemberton et al. (1991) and DDH that intersect the CVC SW of Mount Charter (DDH BHD-10 and MAC-16; McNeill, 1989; Stewart, 2009; this thesis). This stage involved the growth of a large volcanic complex comprising overlapping feldspar-phyric rhyolitic to dacitic and minor feldspar-quartz-phyric rhyolitic lavas, domes and minor cryptodomes in the Sock Creek-Burns Peak area (USB1a; Figure 6.4 - B), and feldspar-phyric rhyolitic lavas and domes in the White Spur-Howards Road area (UWH1; Figure 6.4 - A). In the White Spur area, minor polymictic rhyolite sandstone was resedimented from the margins of the rhyolitic lavas and domes by density currents (Figure 6.1 - DDH WSP-15; Figure 6.4 - A).

In the Rosebery-Hercules area, very thick, poorly stratified, feldspar-phyric, rhyolitic pumiceous, explosive eruption-fed mass flow units (Footwall Member of the Hercules Pumice Formation, Gifkins, 2001) were rapidly emplaced on the seafloor (Figure 6.4 - A). Abundant, fine pyroclasts including pumice clasts, shards and feldspar crystals were temporarily suspended in the water column and began to settle. The Footwall

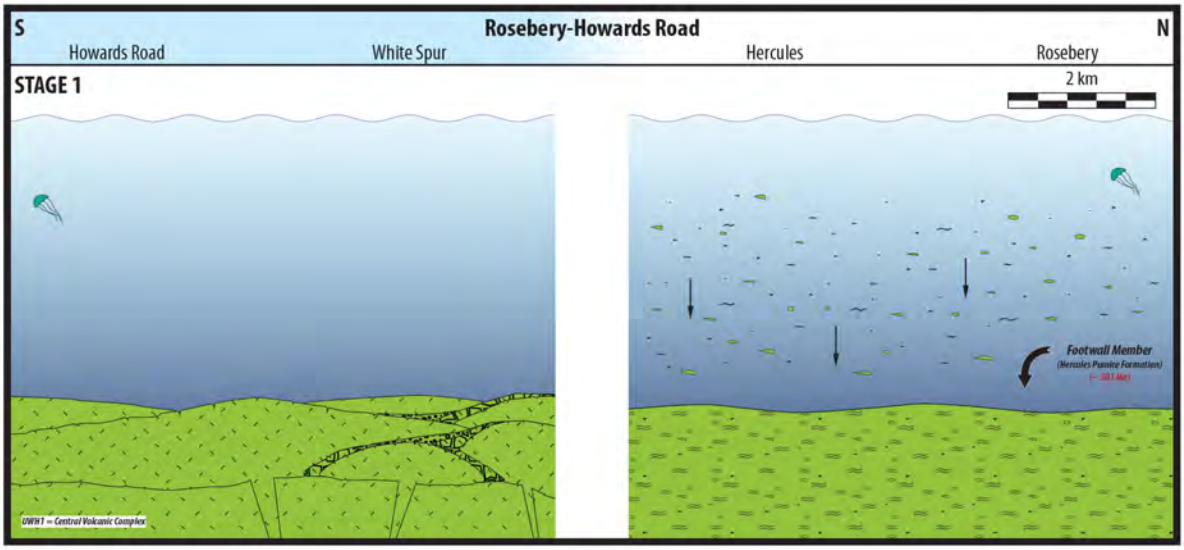

A: Rosebery-Howards Road area

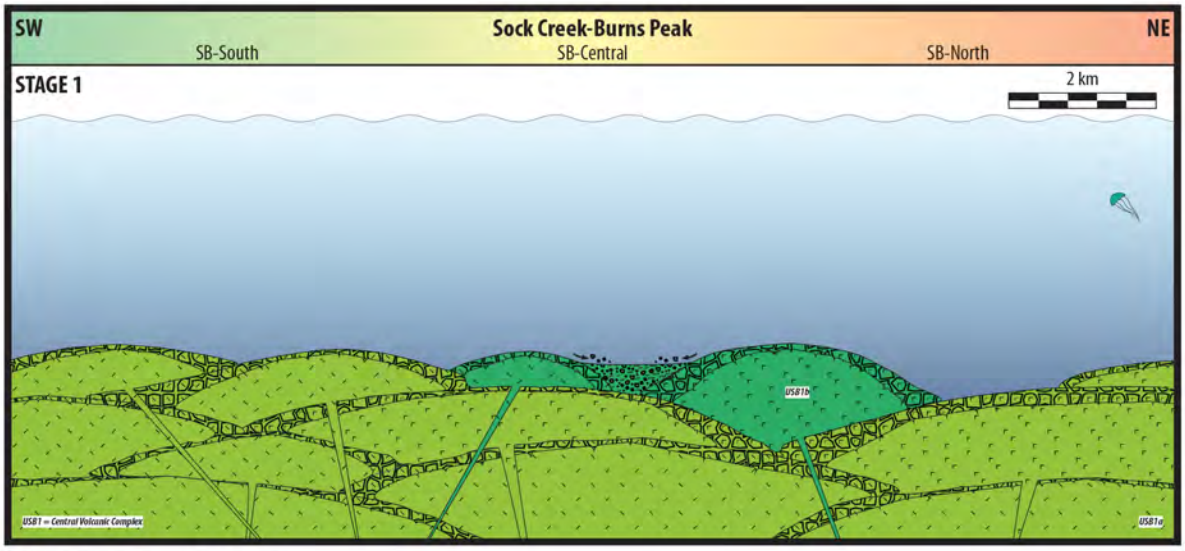

B: Sock Creek-Burns Peak area

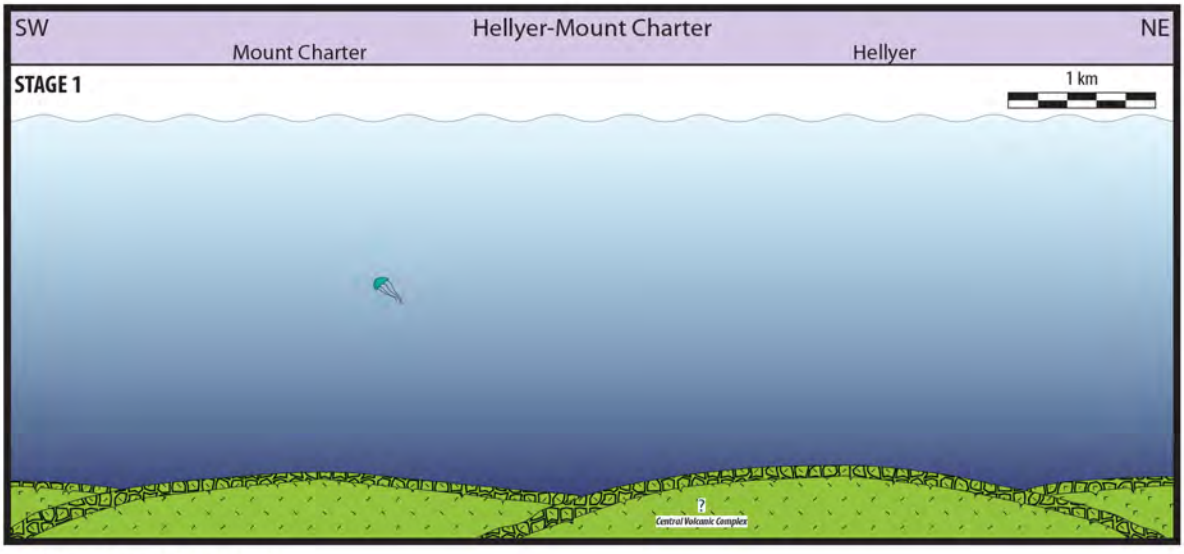

C: Hellyer-Mount Charter area

Figure 6.4: Stage 1 reconstruction diagrams. (CA) ID-TIMS U-Pb age in red from Mortensen et al. (2015).

Member of the Hercules Pumice Formation (Gifkins, 2001) is presently accepted to have been emplaced at approximately 503 Ma (Mortensen et al., 2015).

Later in stage 1, feldspar-quartz-phyric rhyolitic and feldspar-phyric dacitic lavas and domes erupted in the SB-Central area (USB1b; Figure 6.4 - B), and the associated autobreccia and hyaloclastite were resedimented down slope. Syn- to post-eruptive polymictic felsic breccia and sandstone were deposited from density currents derived from the rhyolitic to dacitic volcanic complex.

The intrusive versus extrusive nature of many rhyolites and dacites within the CVC in the Sock Creek-Burns Peak area (USB1a; Figure 6.4 - B) has not been resolved, as the textures and contact relationships are commonly ambiguous in drill core. The paucity of other volcano-sedimentary units (e.g., black mudstone, polymictic volcanic sandstone) and the thicknesses (up to 500 m) imply that the rhyolite and dacite units either accumulated rapidly from adjacent vents or fissures, or that they constructed significant topography, which strongly limited sedimentation.

Stage 2: Syn- to post-eruptive suspension sedimentation and density currents

During stage 2 (Figure 6.5), widespread deposition of fine pyroclasts derived from post-eruptive suspension sedimentation subsequent to the major rhyolitic explosive eruption (stage 1) occurred in the Rosebery-Howards Road area (Figure 6.5 - A). The Host-rock Member of the Hercules Pumice Formation (Gifkins, 2001) began accumulating (Figure 6.5 - A). The Host-rock Member includes components derived by water-settling from suspension, reworking and redeposition of freshly erupted local pyroclastic debris, and quartz-bearing volcaniclastic turbidity current deposits generated at distal rhyolitic volcanic centres (Allen, 1990b, 1991, 1994a; Gifkins and Allen, 2001; Large et al., 2001a).

The Black Harry Beds (BHB) were emplaced from density currents in the SB-North and SB-Central areas (USB2; Figure 6.5 - B), and Hellyer-Mount Charter area (Figure 6.5 - C). The density currents were volcanic quartz-bearing and probably partly explosive eruption-fed because the deposits contain abundant shards. The presence of basement-derived fragments (schist, phyllite and quartzite) suggests that the currents originated within exposed metamorphic basement at the basin margin.

Stage 3: Uplift, basement-derived density currents and suspension sedimentation

Stage 3 (Figure 6.6) involves the deposition of the Animal Creek Greywacke in the Sock Creek-Burns Peak (USB3; Figure 6.6 - B) and Mount Charter (UMC1; Figure 6.6 - C) areas. This unit comprises abundant metamorphic fragments (muscovite, biotite, quartzite and schist) interpreted to have been derived from erosion of exposed basement at the basin margin. Detrital chromite within the Animal Creek Greywacke indicates that obduction of the mafic-ultramafic complexes (Berry and Crawford, 1988; Crawford and Berry, 1992) had occurred and that one or more of these complexes were being eroded. The density currents that deposited this unit were probably generated by slope failure associated with tectonic earthquakes or movement along syn-depositional faults.

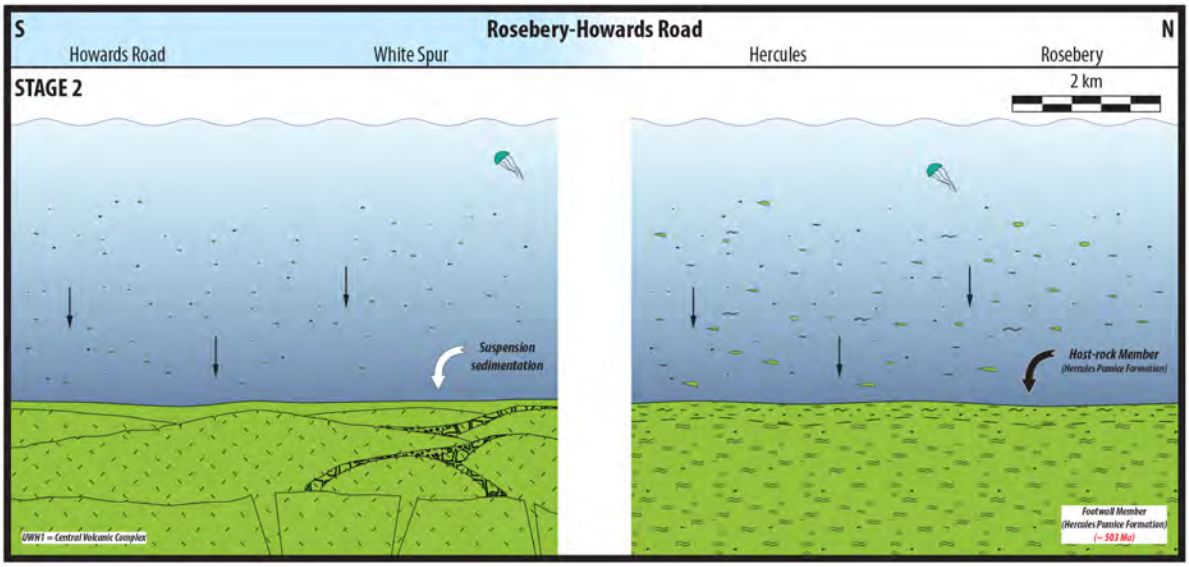

A: Rosebery-Howards Road area

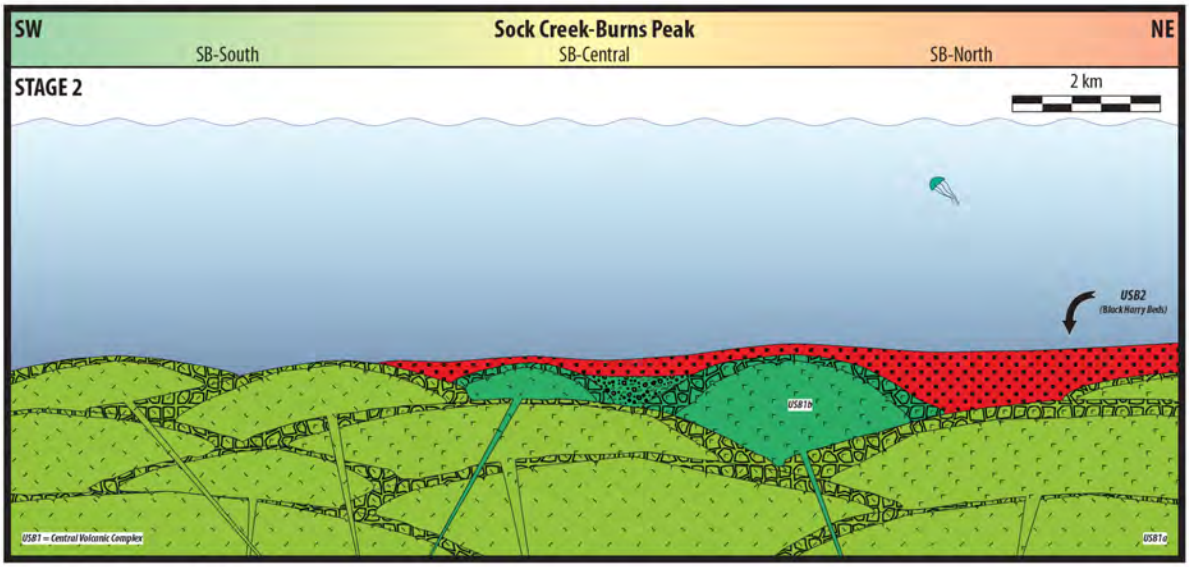

B: Sock Creek-Burns Peak area

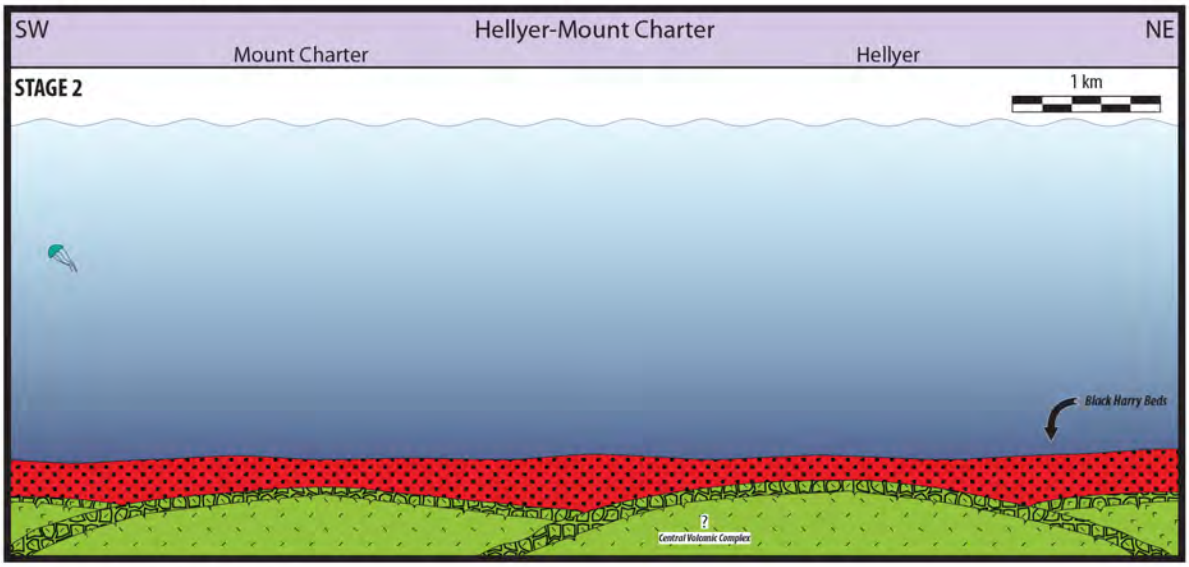

C: Hellyer-Mount Charter area

Figure 6.5: Stage 2 reconstruction diagrams. (CA) ID-TIMS U-Pb age in red from Mortensen et al. (2015).

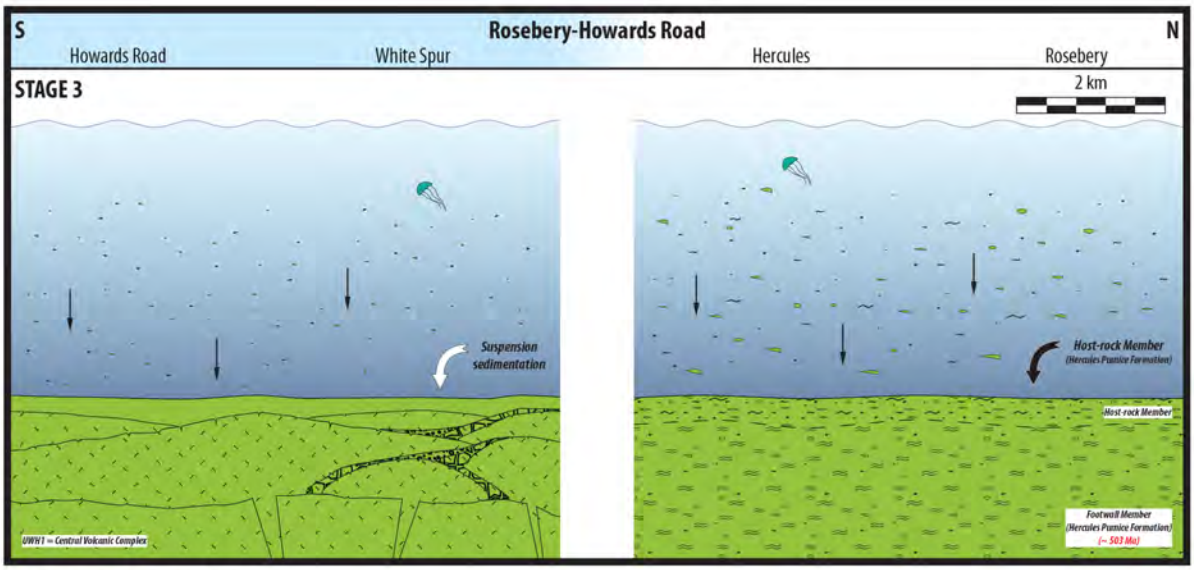

A: Rosebery-Howards Road area

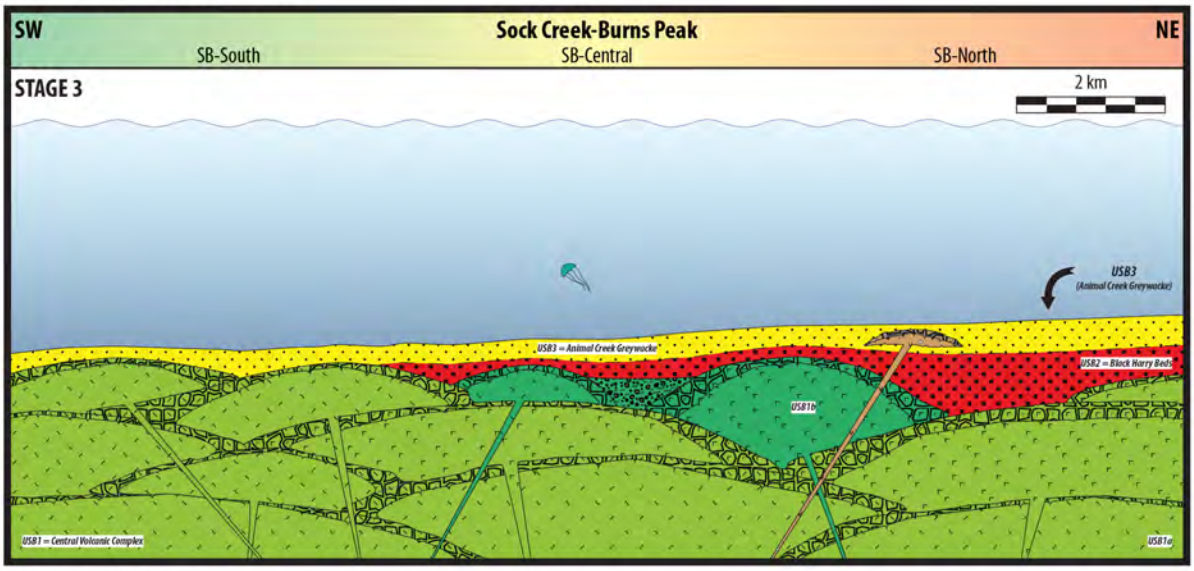

B: Sock Creek-Burns Peak area

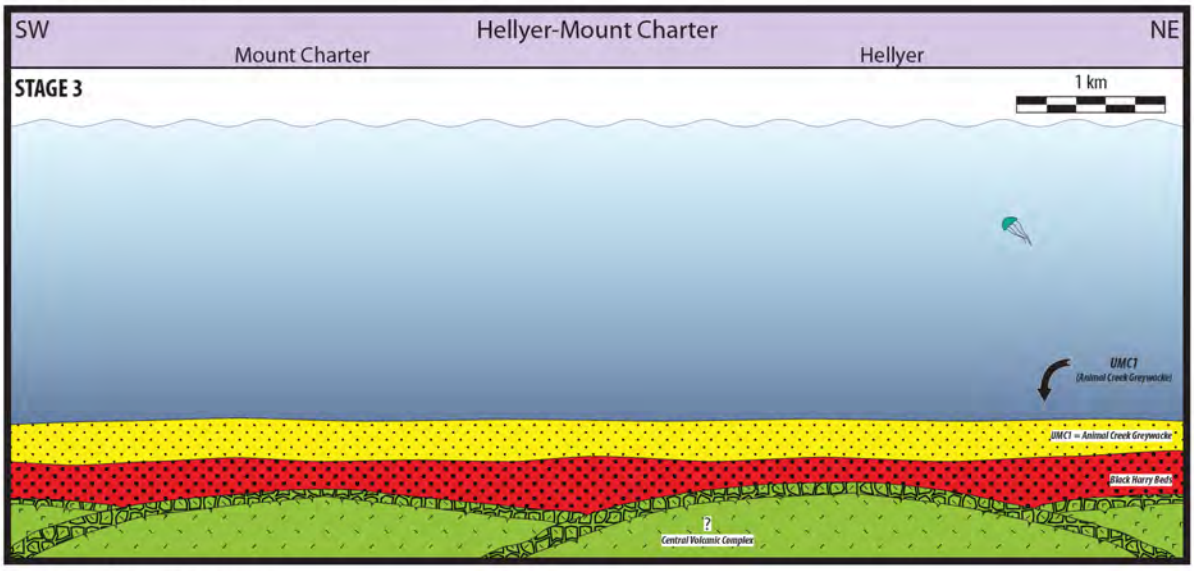

C: Hellyer-Mount Charter area

Figure 6.6: Stage 3 reconstruction diagrams. (CA) ID-TIMS U-Pb age in red from Mortensen et al. (2015).

In the Sock Creek South area (Figure 6.6 - B), the Animal Creek Greywacke was intruded by a feldspar-pyroxene-phyric mafic sill/dyke at the end of stage 3. The presence of monomictic mud-matrix mafic breccia facies (interpreted as peperite - section 3.3.3.10) at the top contact indicates that the Animal Creek Greywacke was unlithified when intruded. The mafic intrusion matches both suite III (calc-alkaline and shoshonitic) and IV (tholeiitic) of Crawford et al. (1992) (Figure 3.1; Table 3.2; DDH SCS-5, 397.0 m).

Post-eruptive suspension sedimentation continued in the Rosebery-Howards Road area (Figure 6.6 - A). In the Rosebery-Hercules area, the Host-rock Member continued accumulating from suspension sedimentation and turbidity currents.

Stage 4: Intrabasinal rhyolitic to basaltic effusive volcanism

Stage 4 (Figure 6.7) encompasses the emplacement of the QHV in the Hellyer-Mount Charter area (UMC2a and UMC2b; Figure 6.7 - C) and its correlates in the Sock Creek-Burns Peak area (USB4a; Figure 6.7 - B). Partly extrusive feldspar-phyric rhyolitic to dacitic cryptodomes, andesitic lavas and domes, and minor basaltic facies were emplaced on the seafloor in the Sock Creek-Burns Peak area, contemporaneous with the lower basalt and lower andesites and basalts of the QHV in the Hellyer-Mount Charter area. An andesite breccia collected from the lower andesites and basalts, approximately 100 m below the mixed sequence, yielded an age of 500.4 ± 1.0 Ma (Mortensen et al., 2015) (Figure 6.7 - C). Basaltic lava fountaining from vents in the Burns Peak area produced monomictic fluidal-clast breccia during extrusion of the Hollway Andesite (Figure 6.7 - B), contemporaneous with eruption of the Boco Road Dacite at Boco Road (McNeill, 2002b; McIntyre, 2006).

The Host-rock Member of the Hercules Pumice Formation (Gifkins, 2001) continued accumulating in the Rosebery-Hercules area (Figure 6.7 - A), and deposition of black mudstone occurred in places in the Rosebery-Howards Road area. A quartz-feldspar-(biotite) rhyolitic porphyry sill was intruded at Rosebery at the end of stage 4. The best estimate for the crystallization age of the rhyolite sill is presently accepted to be 499.4 ± 0.9 Ma (Mortensen et al., 2015).

6.3.3 Syn-mineralisation reconstruction of the northern Mount Read Volcanics

Stage 5: Formation of VHMS deposits at and below the seafloor

In the beginning of stage 5 (Figure 6.8), volcanic quartz-bearing polymictic volcanic breccia and sandstone facies derived from partly explosive eruption-fed density currents were deposited exclusively in the SB-North area (USB4b; Figure 6.8 - B) while the mixed sequence (dacitic to basaltic domes and lavas, monomictic dacitic to basaltic breccia, polymictic breccia and sandstone, and minor mudstone; Corbett and Komyshan, 1989) of the QHV was accumulating in the Hellyer-Mount Charter area (UMC2c; Figure 6.8 - C). Deposition of black mudstone occurred in the Rosebery-Howards Road area (Figure 6.8 - A).

The Rosebery and Hercules sub-seafloor and the Hellyer and Que River seafloor VHMS deposits formed during this stage, at approximately 500 Ma (Mortensen et al., 2015). In the Rosebery-Hercules area (Figure

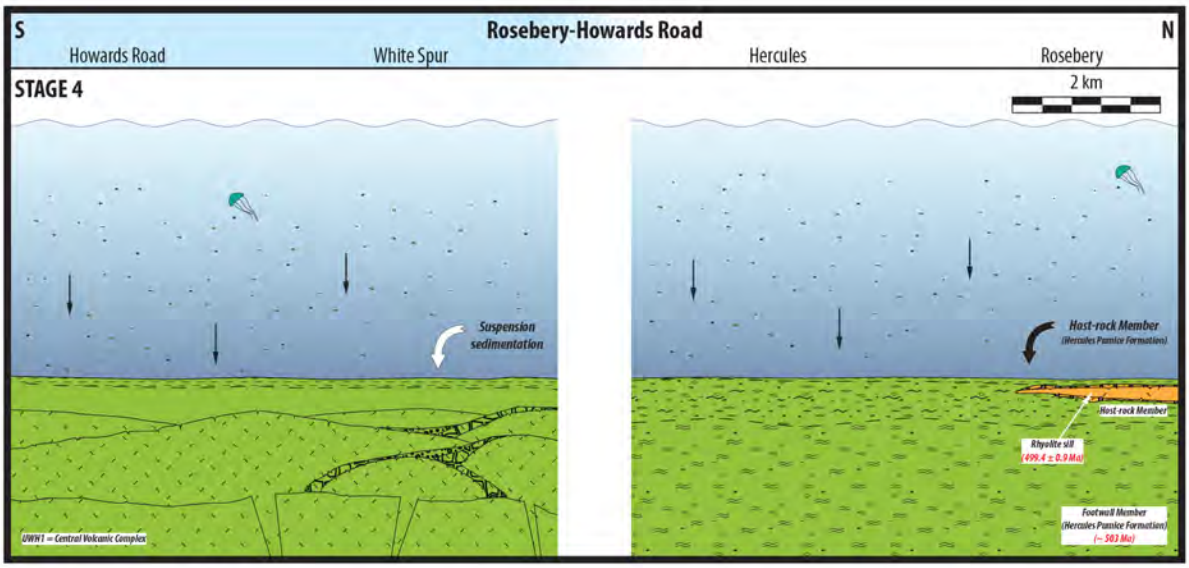

A: Rosebery-Howards Road area

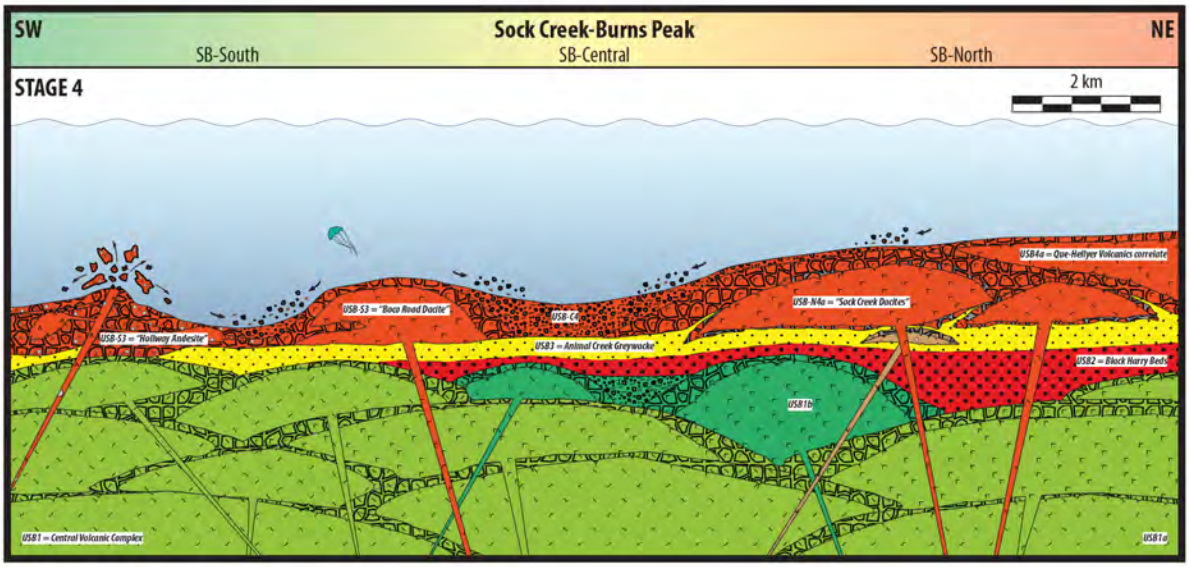

B: Sock Creek-Burns Peak area

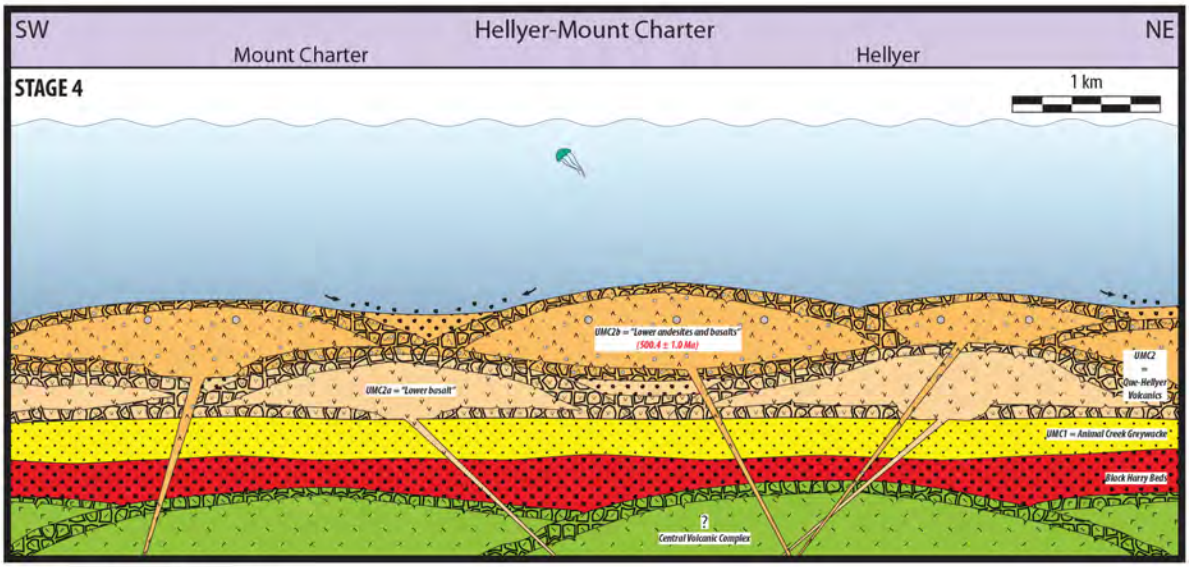

C: Hellyer-Mount Charter area

Figure 6.7: Stage 4 reconstruction diagrams. (CA) ID-TIMS U-Pb ages in red from Mortensen et al. (2015).

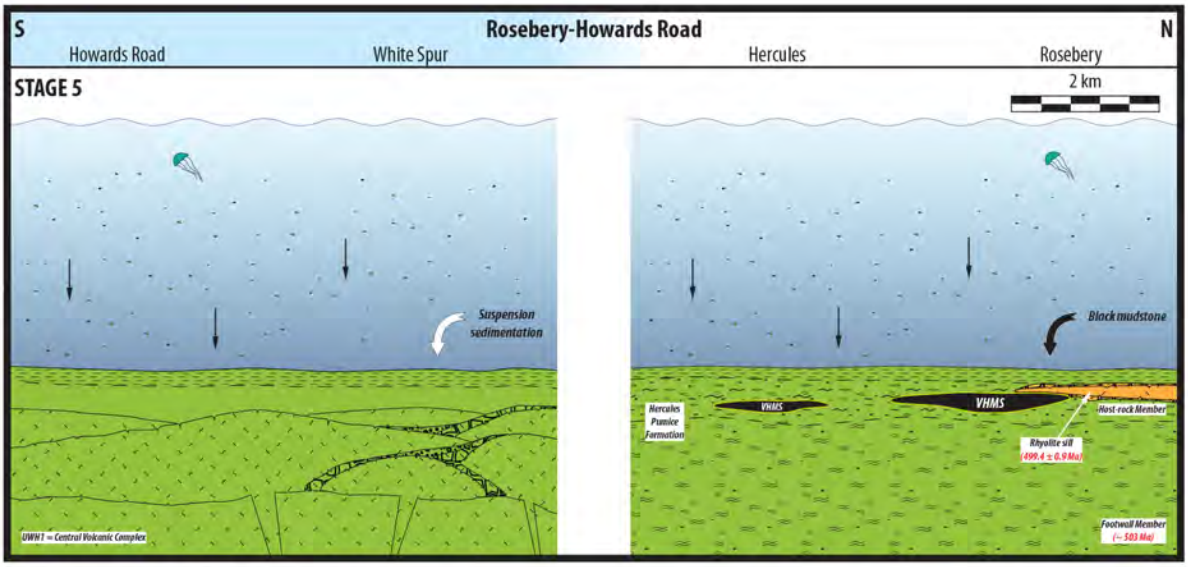

A: Rosebery-Howards Road area

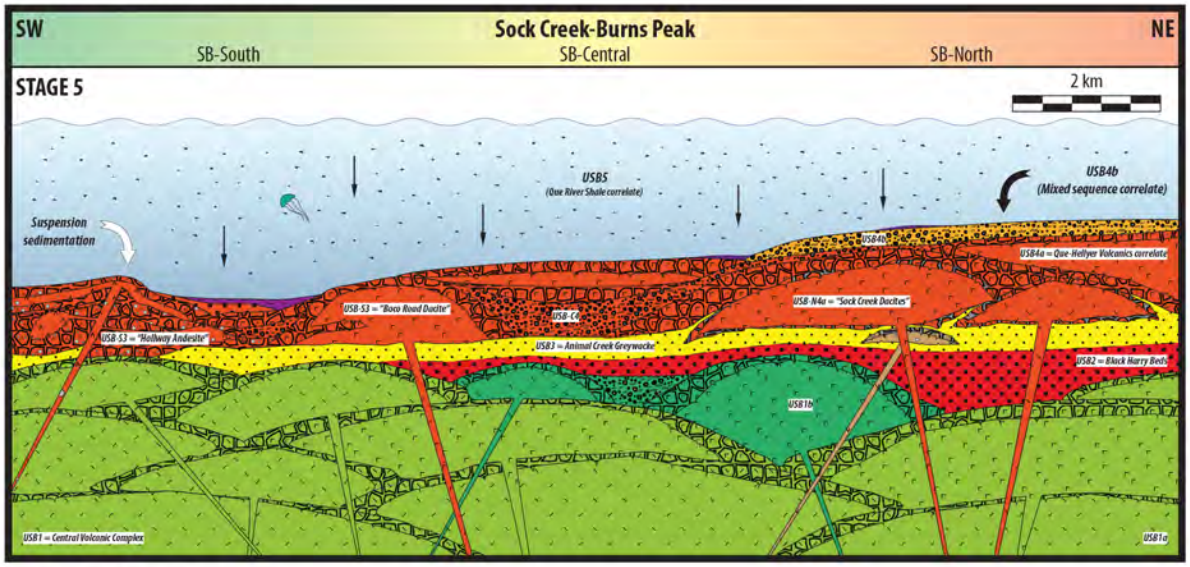

B: Sock Creek-Burns Peak area

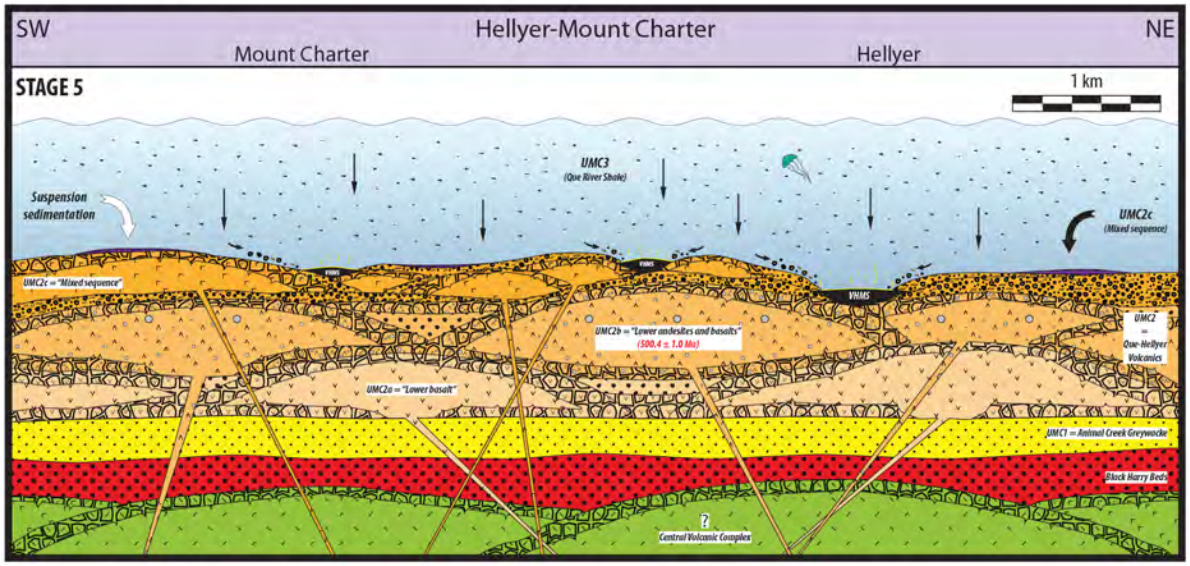

C: Hellyer-Mount Charter area

Figure 6.8: Stage 5 reconstruction diagrams. (CA) ID-TIMS U-Pb ages in red from Mortensen et al. (2015).

6.8 - A), the Rosebery and Hercules VHMS deposits formed by sub-seafloor replacement at the same time as black mudstone was being deposited higher in the stratigraphy; the VHMS deposits in the Hellyer-Mount Charter area (Figure 6.8 - C) formed synchronously to immediately after the emplacement of the mixed sequence of the QHV, and before the deposition of the Que River Shale. This correlation means that the base of the black mudstone in the Rosebery-Hercules area is probably older than the base of the Que River Shale in the Hellyer-Mount Charter area, which suggests that the lower part of the black mudstone in the Rosebery-Hercules area is probably contemporaneous with the mixed sequence of the QHV in the Hellyer-Mount Charter area (Figure 6.8 - A and C). Hence, the base of the black mudstone in the Rosebery-Hercules area and the base of the Que River Shale in the Hellyer-Mount Charter area are excellent lithological markers, but probably diachronous.

Deposition of black mudstone continued in the Rosebery-Hercules area and started in the Sock Creek-Burns Peak (USB5; correlated with the Que River Shale) and Hellyer-Mount Charter (Que River Shale) areas at the end of stage 5 (Figure 6.8 - B and C).

Stage 6: Regional deposition of black mudstone

Stage 6 (Figure 6.9) was a basin-wide period of volcanic quiescence during which black mudstone accumulated (black mudstone in the Rosebery-Hercules area, Figure 6.9 - A; USB5 in the Sock Creek-Burns Peak area, Figure 6.9 - B; Que River Shale in the Hellyer-Mount Charter area, Figure 6.9 - C).

6.3.4 Post-mineralisation reconstruction of the northern Mount Read Volcanics

Stage 7: Partly extrusive rhyolite cryptodomes

Stage 7 (Figure 6.10) involved the emplacement of two partly extrusive feldspar-quartz-phyric rhyolite cryptodomes (USB6a and USB6b; Figure 6.10 - B) into and onto black mudstone (USB5; Figure 6.10 - B) in the Sock Creek and Burns Peak areas. These partly extrusive rhyolite cryptodomes contain peperite, implying that USB5 (black mudstone; Figure 6.10 - B) was still unconsolidated when intruded. Geochemical analyses of two samples of the rhyolite in the Burns Peak area, one from DDH BPD-80 (377.4 m) and one from DDH BPD-89 (85.5 m) (Figure 3.1; Table 3.2), indicate that they match suite I (calc-alkaline) of Crawford et al. (1992), and suggest they could be related. Black mudstone was still accumulating in the Rosebery-Howards Road (Figure 6.10 - A), Sock Creek-Burns Peak (USB5; Figure 6.10 - B), and Hellyer-Mount Charter (Figure 6.10 - C) areas.

Stage 8: Rhyolitic explosive eruption, syn- and post-eruptive density currents, and intrusion of the Hellyer Basalt

In the beginning of stage 8 (Figure 6.11), the Hellyer Basalt (UMC2d; coherent feldspar-phyric mafic facies, monomictic mafic breccia and sandstone, and monomictic mud-matrix mafic breccia facies; Corbett and Komyshan, 1989) intruded the Que River Shale in the Hellyer-Mount Charter area (Figure 6.11 - C). The

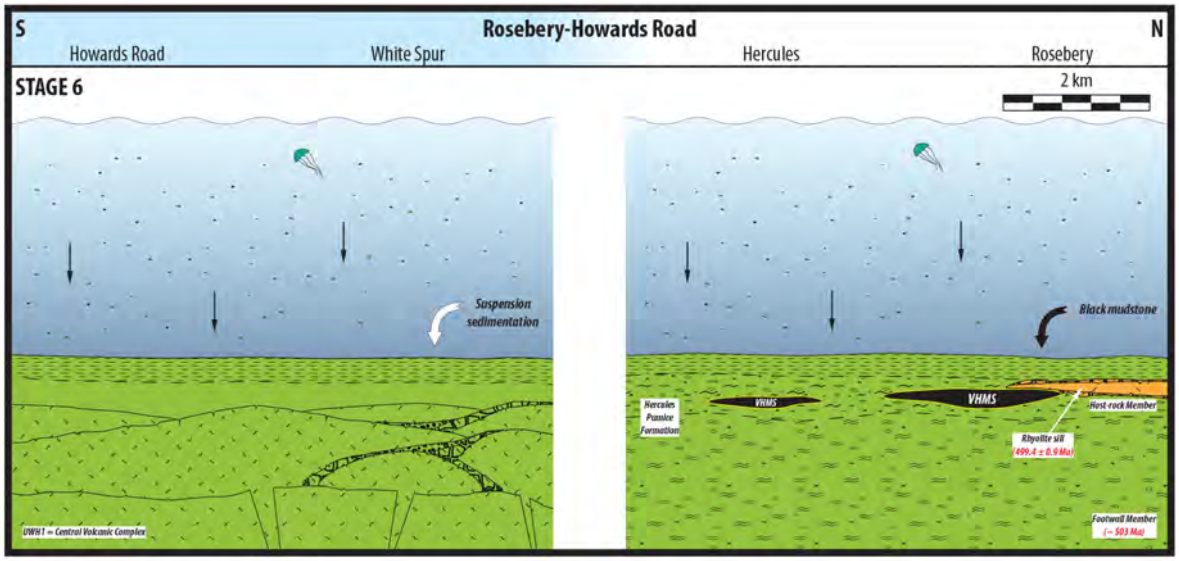

A: Rosebery-Howards Road area

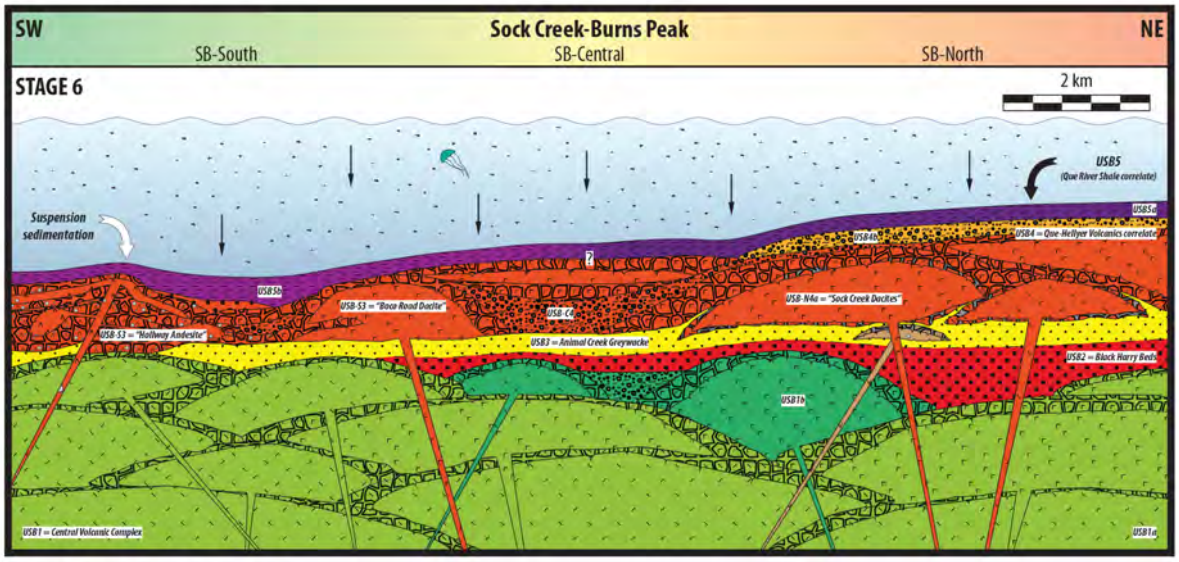

B: Sock Creek-Burns Peak area

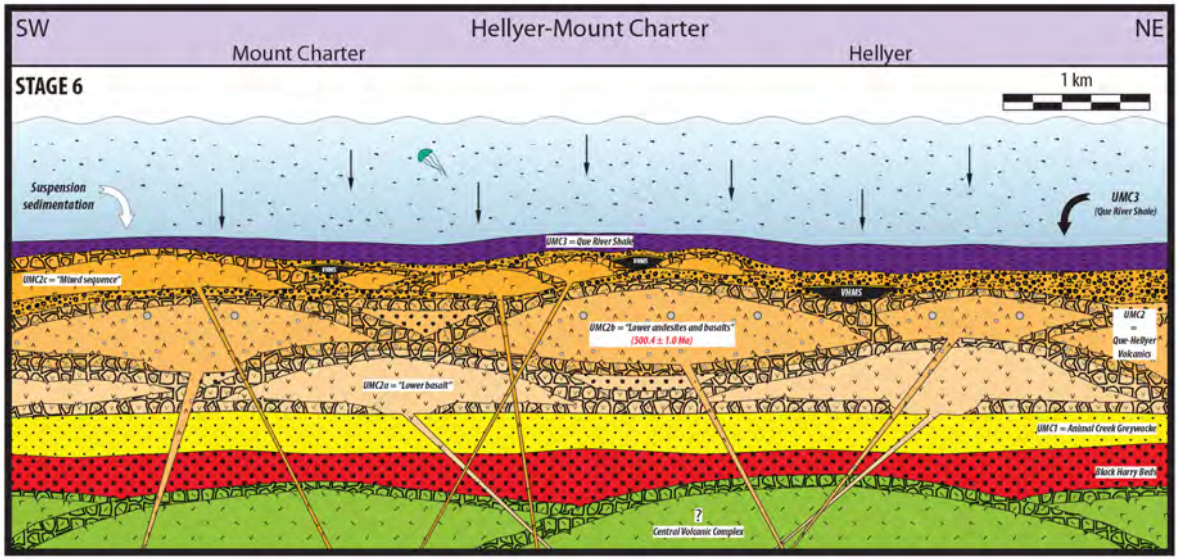

C: Hellyer-Mount Charter area

Figure 6.9: Stage 6 reconstruction diagrams. (CA) ID-TIMS U-Pb ages in red from Mortensen et al. (2015).

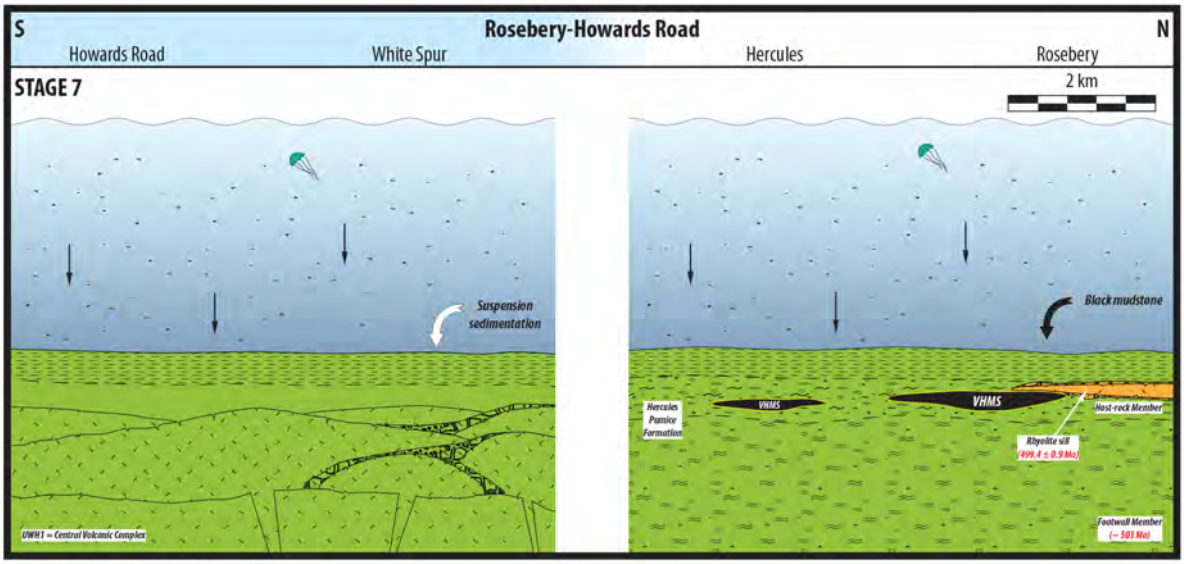

A: Rosebery-Howards Road area

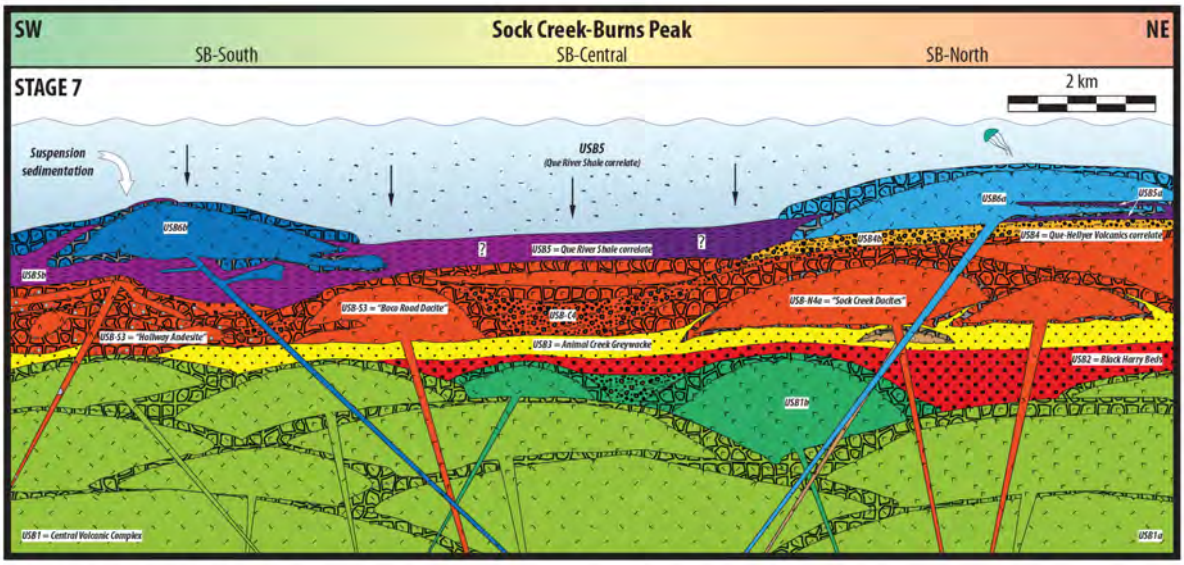

B: Sock Creek-Burns Peak area

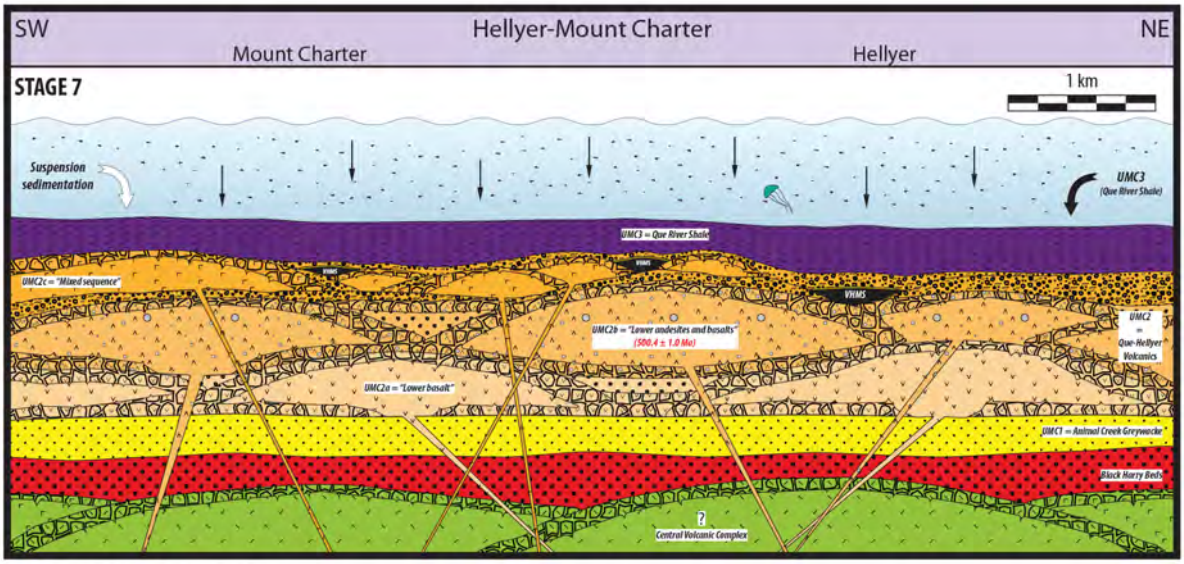

C: Hellyer-Mount Charter area

Figure 6.10: Stage 7 reconstruction diagrams. (CA) ID-TIMS U-Pb ages in red from Mortensen et al. (2015).

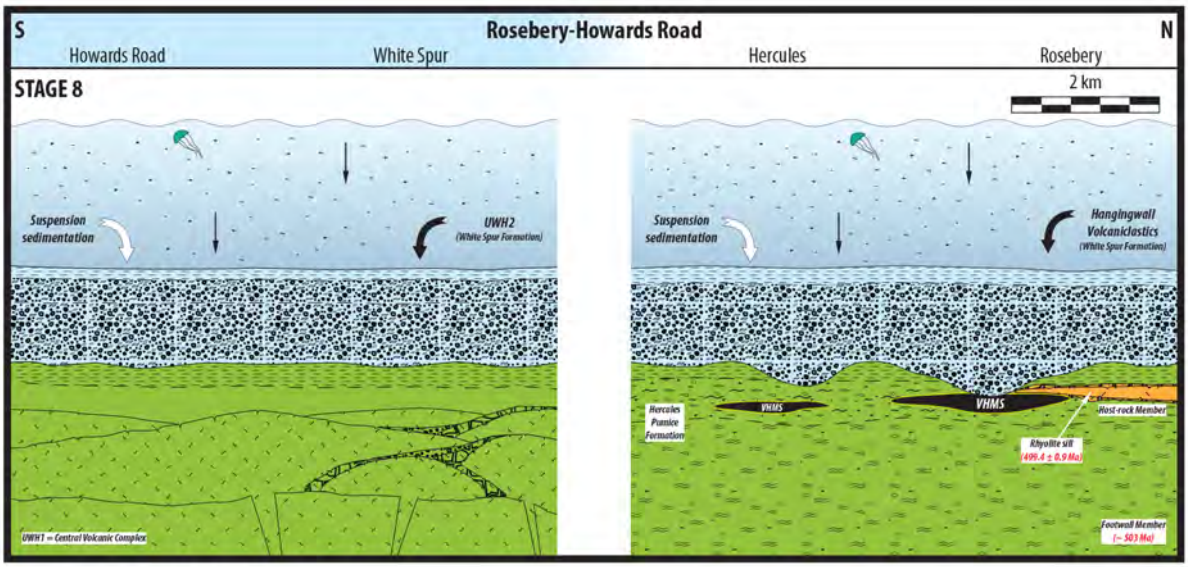

A: Rosebery-Howards Road area

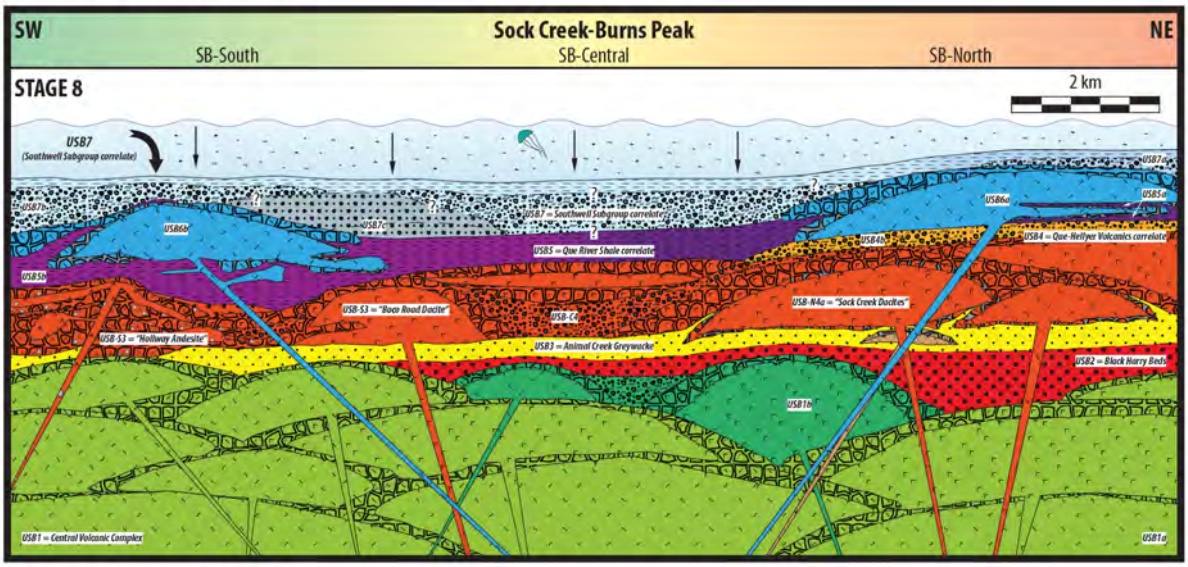

B: Sock Creek-Burns Peak area

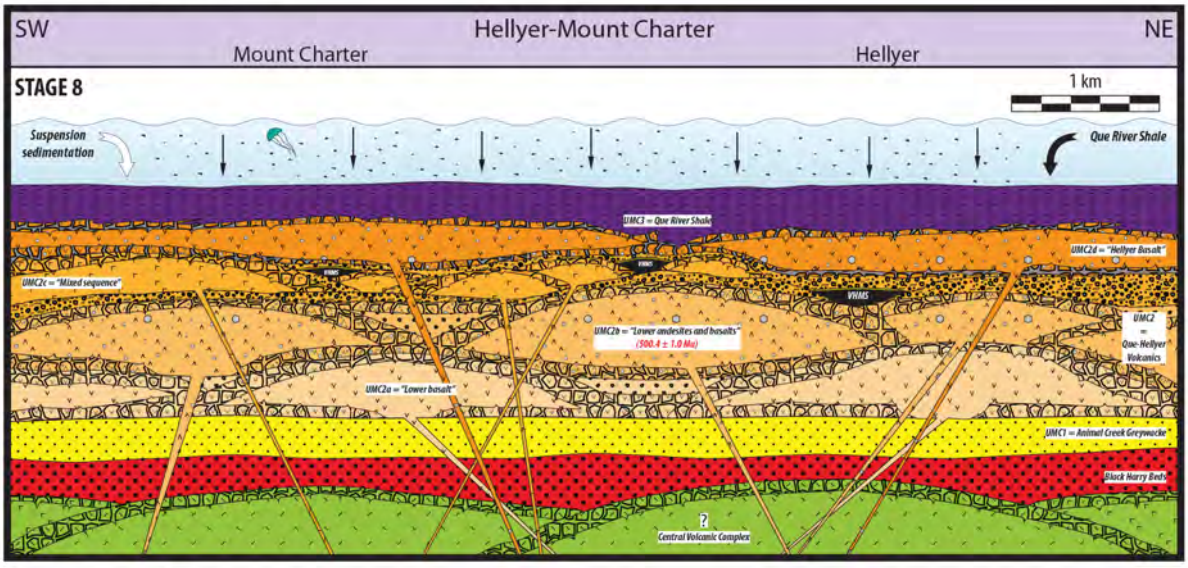

C: Hellyer-Mount Charter area

Figure 6.11: Stage 8 reconstruction diagrams. (CA) ID-TIMS U-Pb ages in red from Mortensen et al. (2015).

presence of peperite throughout the Hellyer Basalt (Waters and Wallace, 1992; Tomes, 2011; this study; UMC2; Figure 6.11 - C) indicates that it intruded unconsolidated Que River Shale (UMC3; Figure 6.11 - C). The intrusive emplacement of the Hellyer Basalt was thus synchronous with or later than the deposition of the lower part of the Que River Shale.

The emplacement of thick (>90 m), normally graded, volcanic quartz-bearing, polymictic rhyolite breccia and sandstone units followed in the Rosebery-Howards Road (UWH2; Figure 6.11 - A) and Sock Creek-Burns Peak (USB7a and USB7b; Figure 6.11 - B) areas. These units were derived from explosive eruption-fed density currents, most likely generated by intrabasinal rhyolitic explosive eruptions. Suspension sedimentation produced black mudstone intervals. The Hangingwall Volcaniclastics units (correlated with the WSF; Corbett and Lees, 1987; Allen, 1990b, 1994a; McPhie and Allen, 1992; Gifkins, 2001) were deposited in the Rosebery-Hercules area (Figure 6.11 - A). Syn- and/or post-eruptive density currents deposited thick intervals of quartz-bearing polymictic crystal-rich sandstone in the Boco Road area (USB7c; Figure 6.11 - B).

The Que-River Shale continued accumulating in the Hellyer-Mount Charter area (Figure 6.11 - C). The Que River Shale is conformably overlain by the Southwell Subgroup in the Hellyer-Mount Charter area (Corbett and Komyshan, 1989), which is a possible lithostratigraphic correlate of the WSF in the White Spur-Howards Road area and the Hangingwall Volcaniclastics in the Rosebery-Hercules area (Corbett and Lees, 1987; Allen, 1990b, 1994a; Corbett, 1992; McPhie and Allen, 1992; Gifkins, 2001). The top of the Que River Shale and the lowermost unit of the Southwell Subgroup are intruded by the "lower rhyolite", which has an age of 499.3 ± 0.9 Ma (Mortensen et al., 2015), and the Que River Shale is significantly thicker (<150 m) at Hellyer compared to the black mudstone (5 to 20 m thick) in the Rosebery-Hercules area. The Hangingwall Volcaniclastics and WSF were deposited at around 500 Ma (Mortensen et al., 2015) because the WSF is intruded by two rhyolite sills dated at 500.4 ± 0.8 Ma and 499.6 ± 0.8 Ma (Mortensen et al., 2015). Hence, the deposition of the WSF in the White Spur-Howards Road area (UWH2; Figure 6.11 - A) and the Hangingwall Volcaniclastics in the Rosebery-Hercules area was probably synchronous with the deposition of the top of Que River Shale in the Hellyer-Mount Charter area (Figure 6.11 - A and C).

6.3.5 Alternative scenario: formation of the Rosebery-Hercules VHMS deposits on the seafloor and implications for the paleogeography and mineralisation reconstruction in the northern Mount Read Volcanics

From a stratigraphic perspective, the genetic models of Brathwaite (1974), Solomon and Walshe (1979), Green et al. (1981), Sainty (1986), Huston and Large (1988), Solomon et al. (1990), and Solomon and Groves (1990) for the formation of the Rosebery and Hercules VHMS deposits on the seafloor, have the following major implications:

1. The Rosebery and Hercules VHMS deposits formed after the emplacement of the Footwall Member and at the same time to immediately before the emplacement of most of the Host-rock Member. The Footwall Member and Host-rock Member comprise the Hercules Pumice Formation, which is part of the

upper CVC (Gifkins, 2001). This implication means that the Rosebery and Hercules VHMS deposits are synchronous with the emplacement of the upper CVC, which has been correlated with USB1 in the Sock Creek-Burns Peak area (Figure 6.1).

2. The Rosebery and Hercules VHMS deposits are older than the Hellyer and Que River VHMS deposits, which formed immediately after the emplacement of the mixed sequence of the QHV (Waters and Wallace, 1992) in the Hellyer-Mount Charter area, and USB4b (polymictic volcanic breccia and sandstone facies - section 3.3.4) in the SB-North area (Figure 6.1). The QHV are part of the Mount Charter Group and younger than the CVC (Corbett, 1992).

3. There were two major seafloor VHMS-forming events in the northern Mount Read Volcanics: the first corresponded to the formation of the Rosebery and Hercules VHMS deposits in the Rosebery-Hercules area during the emplacement of the upper CVC (including USB1 in the Sock Creek-Burns Peak area - Figure 6.1); the second coincided with the formation of the Hellyer and Que River VHMS deposits in the Hellyer-Mount Charter area immediately after the deposition of the mixed sequence of the QHV and USB4b in the SB-North area (Figure 6.1).

6.3.6 Summary

The Hellyer and Que River seafloor VHMS deposits formed during accumulation of the mixed sequence of the QHV in the Hellyer-Mount Charter area; its correlate (USB4b, polymictic volcanic breccia and sandstone facies) was deposited in the Sock Creek-Burns Peak North area. At the same time, black mudstone had already been accumulating in the Rosebery-Howards Road area stratigraphically above the Rosebery and Hercules sub-seafloor VHMS deposits. Regional, basin-wide deposition of black mudstone followed in the Sock Creek-Burns Peak (correlated with USB5), and Hellyer-Mount Charter (Que River Shale) areas at the same time as black mudstone continued accumulating in the Rosebery-Howards Road area. Two partly extrusive feldspar-quartz-phyric rhyolite cryptodomes (USB6a and USB6b) were subsequently emplaced into and onto black mudstone in the Sock Creek and Burns Peak areas while black mudstone was still accumulating in the Rosebery-Howards Road, Sock Creek-Burns Peak (USB5) and Hellyer-Mount Charter (Que River Shale) areas.

The deposition of black mudstone (USB5) marks a break in the accumulation of volcanic facies, and was either synchronous with (Rosebery-Howards Road) or closely followed (Hellyer-Mount Charter) major VHMS-forming hydrothermal processes operating at approximately 500 Ma (Mortensen et al., 2015) in the northern Mount Read Volcanics. The base of the black mudstone immediately overlying the Rosebery and Hercules sub-seafloor VHMS deposits in the Rosebery-Hercules area and the base of the black mudstone in the Sock Creek-Burns Peak (USB5) and Hellyer-Mount Charter (Que River Shale) areas are excellent lithological markers, but they are probably diachronous because the Rosebery and Hercules sub-seafloor VHMS deposits formed at the same time as black mudstone was being deposited higher in the stratigraphy, and the seafloor VHMS deposits in the Hellyer-Mount Charter area formed at the same time to immediately after the emplacement of the mixed sequence of the QHV, and before the deposition of the Que River Shale (Figure 6.8).

6.4 Implications and directions for VHMS exploration in the northern Mount Read Volcanics

6.4.1 Sock Creek-Burns Peak area

In the Sock Creek-Burns Peak area (this study), the lithostratigraphic unit favorable for the formation of economically significant seafloor VHMS deposits is USB4b (polymictic volcanic breccia and sandstone facies - section 3.3.4), which occurs at the top of USB4 (coherent feldspar-phyric rhyolite, dacite and mafic facies, monomictic rhyolite, dacite and mafic breccia, monomictic mud-matrix rhyolite and dacite breccia, monomictic fiamme-rich dacite breccia, monomictic dacite sandstone, coherent feldspar-pyroxene-phyric and aphyric mafic facies, monomictic fluidal-clast mafic breccia, polymictic volcanic breccia and sandstone, polymictic felsic breccia and sandstone, and black mudstone facies - section 3.3; correlated with the QHV in the Hellyer-Mount Charter area and Host-rock Member of the Hercules Pumice Formation in the Rosebery-Hercules area) (Figure 6.3).

USB4b is inferred to have accumulated at the same time the mixed sequence of the QHV was emplaced in the Hellyer-Mount Charter area, and immediately before to synchronously with the formation of the seafloor VHMS deposits in the Hellyer-Mount Charter area (Hellyer, Fossey, Que River and Mount Charter). The emplacement of USB4b is inferred to have occurred before the deposition of black mudstone in the Sock Creek-Burns Peak (USB5) and Hellyer-Mount Charter (Que River Shale) areas, and synchronously with the deposition of black mudstone in the Rosebery-Howards Road areas. During this period, distinct facies formed at different locations.

Assuming that the Rosebery and Hercules VHMS deposits formed by syn-volcanic, sub-seafloor replacement (Allen, 1994b; Martin, 2004), correlations between the Sock Creek-Burns Peak area with the areas to the NE (Hellyer-Mount Charter) and SSW (Rosebery-Hercules) (Figure 6.1) suggest that the stratigraphic interval potentially prospective for sub-seafloor VHMS deposits is represented by the volcano-sedimentary succession below the top of USB4 (correlated with the QHV in the Hellyer-Mount Charter area and Host-rock Member of the Hercules Pumice Formation in the Rosebery-Hercules area) (Figures 6.2 and 6.3). This stratigraphic interval includes the top of USB1 (coherent feldspar-quartz-phyric rhyolite and feldspar-phyric dacite, monomictic rhyolite and dacite breccia, monomictic fiamme-rich rhyolite breccia, and polymictic volcanic breccia facies - section 3.3; correlated with the CVC - section 4.3).

The top of USB1 has been intersected in DDH BHD-10 (SB-North), BOC-1, BOC-2 and BOC-6 (SB-Central), and BOC-3 and BOC-4 (SB-South) (Figure 6.1). In the SB-Central area, USB1 has been divided into USB-C1a and USB-C1b (Figure 6.1). The top contact of USB-C1a was not intersected by any of the DDH in this study, and the uppermost part of USB-C1b in DDH BOC-6 contains minor evidence of sulfides (2-cm sphaleritic clast within pyritic fine-grained sandstone). In the SB-North and SB-South areas, the top contacts of USB1 have been interpreted as faults (Figure 6.1) and the evidence for mineralisation at the uppermost part of USB1 is also minor (<1% sulfides).

The top of USB4 was intersected in both the SB-North and SB-South areas (Figure 6.1). In DDH BPD-89 (SB-South) the top of USB4 does not show any macroscopic evidence of sulfides. In the SB-North area, USB4b (polymictic volcanic breccia and sandstone facies - section 3.3.4) has been correlated with the mixed sequence of the Que-Hellyer Volcanics and constitutes an excellent stratigraphic marker extending for approximately 3 km (Figure 6.1), but it also does not contain any visible sulfides. USB4b was not intersected by any DDH in this study in the SB-Central and SB-South areas (Figure 6.1).

It seems that the zinc-dominated and gold/silver-poor sulfide prospects at Sock Creek and Sock Creek South (Purvis, 1993; McNeill, 2002), the large "barren" sericite-pyrite Boco Alteration Zone (Skirka and McNeill, 2006; Herrmann et al., 2009), and minor base metals at the Hollway prospect (Skirka and McNeill, 2006) remain the only evidence that minor mineralisation occurred in the Sock Creek-Burns Peak area. The prospect at Sock Creek occurs stratigraphically on the contact between black mudstone (correlated with USB5 and the Que River Shale in this thesis) and the feldspar-quartz-phyric rhyolite porphyry (correlated with USB6 in this thesis) (McNeill, 2002); the prospect at Sock Creek South occurs stratigraphically in the black mudstone (McNeill, 2002); the minor base metals in the Boco Alteration Zone occur stratigraphically within the Black Harry Beds and equivalents of the lower Southwell Subgroup (Skirka and McNeill, 2006); the minor base metals at the Hollway prospect occur within the lower part of the Hollway Andesite and the upper part of the Central Volcanic Complex. Only the minor base metals at the Hollway prospect occur stratigraphically where mineralisation would be predicted.

Nevertheless, and despite the lack of evidence for the presence of economically significant mineral deposits in the Sock Creek-Burns Peak area (McNeill, 2001), tracing USB4b further to the SW and further investigating the top of USB1 in the Sock Creek-Burns Peak area may assist in future VHMS exploration.

6.4.2 Other parts of the northern Mount Read Volcanics

The footwall and host-rock successions to the VHMS deposits at Hellyer and Que River in the Hellyer-Mount Charter area (NE of Sock Creek-Burns Peak) and at Rosebery and Hercules in the Rosebery-Hercules area (SSW of Sock Creek-Burns Peak) are quite different in character, and no generalisations can be made regarding the footwall and host-rock lithologies to other VHMS deposits elsewhere in the northern Mount Read Volcanics.

However, in both the Hellyer-Mount Charter and Rosebery-Hercules areas, the host rocks to the VHMS deposits are overlain by black mudstone (Que River Shale in the Hellyer-Mount Charter area and black mudstone in the Rosebery-Hercules area). The presence of finely laminated mudstone represents a period of very low-energy, below-wave-base sedimentation and a break in volcanic aggradation that allowed the hydrothermal systems to properly develop and produce massive sulfides on the seafloor at Hellyer and Que River and below the seafloor at Rosebery and Hercules. The occurrence of black mudstone above the CVC in the northern Mount Read Volcanics thus constitutes a good exploration tool and the stratigraphic interval immediately below it should be regarded as potentially prospective.

Above the black mudstone, the hangingwall successions to the Hellyer, Que River, Rosebery and Hercules VHMS deposits also comprise mass flow-type volcanic quartz-bearing volcaniclastic facies (UNMRV7), including polymictic rhyolite breccia and sandstone, polymictic mud-matrix rhyolite breccia and mudstone (section 3.3). These facies occur in the Sock Creek-Burns Peak (USB7; correlated with the Southwell Subgroup) and White Spur-Howards Road (UWH2; correlated with the WSF) areas. The implication for other areas of the northern Mount Read Volcanics is that the stratigraphic level comprising black mudstone below and mass flow-type volcanic quartz-bearing successions above may represent an excellent syn- to post-mineralisation stratigraphic marker, and further exploration endeavours should be aimed for the stratigraphic interval immediately below it (Figures 6.2 and 6.3).

6.4.3 Summary

The footwall and host-rock facies to the Hellyer, Que River, Rosebery and Hercules VHMS deposits in the northern Mount Read Volcanics are very different in character and do not constitute good exploration guides. However, the hangingwall successions at all deposits comprise black mudstone and volcanic quartz-bearing polymictic volcaniclastic units that are excellent stratigraphic markers for VHMS exploration.

6.5 Summary

Assuming the syn-volcanic, sub-seafloor replacement model of Allen (1994b) and Martin (2004) for the formation of the Rosebery and Hercules VHMS deposits, the following conclusions can be summarized:

1. Normally graded units comprising volcanic quartz-bearing, polymictic volcanic breccia and sandstone facies of USB4b (correlated with the mixed sequence of the Que-Hellyer Volcanics) represent the lithostratigraphic unit in the Sock Creek-Burns Peak area favorable for the formation of economically significant Hellyer-Que River-like seafloor VHMS deposits.

2. The emplacement of USB4b in the Sock Creek-Burns Peak North area is inferred to have occurred (a) immediately before, to synchronously with, the main mineralising event during which the Rosebery and Hercules sub-seafloor, and Hellyer and Que River seafloor VHMS deposits formed, (b) synchronously with the deposition of the mixed sequence of the QHV in the Hellyer-Mount Charter area, (c) partly at the same time as the deposition of black mudstone in the Rosebery-Howards Road area, and (d) before the initial stage of deposition of black mudstone in the Sock Creek-Burns Peak (USB5) and Hellyer-Mount Charter (Que River Shale) areas.

3. The volcano-sedimentary succession in the Sock Creek-Burns Peak area below the top of USB4 (correlated with the QHV in the Hellyer-Mount Charter area and Host-rock Member of the Hercules Pumice Formation in the Rosebery-Hercules area) is potentially prospective for sub-seafloor VHMS deposits. This stratigraphic interval includes dominantly coherent feldspar-quartz-phyric rhyolite and feldspar-phyric dacite, and monomictic rhyolite and dacite breccia facies of USB1 (upper CVC) that are

equivalent to the stratigraphic level at which the Rosebery and Hercules sub-seafloor VHMS deposits occur. It also includes: (a) normally graded units of volcanic quartz- and shard-bearing polymictic felsic breccia, micaceous sandstone and shard-rich mudstone of USB2 (equivalent to the Black Harry Beds) and USB3 (equivalent to the Animal Creek Greywacke), and (b) partly extrusive feldspar-phyric rhyolitic to dacitic cryptodomes, andesitic lavas and domes and minor basaltic facies of USB4a (correlated with the lower basalt and lower andesites and basalts of the QHV in the Hellyer-Mount Charter area). USB2 and USB3 comprise abundant metamorphic and basement-derived fragments, which distinguish them from USB4b in the Sock Creek-Burns Peak area and the VHMS-hosting mixed sequence of the QHV in the Hellyer-Mount Charter area.

4. Tracing USB4b further to the SW and further investigating the top of USB1 in the Sock Creek-Burns Peak area may assist in future VHMS exploration.

5. The facies comprising the footwall and host-rocks of the Hellyer, Que River, Rosebery and Hercules VHMS deposits in the northern Mount Read Volcanics are very different in character and do not constitute good exploration guides, but black mudstone and mass flow-type volcanic quartz-bearing polymictic volcaniclastic units within the hangingwall successions at all deposits are excellent stratigraphic markers, and further VHMS exploration endeavours should be aimed for the stratigraphic interval immediately below the base of these successions.

CHAPTER 7

Conclusions, discussion and recommendations

7.1 Conclusions

The most important and significant aim of this project is to establish the lithostratigraphic correlations of the Sock Creek-Burns Peak area with the areas to the NE (Hellyer-Mount Charter) and SSW (Rosebery-Howards Road), and to discuss the most prospective stratigraphic position in the Sock Creek-Burns Peak area and elsewhere in the Mount Read Volcanics (MRV). This aim has been achieved by combining facies analysis, local and regional correlations and whole-rock compositional data in the Sock Creek-Burns Peak, Mount Charter, Rosebery-Hercules and White Spur-Howards Road areas, and examining the different genetic models, local geological settings and host volcanic successions of the Hellyer, Que River, Rosebery and Hercules VHMS deposits.

An improved understanding of the stratigraphic framework, volcanic and sedimentary facies architecture, and paleogeography of the Sock Creek-Burns Peak area has also been achieved. The stratigraphy of the Sock Creek-Burns Peak area can be considered in terms of seven regional stratigraphic units (USB), and the volcanic and sedimentary facies architecture and paleogeography of the Sock Creek-Burns Peak area can be related to the Hellyer-Mount Charter (NE of Sock Creek- Burns Peak) and Rosebery-Howards Road (SSW of Sock Creek-Burns Peak) areas.

At approximately 503 Ma (Mortensen et al., 2015), prior to the formation of the Hellyer, Que River, Rosebery and Hercules VHMS deposits, the pumice breccia of the Footwall Member of the Hercules Pumice Formation (Gifkins, 2001) was rapidly emplaced in the Rosebery-Hercules area, and feldspar-phyric rhyolitic to dacitic and minor feldspar-quartz-phyric rhyolitic lavas, domes and minor cryptodomes were emplaced in the Sock Creek-Burns Peak (USB1, correlated with the CVC) and White Spur-Howards Road (UHW1, correlated with the CVC) area, and presumably also in the Hellyer-Mount Charter area (McNeill, 1989; Pemberton et al., 1991; Stewart, 2009). Dacitic-andesitic volcanic centres in the Sock Creek-Burns Peak area and basaltic-andesitic-dacitic volcanic centres in the Hellyer-Mount Charter area developed probably at the same time as the Host-rock Member of the Hercules Pumice Formation (Gifkins, 2001) accumulated slowly over an approximately 3-million-year period immediately followed by accumulation of black mudstone in the Rosebery-Hercules area.

The Hellyer and Que River seafloor and the Rosebery and Hercules sub-seafloor VHMS deposits formed during the same time interval, presently accepted to be approximately 500 Ma (Mortensen et al., 2015). The mixed sequence of the Que-Hellyer Volcanics (QHV) accumulated in the Hellyer-Mount Charter area and its correlate (USB4b, polymictic volcanic breccia and sandstone facies) was deposited in the Sock Creek-Burns Peak North area while black mudstone continued accumulating in the Rosebery-Howards Road area.

Regional, basin-wide deposition of black mudstone followed in the Hellyer-Mount Charter (Que River Shale) and Sock Creek-Burns Peak (correlated with USB5) areas at the same time as black mudstone was still accumulating in the Rosebery-Howards Road area. The black mudstone in the Sock Creek and Burns Peak areas was subsequently intruded by two partly extrusive feldspar-quartz-phyric rhyolite cryptodomes (USB6a and USB6b). The volcanic quartz-bearing units of the Hangingwall Volcaniclastics in the Rosebery-Hercules area and the White Spur Formation (WSF) in the White Spur-Howards Road area were deposited at about 500 Ma (Mortensen et al., 2015) because the WSF is intruded by two rhyolite sills dated at 500.4 ± 0.8 Ma and 499.6 ± 0.8 Ma (Mortensen et al., 2015). Similar volcanic quartz-bearing lithofacies of USB7 are inferred to have been deposited approximately at the same time in the Sock Creek and Burns Peak areas while the Que River Shale continued accumulating in the Hellyer-Mount Charter area.

The Southwell Subgroup, which conformably overlies the Que River Shale in the Hellyer-Mount Charter area, is a possible lithostratigraphic correlate of the Hangingwall Volcaniclastics and WSF in the Rosebery-Howards Road area because it comprises very similar lithofacies and volcanic quartz. The Southwell Subgroup, Hangingwall Volcaniclastics and WSF were derived from explosive eruption-fed density currents most likely generated by intrabasinal rhyolitic explosive eruptions, which contrasts with the basaltic-andesitic-dacitic-dominated volcanic centres occurring in the Hellyer-Mount Charter and Sock Creek-Burns Peak areas immediately before the VHMS-forming hydrothermal systems in the Hellyer-Mount Charter and Rosebery-Hercules areas.

The Southwell Subgroup could have a longer duration than the Hangingwall Volcaniclastics and WSF. The lowermost unit of the Southwell Subgroup is intruded by the 499.3 ± 0.9 Ma "lower rhyolite" (Mortensen et al., 2015) which is close to the age of two rhyolite sills dated at 500.4 ± 0.8 Ma and 499.6 ± 0.8 Ma that intrude the WSF (Mortensen et al., 2015). Assuming that sedimentation rates were similar, the significantly greater thickness of the Southwell Subgroup (approximately 1000 in the Hellyer-Mount Charter area, compared to the Hangingwall Volcaniclastics (up to 400 m) in the Rosebery-Hercules area (Figure 6.3), could reflect a longer duration of volcanic quartz bearing accumulation in the Hellyer-Mount Charter area compared with the Rosebery-Hercules area.

The VHMS deposits mark the only chronostratigraphic horizon at approximately 500 Ma (Mortensen et al., 2015). The Que River Shale is immediately overlying the Hellyer-Mount Charter seafloor VHMS deposits and the black mudstone is a few tens of metres above the Rosebery-Hercules sub-seafloor VHMS deposits. Hence, the age difference at the base of the black mudstone in the Rosebery-Hercules area and at the base of the Que River Shale in the Hellyer-Mount Charter area is probably small.

The major outcomes of this research allow discussion of the location of the most prospective stratigraphic position for VHMS deposits in the northern MRV.

1. The lithostratigraphic interval in the Sock Creek-Burns Peak North area favorable for the formation of economically significant Hellyer-Que River-like seafloor VHMS deposits is represented by normally

graded units comprising volcanic quartz-bearing, polymictic volcanic breccia and sandstone facies of USB4b, which is correlated with the mixed sequence of the QHV in the Hellyer-Mount Charter area.

2. The emplacement of USB4b in the Sock Creek-Burns Peak North area is inferred to have occurred (a) synchronously with the deposition of the mixed sequence of the QHV in the Hellyer-Mount Charter area, (b) partly at the same time as the deposition of black mudstone in the Rosebery-Howards Road area, and (c) before the initial stage of deposition of black mudstone in the Sock Creek-Burns Peak (USB5) and Hellyer-Mount Charter (Que River Shale) areas. The emplacement of USB4b occurred immediately before, to at the same time as, the main mineralising event during which the Rosebery and Hercules sub-seafloor, and Hellyer and Que River seafloor VHMS deposits formed.

3. The volcano-sedimentary succession in the Sock Creek-Burns Peak area below the top of USB4b is potentially prospective for sub-seafloor VHMS deposits. This stratigraphic interval includes dominantly coherent feldspar-quartz-phyric rhyolite and feldspar-phyric dacite, and monomictic rhyolite and dacite breccia facies of USB1, which is correlated with the CVC, equivalent to the stratigraphic level at which the Rosebery and Hercules sub-seafloor VHMS deposits occur. It also includes normally graded units of volcanic quartz- and shard-bearing polymictic felsic breccia, micaceous sandstone and shard-rich mudstone of USB2 (equivalent to the Black Harry Beds) and USB3 (equivalent to the Animal Creek Greywacke). These units comprise abundant metamorphic and basement-derived fragments, which distinguish them from USB4b in the Sock Creek-Burns Peak area and the VHMS-hosting mixed sequence of the QHV in the Hellyer-Mount Charter area. The potentially prospective stratigraphic interval for sub-seafloor VHMS deposits in the Sock Creek-Burns Peak area still includes partly extrusive feldspar-phyric rhyolitic to dacitic cryptodomes, andesitic lavas and domes and minor basaltic facies of USB4a, which is correlated with the lower basalt and lower andesites and basalts of the QHV in the Hellyer-Mount Charter area. Tracing USB4b further to the SW and further investigating the top of USB1 in the Sock Creek-Burns Peak area may assist in future VHMS exploration.

4. The succession including and above the VHMS deposits shows marked lateral variations that relate to differences in accumulation rate and in facies associations. Assuming that sedimentation rates were comparable, the significantly greater thickness of the Southwell Subgroup in the Hellyer-Mount Charter area could reflect a longer duration. Similarly, the significantly greater thickness (<150 m) of the Que River Shale, which conformably underlies the Southwell Subgroup in the Hellyer-Mount Charter area, compared to the black mudstone (5 to 20 m thick) in the Rosebery-Hercules area, which immediately underlies the Hangingwall Volcaniclastics (Figure 6.3), could reflect a longer duration. Furthermore, there is a section up to approximately 1500 m thick above the CVC and below the Que River Shale in the Hellyer-Mount Charter area comprising the Black Harry Beds, Animal Creek Greywacke and the QHV, and no equivalent section in the Rosebery-Hercules area (Figure 6.3).

5. The footwall and host-rock successions to the VHMS deposits at Hellyer and Que River in the Hellyer-Mount Charter area (NE of Sock Creek-Burns Peak) and at Rosebery and Hercules in the Rosebery-Hercules area (SSW of Sock Creek-Burns Peak) are very different in character, and do not constitute good exploration guides to other VHMS deposits elsewhere in the northern MRV. However, the hangingwall successions at all deposits comprise black mudstone and mass flow-type volcanic quartz-bearing polymictic volcaniclastic units that are excellent stratigraphic markers, and further VHMS exploration endeavours should be aimed at the stratigraphic interval immediately below the base of these marker units.

7.2 Discussion

The results of this study are relevant to correlation approaches and correlation problems in other comparable VHMS districts worldwide and will ultimately contribute to the global VHMS research project (Allen et al., 2002). The reconstruction of the volcanic and sedimentary facies architecture of VHMS-hosting successions based on facies analysis and correlations is a powerful approach to constraining VHMS depositional environments and understanding the stratigraphy, structure, tectonic setting and genesis of mineralised submarine volcanic successions.

Facies analysis and correlations of the footwall and host successions to VHMS deposits

In the northern MRV, the footwall and host-rock successions to the Hellyer, Que River, Rosebery and Hercules VHMS deposits are very different in character. The Hellyer and Que River VHMS deposits are associated with andesitic and dacitic facies of the QHV whereas the Rosebery and Hercules VHMS deposits are associated with thick, laterally extensive rhyolitic pumice breccia facies of the upper CVC. Consequently, the footwall and host-rock successions to the VHMS deposits in the northern MRV do not constitute good exploration guides to other VHMS deposits across the MRV. Regional stratigraphic relationships are complex, laterally variable, and regional correlations are difficult to demonstrate (McPhie and Allen, 1992; Corbett, 1992). Similarly, most VHMS deposits in the Early Proterozoic Skellefte district in northern Sweden are associated with at least two stratigraphic levels (Billström and Weihed, 1996; Allen et al., 1997, 2002) in a volcano-sedimentary succession that is very complex and laterally variable (Allen et al., 2002), hampering regional stratigraphic correlations.

The different footwall and host successions indicate that the hydrothermal systems responsible for the VHMS deposits in these districts operated in a variety of volcanic hosts and settings, and that both coherent and volcaniclastic facies associations are prospective for VHMS deposits. Some major VHMS deposits are hosted within the top or the upper part of relatively thick and laterally extensive, rapidly emplaced, felsic pyroclastic facies (e.g., MRV, McPhie and Allen, 2003; Skellefte district, Allen et al., 1997). Other major VHMS deposits occur associated with coherent facies (e.g., Mount Windsor Volcanics, Paulick and McPhie, 1999, Doyle and

McPhie, 2000; Iberian Pyrite Belt, Tornos, 2006, Rosa et al., 2008; Kuroko district; Glasby et al., 2008, Yamada and Yoshida, 2011; Yilgarn Craton, Belford et al., 2015).

Independently of the coherent or volcaniclastic nature of the major VHMS deposits host facies, it is widely recognized that the formation of VHMS deposits is closely associated with a break in volcanic accumulation (e.g., marked by black mudstone) (Sangster, 1972; Franklin et al., 1981, 2005; Lydon, 1984, 1988; Gibson et al., 1999), which represents the time necessary for active VHMS-forming hydrothermal systems to develop properly and allow sulfides to accumulate. In the Sock Creek-Burns Peak area (this study), the break in volcanic accumulation is represented by black mudstone of USB5, which immediately overlies polymictic volcanic breccia and sandstone facies of USB4b (correlated with the mixed sequence of the QHV, which hosts the Hellyer and Que River VHMS deposits in the Hellyer-Mount Charter area NE of Sock Creek-Burns Peak). In the Rosebery-Hercules area, the break during which aggradation was very slow could have been in the order of 3 million years because the Footwall Member of the Hercules Pumice Formation (Gifkins, 2001) has an age of approximately 503 Ma (Mortensen et al., 2015) whereas the overlying Host-rock Member of the Hercules Pumice Formation (Gifkins, 2001), black mudstone and sub-seafloor VHMS deposits are all approximately 500 Ma (Mortensen et al., 2015). In contrast, the Hellyer-Mount Charter area was volcanically active immediately before the Hellyer and Que River VHMS deposits formed.

In other VHMS districts (e.g., Iberian Pyrite Belt, Tornos, 2006; Mount Windsor Volcanics, Large, 1992; Abitibi Greenstone Belt, Thurston et al., 2008; Yilgarn Craton, Hollis et al., 2015), the major VHMS deposits are closely associated with volcanic facies that are intercalated with or overlain by sedimentary facies (e.g., black mudstone) which represent a break in volcanic accumulation. The identification of mappable sedimentary facies that represent breaks in VHMS-forming volcanic activity (e.g., Sedimentary Interface Zones, Thurston et al., 2008) is crucial for exploration because it constrains the VHMS prospective stratigraphy (e.g., Belford et al., 2015).

Diachronism of the hangingwall successions and implications for VHMS exploration

In the northern MRV, black mudstone and overlying mass flow-type, laterally extensive, volcanic quartz-bearing polymictic volcaniclastic units constitute the hangingwall successions at all deposits and are excellent stratigraphic markers for VHMS exploration. However, the base of the black mudstone in the Rosebery-Howards Road area and the base of the black mudstone in the Sock Creek-Burns Peak (USB5) and Hellyer-Mount Charter (Que River Shale) areas are probably diachronous.

The initial stage of deposition of black mudstone in the Sock Creek-Burns Peak (USB5) and Hellyer-Mount Charter (Que River Shale) areas most likely occurred at some time after black mudstone deposition had begun in the Rosebery-Howards Road area because the emplacement of USB4b (polymictic volcanic breccia and sandstone facies; correlated with the mixed sequence of the QHV) in the Sock Creek-Burns Peak North (SB-North) area is inferred to have occurred partly at the same time as the deposition of black mudstone in the

Rosebery-Howards Road area, and before the initial stage of deposition of black mudstone in the Sock Creek-Burns Peak (USB5) and Hellyer-Mount Charter (Que River Shale) areas. Similarly, the polymictic rhyolite breccia and sandstone of the WSF and Hangingwall Volcaniclastics in the Rosebery-Howards Road area and similar lithofacies in the Sock Creek-Burns Peak (USB7) and Hellyer-Mount Charter (Southwell Subgroup) areas can be correlated stratigraphically but deposition was probably not synchronous if sedimentation rates were uniform. The significantly greater thickness (approximately 1000 m) of the Southwell Subgroup in the Hellyer-Mount Charter area compared to the Hangingwall Volcaniclastics and WSF (both approximately up to 400 m) in the Rosebery-Howards Road area could reflect a longer duration of volcanic quartz-bearing sedimentation in the north compared with the south. If the base of the black mudstone in the Rosebery-Hercules, Sock Creek-Burns Peak and Hellyer-Mount Charter areas is not diachronous, that would mean that accumulation rates were different regionally, even though the facies are very similar throughout the area. If so, deposition of the Que River Shale in the Sock Creek-Burns Peak and Hellyer-Mount Charter areas would have occurred with higher accumulation rate compared to the black mudstone in the Rosebery-Hercules area.

The diachronism means that whereas black mudstone and volcanic quartz-bearing volcaniclastic units are important lithological markers of the hangingwall position, they are not necessarily time-equivalent and hence, their time relationship with the VHMS deposits is different in different areas. In the Rosebery-Hercules area, the sub-seafloor VHMS deposits formed during the time period when the relatively thin (5 to 20 m) interval of black mudstone was being deposited higher in the stratigraphy. In the Hellyer-Mount Charter area, the seafloor VHMS deposits formed immediately before the deposition of up to 150 m of Que River Shale. Despite the diachronism, the hangingwall successions of the major VHMS deposits in the northern MRV offer a way of establishing regional correlations and constraining the relative age and stratigraphic position of the VHMS deposits.

If the diachronism is not recognized, correlation of the hangingwall successions can lead to wrong conclusions regarding the relative age and stratigraphic position of the VHMS deposits. For example, the Hangingwall Volcaniclastics and WSF in the Rosebery-Howards Road area and the Southwell Subgroup in the Hellyer-Mount Charter area can be correlated on lithological/stratigraphic grounds. The base of the Hangingwall Volcaniclastics/WSF is only approximately 5 to 20 m above the VHMS deposits at Rosebery-Hercules, but the base of the Southwell Subgroup is approximately 150 m above the VHMS deposits in the Hellyer-Mount Charter area. If it is assumed that the base of the Hangingwall Volcaniclastics/WSF/Southwell Subgroup is a synchronous surface, and that accumulation rates are uniform, the correlation would imply that the Rosebery and Hercules VHMS deposits are younger than the Hellyer and Que River VHMS deposits. This is obviously of major importance for VHMS deposit exploration.

Similar relationships occur in the Early Proterozoic Skellefte district in northern Sweden (Allen et al., 1997), where the volcano-sedimentary successions associated with the VHMS deposits are laterally variable and diachronous, and time-equivalent marker horizons are rare (Allen et al., 2002). Therefore, when searching for stratigraphic markers for VHMS exploration in the MRV and other VHMS-hosting districts, local and regional correlations need necessarily to be carefully considered and coupled with biostratigraphic and

radiometric age determinations in order to distinguish between lithostratigraphic and chronostratigraphic markers (e.g., Pereira et al., 1996; Oliveira et al., 1997a, 1997b, 2004, 2005; Marcoux, 1998; Mathur et al., 1999; Relvas et al., 2001; Barrie et al., 2002; Gonzalez et al., 2002; Rodríguez et al., 2002; Munhá et al., 2005; Rosa et al., 2009; Rosa et al., 2010; Matos et al., 2011; Mortensen et al., 2015).

Seafloor versus sub-seafloor VHMS deposits

It is of extreme importance to correctly identify seafloor vs. sub-seafloor VHMS deposits (Doyle and Allen, 2003) when constraining prospective stratigraphy (e.g., Piercey et al., 2014). The correct identification of the emplacement mechanism and origin of the unit that hosts a VHMS deposit using facies analysis, and the recognition of any paleo-seafloor positions, are critical in deciphering whether the deposit formed at the seafloor or sub-seafloor, and consequently should be considered at an early stage in exploration. Furthermore, seafloor VHMS deposits are important in constraining the location of the prospective stratigraphic interval within a given VHMS province because they mark the paleo-seafloor position at the time of ore formation and delineate the stratigraphic level at or below which other seafloor and sub-seafloor VHMS deposits will most likely occur.

This study has demonstrated how the seafloor versus sub-seafloor setting of a VHMS deposit changes the outcome of a prospectivity assessment of the host-succession. The identification of the prospective interval in the Sock Creek-Burns Peak area has been strongly influenced by assuming the VHMS deposits in the Hellyer-Mount Charter area formed on the seafloor (Gemmell and Large, 1992; Waters and Wallace, 1992; Solomon and Khin Zaw, 1997; Gemmell and Fulton, 2001) and the VHMS deposits in the Rosebery-Hercules area formed below the seafloor by sub-seafloor replacement (Allen, 1994b; Martin, 2004). Therefore, the prospective interval for VHMS deposits in the Sock Creek-Burns Peak area is represented by the volcano-sedimentary succession below the top of USB4b (correlated with the mixed sequence on the QHV in the Hellyer-Mount Charter area), which includes not only USB1 (correlated with the upper CVC, equivalent to the stratigraphic level at which the sub-seafloor VHMS deposits in the Rosebery-Hercules area occur), but also USB2 and USB3 (equivalents of the Black Harry Beds and Animal Creek Greywacke, respectively) and USB4a (correlated with the lower basalt and lower andesites and basalts of the QHV in the Hellyer-Mount Charter area).

If, on the other hand, the VHMS deposits in the Rosebery-Hercules area are considered to have formed on the seafloor (Brathwaite, 1974; Solomon and Walshe, 1979; Green et al., 1981; Sainty, 1986; Huston and Large, 1988; Solomon et al., 1990; and Solomon and Groves, 1990), the prospective interval for VHMS deposits in the Sock Creek-Burns Peak area would be restricted to the top of USB4b and the upper part of USB1. In this scenario, the stratigraphic interval between the top of USB4b and the top of USB1 (which includes USB2 and USB3) would be considered unprospective.

Paleogeography reconstruction and tectonic setting

In this study, the use of facies analysis and correlations in the paleogeography and mineralisation reconstruction of the northern MRV provides useful links to understanding the regional tectonic setting and major tectonic events that occurred in the northern MRV before, during and after mineralisation. Specifically, the identification of basement-derived fragments (e.g., schist, phyllite and quartzite) within volcanic quartz-bearing volcaniclastic units of USB2 and USB3 (correlated with the Black Harry Beds and Animal Creek Greywacke, respectively) suggests that the source of at least some of the volcanic components was most likely extrabasinal. The presence of basement-derived fragments within these units also indicates that erosion of exposed basement at the basin margin occurred after the obduction event emplacing not just the forearc crust sheets of the mafic-ultramafic complexes (MUC) but also thrust slices of deeper continental basement rocks, and before the main mineralising event responsible for the formation of the Hellyer, Que River, Rosebery and Hercules VHMS deposits in the northern MRV.

Additionally, the presence of detrital chromite within these units indicates that obduction and erosion of the MUC (Berry and Crawford, 1988; Crawford and Berry, 1992) predated the MRV succession. These features help constrain the time of VHMS formation in relation to the different tectonic stages considered in the most recently accepted tectonic model of the MRV (Berry and Crawford, 1988; Crawford and Berry, 1992), and ultimately add to a better understanding of how and when extensional basin environments constitute locations of excellence for VHMS deposit formation. The comprehensive connection between the paleogeography reconstruction and the tectonic setting of the northern MRV may be relevant to other VHMS districts and contributes to a better understanding of the tectonic influences on the architecture of the successions associated with VHMS deposits.

7.3 Recommendations

The use of biostratigraphic and radiometric age determinations in some of the volcano-sedimentary units occurring in the Sock Creek-Burns Peak area would establish the relative and absolute ages of these units and help confirm the lithostratigraphic correlations, ultimately providing a better understanding of the depositional environment of the volcano-sedimentary successions associated with the VHMS deposits in the northern MRV. Further biostratigraphy of black mudstone units and high-precision dating of the volcanic units with which they are associated would provide information on the duration they represent and further constrain the relative time of formation of these units in relation to the VHMS-hosting successions (e.g., IPB, Pereira et al., 1996; Oliveira et al., 1997a, 1997b, 2004, 2005; Gonzalez et al., 2002; Rodríguez et al., 2002; Rosa et al., 2010; Matos et al., 2011).

In the IPB (Portugal and Spain), biostratigraphic correlations mostly based on palynology and ammonoids biozonation, together with radiometric age determinations, have been of extreme importance in precisely dating the lithostratigraphic units associated with the VHMS deposits, and have provided a better understanding

of the local geodynamic basin development and regional depositional environment of the VHMS host successions. Recent biostratigraphy of dark grey and black mudstone hosting the Neves Corvo (Oliveira et al., 1997a, 1997b; Oliveira et al., 2004), Tharsis (Gonzalez et al., 2002) and Aznalcóllar (Pereira et al., 1996) VHMS deposits indicates they contain similar miospore assemblages of Strunian (Upper Famennian) age (Rosa et al., 2010; Matos et al., 2011), attributed to the LN, Western Europe biozone zonation that ranges for approximately 0.7 Ma, corresponding to the 361.4-360.7 ± 2.7 Ma interval (Kaufmann, 2006). The fossil ages obtained for the VHMS host mudstone of the Volcanic Sedimentary Complex (VSC) (Pereira et al., 1996; Rodríguez et al., 2002; Gonzalez et al., 2002; Oliveira et al., 2004, 2005) are in accordance with the U/Pb, Pb/Pb, Re/Os and Rb/Sr radiometric ages obtained for the felsic volcanic rocks and VHMS deposits (Marcoux, 1998; Mathur et al., 1999; Relvas et al., 2001; Barrie et al., 2002; Munhá et al., 2005; Rosa et al., 2009).

In addition, further systematic whole-rock geochemistry of VHMS-associated coherent felsic units would provide subtle, important information that cannot be obtained solely using drill core logging and field mapping. In the Yilgarn and Pilbara Cratons in western Australia and the Abitibi greenstone belt in Canada, prospective VHMS-associated felsic rocks are characterized by high SiO_2 in unaltered rocks, tholeiitic to transitional Zr/Y and La/Yb values, flattish REE profiles (La/SmCN<3; Dy/YbCN ratios ≈ 1), high HFSE (Y, Nb, Zr, Sc) concentrations, high Sc/TiO_2 and Sc/V, and low V and Th/Yb (Th/Yb<2 and Th>5ppm) (Hollis et al., 2015). Similar studies are recommended for the northern MRV.

Provenance studies focusing on dating of detrital zircons and mineral chemistry (e.g., detrital chromite, clinopyroxene) of mixed provenance sandstone, and lithogeochemistry of mudstone are recommended in order to support correlations and tectonic interpretations. The stratigraphic analysis recommended for the northern MRV ought to be extended to the southern MRV, where the major VHMS deposits occur associated with the CVC (Mount Lyell field) and the Tyndall Group (Henty) (Corbett et al., 2014).

References

Adabi, M. H., 1997. Application of carbon isotope chemostratigraphy to the Renison dolomites (Tasmania, Australia): a Neoproterozoic age. Australian Journal of Earth Sciences, vol. 44, p. 767-776.

Adams C. J., Black, L. P., Corbett, K. D., and Green, G. R., 1985. Reconnaissance isotopic studies on the tectonothermal history of Early Paleozoic and Late Proterozoic sequences in western Tasmania. Australian Journal of Earth Sciences, vol. 32, p. 7-36.

Aerden, D. G. A. M, 1990. Formation of a massive sulphide orebody by syn-deformational host-rock replacement in a ductile shear zone, Rosebery, Tasmania. Geological Society of Australia, Abstracts, vol. 25, p. 174-175.

Aerden, D. G. A. M, 1991. Foliation-boudinage control on the formation of the Rosebery Pb-Zn orebody, Tasmania. Journal of Structural Geology, vol. 13, p. 759-775.

Aerden, D. G. A. M, 1992. Macro- and Micro-Structural Controls on the Genesis of the Rosebery and Hercules Massive-Sulphide Deposits, Tasmania. Unpublished PhD thesis, James Cook University, 260 p.

Aerden, D. G. A. M, 1993. Formation of massive sulfide lenses by replacement of folds: the Hercules Pb-Zn mine, Tasmania. Economic Geology, vol. 88, p. 377-396.

Aerden, D. G. A. M, 1994a. Formation of the Rosebery and Hercules ore deposits, Tasmania by syntectonic mobilization of metals and wallrock replacement about structural traps, in Cooke, D. R., and Kitto, P. A., eds., Contentious issues in Tasmanian Geology: a Symposium: Hobart, Tasmania, Geological Society of Australia, Tasmanian Division, p. 101-106.

Aerden, D. G. A. M, 1994b. Microstructural timing of the Rosebery massive sulphides, Tasmania: evidence for a metamorphic origin through mobilisation of disseminated base metals. Journal of Metamorphic Geology, vol. 12, p. 505-522.

Allen, P. A. and Allen, J. R., 2005. Basin analysis: principles and applications. Blackwell Scientific Publications, Oxford. 451 p.

Allen, R. L., 1988. False pyroclastic textures in altered silicic lavas, with implication for volcanic associated mineralisation. Economic Geology, vol. 83, p. 1424-1446.

Allen R. L., 1990b. Stratigraphy, volcanology and structure of the Rosebery-Hercules mine leases. Unpublished report to Pasminco Exploration and Mining, Rosebery.

Allen R. L., 1991. Structure, stratigraphy and volcanology of the Rosebery-Hercules Zn-Pb-Cu-Au massive sulphide district, Tasmania: results 1988-1990. Volume 1. Unpublished internal report RML98 to Pasminco Exploration and Mining, Rosebery, 59 p.

Allen, R. L., 1992b. Construction of geological cross-sections at the Rosebery Mine, Tasmania, Jan-Feb 1992, unpublished report for Pasminco Exploration and Pasminco Mining Rosebery, p. 22.

Allen, R. L., 1993. Geological cross section and interpretation, 1320 mN Rosebery Mine north end. Unpublished report for Pasminco Exploration Mining, Rosebery.

Allen, R. L., 1994a. Volcanic facies analysis indicates large pyroclastic eruptions, sill complexes, syn-volcanic grabens and subtle thrusts in the Cambrian "Central Volcanic Complex" volcanic centre, western Tasmania. In Cooke, D. R. and Kitto, P. A. (eds.) Contentious issues in Tasmanian geology. Geological Society of Australia abstracts, vol. 39, p. 41-43.

Allen R. L., 1994b. Syn-volcanic, sub-seafloor replacement model for Rosebery and other massive sulphide ores. In Cooke, D. R. and Kitto, P. A. (eds.) Contentious issues in Tasmanian geology. Geological Society of Australia abstracts, vol. 39, p. 107-108.

Allen, R. L., 1997. Rosebery alteration study and regional alteration studies in the Mount Read Volcanics. The record of diagenetic alteration in the strongly deformed, felsic volcaniclastic succession enclosing the Rosebery and Hercules massive sulphide deposits: Australian Mineral Industry Research Association (AMIRA), Unpublished Project P439, Report 5, October 1997, p. 135-173.

Allen R. L., 1998. Review of RGC's base and precious metals exploration projects at White Spur and South Henty, Western Tasmania. Report to RGC Exploration Pty Limited, Zeehan, Tasmania, Australia, 28 p.

Allen, R. L., and Cas, R. A. F., 1990. The Rosebery controversy: Distinguishing prospective submarine ignimbrite-like units from true ignimbrites in the Rosebery-Hercules Zn-Cu-Pb massive sulphide district, Tasmania [abs.], 10th Australian Geological Convention: Hobart, Geological Society of Australia, p. 31-32.

Allen, R. L., Weihed, P. and the global VMS research project team, 2002. Global comparisons of volcanic-associated massive sulphide districts. Geological Society of London Special Publication 204, p. 13-37.

Allen, R. L., Weihed, P. and Svenson, S-Å, 1997. Setting of Zn-Cu-Au-Ag massive sulfide deposits in the evolution and facies architecture of a 1.9 Ga marine volcanic arc, Skellefte district, Sweden. Economic Geology, vol. 91, p. 1022-1053.

Ashley, P. M., Dudley, R. J., Lesh, R. H., Marr, J. M., and Ryall, A. W., 1988. The Scuddles Cu-Zn prospect, an Archean volcanogenic massive sulfide deposit, Golden Grove district, Western Australia. Economic Geology, v. 83, p. 918-951.

Baillie, P. W., 1989. Stratigraphy, sedimentology and structural setting of the Cambrian Sticht Range Formation, western Tasmania: Tasmanian Geological Survey, Bulletin 65, 34p.

Baillie, P. W., and Jago, J. B., 1995. Sedimentology of an Upper Cambrian turbidite succession, Smithton Basin, northwest Tasmania. Australian Journal of Earth Sciences, vol. 42, p. 75-82.

Baillie, P. W., Powell, C. McA., Banks, M. R. and Hills, P. B., 1989. The Eastern Tasmanian Terrane. In: Burrett, C. F. and Martin, E. L., editors, Geology and Mineral Resources of Tasmania. Geological Society of Australia Special Publication, vol. 15, p. 234-237.

Banks, M. R. and Williams, E., 1986. The Wurawina Supergroup, Late Cambrian to Early Devonian, Tasmania. Papers and Proceedings of the Royal Society of Tasmania, vol. 120, p. 95-96.

Barrett, T. J., and MacLean, W. H., 1994. Chemostratigraphy and hydrothermal alteration in exploration for VHMS deposits in greenstone belts and younger volcanic rocks. Geological Association of Canada short course notes 11, p. 433-467.

Barrett, T. J., and Sherlock, R. L., 1996. Geology, lithogeochemistry and volcanic setting of the Eskay Creek Au-Ag-Cu-Zn deposit, northwestern British Columbia. Exploration and Mining Geology, vol. 5, p. 339-368.

Barrie, C. T., Amelin, Y., Pascual, E., 2002. U-Pb geochronology of VMS mineralization in the Iberian Pyrite Belt. Mineralium Deposita, vol. 37, p. 684-703.

Belford, S. M., Davidson, G. J., McPhie, J. and Large, R. R., 2015. Architecture of the Neoarchaean Jaguar VHMS deposit, Western Australia: Implications for prospectivity and the presence of depositional breaks. Precambrian Research, vol. 260, p. 136-160.

Berry, R. F., 1989. The history of movement on the Henty Fault Zone, western Tasmania - an analysis of fault striations. Australian Journal of Earth Sciences, vol. 36, p. 189-205.

Berry, R. F., and Crawford, A. J., 1988. The tectonic significance of Cambrian allochthonous mafic- ultramafic complexes in Tasmania. Australian Journal of Earth Sciences, vol. 35, p. 523-533.

Berry, R. F. and Keele, R. A., 1993. Cambrian structure in western Tasmania. CODES/AMIRA Project P291 Final Report, p. 55-68. Centre for Ore Deposit and Exploration Studies, University of Tasmania.

Berry, R. F., and Keele, R. A., 1997. Cambrian tectonics and mineralisation in western Tasmania. AusIMM 3rd International Mining Conference, November 1997, p. 13-16.

Berry, R. F., Chmielowski, R. M., Steele, D. A. and Meffre, S., 2007. Chemical U-Th-Pb monazite dating of the Cambrian Tyennan Orogeny, Tasmania. Australian Journal of Earth Sciences, vol. 54, p. 757-771.

Berry, R. F., Holm, O. H. and Steele, D. A., 2005. Chemical U-Th-Pb dating and the Proterozoic history of King Island, southeast Australia. Australian Journal of Earth Sciences, vol. 52, p. 461–471.

Billstrom, K. And Weihed, P., 1996. Age provenance of host rocks and ores in the Paleoproterozoic Skellefte district, northern Sweden. Economic Geology, vol. 91, p. 1054-1072.

Black, L. P., Calver, C. R., Seymour, D. B. and Reed, A., 2004. SHRIMP U-Pb detrital zircon ages from the Proterozoic and Early Palaeozoic sandstones and their bearing on the early geological evolution of Tasmania. Australian Journal of Earth Sciences, vol. 51, p. 885-900.

Black, L. P., Everard, J. L., McClenaghan, M. P., Korsch, R. J., Calver, C. R., Fioretti, A. M., Brown, A. V. and Foudoulis, C., 2010. Controls on Devonian-Carboniferous magmatism in Tasmania, based on inherited zircon age patterns, Sr, Nd and Pb isotopes, and major and trace element geochemistry. Australian Journal of Earth Sciences, vol. 57, p. 933-968.

Black, L. P., McClenaghan, M. P., Korsch, R. J., Everard, J. L., and Foudoulis, C., 2005. Significance of Devonian-Carboniferous igneous activity in Tasmania as derived from U-Pb SHRIMP dating of zircon. Australian Journal of Earth Sciences, vol. 52, p. 807-829.

Black, L. P., Seymour, D. B., Corbett, K. D., Cox, S. E., Streit, J. E., Bottrill, R. S., Calver, C. R., Everard, J. L., Green, G. R., McClenaghan, M. P., Pemberton, J., Taheri, J., Turner, N. J., 1997. Dating Tasmania's oldest geological events. Mineral Resources Tasmania and the Australian Geological Survey Organisation. Record 1997/15. 57 p.

Bold, T., 2009. The volcanology and stratigraphy of the Southwell Subgroup, Mount Read Volcanics, west Tasmania. Honours Thesis. University of Tasmania.

Bottrill, R. S. and Taheri, J., 2008. Petrology of the host rocks, including mineralisation and adjacent rock sequences, from the Savage River mine. Tasmanian Geological Survey Record 2007/05.

Branney, M. J. and Sparks, R. S. J., 1990. Fiamme formed by diagenesis and burial compaction in soils and subaqueous

sediments. Journal of the Geological Society (London), vol. 147, p. 919-922.
Branney, M. J., and Suthren, R. J., 1988. High-level peperitic sills in the English Lake District: distinction from block lavas, and implications for Borrowdale Volcanic Group stratigraphy. Geol. J., vol. 23, p. 171-187.
Brathwaite, R. L., 1969. The Geology of the Rosebery Ore Deposit. Unpublished PhD thesis, University of Tasmania, 218p.
Brathwaite, R. L., 1974. The geology and origin of the Rosebery ore deposit, Tasmania. Economic Geology, vol. 69, p. 1086-1101.
Brewer, T. S., Hergt, J. M., Hawkesworth, C. J., Rex, D. and Storey, B. C., 1992. Coats Land dolerites and the generation of Antarctic continental flood basalts. In: Storey, B. C., Alabaster, T. and Pankhurst, R. J., editors, Magmatism and the causes of continental break-up. Geological Society Special Publication, vol. 68, p. 185-208.
Briggs, T., and McNeill, A. W., 2001. Dundas EL 21-96. Final report for the period 9-10-2000 to 8-10- 2001, Pasminco Exploration Ltd.
Briggs, T. J., and McNeill, A. W., 2005. Hercules and South Hercules Zn-Pb-Cu-Ag-Au deposits, western Tasmania, in: C. R. M. Butt, I. D. M. Robertson, K. M. Scott and M. Cornelius (ed.). Regolith Expression of Australian Ore Systems. CRC LEME, Perth, p. 165-167.
Brown, A. V., 1983. Regional geology of the Dundas-Mt Lindsay-Mt Ramsay area. 1:25 000 geological map. Tasmania Department of Mines.
Brown, A. V., 1986. Geology of the Dundas-Mt Lindsay-Mt Youngbuck region. Geological Survey Bulletin 62. Tasmania Department of Mines, Hobart.
Brown, A. V., 1998. Platinum group elements and their host rocks in Tasmania - a summary review. Tasmania Geological Survey. 7p.
Bull, K. F. and McPhie, J., 2007. Fiamme textures in volcanic successions: Flaming issues of definition and interpretation. Journal of Volcanology and Geothermal Research, vol. 164, p. 205-206.
Burrett, C. F. and Martin, E. L., editors, 1989. Geology and Mineral Resources of Tasmania. Geological Society of Australia Special Publication, vol. 15, 574 p.
Callaghan, T., 2001. Geology and host-rock alteration of the Henty and Mount Julia gold deposits, western Tasmania. Economic Geology, vol. 96, p. 1073-1088.
Calver, C. R., 1998. Isotope stratigraphy of the Neoproterozoic Togari Group, Tasmania. Australian Journal of Earth Sciences, vol. 45, p. 865-874.
Calver, C. R., 2007. Some notes on the geology of King Island. Tasmanian Geological Survey Record 2007/2.
Calver, C. R. and Walter, M. R., 2000. The late Neoproterozoic Grassy Group of King Island, Tasmania: correlation and palaeogeographic significance. Precambrian Research, vol. 100, p. 299-312.
Calver, C. R., Black, L. P., Everard, J. L. and Seymour, D. B., 2004. U-Pb zircon age constraints on late Neoproterozoic glaciation in Tasmania. Geology, vol. 32, p. 893-896.
Campana, B., and King, D., 1963. Paleozoic tectonism, sedimentation and mineralization in west Tasmania. Journal of the Geological Society of Australia, vol. 10, p. 1-54.
Carey, S. P. and Berry, R. F., 1988. Thrust sheets at Point Hibbs, Tasmania: palaeontology, sedimentology, and structure. Australian Journal of Earth Sciences, vol. 35, p. 169-180.
Cas, R. A. F., Allen, R. L., Bull, S. W., Clifford, B. A. and Wright, J. V., 1990. Subaqueous, rhyolitic dome-top tuff cones: a model based on the Devonian Bunga Beds, southeastern Australia and a modern analogue. Bulletin of Volcanology, vol. 52, 159-174.
Cas, R. A. F. and Wright, J. V., 1987. Volcanic successions: modern and ancient: a geological approach to processes, products and successions. Allen and Unwin, London, 487 p.
Cas, R. A. F. and Wright, J. V., 1991. Subaqueous pyroclastic flows and ignimbrites: as assessment. Bulletin of Volcanology, vol. 53, pp. 357-380.
Cayley, R. A., 2011. Exotic crustal block accretion to the eastern Gondwanaland margin in the Late Cambrian, Tasmania, the Selwyn Block, and implications for the Cambrian-Silurian evolution of the Ross, Delamerian, and Lachlan orogens. Gondwana Research, vol. 19, p. 628-649.
Chmielowski, R. M., 2009. The Cambrian metamorphic history of Tasmania. PhD thesis. University of Tasmania.
Collins, P. L. F., 1981. The Mount Read Volcanics and associated rocks in the Pinnacles-Que River area, in Collins, P. L. F., Gulline, A. B., Williams, E. (compilers). Geological atlas 1 mile series. Sheet 44 (8014S). Mackintosh. Explanatory Report, Geological Survey, Tasmania.
Collins, P. L. F., and Williams, E., 1986. Metallogeny and tectonic development of the Tasman fold belt system in Tasmania. Ore Geology Reviews, vol. 1, p. 153-201.
Corbett, K. D., 1970. Sedimentology of an upper Cambrian flysch-paralic sequence (Denison Group) on the Denison Range, southwest Tasmania. Unpublished PhD thesis, University of Tasmania, Australia.
Corbett, K. D., 1975. The Late Cambrian to Early Ordovician Sequence on the Denison Range, southwest Tasmania.

Papers and Proceedings of the Royal Society of Tasmania, vol. 109, p. 111-120.
Corbett, K. D., 1979. Stratigraphy, correlation and evolution of the Mt Read Volcanics in the Queenstown, Jukes-Darwin and Mt Sedgwick areas: Tasmania Geological Survey Bulletin 58, 74p.
Corbett, K. D., 1981. Stratigraphy and mineralization in the Mount Read Volcanics, western Tasmania. Economic Geology, vol. 76, p. 209-230.
Corbett, K. D., 1982. Stratigraphy and correlation of the Mt Read Volcanics and associated rocks in the Mt. Sedgwick-Lake Beatrice area and the Lake Dora-Lake Spicer area. Unpublished report 1982/25, Tasmania Department of Mines, 29 p.
Corbett, K. D., 1984. Geological maps and summary of the Cambrian stratigraphic units and relationships in the Henty River-Williamsford area. Tasmanian Geological Survey Record 1984/84, 23 p.
Corbett, K. D., 1985. The Mt. Read drill hole (MR1) through the Central Volcanic Sequence-White Spur Formation contact near Howards Road, western Tasmania. Unpublished report 1985/55, Tasmania Department of Mines, 7 p.
Corbett, K. D., 1989. Stratigraphy, paleogeography and geochemistry of the Mount Read Volcanics, in: Burrett, C. F. and Martin, E. L. (eds.) Geology and mineral resources of Tasmania. Special Publication Geological Society of Australia 15:86-119.
Corbett, K. D., 1992. Stratigraphic-volcanic setting of massive sulfide deposits in the Cambrian Mount Read Volcanics, Tasmania. Economic Geology, vol. 87, p. 564-586.
Corbett, K. D. (compiler) 1995. Digital Geological Atlas 1:25 000 Scale Series. Sheet 3839 Charter. Mineral Resources Tasmania.
Corbett, K. D., 2001a. New mapping and interpretations of the Mount Lyell mining district, Tasmania: a large hybrid Cu-Au system with an exhalative Pb-Zn top. Economic Geology, vol. 96, p. 1089-1122.
Corbett, K. D., 2001b. The geology of the Mount Lyell Mines area, Tasmania - a re-interpretation based on studies at Lyell Comstock, North Lyell and the Iron Blow area. Unpublished M.Sc. (Masters) thesis. University of Tasmania, Australia, 72 p.
Corbett, K. D. (compiler) 2002a. Bedrock Geological Map of the Mt. Read Volcanics Belt and adjacent areas South Darwin Peak to Hellyer. Mineral Resources Tasmania, 1:100 000 Scale map.
Corbett, K. D., 2002b. Western Tasmanian Regional Minerals Program. Mount Read Volcanics Compilation. Updating the geology of the Mount Read Volcanics belt. Tasmanian Geological Survey record 2002/19.
Corbett, K. D., 2005a. A compilation and interpretation of the geology of the Burns Peak area. Unpublished report, Zinifex Exploration, Rosebery.
Corbett, K. D., 2005b. A brief review of geology, exploration and VHMS potential in the North Pinnacles area. Unpublished report for Zinifex Rosebery mine.
Corbett, K. D., 2007. A review of the geology and exploration features of the Browns Tunnel-Burns Peak area. Unpublished report for Zinifex Rosebery mine.
Corbett, K. D. and Komyshan, P., 1989. Geology of the Hellyer-Mount Charter area. Geological Report. Mount Read Volcanics Project Tasmania 1, 48 p.
Corbett, K. D., and Lees, T. C., 1987. Stratigraphic and structural relationships and evidence for Cambrian deformation at the western margin of the Mount Read Volcanics, Tasmania. Australian Journal Earth Sciences, vol. 34, p. 45-67.
Corbett, K. D. and McNeill, A. W., 1986. Geology of the Rosebery-Mount Block area. Mount Read Volcanics Project Map 2, Tasmania Mines Department.
Corbett, K. D. and Solomon, M., 1989. Cambrian Mount Read Volcanics and associated mineral deposits: Chapter 4 in Burrett, C. F. and Martin, E. L. (eds.) "Geology and Mineral Resources of Tasmania". Geological Society of Australia. Special Publication, vol. 15, p. 84-153.
Corbett, K. D., and Turner, N. J., 1989. Early Palaeozoic deformation and tectonics, in Burrett, C. F., and Martin, E. L., eds., Geology and Mineral Resources of Tasmania Special Publication 15, Geological Society of Australia, p. 154-181.
Corbett, K. D., Banks, M. R., and Jago, J. B., 1972. Plate tectonics and the lower Paleozoic of Tasmania. Nature, Physical Science, vol. 240, p. 9-11.
Corbett, K. D., Quilty, P. G., and Calver, C. R. editors, 2014. Geological Evolution of Tasmania. Geological Society of Australia Special Publication 24, Geological Society of Australia (Tasmania Division).
Corbett, K. D., Reid, K. O., Corbett, E. B., Green, G. R., Wells, K. and Sheppard, N., W., 1974. The Mount Read Volcanics and Cambro-Ordovician relationships at Queenstown, Tasmania. Journal of the Geological Society of Australia, vol. 21, p. 173-186.
Coutts, B. P., 1990. The geology, geochemistry and hydrothermal alteration of the Hollway Andesite, Western Tasmania. Unpublished BSc (Hons.) thesis, University of Tasmania, Hobart.

Cox, S. F., 1981. The stratigraphic and structural setting of the Mt. Lyell volcanic-hosted sulfide deposits. Economic Geology, vol. 76, p. 231-245.

Crawford, A. J., and Berry, R. F., 1992. Tectonic implications of late Proterozoic-early Paleozoic igneous rock associations in western Tasmania. Tectonophysics, vol. 214, p. 37-56.

Crawford, A. J., Corbett, K. D., and Everard, J. L., 1992. Geochemistry of the Cambrian volcanic-hosted massive sulfide-rich Mount Read Volcanics, Tasmania and some tectonic implications. Economic Geology, vol. 87, p. 597-619.

Crawford, A. J., Lanyon, R., Elmes, M., and Eggins, S., 1997. Geochemistry and significance of basaltic rocks dredged from the South Tasman Rise and adjacent seamounts. Australian Journal of Earth Sciences, vol. 44, p. 621-632.

Crawford, A. J., Gifkins, C. C. and Allen, R. L., 2000. Tectonic setting of mineralisation, Mt. Read Volcanics, western Tasmania. In: Gemmell, J. B. and Pongratz, J., editors, Volcanic environments and massive sulphide deposits, International conference and field meetings, Program and Abstracts. Hobart, Tasmania, Centre for Ore Deposits Research, p. 31-33.

Crawford, A. J., Meffre, S. and Symonds, P. A., 2003. 120 to 0 Ma tectonic evolution of the southwest Pacific and analogous geological evolution of the 600 to 220 Ma Tasman Fold Belt System. In: Hillis, R. R., and Muller, R. D. (editors), Evolution and dynamics of the Australian plate. Geological Society of Australia Special Publication, vol. 22, p. 383-403.

Crook, K. A. W., 1980. Forearc evolution in the Tasman Geosyncline: the origin of the southeast Australian continental crust. Journal of the Geological Society of Australia, vol. 27, p. 215-232.

Dalziel, I. W. D., 1991. Pacific margins of Laurentia and east Antarctica-Australia as a conjugate rift pair: evidence and implications for an Eocambrian supercontinent. Geology, vol. 19, p. 598-601.

Denwer, K. P., 2012. MMG Rosebery seismic exploration. Bass Metals Ltd. Unpublished presentation. December 2012.

Direen, N. G. and Crawford, A. J., 2003a. The Tasman Line: where is it, what is it, and is it Australia's Rodinian breakup boundary? Australian Journal of Earth Sciences, vol. 50, p. 491-502.

Direen, N. G. and Crawford, A. J., 2003b. Fossil seaward-dipping reflector sequences preserved in southeastern Australia: a 600 Ma volcanic passive margin in eastern Gondwanaland. Journal of the Geological Society, London, vol. 160, p. 985-990.

Doyle, M. G., and Allen, M. R., 2003. Subsea-floor replacement in volcanic-hosted massive sulfide deposits. Ore Geology Reviews, vol. 23, p. 183-222.

Doyle, M. G., and McPhie, J., 2000. Facies architecture of a silicic intrusion-dominated volcanic centre at Highway-Reward, Queensland, Australia. Journal of Volcanology and Geothermal Research, vol. 99, p. 79-96.

Dugdale, J. S., 1992. Lithostratigraphy of the White Spur area, W Tasmania. Honours thesis. University of Tasmania.

Eastoe, C. J., 1973. The Rosebery host rock horizon. Unpublished B.Sc Honours thesis, University of Tasmania, 148 p.

Eastoe, C. J., Solomon, M., and Walshe, J. L., 1987. District-scale alteration associated with massive sulfide deposits in the Mount Read Volcanics, western Tasmania. Economic Geology, vol. 82, p. 1239-1258.

Elliot, D. H. and Fleming, T. H., 2004. Occurrence and dispersal of magmas in the Jurrassic Ferrar Large Igneous Province, Antarctica. Gondwana Research, vol. 7(1), p. 223-237.

Elliston, J., 1954. Geology of the Dundas District, Tasmania. Papers and Proceedings of the Royal Society of Tasmania, vol. 88, p. 161-183.

Everard, J. L., (compiler) 2000. Digital Geological Atlas 1:25 000 Scale Series. Sheet 3638 Parsons. Mineral Resources Tasmania.

Everard, J. L., and Villa, I. M., 1994. Argon geochronology of the Crown Hill Andesite, Mount Read Volcanics, Tasmania. Australian Journal Earth Sciences, vol. 41, p. 265-272.

Everard, J. L., Zhang, M., Lo, C.-H., O´Reilly, S., and Forsyth, S. M., 2004. Overview of Tasmanian Tertiary basalts. Abstracts Geological Society of Australia, 73:74.

Fergusson, C. L., 2014. Late Ordovician to mid-Silurian Benambran subduction zones in the Lachlan Orogen, southeastern Australia. Australian Journal of Earth Sciences, vol. 61, p. 587-606.

Fisher, R., V., 1958. Definition of volcanic breccia. Bulletin of the Geological Society of America, vol. 69, p. 1071-1073.

Fisher, R., V., 1960. Classification of volcanic breccias. Geological Society of America Bulletin, vol. 71, p. 973-982.

Fisher, R., V., 1961. Proposed classification of volcaniclastic sediments and rocks. Geological Society of America Bulletin, vol. 72, p. 1409-1414.

Fisher, R., V., 1966. Rocks composed of volcanic fragments. Earth Science Reviews vol. 1, p. 287-298.

Franklin, J. M., Gibson, H. L., Jonasson, I. R., Galley, A. G., 2005. Volcanogenic Massive Sulfide Deposits: Economic Geology 100th Anniversary Volume, Society of Economic Geologists, p. 523-560.

Franklin, J. M., Lydon, J. W., and Sangster, D. F., 1981. Volcanic-associated massive sulfide deposits, in Skinner, B. J.,

ed., Economic Geology 75th Anniversary Volume, Society of Economic Geologists, p. 485-627.
Galley, A. G., Hannington, M., and Jonasson, I., 2007. Volcanogenic massive sulphide deposits, in Goodfellow, W. D., ed., Mineral Deposits of Canada: A Synthesis of Major Deposit-types, District Metallogeny, the Evolution of Geological Provinces, and Exploration Methods, Special Publication 5, Mineral Deposits Divison, Geological Association of Canada, p. 141-161.
Gee, R. D., 1967. The tectonic evolution of the Rocky Cape Geanticline in northwest Tasmania. Unpublished PhD thesis. University of Tasmania, Australia.
Gee, R. D., 1968. A revised stratigraphy for the Precambrian in north-west Tasmania. Papers and Proceedings of the Royal Society of Tasmania, vol. 102, p. 7-10.
Gee, R. D., 1977. Burnie, Tasmania. Geological atlas 1 mile series explanatory report. Tasmania Department of Mines, 81p.
Gee, C. E., Jago, J. B., and Quilty, P. G., 1970. The age of the Mount Read Volcanics in the Que River area, western Tasmania. Journal of the Geological Society of Australia, vol. 16, p. 761-763.
Gemmell, J. B., and Fulton, R., 2001. Geology, genesis, and exploration implications of the footwall and hanging-wall alteration associated with the Hellyer volcanic-hosted massive sulfide deposit, Tasmania, Australia. Economic Geology, vol. 96, p. 1003-1035.
Gemmell, J. B., and Large, R. R., 1992. Stringer system and alteration zones underlying the Hellyer volcanic-hosted massive sulfide deposit, Tasmania, Australia. Economic Geology, vol. 87, p. 620-649.
Gibson, H. L., Morton, R. L., Hudak, G. L., 1999. Submarine volcanic processes, deposits, and environments favourable for the location of volcanic-associated massive sulfide deposits, In: Barrie, C. T., Hannington, M. D., (editors), Volcanic-Associated Massive Sulfide Deposits: Processes and Examples in Modern and Ancient Settings. Reviews in Economic Geology, vol. 8, p. 13-51.
Gifkins, C. C., 2001. Submarine volcanism and alteration in the Cambrian northern Central Volcanic Complex, Tasmania. PhD thesis. University of Tasmania. 312 p.
Gifkins, C. C., and Allen, R. L., 2001. Textural and chemical characteristics of diagenetic and hydrothermal alteration in glassy volcanic rocks: examples from the Mount Read Volcanics, Tasmania. Economic Geology, vol. 96, p. 973-1002.
Gifkins, C. C., Herrmann, W., and Large, R. R., 2005. Altered volcanic rocks: a guide to description and interpretation. Centre for Ore Deposit Research, University of Tasmania, Hobart, 275 p.
Gifkins, C. C., McPhie, J., and Allen, R. L., 2002. Pumiceous rhyolitic peperite in ancient submarine volcanic successions. Journal of Volcanology and Geothermal Research, vol. 114, p. 181-203.
Glasby, G. P., Iizasa, K., Hannington, M., Kutoba, M. and Notsu, K., 2008. Mineralogy and composition of Kuroko deposits from northeastern Honshu and their possible modern analogues from the Izu-Ogasawara (Bonin) Arc south of Japan: Implications for mode of formation. Ore Geology Reviews, vol. 34, p. 547-560.
Gonzalez, F., Moreno, C., Sáez, R., Clayton, G., 2002. Ore genesis age of the Tharsis Mining District (Iberian Pyrite Belt): a palynological approach. Journal of the Geological Society of London, vol. 159, p. 229-232.
Goto, Y. and McPhie, J., 1988. Endogenous growth of a Miocene submarine dacite cryptodome, Rebun Island, Hokkaido, Japan. Journal of Volcanology and Geothermal Research, vol. 84, p. 273-286.
Green, G. R., 1983. The geological setting and formation of the Rosebery volcanic-hosted massive sulphide orebody, Tasmania. Unpublished PhD thesis, University of Tasmania, Australia, 288 p.
Green, G. R., 1984. The structure of bedded rocks west of Rosebery and their significance in a regional context. In: Proceedings Mineral exploration and tectonic processes in Tasmania, Symposium, Burnie, 1984. Geological Society of Australia, Tasmania Division, p. 28-32.
Green, G. R., Solomon, M., and Walshe, J. L., 1981. The formation of the volcanic-hosted massive sulfide ore deposit at Rosebery, Tasmania. Economic Geology, vol. 76, p. 304-338.
Halley, S. W., and Roberts, R. H., 1997. Henty: a shallow-water gold-rich volcanogenic massive sulfide deposit in western Tasmania. Economic Geology, vol. 92, p. 438-447.
Hergt, J. M., McDougall, I., Banks, M. R., Green, D. H., 1989. Jurassic dolerite. In: Burrett, C. F.; Martin, E. L., editors, Geology and Mineral Resources of Tasmania. Geological Society of Australia Special Publication, vol. 15, p. 375-381.
Hergt, J. M., Peate, D. W. and Hawkesworth, C. J., 1991. The petrogenesis of Mesozoic Gondwana low-Ti flood basalts. Earth and Planetary Science Letters, vol. 105, p. 134-148.
Herrmann, W., Green, G. R., Barton, M. D., and Davidson, G. J., 2009. Lithogeochemical and stable isotopic insights into submarine genesis of pyrophyllite-altered facies at the Boco prospect, western Tasmania. Economic Geology, vol. 104, p. 775-792.
Hollis, S. P., Yeats, C. J., Wyche, S., Barnes, S. J., Ivanic, T. J., Belford, S. M., Davidson, G. J., Roache, A. J., and

Wingate, M. T. D., 2015. A review of volcanic-hosted massive sulfide (VHMS) mineralization in the Archaean Yilgarn Carton, Western Australia: Tectonic, stratigraphic and geochemical associations. Precambrian Research, vol. 260, p. 113-135.

Holm, O. H., and Berry, R. F., 2002. Structural history of the Arthur Lineament, northwest Tasmania - an analysis of critical outcrops. Australian Journal Earth Sciences, vol. 49, p. 167-185.

Huston, D. L. and Kamprad, J., 2001. Zonation of alteration facies at western Tharsis: implications for the genesis of Cu-Au deposits, Mount Lyell field, western Tasmania. Economic Geology, vol. 96, p. 1123-1132.

Huston, H. D., and Large, R. R., 1988. Distribution, mineralogy, and geochemistry of gold and silver in the north end orebody, Rosebery, Tasmania. Economic Geology, vol. 83, p. 1181-1192.

Jago, C. M., 2005. Correlations of the Rosebery-Hercules host sequence at White Spur, Mt. Read Volcanics, western Tasmania: Implications for Exploration. Unpublished B.Sc. (Honours) thesis, Hobart, Australia, University of Tasmania, 89 p.

Jago, J. B., 1973. Cambrian agnostid communities in Tasmania. Lethaia, vol. 6(4), p. 405-422.

Jago, J. B., 1977. A Late Middle Cambrian fauna from the Que River Beds, western Tasmania. Papers and Proceedings of the Royal Society of Tasmania, vol. 111, p. 41-57.

Jago, J. B., 1979. Tasmanian Cambrian biostratigraphy - a preliminary report. Journal of the Geological Society of Australia, vol. 26, p. 223-230.

Jago, J. B., 1986. An early Late Cambrian fauna from Tom Creek, western Tasmania. Papers and Proceedings of the Royal Society of Tasmania, vol. 120, p. 97-98.

Jago, J. B., 1987. Idamean (Late Cambrian) trilobites from the Denison Range, south-west Tasmania. Palaeontology, vol. 30, p. 207-231.

Jago, J. B., 1989. Late Cambrian brachiopods from the Denison Range, south-west Tasmania. Papers and Proceedings of the Royal Society of Tasmania, vol. 123, p. 37-42.

Jago, J. B., and Bentley, C. J., 2010. Geological significance of middle Cambrian trilobites from near Melba Flats, western Tasmania. Australian Journal Earth Sciences, vol. 57, p. 469-481.

Jago, J. B., and Brown, A. V., 1989. Middle to Upper Cambrian fossiliferous sedimentary rocks. In: Burrett, C. F., and Martin, E. L., editors, Geology and Mineral Resources of Tasmania. Geological Society of Australia Special Publication, vol. 15, p. 74-83.

Jago, J. B., and McNeill, A., 1997. A late Middle Cambrian shallow-water trilobite fauna from the Mount Read Volcanics, northwestern Tasmania. Papers and Proceedings of the Royal Society of Tasmania, vol. 131, p. 85-90.

Jago, J. B., Reid, K. O., Quilty, P. G., Green, G. R., and Daily, B., 1972. Fossiliferous Cambrian limestone within the Mount Read Volcanics, Mount Lyell mine area, Tasmania. Journal of the Geological Society of Australia, vol. 19, p. 379-382.

Jutzeler, M., McPhie, J., Allen, S. R., 2014. Submarine eruption-fed and resedimented pumice-rich facies: the Dogashima Formation (Izu Peninsula, Japan). Bulletin of Volcanology, 76:867.

Kano, K., Takeuchi, K., Yamamoto, T. and Hoshizumi, H., 1991. Subaqueous rhyolite block lavas in the Miocene Ushikiri Formation, Shimane Peninsula, SW Japan. Journal of Volcanology and Geothermal Research, vol. 46, p. 241-253.

Kaufmann, B., 2006. Calibrating the Devonian time scale: a synthesis of U-Pb ID-TIMS ages and conodont stratigraphy. Earth Science Reviews, vol. 76, p. 175-190.

Kendall, B., Creaser, R. A., Calver, C. R., Raub, T. D. and Evans, D. A. D., 2009. Correlation of Sturtian diamictite successions in southern Australia and northwestern Tasmania by Re-Os black shale geochronology and the ambiguity of "Sturtian"-type diamictite-cap carbonate pairs as chronostratigraphic marker horizons. Precambrian Research, vol. 172, p. 301-311.

Kokelaar, B. P., 1982. Fluidization of wet sediments during the emplacement and cooling of various igneous bodies. J. Geol. Soc. London, vol. 139, p. 21-33.

Komyshan, P., 1986a. Mount Read Volcanics Project. Map 1, Geology of the Mount Charter-Hellyer area. Department of Mines, Tasmania.

Komyshan, P., 1986b. Geology of the Hellyer-Mount Charter area, in Large, R. R., ed., The Mount Read Volcanics and associated ore deposits: Symposium, Burnie, November 1986, Geological Society of Australia, Tasmanian Division, Abstracts, p. 53-55.

Kruse, P. D., Jago, J. B. and Laurie, J. R., 2009. Recent developments in Australian Cambrian stratigraphy. Journal of Stratigraphy, vol. 33, p. 35-47.

Large, R. R., 1992. Australian Volcanic-Hosted Massive Sulfide Deposits - Features, Styles, and Genetic Models. Economic Geology, vol. 87, p. 471-510.

Large, R. R., Allen, R. L., Blake, M. D., and Herrmann, W., 2001a. Hydrothermal alteration and volatile element halos for the Rosebery K lens volcanic-hosted massive sulfide deposit, western Tasmania. Economic Geology, vol. 96, p. 1055-1072.

Large, R. R., Doyle, M., Raymond, O., Cooke, D., Jones, A., and Heasman, L., 1996. Evaluation of the role of Cambrian granites in the genesis of world class VHMS deposits in Tasmania. Ore Geology Reviews, vol. 10, p. 215-230.

Large, R. R., Gemmell, J. B., Paulick, H. and Huston, D. L., 2001b. The alteration box plot: a simple approach to understanding the relationship between alteration mineralogy and Lithogeochemistry associated with volcanic-hosted massive sulfide deposits. Economic Geology, vol. 96, p. 957-971.

Large, R. R., McPhie, J., Gemmell, J. B., Herrmann, W., and Davidson, G. J., 2001c. The spectrum of ore deposit types, volcanic environments, alteration halos, and related exploration vectors in submarine volcanic successions: Some examples from Australia. Economic Geology and the Bulletin of the Society of Economic Geologists, vol. 96, p. 913-938.

Laurie, J. R., 1996. Correlation of Lower-Middle Ordovician clastics in Tasmania. Australian Geological Survey record 1995/23, 18 p.

Laurie, J. R., Jago, J. B., and Bao, Jin-Song, 1995. Review of Tasmania Cambrian biostratigraphy. Australian Geological Survey Organ. Record 1995/69:1-32.

Leaman, D. E., 1995. Mechanisms of sill emplacement: comments based on the Tasmanian dolerites. Australian Journal of Earth Sciences, vol. 42, p. 151-155.

Leaman, D. E., 1997. Features of Jurassic dolerite intrusions at Cape Surville, Lymwood, Single Hill and Mount Nelson, Tasmania. Papers and Proceedings of the Royal Society of Tasmania, vol. 131, p. 13-20.

Leaman, D. E., 2012. The Rock That Made Tasmania. Leaman Geophysics, Hobart.

Leaman, D. E., and Richardson, R. G., 1989. The granites of west and north-west Tasmania - a geophysical interpretation. Geological Survey Tasmania, Bulletin 66, Mineral Resources Tasmania, 144 p.

Leaman, D. E., and Richardson, R. G., 2003. A geophysical model of the major Tasmanian granitoids. Mineral Resources Tasmania, Tasmanian Geological Survey, Record 2003/11, 8 p.

Leaman, D. E., Richardson, R. G., and Shirley, J. E., 1980. Tasmania – the gravity field and its interpretation. Report Mineral Resources Tasmania, 37p.

Lees, T. C., 1987. Geology and Mineralisation of the Rosebery-Hercules area, Tasmania. Unpublished MSc. thesis, University of Tasmania, 160p.

Lees, T. C., Khin Zaw, Large, R. R: and Huston, D. L., 1990. Rosebery and Hercules copper-lead-zinc deposits. In: Hughes, F. E., editor, Geology of the Mineral Deposits of Australia and Papua New Guinea, p. 1241-1247. The Australasian Institute of Mining and Metallurgy, Melbourne.

Li, Z.X., Baillie, P.W., Powell, C.M., 1997. Relationship between northwestern Tasmania and east Gondwanaland in the late Cambrian/early Ordovician: Paleomagnetic evidence. Tectonics, vol. 16, p. 161-171.

Li, Z. X., Bogdanova, S. V., Collins, A. S., Davidson, A., De Waele, B., Ernst, R. E., Fitzsimons, I. C. W., Fuck, R. A., Gladkochub, D. P., Jacobs, J., Karlstrom, K. E., Lu, S., Natapovm, L. M., Pease, V., Pisarevsky, S. A., Thrane, K., Vernikovsky, V., 2008. Assembly, configuration, and break-up history of Rodinia - a synthesis. Precambrian Research, vol. 160, p. 179-210.

Lorrigan, A. N., 1991. Bulgobac Hill annual report EL 37-38 for the period March 1990 to January 1991. Pasminco Exploration 91-3225.

Lowe, D. R., 1976. Grain flow and grain flow deposits. Journal of Sedimentary Research, vol. 46, p.188-199.

Lowe, D. R., 1982. Sediment Gravity Flows: II Depositional models with special reference to the deposits of high-density turbidity currents. Journal of Sedimentary Research, vol. 52 (1), p. 279-297.

Lydon, J. W., 1984. Volcanogenic massive sulfide deposits. Part I: A descriptive model: Geoscience Canada, vol. 11, p. 195-202.

Lydon, J. W., 1988. Volcanogenic massive sulfide deposits. Part 2 Genetic models: Geoscience Canada, vol. 15, p. 43-65.

MacLean, W. H., and Kranidiotis, P., 1987. Immobile elements as monitors of mass-transfer in hydrothermal alteration - Phelps Dodge massive sulfide deposit, Matagami, Quebec. Economic Geology, v. 82, p. 951-962.

Marcoux, E., 1998. Lead isotopic systematic in the giant massive sulphide deposits in the Iberian Pyrite belt. Mineralium Deposita, vol. 33, p. 45-58.

Martin, N. K., 2004. Genesis of the Rosebery massive sulfide deposit, western Tasmania, Australia. PhD thesis, University of Tasmania, 273 p.

Mathur, R. Ruiz, J. and Tornos, F., 1999. Age and sources of the ore at Tharsis and Rio Tinto, Iberian Pyrite Belt, from Re-Os isotopes. Mineralium Deposita, vol. 34, p. 790-793.

Matos, J. X., Pereira, Z., Rosa, C. J. P., Rosa, D. R. N., Oliveira, J. T. and Relvas, J. M. R. S., 2011. Late Strunian age: a key time frame for VMS deposit exploration in the Iberian Pyrite Belt. 11th SGA biennial meeting,

4th edition. Abstracts Book, Antofagasta, Chile, p. 790-792.
McArthur, G. J., 1986. The Hellyer massive sulphide deposit. In: Large, R. R., editor, Cambrian Mt. Read Volcanics and associated ore deposits. Hobart, Geological Society of Australia, Tasmania Division.
McArthur, G. J., 1996. Textural evolution of the Hellyer Massive Sulphide Deposit. Unpublished PhD thesis, University of Tasmania, Hobart, 272 p.
McArthur, G. J. and Dronseika, E. V., 1990. The Que River and Hellyer volcanogenic Ag-Pb-Zn sulphide deposits. In: Hughes, F. E., editor, Geology of the Mineral Deposits of Australia and Papua New Guinea, p. 1229-1239. Australasian Institute of Mining and Metallurgy Monograph 14.
McClenaghan, M. F., 2006. The geochemistry of Tasmanian Devonian-Carboniferous granites. Tasmania Geological Survey Record 2006/06. Mineral Resources Tasmania. 31 p.
McClenaghan, M. P. (compiler) 2003. Digital Geological Atlas 1:25 000 Scale Series. Sheet 3635. Oceana. Mineral Resources Tasmania.
McClenaghan, M. P., and Corbett, K. D., 1985. Geochemical diagrams of Cambrian rocks and associated intrusions from western Tasmania. Tasmania Department of Mines. Unpublished report 1985/63, p. 1-14.
McDougall, I., and Leggo, P. J., 1965. Isotopic age determinations of granitic rocks in Tasmania. Journal of the Geolgical Society of Australia, vol. 12, p. 295-332.
McIntyre, D., 2006. The volcanology and geochemistry of the Hollway Andesite. Unpublished BSc (Hons.) thesis, University of Tasmania, Hobart.
McGoldrick, P. J., and Large, R. R., 1992. Geologic and geochemical controls on gold-rich stringer mineralization in the Que River deposit, Tasmania. Economic Geology, vol. 87, p. 667-685.
McNeill, A. W., 1985. The structure and petrology of the Nye Bay area, south west Tasmania. Unpublished B.Sc. (Honours) thesis. University of Tasmania, Australia.
McNeill, A. W., 1989. Lake Mackintosh, Exploration Licence 106-87 Tasmania, Technical Progress Report for the Period February 1988 to February 1989. 89-2948.
McNeill, A.W., 1999. Mt. Charter EL 10-98. Annual Report for the period ending June 1999. Pasminco Exploration.
McNeill, A. W., 2001. Burns Peak EL 44-88 Annual and Final Relinquishment Report for the period 1 November 2000 to 31 May 2001. Pasminco Exploration. TCR01-4567.
McNeill, A. W., 2002a. EL 30/2000 Sock Creek, annual report for the period ending 23rd January 2002. Unpublished Pasminco Exploration Report BH76.
McNeill, A. W., 2002b. EL 4/2000 Bulgobac (Boco Siding), annual report for the period ending 16th May 2002. Unpublished Pasminco Exploration Report BH77.
McNeill, A. W. and Corbett, K. D., 1989. Geology of the Tullah - Mount Block area. Mount Read Volcanics Project Geological Report 2, 19 p. Tasmania Department of Mines.
McNeill, A. W., and Corbett, K. D., 1992. Geology and mineralization of the Mount Murchison area: Tasmania Department of Mines, Mount Read Volcanics Project Geological Report 3, 39p.
McPhie, J., 1993. The Tennant Creek porphyry revisited: a syn-sedimentary sill with peperite margins, early Proterozoic, Northern Territory. Australian Journal of Earth Sciences, vol. 40, p. 545-558.
McPhie, J., and Allen, R. L., 1992. Facies architecture of mineralized submarine volcanic sequences, Cambrian Mount Read Volcanics, western Tasmania. Economic Geology, vol. 87, p. 587-596.
McPhie, J. and Allen, R., 2003. Submarine, silicic, syn-eruptive pyroclastic units in the Mount Read Volcanics, western Tasmania; influence of vent setting and proximity on lithofacies characteristics. Geophysical Monograph 140, 245-258.
McPhie, J., Doyle, M. and Allen, R., 1993. Volcanic Textures: a guide to the interpretation of textures in volcanic rocks. 198 p.
Meffre, S., Berry, R. F., and Hall, M., 2000. Cambrian metamorphic complexes in Tasmania, tectonic implications. Australian Journal of Earth Sciences, vol. 47, p. 971-985.
Meffre, S., Direen, N. G., Crawford, A. J. and Kamenetsky, V., 2004. Mafic Volcanic rocks on King Island, Tasmania: Evidence for 579 Ma break-up in east Gondwana. Precambrian Research, vol. 135, p. 177-191.
Mielke, J. E., 1979. Composition of the Earth's crust and distribution of the elements, in Siegel, F. R., ed., Review of research on modern problems in geochemistry, International Association for Geochemistry and Cosmochemistry, Earth Science Series No. 16, UNESCO Report SC/GEO/544/3, p. 13-37.
Mortensen, J. K., Gemmell, J. B., McNeill, A. W., and Friedman, R. M., 2015. High-precision, U-Pb Zircon Chronostratigraphy of the Mount Read Volcanic Belt in Western Tasmania, Australia: Implications for VHMS deposit formation. Economic Geology, vol. 110, pp. 445-468.
Munhá, J., Relvas, J. M. R. S., Barriga, F. J. A. S., Conceição, P., Jorge, R. S., Mathur, R., Ruiz, J., Tassinari, C. C. G., 2005. Osmium isotope systematics in the Iberian Pyrite Belt. Meeting the Global Challenge, Beijing, p. 663-666.
Murphy, T., 2007. Mt Charter Project, Tasmania, RL11-1997. Annual Progress Report for period ended 5 June 2007.

Bass Metals Ltd.
Niem, A. R., 1977. Mississippian pyroclastic flow and ash-fall deposits in the deep-marine Ouachita flysch basin, Oklahoma and Arkansas. Geological Society of America Bulletin, vol. 88, p. 49-61.
Noll, C. A., and Hall, W. D. M., 2005. Great Lyell Fault, western Tasmania - a collage of Middle and Late Cambrian growth faults reactivated during the Devonian orogenesis. Australian Journal of Earth Sciences, vol. 52, p. 427-442.
Nunn, T., 1995. The sedimentology, volcanology, and structure of the Lower Dundas Group, Hall Rivulet Canal, western Tasmania. Honours thesis. University of Tasmania.
Offler, R. and Whitford, D. L., 1992. Wall-rock alteration and metamorphism of a volcanic-hosted massive sulfide deposit at Que River, Tasmania - Petrology and Mineralogy. Economic Geology, vol. 87, p. 686-705.
Oliveira, J. T., Carvaljo, P., Pereira, Z., Pacheco, N., Fernandes, J. P., Korn, P., 1997a. Neves Corvo Field Conference Abstracts, Lisbon, p. 86-87.
Oliveira, J. T., Pacjeco, N., Carvalho, P., Ferreira, A., 1997b. The Neves Corvo Mine and the Palaeozoic geology of Southern Portugal. In: Barriga, F. J. A. S., Carvalho, D. (editors), Geology and VMS deposits of the Iberian Pyrite Belt: SEG Guide Book Series, 27, p. 21-71.
Oliveira, J. T., Pereira, Z., Carvalho, P., Pacheco, N., Korn, P., 2004. Stratigraphy of the tectonically imbricated lithological succession of the Neves Corvo mine area, Iberian Pyrite Belt, Portugal. Mineralium Deposita, vol. 39, p. 422-436.
Oliveira, J. T., Pereira, Z., Rosa, C. J. P., Rosa, D., Matos, J., 2005. Recent advances in the study of the stratigraphy and the magmatism of the Iberian Pyrite Belt, Portugal. In: Carosi, R., Dias, R., Iacopini, D., Rosenbaum, G. (editors), The southern Variscan belt. Journal of the Virtual Explorer, Electronic Edition, vol. 19, ISSN 1441-8142, Paper 9.
Palmeri, P., Chmielowski, R., Sandroni, S., Talarico, F. And Ricci, C. A., 2009. Petrology of the eclogites from western Tasmania: Insights into the Cambro-Ordovician evolution of the paleo-Pacific margin of Gondwana. Lithos, vol. 109, p. 223-239.
Paulick, H. And McPhie, J., 1999. Facies architecture of the felsic lava-dominated host sequence to the Thalanga massive sulfide deposit, Lower Ordovician, northern Queensland. Australian Journal of Earth Sciences, vol. 46, p. 391-405.
Pearce, J. A., and Cann, J. R., 1973. Tectonic setting of basic volcanic-rocks determined using trace-element analyses. Earth and Planetary Science Letters, v. 19, p. 290-300.
Pemberton, J., McNeill, A. W., Corbett, K. D. and Vicary, M. J. (compilers) 1995. Digital Geological Atlas 1:25 000 Scale Series, Sheet 3838, Block, Mineral Resources Tasmania.
Pemberton, J., Vicary, M. J., and Corbett, K. D., 1991. Geology of the Cradle Mountain Link Road-Mt Tor area. Geological Survey of Tasmania. Geological Report, Mount Read Volcanics Project Tasmania 4.
Pereira, Z., Sáez, R., Pons, J. M., Oliveira, J. T., Moreno, C., 1996. Edad devonica (struniense) de las mineralizaciones de Aznalcóllar (Faja Piritica Iberica) en base a palinologia. Geogaceta, vol. 20, p. 1609-1612.
Perkins, C., and Walshe, J. L., 1993. Geochronology of the Mount Read Volcanics, Tasmania, Australia. Economic Geology, vol. 88, p. 1176-1197.
Peterson, D. W., 1979. Significance of the flattening of pumice fragments in ash-flow tuffs. In: Chapin, C E., Elston, W. E. (Eds.), Ash flow tuffs. Special Paper Geological Society of America, vol. 180, p. 195-204.
Pichler, H., 1965. Acid Hyaloclastites. Bulletin of Volcanology, vol. 28, p. 293-310.
Piercey, S. J., Squires, G. C. And Brace, T. D., 2014. Lithostratigraphy, hydrothermal, and tectonic setting of the Boundary volcanogenic massive sulfide deposit, Newfoundland Appalachians, Canada: formation by subseafloor replacement in a Cambrian rifted arc. Economic Geology, vol. 109, p. 661-687.
Polya, D. A., Solomon, M., Eastoe, C. J., and Walshe, J. L., 1986. The Murchison Gorge, Tasmania - a possible cross section through a Cambrian massive sulfide system. Economic Geology, vol. 81, p. 1341-1355.
Powell, C. McA. and Baillie, P. W., 1992. Tectonic affinity of the Mathinna Group in the Lachlan Fold Belt. Tectonophysics, vol. 214, p. 193-209.
Powell, C. McA., Baillie, P. W., Conaghan, P. J. and Turner, N. J., 1993. The Mid-Palaeozoic turbiditic Mathinna Group, northeast Tasmania. Australian Journal of Earth Sciences, vol. 40, p. 169-196.
Purvis, J. G., 1993. EL 37-89 Bulgobac Hill Annual Report for the Period February 1992 to July 1993. Unpublished Pasminco Exploration Report T93-10 (TCR93-3478).
Quilty, P. A., 1971. Cambrian and Ordovician hydroids and dendroids of Tasmania. Journal of the Geological Society of Australia, vol. 17, p. 171-189.
Quilty, P. A., 1972a. A middle Cambrian xiphosuran (?) from western Tasmania. Papers and Proceedings of the Royal Society of Tasmania, vol. 106, p. 21-23.

Quilty, P. A., 1972b. The biostratigraphy of the Tasmanian marine Tertiary. Papers and Proceedings of the Royal Society of Tasmania, vol. 106, p. 25-44.

Quilty, P. A. and Seymour, D. B., 1994. Marine Neogene samples from around Tasmania: an extension to the Miocene/Pliocene marine record in Tasmania. Papers and Proceedings of the Royal Society of Tasmania, vol. 128, p. 41-56.

Quilty, P. A. and Seymour, D. B., 2010. Early Miocene silicified limestone from Temma, northwestern Tasmania: further evidence of substantial post-early Miocene uplift or tilting of Tasmania. Papers and Proceedings of the Royal Society of Tasmania, vol. 144, p. 43-50.

Reed, A. R., 2001. Pre-Tabberabberan deformation in eastern Tasmania: a southern extension of the Benambran Orogeny. Australian Journal of Earth Sciences, vol. 48, p. 785-796.

Reed, A. R., Calver, C. and Bottrill, R. S., 2002. Palaeozoic suturing of eastern and western Tasmania in the west Tamar region: implications for the tectonic evolution of southeast Australia. Australian Journal of Earth Sciences, vol. 49, p. 809-830.

Reid, R. O., 1990. The geology of the Burns Peak-Boco Road area. Unpublished BSc. (Honours) thesis, University of Tasmania, Hobart, 123 p.

Relvas, J. M. R. S., Tassinari, C. C. G., Munhá, J., Barriga, F. J. A. S., 2001. Multiple sources for ore-forming fluids in the Neves Corvo VHMS Deposit of the Iberian Pyrite Belt (Portugal): strontium, neodymium and lead isotope evidence. Mineralium Deposita, vol. 36, p. 416-427.

Rodríguez, R. M., Díez, A., Leyva, F., Matas, J., Almarza, J., Donaire, M., 2002. Datación palinoestratigráfica del volcanismo de la sección de la Ribera del Jarama, Faja Pirítica Ibérica, Zona Surportuguesa. Geogaceta, vol. 32, p. 247-250.

Rosa, C. J. P., McPhie, J. and Relvas, J. M. R. S., 2010. Type of volcanoes hosting the massive sulfide deposits of the Iberian Pyrite Belt. Journal of Volcanology and Geothermal Research, vol. 194, p. 107-126.

Rosa, C. J. P., McPhie, J., Relvas, J. M. R. S., Pereira, Z., Oliveira, T. and Pacheco, N., 2008. Volcanic setting of the giant Neves Corvo massive sulfide deposit, Iberian Pyrite Belt, Portugal. Mineralium Deposita, vol. 43, p. 449-466.

Rosa, D., Finch, A., Andersen, T., and Inverno, C., 2009. U-Pb geochronology and Hf isotope ratios of magmatic zircons from the Iberian Pyrite Belt, Portugal. Mineralogy & Petrology, vol. 95, p. 47- 69.

Ross, C. S. and Smith, R. L., 1955. Water and other volatiles in volcanic glass. American Mineralogist, vol. 40, p. 1071-1089.

Sangster, D. F., 1972. Precambrian volcanogenic massive sulphide deposits in Canada. A review: Canada Geological Survey Paper 72-22, 44 p.

Sainty, R. A., 1986. Volcanic stratigraphy and a speculative model for the Rosebery deposit, in Large, R. R., ed., The Mount Read Volcanics and Associated Ore Deposits: A Symposium: Burnie, Tasmania, Geological Society of Australia, Tasmanian Division, p. 75-80.

Scutter, C. R., Cas, R. A. F., and Moore, C. L., and D. de Rita 1998. Facies architecture and origin of a submarine rhyolitic lava flow-dome complex, Ponza, Italy. Journal of Geophysical Research, vol. 103, no. B11, pages 27,551-27,566, November 10, 1998.

Selley, R. C., 1978. Ancient sedimentary environments. 2nd edn, Chapman & Hall, London, 408 p.

Seymour, D. B., Green, G. R., and Calver, C. R., 2007. The geology and mineral deposits of Tasmania - a summary. Tasmanian Geological Survey, Bulletin 72, Mineral Resources Tasmania, 29p.

Seymour, D. B. and McMclenaghan, M. P. (compilers) 2003. Digital Geological Atlas 1:25 000 Scale Series. Sheet 3636. Dundas. Mineral Resources Tasmania.

Seymour, D. B. and McClenaghan, M. P. (compilers) 2003. Digital Geological Atlas 1:25 000 Scale Series. Sheet 3637. Rosebery. Mineral Resources Tasmania.

Simpson, K., and McPhie, J., 2001. Fluidal-clast breccia generated by submarine fire fountaning, Trooper Creek Formation, Queensland, Australia. Journal of Volcanology and Geothermal Research, volume 109, p. 339-355.

Skilling, I. P., White, J. D. L., McPhie, J., 2002. Peperite: A Review of Magma-Sediment Mingling, Journal of Volcanology and Geothermal Research, vol. 114, p. 1-17.

Skirka, M. and McNeill, A.W., 2006. Bulgobac (Boco Siding) EL 4/2000, Sixth and Final Annual Report for the period ending 15-12-2006. Unpublished Zinifex Exploration Report BH89.

Smith, R. N. and Huston, D. L., 1992. Distribution and association of selected trace elements at the Rosebery deposit, Tasmania. Economic Geology, vol. 87, p. 706-719.

Solomon, M., 1962. The tectonic history of Tasmania. Australian Journal of Earth Sciences, vol. 9, p. 311-339.

Solomon, M., 1981. An introduction to the geology and metallic ore deposits of Tasmania. Economic Geology, vol. 76, p. 194-208.

Solomon, M., and Gaspar, O. C., 2001. Textures of the Hellyer volcanic-hosted massive sulfide deposit, Tasmania - the

aging of a sulfide sediment on the sea floor. Economic Geology, vol. 96, p. 1513-1534.
Solomon, M. and Griffiths, J. R., 1972. Tectonic evolution of the Tasman Orogenic Zone, eastern Australia. Nature, vol. 237, p. 3-6.
Solomon, M., and Groves, D. I., 1994. Volcanic-Hosted Massive Sulphide Deposits of the Tasman Fold Belt System. The Geology and Origin of Australia's Mineral Deposits. Oxford, Clarendon Press, p. 580-647.
Solomon, M., and Groves, D. I., 2000. The geology and origin of Australia's mineral deposits, reprinted with additional material. Centre for Ore Deposit Research, University of Tasmania and Centre for Global Metallogeny, University of Western Australia.
Solomon, M. and Walshe, J. L., 1979. The formation of massive sulfide deposits on the seafloor. Economic Geology, vol. 74, p. 797-813.
Solomon, M., and Zaw, K., 1997. Formation on the sea floor of the Hellyer volcanogenic massive sulfide deposit. Economic Geology, vol. 92, p. 686-695.
Solomon, M., Eastoe, C. J., Walshe, J. L., and Green, G. R., 1988. Mineral deposits and sulfur isotope abundances in the Mount Read Volcanics between Que River and Mount Darwin, Tasmania. Economic Geology, vol. 83, p. 1307-1328.
Solomon, M., Gemmell, J. B., and Zaw, K., 2004. Nature and origin of the fluids responsible for forming the Hellyer Zn–Pb–Cu, volcanic-hosted sulfide deposit, Tasmania, using fluid inclusions, and stable and radiogenic isotopes. Ore Geology Reviews, vol. 25, p. 89-124.
Solomon, M., Rafter, T. A., and Jensen, M. L., 1969. Isotope studies on the Rosebery, Mount Farrell and Mount Lyell ores, Tasmania. Mineralium Deposita, vol. 4, p. 172-199.
Solomon, M., Walshe, J. L., and Heinrich, C. A., 1990. The formation of Rosebery-type, volcanogenic massive sulphide deposits. Geological Society of Australia, Abstracts, vol. 25, p. 6.
Spry, A. H., 1957. The Precambrian rocks of Tasmania, Part I. Dolerites of the north-west coast of Tasmania. Papers and Proceedings of the Royal Society of Tasmania, vol. 91, p. 81-93.
Spry, A. H., 1958. The Precambrian rocks of Tasmania, Part III. Mersey-Forth area. Papers and Proceedings of the Royal Society of Tasmania, vol. 92, p. 117-137.
Spry, A. H., 1962. Precambrian rocks. In: Spry, A. H. and Banks, M. R., editors. The Geology of Tasmania. Journal of the Geological Society of Australia, vol. 9, p. 107-126.
Spry, A. H., 1963. The Precambrian rocks of Tasmania, Part V. Petrology and structure of the Frenchmans Cap area. Papers and Proceedings of the Royal Society of Tasmania, vol. 97, p. 105-127.
Spry, A. H., 1964. Precambrian rocks of Tasmania, Part VI. The Zeehan-Corinna area. Papers and Proceedings of the Royal Society of Tasmania, vol. 98, p. 23-48.
Stacey, A. R., and Berry, R. F., 2004. The structural history of Tasmania - a review for petroleum explorers. PESA Eastern Australasian Basins Symposium II, Adelaide.
Stait, B. and Laurie, J., 1980. Lithostratigraphy and biostratigraphy of the Florentine Valley Formation in the Tim Shea area, southwest Tasmania. Papers and Proceedings of the Royal Society of Tasmania, vol. 114, p. 201-208.
Stewart, L. F., 2009. Exploration Licence 33/2006, Bulgobac River. Final report for the period April 2007 to September 2009. Mineral Resources Tasmania.
Thurston, P. C., Ayer, J. A., Goutier, J. and Hamilton, M. A., 2008. Depositional Gaps in Abitibi Greenstone Belt Stratigraphy: A Key to Exploration for Syngenetic Mineralization. Economic Geology, vol. 103, p. 1097-1134.
Tomes, K. L., 2011. The Textures and Geochemistry of the Hellyer Basalt, western Tasmania. Honours Thesis. University of Tasmania. Hobart.
Tornos, F., 2006. Environment of formation and styles of volcanogenic massive sulfides: Iberian Pyrite Belt. Ore Geology Reviews, vol. 28, p. 259-307.
Turner, N. J., 1989. Precambrian. In: Burrett, C. F. and Martin, E. L., editors, Geology and Mineral Resources of Tasmania. Geological Society of Australia Special Publication 15, p. 5-46.
Turner, N. J. and Bottrill R. S., 2001. Blue amphibole, Arthur Metamorphic Complex, Tasmania: composition and regional tectonic setting. Australian Journal of Earth Sciences, vol. 48, p. 167- 181.
Turner, N. J., Black, L. P., and Kamperman, M., 1998. Dating of Neoproterozoic and Cambrian orogenies in Tasmania. Australian Journal of Earth Sciences, vol. 45, p. 789-806.
Varne, R., and Foden, J. D., 1987. Tectonic setting of Cambrian rifting, volcanism and ophiolite formation in western Tasmania. Tectonophysics, vol. 140, p. 275-295.
Vicary, M. 1998. Tasmanian Base Metals Project EL 5/96. White Spur. AGC Exploration Annual report EL 5/96 for the period March 1997 to March 1998, unpublished.
Walshe, J. L., and Solomon, M., 1981. An investigation into the environment of formation of the volcanic-hosted

Mount Lyell copper deposits using geology, mineralogy, stable isotopes, and a six-component chlorite solid solution model. Economic Geology, vol. 76, p. 246-284.

Waters, J. C., 1995. Volcanology and sedimentology of the host succession to VHMS style mineralisation within the Cambrian Que-Hellyer Volcanics, northwestern Tasmania. Unpublished PhD thesis. University of Tasmania.

Waters, J. C., and Wallace, D. B., 1992. Volcanology and sedimentology of the host succession to the Hellyer and Que River volcanic-hosted massive sulfide deposits, northwestern Tasmania. Economic Geology, vol. 87, p. 650-666.

White, A. J. R. and Chappell, B. W., 1977. Ultrametamorphism and granitoids genesis. Tectonophysics, vol. 43, p. 7-22.

White, J. D. L., 2000. Subaqueous eruption-fed density currents and their deposits. Precambrian Research, vol. 101, pp. 87-109.

White, J. D. L., McPhie, J., and Skilling, I., 2000. Peperite: a useful genetic term. Bulletin of Volcanology, vol. 62, p. 65-66.

White, M. J., and McPhie, J., 1996. Stratigraphy and palaeovolcanology of the Cambrian Tyndall Group, Mount Read Volcanics, western Tasmania. Australian Journal of Earth Sciences, vol. 43, p. 147-159.

White, M. J., and McPhie, J., 1997. A submarine welded ignimbrite-crystal-rich sandstone facies association in the Cambrian Tyndall Group, western Tasmania, Australia. Journal of Volcanology and Geothermal Research, vol. 76, p. 277-295.

Wilde, A. R., and Kerr, T. L., 1989. Exploration licence 5/63 Comstaff J. V., N. W. Tasmania. Final report, May 1989: Tasmania Department of Mines Open-File Rept. TCR 89-2968, 35 p.

Williams, E., 1978. Tasman fold belt system in Tasmania. Tectonophysics, vol. 48, p. 159-205.

Williams, L. P. (2009). Stratigraphy, volcanology, and geology of the Rosebery hangingwall sequence. Unpublished PhD thesis. University of Tasmania, Hobart. 85 p.

Winchester, J. A., and Floyd, P. A., 1977. Geochemical discrimination of different magma series and their differentiation products using immobile elements. Chemical Geology, vol. 20, p. 325-343.

Wingate, M. T. D., Campbell, I. H., Compston, W. and Gibbon, G. M., 1998. Ion microprobe U-Pb ages for Neoproterozoic basaltic magmatism in south-central Australia and implications for the breakup of Rodinia. Precambrian Research, vol. 87, p. 135-179.

Yamada, R. and Yoshida, T., 2011. Relationships between Kuroko volcanogenic massive sulfide (VMS) deposits, felsic volcanism, and island arc development in the northeast Honshu arc, Japan. Mineralium Deposita, vol. 46, p. 431-448.

Yamagishi, H., 1987. Studies on the Neogene subaqueous lavas and hyaloclastites in Southwest Hokkaido. Report of the Geological Survey of Hokkaido, 59, 55-117.

Yamagishi, H., 1991. Morphological and sedimentological characteristics of the Neogene submarine coherent lavas and hyaloclastites in Southwest Hokkaido, Japan. Sedimentary Geology, vol. 74, p. 5-23.

Zaw, K., and Large, R. R., 1992. The precious metal-rich south Hercules mineralization, western Tasmania: a possible subsea-floor replacement volcanic-hosted massive sulfide deposit. Economic Geology, vol. 87, p. 931-952.

Zaw, K., Huston, D. L., and Large, R. R., 1999. A chemical model for the Devonian remobilization process in the Cambrian VHMS Rosebery deposit, W Tasmania. Economic Geology, vol. 94, p. 529-546.

APPENDIX A
Graphic logs

In the course of this study, twenty four diamond drill holes (DDH) intersecting the northern Mount Read Volcanics were logged at 1:400 scale. The inclusion of all of these graphic logs in this thesis would be cumbersome. Therefore, six examples of original field graphic logs are presented herein. Together, these examples provide a good representation of the stratigraphy in the Sock Creek-Burns Peak (SB) area. Graphic logs of DDH not included in this appendix may be made available electronically by the author on request.

The six examples are: BHD-4 and BHD-10 (SB-North area); AK-1 and BOC-2 (SB-Central area) and BOC-4 and BPD-80 (SB-South area).

Other graphic logs of DDH used in this study were: BBP-207, BBP-209, BBP-242, BHD-7, BHD-8, BHD-9, BOC-1, BOC-3, BOC-6, BPD-89, MAC-16, MCH-1, SCS-2, SCS-3, SCS-4, SCS-5, WSP-14 and WSP-15.

LOG AK-1 (ANIMAL CREEK)
Location: BULGOBAC HILL MRT core stove

Date: 6/MAY/2010
Logged by: PEDRO FONSECA

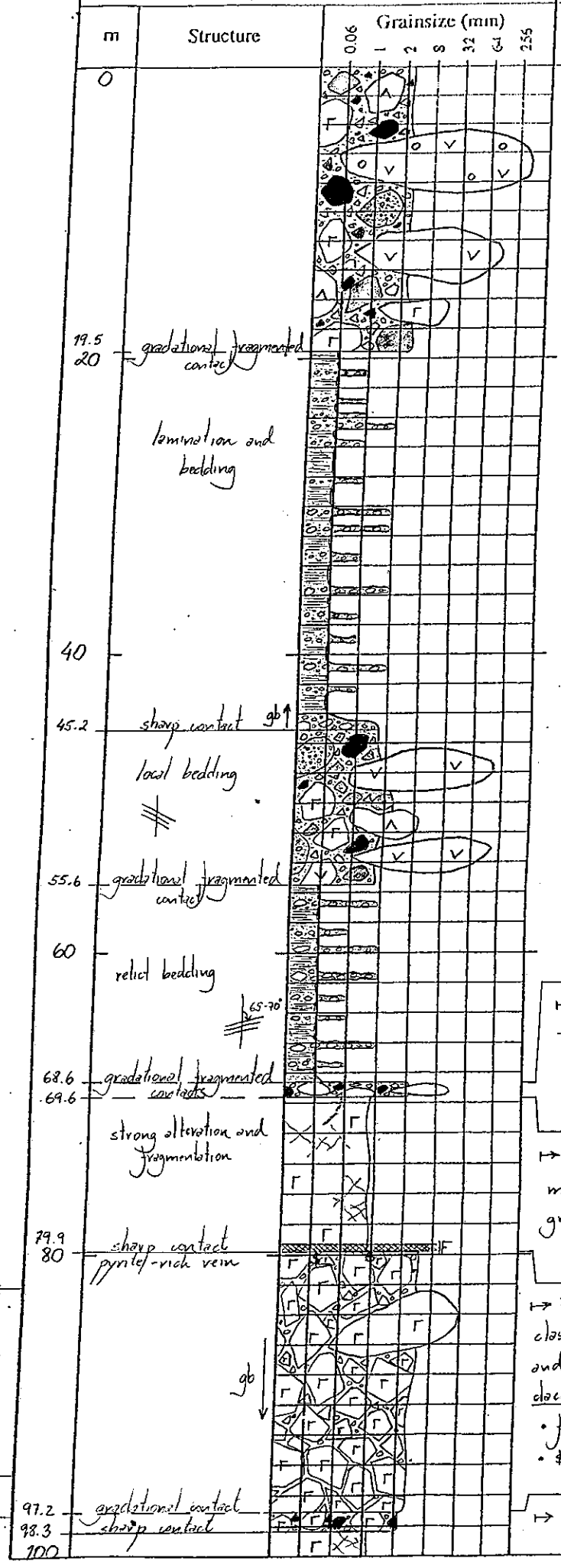

↦ 0 - 19.5 + 45.2 - 55.6 : Weakly altered, semi-consolidated, locally bedded intercalated mudstone, coarse sandstone, granule breccia and very poorly-sorted sand matrix-supported polymictic conglomerate.

Glacial till

- mudstone beds up to 25 cm
- cobble to boulder basaltic clasts (< 30 cm)
  - vesicular; feldspar-phyric
- dacitic + andesitic? clasts: porphyritic; multicolored
- lithics: reddish; homogeneous; hematitic.
- quartz: 1-3 cm; white + grey
- volcanic sand clasts up to 3-4 cm
- 20-30% conglomerate; 70-80% matrix.

↦ 19.5 - 45.2 + 55.6 - 68.6 : Weakly altered, semi-consolidated, relict-bedded, intercalated creamy mudstone (clays) and mud matrix-supported, poorly-sorted sandstone and breccia → Varved clays

- 15-25% clasts and 75-85% clays (matrix).
- clasts within clays: 1%
  - quartz: < 3 cm
  - andesite?: < 5 cm
  - dacite: 6-7 cm; feldspar-phyric

> soft-sediment deformation: folded lamination and loading structures.

68.6m

↦ 68.6 - 69.6 : Strongly altered, poorly-sorted, matrix-supported, polymictic? breccia.

- coarse sand matrix (55%)
- gravel clasts (45%)
- clays at upper and lower contacts.

69.6m

↦ 69.6 - 79.9 : Highly altered/sericitic, feldspar-phyric, massive to locally brecciated, yellowish, orangish and greenish dacite

- feldspar phenocrysts: 10%; 1-2 mm; yellow; irregular.
- fault zone near lower contact.

79.9m

↦ 79.9 - 97.2 : Weakly sericitic/chloritic, poorly-sorted, clast-supported, jigsaw-fit, locally feldspar crystal-rich and vein-rich monomictic dacite breccia and massive dacite near lower contact.

- feldspar phenocrysts: 15-20%; 2-3 mm; creamy, white, tabular
- $-rich vein supported jigsaw-fit texture at lower contact.

97.2m

↦ 97.2 - 98.3 : Next page...

LOG AK-1 (ANIMAL CREEK)
Location: BULGOBAC HILL · MRT core store

Date: 6/MAY/2010
Logged by: PEDRO FONSECA

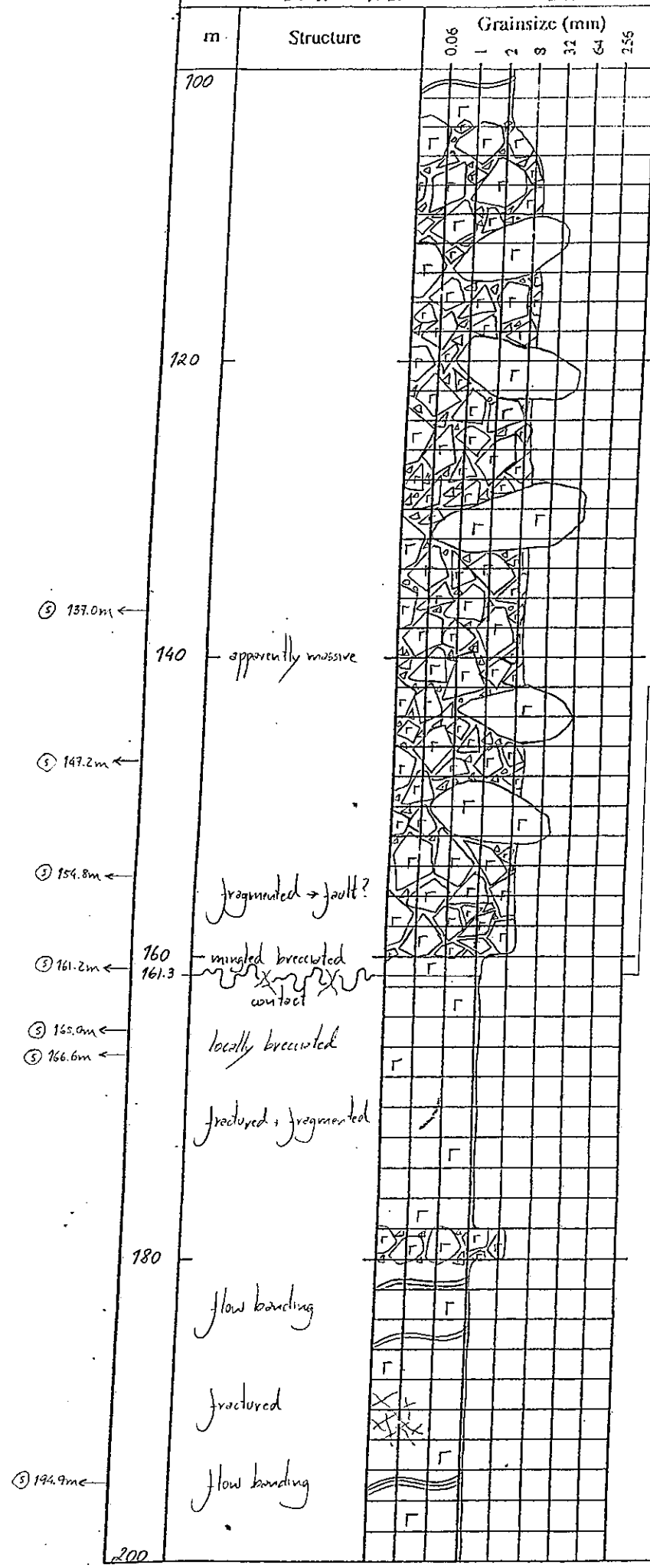

↦ 97.2 - 98.3 : Weakly sericitic/chloritic, pyritic, moderately-sorted, clast-supported, dark green, polymictic? dacite breccia.

- dacite clasts : 40-50%; < pebble-size; aphyric
- lithics? : 5%; < 6mm; grey
- pyrite : 2-3%, round

– feldspar-rich.

98.3m

↦ 98.3 - 161.3 : Weakly to moderately sericitic, chloritic and silicified, poorly-sorted, clast-supported, jigsaw-fit, vein-rich, monomictic dacite breccia and weakly sericitic, silicified, locally flow-banded, feldspar-phyric, massive dacite.

- frequent yellow patchy zones
- strong vein-controlled near lower contact (fault?)
- disseminated sulfides

161.3m

↦ 161.3 - 218.3 : Weakly to moderately sericitic and altered, feldspar-phyric, locally strongly flow-banded, locally fractured, creamy, reddish, greenish massive dacite and local jigsaw-fit, monomictic dacite breccia.

- disseminated sulfides
- sericitization + silicification throughout
- feldspar phenocrysts : 5-10%, 2-3mm; white, tabular + irregular

– strongly flow-banded zone at 195.0m.

LOG AK-1 (ANIMAL CREEK)
Location: BUCCHANAN HILL MRT core store

Date: 6/MAY/2010
Logged by: PEDRO FONSECA

m | Structure | Grainsize (mm) 0.06 | 1 | 2 | 8 | 32 | 64 | 256 | Description

200 — fractured + fragmented — minor fault L.C.A. 45° F — brecciated — mingled contact? — ⑤ 218.3m ← 218.3 — ⑤ 219.5m ← 220 — flow banding — ⑤ 228.6m ← — fractured — 240 — mingled contact — ⑤ 241.7m ← 241.7 — flow banding — ⑤ 259.5m ← 260 — fragmentation / fault/shear zone? — flow banding — fractured + fragmented — 280 — fractured + fragmented — flow banding — ⑤ 291.6m ← — 295.4 sharp irregular 10°LCA contact — fault? 15° F — 300

↦ 161.3 – 218.3 : Weakly to moderately sericitic and altered, feldspar-phyric, locally flow-banded, locally fractured, creamy, reddish, greenish, massive dacite, and locally jigsaw-fit, monomictic dacite breccia.

- disseminated sulfides
- sericitization + silicification throughout
- o feldspar phenocrysts: 5-10%; 2-3mm; white; tabular + irregular.
- > minor fault at 207.1m
- > flow banding with disseminated $ at ~ 204.0m.

218.3m

↦ 218.3 – 241.7 : Weakly sericitic, creamy, feldspar-phyric massive dacite and locally flow-banded, monomictic dacite breccia.

- feldspar phenocrysts: 5-10%; 3mm; tabular; white.
- o sericitic/siliceous patchy alteration
- > carbonate vein-rich zone with disseminated $ at ~ 227.0m.

↦ 241.4 – 241.7 : Monomictic dacite breccia with "flow fabric".

- flow matrix supported
- heterogeneous pumice clasts? (original?)
- feldspar-phyric + amygdaloidal!

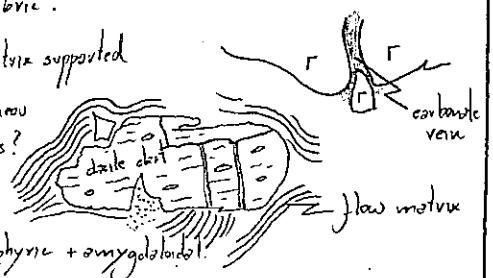

241.7m

↦ 241.7 – 295.4 : Weakly sericitic and chloritic, creamy, pink, reddish and green, flow-banded to massive, feldspar-phyric dacite and local jigsaw-fit, monomictic dacite breccia.

- feldspar phenocrysts: <15%; 2-4mm; creamy; tabular
- fault zone at ~ 262.0m
- o local silicification at ~ 270.0m
- > $-rich crystalline carbonate veins with iron oxide cover at ~ 278.0m.

295.4m

↦ 295.4 – 310.7 : Weakly sericitic, aphyric, very poorly amygdaloidal (near lower contact), homogeneous, massive dark green basalt.

- locally cross-cut by carbonate veins

⇒ dyke / mafic intrusion

LOG AK-1 (ANIMAL CREEK)
Location: BULGOBAL HILL MRT ore store

Date: 6/MAY/2010
Logged by: PEDRO FONSECA

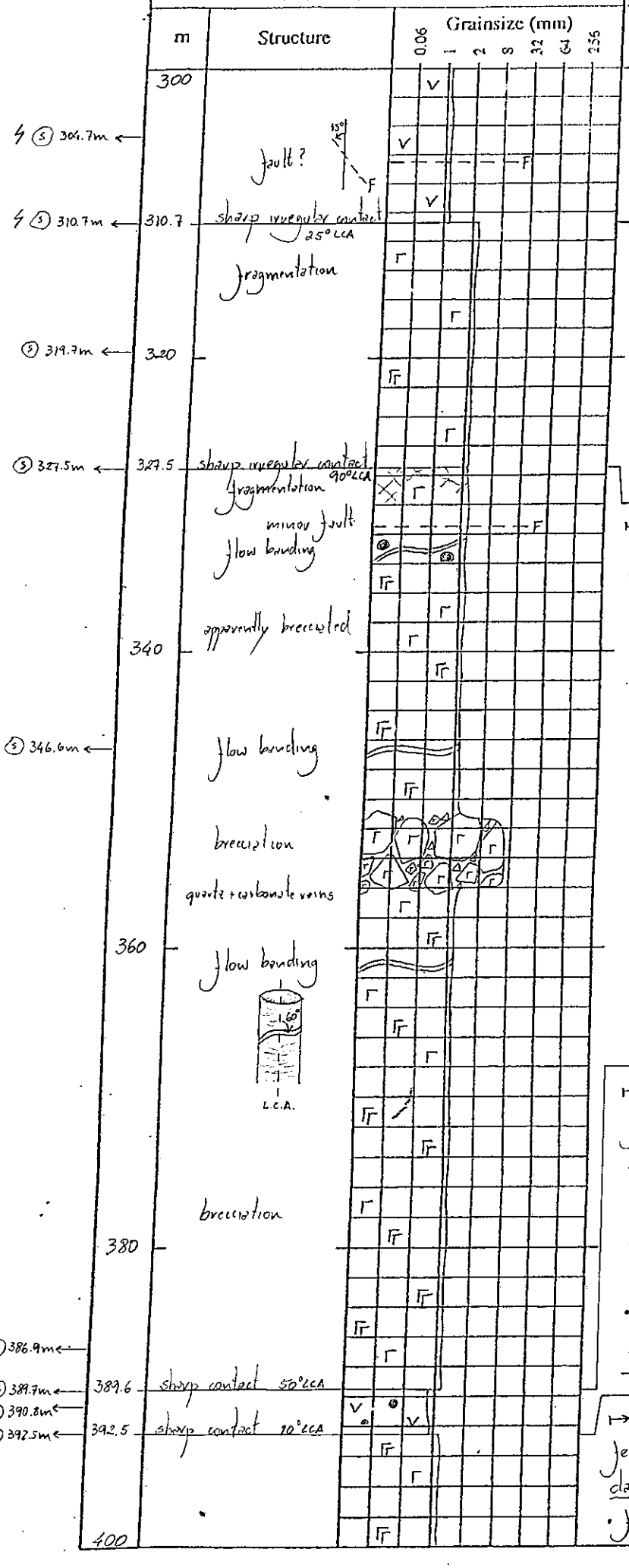

Description

↦ 295.4 - 310.7 : Weakly sericitic, aphyric, very poorly amygdaloidal (near lower contact), homogeneous, massive dark green basalt.

- locally cross-cut by carbonate veins
  ⇒ dyke/mafic intrusion

310.7m

↦ 310.7 - 327.5 : Weakly sericitic, feldspar-phyric to apparently aphyric, massive, pale pink, cream and green dacite.

- feldspar phenocrysts : 5-10% ; 2-3mm ; pink ; tabular
- chlorite spots (amygdales) : 2% ; 1-2mm, elongated ; dark green
- carbonate veins

327.5m

↦ 327.5 - 389.6 : Weakly sericitic and chloritic, feldspar - quartz? - phyric, massive and locally flow-banded, creamy pink to green dacite.

- feldspar phenocrysts : 20-25% (up to 30%) ; 2-4mm (up to 5mm) ; creamy white ; tabular and irregular ; chloritic/sericitic and siliceous.
- amygdales up to 1.5cm at ~ 333.0m.
- many overprinting alteration zones create apparent variability in the generally monotonous/homogeneous feldspar-phyric dacite.
- carbonate + quartz? veins.
- "pseudo-clastic" brecciated zones due to alteration
  - some silicified feldspar phenocrysts throughout
  - some disseminated & around veins + brecciated zones
- minor fault + brecciation at ~ 331.6m.

389.6m

↦ 389.6 - 392.5 : Weakly sericitic and chloritic, feldspar-phyric, fine-grained, amygdaloidal, massive dark green basalt.

- feldspar phenocrysts : 5-10% ; 2-3mm ; irregular
- chloritic spots (amygdales) : 2% ; 1-2mm ; elongated dark green
- amygdales : 2-3% ; <5mm ; carbonate + quartz-filled ; round ; white + creamy.
- disseminated sulfides near upper and lower contacts

392.5m

↦ 392.5 - 413.0 : Weakly sericitic and chloritic, massive, feldspar - quartz? - phyric, creamy pink to orange green dacite.

- feldspar phenocrysts : 10% (up to 15%) ; 2-4mm ; creamy pink tabular and irregular.

LOG AK-1 (ANIMAL CREEK)
Location: BULGOBAC HILL MRT core store

Date: 6/MAY/2010
Logged by: PEDRO FONSECA

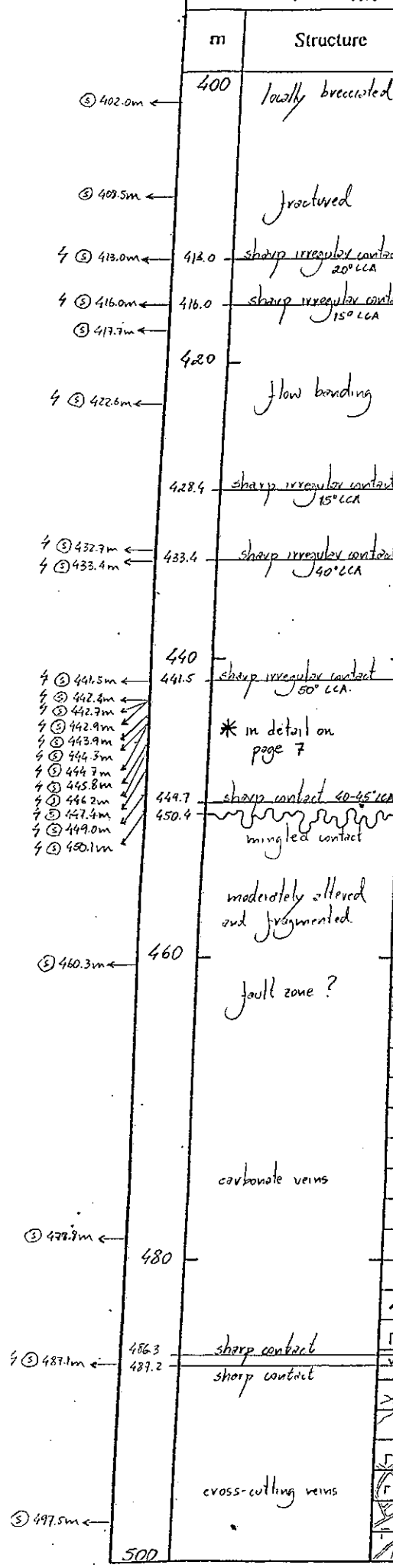

↦ 392.5 - 413.0: Weakly sericitic and chloritic, massive feldspar-quartz?-phyric, creamy pink to orange green dacite and local monomictic dacite breccia.
- feldspar phenocrysts: 10% (up to 15%); 2-4mm; creamy pink, tabular and irregular
- disseminated sulfides

413.0m

↦ 413.0 - 416.0: Weakly sericitic and chloritic, massive, feldspar-phyric, greenish/reddish basalt.
- feldspar phenocrysts: 5-10%; 1-2mm (up to 3-4mm); irregular; one large zoned (1cm) and sericitic
- felsic xenoliths
- chloritic spots.

416.0m

↦ 416.0 - 428.4: Weakly sericitic and chloritic, massive, feldspar-quartz?-phyric greenish, yellowish dacite.
- feldspar phenocrysts: 15-20%; 2-4mm; light grey, tabular
- quartz phenocrysts?: 1%; 1-4mm, round, elongated, incolor
- feldspar phenocrysts often present chloritic coves.

428.4m

↦ 428.4 - 433.4: Weakly sericitic and chloritic, massive, fine-grained, feldspar-phyric, dark green andesite.
- feldspar phenocrysts: 5%; 2-3mm, irregular
- feldspar-phyric felsic xenoliths
- > chloritic spots: 2%; 1-2mm

433.4m

↦ 433.4 - 441.5: Weakly sericitic and chloritic, massive, feldspar-quartz?-phyric, greenish dacite.
- feldspar phenocrysts: 25-30%; 2-5mm; light grey, creamy, tabular
- quartz phenocrysts?: < 2%; 2-3mm; round; incolor.

441.5m

↦ 441.5 - 449.7: Interbedded, weakly to moderately sericitic and chloritic, heterogeneous, multicolored, well-sorted, locally bedded and laminated, grey volcaniclastic mudstone, green quartz + feldspar crystal-rich siltstone and sandstone and strongly silicified feldspar crystal-rich volcaniclastic sandstone
- feldspar: 20-25%; 2-4mm; orange; tabular

449.7m

↦ 449.7 - 450.4: Weakly sericitic and altered, very poorly feldspar-phyric to apparently aphyric, fine-grained, massive green andesite.

450.4m

↦ 450.4 - 486.3: Weakly sericitic and chloritic, aphyric to weakly feldspar-phyric, amygdaloidal massive dacite and moderately to highly altered, poorly-sorted, clast-supported, monomictic dacite breccia.
- feldspar phenocrysts: <5%; 3-4mm; creamy white, irregular
- amygdales: 5%; 2-4mm (up to 1cm); elongated; dark green
- > faults at ~ 454m and 463m (454 - 463 → fault zone ?).

486.3m

↦ 486.3 - 487.2: Weakly altered, feldspar-phyric, massive, fine-grained dark brown basalt
- feldspar phenocrysts: 5-10%; 1-2mm; dark; irregular
- disseminated sulfides

487.2m

↦ 487.2 - 506.6: Weakly to moderately sericitic and chloritic, aphyric to feldspar-phyric, massive green dacite.
- feldspar phenocrysts: 15%; 2-4mm; brown (altered), irregular
- carbonate + chlorite-rich veins.

LOG AK-1 (ANIMAL CREEK)
Location: BULGOBAC HILL MRT core store

Date: 6/MAY/2010
Logged by: PEDRO FONSECA

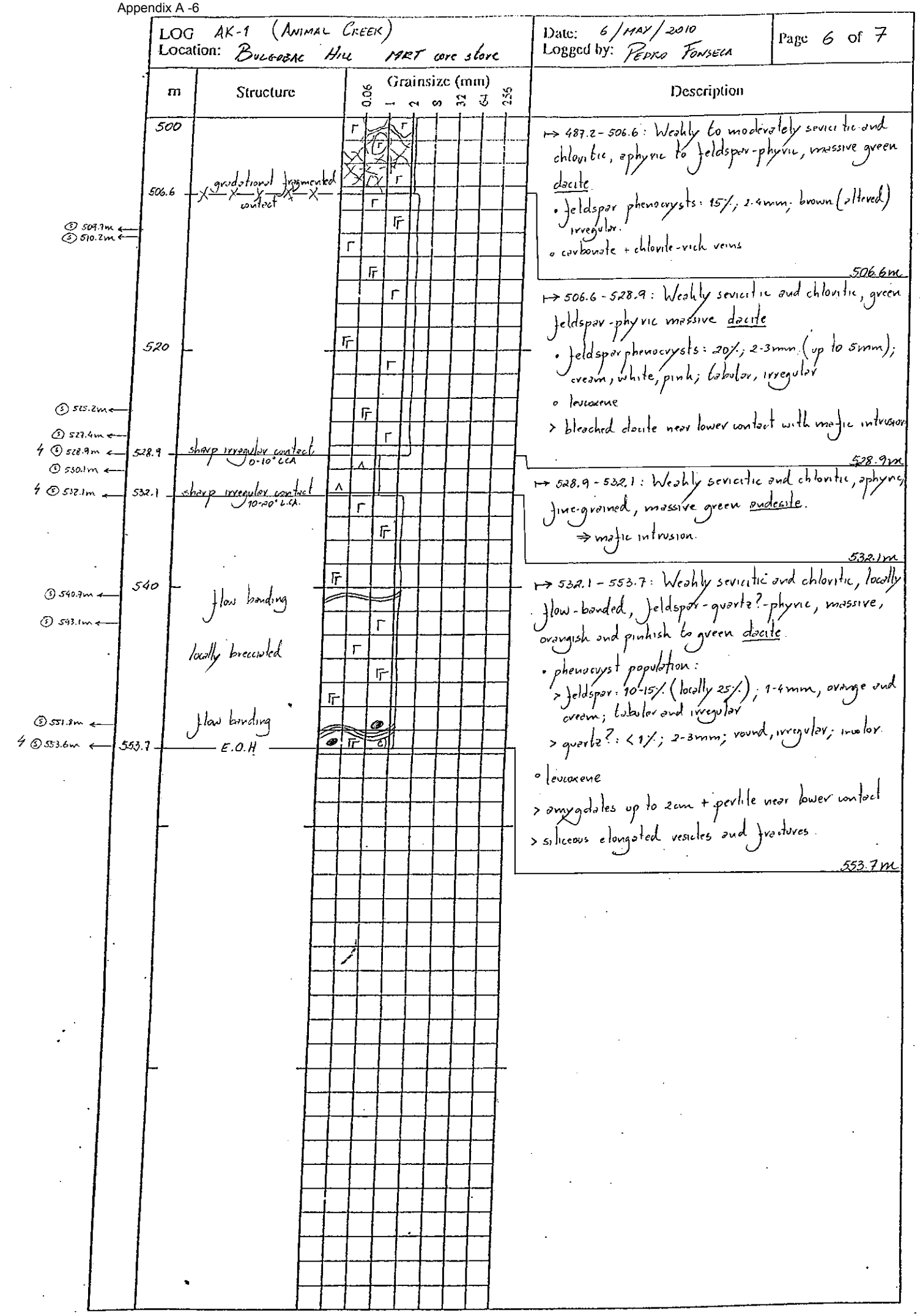

↦ 487.2 - 506.6 : Weakly to moderately sericitic and chloritic, aphyric to feldspar-phyric, massive green dacite

- feldspar phenocrysts : 15%; 2-4mm; brown (altered) irregular.
- carbonate + chlorite-rich veins

506.6m

↦ 506.6 - 528.9 : Weakly sericitic and chloritic, green feldspar-phyric massive dacite

- feldspar phenocrysts : 20%; 2-3mm (up to 5mm); cream, white, pink; tabular, irregular
- leucoxene
- > bleached dacite near lower contact with mafic intrusion

528.9m

↦ 528.9 - 532.1 : Weakly sericitic and chloritic, aphyric, fine-grained, massive green andesite.

⇒ mafic intrusion.

532.1m

↦ 532.1 - 553.7 : Weakly sericitic and chloritic, locally flow-banded, feldspar-quartz?-phyric, massive, orangish and pinkish to green dacite.

- phenocryst population :
  - > feldspar : 10-15% (locally 25%) ; 1-4mm, orange and cream; tabular and irregular
  - > quartz? : < 1%; 2-3mm; round, irregular; inolor.
- leucoxene
- > amygdales up to 2cm + perlite near lower contact
- > siliceous elongated vesicles and fractures.

553.7m

LOG AK-1 (ANIMAL CREEK)
Location: BULGOBAC HILL MRT core store

Date: 6/MAY/2010
Logged by: PEDRO FONSECA

m | Structure | Grainsize (mm) 0.06 — 2 8 32 64 256 | Description

440.0m

↦ 440.0-441.5: Weakly sericitic and chloritic, massive feldspar-quartz?-phyric, greenish dacite.
- feldspar phenocrysts: 25-30%; 2-5mm; light grey, creamy, tabular
- quartz phenocrysts?: <2%; 2-3mm; round; incolor
- o pervite + pyrite near lower contact

440

441.5m

↦ 441.5-442.4: Strongly silicified, flow-banded, leucoxene-bearing + feldspar crystal-bearing (phenocrysts?), fine-grained dacite
- o sulfides near top contact.

441.5 — sharp irregular contact 50° LCA

442.4m

↦ 442.4-442.7: Grey yellowish, homogeneous mudstone

442.4 — sharp irregular contact

442.7m

↦ 442.7-443.9: Poorly-sorted, pumiceous and fiamme-rich monomictic mud-matrix dacite breccia.
- o mudstone beds
- o sandy and granule dacite near lower contact

442.7 — sharp irregular contact

pumice + fiamme ≈ mudstone

443.9m

443.9 — sharp contact

443.9-444.7: Chloritic, flow-banded, laminated, pyritic, fiamme-rich, matrix-supported, feldspar crystal-rich, monomictic dacitic fiamme breccia.
- o feldspar crystals: 25-30%, 2-5mm; reddish, tabular

444.7 — sharp contact

444.7m

↦ 444.7-445.5: Phenocryst-rich, vesicular basalt
⇒ intrusion

445.5 — sharp contact

445.5m

↦ 445.5-445.8: Chloritic, matrix-supported, monomictic dacitic fiamme breccia

445.8 — sharp contact

445.8m

↦ 445.8-446.2: Aphyric, partly brecciated, massive dacite.

446.2 — sharp irregular contact

446.2m

↦ 446.2-447.8: Strongly feldspar-phyric massive dacite
- o disseminated sulfides
- fiamme near lower contact (4-5m thick)

447.4m

447.8 — sharp contact

447.8m

↦ 447.8-449.0: Aphyric, partly brecciated, massive dacite.

449.0m

449.0 — gradational contacts
449.1

↦ 449.0-449.1: Strongly feldspar-phyric, massive dacite
- o disseminated sulfides

449.1m

↦ 449.1-449.7: Aphyric, partly brecciated, massive dacite.

449.7 — sharp contact 40-45° LCA

449.7m

450

↦ 449.7-450.0: Weakly sericitic and altered, very poorly feldspar-phyric to apparently aphyric, fine-grained, massive green andesite

450.0m

LOG: BHD-4
Location: MRT core store

Date: 15 - 23/NOV/2011
Logged by: Pedro Fonseca

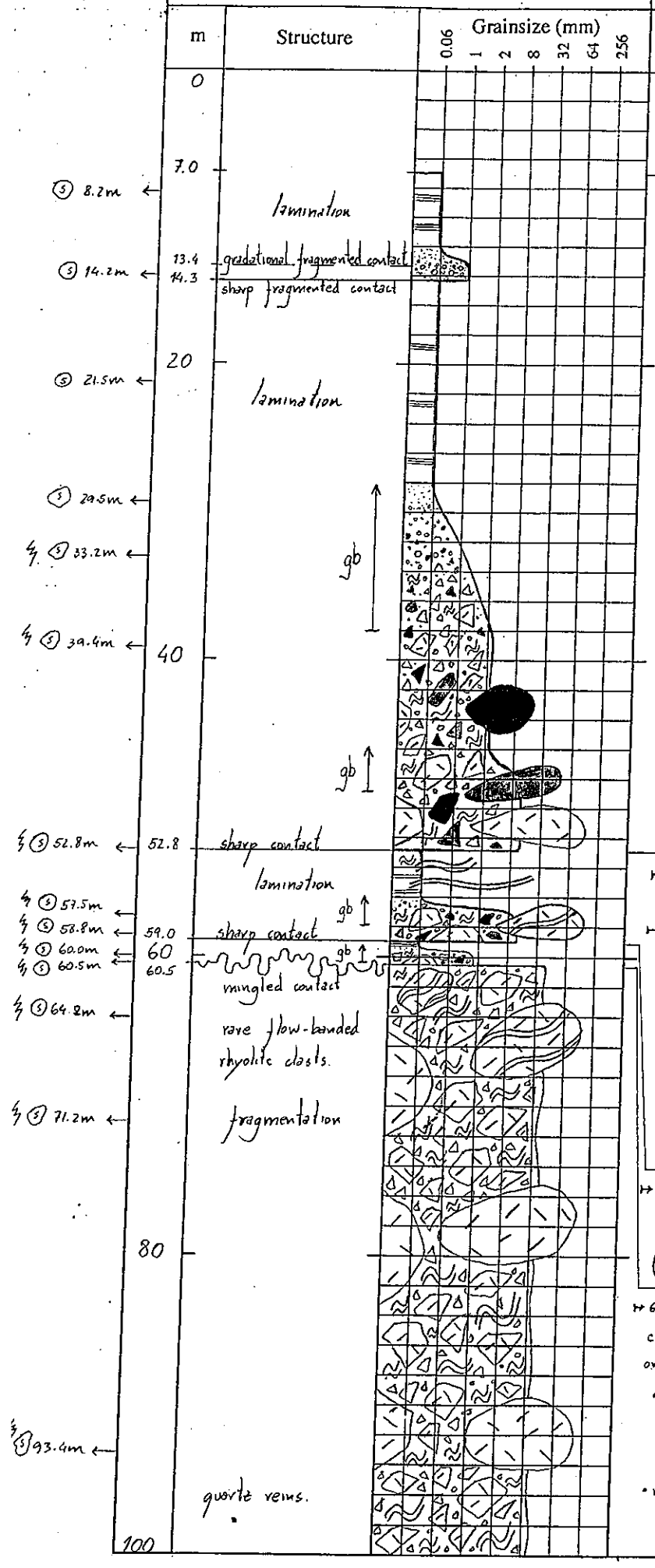

no core 7.0m

↦ 7.0 - 13.4 : Homogeneous, locally laminated, greenish brown to grey mudstone.

↦ 13.4 - 14.3 : Graded, moderately-sorted, qtz+fds-rich, yellow volcaniclastic sandstone.

↦ 14.3 - 28.5 : Homogeneous, locally laminated, greenis brown to black mudstone. 14.3m

- disseminated chalcopyrite/pyrite : 1%, < 0.5mm.

↦ 28.5 - 38.0 : Graded, moderately sericitic, well-sorted, polymictic, volcaniclastic, greyish green, qtz+fds-rich sandstone

- qtz : 25-30%, 0.1-2mm, whitish + incolor, round
- fds : 30-35%, 0.1-2mm, creamy + orange, tabular + round
- lithics : 1%, 0.5-1mm, brown, irregular
- pumice : 2-3%, 1-2mm, dark green, wispy + irregular.
- chalcopyrite/pyrite spots : < 1%, 1-2mm, round.

↦ 38.0 - 52.8 : Graded, moderately sericitic/chloritic, poorly-sorted, matrix-supported, polymictic, volcaniclastic, granule to cobble, pumiceous rhyolite breccia.

- qtz : 5-10%, < 4mm, incolor + whitish, round + irregular
- fds : 25-30%, < 5mm, creamy + orange, tabular + irregular.
- lithics : 10%, < 12cm, creamy + brown, round + irregular
- mudstone : 2-3%, < 7cm, black, elongated + irregular
- rhyolite clasts : 25%, < 15cm, qtz+fds-phyric, green+orange, irregular
  - > qtz : 5-10%, < 1cm, incolor, round + elongated
  - > fds : 10-15%, < 8mm, orange + creamy, tabular + irregular
- rhyolitic pumice : 20%, < 10cm, dark green, wispy + wavy + irregular
  - > qtz : 10-15%, < 1cm, incolor, round + elongated
  - > fds : 15-20%, < 8mm, orange + creamy, tabular + irregular.

52.8m

↦ 52.8 - 56.0 : Homogeneous, locally laminated, qtz+fds-rich rhyolitic pumice-bearing black mudstone.

↦ 56.0 - 59.0 : Graded, moderately-sorted, qtz+fds-rich, volcaniclastic siltstone + sandstone and moderately to poorly-sorted, matrix-supported, polymictic, volcaniclastic, granule to cobble pumiceous rhyolite breccia.

- rhyolite clasts : 15-20%, < 15cm, creamy, irregular
  - > qtz : 5-10%, < 1cm, incolor, round + irregular
  - > fds : 10-15%, < 8mm, orange + creamy, tabular + irregular
- rhyolitic pumice : 10-25%, < 10cm, dark green, wispy + irregular.
  - > qtz : 10-15%, < 1cm, incolor, round + irregular
  - > fds : 15-20%, < 8mm, orange + creamy, tabular + irregular

59.0m

↦ 59.0 - 60.5 : Graded, homogeneous, locally laminated, black mudstone and moderately sorted, qtz+fds-rich, volcaniclastic, rhyolite and pumice-bearing sandstone.
(note : rhyolite and pumice abundances + compositions as above).

60.5m

↦ 60.5 - 104.5 : Moderately sericitic/chloritic, poorly-sorted, clast-supported, monomictic, granule to cobble, volcaniclastic, orangish to green pumiceous rhyolite breccia.

- rhyolite clasts : 45%, < 90cm, qtz+fds-phyric, orange + creamy round + irregular.
  - > qtz : 5-10%, < 1cm, incolor, round + elongated
  - > fds : 10-15%, < 8mm, orange + creamy, tabular + irregular
- rhyolitic pumice : 40%, < 10cm, dark green, wispy + irregular
  - > qtz : 10-15%, < 1cm, incolor, round + elongated
  - > fds : 15-20%, < 3mm, orange + creamy, tabular + irregular.

LOG: BHD-4
Location: MRT core store

Date: 15-23/NOV/2011
Logged by: Pedro Fonseca

m	Structure	Grainsize (mm) 0.06 1 2 8 32 64 256	Description
100			↦ 60.5-104.5: Perlitic pumiceous rhyolite breccia. (note: details as above).
ϟ ⑤ 102.4m ←			
ϟ ⑤ 104.3m ←	104.5 gradational contact		104.5m
	flow banding		↦ 104.5-135.2: Weakly sericitic/chloritic, locally flow-banded, fds+qtz-phyric, ovarigish to green massive rhyolite. • qtz: ~5-10%, <6-8mm, incolor, rounded+irregular • fds: ~10-15%, <3-6mm, white+pink, tabular+irregular. o phenocryst size+amount decrease downhole.
ϟ ⑤ 112.8m ←	fracturation quartz+carbonate veins		
120			135.2m
	flow banding		↦ 135.2-136.0: Homogeneous, poorly laminated, black mudstone • disseminated chalcopyrite. 136.0m
ϟ ⑤ 131.5m ←			↦ 136.0-138.1+151.5-152.0: Weakly to moderately sericitic/chloritic, poorly-sorted, matrix-supported, monomictic, granule to cobble, volcaniclastic, locally perlitic, pumiceous rhyolite breccia. • rhyolite clasts: ~15%, <6cm, green+grey, irregular > fds: 20-25%, <1cm, orange, tabular > qtz: 10-15%, <8mm, incolor, rounded • rhyolitic pumice: ~10%, <4cm, dark green, wispy+wavy. > qtz: ~15%, <8mm, incolor, rounded > fds: ~60%, <1cm, orange, tabular.
135.2	missing fragmented contact		
136.0			
ϟ ⑤ 137.7m ←	mingled contact		
138.1			↦ 138.1-151.5: Weakly sericitic, locally flow-banded, fds+qtz-phyric massive rhyolite. • qtz: ~15%, <1cm, incolor, rounded+irregular • fds: ~20-25%, <7mm, orange+creamy, tabular
140			
ϟ ⑤ 147.5m ←			152.0m
ϟ ⑤ 151.5m ←			↦ 152.0-153.2: Heterogeneous, weakly locally laminated, grey to black, fds+qtz-phyric rhyolite-bearing mudstone. o disseminated chalcopyrite. 153.2m
151.5	mingled contact		
152.0			
ϟ ⑤ 153.4m ←			
153.2			
154.0			↦ 153.2-154.0: Weakly to moderately sericitic/chloritic, poorly-sorted, clast-supported, monomictic, granule to cobble, volcaniclastic, perlitic rhyolite breccia. • rhyolite clasts: 85%, <6cm, green+brownish, rounded+irregular > qtz: ~10%, <8mm, incolor, rounded > fds: 15-20%, <6mm, orange+pink+creamy, tabular+irregular • pumice: 1%, <3mm, dark green, wispy+wavy+irregular.
ϟ ⑤ 155.2m ←			↦ 154.0-155.5: Sericitic, perlitic, fds+qtz-phyric massive rhyolite. • qtz: ~10%, <8mm, incolor, rounded • fds: 15-20%, <6mm, orange+creamy, tabular+irregular.
155.5	mingled contact		↦ 155.5-161.0: Weakly to strongly sericitic/chloritic, poorly-sorted, mud matrix-supported, monomictic, granule to boulder, volcaniclastic, perlitic, fds+qtz-phyric rhyolite breccia. ⇒ peperite • rhyolite clasts: 30-40%, <40cm, green, irregular > qtz: 15-20%, <1cm, incolor, rounded+irregular > fds: 40-45%, <1cm, orange+creamy, tabular+irregular.
ϟ ⑤ 158.0m ←			
ϟ ⑤ 160.8m ←			
160			
161.0	fragmentation		↦ 161.0-162.8: Heterogeneous, massive, fragmented grey mudstone.
162.8			↦ 162.8-175.3: Weakly to strongly sericitic/chloritic, poorly-sorted, matrix to locally mud matrix-supported, monomictic, granule to cobble, volcaniclastic, perlitic, pumiceous rhyolite breccia. • rhyolite clasts: 30-85%, <10cm, green+creamy, rounded+irregular > qtz: 5-10%, <8mm, incolor, rounded > fds: 10-15%, <5mm, orange, tabular • pumice clasts: 15-20%, <6cm, dark green+green, wispy+irregular > qtz: 15-20%, <8mm, incolor, rounded > fds: 20-25%, <4mm, brown, tabular
ϟ ⑤ 165.4m ←			
ϟ ⑤ 166.2m ←			
ϟ ⑤ 167.8m ←			
⑤ 171.8m ←			
ϟ ⑤ 172.5m ←			
⑤ 175.9m ←	175.3 fragmentation		↦ 175.3-213.4: Weakly to moderately sericitic/chloritic, very locally flow-banded, fds+qtz-phyric, massive green rhyolite. • qtz: 10-15%, <1cm, incolor, rounded+irregular • fds: 20-25%, <8mm, creamy+green, tabular+irregular • chlorite: 1-2%, <3mm, dark green/black, rounded+irregular.
	quartz veins		
180	flow banding		
200			

LOG BHD-4
Location: MRT core store

Date: 15-23/NOV/2011
Logged by: Pedro Fonseca

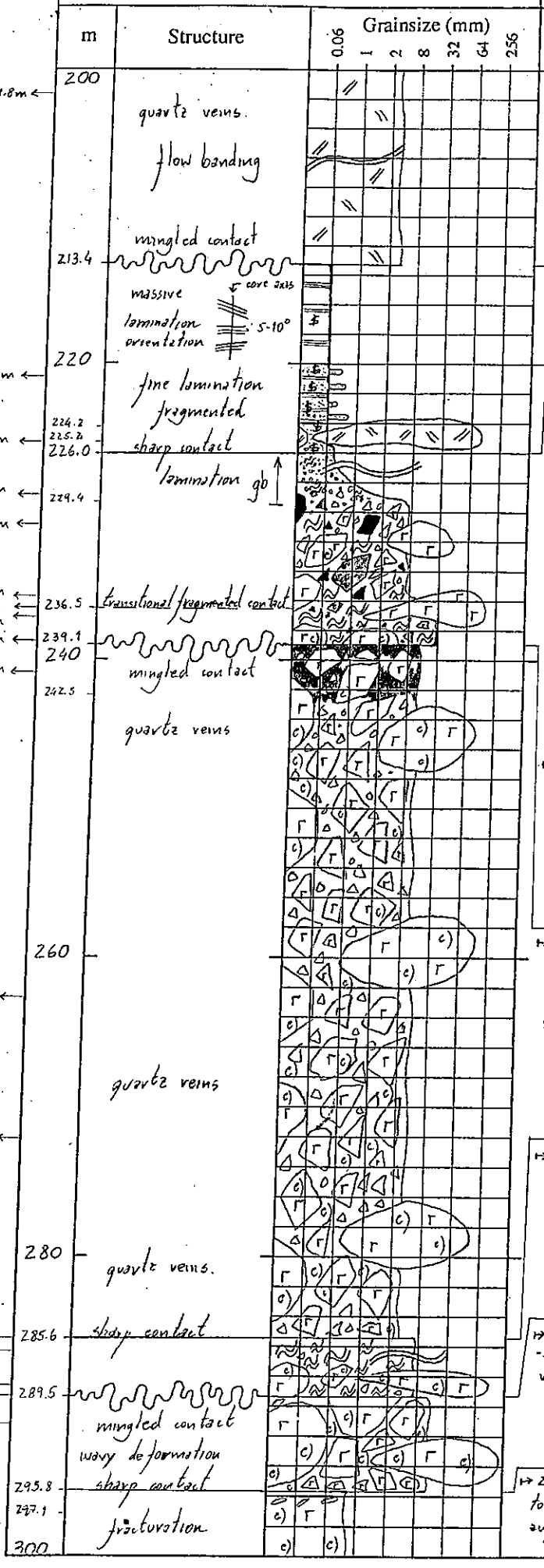

↦ 175.3 - 213.4 : Weakly to moderately sericitic/chloritic, very lowly flow-banded, fds+qtz-phyric, massive green rhyolite.
- qtz : 10-15%, <1cm, incolor, round + irregular
- fds : 20-25%, <8mm, creamy + green, tabular + irregular
- chlorite : 1-2%, <3mm, dark green/black, round+irregular

213.4m

↦ 213.4 - 226.0 : Heterogeneous, massive to finely laminated, pyritic, grey to black mudstone, siltstone + fine sandstone.
- pyritic lenses (<2-3cm x 1cm), thin beds (<3mm) + veins.
- rhyolite clasts + pumice (224.2 - 225.4) : ~40%, <10cm
  - > qtz : 10-15%, <6mm, incolor, round + irregular
  - > fds : 20-25%, <4mm, pink + creamy, tabular + irregular.

226.0m

↦ 226.0 - 229.4 : Graded, weakly to moderately sericitic/chloritic, heterogeneous, weakly laminated, well- to poorly-sorted, fds-rich, very fine to very coarse, pinkish to greyish pumice-rich sandstone.
- pumice : 10-15%, <4cm, dark green + black, wispy + irregular

↦ 229.4 - 236.5 : Weakly to moderately sericitic/chloritic, poorly-sorted, matrix-supported, polymictic, granule to cobble, volcaniclastic, perlitic, pumiceous dacite breccia.
- qtz : 5-10%, <5mm, incolor, round + irregular
- fds : 10-15%, <4mm, pink + orange, tabular + irregular
- mudstone : <5%, <2cm, black, homogeneous, round + irregular
- lithics : 5-10%, <1cm, orange + grey, round + irregular
- perlitic clasts : 5%, <1cm, black + pinkish, round + irregular
- pumice : 10%, <3cm, dark green + black, wispy + irregular.
- dacite clasts : 15-20%, <4cm (up to 15cm), qtz+fds-phyric to aphyric, rarely perlitic, multicoloured, round + irregular.
  - > fds : 5%, <2mm, pink + orange, tabular + irregular
  - > qtz : 1%, <1mm, incolor, round.

↦ 236.5 - 239.1 : Weakly to moderately sericitic/chloritic, poorly-sorted, matrix-supported, monomictic, granule to cobble, strongly perlitic, volcaniclastic, dacite pumice breccia.
- pumice : 20-25%, <2cm, dark green, wispy + irregular
- dacite clasts : 15-20%, <12cm, fds+qtz-phyric to aphyric, pink + orange, irregular, perlitic.
- lithics : 1%, <1cm, pink/orange, round + irregular.

239.1m

↦ 239.1 - 285.6 : Weakly sericitic/chloritic, poorly-sorted, matrix-supported (locally clast-supported with mud matrix at the top), monomictic, granule to cobble, volcaniclastic, perlitic, dacite breccia.
- dacite clasts : 35-40%, <25cm, green, irregular, perlitic, aphyric to weakly qtz+fds-phyric.
  - > fds=qtz : 1%, <3mm, irregular
- glassy matrix.

285.6m

↦ 285.6 - 289.5 : Weakly to moderately sericitic/chloritic, poorly-sorted, matrix-supported, monomictic, granule to cobble, perlitic, dacitic pumice breccia.
- dacitic clasts : ~30% (concentrated at the bottom), <35cm, green, irregular, perlitic, aphyric to weakly qtz+fds-phyric
- pumice : 70% (100% at the top), <5cm, dark green, wispy + irregular

289.5m

↦ 289.5 - 295.8 : Weakly sericitic/chloritic, poorly-sorted, matrix-supported to clast-supported, monomictic, granule to boulder, perlitic, volcaniclastic dacite breccia.
- dacite clasts : 55-60%, <40cm, green, irregular, perlitic, aphyric to weakly fds+qtz-phyric
  - > fds : qtz : 1%, <3mm, irregular

295.8m

↦ 295.8 - 301.2 : Weakly to moderately sericitic/chloritic, aphyric to very weakly fds-phyric, strongly perlitic, weakly and locally amygdaloidal, massive dark green dacite.
(note: details as below).

LOG BHD-4
Location: MRT core stove

Date: 15-23/NOV/2011
Logged by:

Page 4 of 7

m	Structure	Grainsize (mm) 0.06 1 2 8 32 64 256	Description
300			↦ 295.8-301.2 + 307.5-313.8 + 338.0-344.0 + 363.5-366.0: Weakly to moderately sericitic/chloritic, aphyric to very weakly fds-phyric, strongly perlitic, weakly and locally amygdaloidal, massive, dark green dacite. • fds: 1%, <3mm, creamy + pink + green, tabular + irregular • amygdales: 1%, <5mm, incolor + green, elipsoidal + irregular.
301.2			
307.5	massive		
313.8			
320	shear...		↦ 301.2-307.5 + 313.8-338.0 + 344.0-363.5 + 366.0-382.2: Weakly sericitic/chloritic, poorly-sorted, clast-supported, monomictic, strongly perlitic, granule to cobble, locally jigsaw-fit, volcaniclastic dacite breccia. • dacite clasts: 50-55%, <10cm, dark green, irregular, aphyric to weakly fds-phyric, perlitic > fds: 1%, <3mm, pink + creamy, tabular + irregular.
338.0			
340	massive fracturation		
344.0			
360			
363.5	fracturation massive		
366.0			
380			↦ 384.5-389.3 + 390.0-392.8: Weakly to moderately sericitic/chloritic, poorly-sorted, clast-supported, monomictic, perlitic, granule to cobble, volcaniclastic dacite breccia. • dacite clasts: 30-35%, <10cm, orange + green, round + irregular, fds + qtz-phyric > fds: 5-10%, <4mm, creamy + green, tabular + irregular > qtz: 2-3%, <2mm, incolor, round ○ ~399.0m: phenocryst-rich: 20-25%
381.5			
382.2/4	sharp contact		
382.7			
383.0			
384.5	mingled contact		
389.3			
390.0	flow banding		
392.8	fracturation + fragmentation		
400			

382.2m

↦ 382.2-382.4: Heterogeneous, massive, pyritic, fds + qtz-rich pumice-bearing grey to black mudstone.

• pumice: 40%, <5cm, dark green, wispy, fds + qtz-phyric.
> fds: 20-25%, <4mm, orangish + pinkish + creamy, tabular + irregular
> qtz: 5-10%, <2mm, incolor + whitish, round

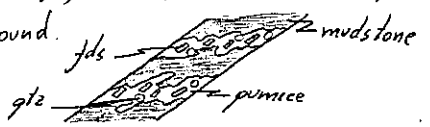

382.4m

○ 301.4m
○ 304.3m
○ 309.7m
○ 322.8m
○ 339.5m
○ 343.5m
○ 358.8m
○ 363.5m
○ 369.8m
○ 381.5m
○ 382.2/4m
○ 382.7m
○ 383.0m
○ 399.1m

LOG: BHD-4
Location: MRT cove stove

Date: 15-23/NOV/2011
Logged by: Pedro Fonseca

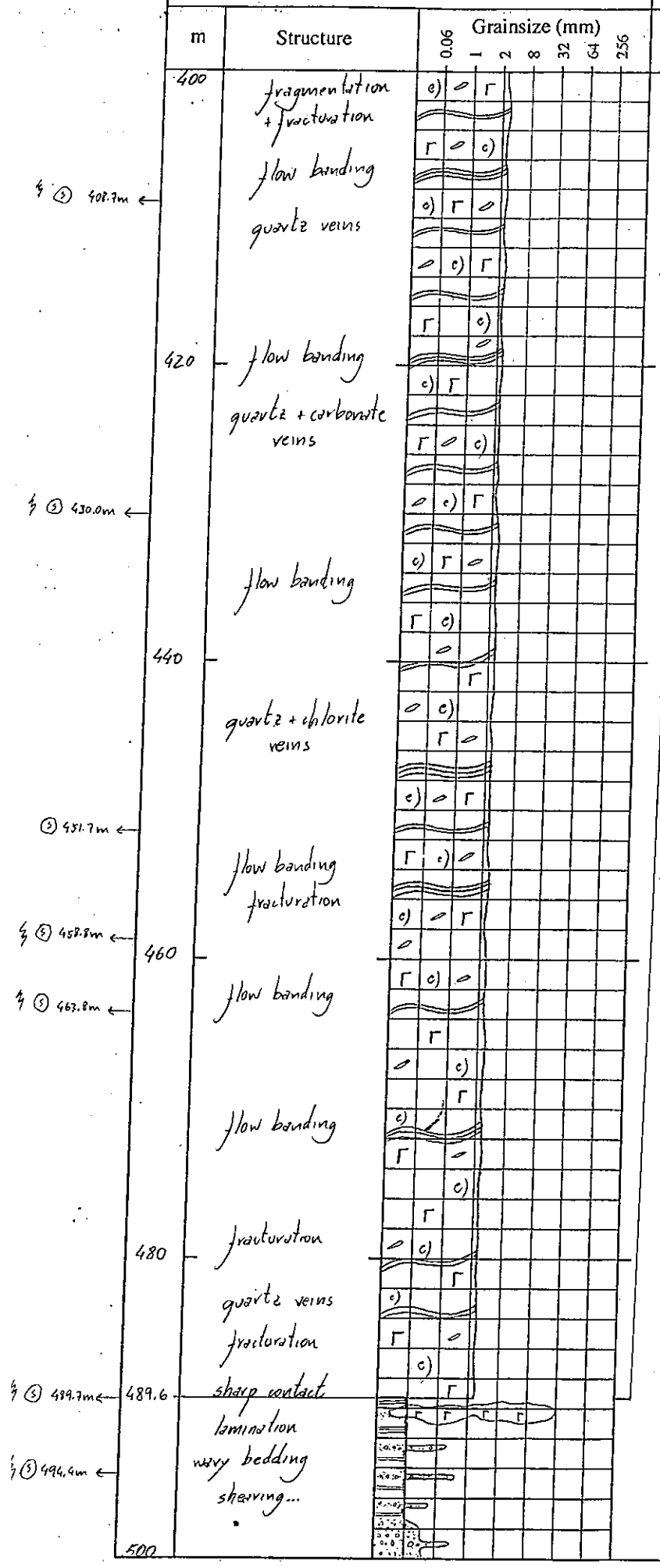

↦ 382.7 - 384.5 + 389.3 - 390.0 + 392.8 - 489.6:

Weakly sericitic/chloritic, flow-banded, fds + qtz-phyric, weakly perlitic, very weakly amygdaloidal and pyritic, creamy green massive dacite.

- fds: 5%, <4mm, creamy + pink + green, tabular + irregular
- qtz: 2-3%, <2mm, incolor, round
- amygdales: 1%, <8mm, dark green, elongated + irregular, chloritic
- pyrite/chalcopyrite: 1%, <2mm, round

489.6m

↦ 489.6 - 615.1:

Animal Creek Greywacke

Interbedded, moderately pyritic and weakly micaceous, homogeneous, well-sorted, fine- to coarse-grained greenish grey, massive to weakly bedded to locally graded sandstone, pale grey to dark grey, homogeneous, laminated, siltstone, and very weakly pyritic, laminated, homogeneous black mudstone.

- sandstone beds: >1-10m
- chalcopyrite/pyrite nodules/lenses: <2cm
- dacite clasts: 1%, <7cm, green, irregular
  - > fds: 10%, <3mm, orange, tabular + + irregular.
  - > qtz: 1%, <2mm, incolor, round + + irregular.

LOG: BHD-4
Location: MRT core store

Date: 15-23/NOV/2011
Logged by: Pedro Fonseca

m	Structure	Grainsize (mm) 0.06 1 2 8 32 64 256	Description

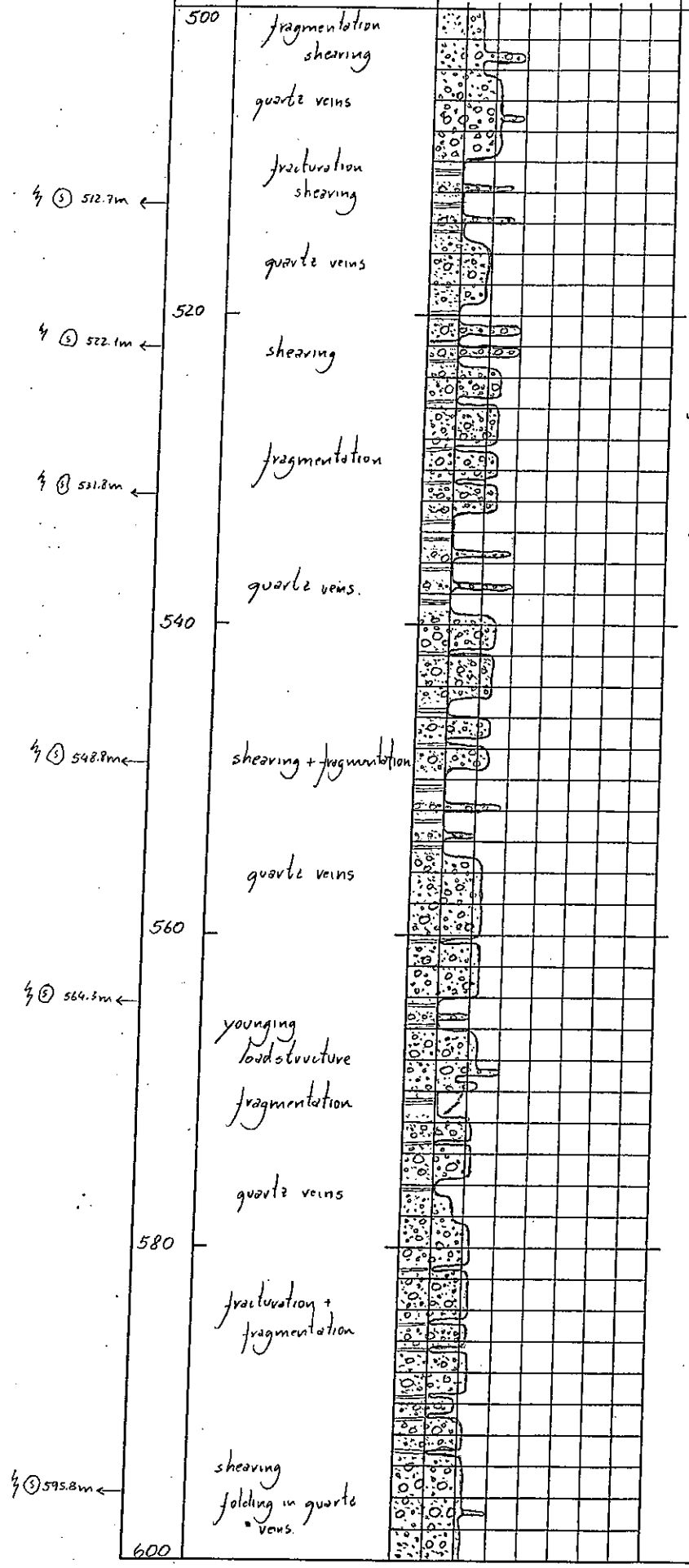

↦ 489.6 - 615.1 :

Animal Creek Greywacke

Interbedded, moderately pyritic and weakly micaceous, homogeneous, well-sorted, fine- to coarse-grained, greenish grey, massive to weakly bedded to locally graded sandstone, pale grey to dark grey, homogeneous, laminated, siltstone, and very weakly pyritic, laminated, homogeneous black mudstone.

- sandstone beds : > 1-10 m
- chalcopyrite/pyrite nodules/lenses : < 2 m.

LOG BHD-4
Location: MRT - core store

Date: 15-23/NOV/2011
Logged by: Pedro Fonseca

Page 7 of 7

m	Structure	Grainsize (mm) 0.06 1 2 8 32 64 256	Description
600			↳ 489.6 - 615.1:
ϟ ⑤ 606.1m ←			**Animal Creek Greywacke**
ϟ ⑤ 614.9m ← 615.1	E.O.H.		Interbedded, moderately pyritic and weakly micaceous, homogeneous, well-sorted, fine- to coarse-grained, greenish grey, massive to weakly bedded to locally graded sandstone pale grey to dark grey, homogeneous, laminated, siltstone, and very weakly pyritic, laminated, homogeneous, black mudstone.
620			o sandstone beds: > 1-10 m
			o chalcopyrite/pyrite nodules/lenses: < 2m

LOG BHD-10
Location: MRT core store

Date: 24/APR/2012
Logged by: PEDRO FONSECA

m | Structure | Grainsize (mm): 0.06, 1, 2, 8, 32, 64, 256 | Description

0 — Alteration + fragmentation

6.5m

lamination...

13.1m

18.5m

20 — wavy lamination

25.6m

30.8m

fragmentation

36.5m

wavy lamination

38.0m

40 — fragmentation

lamination + fragmentation

55.0m

58.2m

60 — lamination

64.5m

wavy lamination

80 — fragmentation.

mingled contact

88.0

89.5m

97.4 — sharp contact

lamination.

100

↦ 0 - 88.0: Interbedded, locally pyritic and micaceous, heterogeneous, well-sorted, fine- to coarse-grained, massive to weakly bedded to locally graded and laminated, polymictic, volcaniclastic, yellowish greyish brown sandstone and siltstone and weakly pyritic, massive to locally laminated, homogeneous, dark grey to black mudstone.

- altered zones ("ghosts") up to 4cm long.
- pyritic clusters (< 1cm) + mudstone lenses (< 8cm)

Black Heavy Beds

88.0m

↦ 88.0 - 97.4: Weakly sericitic and chloritic, pyritic, moderately sorted, mud-matrix-supported, polymictic, granule to pebble-sized, volcaniclastic breccia.

- fds: 5%, < 5mm, white, tabular + rectangular + irregular
- qtz: 2%, < 2mm, inicolor, round + irregular
- lithics: 1%, < 4mm, creamy + reddish, irregular
- chloritic + pyritic + sphaleritic, fds + qtz ? - phyric to aphyric, dacitic? flamme (pumice): 3%, < 3cm, dark green, irregular + wispy + elongated
- fds-phyric dacite clasts: < 1%, < 3cm, light green, round, + elongated + irregular, chloritic + perlitic?
- mudstone: 2%, < 4cm, dark grey, elongated
- pyrite + sphalerite: 1%, < 2mm, irregular.

97.4m

↦ 97.4 - 103.6: Weakly sericitic and chloritic, graded, locally laminated, homogeneous, dark grey to black mudstone, very well-sorted, volcaniclastic siltstone and moderately- to poorly-sorted, mud-matrix- to locally matrix-supported, polymictic, volcaniclastic breccia.

- fds: 5%, < 4mm, creamy + grey, tabular + rectangular + irregular
- qtz: 5%, < 2mm, inicolor, round + irregular
- fds-phyric dacite: < 5%, < 15mm, light greyish green, round + irregular.
- amygdaloidal clasts: < 1%, < 1cm, grey, irregular, chlorite + qtz + carbonate-filled amygdales (< 4mm, elongated)

sand dykes throughout...

100.9m.

LOG BHD-10
Location: MRT core store

Date: 24/APR/2012
Logged by: PEDRO FONSECA

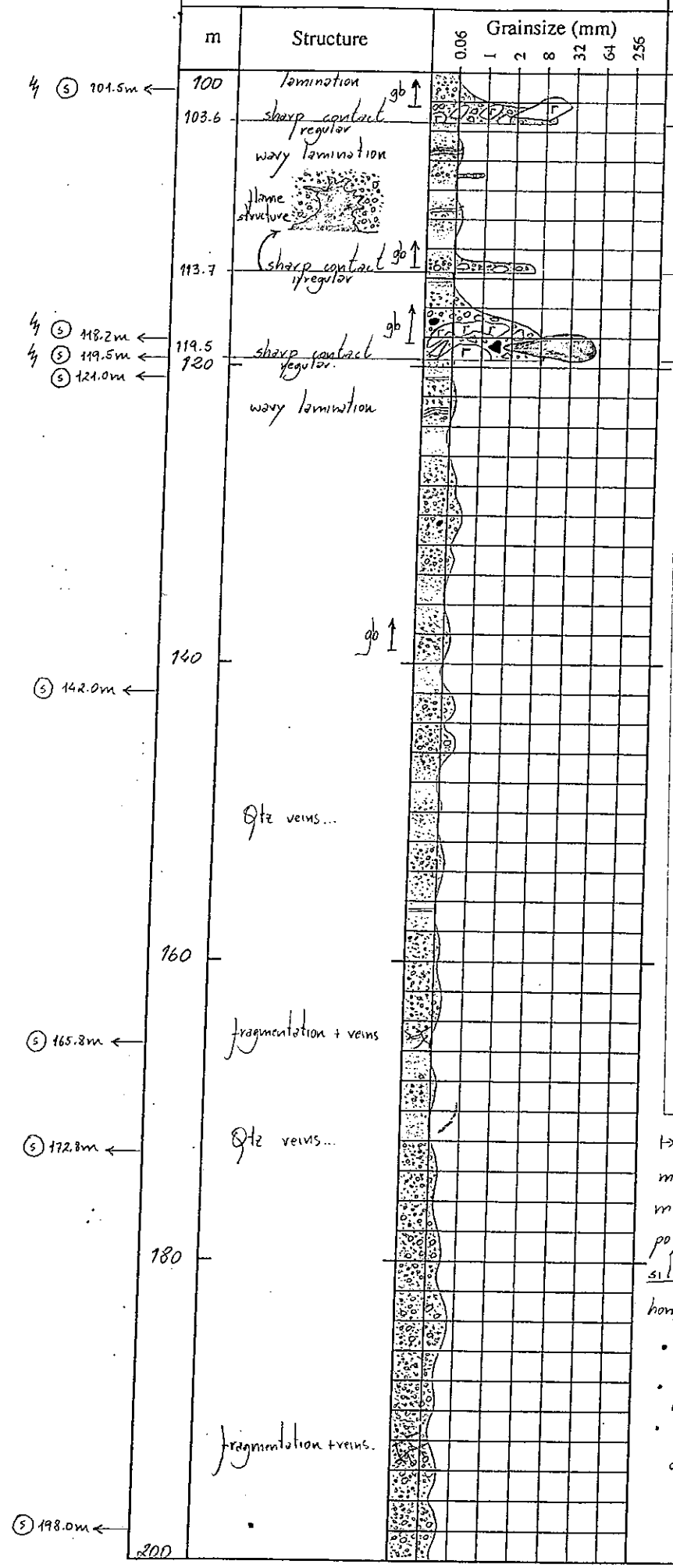

Description

↦ 97.4 - 103.6 : Weakly sericitic and chloritic, graded, locally laminated, homogeneous, dark grey to black mudstone, very well-sorted, volcaniclastic siltstone and moderately to poorly-sorted, mud matrix- to locally matrix-supported polymictic, volcaniclastic sandstone and breccia.

103.6m

↦ 103.6 - 119.7 : Weakly sericitic and chloritic, graded, locally laminated, pyritic and sphaleritic, homogeneous, dark grey to black mudstone, very well-sorted, volcaniclastic siltstone and moderately-sorted, mud matrix- to locally matrix-supported polymictic, volcaniclastic sandstone and breccia.

- sandstone and breccia from 113.2m to 113.7m :
  - fds : <10%, <3mm, white + creamy, tabular + irregular
  - qtz : <10%, <6mm, incolor, round + irregular
  - dacite? : <5%, <5mm, green, irregular, aphyric
  - chlorite (glass shards?) : 1%, <5mm, dark green + black, irregular
  - pyrite : <5%, <4mm, irregular + round
  - sphalerite : 1%, <5mm, red, irregular.

113.7m

↦ 119.7 - 119.5 : Weakly sericitic and chloritic, graded, locally laminated, pyritic and sphaleritic, homogeneous, dark grey to black mudstone, very well-sorted, volcaniclastic siltstone and moderately to poorly-sorted, mud matrix to locally matrix-supported, polymictic, volcaniclastic sandstone and breccia.

- fds : 5%, <5mm, white, tabular + rectangular + irregular
- qtz : <5%, <2mm, incolor, round + irregular
- fds-phyric to aphyric, chloritic + pyritic + sphaleritic, flamme (pumice) dacite : <5%, <3cm, dark green, wispy + irregular
- lithics : 1%, <6mm, brown, round + irregular
- mudstone : 1-2%, <5cm, elongated, black, laminated
- pyrite + sphalerite : 2%, <1cm, red + yellow, elongated.

o 5cm long mudstone clast at 118.0m.

119.5m

↦ 119.5 - 202.0 : Interbedded, locally pyritic and micaceous, heterogeneous, well-sorted, fine- to coarse-grained massive to weakly bedded to locally graded and laminated polymictic, volcaniclastic, greyish green sandstone and siltstone and weakly pyritic, massive to locally laminated, homogeneous, dark grey to black mudstone.

- 4cm long mudstone clast at 135.2m
- pyrite clusters (<15mm) at 182.9m
- fds-phyric, pyritic, chloritic, dark green, pumiceous? dacite clast at 184.0m : <1%, <3cm, dark green, elongated.

Black Harry Beds

LOG BHD-10
Location: MRT core store

Date: 24/APR/2012
Logged by: PEDRO FONSECA

Page 3 of 3

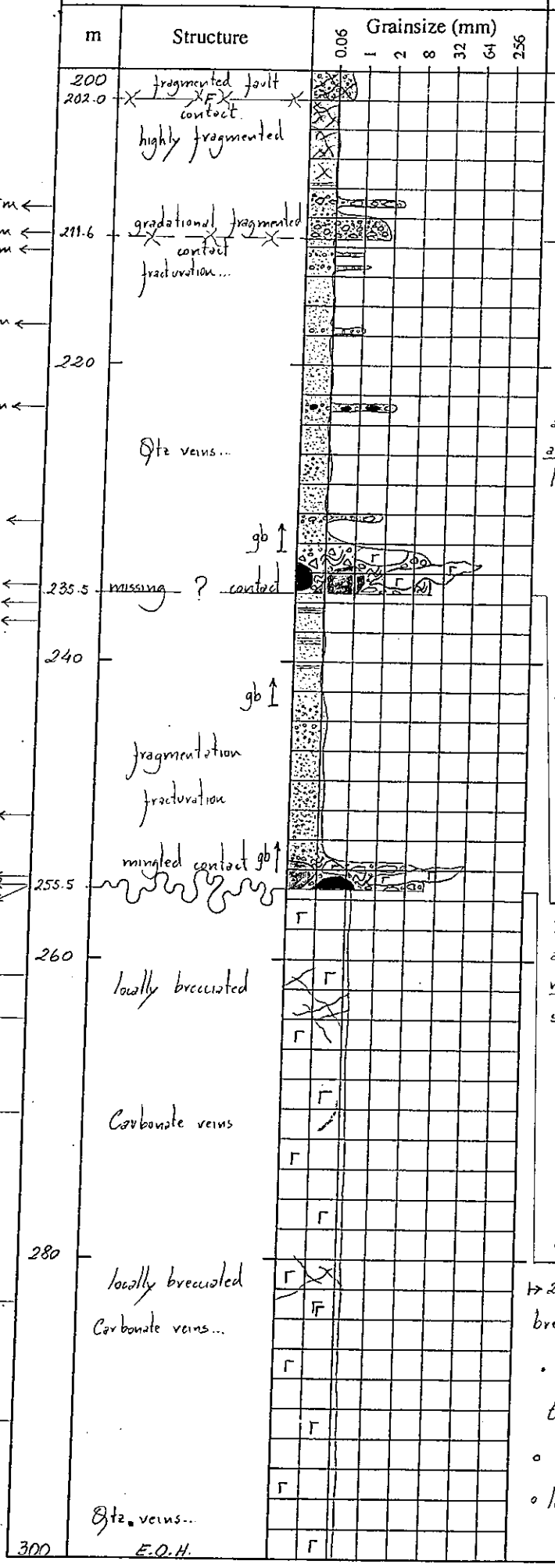

↦ 119.5 - 202.0: Black Hawy Beds.

202.0m

↦ 202.0 - 211.6: Weakly sericitic and chloritic, locally graded and laminated, weakly pyritic, heterogeneous, dark grey to black silicified mudstone and siltstone and moderately-sorted, matrix-supported, polymictic, volcaniclastic sandstone and breccia.

- fds: 10%, <4mm, cream+orange, tabular+round+irregular
- qtz: 5%, <1mm, incolor, round+irregular
- chlorite: 1%, <3mm, dark green, irregular
- disseminated sulfides.

211.6m

↦ 211.6 - 235.5: Weakly sericitic and chloritic, locally graded and laminated, locally pyritic, homogeneous, dark grey to black mudstone and siltstone, and moderately-sorted, matrix-supported, polymictic lithic-rich volcaniclastic sandstone and breccia.

- fds+qtz+pyrite-rich breccia at 223.0 - 223.3m + 230.1 - 230.4m:
  - fds: 10%, <5-6mm, creamy, tabular+irregular
  - qtz: 5%, <4mm, incolor, round+irregular
  - lithics: 5%, <6mm, creamy, round+irregular
  - mudstone: 1%, <2-5cm, black, round+elongated.
- big carbonate clast at 230.0m: 6cm long.
- sandstone stevls at 231.5m:
  - fds: 15%, <7mm, creamy, tabular+rectangular+irregular
  - qtz: <5%, <3mm, incolor, round+irregular
  - mudstone: 1%, <15mm, black, round+elongated, homogeneous.
  - lithics: 1%, <10mm, brownish cream, round+elongated
  - pumice: 15-20%, <4cm, dark green+light green, wispy+irregular+elongated, rarely fds-phyric, often aphyric, dacitic?
  - fds-phyric dacite: 1%, <1cm, light green, round+irregular, chloritic/sericitic
  - pyrite: <5%, <30mm, elongated.

235.5m

↦ 235.5 - 255.5: Weakly sericitic and chloritic, locally graded and laminated, pyritic, homogeneous, dark grey to black mudstone and siltstone, and moderately sorted, matrix-supported, polymictic volcaniclastic sandstone and breccia.

- fds: 15%, <7mm, creamy, tabular+rectangular+irregular
- qtz: <5%, <3mm, incolor, round+irregular
- mudstone: <5%, <30mm, black, round+elongated, homogeneous
- lithics: <5%, <10mm, brownish cream, round+elongated
- pumice: 15-20%, <4cm, dark green+light green, wispy+irregular+elongated+rarely fds-phyric, often aphyric, dacitic?
- fds-phyric dacite: 1%, <1cm, light green, round+irregular, chloritic/sericitic
- pyrite: <5%, <30mm, elongated

255.5m

↦ 255.5 - 300.0: Weakly sericitic and silicified, locally brecciated, fds-phyric massive green dacite.

- fds: 15%, <3mm, pink+orange+cream+white, tabular+rectangular+irregular.
- disseminated sulfides (pyrite+chalcopyrite)
- local fds abundance of 20-25% at 283.5m

LOG BOC-2 Boco Alteration Zone
Location: Tullok core shed

Date: 16/MAR/2011
Logged by: Pedro Fonseca

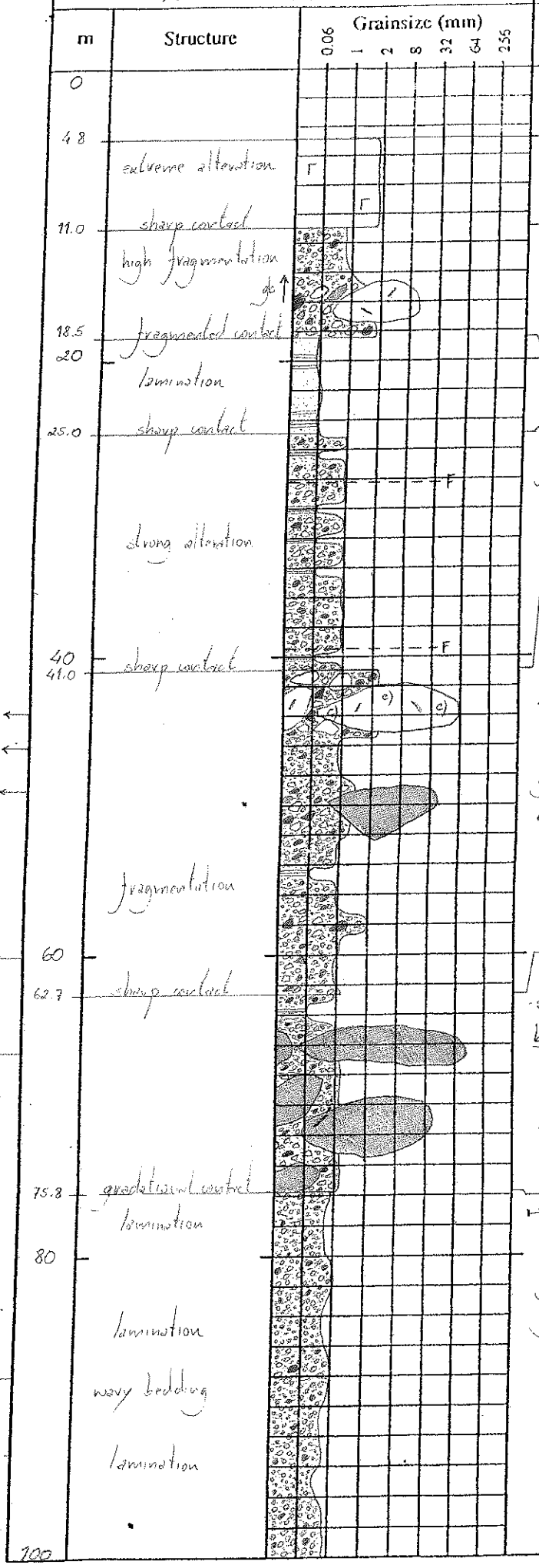

↦ 0 - 4.8: No hole...

4.8m

↦ 4.8 - 11.0: Strongly altered, feldspar-phyric, massive dacite.

- fds: <5%, 2-3mm, tabular, irregular, greenish

11.0m

↦ 11.0 - 18.5: Strongly altered, moderately-sorted, fragmented, fine to coarse-grained volcaniclastic lithic sandstone and polymictic volcaniclastic breccia.

- quartz + lithics + rhyolite clasts + mudstone

18.5m

↦ 18.5 - 25.0: Weakly altered, pyritic, laminated, brown and black mudstone.

25.0m

↦ 25.0 - 41.0: Interbedded, fine to coarse-grained, feldspar-quartz crystal-rich volcaniclastic lithic sandstone and pyritic, laminated brown and black mudstone.

- lithic fragments in sandstone beds?
- minor faults at: 28.2m, 39.5m

41.0m

↦ 41.0 - 62.7: Moderately altered, poorly-sorted, feldspar-quartz? crystal-rich, matrix-supported, polymictic volcaniclastic breccia and perlitic feldspar-phyric rhyolite breccia, and strongly silicified, well to poorly-sorted, quartz-rich, fine to coarse-grained, grey volcaniclastic lithic sandstone, and laminated black mudstone.

- sandstone and mudstone clasts up to 4cm across and strongly silicified.
- lithics in sandstone are probably dacitic in composition
- <1% sphalerite

62.7m

↦ 62.7 - 75.8: Weakly to moderately sericitic, poorly-sorted, matrix-supported volcaniclastic mudstone breccia.

- mudstone clasts: up to 10cm across, laminated, become rare and smaller downhole
- matrix: feldspar-quartz crystal-rich and lithic-bearing, fine to coarse-grained volcaniclastic sandstone.

75.8m

↦ 75.8 - 112.0: Weakly sericitic to moderately silicified, interbedded laminated, weakly pyritic and sphaleritic grey siltstone and well-sorted, fine to medium-grained, locally feldspar-quartz crystal-rich, bedded to massive volcaniclastic lithic sandstone.

- feldspar crystal-rich zones: 5%, ~2mm, creamy, irregular.

LOG BOC-2 Boco Alteration Zone
Location: Tulloh core shed

Date: 16/MAR/2011
Logged by: Pedro Fonseca

m | Structure | Grainsize (mm) 0.06 1 2 8 32 64 256 | Description

100

111.8m
112.0
113.1m
mingled contact

↦ 75.8 - 112.0 : Weakly sericitic to moderately silicified, interbedded laminated, weakly pyritic and sphalenitic, grey siltstone and well-sorted, fine to medium-grained, locally feldspar-quartz crystal-rich, bedded to massive volcaniclastic lithic sandstone.

- feldspar crystal-rich zones: 5%, ≈2mm, creamy, irregular.

112.0m

120

↦ 112.0 - 158.9 : Weakly to strongly altered, laminated to massive, dark grey to black pyritic mudstone and siltstone, and poorly-sorted, matrix-supported volcaniclastic mudstone breccia.

- mudstone clasts: up to 5cm across,
- matrix: feldspar-quartz crystal-rich and lithic-bearing fine to coarse-grained volcaniclastic sandstone.
- rhyolite clasts: feldspar (2-3%, ≈1mm, creamy, irregular), quartz? (2-3%, ≈1mm, round, incolor)
- crystal-rich sandstone clasts: up to 10cm long; probably of dacitic or rhyolitic composition
- pyrite: 1-3%, disseminated, veinlets, blobs up to 2-3cm.

140

146.4m

158.9m

↦ 158.9 - 177.9 : Weakly to strongly altered (silicified), feldspar-phyric, massive, greyish rhyolite

- feldspar: 3%, 1-4mm, rectangular, irregular, whitish
- quartz ??? : 1%, 1-2mm, round, incolor.

158.9
mingled contact
160
160.8m

177.9m

↦ 177.9 - 194.7 : Weakly to strongly altered (silicified), laminated to massive, dark grey to black mudstone and siltstone, volcaniclastic lithic sandstone with local amygdaloidal basaltic clasts.

- mafic clasts (basalt/andesite): chlorite-filled amygdales; up to 5cm across
- rare feldspar-quartz-lithics crystal-rich zones in volcaniclastic lithic sandstone

minor fault 166.0m
fractures + qtz veins
fault zone 172.0-175.0
177.9
fault contact
180
lamination

194.7m

↦ 194.7 - 243.0 : Weakly to moderately altered, weakly bedded, moderately to poorly-sorted fine to coarse-grained volcaniclastic lithic sandstone and poorly-sorted, matrix-supported polymictic volcaniclastic breccia.

- siltstone/mudstone and sandstone clasts up to 5cm.
- feldspar: ≈15%, 1-2mm, orangish, irregular
- lithics: 5-10%, 2-3mm, orangish
- quartz: 2-3%, 1-2mm, round, incolor
- rhyolite clasts: fds+qtz?-phyric, up to 5cm long, light grey.

189.6m
194.7
sharp contact
195.6m
weak bedding
200

LOG BOC-2 Boco Alteration Zone
Location: Tullok core shed

Date: 16/MAR/2017
Logged by: Pedro Fonseca

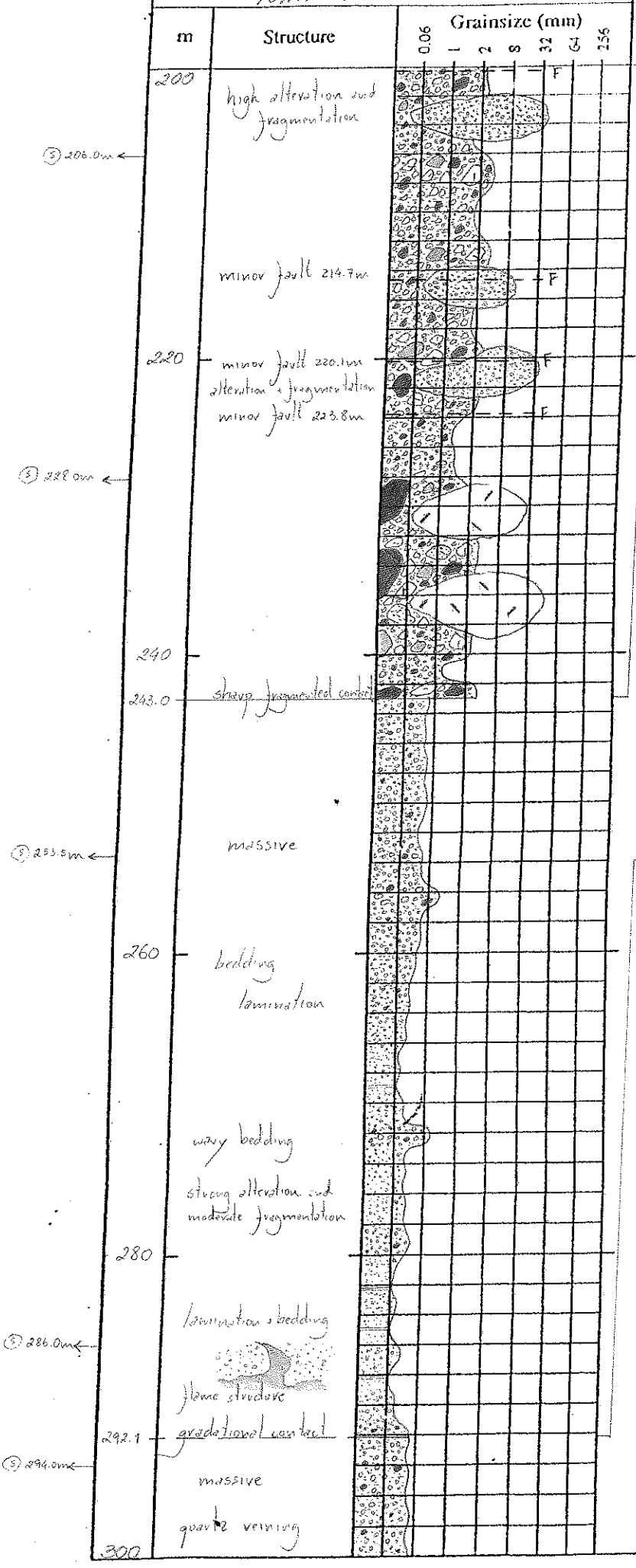

↦ 194.7 - 243.0: Weakly to moderately altered, weakly bedded, moderately to poorly-sorted, fine to coarse-grained volcaniclastic lithic sandstone and poorly-sorted, matrix-supported polymictic volcaniclastic breccia.

- siltstone/mudstone and sandstone clasts up to 5cm
- feldspar: ~15%, 1-2mm, orangish, irregular
- lithics: 5-10%, 2-3mm (up to 1-2cm), orangish.
- quartz: 2-3%, 1-2mm, round, incolor
- rhyolite clasts: fds+qtz?-phyric, up to 5cm long, light grey

243.0m

↦ 243.0 - 292.1: Weakly to strongly altered, interbedded laminated pale to dark grey and black mudstone and volcaniclastic siltstone, and well-sorted, fine to coarse-grained, pyritic, bedded to massive, feldspar-quartz crystal-rich volcaniclastic lithic sandstone.

- sandstone interbeds < 2cm
- flame structure at ~ 288.0m
- quartz and carbonate veins and fractures downholes.

292.1m

↦ 292.1 - 314.2: Weakly altered, well-sorted, fine to coarse-grained, bedded to massive, feldspar-quartz crystal-rich, volcaniclastic lithic sandstone and moderately altered, poorly-sorted, matrix-supported polymictic volcaniclastic breccia.

- pyrite cluster with 2cm across at ~ 299.0m
- trace pyrite downhole
- lithic clasts up to 2cm across, probably of volcanic origin.
- matrix in breccia is feldspar+quartz crystal-rich and lithic-bearing volcaniclastic sandstone and siltstone

LOG BOC-2 Boco Alteration Zone
Location: Tuffish cove shed

Date: 16/MAR/2017
Logged by: Pedro Fonseca

m	Structure	Grainsize (mm) 0.06 — 1 — 2 — 8 — 32 — 64 — 255
300	massive weakly bedded strong alteration + fragmentation minor fault 312.7m	F
314.2	sharp contact	
	minor fault 317.0m lamination	F
320	⚡ ⑤ 320.0m ←	
	minor fault 322.9m minor fault 324.7m bedding	F F
	massive strong alteration minor fault 337.1m	F
340	lamination	
	minor fault 345.8m moderate fragmentation minor fault 350.2m	F F
360	bedding	
	minor fault 366.6m lamination	F
	bedding	
	⚡ ⑥ 379.0m ←	
380	cross-bedding bedding fragmentation lamination	
	moderate alteration + fragmentation	
400	lamination	

↦ 292.7 - 314.2: Weakly altered, well-sorted, fine to coarse-grained, bedded to massive, feldspar and quartz crystal-rich, volcaniclastic lithic sandstone and moderately altered, poorly-sorted, matrix-supported polymictic volcaniclastic breccia.

- trace pyrite
- lithic clasts up to 2cm across, probably of volcanic origin.
- matrix in breccia is feldspar+quartz crystal-rich and lithic-bearing volcaniclastic sandstone and siltstone

314.2m

↦ 314.2 - 454.7: Animal Creek Greywacke

Interbedded, moderately to weakly pyritic and weakly micaceous, homogeneous, well-sorted, and well-bedded, fine to coarse-grained grey to greenish massive to graded sandstone, pale grey to dark grey, laminated siltstone, and very weakly pyritic, laminated, homogeneous, black mudstone.

- some pyritic-rich beds
- 1% pyrite in clusters/blobs/lenses/spots
- sandstone + mudstone bed thicknesses are very variable
- minor faults at: 317.0m, 322.9m, 324.7m, 337.1m, 345.8m, 350.2m, 366.6m.
- carbonate veins
- large (5cm across) mudstone clast at ~ 379.0m

LOG BOC-2 Boco Alteration Zone
Location: Tullok cove shed

Date: 16/MAR/2017
Logged by: Pedro Fonseca

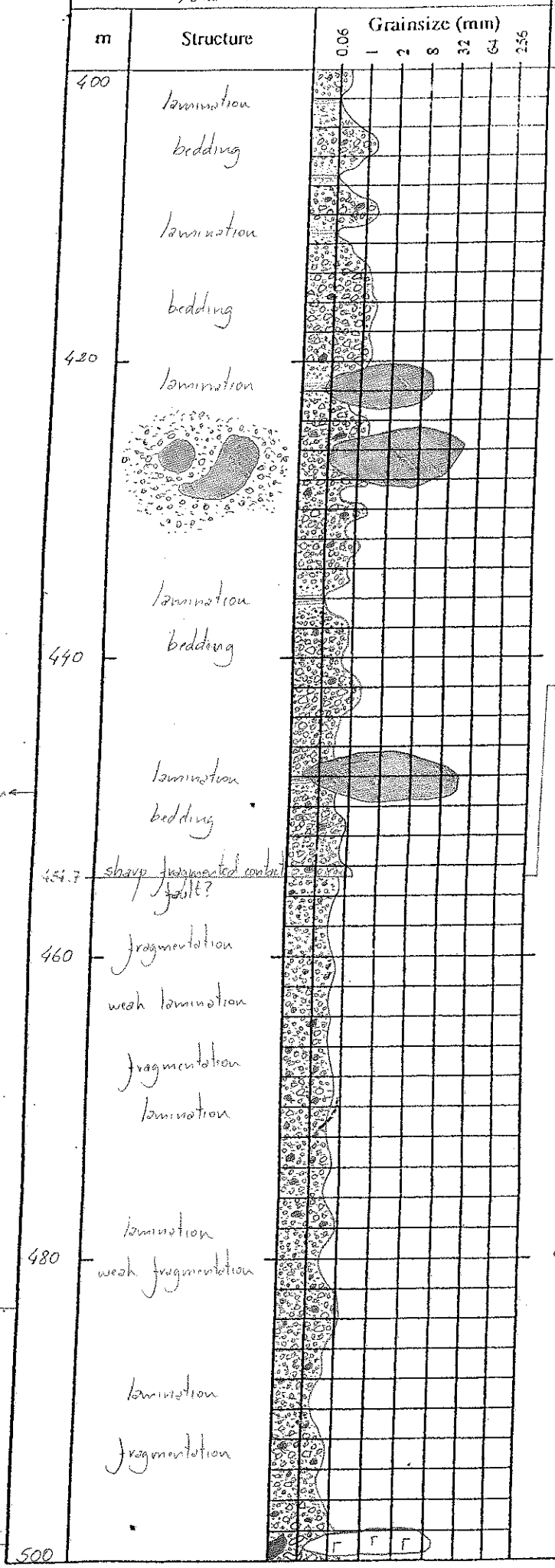

Description

↦ 314.2 - 454.7 : Animal Creek Greywacke

Interbedded, moderately to weakly pyritic and weakly micaceous, homogeneous, well-sorted and well-bedded, fine to coarse-grained grey to greenish massive to graded sandstone, pale grey to dark grey, laminated siltstone and very weakly pyritic, laminated, homogeneous black mudstone.

- some pyritic-rich beds
- 1% pyrite in clusters/blobs/lenses/spots
- sandstone + mudstone bed thicknesses are very variable
- carbonate veins
- large (up to 5cm across), laminated, mudstone clasts.

454.7m

↦ 454.7 - 546.7 : Plank Heavy Beds

Interbedded, weakly sericitic, locally pyritic and micaceous, heterogeneous, well to moderately-sorted, fine to coarse-grained, massive to weakly-bedded and locally graded and laminated, shard and lithic-bearing, grey to brownish green volcaniclastic sandstone, siltstone, and weakly pyritic, massive to laminated, homogeneous dark grey to black mudstone

- trace sulfides
- flattened feldspar-phyric dacite clasts, lithic clasts and siltstone + sandstone clasts up to 4cm across at ~ 499m.

LOG BOC-2 Bolo Alteration Zone
Location: Tullok core shed

Date: 16/MAR/2011
Logged by: Pedro Fonseca

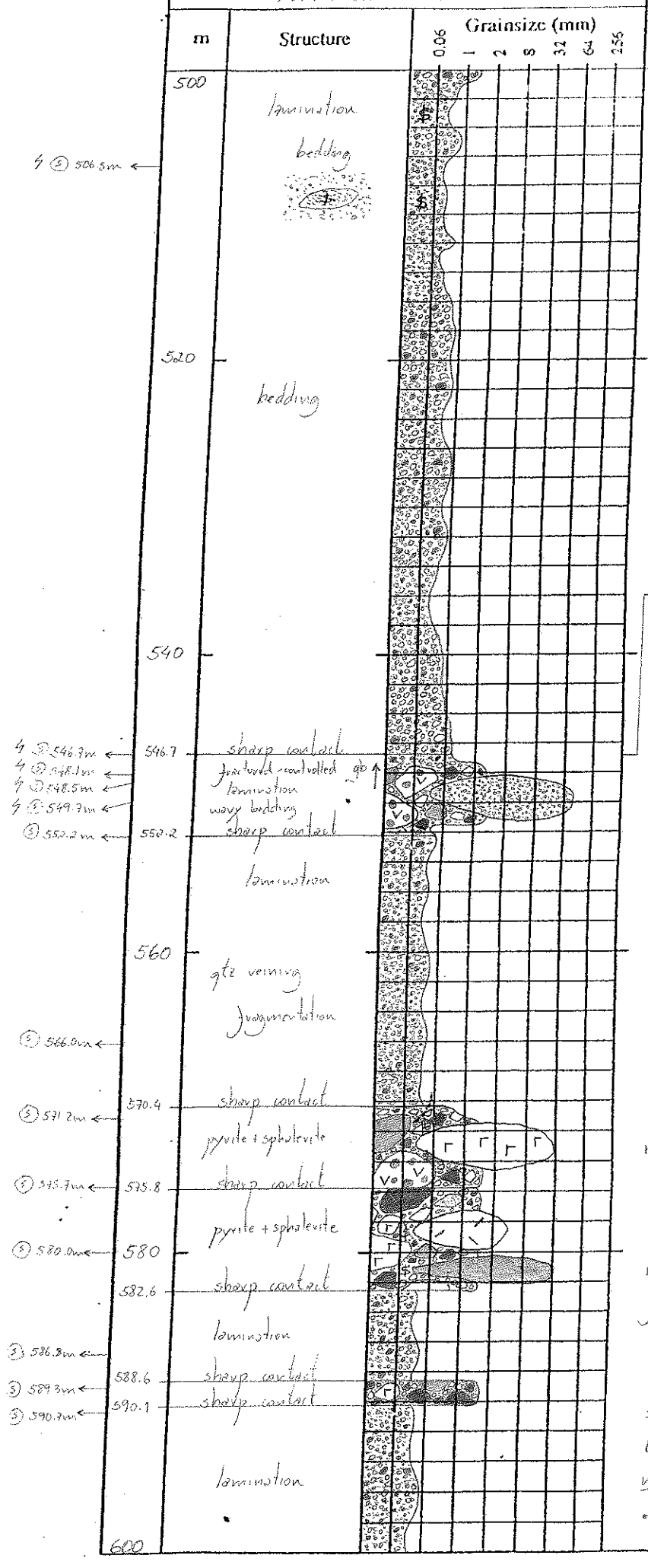

→ 454.7 - 546.7 : Black Harry Beds

Interbedded, weakly sericitic, locally pyritic and micaceous, heterogeneous, well to moderately-sorted, fine to coarse-grained, massive to weakly-bedded and locally graded and laminated, shard and lithic-bearing, grey to brownish green volcaniclastic sandstone siltstone, and weakly pyritic, massive to laminated, homogeneous, dark grey to black mudstone.

- trace sulfides
- pyrite blobs up to 2cm across

546.7m

↦ 546.7 - 552.2 ; 570.4 - 575.8 ; 575.8 - 582.6 ; 588.6 - 590.1 : Interbedded, weakly to moderately sericitic/chloritic and silicified, locally graded and micaceous, moderately to poorly-sorted, laminated volcaniclastic siltstone, fine to very coarse-grained, feldspar-quartz crystal-rich, volcaniclastic lithic sandstone, and polymictic volcaniclastic breccia.

- mudstone clasts up to 6cm across
- sandstone/siltstone clasts up to 7cm across
- rhyolite/dacite clasts.
- amygdaloidal (chloritized) andesite/basalt clasts.
- lithic clasts.

↦ 552.2 - 570.4 ; 582.6 - 588.6 ; 590.1 - 603.5 : Black Harry Beds

Interbedded, weakly sericitic, locally pyritic and micaceous, heterogeneous, well to moderately-sorted, fine to coarse-grained, massive to weakly-bedded and locally-graded and laminated, shard and lithic-bearing, grey to brownish green volcaniclastic sandstone, siltstone, and weakly pyritic, massive to laminated, homogeneous, dark grey to black mudstone.

- trace sulfides

LOG BOC-2 Boco Alteration Zone
Location: Tulsh core shed

Date: 16/MAR/2011
Logged by: Pedro Fonseca

m | Structure | Grainsize (mm): 0.06 — 1 — 2 — 8 — 32 — 64 — 256 | Description

600 — mirror fault 600.6m

603.5 — mingled contact

brecciation

(S) 612.5m

617.4 — sharp contact

(S) 617.7m

620

624.1 — sharp contact

lamination

(S) 626.5m

635.0 — sharp? fragmented contact

640

(S) 641.0m

643.4 — sharp contact

(S) 644.8m

646.6 — mingled brecciated contact

(S) 648.5m

653.0 — mingled fragmented contact

658.2 — sharp fragmented contact

660

weak foliation

(S) 667.1m

667.2 — E.O.H.

→ 590.1 - 603.5: Black Hawy Beds

details on previous page.

603.5m

↦ 603.5 - 617.4: Weakly sericitic/chloritic, poorly-sorted, clast-supported, feldspar-phyric, monomictic dacite breccia and amygdaloidal massive feldspar-phyric dacite.

- feldspar phenocrysts: 5-10%, 1-4mm, rectangular, creamy
- quartz blebs/amygdules: up to 3%, up to 1cm, elongated.

617.4m

↦ 617.4 - 624.1: Weakly sericitic/chloritic, sphaleritic, poorly-sorted, clast-supported, feldspar-phyric, polymictic volcaniclastic dacite breccia.

- dacite clasts up to 10cm.

624.1m

↦ 624.1 - 635.0: Black Hawy Beds

Interbedded, weakly sericitic, locally pyritic and micaceous, heterogeneous, well to moderately-sorted, fine to coarse-grained, massive to weakly-bedded and locally graded, laminated, shaved and lithic-bearing, grey to brownish green volcaniclastic sandstone, siltstone, and weakly pyritic, massive to laminated, homogeneous, dark grey to black mudstone.

- trace sulfides

635.0m

↦ 635.0 - 643.4: Weakly sericitic/chloritic, moderately to poorly-sorted, coarse to very-coarse-grained feldspar crystal-rich volcaniclastic lithic sandstone and polymictic volcaniclastic dacite breccia.

- feldspar: 10-15%, ~2mm, creamy, irregular
- lithics: 1-2%, up to 1cm, chloritized

643.4m

↦ 643.4 - 646.6: Weakly sericitic, poorly-sorted and clast-supported, monomictic dacite breccia.

- feldspar phenocrysts: 2-3%, 2-3mm, irregular.

646.6m

↦ 646.6 - 653.0: Weakly sericitic, moderately-sorted, feldspar crystal-rich coarse-grained dacite sandstone and monomictic dacite breccia.

653.0m

↦ 653.0 - 658.2: Weakly sericitic, poorly-sorted and clast-supported, fractured, feldspar-phyric monomictic dacite breccia:

- feldspar phenocrysts: 2-3%, 2-3mm, irregular

658.2m

↦ 658.2 - 667.2: Weakly to moderately sericitic, fractured, feldspar-phyric massive dacite.

- feldspar: 5-10%, 2-3mm, creamy, irregular

LOG BOC-4 (BOCO) - BURNS PEAK
Location: Tullah core shed

Date: 23/FEB/2011
Logged by: PEDRO FONSECA

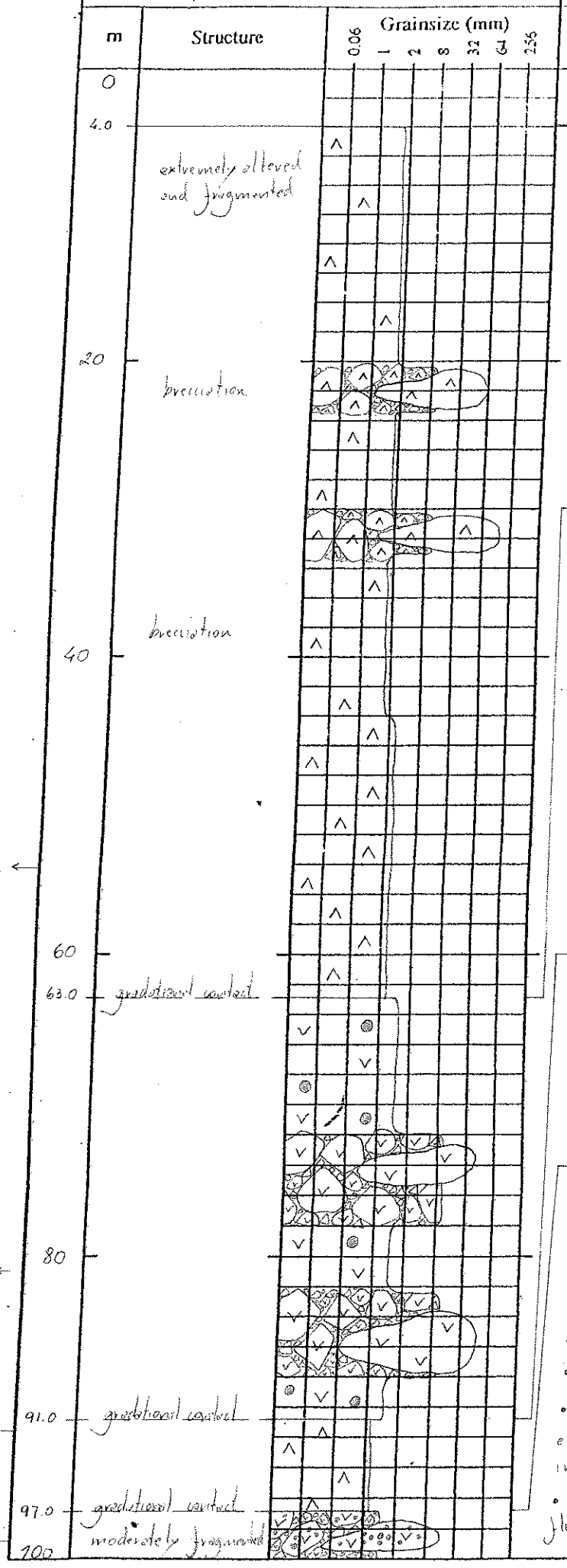

Description

↦ 0 - 4.0 : No hole ...

4.0m

↦ 4.0 - 63.0 : Weakly sericitic, locally vesicular, feldspar - pyroxene? - hornblende? - phyric, massive andesite and poorly-sorted, clast-supported, feldspar - pyroxene? - hornblende? - phyric, monomictic andesite breccia.

- feldspar : 5-10%; 1-3mm; ovoid; greenish, weakly sericitized downhole; content and grainsize seems to increase at ~ 44.0m; irregular, tabular
- pyroxene? hornblende? : < 1-3%, ~ 1mm (up to 5mm); dark green, altered; tabular.

63.0m

↦ 63.0 - 91.0 : Weakly to moderately sericitic and chloritic, amygdaloidal, feldspar - phyric, massive, green basalt and weakly sericitic and chloritic, poorly-sorted, clast-supported, feldspar - phyric, monomictic basalt breccia.

- feldspar : 5%; 2-4mm; tabular, rectangular; green - sericitized
- amygdules : < 10%; 1-2mm; round; dark green and chloritized or 2-3%; < 3-4cm, white, creamy; carbonate + quartz - filled.

- < 1% pyrite spots

91.0m

↦ 91.0 - 97.0 : Weakly sericitic, weakly amygdaloidal, feldspar - phyric, massive andesite.

- feldspar : 10%; 2-3mm; rectangular, creamy, pink.

97.0m

↦ 97.0 - 171.3 : Weakly to moderately chloritic, poorly-sorted, clast-supported to locally matrix-supported, locally massive, strongly amygdaloidal, weakly feldspar - phyric, monomictic basalt breccia.

- feldspar : 1-2%; 1-2mm, rectangular; green - sericitized
- amygdules : < 20%, < 4mm, dark green; round and elongated; chloritized or quartz-carbonate - filled; mainly inside basalt clasts
- basalt clasts : < 15cm; strongly amygdaloidal, some flow-banded; weakly feldspar - phyric, aphyric or fine-grained

LOG BOC-4 (BAO) - BURNS PEAK
Location: Tullish core shed

Date: 23/FEB/2011
Logged by: PEDRO FONSECA

m	Structure	Grainsize (mm) 0.06 – 1 – 2 – 8 – 32 – 64 – 256	Description

100

(S) 104.2m

sheaving

(S) 109.5m

(S) 113.0m

(S) 119.0m

120

strongly amygdaloidal

140

amygdale size grading

160

171.3 sharp contact

(S) 174.3m

(S) 179.0m

178.9 sharp contact

180 sharp contact

180.3

(S) 183.2m

(S) 186.5m

186.3 sharp contact

(S) 189.9m

188.8 sharp contact

amygdales

pevlite

moderately fragmented and fractured.

(S) 194.0m

200

↦ 97.0 - 171.3: Weakly to moderately chloritic, poorly-sorted, clast-supported to locally matrix-supported, locally massive, strongly amygdaloidal, weakly feldspar-phyric, monomictic basalt breccia.

- feldspar: 1-2%; 1-2 mm; rectangular; green; sericitized
- amygdales: <20%; <4mm; dark green; round and elongated; chloritized or quartz-carbonate-filled, mainly inside basalt clasts.
- basalt clasts: <15cm; strongly amygdaloidal, some flow-banded; weakly feldspar-phyric, aphyric or fine-grained.

171.3m

↦ 171.3 - 178.9: Weakly to moderately chloritic, poorly-sorted, clast-supported, weakly feldspar-phyric to aphyric, strongly amygdaloidal, monomictic basalt breccia.

- amygdales: 5%; <2cm; elongated, chloritic or quartz + carbonate-filled.

178.9m

↦ 178.9 - 180.3: Weakly to moderately chloritic, poorly-sorted, clast-supported, fine to coarse-grained, polymictic volcanic basalt breccia.

- basalt clasts: aphyric, amygdaloidal, main part of breccia
- lithics: 1-2%; <0.5cm; round; pink

180.3m

↦ 180.3 - 186.3: Moderately chloritic, aphyric to weakly feldspar-phyric; strongly amygdaloidal, massive, green basalt.

- amygdales: 10%; <4mm; elongated; chloritic.

186.3m

↦ 186.3 - 188.8: Moderately chloritic, lithic-bearing, poorly-sorted, matrix-supported, polymictic volcanic andesite breccia and sandstone.

- lithics: 2-3%; <4-5cm; pink, creamy
- matrix is andesitic.

188.8m

↦ 188.8 - 224.0: Weakly to moderately sericitic and chloritic, locally perlitic, amygdaloidal, poorly-sorted, clast-supported, feldspar-phyric, monomictic andesite breccia and weakly to moderately chloritic, very weakly feldspar-phyric to aphyric, amygdaloidal, massive green andesite.

- breccia feldspar phenocrysts: 2-3%; 1-2mm; creamy
- andesite feldspar phenocrysts: <1%; 1-2mm; tabular, light green; sericitized
- amygdales: 1-2%; <8mm; elongated, round; dark green; chloritized
- <1% sulfides

LOG BOC-4 (BOCO) - BURNS PEAK
Location: Tullah core shed

Date: 23/FEB/2011
Logged by: PEDRO FONSECA

m	Structure	Grainsize (mm) 0.06 — 2 8 32 64 256	Description
200	fragmented		↦ 188.8 - 224.0: Weakly to moderately sericitic and chloritic, locally perlitic, amygdaloidal, poorly-sorted, clast-supported, feldspar-phyric, monomictic andesite breccia and weakly to moderately chloritic, very weakly feldspar-phyric to aphyric, amygdaloidal, massive, green andesite. • feldspar phenocrysts: > breccia: 2-3%; 1-2mm; creamy > andesite: <1%; 1-2mm; tabular, light green; sericitised • amygdules: 1-2%; <8mm; elongated, round; dark green; chloritised – <1% sulfides.
220			224.0m
224.0	gradational contact		↦ 224.0 - 237.5: Weakly to moderately chloritic, very weakly amygdaloidal, weakly feldspar-phyric, massive green andesite. • feldspar: 2-3%; 1-3mm, tabular, rectangular; pale cream and light green; sericitised • amygdules: <1%; 1-2mm; round, green; chloritic.
237.5	gradational contact fractured		237.5m ↦ 237.5 - 277.2: Weakly to moderately sericitic and chloritic, poorly-sorted, clast-supported, strongly amygdaloidal; weakly feldspar-phyric, green, monomictic andesite breccia and massive andesite. • feldspar: 1% (1-3% locally); 1-3mm; tabular, rectangular; white, creamy (some green and sericitised) • amygdules: <5% (up to 25% locally), both in massive andesite and andesite clasts; 1-3mm (green, elongated and strongly chloritised) or <2cm (carbonate + quartz-filled, round to elongated).
240			
	strongly amygdaloidal		
260			277.2m ↦ 277.2 - 278.6: Weakly sericitic to moderately hematitic, graded, moderately-sorted, matrix-supported, lithic-rich and feldspar-bearing, polymictic volcanic breccia, sandstone and siltstone. • feldspar: 10%; 2-4mm; red, rectangular – some lithics are feldspar-phyric
	andesite clasts with amygdule size gradient		278.6m ↦ 278.6 - 284.0: Weakly to moderately sericitic and chloritic, poorly-sorted, clast-supported, moderately amygdaloidal, very weakly feldspar-phyric, green monomictic andesite breccia and massive andesite. – <1% pyrite
277.2	sharp contact		
278.6	sharp contact		284.0m ↦ 284.0 - 287.4: Interbedded, moderately pyritic and weakly micaceous, homogeneous, well-sorted, fine to medium grained, quartz-feldspar-lithic-bearing siltstone and sandstone and minor local breccia.
280			
284.0	undulated contact brecciated		Animal Creek Greywacke?
287.4	faulted brecciated contact	— — — F	287.4m ↦ 287.4 - 360.0: Weakly to moderately sericitic/altered, feldspar-quartz-phyric, massive rhyolite and local, altered, monomictic rhyolite breccia.
300			details on next page..

(5) 223.3m ←
(4) (3) 258.0m ←
(4) (2) 278.4m ←
(4) (3) 284.2m ←
(5) 286.0m ←
(3) 296.2m ←

LOG BOC-4 (BOCO) - BURNS PEAK
Location: Tullok core shed

Date: 23/FEB/2011
Logged by: PEDRO FONSECA

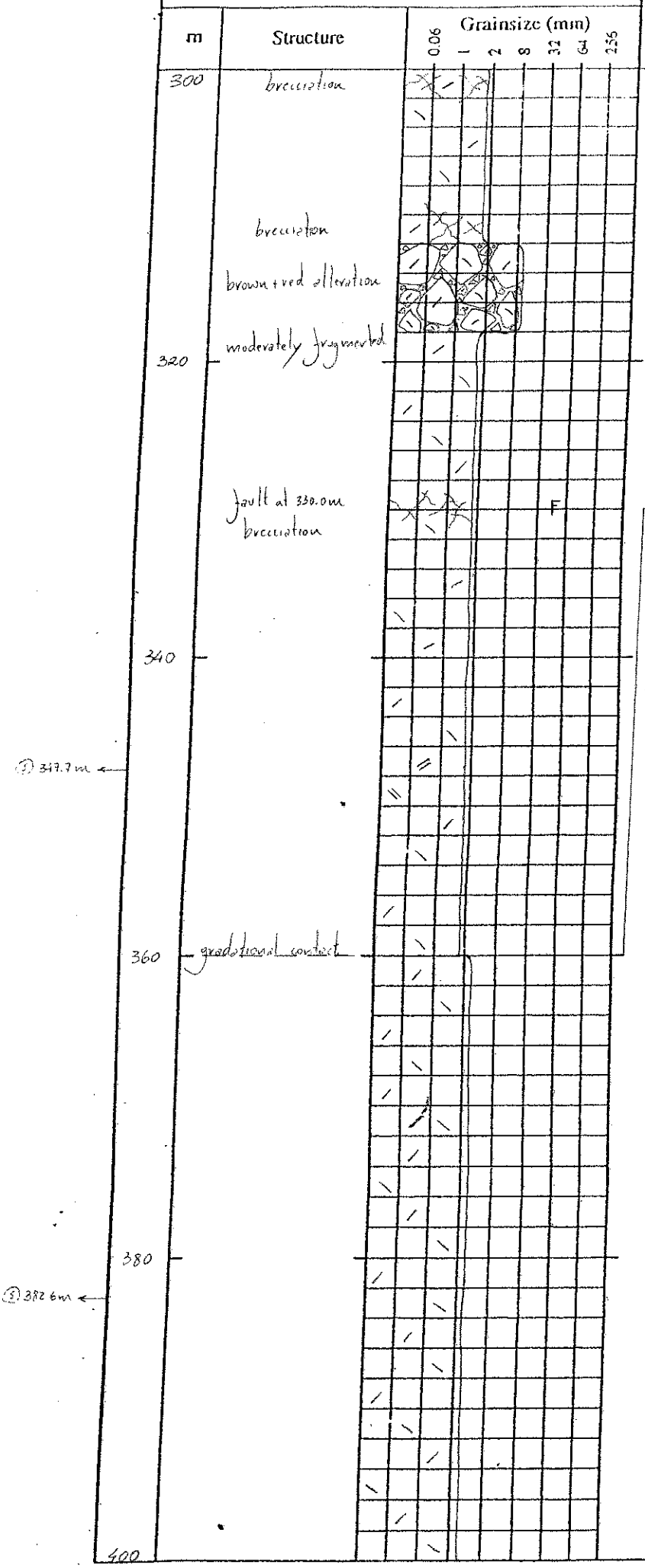

Description

↦ 287.4 - 360.0: Weakly to moderately sericitic / altered, feldspar-quartz-phyric, massive rhyolite and local, altered, monomictic rhyolite breccia.

- feldspar: 3-5%; 1-4mm; tabular; light pink to brown; strongly altered
- quartz: < 1%; 1-3mm; round; inolor

– < 1% sulfides

> yellowish / greenish colour

+ 10-15% feldspar phenocrysts at ~ 348.0m.

360.0m

↦ 360.0 - 436.8: Weakly altered (hematitic, sericitic), feldspar-quartz-phyric, massive brownish, reddish and greenish rhyolite.

- feldspar: 5%; 1-5mm; tabular, irregular; light pink
- quartz?: 1%; 1-3mm; round, inolor

– < 1% sulfides.

> 360.0 - 436.8 rhyolite is feldspar-phyric-richer than 287.4 - 360.0 rhyolite.

LOG BOC-4 (BOO) - BURNS PEAK
Location: Tullah core shed

Date: 23/FEB/2011
Logged by: PEDRO FONSECA

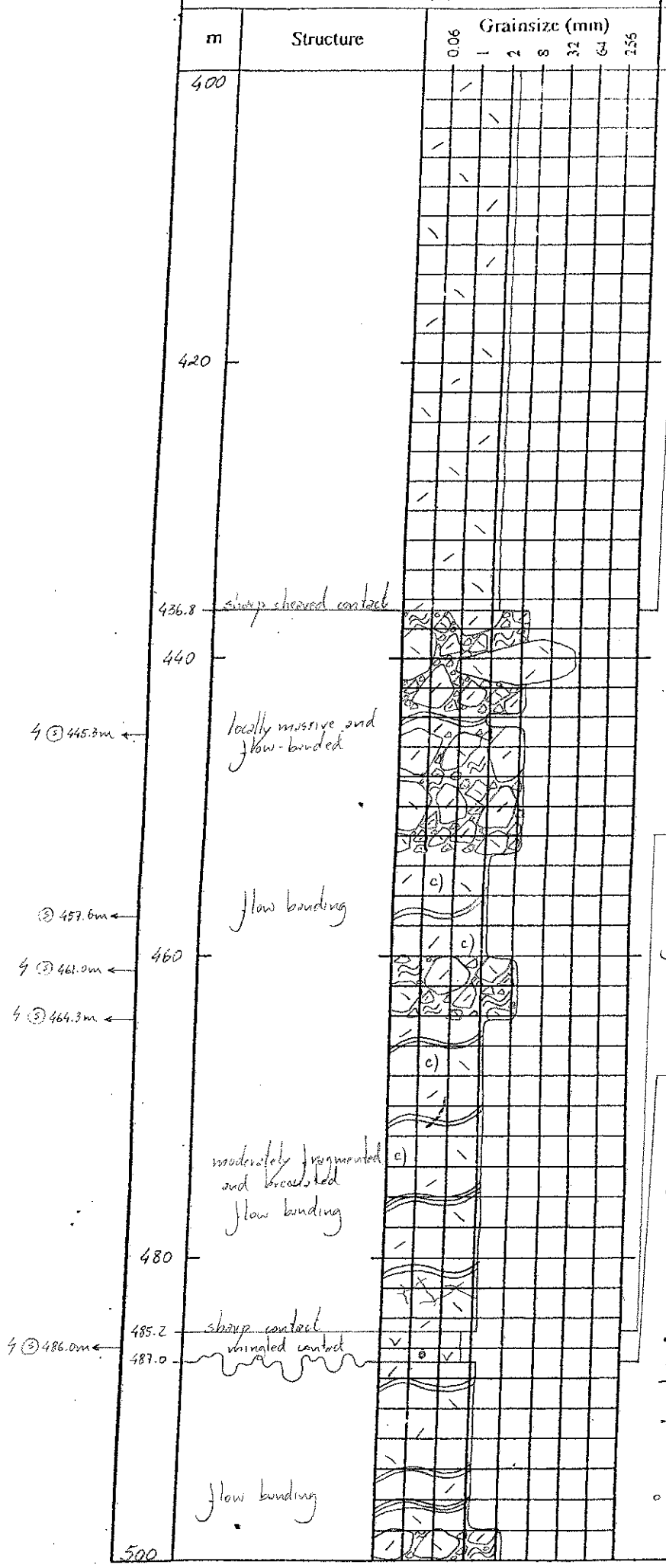

↦ 360.0 - 436.8 : Weakly altered (hematitic and sericitic), feldspar-quartz-phyric, massive, brownish reddish and greenish rhyolite.

- feldspar: 5%; 1-5mm; tabular; irregular; light pink
- quartz? 1%; 1-3mm; round; inolor
- < 1% sulfides

436.8m

↦ 436.8 - 485.2 : Weakly to moderately sericitic and chloritic, poorly-sorted, clast-supported, feldspar-phyric, pumiceous monomictic rhyolite breccia, rhyolite breccia and flow-banded, weakly perlitic, massive rhyolite.

- feldspar: < 5%; 1-4mm; tabular; altered
- quartz?: < 1%; 1-2mm; round; inolor
- rhyolite clasts up to 5cm long; irregular
- pumice up to 3cm long, wispy
- o perlites are visible on rhyolite clasts in brecciated zones and together with flow-banded rhyolite
- o visible perlite at ~ 445.5 m.

485.2m

↦ 485.2 - 487.0 : Weakly to moderately sericitic and chloritic, fine-grained, weakly amygdaloidal, feldspar-phyric, massive, dark green basalt

- feldspar: < 5%; 1-2mm; rectangular
- amygdales: 1-2%; 1-2mm; round; chloritic

487.0m

↦ 487.0 - 545.7 : Weakly to moderately sericitic and chloritic, poorly-sorted, clast-supported, feldspar-phyric, pumiceous monomictic rhyolite breccia, and flow-banded, weakly perlitic?, massive rhyolite.

- feldspar: < 5%; 1-4mm; tabular; altered
- quartz?: < 1%; 1-2mm; round; inolor
- rhyolite clasts up to 5cm long; irregular
- pumice up to 3cm long; wispy, some are feldspar-phyric
- o pumice breccia zones may contain glass shards?

LOG BOC-4 (BOC4) - BURNS PEAK
Location: Tuttoh core shed

Date: 23/FEB/2011
Logged by: PETRA FAYRAM

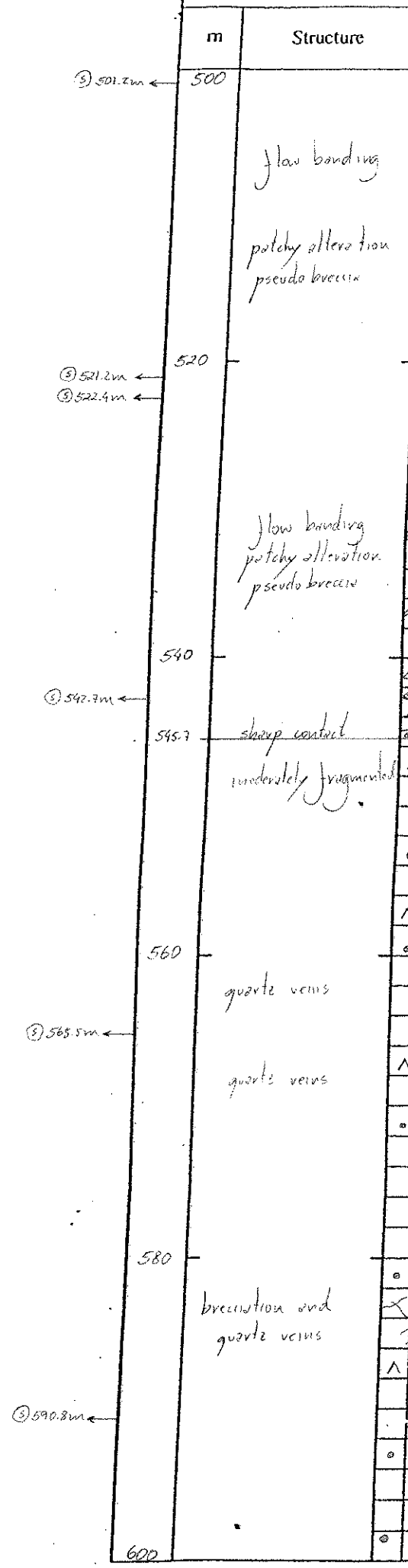

↦ 487.0 - 545.7: Weakly to moderately sericitic and chloritic, poorly-sorted and clast-supported, feldspar-phyric, pumiceous monomictic rhyolite breccia and flow-banded weakly perlitic?, massive rhyolite.

- feldspar: <5%; 1-4mm; tabular, altered
- quartz: <1%; 1-2mm; round, inwater
- rhyolite clasts up to 5cm long; irregular
- pumice up to 3cm long; wispy; some are feldspar-phyric
- pumice breccia zones may contain glass shards?

545.7m

↦ 545.7 - 603.7: Weakly to moderately chloritic and sericitic, weakly amygdaloidal, weakly feldspar-phyric, fine-grained, massive green andesite.

- feldspar: 1-2%; 1-2mm; tabular, rectangular white and creamy and light green, sericitized.
- amygdules: 0-3%; ~2mm; round and elongated; dark green (chloritic); some <2cm and carbonate + quartz filled

LOG BOC-4 (BOCO) - BURNS PEAK
Location: Tullish core shed

Date: 23/FEB/2011
Logged by: PEDRO FONSECA

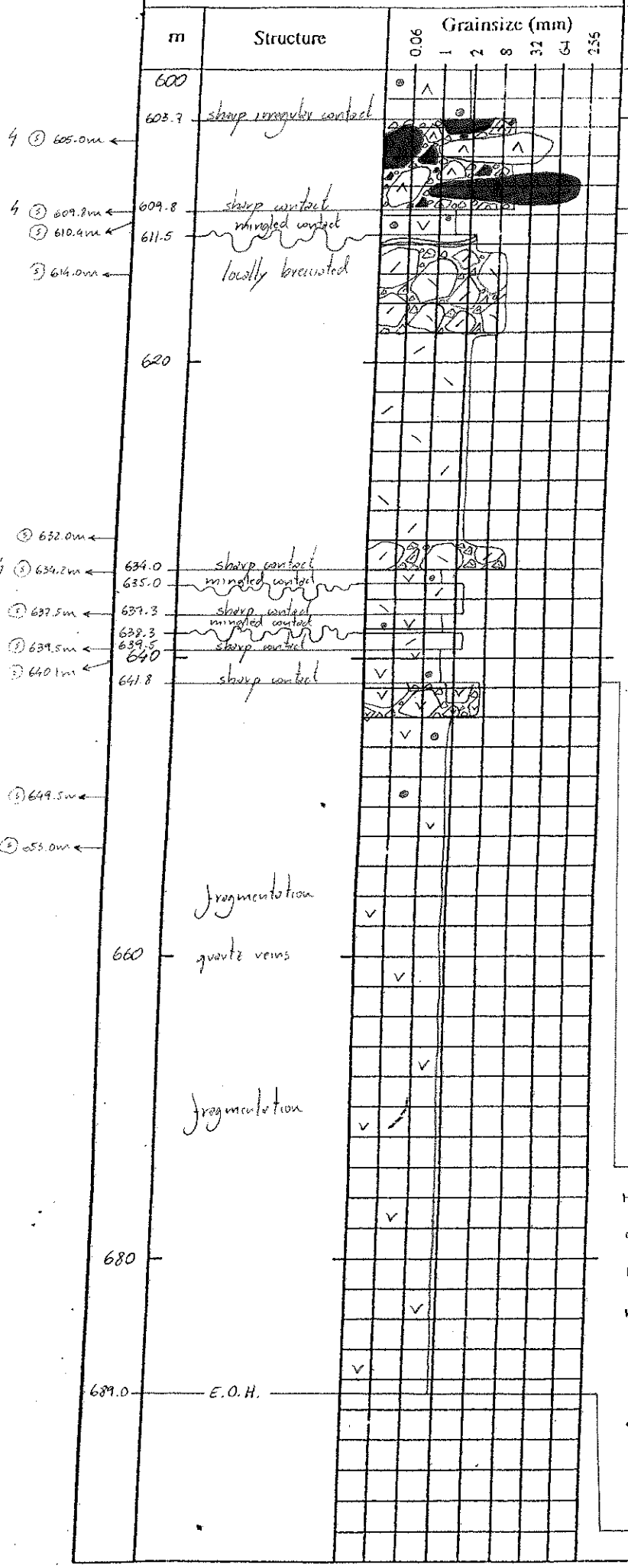

↦ 545.7 - 603.7: Weakly to moderately chloritic and sericitic, weakly amygdaloidal, weakly feldspar-phyric, fine-grained, massive green andesite.

details on previous page...

603.7m

↦ 603.7 - 609.8: Weakly sericitic and chloritic, poorly-sorted, clast-supported, feldspar-phyric, lithic-rich, polymictic volcanic andesite breccia

- andesite clasts: 90%; <5cm
- lithics: reddish in colour (possibly rhyolitic)

609.8m

↦ 609.8 - 611.5: Weakly to moderately chloritic, fine-grained, amygdaloidal, feldspar-phyric, dark green, massive basalt.

- feldspar: 2%; 1-2mm; rectangular; light green
- amygdales: 2-3%; 1-2mm; round; chloritic.

611.5m

↦ 611.5 - 634.0 + 635.0 - 637.3 + 638.3 - 639.5: Weakly altered (hematitic), feldspar-phyric, reddish, massive rhyolite, and poorly-sorted, clast-supported, reddish, monomictic rhyolite breccia.

- feldspar: 5%; 2-3mm; pink; rectangular
- quartz ?: 1%; 2mm; round
- devitrification textures in rhyolite at ~ 639.0m.

↦ 634.0 - 635.0 + 637.3 - 638.3 + 639.5 - 641.8: Weakly sericitic and chloritic, fine-grained, weakly amygdaloidal, feldspar-phyric, massive to locally brecciated, green basalt.

- feldspar: 2-3%; 1-2mm; rectangular; orange
- amygdales: 1%; 1-2mm; round; elongated; dark green

641.8m

↦ 641.8 - 689.0: Weakly to moderately sericitic and chloritic, fine-grained, weakly amygdaloidal, weakly feldspar-phyric to aphyric, dark green, massive basalt

- feldspar: 1-2% (locally); 1-2mm; rectangular; creamy.
- amygdales: 0-1% (rare); 1-2mm; round; dark green, chloritic; some < 1-2cm and carbonate + quartz-filled.

689.0m

LOG BPD-80 (BURNS PEAK DRILL HOLE)
Location: MRT core store

Date: 17/JAN/2011
Logged by: PEDRO FONSECA

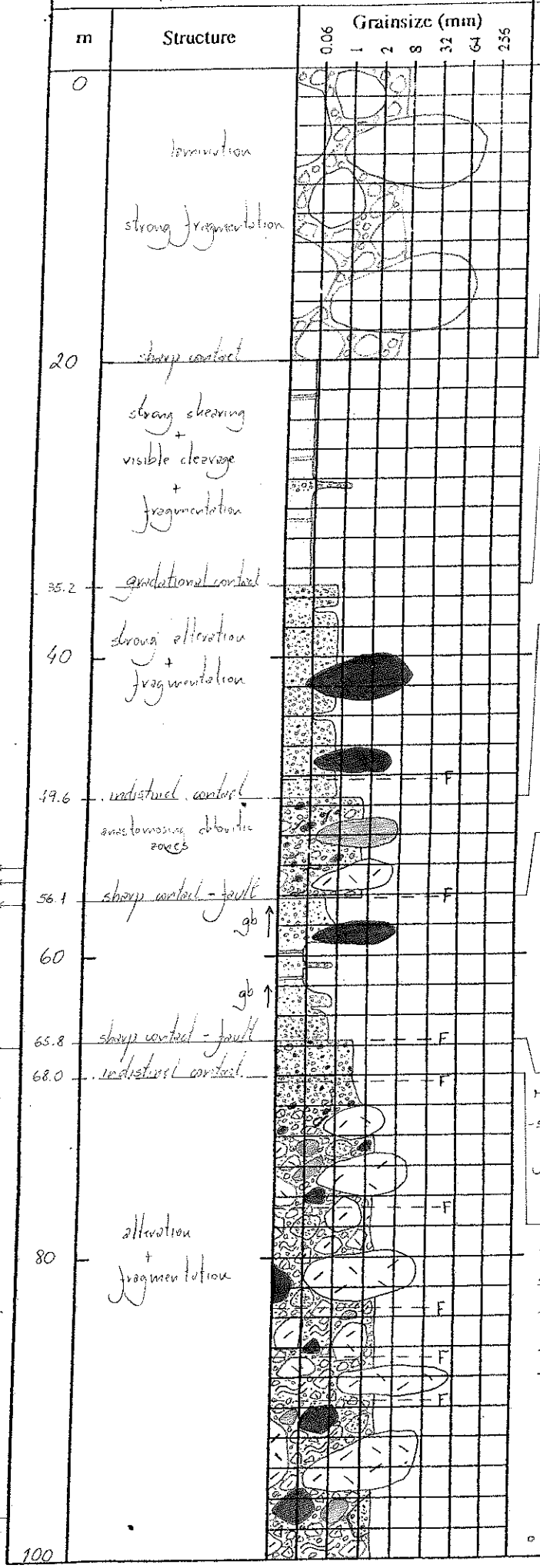

↦ 0 - 20.0: Fluvio-glacial deposits. Moderately to strongly altered, very poorly-sorted, matrix-supported, polymictic, quartz-rich, locally laminated, creamy orange breccia.

20.0m

↦ 20.0 - 35.2: Weakly altered, strongly sheared and cleaved, homogeneous, finely laminated, massive, black to dark grey mudstone and minor polymictic sandstone.

- sandstone beds < 20cm thick.

35.2m

↦ 35.2 - 49.6: Interbedded strongly altered, moderately- to locally poorly-sorted, matrix-supported, medium to coarse-grained, feldspar crystal-rich, greyish polymictic sandstone and laminated, grey to black mudstone.

- rare lithic clasts < 2cm.
- fault at ~ 48.3m

49.6m

↦ 49.6 - 56.1: Moderately to strongly sericitic and altered, moderately-sorted, matrix-supported, medium to very coarse-grained, lithic-bearing, feldspar crystal-rich polymictic volcanic sandstone and breccia.

- mudstone, lithic and rhyolite clasts < 2cm.
- fault at lower contact ~ 56.1m.

56.1m

↦ 56.1 - 65.8: Interbedded and graded-bedded, moderately to strongly altered, well-sorted, feldspar crystal-rich polymictic volcanic sandstone, laminated and massive siltstone, and black to dark grey mudstone

- rare (<1%) lithic clasts in sandstone:
  - < 1cm; round; grey
- fault at lower contact ~ 65.8m

65.8m

↦ 65.8 - 68.0: Moderately sericitic and strongly altered, well-sorted, clast-supported, medium to very coarse-grained, feldspar crystal-rich dark green polymictic volcanic sandstone

- feldspar crystals < 2-3mm

68.0m

→ 68.0 - 103.0: Weakly to strongly sericitic, locally silicified, poorly-sorted, matrix-supported, feldspar crystal-rich, pumiceous, lithic-bearing, greyish green polymictic rhyolitic breccia and sandstone.

- clast population:
  - rhyolite: 10-15%; < 6cm; irregular; feldspar-quartz-phyric
  - lithics: < 10%; < 1-2cm, pale pink; some pumiceous
  - mudstone: < 5%; < 1cm; long; black; massive or laminated
  - sandstone/siltstone: < 5%; < 2cm, massive or laminated
  - pumice: ~ 5%; < 1cm; wispy
- matrix: 80%; feldspar crystal-rich

LOG BPD-80 (BURNS PEAK DRILL HOLE)
Location: MRT core store

Date: 17/JAN/2019
Logged by: PEDRO FONSECA

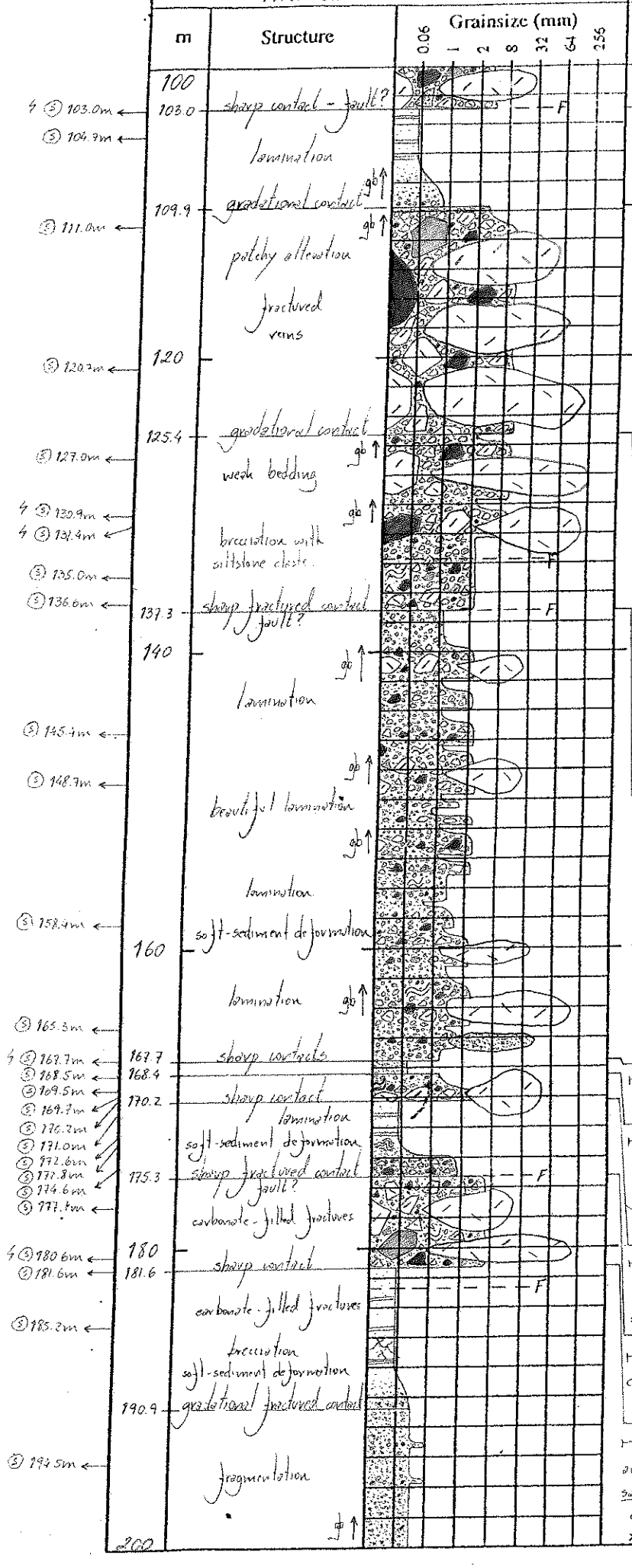

LOG BPD-80 (BURNS PEAK DRILL HOLE)
Location: MRT core store

Date: 17/JAN/2011
Logged by: PEDRO FONSECA

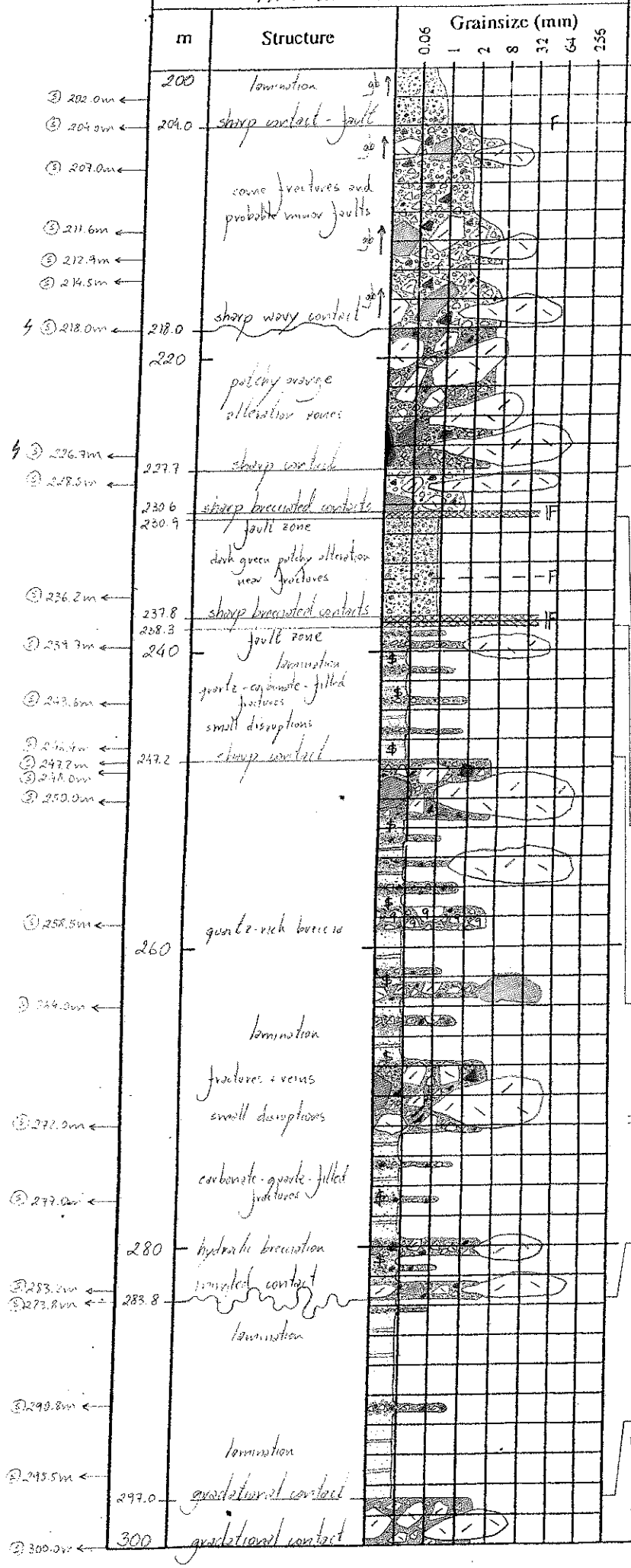

↦ 181.6 - 204.0: Details on previous page...
o fault at lower contact ~ 204.0m.
204.0m

↦ 204.0 - 218.0: Weakly to moderately sericitic, graded, poorly- to moderately-sorted, clast-supported, polymictic rhyolite breccia and sandstone.
• rhyolite clasts: ~5%; < 3cm > leucoxene
• mudstone clasts: < 5%; < 1cm; in sandstone + breccia
o quartz - 15-20%; 3-4mm, round
o feldspar: 25-30%; 2-3mm; tabular
218.0m

↦ 218.0 - 227.7: Weakly to moderately sericitic and chloritic, poorly- to moderately-sorted, dark green polymictic mud-matrix rhyolite breccia and minor sandstone
• rhyolite clasts: dark green, wispy; feldspar-quartz-phyric:
> quartz: 10-15%; 3-4mm, round, incolor
> feldspar: 20-25%; 2-3mm; tabular, white + pink
o sandstone with high % of quartz + feldspar
> mudstone + lithic clasts: < 5% (below ~ 224.9m)
+ local black mudstone zones ⇒ peperite?
227.7m

↦ 227.7 - 230.9: Weakly sericitic, moderately-sorted, clast-supported, interbedded polymictic-rhyolite breccia and quartz-feldspar-rich sandstone.
• quartz: 10-15%, < 5mm; round; incolor • leucoxene
• mudstone clasts: 2-3%; 1-3mm (< 2cm)
230.9m

↦ 230.9 - 238.3: Homogeneous, well-sorted, lithic-bearing and feldspar-quartz-leucoxene-rich, pale green polymictic rhyolite sandstone and siltstone.
238.3m

↦ 238.3 - 247.2: Interbedded, homogeneous to finely laminated pyritic, black mudstone and weakly sericitic, silicified, moderately to well-sorted, pyritic-rich polymictic rhyolite sandstone and siltstone
• 1cm to very thin beds of siltstone/mudstone
• local quartz-rich coarse and very coarse sandstone and breccia
247.2m

↦ 247.2 - 283.8: Interbedded, homogeneous to finely laminated pyrite-rich black mudstone, siltstone and sandstone, and weakly to moderately sericitic, poorly-sorted, mud- to sand-matrix-supported green to grey polymictic rhyolite breccia and well- to moderately-sorted polymictic rhyolite sandstone.
• black mudstone clasts in sandstone and breccia: < 3-4cm, < 5%
• beds of pyrite-rich mudstone, siltstone and sandstone are thin to medium
⇒ peperite?
283.8m

↦ 283.8 - 297.0: Homogeneous to finely laminated pyritic black mudstone and interbedded siltstone
• pyrite-rich beds near top contact and in fractures
• mud-matrix rhyolite sandstone bed at ~ 290.8m
• siltstone beds are thin to medium
⇒ Que River Shale
297.0m

↦ 297.0 - 300.0: Moderately sericite/chloritic, poorly-sorted, mud-matrix-supported, dark green, monomictic rhyolite breccia
⇒ peperite

LOG BPD-80 (BURNS PEAK DRILL HOLE)
Location: MRT core store

Date: 17/JAN/2011
Logged by: PEDRO FONSECA

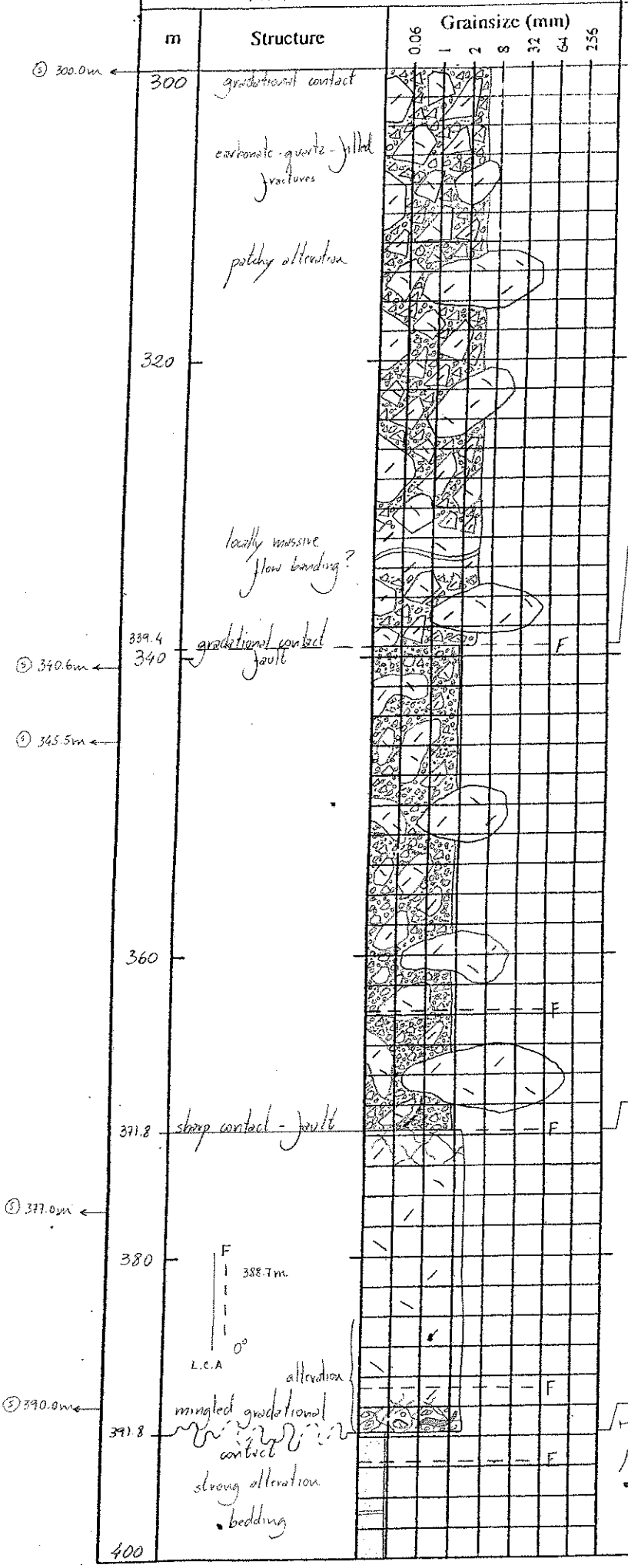

↦ 300.0 - 339.4: Weakly to moderately sericitic and chloritic, and strongly silicified, poorly-sorted, clast-supported monomictic rhyolite breccia with local very coarse-grained, quartz-feldspar-bearing monomictic rhyolite sandstone matrix and local massive quartz-feldspar-phyric rhyolite.

- patchy alteration texture + leucoxene
- ○ rhyolite clasts are more abundant and larger than the ones found in the unit below.
- > fault at lower contact @ 339.4m.

339.4m

↦ 339.4 - 371.8: Weakly to moderately sericitic and chloritic, and strongly silicified, poorly-sorted, clast-supported, monomictic rhyolite breccia with local very coarse-grained, quartz-feldspar-bearing monomictic rhyolite sandstone matrix.

- rhyolite clasts: 20-25%; >10cm; wavy, irregular; greyish green; feldspar-quartz-phyric
- ○ sandstone matrix:
  - > quartz: 10-15%; <6mm (average 3mm); round, incolor
  - > feldspar: 20-25%; <5mm (average 2mm); tabular; altered
- + patchy alteration pattern
- + wispy, fiamme-like structures (maybe glassy or vesicular in origin).
- ○ fault at ~ 363.8m

371.8m

↦ 371.8 - 391.8: Weakly sericitic to locally moderately altered, feldspar-quartz-phyric, massive to locally brecciated greenish grey rhyolite.

- phenocryst population:
  - > quartz: 10%; 1-8mm (average 3-4mm); round; incolor
  - > feldspar: 5%; 1-6mm (average 2-3mm); tabular; white
- ○ fault at ~ 388.7m
- + quartz + carbonate veins + leucoxene near lower contact

391.8m

↦ 391.8 - 427.4: Homogeneous, finely laminated, pyritic black mudstone and interbedded siltstone.

- very thin siltstone beds.

⇒ Que River Shale

LOG BPD-80 (BURNS PEAK DRILL HOLE)
Location: MRT core store

Date: 17/JAN/2011
Logged by: PEDRO FONSECA

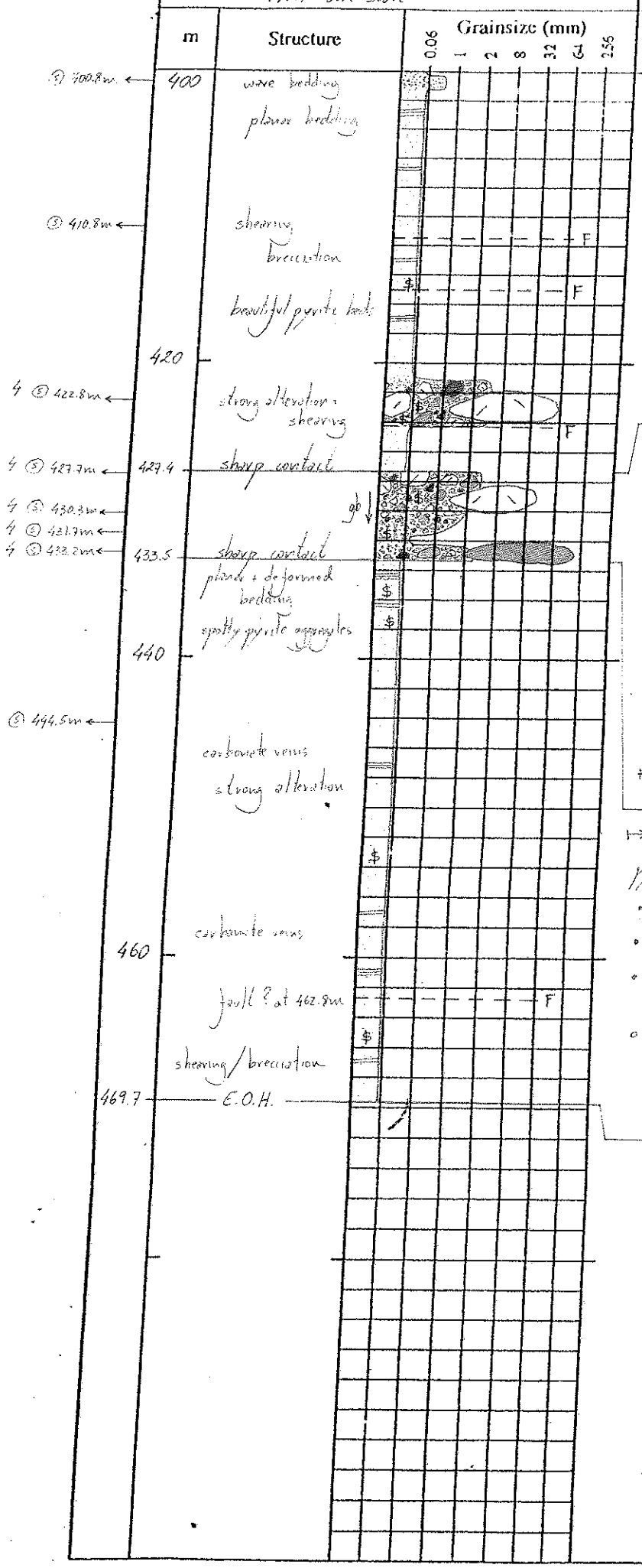

Description

↦ 391.8 - 427.4: Homogeneous, finely laminated, pyritic black mudstone and interbedded siltstone.
- very thin siltstone beds

⇒ Que River Shale

↦ 421.0 - 424.2: Weakly altered, pyritic, moderately sorted, clast-supported polymictic rhyolite breccia and very coarse sandstone.
- 10cm-thick porphyritic ? rhyolite bed or sandstone at ~ 410.7m
- faults at ~ 411.4m, 415.0m, 424.2m.

427.4m

↦ 427.4 - 433.5: Heterogeneous, weakly altered, pyritic, graded, moderately-sorted, clast-supported, dark grey to greyish green polymictic rhyolite breccia and sandstone

- clast population in breccia:
  - rhyolite: 10-20%; < 6cm; feldspar-rich; porphyritic
  - mudstone: 10-80% (max. 432.0m); < 18cm; black; homogeneous
  - feldspar + quartz + pyrite: < 1cm

> sandstone is rhyolite- and feldspar-rich

+ porphyritic felsic clasts at ~ 431.0m

433.5m

↦ 435.5 - 469.7: Homogeneous, finely laminated, pyritic black mudstone and interbedded siltstone.
- very thin siltstone beds
- carbonate-filled fractures
- pyrite: very thin interbeds; spots; veins; patches ~ 5%
- bedding variation: commonly 65° to core axis, but also 45° and 90°.

⇒ Que River Shale

469.7m

APPENDIX B

Geological mapping (Boco Road section)

In this study, an approximately 2-km-long road section of Boco Road located east of Burns Peak and west of the Boco Alteration Zone was mapped at 1:5 000 scale. The topographic map was published by the Mineral Resources Tasmania and made available by the Minerals and Metals Group (MMG) at Rosebery.

Boco Creek

380 000mE.

381 000mE.

5 385 000mN.

5 385 000mN.

475

450

425

425

450

475

Mudstone + siltstone

Lithic-bearing qtz+fds crystal-rich volcaniclastic sandstone

Mudstone + siltstone

Lithic-bearing qtz+fds crystal-rich volcaniclastic sandstone

Qtz+fds-phyric massive rhyolite

Mudstone + siltstone

Fds-phyric massive dacite

Fds-phyric massive dacite

Fds-phyric massive dacite + dacite breccia

Micaceous sandstone + siltstone

Fds-phyric massive dacite

Glacials

Mudstone + siltstone

Glacials

Mudstone + siltstone

Glacials

Lithic-bearing qtz+fds crystal-rich volcaniclastic sandstone

APPENDIX C

Boco Road lithologies and true thickness calculations

The data acquired from mapping of the approximately 2-km-long road section of Boco Road have been transposed onto a true-thickness log to allow direct correlations with the logs from the surrounding areas. The true thickness calculations of the lithologies mapped at Boco Road are presented in the table below considering that:

True thickness = Surface length x cos 60º

Stop	Lithology	Outcrop lenght (m)	Bedding strike (º)	Bedding dip (º)	Bedding dip direction (º)	Surface lenght (m)	True thickness (m)
1	Fds-phyric massive **Dacite**	40	-	-	-	35	**30.3**
2	Micaceous **Sandstone + Siltstone**	45	-	-	-	45	**39.0**
3	**Glacial cover**	100	-	-	-	70	**60.6**
4	Fds-phyric massive **Dacite + Dacite breccia**	150	-	-	-	115	**99.6**
5	Fds-phyric massive **Dacite**	155	-	-	-	95	**82.3**
6	Fds-phyric massive **Dacite**	180	-	-	-	105	**90.9**
7	Qtz+Fds-phyric massive **Rhyolite**	25	-	-	-	45	**39.0**
8	**Mudstone + Siltstone**	20	-	-	-	25	**21.7**
9	Lithic-bearing, qtz+fds crystal-rich volcaniclastic **Sandstone**	125	-	-	-	90	**77.9**
10	Lithic-bearing, qtz+fds crystal-rich volcaniclastic **Sandstone**	15	-	-	-	10	**8.7**
11	**Mudstone + Siltstone**	15	40	78	310	15	**13.0**
12	Lithic-bearing, qtz+fds crystal-rich volcaniclastic **Sandstone**	30	-	-	-	20	**17.3**
13	**Mudstone + Siltstone**	225	28	74	298	160	**138.6**
14	**Mudstone + Siltstone**	10	-	-	-	5	**4.3**
15	Lithic-bearing, qtz+fds crystal-rich volcaniclastic **Sandstone**	175	-	-	-	135	**116.9**
16	**Glacial cover**	40	-	-	-	30	**26.0**
17	**Mudstone + Siltstone**	60	52	66	322	35	**30.3**
18	**Glacial cover**	120	-	-	-	55	**47.6**
19	**Mudstone + Siltstone**	10	18	84	108	10	**8.7**
20	Lithic-bearing, qtz+fds crystal-rich volcaniclastic **Sandstone**	50	-	-	-	40	**34.6**

APPENDIX D
Analytical methods and data

This appendix presents the whole-rock analysis of 21 representative samples of the northern MRV. The major and trace elements were analysed by automated X-Ray Fluorescence (XRF) spectrometry and Induced Coupled Plasma Mass Spectrometry (ICP-MS) at the University of Tasmania. Analyses have been recalculated to 100% on an anhydrous basis to remove variations resulting from loss on ignition (L.O.I.) values.

The abbreviations used in the table below are:

Rpq = coherent quartz-poor rhyolite sub-facies; **Rqr** = coherent quartz-rich rhyolite sub-facies; **Rf** = coherent feldspar-phyric rhyolite facies; **Df** = coherent feldspar-phyric dacite facies; **Mfp** = coherent feldspar-pyroxene-phyric mafic facies; **PfS** = polymictic felsic sandstone facies; **Pol. sst.** = polymictic sandstone.

Sample	179333	179336	179337	179356	179359	179361	179376
Location	AK-1 (304.7 m)	BBP-209 (102.8 m)	BBP-209 (152.4 m)	BHD-7 (40.7 m)	BHD-7 (121.2 m)	BHD-7 (277.5 m)	BHD-9 (351.1 m)
Facies	*Mfp*	*Mfp*	*Rqp*	*Rqr*	*Df*	*Rf*	*Rf*
Rock type	Basalt	Basalt	Rhyolite	Rhyolite	Dacite	Rhyolite	Rhyolite
Major elements (wt. %)							
SiO_2	48.49	50.14	76.46	76.11	71.71	76.24	71.24
TiO_2	0.92	0.90	0.24	0.25	0.60	0.35	0.38
Al_2O_3	18.11	17.27	13.10	13.29	14.10	13.43	15.09
Fe_2O_3	13.19	12.08	2.43	2.07	4.54	1.49	2.18
MnO	0.45	0.15	0.06	0.05	0.18	0.03	0.05
MgO	6.18	6.31	0.50	0.58	1.68	0.64	0.66
CaO	9.67	10.50	0.19	0.20	1.73	0.41	1.60
Na_2O	1.89	1.53	3.81	5.40	3.29	4.17	4.18
K_2O	0.94	0.97	3.17	2.01	2.05	3.19	4.56
P_2O_5	0.16	0.15	0.04	0.04	0.12	0.06	0.06
Total	100.00	100.00	100.00	100.00	100.00	100.00	100.00
L.O.I.	5.01	2.70	1.05	0.83	2.90	1.79	2.07
Trace elements (ppm)							
As (ICP-MS)	3.6	16.0	<3	<2	<2	<2	<2
Ba	1341	514	1338	806	802	767	1322
Be (ICP-MS)	0.8	0.7	2.4	1.0	2.4	1.2	1.6
Bi (ICP-MS)	0.5	<2	<2	0.0	0.2	0.0	0.0
Ce (ICP-MS)	37.3	35.1	116.9	45.3	101.5	77.4	121.0
Co (ICP-MS)	50.9	44.9	32.9	22.8	13.8	27.5	19.3
Cr	9.1	7.1	<1	2	1.7	2.4	1.5
Cu (ICP-MS)	105.6	12.8	1.6	0.7	8.1	0.7	1.8
Dy (ICP-MS)	3.7	3.3	6.1	4.1	6.0	3.5	6.1
Er (ICP-MS)	2.1	1.9	3.7	3.0	3.6	2.5	3.7
Eu (ICP-MS)	1.2	1.2	1.2	0.8	1.8	0.9	1.9
Ga	17.4	17.3	10.3	11.8	13.9	10.5	14.4
Gd (ICP-MS)	4.1	3.7	6.5	3.2	6.8	3.5	6.8
Ho (ICP-MS)	0.7	0.7	1.3	0.9	1.2	0.8	1.2
La (ICP-MS)	18.4	17.4	56.3	22.8	50.6	39.0	61.4
Li (ICP-MS)	12.3	17.4	5.6	5.6	13.6	13.6	4.0
Lu (ICP-MS)	0.3	0.3	0.6	0.5	0.6	0.4	0.6
Mo (ICP-MS)	1.2	2.7	2.3	0.2	2.9	0.6	0.7
Ni	9.4	9.4	2.9	1.2	1.5	1.8	2
Nb	2.5	2.3	11.1	8.9	11.9	12.2	13.8
Nd (ICP-MS)	19.0	17.8	46.7	17.5	43.1	29.1	48.5
Pb (ICP-MS)	405.3	8.8	18.8	3.8	14.0	3.1	4.1
Pr (ICP-MS)	4.6	4.3	13.1	4.9	11.7	8.5	13.6
Rb	38.6	33.7	103	35.5	84.8	79.7	94.6
Sc	35.3	31.7	4.1	5.5	16.2	5.7	8.9
Sm (ICP-MS)	4.4	4.1	8.5	3.4	8.5	4.9	8.6
Sn (ICP-MS)	0.4	<1	3.9	0.9	1.4	1.3	1.5
Sr	481	527	176	133	213	88.7	169
Tb (ICP-MS)	0.7	0.6	1.0	0.6	1.0	0.5	1.1
Th	2	3	22.2	12.4	20.2	21.5	24.8
Tl (ICP-MS)	0.2	0.2	0.4	0.2	0.4	0.4	0.3
Tm (ICP-MS)	0.3	0.3	0.6	0.5	0.5	0.4	0.6
U (ICP-MS)	0.9	0.9	5.4	2.9	5.4	5.4	6.2
V	348	364	8.9	20.4	31.7	16.7	15.8
W (ICP-MS)	34.3	67.7	280.1	203.1	104.4	248.1	149.7
Y	18.4	16.8	34.6	26.2	34.6	21.1	34.6
Yb (ICP-MS)	1.9	1.7	3.6	3.2	3.5	2.5	3.5
Zn (ICP-MS)	385.9	58.1	54.0	45.6	100.3	23.7	33.5
Zr	45.1	42.1	179	160	678	334	382
Ti/Zr	122.4	128.4	8.0	6.2	9.5	5.3	6.0
P_2O_5/TiO_2	0.2	0.2	0.2	0.2	0.2	0.2	0.2

Sample	179383	179391	179392	179394	179400	179411	179416
Location	BOC-1 (91.7 m)	BOC-1 (483.5 m)	BOC-1 (543.4 m)	BOC-2 (160.9 m)	BOC-2 (612.5 m)	BOC-3 (400.1 m)	BOC-4 (382.6 m)
Facies	*Rqp*	*PfS*	*Rqr*	*Rf*	*Df*	*Rf*	*Rf*
Rock type	Rhyolite	Pol. sst.	Rhyolite	Rhyolite	Dacite	Rhyolite	Rhyolite
Major elements (wt. %)							
SiO_2	77.04	71.09	74.46	71.05	66.11	76.63	72.26
TiO_2	0.22	0.47	0.33	0.38	0.62	0.19	0.27
Al_2O_3	13.09	13.53	12.94	15.40	14.61	13.54	14.33
Fe_2O_3	1.79	3.48	4.12	3.19	5.98	0.97	3.42
MnO	0.06	0.16	0.11	0.12	0.53	0.05	0.08
MgO	0.54	0.82	0.82	1.61	2.90	0.29	0.58
CaO	0.25	2.28	0.96	0.40	4.14	0.46	1.05
Na_2O	5.64	2.25	4.40	4.08	3.53	6.67	5.66
K_2O	1.34	5.83	1.79	3.71	1.41	1.19	2.27
P_2O_5	0.04	0.10	0.06	0.07	0.15	0.02	0.07
Total	100.00	100.00	100.00	100.00	100.00	100.00	100.00
L.O.I.	0.76	1.99	2.06	1.72	2.73	0.83	1.52
Trace elements (ppm)							
As (ICP-MS)	<3	5.4	<3	<3	7.0	<3	<3
Ba	988	1779	496	2470	753	498	871
Be (ICP-MS)	1.4	1.9	1.3	2.2	1.8	1.2	1.9
Bi (ICP-MS)	<2	<2	<2	<2	<2	<2	<2
Ce (ICP-MS)	108.9	90.3	124.7	52.6	94.7	28.2	110.8
Co (ICP-MS)	22.6	18.6	34.3	21.3	28.3	35.7	18.3
Cr	1.4	4.8	2.8	<1	21.7	1.6	<1
Cu (ICP-MS)	5.8	9.5	1.7	3.6	3.2	1.3	1.2
Dy (ICP-MS)	3.5	5.8	6.3	5.0	6.1	4.6	5.6
Er (ICP-MS)	2.3	3.5	3.3	3.2	3.7	3.4	3.5
Eu (ICP-MS)	1.4	1.7	1.9	1.2	1.7	0.5	1.6
Ga	10.1	11.5	13.7	15.2	14.6	5.4	15.1
Gd (ICP-MS)	4.1	6.4	7.5	4.9	6.9	2.6	6.1
Ho (ICP-MS)	0.8	1.2	1.2	1.1	1.3	1.1	1.2
La (ICP-MS)	60.8	44.3	64.6	21.8	46.6	14.8	55.4
Li (ICP-MS)	5.8	7.8	7.3	16.1	14.8	1.7	8.5
Lu (ICP-MS)	0.4	0.5	0.5	0.5	0.6	0.5	0.6
Mo (ICP-MS)	0.6	5.0	0.9	4.8	4.1	0.9	1.0
Ni	1.1	5	2.6	3.2	10.2	1.1	1.4
Nb	8.4	10.5	11	12.8	11.1	9.6	11
Nd (ICP-MS)	36.5	39.4	50.5	27.6	41.6	11.6	44.3
Pb (ICP-MS)	45.1	156.8	3.2	22.6	6.8	6.8	3.8
Pr (ICP-MS)	11.0	10.4	13.7	6.7	11.1	3.2	12.3
Rb	32.1	167	70.8	89.2	34.4	27.6	47.9
Sc	5.8	8.3	9.6	5.8	19	2.8	5.1
Sm (ICP-MS)	5.7	7.7	9.4	6.0	8.3	2.6	7.9
Sn (ICP-MS)	<1	<1	4.5	<1	<1	<1	<1
Sr	221	195	148	212	457	156	161
Tb (ICP-MS)	0.6	1.0	1.1	0.8	1.1	0.6	1.0
Th	18.6	17.6	24.6	28.8	19	19.8	20.3
Tl (ICP-MS)	0.2	1.0	0.3	0.8	0.3	0.2	0.3
Tm (ICP-MS)	0.4	0.5	0.5	0.5	0.6	0.5	0.5
U (ICP-MS)	3.8	4.6	5.8	6.2	4.6	5.2	4.6
V	<3	38.6	49	17.7	104	<3	7.6
W (ICP-MS)	201.3	125.5	279.2	160.1	103.0	292.3	157.3
Y	19.5	31.9	31.2	31.3	35.1	28.4	33
Yb (ICP-MS)	2.5	3.4	3.1	3.3	3.6	3.4	3.6
Zn (ICP-MS)	53.8	562.2	67.2	38.0	194.1	24.5	56.5
Zr	197	216	161	414	213	162	193
Ti/Zr	12.5	6.6	13.1	5.5	17.6	7.0	8.5
P_2O_5/TiO_2	0.2	0.2	0.2	0.2	0.2	0.1	0.3

Sample	179421	179441	179443	179463	179464	179470	179486
Location	BOC-6 (156.4 m)	BPD-80 (377.4 m)	BPD-89 (85.5 m)	SCS-5 (96.3 m)	SCS-5 (152.0 m)	SCS-5 (397.0 m)	WSP-15 (388.8 m)
Facies	*Rqp*	*Rqr*	*Rqr*	*Mfp*	*Mfp*	*Mfp*	*Rf*
Rock type	Rhyolite	Rhyolite	Rhyolite	Basalt	And/Bas	And/Bas	Rhyolite
Major elements (wt. %)							
SiO_2	71.33	82.09	71.55	51.28	53.68	51.64	76.44
TiO_2	0.53	0.19	0.27	0.43	0.58	0.92	0.26
Al_2O_3	16.07	11.20	15.73	15.05	11.42	17.30	13.08
Fe_2O_3	3.53	0.31	4.46	9.89	9.88	11.22	1.82
MnO	0.13	0.02	0.11	0.19	0.30	0.26	0.04
MgO	1.36	0.23	0.88	9.44	13.52	5.51	0.39
CaO	0.59	0.95	0.35	11.92	8.84	8.45	0.90
Na_2O	2.99	3.80	5.10	1.36	1.27	3.44	4.15
K_2O	3.37	1.18	1.50	0.37	0.04	1.08	2.87
P_2O_5	0.10	0.03	0.04	0.07	0.45	0.18	0.03
Total	100.00	100.00	100.00	100.00	100.00	100.00	100.00
L.O.I.	2.32	1.83	1.95	2.58	5.52	2.76	1.37
Trace elements (ppm)							
As (ICP-MS)	13.0	<3	<3	<2	5.8	<2	<2
Ba	818	463	528	217	112	1150	874
Be (ICP-MS)	2.9	0.9	1.5	0.4	2.0	1.0	2.2
Bi (ICP-MS)	<2	<2	<2	0.0	0.1	0.0	0.1
Ce (ICP-MS)	190.8	38.2	68.8	17.9	159.3	35.3	92.3
Co (ICP-MS)	16.6	40.8	20.9	49.6	51.2	36.2	18.1
Cr	3.9	1.8	1.5	347	1185	25.4	2.5
Cu (ICP-MS)	10.2	1.5	1.8	25.2	51.5	22.4	1.1
Dy (ICP-MS)	5.4	2.9	4.4	2.4	4.6	3.6	5.6
Er (ICP-MS)	3.2	2.3	3.3	1.6	2.0	2.2	3.5
Eu (ICP-MS)	1.9	0.6	0.8	0.6	2.9	1.1	1.3
Ga	16.2	7.2	15.7	12.9	11.5	16.5	12.8
Gd (ICP-MS)	6.9	2.5	4.2	2.1	7.8	3.8	5.8
Ho (ICP-MS)	1.1	0.7	1.0	0.5	0.8	0.7	1.2
La (ICP-MS)	103.5	19.5	34.9	8.7	83.2	17.0	45.7
Li (ICP-MS)	16.3	39.8	18.0	20.1	49.7	17.0	6.1
Lu (ICP-MS)	0.5	0.5	0.6	0.2	0.3	0.3	0.6
Mo (ICP-MS)	2.2	0.6	1.7	0.7	1.0	0.7	0.3
Ni	2.5	1.5	2.4	119	319	10.8	2.7
Nb	11.5	7.3	9.4	1.6	6.5	3.3	13.6
Nd (ICP-MS)	68.5	14.4	26.7	8.8	67.5	18.0	38.0
Pb (ICP-MS)	17.2	15.5	12.3	2.8	10.0	70.8	3.7
Pr (ICP-MS)	19.9	4.1	7.5	2.2	18.5	4.4	10.7
Rb	145	35.6	43.2	11.2	1.6	27.8	112
Sc	10.7	4.9	9.2	38.8	31.9	29.8	4.4
Sm (ICP-MS)	10.2	2.8	4.9	2.1	11.9	4.1	7.3
Sn (ICP-MS)	<1	<1	<1	0.3	0.9	0.7	1.8
Sr	205	142	213	315	242	582	192
Tb (ICP-MS)	1.0	0.5	0.7	0.4	1.0	0.6	1.0
Th	26	12.6	17.9	2.4	22.8	3.5	20.7
Tl (ICP-MS)	0.6	0.3	0.3	0.1	0.0	0.2	0.3
Tm (ICP-MS)	0.5	0.4	0.5	0.2	0.3	0.3	0.5
U (ICP-MS)	5.6	3.1	3.9	0.6	4.6	1.2	5.8
V	43.6	7.6	18	259	221	322	4.6
W (ICP-MS)	91.3	376.0	156.4	79.9	26.4	48.3	135.6
Y	31.4	17.1	28.2	13.3	21.2	18.9	32.5
Yb (ICP-MS)	3.1	2.8	3.7	1.5	1.7	2.0	3.5
Zn (ICP-MS)	64.2	35.3	286.3	49.7	85.6	125.6	21.7
Zr	459	138	180	29.4	155	54.8	203
Ti/Zr	6.9	8.3	9.1	100.8	88.2	22.6	7.8
P_2O_5/TiO_2	0.2	0.2	0.2	0.2	0.2	0.8	0.1